ATLANTIS PRESS

Philippe Dillmann
Ludovic Bellot-Gurlet
Irène Nenner
Editors

Nanoscience and Cultural Heritage

Nanoscience and Cultural Heritage

Philippe Dillmann · Ludovic Bellot-Gurlet
Irène Nenner
Editors

Nanoscience and Cultural Heritage

ATLANTIS PRESS

Editors
Philippe Dillmann
LAPA-IRAMAT, NIMBE, CEA, CNRS
Université Paris-Saclay
Gif sur Yvette Cedex
France

Irène Nenner
Nenner.conseil Ltd.
Chaville
France

Ludovic Bellot-Gurlet
MONARIS "de la Molécule aux Nano-objets: Réactivité, Interactions et Spectroscopies", UMR 8233, UPMC-CNRS
Sorbonne Universités, UPMC Université Paris 6
Paris Cedex 05
France

ISBN 978-94-6239-197-0 ISBN 978-94-6239-198-7 (eBook)
DOI 10.2991/978-94-6239-198-7

Library of Congress Control Number: 2016936968

Foreword

The book forms an excellent blueprint and a welcome step in bringing nanosciences to the tangible cultural heritage community deriving from archaeological sites and artefacts, collections in museums, masterpieces, buildings and monuments. It gives a good overview on the uniqueness of cultural heritage systems that need to be studied by physico-chemical sciences in an interdisciplinary way, with the help of specialists of pure disciplines (physics, chemistry, material sciences) associated with those practicing interface disciplines such as archaeometry, and conservation science. This complexity of approaches to investigate a large number of objects, with a large heterogeneity at different scales, explains why the nanoaspects of cultural heritage systems have only appeared fairly recently. Indeed, this book is the first attempt to review how nanoscience is bringing new insights into this area.

I find the ambitious approach to cover the whole value chain from the importance of nanoaspects in ancient technologies of cultural heritage systems, through nanotechnologies and analytical strategies to characterise cultural heritage objects, up to the stage of their conservation and protection, in addition to new technologies, as well as the implications for societies including environmental aspects, very impressively. The book covers all topics from nanoparticles, nanomaterials and nanocomponents, from fundamentals of composition, structure and properties to nanosyntheses and processing aspects, characterisation, analytical techniques, and modelling. It also covers the conservation and protection of cultural heritage with nanomaterials, e.g., aspects such as corrosion, de-acification, etc., and cleaning and restoring.

The book introduces a large panel of prospect developments, largely due to the fact that the use of suitable nano-analytical methods within a multiscale-investigation, is still in its infancy and also because possible applications in specific material science (i.e., bio-inspired materials) and conservation methods, motivates education and offers an emerging field of research and innovation. It is a source of information and pinpoints new ideas and lists a large number of recommendations for all those involved in cultural heritage and restoration of historical

buildings; finally it provides an enormous potential for societal and economic benefits, including job creation.

The book is a great initiative and should receive the attention of specialists of cultural heritage, scientists interested in the application of nanosciences searching for reviews in this emerging field, but also citizens, policy-making bodies, research agencies or foundations who are searching for support of societal applications of nanosciences.

Marcel H. Van de Voorde
Prof. emer. University of Technology Delft
The Netherlands European Institutions Member, Science Council
French Senate and National Assembly Ret. European Commission, CERN
Science Advisor to Research Ministers, Universities
Research Institutes throughout the world

Contents

Contributors

Michele Baglioni Department of Chemistry and CSGI, University of Florence, Florence, Italy

Piero Baglioni Department of Chemistry and CSGI, University of Florence, Florence, Italy

Ludovic Bellot-Gurlet de la Molécule aux Nano-Objets: Réactivité, Interactions et Spectroscopies (MONARIS), UMR 8233, UPMC-CNRS, Sorbonne Universités, UPMC Université Paris 6, Paris Cedex 05, France

Nicole Bonelli Department of Chemistry and CSGI, University of Florence, Florence, Italy

Francesca Casadio Department of Conservation, Art Institute of Chicago, Chicago, USA

Lisa Chan EDAX, TESCAN USA, Warrendale, PA, USA

David Chelazzi Department of Chemistry and CSGI, University of Florence, Florence, Italy

Philippe Colomban MONARIS "de la Molécule aux Nano-Objets: Réactivité, Interactions et Spectroscopies", UMR 8233, CNRS, IP2CT, Sorbonne Universités, UPMC Université Paris 6, Paris, France

Philippe Dillmann LAPA-IRAMAT, NIMBE, CEA, CNRS, Université Paris-Saclay, Gif-sur-Yvette, France

Rodorico Giorgi Department of Chemistry and CSGI, University of Florence, Florence, Italy

Aurélien Gourrier University of Grenoble Alpes, LIPHY, Grenoble, France; CNRS, LIPHY, Grenoble, France

Marco Leona Department of Scientific Research, Metropolitan Museum of Art, New York, NY, USA

Lingjia Li TESCAN USA Inc., Warrendale, PA, USA

John R. Lombardi Department of Chemistry, City College of New York, New York, NY, USA

Rob McElroy Archive Studio, Buffalo, NY, USA

Delphine Neff LAPA-IRAMAT, NIMBE, CEA, CNRS, Université Paris-Saclay, Gif-sur-Yvette, France

Giovanna Poggi Department of Chemistry and CSGI, University of Florence, Florence, Italy

Federica Pozzi Department of Conservation, Solomon R. Guggenheim Museum, New York, NY, USA

Trinitat Pradell Physics Department and Center for Research in Nano-Engineering, Universitat Politècnica de Catalunya, Castelldefels, Catalunya, Spain

Patrick Ravines Art Conservation Department, State University of New York College, Buffalo, NY, USA

Ina Reiche CNRS, UMR 8220, Laboratoire d'Archéologie Moléculaire et Structurale (LAMS), Sorbonne Universités, UPMC Université Paris 6, Paris, France; Rathgen-Forschungslabor, Staatliche Museen zu Berlin-Preußischer Kulturbesitz, Berlin, Germany

Philippe Sciau CEMES, CNRS, Université de Toulouse, Toulouse, France

Richard P. Van Duyne Department of Chemistry, Northwestern University, Evanston, IL, USA

Huiping Xing Department of Chemistry and CSGI, University of Florence, Florence, Italy

Stephanie Zaleski Department of Chemistry, Northwestern University, Evanston, IL, USA

Introduction

We may consider that when Theodoric the great (6th AD) listed the seven marvels of the world, this was a first but probably unconscious attempt to define a kind of Cultural Heritage. More later, in several European countries, exists the willing of stressing the value of the heritage of ancient generations. For example during the French revolution, in 1794, the "*Instruction sur la manière d'inventorier et de conserver, dans toute l'étendue de la République, tous les objets qui peuvent servir aux arts, aux sciences, et à l'enseignement*" of the *Commission temporaire des arts, Comité d'instruction publique de la Convention nationale, l'an II de la République* declared: "the objects that serve to instruction [ ] will be found in libraries, museums, in cabinets, in collections [ ], in workshops were are gathered instruments, in palaces and temples decorated by masterpieces of arts; in all places where monuments shows what were humans, people, everywhere where lessons from past can be collected and transmitted to posterity". The contemporary definition of Cultural Heritage considers both tangible heritage (such as archaeological sites and artefacts, collections in museums, masterpieces, buildings and groups of buildings, monuments, landscapes, etc.[1]) and also intangible attributes of human groups (languages, folklore, traditions, biodiversity, etc.[2]) inherited from past generations. As stated by International Council of Museums (ICOM[3]) the main international organisation representative of museums and professional of museums, or the International Council of Monuments and Sites (ICOMOS[4]), both linked to UNESCO, this heritage must be protected and preserved for future generations.

Concerning tangible Cultural Heritage, in addition to other approaches (historical, ethnographical, archaeological, art history, conservation, etc.), physico-chemical

[1]Convention Concerning the Protection of the World Cultural and Natural Heritage: http://whc.unesco.org/en/conventiontext/; and Convention on the Protection of the Underwater Cultural Heritage: http://www.unesco.org/new/en/culture/themes/underwater-cultural-heritage/2001-convention/.

[2]Convention for the Safeguarding of the Intangible Cultural Heritage: http://www.unesco.org/culture/ich/en/convention.

[3]http://icom.museum/.

[4]http://www.icomos.org/en/.

sciences can be used to study what can be considered as Cultural Heritage systems (in the physico-chemical sense). Contrary to a large part of systems that are studied in experimental sciences and that can be synthetised, authorising reproducibility of measurement, heritage systems (as the other one studied in natural sciences or geology for examples) present several particularly as their uniqueness, their heterogeneity at different scales or their variability. For that reason their study using physico-chemical methods needs a high interdisciplinarity and the involvement, in addition to specialists of pure disciplines (physics, chemistry, material sciences, etc.), of "intermediaries" as scientists practicing archaeometry, conservation science, etc.

Moreover, the challenges on the one hand of understanding and preserving objects and buildings of the past and, on the other hand linked to the difficulty of setting adapted methodologies and scientific concepts, leaded scientists to implement, since the beginning of positive sciences during the nineteenth century, new analytical methods or disciplines on heritage systems. For example, one of the first experiment proceeded after the development of metallographic microscope and metallurgy was to observe damasked swords and to try to decipher their structure (see for example the works of G. Pearsonen, P. Anossov, Faraday and J.-R. Bréant). Besides, Willhelm C. Röntgen, the inventor of X-rays, has very early used his invention to investigate painting, polychromed sculptures and metallic archaeological artefacts. Soon after the discovery of X-rays, they were employed to better understand the structure of archaeological artefacts. After the Second World War, the development of analytical techniques (as neutron activation, X-ray fluorescence, magnetism, etc.) was quickly followed by applications to heritage artefacts; furthermore some specific methods dedicated to heritage problematics were invented, as radiocarbon dating (for which Willard Frank Libby received the Nobel Prize in 1960) or thermoluminescence dating (proposed by Martin J. Aitken). The development of these researches, with dedicated laboratories, leads to the first scientific journal dedicated to this field: "Archaeometry", which is published since 1958. Still at the end of the twentieth century and today, scientists follow the development of analytical techniques to implement their performances to enhance the deciphering of challenges (ancient techniques, materials, conservation) offered by Cultural Heritage systems. Nowadays because of their pluridisciplinarity and impacts in various fields, researches dealing with cultural heritage are accepted for publication in diverse categories of journals. It could be "multidisciplinary sciences", general or specialised journal in a scientific field (as chemistry, physics, earth sciences, analytical sciences), or journals dedicated to heritage problematics which more recently flowered with the multiplication of journals and publications [e.g. some of the most ancient ones: Studies in Conservation (since 1952), Journal of Archaeological Science (since 1974), ArcheoSciences-Revue d'archéométrie (since 1977), Journal of Cultural Heritage (since 2000)]. Sometimes the recall of new analytical techniques are only "one-shot" tries with low significant added-value in the domain of heritage, but often the use of these cutting-edge methods brings key results to the understanding of ancient systems. Some examples of this dynamic trend are the following journals special issues corresponding to papers given in international

conferences: Synchrotron Radiation in Art and Archaeology (SR2A) (Journal of Analytical Atomic Spectroscopy, issue 3, 2015), International Conference on Particle Induced X-ray Emission (Nuclear Instruments and Methods in Physics Research Section B: Beam Interactions with Materials and Atoms, volume 363, 2015). Thus, naturally, with the development of nanosciences and nanotechnologies at the end of the twentieth century and the beginning of the twenty-first century, scientists tried to benefits of these new approaches, methodologies and concepts for studying systems of Cultural Heritage. First attempts could be sometimes clumsy or artificial, but they have the merit to open the doors of nanoscale to conservation scientists and archaeometers.

Nanoscience and nanotechnology are based on the control of the knowledge, structure and function of materials on the nanometer scale, i.e. on the scale of one billionth of a metre. The gateway to this domain has been opened since 100 years, when W.C. Röntgen discovered the X-rays which allowed us to unravel the nanoscale structure of matter and when M. Planck, W.K. Heisenberg, E. Schrödinger and A. Einstein developed the language of quantum mechanics. Indeed, the nanometer world is governed by quantum mechanics and represents the interface between quantum and classical physics. As material systems and device structures become nanosized and nanostructured, new challenges have emerged: how to grow and design these artificial material structures in a precise and reproducible way and how to analyse their three-dimensional structure, properties and functions with the highest level of precision. In the past 40 years, the development of analytical techniques, capable to investigate the chemical, electronic and magnetic structure of any given material structure in any possible environment in a non-destructive way, has been spectacular. Among them, synchrotron radiation facilities providing micro-sized X-ray beams has a specific position because diffraction, diffuse scattering, tomography, spectroscopy, microscopy have produced unprecedented information in the nanoscale world. Generally, nanoscience and nanotechnology is an interdisciplinary ensemble of several fields of sciences such as materials science, physics, chemistry, biology and engineering. It is producing a true revolution because there are opportunities of connecting nanostructures with various functions and macroscopic properties as well as designing and fabricating new objects with specific functionalities. This explains why major consequences are expected in health and medicine, energy and environment, transport and space, communication and information.

Considering this short definition of nanoscience and nanotechnologies, one can think that “nano” is only a contemporary reality. Nevertheless, nanoscale can be addressed by looking ancient nanosystems. As illustrated by the various chapters of this book, “nano” plays a role at various step of the “ancient object life”. Nanoscaled systems have been manufactured since a long time, or nanostructures of natural materials are anciently exploited during manufacturing processes. The understanding of the processes to form such nano-features could reveal the selection of some specific raw materials and/or the setting of precise know-how. These impacts on the knowledge and organisation of ancient societies answer or renew some historical questions. Part I of this book dedicated to “Nanostructuration in

Ancient Materials" illustrates from diversified examples (materials, periods) such relations between nano-features and Cultural Heritage. This is demonstrated for multiple artificial materials and their related manufacturing techniques with: metallic-lustre ware (Chapter "Lustre and Nanostructures-Ancient Technologies Revisited"), nano-crystallisation in decorative layers of Greek and Roman ceramics (Chapter "Nano-crystallization in Decorative Layers of Greek and Roman Ceramics"), natural nanosized raw materials and sol-gel technology in pottery (Chapter "Natural Nanosized Raw Materials and Sol-Gel Technology: The Base of Pottery Since Millenniums") or for a more recent technique one of the first photographic process at the beginning of the XIXth century: daguerreotypes (Chapter "The Science Behind the Daguerreotype: Nanometer and Sub-micrometer Realities On and Beneath the Surface"). Besides, natural biomaterials (bones, ivories, antler) intensively used by men along their history are complex organic/mineral composites which must be studied down to the nanoscale in order to ensure their identification (nature and associated species), to understand their properties, to reveal treatments and to undertake adapted conservation strategies (Chapter "Informative Potential of Multiscale Observations in Archaeological Biominerals Down to Nanoscale"). Through scales the understanding of the influences of the nanoscale on the macroscopic properties (aesthetic, mechanic, durability, etc.) is challenging. Ancient societies prepared some objects with nano-features to obtain some "macro" properties, readily evaluable at these periods. One can even consider that ancients were practicing nanotechnologies but with no means to observe the results of their "trial-and-error" approach with probes revealing the nanoscale and models explaining the properties. The challenge offered nowadays is to understand the effects of "nano" on the macro-scale in quite complex samples prepared in the past by an often currently unknown process or of natural ones not already fully understood. It has to be stressed that these concerns about relations between structures from the nanoscale and properties are the same than the current challenges in new material design. Tackling these challenges in ancient artefacts could inspire modern material designs, as one searches some concepts in "bio-inspired materials" (see for example: Sanchez et al. 2005; Nicole et al. 2010).

Besides, the needs to investigate objects at the nanoscale level (especially through the chemistry and material scientific aspects), conducted scientists to use new suitable characterisation techniques. These analytical techniques which open the "nano world" and which can be of great interest for the study of heritage systems are discussed in Part II "Nanotechnologies and Analytical Strategies to Characterise Cultural Heritage" with the Chapters "Surface-Enhanced Raman Spectroscopy: Using Nanoparticles to Detect Trace Amounts of Colorants in Works of Art" and "From Archaeological Sites to Nanoscale: The Quest of Tailored Analytical Strategy and Modelling". Nevertheless, some specific precautions should be taken for an efficient and significant use of nanotechniques. Lastly, new insights at nanoscale bring other point of views and new challenges concerning the bridging of the gaps between functional scale (macroscopic scale) and nanoscale, as especially discussed in Chapter "From Archaeological Sites to Nanoscale: The Quest of Tailored Analytical Strategy and Modelling".

A third aspect linked to heritage artefacts and systems is the understanding and the management of the alteration processes. First because it is needed to properly identify and differentiate anthropic information from alteration effects; second to propose suitable and efficient conservation (preventive or curative) and restoration strategies. These aspects are presented in Part III "Conserve and Protect the Cultural Heritage using Nanomaterials and Nanoscience". Altered materials are heterogeneous at all scales, and the setting of a global mechanism requires starting from the nanoscale at which the chemical reactions occur. Studying transport mechanisms or reactivity underlines the role of nanostructures or interfaces in the complex thick layers of alterations. Moreover heritage systems give an unique opportunity to explore the very long time span, for which mechanisms are specific and with given material characteristics produced over long periods which could not be reproduced by accelerated processes in laboratories. Studying ancient artefacts as "analogues" of modern ones in order to predict their very long term behaviour could answer: on the one hand questions about modern material durability; and on the other hand issues on the ways to conserve the heritage artefacts, gathering for the future the becoming of ancient and present objects. An illustration is given in Chapter "Nanoscale Aspects of Corrosion on Cultural Heritage Metals" with the case of the corrosion of metallic heritage artefacts and their protection.

As stated in the beginning of this introduction, a crucial aspect is the protection of cultural heritage objects by setting adapted treatments. As indicated by the International Centre for the Study of the Preservation and Restoration of Cultural Property (ICCROM[5]), the restoration or protection treatment must be adapted to the specific case of heritage systems, must easily be removable and should not alter the aspect of the artefact or heritage system. Additional requirements are also practical ones, as a quick preparation, a relatively low cost and a straightforward use, because the global costs should be controlled and accordingly only few museum laboratories have the extensive sample preparation capabilities of university-based facilities. Besides, dealing with archaeological artefacts on the field or monuments requires procedures adapted to on-site work. Two chapters will present several cases where the nanotechnologies propose innovative solutions for preserving the Heritage. The systems presented are linked to paper with alkaline nanoparticles for deacidification and pH control (Chapter "Alkaline Nanoparticles for the Deacidification and pH Control of Books and Manuscripts"), or cleaning procedures using gels and nanofluids (Chapter "Confined Aqueous Media for the Cleaning of Cultural Heritage: Innovative Gels and Amphiphile-Based Nanofluids").

The studies around cultural heritage systems, dealing with nano-aspects, are obviously relatively recent. One could expect many developments with the current possible increasing access to the nanoscale, through analytical approaches or mechanisms description across scales from the element, the molecules, to the functional scale of the artefacts or the system. Thus the aim of this book, mixing general review and some more specific case studies, is to provide a global overview

[5] http://www.iccrom.org/.

of the up-to-date and significant aspects of nanoscience and nanotechnologies in the domain of Cultural Heritage to give examples of potentialities and good practice of these axis of researches, integrated in the large panel of approaches and scales dealing with the study of tangible cultural heritage for the next decades.

References

Nicole L, Rozes L, Sanchez C (2010) Integrative approaches to hybrid multifunctional materials: from multidisciplinary research to applied technologies. Adv Mater 22:3208–3214

Nuclear Instruments and Methods in Physics Research Section B: Beam Interactions with Materials and Atoms, vol 363, 2015

Sanchez C, Arribart H, Guille MMG (2005) Biomimetism and bio-inspiration as tools for the design of innovative materials and systems. Nat Mater 4:277–288

Synchrotron radiation and neutrons in Art and Archaeology 2014 (2015) J Anal At Spectrom 30(3):529–840

Part I
Nanostructuration in Ancient Materials

Lustre and Nanostructures—Ancient Technologies Revisited

Trinitat Pradell

Abstract *Lustre* is a glaze decoration with a colourful metallic and iridescent appearance of sparkling beauty. It is among the first technologies which made use of the peculiar optical properties of nanostructures, and in particular, of metallic nanoparticles. It involves also a scientifically advanced method of production which is able to trigger the lustre optical properties (colour and shine) of the decorated object. Consequently, among the various technologies developed in historical times able to generate nanostructures and modify the physical properties of the materials, *lustre* is unquestionably the one involving the utmost technological advance. The chapter unveils the science behind lustre, how the nanostructure is obtained, how it is related to the lustre colour and shine, and explores the main features of historical lustre productions.

1 Introduction

Metallic and iridescent glazes containing metallic particles (gold, silver, copper, iron) were produced since early medieval times with the object of either imitating metal objects to give to the ceramics an extra value or simply producing objects of sparkling beauty. Many different methods for producing metallic and iridescent glazes and glaze decorations have been developed since then but, among them, *lustre* decorations (Figs. 1, 2 and 3) are unquestionably those involving the utmost technological advance and are distinguished fundamentally by the total absence of relief.

In fact, *lustre* is a micrometric layer made of silver and/or copper metallic nanoparticles lying beneath the glass surface of an artefact (Fig. 1b, c) which shows a large variety of colours (green, yellow, amber, red, brown, white) (Fig. 2) and metallic (golden, coppery, silvery) (Fig. 3a) and iridescent (bluish, purplish)

T. Pradell (✉)
Physics Department and Center for Research in Nano-Engineering,
Universitat Politècnica de Catalunya, Campus Baix Llobregat,
Esteve Terrades 8, Castelldefels 08860, Catalunya, Spain
e-mail: Trinitat.Pradell@upc.edu

P. Dillmann et al. (eds.), *Nanoscience and Cultural Heritage*,
DOI 10.2991/978-94-6239-198-7_1

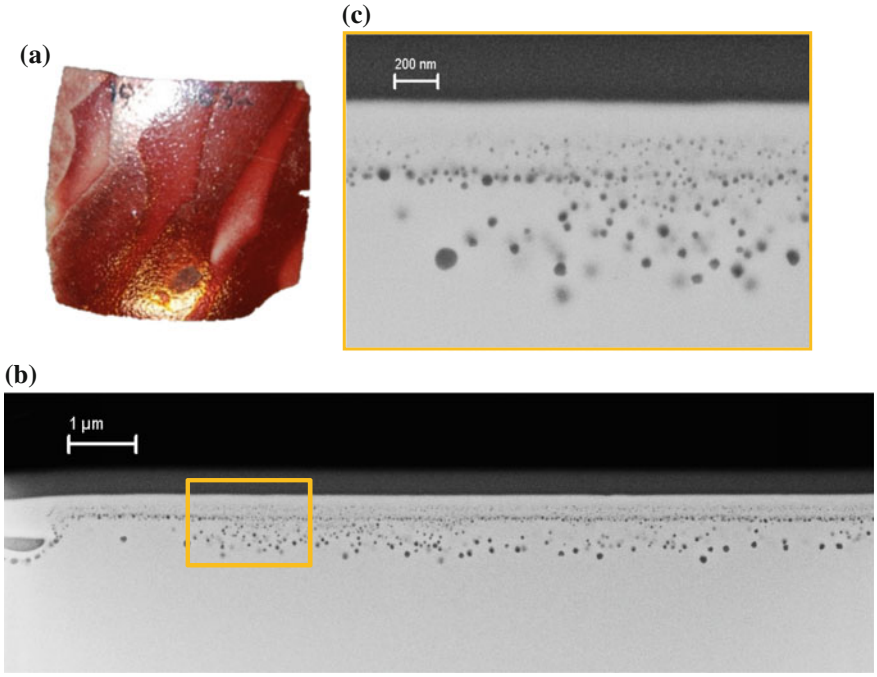

Fig. 1 **a** Red coppery lustre (Iraq, 9th century AD); **b** Nanostructure of the lustre layer; **c** Magnification of the *yellow square area* in **b**

appearance (Fig. 3b). Among them, a most remarkable feature is the high specular reflectance which conveys to the decoration a metallic-like shine (Fig. 3a). Although all this may suggest a product of modern nano-science and technology, the fact is that the first *lustre* was produced at least 1300 years ago. Consequently, the study of historic *lustre* layers, the materials and processes used in their production, as well as their optical properties and in particular the link between the optical properties and the lustre nanostructure have attracted much interest among the scientific community. (Pérez-Arantegui et al. 2001; Jembrih-Simbürger et al. 2002; Bobin et al. 2003; Padovani et al. 2003; Padeletti and Fermo 2004, 2013, Pradell et al. 2005, 2006, 2007, 2012; Bethier and Reillon 2006, Reillon and Bethier 2013; Molera et al. 2007; Polvorinos del Rio et al. 2008; Colomban 2009; Sciau et al. 2009; Gutierrez et al. 2010; Delgado et al. 2011; Chabanne et al. 2012).

Although *lustre* is not the only historic material where metallic nanoparticles are present, it is the one implying the utmost scientific and technological achievement. Among the many materials containing metallic nanoparticles we can mention the dichroic Roman glass, i.e. Lycurgus cup (Barber and Freestone 1990), which appears red in transmitted light and green in reflected light as a consequence of the presence of gold and silver nanoparticles; the red glasses, glazes and enamels (Freestone et al. 2003; Kunicki-Goldfinger et al. 2014; Wood 1999), the colour of which is due to the

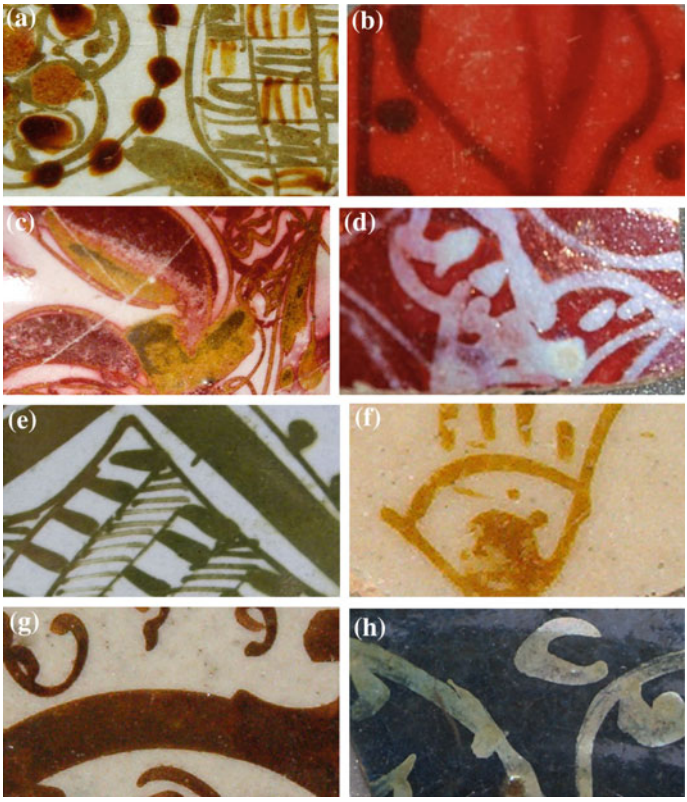

Fig. 2 Colours of lustre. **a**–**d** Iraqi polychrome 9th century; **e** Iraqi monochrome 10th century; **f**, **g** Fatimid late 10th–12th century; **h** Syrian or Egypt 14th century

presence of metallic copper and cuprite nanoparticles; and also, the gold ruby glasses whose colour is due to the presence of metallic gold nanoparticles. However, none of them has a lustrous appearance and the nanoparticles are present in the whole glass thickness.

The term *lustre* is often used among the potters to define any type of metallic-iridescent glaze, and *clay-paste lustre* or *transmutation lustre* is used to distinguish the *historic lustre* from other types of lustrous glazes (Clinton 1991; Caiger-Smith 1991; Hamer and Hamer 2004). In fact, metallic-iridescent glazes were also made following other methods of production. For instance, in *raku ware*, copper, silver or other metals are added to the glaze mixture, the ceramics are covered with clay and combustible material which produces a strong reducing atmosphere during the firing after which the ceramic is cooled in an oxidising atmosphere in flowing water when metallic particles precipitate in the glaze (Hamer and Hamer 2004). Another method consists in applying a *resinate* over the glaze, a *resinate* being a low temperature glass mixture which contains metals and reducing

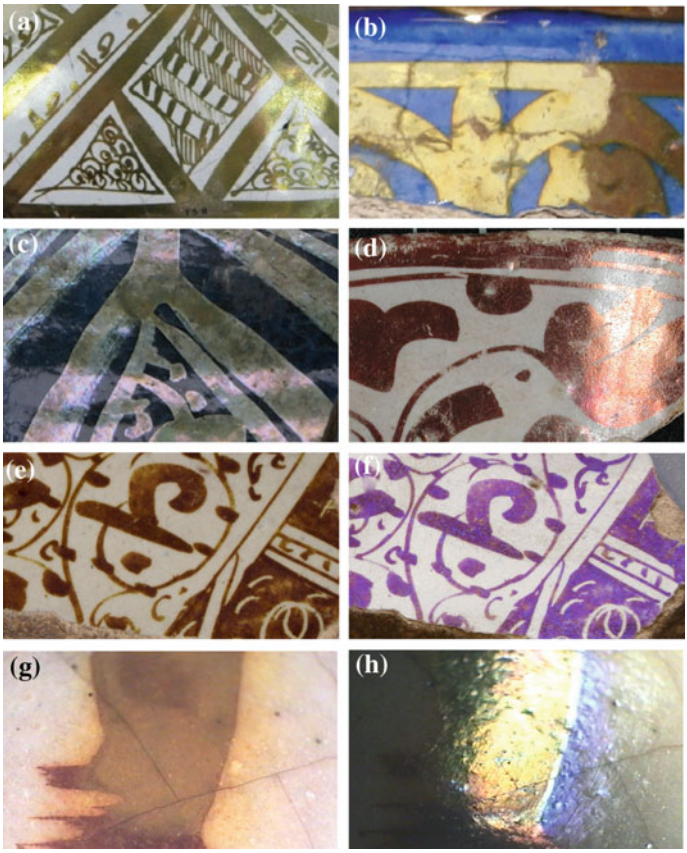

Fig. 3 Metallic like shine of lustre: **a** Green-golden (Iraq 10th century AD); **b** yellow golden (Syrian 14th century AD); **c** white-silvery (Syria, 14th century AD); **d** Red coppery (Barcelona, 16th century AD). Iridescent lustre (Fatimid, Egypt, 11th–12th century AD): **e** and **f** Brown-purplish; **g** and **h** yellow golden-bluish iridescences

agents which after firing forms a glass layer attached to the glaze surface like an enamel, but containing metallic nanoparticles (Clinton 1991). Furthermore, a metal foil may be fused onto the glaze surface after firing. In all the cases a metallic surface finishing may be obtained provided that the adequate firing conditions are applied. *Resinates* and metal foils are distinguished from *lustre* because they protrude or stand in relieve above the glaze surface in contrast to *lustre* which shows a total absence of relief. *Raku* and all types of reduced glazes are also distinguished from *lustre* because the metallic particles are present in the whole glaze thickness.

All of them are characterised by a production process where simply the mixing of metals into the glass and the control of kiln temperature and atmosphere induce the development of the nanostructures. Contrariwise, *lustre* is the result of a complex process with very close connections to modern nanotechnologies.

Consequently, *lustre* will be more precisely defined by the method of production rather than by the small thickness of the layer or the presence of metallic nanoparticles.

A lustre pigment is constituted basically by salts of copper and silver and a sulfur compound all of which are finely ground and mixed together with some organic medium or clay. The lustre pigment is painted over the glass surface and placed in the kiln at relatively low temperatures to avoid the glass softening. After firing the lustre pigment relic is rubbed off revealing the lustre layer beneath.

From this description, two important facts are revealed, on the one hand that the lustre layer is the result of some kind of reaction between the lustre pigment and the glass surface and, on the other hand, that the lustre pigment is missing from the finished objects. Moreover, the lustre layer microstructure, i.e. nature and size of the nanoparticles, position and thickness of the layer and distribution of the particles in the layer, depends on the materials (lustre pigment and glass substrate) and firing protocols. Therefore, variation on the materials and firing protocols in different epochs and places is responsible for the various appearances shown by the lustre decorations.

We will first give some historical background and describe the historical context of the main lustre productions; then we will explore the historical information available about the lustre technology. We will discuss the science behind lustre, including the chemistry (materials and reactions) and physics (nanostructure and optical properties) and how they are connected. We will present what is known about the materials and methods used in the various historic lustre productions, how they changed and how the changes relate to the appearance of the objects. A final section will be dedicated to the link existing between lustre and Alchemy.

2 Historical Setting

The first *lustre* decorations were applied on glass, the earliest identified objects dating to between 772 AD and 779 AD (Brill 1979; Jenkins 1986; Carboni 2002). Those *lustr*e painted glass objects were produced in Egypt or Syria (there is not full agreement between scholars about the place) and probably dated earlier (there is no agreement either but it has been suggested that as early as the 6th century AD). Lustre glass continued being produced by the Fatimid (10th–12th centuries AD) and also Byzantine glassworkers (10th–13th centuries AD) (Pilosi and Whitehouse 2013). Later, in the 13th century, lustre paints were also used to produce the so-called yellow stained glass for the windows of the cathedrals in central Europe. Soon after, in the Renaissance (15th–16th centuries) the palette of colours was expanded and not only yellow but also amber, orange and red stained glasses were produced.

Actually, lustre painted glass is often referred as stained glass due to the fact that it rarely shows distinct metallic lustre (Brill 1979). Robert H. Brill studied a large amount of lustre painted glass fragments (above 700 fragments) from an excavation

in Fustat (Cairo) and less than 15 % showed any metallic lustre effect. Only a few showed a mirrorlike effect, what we call silvery, and most of the lustre appeared only ephemeral, although they all appeared in very good conservation conditions. Here lated this to a possible loss of the lustrous effect over the centuries. However, as we will see when discussing about lustre technology, this is not wholly unexpected.

Following Lamm (1941), (Carboni 2002) lustre painted glass is classified into three main periods. The earliest, amber-brown lustre, often two sided, painted over clear or lightly tinged glass dates to the 8th century. Opaque deep yellow-orange lustre painted over a cobalt blue transparent glass, opaque red ruby lustre painted over a dark olive glass as well as polychrome glass, date to the 9th or 10th century. Finally, amber, brown or greenish lustre paintings applied over a clear glass with a high artistic quality were produced during the Fatimid period (10th–12th centuries). Actually, the rich range of colours shown by the lustre painted glasses seems more the desired purpose than the lustrous effect itself. Later on, we will see that, in fact, the *lustre* painted glass and *lusterware* decoration nanostructures also show distinctive microstructural features.

There is quite wide agreement between scholars that lustre decorated glaze ceramics started being produced in the 9th century in Iraq, under the Abbasid rule (750–1258) (Watson 1985; Caiger-Smith 1991). Künel (1934) dated the polychrome (brown-green-amber) lustres as the earliest (Fig. 2a), followed by the bichrome (red-black, red-yellow or red-silvery and brown-green) (Figs. 1, 2b, 3c, d) and then by the monochrome green lustres (Fig. 2e). Green and yellow often show a golden shine (Fig. 3a, b) while red lustre sometimes shows a coppery shine (Fig. 3b). Generally speaking polychrome and bichrome lustres are dated to the 9th century while the monochrome lustres to the 10th century. This dating corresponds well with the lustre painted glass studied by Brill (1979) as mentioned above with the sole difference that the lustre painted glasses were found in Cairo and attributed to the Egyptian glass workshops. Nevertheless, besides this large lustre painted glass production there is no evidence of a contemporary Egyptian lusterware production (Figs. 2f–h and 3e–h). Lustreware stopped being produced in Iraq by the end of the 10th century. Some theories suggest the fracture of the Abbasid caliphate that was forced to cede authority to the Fatimid in Egypt and which may have been accompanied by the migration of the potters. In fact the complexity of the lustre production suggested that copying is unlikely and that direct transmission of knowledge is more probable, as a consequence, the migration of potters has traditionally been considered the main mechanism of geographical expansion of lustre. However, this seems not to apply for the transmission between lustre painted glass and lustre decorated ware, as the early Egyptian lustre glass production mentioned above is not accompanied by a contemporary lustreware production.

After the Abbasid lustreware, the next unquestionable lustre production was set in Egypt (Fustat) during the Fatimid rule (909–1171), earliest datable objects being around the year 1000. Fatimid lustre is monochrome green-yellow later shifting to stronger orange (Fig. 2f, g) and brown (Figs. 2g and 3e–h) colours and showing often a golden shine (Philon 1980) (Fig. 3g, h). The Fatimid lusterware stopped

probably due to the take-over of Egypt by Saladin who established the Ayyubid dynasty, although the political and social instability at the end of the Fatimid dynasty may have helped an earlier movement of potters to other more peaceful areas (Watson 1985).

A clear direct connexion between the end of the Fatimid production and the beginning of lustre production in Iran (Kashan) can be established (the earliest object dates 1179). Watson firmly states, that the sudden start of Iranian lusterware was due to the migration of Egyptian potters after the Saladin destruction at Fustat (Watson 1985). A large lustre decorated tile production started in the second half of the 13th century and 14th century. After this period lustre nearly disappears in the Middle East until the 17th century under the rule of the Safavids. Well fired Kashan lustre is brown with golden shine and often appears combined with cobalt blue and copper turquoise decorations, and is also applied over cobalt tinged transparent glazes. Safavid lustre is red with golden and coppery shine often combined with cobalt blue and yellow decorations and also applied over cobalt tinged transparent glazes.

Besides the Iranian production, during the Fatimid regime lustre appears already spread all over the Islamic lands. Some recent findings suggest the existence of local productions in Tunisia dating before second half of the 11th century (Waksman et al. 2014) and in Al-Andalus, second half of the 11th and 12th century (Albarracín, Almeria, Zaragoza) (REMAI 2015). Yellow golden and red lustre are found in Zaragoza and Albarracín, and red coppery lustre is found in moulded objects from Almeria (Rosser-Owen 2010).

Syrian lusterware begins in the first half of the 12th century, it is called *Tell Minis* lustre (Porter and Watson 1987) showing a clear Egyptian influence (i.e. similar colours and designs). At the end of the 12th century, without clear continuity between them, a very distinct lusterware production (red-brown lustre) appears in Raqqa (Porter 1981; Jenkins-Madina 2006). Raqqa lusterware is contemporary to, and shows also clear stylistic similarities with the Iranian lusterware; it ends in 1260 due to the destruction of the city by the Mongols invasion. Again without continuity with the earlier lustres, it reappears in Damascus by the end of the 13th century, with a yellow golden over cobalt tinged transparent glaze (Figs. 2h and 3b).

The next production in importance, mainly due to the high quality of the few objects preserved, is the 13th–14th century lustre from Malaga (Rosser-Owen 2010). Contemporarily, a mass lustre ware production, the first outside the Islamic lands, begins in Manises (second half of the 14th century and 15th century) (Fig. 3d). Hispano-Moresque lusterware (Fig. 3d) was exported all over Europe and can be found in all the noble and rich houses in central Europe. 14th century lustres are brownish golden. Lustre does not disappear but continued being produced in other places in Spain until the first half of the 20th century although the objects tend to be of low quality and with a coppery finish.

During the 16th century, lustre was introduced in the Italian majolica produced in Deruta and Gubbio (Caiger-Smith 1991; Padeletti and Fermo 2004; Padeletti et al. 2004; Padeletti 2013). The most remarkable characteristic of Gubbio

lusterware is the reintroduction of the red ruby lustre which is found together with the characteristic Italian yellow golden lustre. This is the first time that red ruby lustre and polychrome lustre is produced since the 9th century.

During the second half of the 19th century lustre is rediscovered by some companies (red ruby lustres from William de Morgan in England, Vilmos Zsolnay in Hungary or Clément Massier in France) (Clinton 1991; Caiger-Smith 1991). By the turn of the 20th century, various potters all over Europe reintroduced lustre to obtain beautifully coloured, iridescent and metallic surfaces for their objects (Allan Caiger-Smith, Margery Clinton, Said El Sadr, Jordi Serra Moragas among many others). With them lustre became an art object appreciated by the beauty and singularity of each piece and the great difficulty in producing them.

3 Chemistry and Physics Behind Lustre Nanotechnology

3.1 The Chemistry of Lustre

As we have mentioned above, the lustre layer is the result of some kind of reaction between the lustre pigment and the glass surface. Moreover, the lustre pigment is rubbed off from the finished objects and consequently missing. In a very few cases, workshop structures and within them, samples of the original lustre pigment, or fragments of unfired lustre-painted ceramics have been found; for instance those associated with 14th century AD Islamic and Hispano-Moresque lusterware from Spain (Molera et al. 2001a, b).

Consequently, the composition of the lustre pigment is still unknown for most of the lusterware productions, although in some cases information can be inferred from analysis of the lustre layer (Brill 1979; Padeletti and Fermo 2004; Molina et al. 2014; Pradell et al. 2016). Recipes for lustre production are given in a small number of treatises among the earliest of which is the "Kitab Al-Durra Al-Maknuzna (The book of the hidden pearl)" by Jazbir Ibn Hayyan (c. 721–c. 815 AD) (Al-Hassan 2009) where a series of recipes for the production of lustre on glass are detailed.

Jabir Ibn Hayyan's treatise describes a series of 118 recipes for *talawıh* (lustre painted or stained glass), in which the metals are mainly added as "*burnt silver*" and "*copper burnt with sulphur*". In addition, cinnabar (HgS), *vitriol,* sulphates of metals (copper and iron), realgar (AsS), orpiment (As_2S_3) or sulphur and magnesia are added. Finally, in some cases "*ceruse*" (white) of lead and/or tin is also described (probably lead carbonate $PbCO_3$ and tin oxide SnO_2). The ingredients mixed with some vinegar and citrus juice and thickened by small amount of Arabic gum, are applied to the glass surface.

With regard to the production of ceramics, the earliest treatise is Abu'l Qassim (Abd Allah Ibn Ali Al Qashani) dated to 1301 AD (Brill 1979; Allan 1973) which describes the materials and procedures followed in the production of Kashan lustreware. The pigment is made of silver or gold marcasite (probably chalcopyrite—

$CuFeS_2$) and red and yellow arsenic (i.e., realgar and orpiment) with "*burnt silver*" and "*roasted copper*"; everything being ground very fine and mixed with vinegar and grape juice. It is also indicates that *sirinj*, which is interpreted as a lead-tin mixture is sometimes added. It has to be fired with little smoke in a second oven made especially for this purpose. After cooling the pigment has to be rubbed off with wet earth.

Later Islamic treatises on lustre painting on glass appear to be a compilation from earlier treatises (Heaton 1948). The earliest European text where a recipe of lustreware is given in "El llibre de les fornades" from Nicolau de Reyner, Barcelona dated to 1514–1519 AD (Ainaud de Lasarte 1942) and Cipriano Picolpasso's "Three books of potters art" dated to 1558 AD (Caiger-Smith and Lightbown 1980). They describe the same basic recipe which includes cinnabar, an earth rich in iron oxides, copper sulphide, sulphur and silver. In fact the lustre pigment found in the excavation of workshops from Paterna and Manises, show also the same ingredients (Molera et al. 2001b).

In summary, the basic ingredients are silver and copper salts, obtained after burning silver and copper (some indicate with sulphur) and a sulphur containing compound such as cinnabar, copper, iron and arsenic sulphide or iron/copper sulphates. Earlier recipes indicate also the addition of some tin/lead compound (probably mixed lead-tin oxides) together with Arabic gum, substituted in later recipes by an earth rich in iron oxides. The ingredients have to be ground and mixed with vinegar and grape juice or citrus juice before application.

Replication of the process using any of the previous recipes has been undertaken (Brill 1979; Jembrih-Simbürger et al. 2002; Delgado et al. 2011 for lustre painted glass and Molera et al. 2007 also for lustreware) and the science behind lustre has unfolded. The mechanism by which silver and copper react with the glass surface is what is known as "ionic exchange" which happens between the silver ions (Ag^+) but also copper ions (Cu^+ or Cu^{2+}) from the lustre paint and the sodium (Na^+) and potassium (K^+) ions from the glass. Ag^+ is very similar in size and also has the same electric charge as Na^+, but it may also substitute K^+ and the same happens with Cu^+. Figure 4 shows how the process takes place. A copper lustre pigment containing 30 % HgS, 10 % CuO, 60 % clay in water is applied over a modern glass (Fig. 4a-1) and fired at 550 °C for 10 min under oxidising conditions; after removing the lustre pigment the glass appears yellow tinged (Fig. 4a-2) due to the precipitation of cuprite (Cu_2O) nanoparticles (Fig. 4b-2); if a reducing gas is introduced for 5 more minutes, the glass appears red tinged (Fig. 4a-3) due to the precipitation of metallic copper (CuO) nanoparticles as a result of the reduction of most of the cuprite (Fig. 4b-3). Chemical analysis of the red lustre (Fig. 4c) shows an inverse linear correlation between sodium and copper atoms demonstrating that each sodium ion has been replaced by a copper ion, the so called "ionic exchange", which happens during the lustre firing.

Moreover, Fig. 5 shows the X-ray Diffraction pattern corresponding to the lustre pigment after firing; among the compounds expected to be formed during the firing, sodium sulphate (thenardite) is most probably formed during the cooling. Its presence gives a good clue that the compound responsible for the ion-exchange mechanism is a mixed sulphate melt. As a consequence, sulphur needs to be present

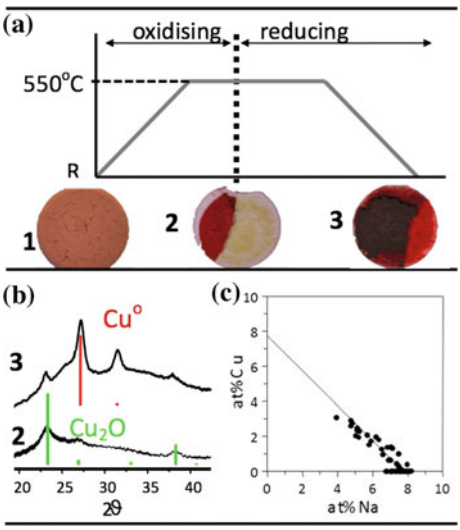

Fig. 4 **a** Firing protocol (10 °C/min heating rate, 20 min at 550 °C and free cooling). *1* copper lustre pigment (10 % CuO, 30 % HgS, 60 % clay; *2* After firing for 10 min under oxidising conditions; *3* then after firing for 5 more minutes under a reducing firing. **b** XRD-patterns of the glass surface *2* and *3* after removing the lustre paint. **c** Analysis of the glass surface *3* showing the substitution of sodium by copper

in the lustre pigment. In the case studied, sulphur has been added as cinnabar (HgS), and a more complete study of the reactions taking place (Pradell et al. 2004) shows how at temperatures above 400 °C the sulphur reacts with the copper and silver compounds producing copper and silver sulphates and sulphides. Moreover, the decomposition of cinnabar produced a sulpho-reducing atmosphere able to reduce Cu^{2+} to Cu^{+}, and result in the formation of a silver-mercury amalgam.

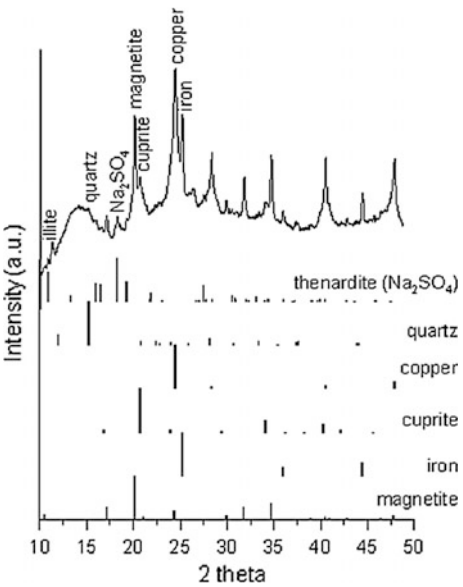

Fig. 5 XRD-pattern obtained of the lustre pigment from Fig. 4 after firing

Looking at the recipes we can see that sulphur was also added as copper sulphide; and other recipes indicate that the silver (and also copper) was sometimes previously burnt with sulphur. Finally, the addition of sulphur itself to the pigment mixture is also sometimes indicated, and its role would be to generate a sulpho-reducing atmosphere and produce copper and silver sulphides and sulphates.

Although all the lustre recipes found or described in the ancient treatises add sulphur as main ingredient in the lustre pigment, other silver and copper salts, such as silver and copper chlorides (AgCl, CuCl) and silver nitrate ($AgNO_3$), may also act as vehicles for ionic exchange, if they become molten at the right temperature range. It is not improbable that some chlorides could be present in the lustre pigment resulting from the complex preparation procedures described in the treatises. However, silver nitrate was not yet discovered in early Islamic times. What is true is that later, with the industrial revolution (18th and the 20th century) both AgCl and $AgNO_3$ were used in the production of the silver yellow lustre paints (Caiger Smith 1991; Jembrih-Simbürger et al. 2002). Some replication experiments of silver painted lustre glasses (Jembrih-Simbürger et al. 2002) demonstrated that modifying the glass paint, using either silver nitrate, sulphate (Ag_2SO_4), chloride and phosphate (Ag_3PO_4) together with different optimal firing temperatures, resulted in larger or smaller silver nanoparticles. However, only $AgNO_3$ gave rise to a homogeneous yellow colour.

The addition of clay or Arabic gum is related to the need of a dispersal medium that gives some plasticity to the paint, although some clay minerals may also act as an ion-exchange medium. Other compounds such as tin and iron oxides could act as a redox buffer, controlling the reducing process, in the pigment during firing.

The recipes also often describe very finely grinding together at the compounds with vinegar, grape or citrus juice to obtain a fine homogeneous pigment. The reason for the addition of vinegar has been discussed in terms of either producing copper and silver acetates which during firing would presumably generate a reducing atmosphere; assisting the drying of the painted pigment; acid attacking the glass surface and generating more free surface for the lustre to form in; or acting as a deflocculant preventing the particles in the paint from agglomerating or settling (Brill 1979). The last is the most probable reason, as laboratory replications showed that copper and silver acetates are not decomposed during the firing and lustre does not take in those areas where acetates are present (Molera et al. 2007).

Once copper and/or silver ions enter the glass surface they diffuse inside the glass, the inter-diffusion process depending on the cations from the glass involved in the ionic exchange. We have to mention that the firing temperature has to be higher than the glass transition temperature (T_g, temperature at which the viscosity of the liquid is 10^{12} Pa s) of the substrate glass. This is necessary because at temperatures above T_g, the glass behaves as a liquid and, as a consequence, atomic diffusion coefficients show a great increase (Doremus 1994). However, T_g depends on the heating rate and is lower at low heating rates, so that heating a soda-lime glass (16 % Na_2O and 10 % CaO) at 20 °C/min, T_g is 578 °C, while heating it at 2.5 °C/min the T_g is reduced by 33°. Finally, the glass softening temperature should not be reached to avoid the pigment sticking onto the glass surface. These

restrictions leave a relative narrow range and a dependence on the composition of the substrate glass for the lustre firing temperature.

The glass transition temperature decreases with increasing the alkali (Na_2O and K_2O) and contrariwise, it increases with increasing CaO, MgO or Al_2O_3. Finally, the incorporation of PbO results in a decrease by more than 100 °C in the glass transition temperature. Most of the early Islamic glasses are of the soda-lime type (between 17–20 % Na_2O, 7–15 % CaO, 1–5 % MgO, 1–3 % K_2O and 1–3 % Al_2O_3) which means typical glass transition temperatures between 550 and 650 °C, and therefore optimal firing temperatures above 600 °C. This agrees with the firing temperatures found to be adequate by Brill (1979). Moreover, soda-lime and potash-lime glasses were tested to replicate lustre painted glass (Delgado et al. 2011), and for a soda-lime glass firing temperatures between 600 and 650 °C were required while for potash glasses the optimal firing temperature was 550 °C. On the contrary, the composition of the glazes may vary a lot between productions and large amounts of PbO are incorporated in many cases. Consequently, the firing temperatures are expected to be lower than for glass, in particular, replication experiments have shown that 550 °C is the most frequent optimal firing temperature.

One of the most astonishing results from the replication work (Molera et al. 2007) is undoubtedly the difference in the lustrous appearance shown by lustres produced over lead-free and lead-containing glazes. The composition of the glaze was found to be strikingly important. Lustres produced following the same firing protocol on lead free glazes did not show metallic shine in contrast to those obtained on lead containing glazes (32 % PbO). Moreover, for lead free glazes, lustres produced at higher temperatures (up to 600 °C) and longer reducing times (up to 30 min) showed a similar, but more intense colour as a result of increases in the size of the nanoparticles and the total amount of the metals but the metal shine was not achieved. On the contrary, for the lead containing glaze, the metal shine was always obtained provided that temperatures close to or higher than 550 °C were reached even for shorter reducing times (5 min). The explanation could be related either to the presence of large metallic particles or to a higher concentration of metallic particles in the lustre layers.

In order to check which one was the right explanation, detailed chemical composition of the lustres was obtained by Rutherford Backscattering Spectroscopy (Pradell et al. 2007, 2012). The chemical cross section profiles of copper and silver lustres produced over lead free and lead containing glazes are shown in Fig. 6a, b respectively. The copper lustres, j6 for a lead free glaze and j65 for the same glaze to which 32 % PbO was added, were obtained following the same firing protocols (50 °C/min heating ramp, dwell at 550 °C, 20 min under oxidising conditions and 10 min reducing conditions, free cooling). The silver lustres, j126 for the lead free glaze and r254 for the lead containing glaze, were obtained following same firing protocol as before for j126 but with a shorter reducing stage for r254; this was done to obtain a nanostructure with similar nanoparticle sizes for both glazes. j6 is red ruby and j126 green with neither showing metallic shine, while j65 is red coppery and r254 green golden.

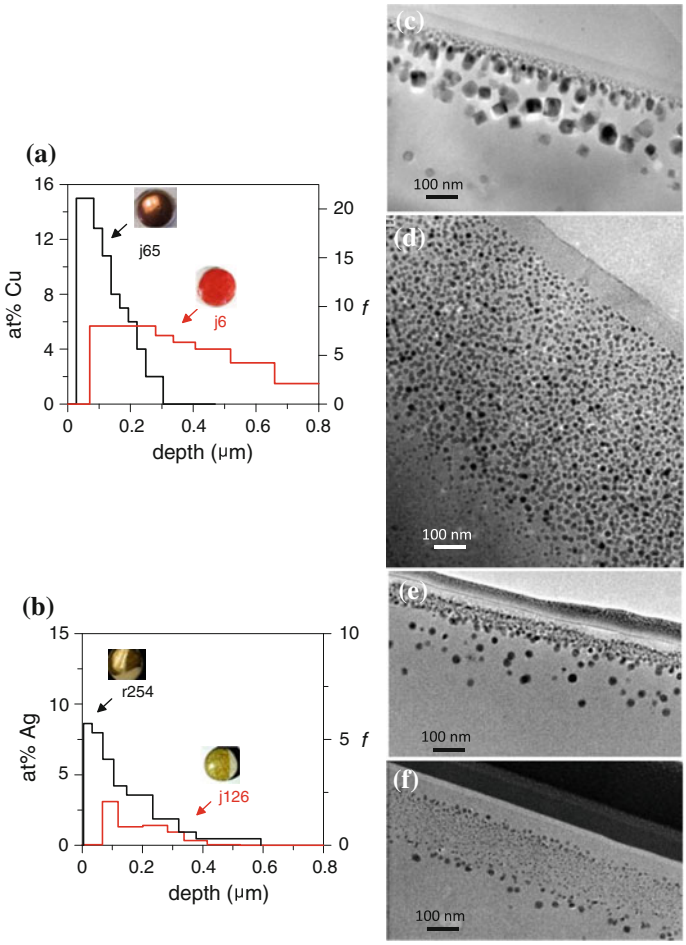

Fig. 6 Atomic concentration profiles corresponding to **a** copper lustres produced on a lead free glaze (j6) and on a lead containing glaze (j65) and the corresponding TEM images **c** j6, **d** j65, **b** silver lustres produced on a lead free glaze (j126) and on a lead containing glaze (r254) and the corresponding TEM images **e** j126, **f** r254

Figure 6a, b shows that the lustres obtained over lead containing glazes are more concentrated, the layer appears closer to the surface and is also thinner. Moreover, the nanoparticles are larger for the lead containing glaze, as is shown in the TEM images of the nanostructures for the copper lustres obtained on a lead-free and a lead containing glaze respectively (Fig. 6c, d). However, nanoparticles of similar size can be obtained by shortening the reducing stage of the lustre firing for the lead containing glaze. This was done for the silver lustres, and we can see the nanostructures formed on a lead-free and a lead containing glaze in Fig. 6e, f respectively. This demonstrates that the metallic shine observed is mainly due to the high

concentration of nanoparticles in the layer, which it is more easily obtained for lead containing glazes than for lead free glazes.

This may be understood considering the differences of the kinetic properties of the substrate glazes. We can clearly see in the chemical concentration profiles corresponding to the lustre layers, shown in Fig. 6a, b, that the penetration of the metal cations is greater for the lead free glazes and also that copper also penetrates deeper than silver. The penetration of copper and silver in the glazes is related to the diffusion coefficients of copper and silver but also of the alkali ions, as they are displaced and removed outside the glaze. Thus, in an ionic exchange process the reduced diffusivity of silver/copper ions in the lead containing glazes is also related to the reduced ionic mobility of the alkali ions in the lead containing glaze. It may be found surprising that a flux like lead that it is known to reduce the viscosity of the melt could be responsible for a reduced diffusivity of the cations in the undercooled liquid. However, it is known that the addition of an oxide of a higher-valence metal ion such as Pb^{2+} to an alkali silicate glass decreases the ionic mobility of the alkali ions; in fact the ionic mobility is inversely related to the ionic size of the added divalent ions (Doremus 1994). This effect is known to happen at all temperatures although it is more important at low temperatures, such as those used in lustre production (Greaves and Ngai 1995).

This explains why the lustre painted glass produced over lead free glasses rarely show lustrous shine (Brill 1979) in contrast to lusterware which was mainly made over lead containing glazes. Moreover, European Medieval lustre painted glass does not show any lustrous effect and even modifying the glass paint (using $AgNO_3$, Ag_2SO_4, AgCl and Ag_3PO_4), different optimal firing temperatures and larger or smaller silver nanoparticles were obtained but never a lustrous effect. We will discuss this in more detail later while considering the optical properties of lustre.

The precipitation of the metallic nanoparticles requires reducing conditions. The necessary reducing conditions may be achieved in the glass by incorporating other cations (Fe^{2+}, Sn^{2+}, As^{3+} or Sb^{3+}) which generate redox conditions adequate for the reduction of Ag^+ and Cu^+/Cu^{2+} to the metallic state. Moreover, the introduction of an external reducing atmosphere may also favour the precipitation and growth of the metallic nanoparticles. Generally speaking silver lustres may be obtained without any external reduction provided that some reducing cations (Cu^+, Cu^{2+}, Fe^{2+}, Sn^{2+}, As^{3+} or Sb^{3+}) are also present in the glaze. Contrarily, copper is hardly reduced to the metallic state unless assisted by an external reducing atmosphere. In fact, copper is able to reduce silver to the metallic state; when copper and silver are included in the lustre pigment both enter the glass, and Cu^+ is then able to reduce silver to the metallic state helping the growth of the silver nanoparticles producing the oxidation of the copper. This interference between silver and copper can be seen in Fig. 7 (Smith et al. 2006) for a Hispano Moresque lustre; the presence of higher amounts of silver reduce the fraction of metallic copper down to 40 % CuO/(Cu^+ + CuO), in contrast in the silver poor areas up 70 % CuO/(Cu^+ + CuO) is observed. However, we have not to forget that the use of an external reducing

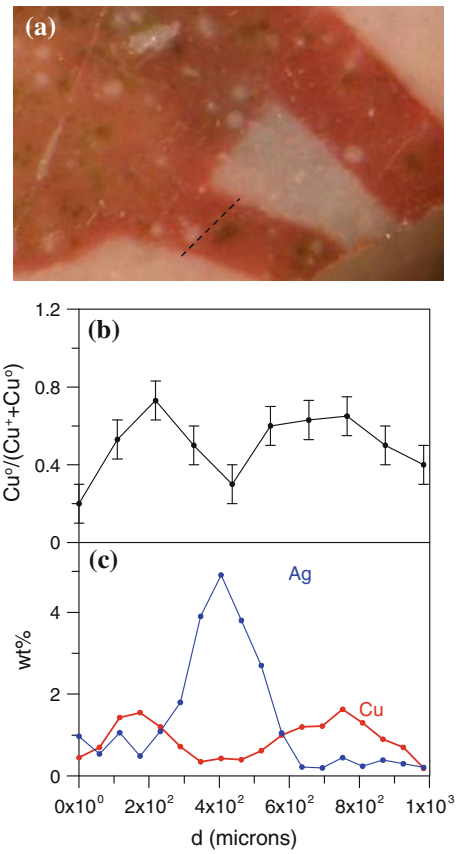

Fig. 7 **a** copper lustre (*red*) with silver spots (*green*) from a lusterware from Paterna (Spain), 14th century. **b** Metallic copper fraction, $CuO/(Cu^{+} + CuO)$ of the line marked in (**a**) determined by EXAFS (Smith et al. 2006). **c** Silver and chemical content of the same line

atmosphere and/or the presence of the reduced form of other cations will also enhance the reduction of copper to the metallic state.

In fact the addition of Fe to the glass melt (which at high temperature is predominantly present as Fe^{2+}) (Doremus 1994) is known to be helpful in the production of red copper glass; during the cooling of the melt, iron is oxidised at the expense of copper which is reduced to cuprite and/or metallic copper.

Tin (Sn^{2+}) is also known to be a powerful reducing agent for copper. Therefore the presence of tin and iron in the glasses as reducing agents for copper was probably well known by the glassmaker. The link between the lustreware production and the glass industry is obvious and therefore, it is expected that the relevant knowledge was transferred from the glass industry through the lustre painted glass to the lusterware production. However, it is also true that tin is commonly associated with copper and could have been added unintentionally if the original copper source used was bronze.

The inclusion of arsenic is also described in the treatises, and the reduced form of arsenic, As^{3+}, if present in the glass would also act as a reducing agent. In fact,

most of the Islamic lustre painted glasses showed also the presence of trace amounts of As, Sn and Bi. The three of them are strong reducing agents, able to reduce copper, and are only present in the lustre painted areas (Brill 1979).

The addition of lead to the lustre pigment is also described in the treatises. In fact, the presence of lead has been determined in the lustre layers themselves, in particular, in some red Iraqi (9th century) lusterware decorations (Molina et al. 2014) and also in Islamic (Brill 1979) and Renaissance (Molina et al. 2013) lustre painted glass. In those cases a lead free substrate glaze/glass was used, and consequently the presence of a diffusion profile of lead in the lustre layer can be distinguished. Figure 8 shows the lustre layer composition of three Renaissance lustre painted glasses (Molina et al. 2013). Two of the lustre painted glasses, AVI15 and PAL15, contain only Ag while AVI16 contain Ag, Cu and Pb. The exact role of lead is not very clear, but it is known that copper is more readily dissolved in a glass containing lead and therefore it may be added together with copper to help the incorporation of copper into the glass. In fact, lead was traditionally added to the copper red glasses. Figure 8 shows how lead is not found in the silver lustres, contrarily to the situation in the silver and copper containing lustres. Consistently, lead was also determined in the Islamic lustre painted glasses (Brill 1979) containing copper and silver, and was also found in the red lusterware decorations of the polychrome Iraq lusterware production (9th century) (Molina et al. 2014).

Considering the complexity of lustre production, one wonders about the reason for using lustre instead of other methods of decorating glass. Actually, glass could be easily coloured by adding metals (copper green and turquoise, cobalt blue, manganese violet, yellow/ochre iron, etc.) or by mixing particles (lead antimonates or stannates for yellow and calcium antimonate or tin oxide for white) in the melt.

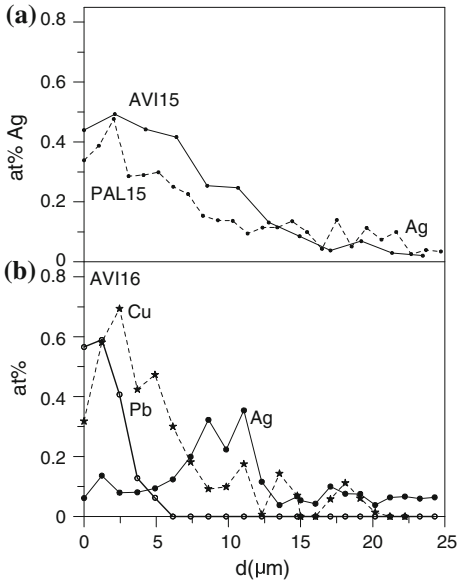

Fig. 8 **a** at.% Ag composition profile corresponding to lustre painted Renaissance glasses Avi15 and Pal15. **b** at.% Ag, Pb and Cu composition profiles corresponding to the lustre painted Renaissance glass Avi16

However, painting the surface with thin lines is not so simple, one way being to apply a thin layer of coloured glass (i.e. enamel). The coloured glass has to be either worked together with the substrate glass, or fired at a lower temperature to avoid the softening of the substrate glass. Consequently, and despite the technical difficulties, lustre gives rise to decorations showing remarkably well defined contours and, the large variety of transparent brilliant colours with iridescent and metallic reflections obtained render lustre painted objects to be unique.

3.2 Optical Properties of Lustre

The fascinating colourful and lustrous appearance of lustre is directly related to the peculiar optical response of the metal nanoparticles. The nanometric size of the metal particles is responsible for a localized resonant absorption and scattering of the visible light which depends on the nature, size, shape and concentration of the particles in the layer. Moreover, in consequence of the mechanism of formation of the lustre layer, the presence of other nanoparticles such as cuprite (Cu_2O, absorption band at about 520 nm) and also of metal ions such as Cu^+, Cu^{2+} or even Ag^+ dissolved in the glass influence also the optical properties of the layer.

Absorption of the light by the metal nanoparticles is dominated by the collective resonance of the free electrons resulting from surface polarization, denoted as surface-plasma resonance (SPR). The wavelength and shape of these resonances depend on the optical functions of the metals and of the dielectric matrix (glass). Spherical nanoparticles will also scatter the light (van de Hulst 1981). Roughly speaking small spherical silver nanoparticles absorb strongly in the blue region of the spectra (around 400–450 nm) but are essentially transparent to the rest of the wavelengths in the visible and this causes the typical yellow colour of silver colloidal solutions. The SPR absorption band (at 560 nm) and electronic inter-band transitions absorbing at shorter wavelengths of copper nanoparticles confer red hues to copper colloidal solutions.

The paths of light through a lustre layer for both a lustre painted glass or a lusterware are shown in Fig. 9a, b respectively. In both cases, the light is partly reflected on both glass surfaces and scattered and absorbed in the nanoparticles.

For a lustre painted glass, although the colour is normally observed in transmission, it may also be looked at in reflection. The colour seen in transmission and far away from the glass corresponds to the light filtered by both absorption and scattering by the metal nanoparticles, and also absorption of other ionic species dissolved in the glass. Consequently the light transmitted (Transmission) is that which is not extinguished (extinction = absorption + scattering). The Reflectance corresponds to the light back-scattered by the nanoparticles (after single or multiple scattering) together with that absorbed on its way back to the surface after being reflected in the exit glass surface. Consequently, the Reflectance depends on the characteristics of the back surface; in the case of a black absorbing background, be the main contribution will correspond to the back-scattered light, while for a white

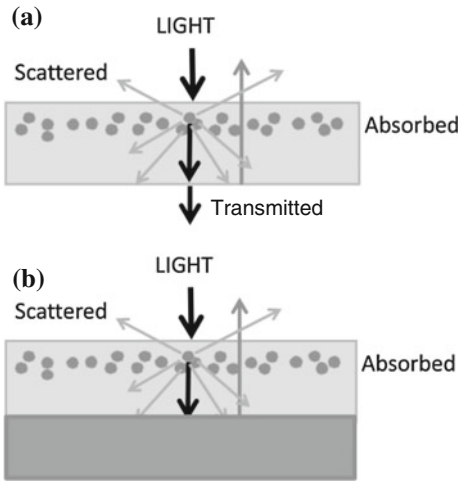

Fig. 9 Scheme of the interactions of light going through a lustre layer on **a** glass and **b** ceramic

reflecting background, the double path of the light through the particles will increase the contribution of the absorption cross section to the Reflectance.

In lustreware only the light exiting backwards will be measured (Reflectance); in its path through the glaze the light will be reflected in the glaze-ceramic interface and also scattered by the cassiterite (SnO_2) microcrystallites when present in the glaze. The ceramic surface, as stonepastes or calcareous pastes are normally used, has a cream colour. The double path through the metallic nanoparticles will give a main extinction contribution to the Reflectance to which the light back-scattered and multiscattered by the particles will add (Fig. 9b).

Multi-scattering will contribute to the Reflectance of the lustre layer in a non-negligible amount even for a low volume fraction of nanoparticles. However, this effect will be significant for large particles for which scattering dominates the optical response and less important for small particles for which absorbance dominates the optical response as will be seen later. But even for small particles, multiscattering will be responsible for the broadening of the SPR peak in the Reflectance spectra. A more realistic calculation of the Reflectance and Transmittance may be obtained by a numerical simulation, such as the Finite Difference Time Domain Method (FDTD), for obtaining numerical solutions of Maxwell equations for extremely complex systems with almost arbitrary geometrical configuration. Although it has been used in some cases for the study of the optical properties of lustre, the explanation of most of the peculiarities shown by lustre may be attained from simple Mie single metal nanoparticle calculations; or by using mean field models for the nanoparticles-glass system such as Maxwell Garnett which is valid for small nanoparticles and highly diluted systems (Maxwell Garnet 1904, 1906), or Torquato–Kreibig–Fresnel which is valid also for small nanoparticles but able to consider three-particle interactions, that is, more concentrated systems (Farbman et al. 1992).

The fraction of light loss (extinct) and also scattered in the nanoparticles is determined by the extinction and scattering cross-sections which are calculated for spherical particles by a series expansion (Mie theory) corresponding to spherical multipolar excitations (dipolar, quadrupolar, and octupolar) (van de Hulst 1980, 1981). Although the dipolar approximation is sufficient for small particles (up to about 20 nm for silver and 50 nm for copper), larger nanoparticles require the use of higher multipolar orders. Consequently, the light absorbed and scattered by the metal nanoparticles is particle size dependent. Figure 10 shows the absorption and scattering cross sections for silver and copper nanoparticles for particle sizes varying between 20 and 80 nm calculated up to third order, using the measured dielectric constants for metallic silver (Johnson and Christy 1972) and taking into account the particles size dependence of the dielectric constants using the Drude approximation (Kreibig and Vollmer 1995). We can see how, for small particle size, absorption dominates the optical response; on the contrary, for large particles, scattering dominates the optical response.

This has important implications for the colour seen in transmission and in reflection. Figure 11 shows the Extinction—log(1/T)—and the Reflectance of the two silver lustre painted glasses (AVI15 and AVI16) dating to the Renaissance period, AVI15 is yellow both in reflection and transmission while AVI16 appears red in transmission and yellow in reflection. The dichroic effect is due to the presence of small (about 20 nm) and large (about 85 nm) silver nanoparticles in the lustre layer which are respectively near and far from the surface as is seen in

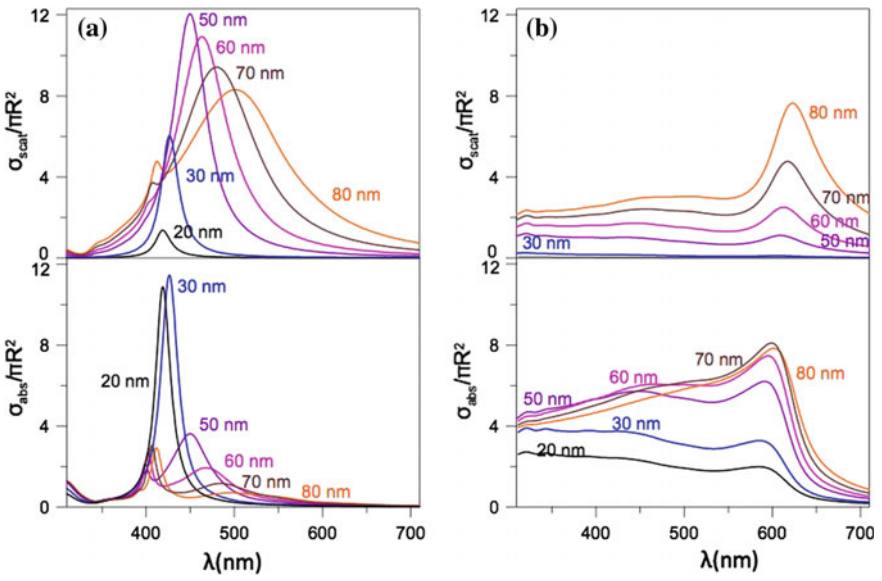

Fig. 10 Absorption cross section (*Bottom*) and Scattering cross section (*top*) for **a** silver and **b** copper nanoparticles of various sizes in a glass of refraction index $n_g = 1.56$

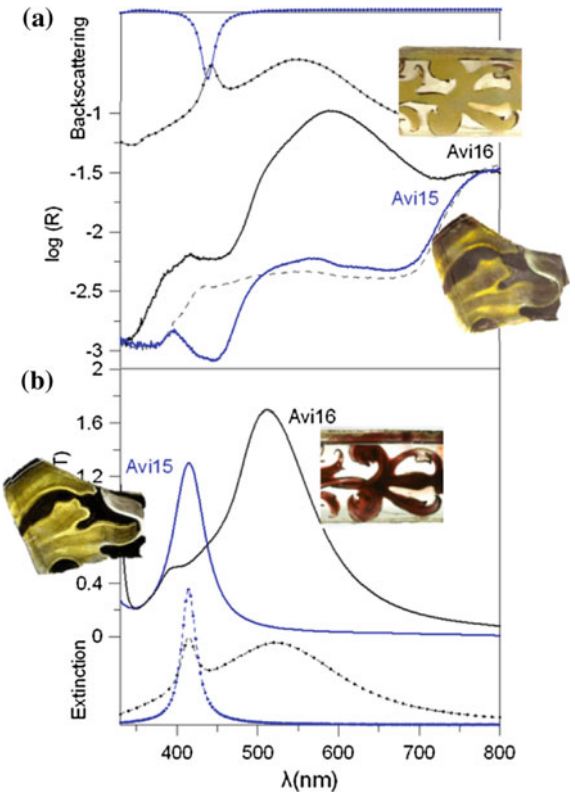

Fig. 11 **a** log(1/T) from AVI15 and AVI16 after subtracting the glass contributions. The *dotted lines* correspond to the extinction constants for 20, and 85 nm spherical particles in glass. **b** log(R) from Av15 and Av16. The glass contribution has not been subtracted and is plotted with a *dashed line*. The *dotted lines* correspond to the backscatter constant minus the absorption constant calculated for 20 and 85 nm spherical particles in glass. The first two compare directly to the log(R) spectra from AVI15. A combination of the small and large particles constants compare to the log(R) spectrum from AVI16

Fig. 12. The small particles absorb light around 420 nm (blue light) while the large nanoparticles scatter light around 530 nm (yellow). For this reason the light transmitted is red while the light reflected is yellow.

AVI15 contain only small particles, and therefore, the colour is yellow both in transmission and in reflection. The formation of large nanoparticles in the dichroic lustre glass AVI16 may be related to the presence of copper and lead (Fig. 8b), we know that copper is able to reduce silver to the metallic state and enhance the growth of silver nanoparticles; and lead improves copper solubility in the glass. The lustre layer in the glasses (see Figs. 8 and 12) is about 25 μm thick or even larger (Vilarigues et al. 2009), and this is one or two orders of magnitude thicker than common lusterware layers (Fig. 1).

Figure 13 shows the calculation of the extinction cross section and the calculated transmitted colour plotted on a CIE-Lab* graph for the colour coordinates. For small silver nanoparticles the colour observed is yellow-green (10–50 nm) shifting to yellow (50–60 nm), orange (60–70 nm), red (70–80 nm) to a very dark magenta (>90 nm).

With regard to lusterware, we have seen how various colours, that is, green, amber, yellow, brown, red, dark red, are obtained. The colours are due mainly to the

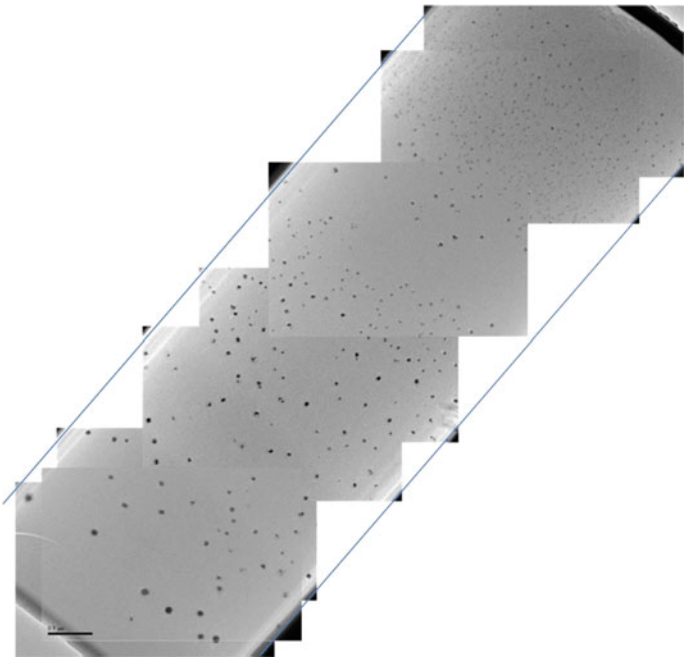

Fig. 12 TEM image of the nanostructure corresponding to the dichroic lustre painted glass Avi16. The size of the particles close to the surface of the glass (*top-right*) is of about 20 nm and of those present inside the glass (*bottom-left*) is of about 85 nm

nature (silver and/or copper metallic nanoparticles) and size of the particles. We will define *silver lustres* as those which contain silver metal nanoparticles and *copper lustres* as those that contain copper metallic nanoparticles.

Silver lustre ware show different colours depending mainly on the size of the silver metal nanoparticles and both absorption and scattering contribute to the colour as shown in Fig. 10a. Although *silver lustres* may also contain copper, it is present as Cu^{+} or Cu^{2+}; in fact the presence of copper favoured the growth of the metal silver nanoparticles, consequently those containing more copper contain also larger metal silver nanoparticles. Moreover, cuprite (Cu_2O) nanoparticles (absorption at about 520 nm) will add a yellow tinge and the presence of Cu^{2+} ions (large absorption band between 600 and 1000 nm) will add a turquoise blue to green tinge to the glaze.

The absorbance spectra corresponding to a selection of Islamic silver lustres (Abbasid polychrome and monochrome and Fatimid lustres), calculated from the Reflectance spectra as log(1/R) which is a good approximation when absorption dominates the optical response, are shown in Fig. 14a. Therefore they may be directly compared to the absorption cross sections calculated in Fig. 10a. The oxidation state of copper for some of the different colour lustre layers are shown in Fig. 14b, c (Pradell et al. 2008a, b), and replicated silver and silver with some

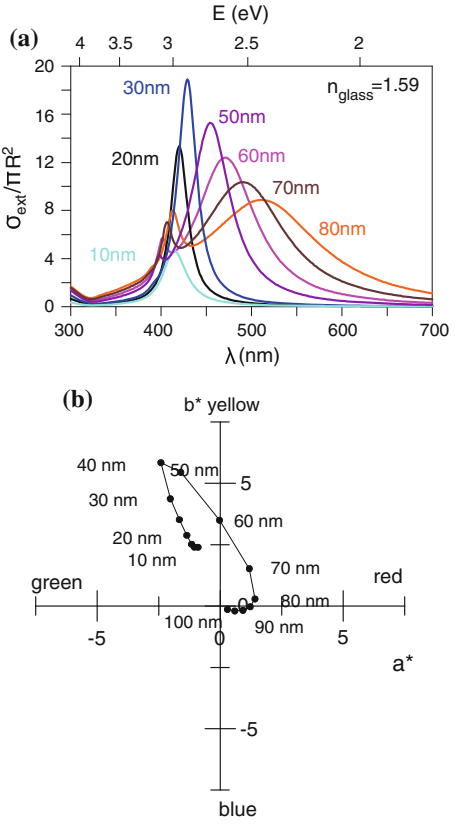

Fig. 13 **a** Extinction cross section for silver nanoparticles of increasing size in a glass similar to AVI16 and **b** colour of the glass seen in transmission as a function of the size of the silver nanoparticles

copper lustres over an alkaline glaze showed the same range of colours (Molera et al. 2007, Pradell et al. 2008a, c) as seen in Fig. 14.

Those containing small silver nanoparticles (20–30 nm) contain also little amounts of Cu^{+} and appear green (Fig. 14c), such as those shown in Fig. 2a, e. Those containing larger silver nanoparticles (30–40 nm) which contain also Cu^{+} and some Cu^{2+} appear amber or yellow (Fig. 14b); such as those of Fig. 2a, f. Finally, those containing an heterogeneous distribution of silver nanoparticles (10–50 nm) and also Cu^{+}, cuprite nanoparticles and a higher amount Cu^{2+} appear brown (Fig. 14b); such as those shown in Fig. 2a, g. In this case, and due to the presence of large silver nanoparticles they also scatter light strongly showing bluish or purplish iridescences. Figure 15a show the Reflectance spectra corresponding to two replications of a silver lustre containing copper; they appear brown-yellowish and show bluish and purplish iridescences similar to those shown in Fig. 3e–h. Figure 15b shows also a TEM image corresponding to the lustre showing the bluish iridescence, we can see the presence of large silver particles 50 nm responsible for the blue scattering.

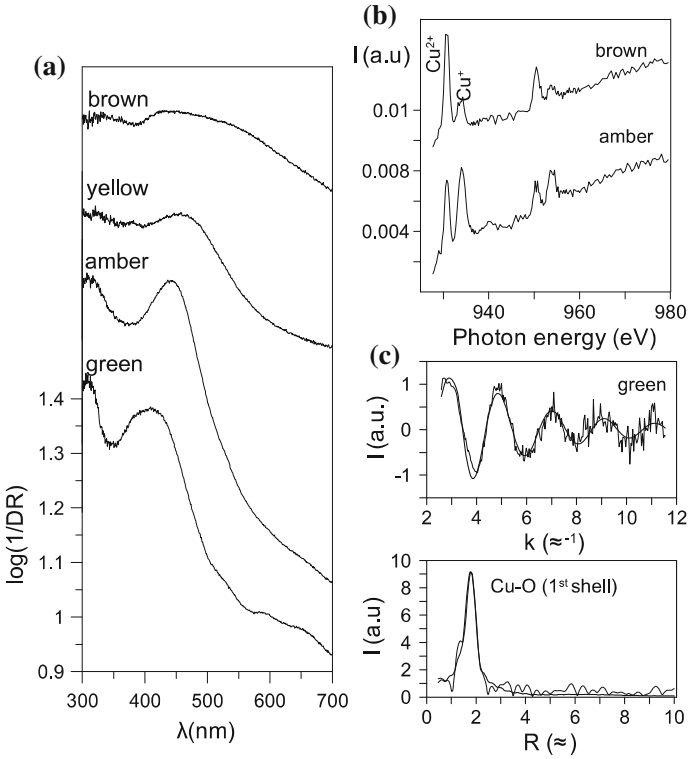

Fig. 14 Selection of Islamic Abbasid and Fatimid colour lustres; **a** log(1/DR) equivalent to the absorbance for low volume fractions (below 5 %) and small sizes (below 30 nm) of silver nanoparticles in the layer. **b** Xanes Cu L_{12}-edge corresponding to the *amber* and *brown* lustre. **c** Micro-EXAFS Cu kα-edge corresponding to the *green lustre*

In fact the peak position and width determines the colour shown by the lustre layers, and it depends not only on the size of the nanoparticles but also on the index of refraction of the glaze. Figure 16 shows the dependence of the peak position and width of the extinction cross section peak for silver nanoparticles in alkali and

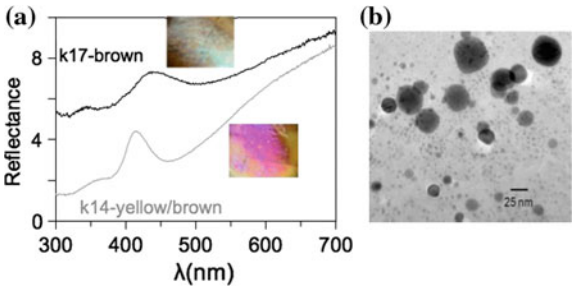

Fig. 15 **a** Reflectance shown by two replicated *brown silver* lustres containing Cu^{+} and Cu^{2+} showing *bluish* and *purplish* iridescences. **b** TEM image of the nanostructure of *k17-brown*

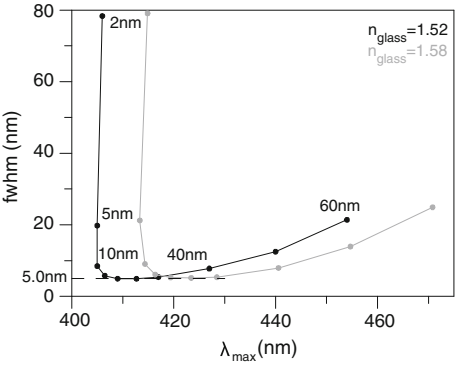

Fig. 16 Full width half maximum versus peak position plot corresponding to silver metal nanoparticles of varying size in a lead free (n_{glass} = 1.52, *black line*) and a lead bearing glass (n_{glass} = 1.58, *grey line*) calculated using the Mie theory

mixed lead-alkali glazes (refraction index 1.52 and 1.58 respectively). We can see that for lead containing glazes the extinction (both absorption and scattering) are red shifted with respect to a lead-free glaze. Consequently, the colour will also depend, although in a lesser extent, of the glass composition.

For *copper lustres*, the colour shown is essentially red in all the cases; Fig. 17 shows the differences in the colour and shine of copper lustres produced at different temperatures and the corresponding absorbance spectra. The spectra can be directly compared to those calculated in Fig. 10b. We can see that at low temperatures, 480 °C, the absorbance corresponds to that of 20–30 nm copper particles; at 550 °C to that of 50 nm copper particles (see the corresponding TEM image in Fig. 6f); and at 580 °C to that of 70–80 nm copper particles.

On the other hand, with an increasing nanoparticles volume fraction, the optical spectrum is modified even further and cannot be attributed anymore to scattering by individual particles but should rather be considered as the result of collective scattering by an ensemble of particles (Dusemund et al. 1991). This type of scattering has been observed in many different systems; such materials are essentially composites consisting of organic dielectric materials and show intense colours and strong reflectance (Wolf and Maret 1985; Kuga and Ishimaro 1984). The corresponding

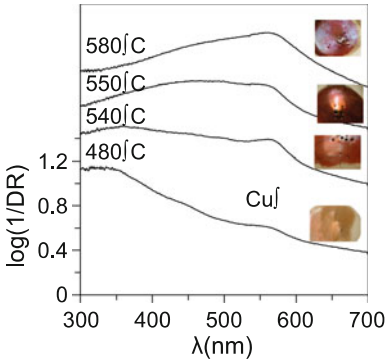

Fig. 17 Absorbance of replicated copper lustres fired following thermal paths at different maximum temperatures. The absorbance SPR peak at 560 nm demonstrates the presence of metallic copper nanoparticles. The profile of the absorbance spectra may be directly correlated to the one calculated in Fig. 10b

structures can be formally divided into ordered and disordered, and can be treated as photonic crystals and photonic glass, respectively. Lustres resemble especially the latter case, but differ from it in that the metal spheres suspended in the glass are much smaller and their dielectric function has a large imaginary part which is why they not only scatter but also absorb strongly.

The study of the optical properties of a composite made of metal nanoparticles embedded in a dielectric matrix may be determined using the Maxwell-Garnett (MG) model (Maxwell Garnet 1904, 1906). The composite may be treated as an optically equivalent medium with an average dielectric constant calculated using the Lorentz–Lorentz–Clausius–Monotti relationship, which considers that each nanoparticle will produce the effect of a Hertzian doublet. However, the MG relationship considers the nanoparticles to be described by a simple dipole and neglects both higher multipolar contributions as well as the interactions between nanoparticles. Therefore, it is valid only for highly diluted systems ($f \ll 1$ %) of small nanoparticles (up to 20 nm for silver or 50 nm for copper nanoparticles). Later a mean field model (Farbman et al. 1992), so-called Torquato–Kreibig–Fresnel model (TKF), able to consider three-particle interactions in a random monodispersed system was also proposed. The model is able to give a better description in the case of more densely packed small nanoparticles, but it does not take into account the retardation effects and high multipolar terms occurring in large nanoparticles. As in the MG model, it evaluates an average dielectric constant of the nanoparticle–glass composite, which in this case includes a structure parameter involving up to three-body correlation functions in space. Using the Fresnel equations, the extinction and reflectivity of the surface can be evaluated for different volume fractions of nanoparticles provided that the size of the nanoparticles is small.

Figure 18a, b shows the calculated reflectance and absorbance for different volume fractions (1–25 %) of 20 nm silver and 50 nm copper nanoparticles for a mixed lead-alkali glaze ($n_{glass} = 1.58$). We can see an important enhancement, broadening, and red shifting of the reflectivity with an increasing volume fraction of the nanoparticles in the layer (Pradell et al. 2012). This red shifts from blue to yellow the colour of the reflected light of an assembly of silver nanoparticles, the golden shine shown in Fig. 3a, b, h. As copper has lower scattering capacity than silver, larger nanoparticles are necessary to obtain a high reflectance, and this is the reason why the calculation is made for 50 nm particles instead 20 nm, resulting in a coppery reflectance similar to those shown in Fig. 3d. This enhancement in the reflectivity, the lustrous effect, is more important for incident angles larger than 0°.

Although for large silver nanoparticles, the reflectance may not be estimated with the above models, a numerical simulation for a volume fraction of 10 % silver nanoparticles of 30 nm resulted in a flat optical response in the visible range, and a silvery shine, as the one shown in Fig. 3c.

The above calculations did not take into account either the thickness of the lustre layer or the absorption in the UV of the glaze matrix. Some other studies about the lustre optical properties have considered also the presence of multilayers (the surface layer being free of nanoparticles, and sub-layers showing different particle

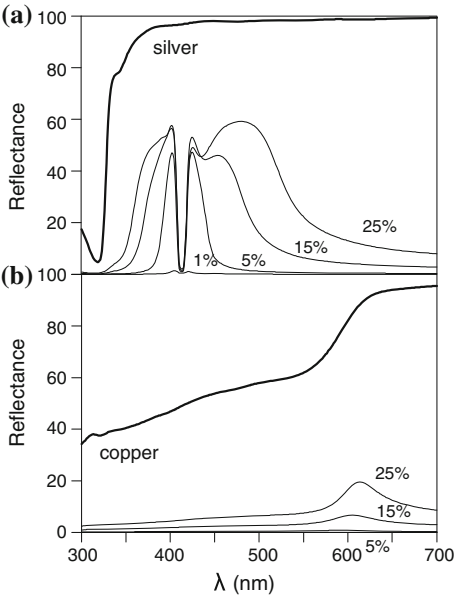

Fig. 18 Reflectivity of a silver lustre for increasing volume fraction of the nanoparticles (30 nm size silver nanoparticles, n_{glass} = 1.58 and normal incidence). Increasing the metal nanoparticle volume fraction the reflectivity increases and red shifts

sizes or concentrations), and also their thickness (Berthier and Reillon 2006; Reillon and Bethier 2013) and how they contribute to the reflectance of the layers. Interference phenomena also occur for those layers filled with small nanoparticles with layer thickness in the light wavelength range, and are responsible for iridescent effects in thin layers with large nanoparticles.

4 Historic Lustre Painted Glass and Lustreware Productions

Among the many relevant studies about lustre, we will highlight those that give some insights in the differences between lustre painted glass and lusterware optical properties and also about the changes happening chronologically in lusterware. We have seen that important differences in the microstructure between lustre painted glass and lustreware, namely thickness of the lustre layer, size and distribution of the nanoparticles in the layer, determine the range of colours and shine observed; see how they compare in Figs. 1 and 6 for lusterware and Fig. 12 for lustre painted glass. Moreover, there are also important differences between the microstructures within different lusterware productions which may be seen in the replications (Figs. 1 and 12) but also in the many TEM pictures related to different historical productions (Pérez-Arantegui et al. 2001, 2004; Fredrickx et al. 2004; Colomban 2009; Sciau et al. 2009; Chabanne et al. 2012; Molina et al. 2014). Those differences are attributed in many cases to the differences in the thermal protocols

followed (temperature, reducing atmosphere, number of firings), then to the composition of the lustre paint and, finally, to the composition of the glass/glaze. However, as we have seen before, those parameters are not wholly independent; on the one hand, the range of optimal firing temperatures depends directly on the glass composition in a more or less complex way. On the other hand, the external reducing conditions depend also on the reducing elements already presence in the glass and in the lustre paint. Consequently, the composition of the glass and those of the lustre paint are among the most important parameters.

Qualitative analysis of the various Islamic lustre painted glasses studied, such as opaque deep yellow-orange lustre painted over a cobalt blue transparent glass, opaque red ruby lustre painted over a dark olive glass (9th or 10th century) and amber lustre paintings over transparent tinged glass (10th–12th centuries) (Brill 1979), showed that lustre contains mainly silver and copper (in variable relative amounts and oxidation states depending on the colour) together with minor or even trace contents of reducing elements such as Sn, Pb, As, Bi. However, the good correlation between Pb and Cu suggested that Pb could have been incorporated with the copper compound. The glasses were of the type soda-lime type (17–20 % Na_2O, containing 7–15 % CaO, 1–4 % K_2O, 0.4–1.3 % Fe_2O_3 and 1–5 % MgO) but showing some different compositions between the early opaque red and yellow lustres and the later amber transparent lustres. The yellow opaque contained 5 % of Mg and 1 % Fe_2O_3, and the red lustres also between 7 and 9 % of Al_2O_3. Brill related these differences to both the base colour of the glass but also to the lustre colours obtained, suggesting different glass compositions could favour the formation of the yellow and red lustres. Consequently, the different substrate glasses and the significant presence of reducing elements in the lustre paints (Brill 1979) are directly responsible for the microstructure developed.

Byzantine lustre painted glass (Pilosi and Whitehouse 2013) shows yellow and also silvery lustre decorations; unfortunately as yet, neither the composition nor microstructure of these lustres has been studied. On the contrary, several studies on European Medieval lustre painted glass (Vilarigues et al. 2009; Delgado et al. 2011; Molina et al. 2013) have shown that yellow silver lustres were produced during the 13th and 14th centuries, while copper was added later in the 15th and 16th centuries to obtain deep yellow, orange and red colours; copper acted as a reducing agent, increasing the size of the metallic silver nanoparticles. The presence of lead in the lustre paint is also demonstrated in many lustre paints to which copper was added but not in all of them. In all the cases the substrate glass was a lead free, soda-lime or potash-lime glass.

However, the thick lustre layers (about 20–30 μm) obtained are essentially related to the glass composition, and we have demonstrated that PbO, among all the glass constituents, is the one which reduces further the ionic interdiffusion coefficients. Consequently, the lack of metallic shine of lustre painted glasses is understandable, only those which experienced strong reducing conditions showing some silvery lustre effect.

The presence or absence of lead in the historic lusterware productions is also expected to affect their optical properties. In fact, when lusterware started being

produced in the *Abbasid* caliphate in the 9th and 10th centuries, the glazed ceramic productions are often classified either as alkali and high lead transparent glazes, or as mixed alkali, low lead, tin opaque glazes (1–15 % PbO and 0.5–10 % SnO_2) (Wood et al. 2007). However, lustreware was produced only over alkali and alkali low lead, tin opaque glazes (Bobin et al. 2003; Mason 2004; Polvorinos del Rio et al. 2008; Pradell et al. 2008a; Chabanne et al. 2012; Molina et al. 2014). Although some studies suggested that early polychrome lusterware was poorer in lead while later monochrome lusterware was richer in lead, in fact both show variable lead contents. The use of alkali glazes can be easily understood in terms not only of the need of alkali ions in the glaze for lustre to develop, but also because the technology came from the glass industry. Moreover, the addition of some lead to the alkaline glazes may also be understood taking into account that it reduced glaze crazing during cooling by making the thermal expansion coefficients of both ceramic body and glaze more similar.

What is also true is that there is a strong correlation between the metallic shine and the lead and tin content of the glazes throughout time. A study of polychrome lustres (Molina et al. 2014) showed how a yellow-golden and red-coppery lustre was produced on a lead tin glaze (9.4 % SnO_2 and 13.3 % PbO), red-black non shiny lustre was produced over a tin and lead free glaze, and the red coppery and white-silvery was produced over a low lead and tin glaze (3.3 % SnO_2 and 5.6 % PbO). The last was obtained after applying a strong reducing atmosphere which resulted in large size (Fig. 1) silver and also copper nanoparticles which appear also welt together (Molina et al. 2014). Other *Abbasid* polychrome productions (Pradell et al. 2008a) such as the amber-brown non-shiny lustre was obtained over a 2 % SnO_2 and 6 % PbO glaze while a green golden-amber-brown lustre was obtained over 2 % SnO_2 and 13 % PbO.

Monochrome green silver *Abbasid* lustreware was produced in the 10th century; it is silver rich containing very little copper if any [well below 10 % Cu/(Cu + Ag)]. Later by the end of the 10th century, when the production moved to Egypt (*Fatimid* lusterware), monochrome silver lustres continued being produced. A more detailed study of Abbasid and Fatimid silver lustres showed that there is an inverse correlation between the depth at which the lustre layer is formed and the lead content of the glazes up to approximately 20 % PbO, as shown in Fig. 19a. Some of the silver concentration cross sections are also shown in Fig. 19b in which differences not only in the position, but also in the thickness and concentration of the layers are observed. Lead containing glazes give rise to lustre layers that are thinner and more concentrated in good agreement with the results obtained from the replications. Moreover, only those lustres showing a high silver concentration appear golden.

The large variation in the glaze composition of the *Abbasid* lustreware may be associated with the work of different workshops which produced also different colour combinations and designs. Moreover, it is also true, that increasing the glaze lead content from 5 to 15 % would raise significantly the probability of obtaining a golden/coppery lustre. However, variations in the position, thickness and concentration of the lustre layers depend also on the firing temperature and reducing

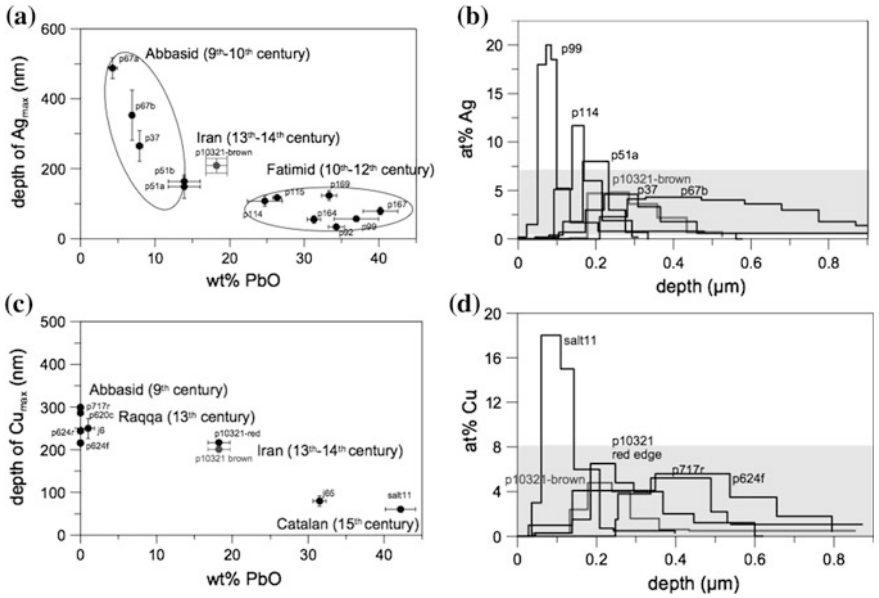

Fig. 19 Depth at which the silver lustre layer forms inside the glaze as a function of the lead oxide (PbO) content of the glaze for Abbasid, Fatimid and Iranian lustreware productions

process, and golden/coppery shinny lustres were obtained only if the appropriate firing procedure was followed. The colour obtained depends mainly on the firing temperature and atmosphere but, other parameters, such as the thickness of the lustre paint applied is also very important (amount of copper and silver available, different reducing conditions in the paint, etc.). Different thicknesses of paint could be voluntarily applied to obtain different colours, but could also be a consequence of the brush application. The effect of the external atmosphere is also clearly seen at the edges of the decoration, producing different colours and shines in these areas. Consequently, green, yellow, amber and brown silver lustres could be obtained without changes in the glaze or lustre composition or even in the firing temperature or reducing atmosphere.

The glazes of *Fatimid* lusterware are lead rich (between 20 and 40 % PbO) although some studies also suggest a slight decrease in the lead content by the end of the Fatimid period (Mason 2004; Pradell et al. 2008b). Early *Fatimid* lustre is green, similar to the monochrome Abbasid production, changing to yellow and amber, and finally to brown applied over a slightly turquoise green glaze (Philon 1980). The change from green to amber and brown is also related to an increase in the amount of copper from less than 10 % Cu/(Cu + Ag) to 30 % Cu/(Cu + Ag) (Pradell et al. 2008b). One important novelty is the re-discovery of *stonepastes* which were used instead of calcareous clays. A *stonepaste* is a synthetic ceramic paste made of sand (above 70 % SiO_2), clay and glass frit. One of the advantages was that the *stonepaste* and the glaze could be fired together reducing the number of

firings from three to two as Abu'l Qassim indicates in his treatise (Allan 1973). Contemporary to the late Fatimid lusterware productions and showing many similarities but also some clear differences is the so-called Syrian *Tell Minis* lustreware (early 12th century) (Porter and Watson 1985). *Tell Minis* lustre shows a similar range of colours but with higher copper contents [between 30 and 50 % Cu/(Cu + Ag)]; the bodies are silica rich *stonepastes* and in many cases lead tin-free transparent glazes are used (Chabanne et al. 2012; Pradell et al. 2013).

Copper lustres first produced in the early *Abbasid* polychrome wares were not produced again until the *Ayyubid* Syrian dynasty (*Raqqa* lustreware from the late 13th and first third of the 14th century) (Porter 1981; Jenkins-Madina 2006). Abbasid red lustres on lead free glazes, and *Ayyubid* red lustre over a lead free glaze are compared to the copper replications from Fig. 6a, c, d and to some later red lustres (a Catalan 15th century coppery lustre and a red edge in a Iranian 13th–14th century lustre) in Fig. 19c, d. Again a thinner, highly concentrated lustre layer forming closer to the surface is also obtained for the lead containing glazes, and again the coppery shine is directly linked to this. However, most of the historical copper lustre productions were obtained over alkaline lead-free glazes (Chabanne et al. 2012; Pradell et al. 2013); among them we can highlight *Ayyubid* (*Raqqa*, 13th century AD) and *Mamluk* (*Damascus*, 14th century AD) Syrian lusterware, and *Kashan* (13th–14th century AD) and *Safavid* (16th–17th century AD) Iranian lustreware. Although *Raqqa* lustre does not show a coppery shine the other productions often show coppery shine. This seems quite contradictory to previous data but we have to keep in mind that the stronger reducing conditions needed for the development of a copper lustre (reduction of copper to the metallic state) are not the best for lead glazes and that other strategies to reduce copper to the metallic state exist such as the addition of reducing elements to the glaze. Most of the Kashan and *Mamluk* copper lustres were obtained over a cobalt blue glaze. Cobalt blue glazes were obtained by dissolving a cobalt containing pigment (cobaltite, an iron sulphide with little cobalt) to the glaze. The resulting glaze will contain very small amounts of cobalt which are known to produce a deep blue colour, but large amounts of iron. We know that iron is able to reduce copper to the metallic state suggesting that the use of cobalt, lead free glazes was an alternative to the production of coppery shiny lustres. More work should be devoted to the study of these productions.

Iranian lustreware (Kashan late 13th–14th century) was produced using *stonepaste* and tin-lead glaze (20–25 % PbO). It is copper richer [40–60 % Cu/(Cu + Ag)] than previous Fatimid productions, similar to *Tell Minis* but poorer than later *Ayyubid*, *Mamluk* and *Safavid* lustres (Pradell et al. 2008b, c; Chabanne et al. 2012). The colour is brown golden, and shows the presence of copper rich red edges to the lustre designs. The brown lustre contains both silver and copper metallic nanoparticles and the red edge copper metallic nanoparticles. The thickness, position and silver and copper concentrations of a brown golden Kashan lustre and of the corresponding red edge are shown in Fig. 19. The brown golden lustre does not show a high silver concentration but in this case it also contains metallic copper nanoparticles, and therefore the shiny effect is the simultaneous response of

both silver and copper. More work should be dedicated to the study of mixed silver and copper lustres.

Al-Andalus is known for several lustreware productions, including Almeria (12th century), Murcia (13th century), Malaga (13–15th century) and Granada (14th–15th century). However, little is known about them; calcareous ceramic pastes and tin lead glazes (30–45 % PbO) were identified (Picon and Navarro Palazón 1986; Remai 2012). On the contrary, Hispano Moresque lustreware productions started being produced in the 14th century in the Valencian area at Manises and Paterna, and were successfully exported all over Europe, followed by later Seville (16th century) and Catalan (Reus and Barcelona 16th–17th century) productions. The huge production and historical records, and the excavation of the Valencian workshops which provide samples of the lustre pigment and shards at all the stages of production have helped their study (Molera et al. 2001a, b; Pérez-Arantegui et al. 2001; Polvorinos del Rio and Castaign 2010; Chabanne et al. 2012). Hispano-Moresque lustreware was produced using calcareous clay and tin-lead glaze (34–40 % PbO), and compared to other coloured productions of the same workshops, they are also potassium richer (Molera et al. 2001b). The 14–15th century lustre is monochrome, mixed brown golden with red edges, and similar to the Iranian productions. However, the productions show also a range of colours typical of variable firing conditions. The brown golden lustres are mixed silver-copper lustres while the red edges are basically copper lustres. Later productions tend to appear coppery and are also copper richer. The lustres are well reduced, but although all the silver appeared as metallic silver copper varied between 70 % CuO/(CuO + Cu^+) in the red edges and 40 % CuO/(CuO + Cu^+) in the silver rich areas (Smith et al. 2006).

The Italian lustreware productions are the result of the adoption of lustre by the Italian potters, and the technology is supposed to come from Spain. Two workshops Derutta and Gubbio started decorating majolica with lustre (Padeletti and Fermo 2004; Padovani et al. 2004; Padeletti et al. 2006, 2010, 2013). A tin-lead glaze (25–35 % PbO) containing also more potassium than polycrome glazes, as in the Hispano-Moresque productions, and a calcareous clay were used. Yellow golden lustre was first produced in Derutta and soon after in Gubbio in combination with red ruby shiny lustres. Yellow golden lustres contained a high silver concentration and between 85 and 95 % Ag/(Ag + Cu); in contrast the red lustres contained between 0 and 10 % Ag/(Ag + Cu). Contrarily to Hispano-Moresque lustres, copper appears fully oxidised (Cu^+) and even some of the silver appears partially oxidised (Padovani et al. 2004; Padeletti and Fermo 2013) in the silver lustres, and mainly as Cu^+ even in the red copper lustres. The presence of cosalite ($Pb_2Bi_2S_5$) indicated on the one hand the use of a bismuth pigment and also sulphur, which is in contradiction with Picolpasso's treatise (Padeletti and Fermo 2004, 2013). The presence of bismuth has been associated with various possible purposes, and could have been added as a reducing element or as a flux, or as a cheaper substitute of silver, or could have been a natural impurity of silver typical of European deposits. Moreover, a deliberate addition of bismuth cannot be fully withdrawn.

5 Lustre and Alchemy

The peculiar optical properties of silver metal nanoparticles, triggered by a process of production which results in placing the particles in a surface submicrometric glassy layer and the control their size and volume fraction, is responsible for the golden shine shown by the lustre layers. Although even Arabian scientists were aware that "not all that glitters is gold", the transmutation of other metals into gold was a piece of fundamental research in Alchemy. Moreover, the connection between lustre and the treatise Kitab Al-Durra Al-Maknuzna (The book of the hidden pearl) by Jazbir Ibn Hayyan who during the Middle Ages in Europe was claimed as the father of Alchemy, sustains further the link.

Jabir Ibn Hayyan was an alchemist (710/730 AD–810 AD) to whom more than 3000 treatises are credited, although most of them are probably compilation works of many authors. He has to be placed in the Islamic Golden Age (Abbasid caliphate) when medicine, mathematics, astronomy, physics and many other scientific disciplines were compiled and developed by scientists under the Muslim rule. During the medieval period he was known in Europe by his Latinised name Gebber and his vast work was translated into Latin. However, many of the translations of supposed Jabir treatises were not presumably written by him. The main corpus of Alchemy extracted ideas from Jabir but was most likely written in Latin by a European author, and at least one of the books attributed to Jabir, *Summa perfectionis magisterii*, is known to be written around the end of the thirteen century by a Franciscan monk, Paulus of Taranto. The so-called Pseudo-Gebber corpus of Alchemy is therefore a product of medieval authors inspired in Jabir work (Newman 1991).

Further, we have to state that many of the products and procedures used in Lustre nanotechnology show close relations with the early metallurgy. Arabian philosophy took Aristotle's classification of all the substances as being composed of five primary elements, water, earth, fire and air, and then they added mercury and sulphur. The idea was that if any substance is formed by different proportions of the primary elements, then it should be possible to transform one substance into other.

Jabir divided the substances into spirits, metallic bodies (metals) and minerals bodies (stones). Gold, silver, copper, tin, lead and mercury were the metals known since Antiquity. All the metals were constituted of mercury and sulphur in various proportions.

Marcasite (sulphides of metals, most commonly iron and copper) included those minerals that showed a metallic lustre. In the weathered areas of those ores, hydrated sulphates of iron and copper (*vitriol*) are found (Karpenko and Norris 2002). *Vitriol* was known since Antiquity for its capability to purify gold and separating it from silver. For example, Pliny the Elder (23 AD–79 AD) described how gold could be purified by heating it together with *vitriol*, salt (sodium chloride) and ceramic powder. During this process silver chloride is formed and adsorbed in the ceramic powder (Scabadváry 1992).

In a 13th century Arabian treatise *Mabahig al-fihar*, Mountains and minerals, from Muhammad ibn Ibrahim al-Watwat (Karpenko and Norris 2002), v*itriol* was included in the subcategory of stones whose nature changes that of other stones. For example, a block of iron could be attacked by a copper sulphate solution (copper vitriol) in the hydrometallurgy of copper, and result in the reduction of copper to the metallic state (Karpenko and Norris 2002). Later Gebber was considered the first person who separated sulphuric and nitric acids; and since then *aqua regia*'s capability to dissolve gold made of it a basic element in medieval alchemy.

Finally, the production of cinnabar (HgS) by heating its constituents, and also the production of mercury by rubbing cinnabar with acetic acid was also known since Antiquity (Theophrastus in his *Book of stones* written the 4th century BC) (Takacs 2000).

Marcasite (iron and copper sulphides), *vitriol* (copper sulphates), cinnabar, acetic acid, sulphur and heat are the main ingredients of lustre; they all fit surprisingly well with the various methods of purification and transmutation of metals known by the Arabian alchemists. A little of chance and a lot of essay-error was probably the right combination that produced lustre. Nevertheless, once the golden shine was obtained, it could be interpreted as a confirmation among the believers of the theory of the transmutation of metals, theory which had already cast serious doubts even to contemporary Alchemists.

In any case, chemical experimentation is the base of many early craft products. However, we have to remember that the discoveries and success seem based largely on the trial-and-error approach, and even lustre technology is not an exception to this.

6 Conclusions

A *lustre* decoration is a sub-micrometric layer containing silver and/or copper metallic nanoparticles lying beneath the glass/glaze surface which shows a large variety of colours and metallic and iridescent appearance. *Lustre* involves a sophisticated process of production which has close connections to modern nanotechnology. The invention of lustre took place in the Islamic Golden Age when the previous knowledge on medicine, mathematics, astronomy, physics and many other scientific disciplines was compiled at the same time that it was further developed by scientists under the Muslim rule. A period characterised by leading chemical experimentation which resulted in the discovery of many new methods of processing and improving the materials properties.

The lustre chemistry, nanostructure and optical properties were far above the contemporary scientific knowledge and its production involved important technical difficulties. Nonetheless, experimentation with materials and processing conditions gave rise to one of the most beautiful and sophisticated decorations made by mankind. Nowadays we have a deeper knowledge of the science behind lustre (materials properties, atomic structure of matter, optical properties, etc.) and

incomparably superior technical capabilities, and yet making *lustre* has difficulties which require of some experimentation.

The difficulty of *lustre* manufacture makes it a very useful tracer of migration movements, commercial trade, regional interconnections, as well as, as a dating object. It is commonly accepted that the beginning of lustre productions in different regions can be related to historical events which resulted in the migration of potters from one place to another. In addition, variations of the *lustre* appearance along history may also be related to changes in materials availability and processing conditions giving rise to the various historic lustre productions.

Lustre is a clear example of engineering materials transformation resulting from the previous knowledge on materials and processing inherited from the glass industry together with lot of experimentation (trial-and-error), which in fact is what science is all about. We do not have to underestimate the science behind lustre technology, though it is a clear example of technology going ahead of science. The cumulative empirical knowledge of the glass and pottery makers took advantage of the parallel development of Chemistry. All together gave rise to a material which still nowadays captivates our eyes.

Acknowledgments The study would not have been possible without the long term funding from Mineco (present project MAT2013-41127-R) and Generalitat de Catalunya (present project 2014SGR581) received and the collaboration of many people. I would also like to express my greatest gratitude to the Ashmolean Museum staff who has supported this study allowing access to their lustre collection.

References

Ainaud de Lasarte J (1942) La loza dorada y la alfareria Barcelonesa de los siglos XIV y XV, Anales y Boletín de los Museos de Barcelona I:89–104

Al-Hassan AY (2009) An eighth century arabic treatise on the colouring of glass: Kitazb Al-Durra Al-Maknuzna (The book of the hidden pearl) of Jazbir Ibn Hayyan (c. 721–c. 815). Arabic Sciences and Philosophy 19:121–156

Allan JW (1973) Abu'l-Qasim's treatise on ceramics. Iran 11:111–120

Barber DJ, Freestone IC (1990) An investigation of the origin of the colour of the Lycurgus cup by analytical transmission electron microscopy. Archaeometry 32(1):33–45

Bethier S, Reillon V (2006) Modelization of the optical colorimetric properties of lustred ceramics. Appl Phys A 83:257–265

Bobin O, Schvoerer M, Ney C, Rammah M, Daoulatli A, Annequin B (2003) Where did the lustre tiles of the Sidi Oqba Mosque (AD 836–863) in Kairouan come from? Archaeometry 45 (4):569–577

Brill RH (1979) Chemical studies of Islamic luster glass. In: Berger R (ed) Scientific methods in medieval Archaeology, chapter XVI. UCLA Centre for Medieval and Renaissance studies. Contributions IV, pp 351–377. Berkeley CA (USA)

Caiger Smith A (1991) Lustre pottery. New Amsterdam Books, New York, EUA

Caiger-Smith A, Lightbown R (1980) The three books of the potter's art by Cipriano Piccolpasso, 1558. The Scolar Press, London

Carboni S (2002) The early period, chap. 2. In: Glass from Islamic lands: the Al-Sabah collection. Thames and Hudson, New York (USA), pp 50–137

Chabanne D, Aucouturier M, Bouquillon A, Darque-Ceretti E, Makariou S, Dectot X, Faÿ-Hallé A, Miroudot D (2012) Ceramics with metallic lustre decoration. A detailed study of Islamic productions from the 9th century until the Renaissance. Matériaux & Techniques 100:47–68
Clinton M (1991) Lustres. In: Cooper E (ed) The complete potter. Kangaroo Press, Kenthurst, New South Wales (Australia)
Colomban P (2009) The use of metal nanoparticles to produce yellow, red and iridescent colour, from bronze age to present times in lustre pottery and glass solid state chemistry, spectroscopy and nanostructure. J Nano Res 8:109–132
Delgado J, Vilarigues M, Ruivo A, Corregidor V, da Silva RC, Alves LC (2011) Characterisation of medieval yellow silver stained glass from Convento de Cristo in Tomar, Portugal, *Nuc*. Instrum Methods Phys Res B 269:2383–2388
Doremus RH (1994) Glass science. Wiley, New York, EUA
Dusemund B, Hoffmann A, Salzmann T, Kreibig U, Smidth G (1991) Cluster matter: the transition of optical elastic scattering to regular reflection. Z Phys D 20:305–308
Farbman I, Levi O, Efrima S (1992) Optical response of concentrated colloids of coinage metals in the near-ultraviolet, visible and infrared regions. J Chem Phys 96(9):6477–6485
Fredrickx P, Helary D, Schryvers D, Darque-ceretti E (2004) A TEM study of nanoparticles in lustre glazes. Appl Phys A 79:283–288
Freestone IC, Stapleton CP, Rigby V (2003) The production of red glass and enamel in the Later Iron Age, Roman and Byzantine periods. In: Entwistle C (ed) Through a glass brightly. Studies in byzantine and medieval art and archaeology presented to David Buckton. Oxbow (UK), pp 142–154
Greaves GN, Ngai KL (1995) Reconciling ionic-transport properties with atomic structure in oxide glasses. Phys Rev B 52(9):6358–6380
Gutierrez PC, Pradell T, Molera J, Smith AD, Climent-Font A, Tite MS (2010) Color and golden shine of silver Islamic luster. J Amer Ceram Soc 93(8):2320–2328
Hamer F, Hamer J (2004) The potter's dictionary of materials and techniques, 5th edn. A&C Black Publishers Ltd., London
Heaton N (1948) The origin and use of silver stain. J British Soc Master Glass Painters 10:9–16
Jembrih-Simbürger D, Neelmeijer C, Schalm O, Fredrickx P, Schreiner M, De Vis K, Mäder M, Schryvers D, Caen J (2002) The colour of silver stained glass—analytical investigations carried out with XRF, SEM/EDX, TEM, and IBA. J Anal At Spectrom 17:321–328
Jenkins M (1986) Islamic glass. A brief history, The Metropolitan Museum of Art Bulletin, fall 1986. New York (USA)
Jenkins-Madina M (2006) Raqqa Revisited. Ceramics of Ayyubid Syria. The Metropolitan Museum of Art, New York
Johnson PB, Christy RW (1972) Optical constants of noble metals. Phys Rev B 6(12):4370–4379
Karpenko V, Norris JA (2002) Vitriol in the history of chemistry. Chem Listy 96:997–1005
Kreibig U, Vollmer M (1995) Optical properties of metal cluster, Springer series 25. Springer, Berlin
Kuga Y, Ishimaro A (1984) Retropreflectance from a dense distribution of spherical particles. J Opt Soc Am 1(8):831–835
Künel E (1934) Die Abbasidischen Lüsterfayencen, Ars Islamica 1(2):148–159
Kunicki-Goldfinger JJ, Freestone IC, McDonald I, Hobot JA, Gilderdale-Scott H, Ayers T (2014) Technology, production and chronology of red window glass in the medieval period a rediscovery of a lost technology. J Archaeolo Sci 41:89–105
Lamm CJ (1941) Oriental glass of medieval date found in Sweden and the early history of lustre-painting, Vitterhets, historie och antikvitets akademien. Wahlström & Widstrand, Stockolm (Sweden)
Mason RB (2004) Shine like the sun. Lustre-painted and associated pottery from the Medieval Middle East. In: Bibliotheca Iranica: Islamic art and architecture series, vol 12. Mazda Publishers, Inc., Costa Mesa, Canada
Maxwell Garnett JC (1904) Colours in metal glasses and in metallic films. Philos Trans R Soc London 203:385–420

Maxwell Garnett JC (1906) Colours in metal glasses, in metallic films and in metallic solutions. Philos Trans R Soc London 205:237–288

Molera J, Pradell T, Vendrell-Saz M (2001a) Características Técnicas y Procesos de Producción de Las Cerámicas del s. XIII en Paterna; chapter 4. In: Mesquida M, E. López Peris J, Prades S, Smolka R (eds) Las ollerías de Paterna. Tecnología y producción del s.XII y s.XIII. Publicaciones del Ayuntamiento de Paterna, (Paterna) 223–253

Molera J, Mesquida M, Pérez-Arantegui J, Pradell T, Vendrell M (2001b) Luster recipes from medieval workshop in Paterna. Archaeometry 43(4):455–460

Molera J, Bayés C, Roura P, Crespo D, Pradell T (2007) Key parameters in the production of medieval lustre colors and shines. J Am Ceram Soc 90(7):2245–2254

Molina G, Murcia S, Molera J, Roldan C, Crespo D, Pradell T (2013) Color and dichroism of silver-stained glasses. J Nanoparticle Res 15:1932

Molina G, Tite MS, Molera J, Climent-Font A, Pradell T (2014) Technology of production of polychrome lustre. J Eur Ceram Soc 34:2563–2574

Newman WR (1991) The Summa Perfectionis of Pseudo-Geber. A critical edition, Translationa and study. EJ Brill, Leiden

Padeletti G, Fermo P (2004) Production of gold and ruby-red lustres in Gubbio (Umbria, Italy) during the Renaissance period. Appl Phys A 79(2):241–245

Padeletti G, Fermo P (2013) Il lustro dall'Islam al Rinascimento: la presenza del bismuto nella produzione italiana. In Mastro Giorgio da Gubbio, art, science and technology of lustred majolicas. Volumnia Editrice (Perugia, Italy), pp 197–204

Padeletti G, Ingo GM, Bouquillon A, Pages-Camagne S, Aucouturier M, Roehrs S, Fermo P (2006) First time observation of Mastro Giorgio masterìeces by means of non-destructive techniques. Appl Phys A 83:475–483

Padeletti G, Fermo P, Bouquillon A, Aucouturier M, Barbe F (2010) A new light on a first example of lustred majolica in Italy. Appl Phys A 100:747–761

Padovani S, Borgia I, Brunetti B, Sgamellotti A, Giulivi A, D'Acapito F (2004) Silver and copper nanoclustres in the lustre decoration of Italian Renaissance pottery: an EXAFS study. Appl Phys A 79(2):229–233

Pérez-Arantegui J, Molera J, Larrea A, Pradell T, Vendrell M, Borgia I, Brunetti BG, Cariati F, Fermo P, Mellini M, Sgamellotti A, Viti C (2001) Luster pottery from the thirteenth century to the Sixteenth century: a nanostructured metallic thin metallic film. J Am Ceram Soc 84(2):442–446

Pérez-Arantegui J, Larrea A, Molera J, Pradell T, Vendrell M (2004) Some aspects of the characterization of decorations on ceramic glazes. Appl Phys A 79(2):235–239

Philon H (1980) Early Islamic ceramics: ninith to twelfth centuries. Islamic art publications, Sotheby Parke and Bernet Pub. London, Benaki Museum, Athens

Picon M, Navarro Palazón J (1986) La loza dorada de la Province de Murcie: étude de laboratoire. In: La ceramica medievale nel mediterraneo occidentale. Siena-Faenza, Edizioni All' Insegna Del Giglio

Pilosi L, Whitehouse D (2013) Early Islamic and Bizantine silver stain. In: Endwistle C, James L (eds) New light on old glass in recent research on byzantine mosaics and glass. The British Museum. Research Publication, chap. 29, vol 179, pp 329–337

Polvorinos del Rio A, Castaig J (2010) Lustre decorated ceramics from a 15th and 16th century production in Seville. Archaeometry 52(1):83–98

Polvorinos del Rio A, Castaing J, Roehrs S, Vallejo-Triano A, Escudero-Aranda J (2008) Estudio arqueométrico de loza dorada de Madinat al'Zahra, Córdoba. Cuadernos de Madinat al-Zahra 6:165–179

Porter V (1981) Medieval Syrian Pottery (Raqqa Ware). Ashmolean Museum publications, Oxford

Porter V, Watson O (1987) Part II: Tell Minis' wares. Syrian and Iran, three studies in medieval ceramics. Oxford studies in Islamic art, IV. Oxford University Press, Oxford (UK), pp 175–248

Pradell T, Molera J, Vendrell M, Pérez-Arantegui J, Pantos E, Roberts M, DiMichiel M (2004) The role of cinnabar in Luster production. J Am Ceram Soc 86(6):1018–1023

Pradell T, Molera J, Roque J, Smith AD, Crespo D, Pantos E, Vendrell M (2005) Ionic-exchange mechanism in the formation of medieval luster decorations. J Amer Ceram Soc 88(5):1281–1289
Pradell T, Molera J, Bayés C, Roura P (2006) Luster decoration of ceramics: mechanisms of metallic luster formation. Appl Phys A 83(2):203–208
Pradell T, Climent-Font A, Molera J, Zucchiatti A, Ynsa MD, Roura P, Crespo D (2007) Metallic and non-metallic shine in luster: an elastic ion backscattering study. J Appl Phys 101 (9):103518 (8 Pages)
Pradell T, Molera J, Smith AD, Tite MS (2008a) The invention of lustre: Iraq 9th and 10th centuries AD. J Archaeol Sci 35:1201–1215
Pradell T, Molera J, Smith AD, Tite MS (2008b) Early Islamic luster from Egypt, Syria and Iran (10th to 13th century AD). J Archaeol Sci 35:2649–2662
Pradell T, Molera J, Pantos E, Smith AD, Martin CM, Labrador A (2008c) Temperature resolved reproduction of medieval luster. Appl Phys A 90:81–88
Pradell T, Pavlov R, Gutiérrez PC, Climent-Font A, Molera J (2012) Composition, nanostructure and optical properties of silver and silver-copper lusters. J App Phys 112(5):054307(10 pages)
Pradell T, Molera J, Molina G, Tite MS (2013) Analysis of Syrian lustre pottery (12th–14th centuries AD). Appl Clay Sci 82:106–112
Pradell T, Molina G, Molera J, Tite MS (2016) Composition of the lustre pigment used in the production of 13th century AD lustreware from Syria. Archaeometry. doi:10.1111/arcm.12211
Reillon V, Bethier S (2013) Optical and colorimetric properties of lustres. In: Mastro Giorgio da Gubbio, Art, Science and Technology of Lustred Majolicas, Volumnia Editrice (Perugia, Italy). pp 115–134
REMAI (2012) Proceedings of the 1st international conference of the European network of museums of Islamic art, Museo de la Alhambra, V&A and Musée du Louvre
Rosser-Owen M (2010) Islamic arts from Spain. V&A Publishing, London
Scabadváry F (1992) History of analytical chemistry. Gordon and Beach Science Pub, London
Sciau Ph, Mirguet C, Roucau C, Chabanne D, Schvoerer M (2009) Double nanoparticle layer in a 12th century lustreware decoration: accident or technological. J Nano Res 8:133–140
Smith AD, Pradell T, Roque J, Molera J, Vendrell-Saz M, Dent AJ, Pantos E (2006) Colour variations in 13th century hispanic luster—an EXAFS study. J Non-Cryst Solids 352:5353–5361
Takacs L (2000) Quiksilver from cinnabar: the first documented mechanochemical reaction? JOM 52(1):12–13
van de Hulst HC (1980) Multiple light scattering; tables, formula and applications, vol 1 and 2. Academic Press, New York
van de Hulst HC (1981) Light scattering by small particles. Dover Publications Inc, New York
Vilarigues M, Fernandes P, Alves LC, da Silva RC (2009) Stained glasses under the nuclear microprobe: a window into history. Nuc Inst Meth Phys Res B 267:2260–2264
Waksman Y, Capelli C, Pradell T, Molera J (2014) The ways of the lustre: looking for the Tunisian connection. In: Martinón-Torres M (ed) Craft and science: international perspectives on archaeological ceramics. UCL Qatar series in archaeology and cultural heritage 1 Doha, Qatar. Bloomsbury Qatar Foundation, pp 109–116
Watson O (1985) Persian lustre ware. Faber and Faber, London (UK)
Wolf PE, Maret G (1985) Weak localization and coherent backscattering of photons in disordered media. Phys Rev Lett 55(24):2696–2699
Wood N (1999) Chinese glazes: their origins, chemistry and recreation. A and C Black publishers, Bedford (UK)
Wood N, Tite MS, Doherty C, Gilmore B (2007) A technological examination of ninth–tenth century AD Abbasid blue-and-white ware from Iraq, and its comparison with eighth century ad Chinese blue-and-white Sancai ware. Archaeometry 49(4):665–684

Nano-crystallization in Decorative Layers of Greek and Roman Ceramics

Philippe Sciau

Abstract Besides metallic nanocrystals of lusterware (Chapter "Lustre and Nanostructures—Ancient Technologies Revisited"), other nanoscale crystals can be found in ancient ceramics and more specifically in their decorative layers or coatings. These crystals can play a major role in the physical properties of these thin layers or can be an indicator of the manufacturing process. These thin layers are formed during firing and result from physicochemical reactions among the diverse compounds of raw preparation. In general, the firing conditions are not suitable for obtaining large crystals and many of the formed phases have crystal sizes of a few tens nanometres. Over a long period of time and throughout the world, the variety of raw preparations and firing conditions used are so diverse that it is not conceivable to give here an exhaustive rundown. In this chapter, we will focus our attention on some decorative layers of Greek and Roman potteries for which oxide nanocrystals play a key role regarding the optical and/or mechanical properties. These decorations were obtained from clay preparations and their physical properties result directly from the nanocrystalline size and the behaviour of clay minerals.

1 Introduction

Metallic lustre decorations of glazed ceramics, which appeared in Mesopotamia during the 9th century AD, are certainly the most famous historical example of controlled nanotechnology for optical devices (cf. Part 1, Chapter "Lustre and Nanostructures—Ancient Technologies Revisited"). But in fact the use of optical properties of metallic particles is older (Colomban 2009; Sciau 2012). Indeed, transmission electron microscopy (TEM) revealed that the dichroic colouring of the amazing 4th century Roman Lycurgus cup, showed at the British Museum, comes from nanocrystals of an Au/Ag alloy dispersed in the glassy matrix (Barber and Freestone 1990;

P. Sciau (✉)
CEMES, CNRS, Université de Toulouse, Toulouse, France
e-mail: philippe.sciau@cemes.fr

P. Dillmann et al. (eds.), *Nanoscience and Cultural Heritage*,
DOI 10.2991/978-94-6239-198-7_2

Freestone et al. 2007). However, only a few fragments of dichroic glasses were found up to now and none of them has the quality of the glass of the Lycurgus cup. It seems unlikely that sufficient craft experience could have been developed to master this highly complex technology.

In fact, the tinting strength of metallic nanocrystal was used earlier for colouring glasses. It was shown that red glasses of the Final Bronze Age (1200–1000 BC) from Frattesina di Rovigo in Italy were coloured thanks to crystalline particles of metallic copper dispersed in the surface layer of a glassy matrix (Angelini et al. 2004). Many other examples can be found in the literature showing that this glass staining process was widely used worldwide and up to present times. Thus, the presence of both copper and cuprite particles was reported in Celtic enamels (Brun et al. 1991). Most of the Roman tesserae of red colour were obtained from a glass containing copper nanocrystal (Ricciardi et al. 2009). These tesserae were produced massively during the Roman period thanks to a scale production of glass ingots (Colomban 2009). Unlike the manufacturing of the dichroic glasses, the achievement of tinted glass by copper nanoparticles was perfectly mastered by the Roman craftsmen. Outside Europe and the Mediterranean basin, copper nanoparticles for colouring glasses and glazes were also massively used in Asia. For instance, the colouring of Japanese Satsuma glasses was obtained in this way (Nakai et al. 1999). The blue-red Jun glazed porcelains made from Song to Qing Chinese Dynasties were manufactured using a similar process leading to a formation of copper nanocrystals in the red zones during the firing (Wood 1999). It is also the case of some Vietnamese porcelains and celadons (Colomban et al. 2003). The process is still used nowadays. It is at the origin of the glaze colour called oxblood of current porcelains (Fig. 1).

Besides metallic nanocrystals exploited for their optical properties, many other nanoscale crystals such as iron oxides can be found in ancient potteries and more specifically in their decorative or coating layers. These crystals can play a major role in the physical properties of these thin layers or merely be an indicator of manufacturing processes. These thin layers are formed during firing and result from physicochemical reactions among the diverse compounds of raw preparation. In general, the firing conditions are not suitable for obtaining large crystals and many

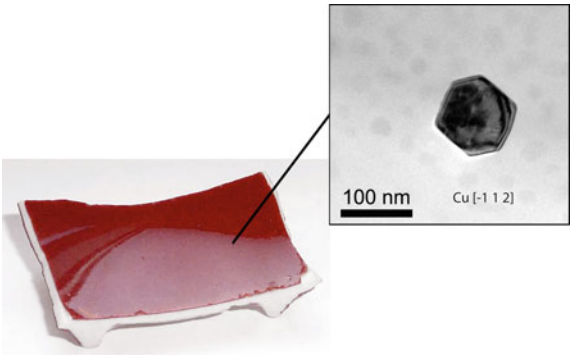

Fig. 1 Copper nanocrystal observed in modern porcelain with *red glaze* called "oxblood"

of them have nano or submicrometric sizes. In time and around the world, the variety of raw preparations and firing conditions used are so diverse that it is not reasonable to give here an exhaustive overview. In this chapter, we will focus our attention on some decorative layers of Greek and Roman potteries for which oxide nanocrystals play a key role for the optical and/or mechanical properties. These decorations were obtained from clay preparations and their physical properties result directly from the nanocrystalline size and the behaviour of clay minerals, which are discussed in detail in the next paragraphs, after a short description of the main characteristics of the surface treatments performed from clay preparations.

2 Potteries and Surface Treatments

The first potteries, or vessels in fired clay, were made several millennia before the Neolithic revolution in various areas of the world but it is during the Neolithic, with the settlement of human communities, that its use becomes widespread, leading to the improvement of manufacturing processes (Garcia et al. 2014; Sciau and Goudeau 2015). In particular, various surface treatments began to be developed for improving the ceramic properties such as waterproofness or surface strength (hardening). Very early on, these surface treatments had also a decorative function with the design of ornamental patterns, which were specific to cultural communities or civilizations. Since the Neolithic time, knowledge and know-how have improved, leading to the manufacturing of high-quality pottery using very sophisticated surface treatments. Lusterware mentioned in the introduction and presented in detail in Sect. 1.1, is a typical example of achievement with a complex surface treatment requiring two well-controlled firings. The first one allows for the formation of glaze, which provides hardness and tightness while the second leads to the growth of metal nanoparticles within the outermost layers of the glaze (Sciau 2012).

Clay preparations were also intensively used to shape thin decorative and water-resistant coatings at the pottery's surface (Tite 2008). By means of settling and decantation, raw clay material was fractionated to keep only the finest particles and thus to obtain a liquid slip. Then, unfired vessels were dipped into the liquid slip or, the liquid slip was used as paint and applied on the vessel surface. These liquid preparations can be naturally rich in iron if raw clay materials containing oxides and/or hydroxides of iron are selected. Most of these Fe-phases are present in small grains and are kept during the preparation step. Furthermore, several clay minerals (illite, smectite, vermiculite,…) can contain a significant rate of iron in their structures (Deer et al. 1992) and as the clay minerals are also constituted of very small particles, the groundwork results in an increase of the iron rate. The colour after the firing of these slips can be controlled through the redox chemistry of iron so that a firing under reducing conditions leads to a black colour by fostering the formation of magnetite and/or hercynite while a firing under an oxidizing atmosphere leads to a red colour by triggering the formation of hematite. Playing on the total iron rate (preparation), the Fe^{2+}/Fe^{3+} ratio and the size of iron oxide particles formed during

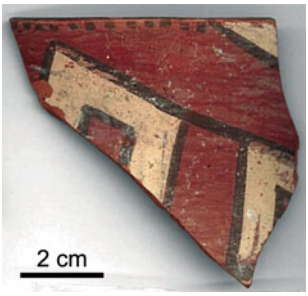

Fig. 2 Fragment of a Cucuteni ceramic. (Micrograph, courtesy D. Popovici and R. Bugoi)

the firing (atmosphere/temperature/time), one can more or less control the final colour from black to bright red. The colour palette can be completed with white slips prepared from raw clay materials containing no iron. The full range was used since the Neolithic times. For example, the flourishing Cucuteni-Tripolye civilization, which was located in the southeastern part of Europe from the Vth to IVth Millennia BC, designed decorative patterns (Fig. 2) using up to 3 colours (Fig. 1) in the same vessel (Bugoi et al. 2008). The red decors were obtained using Fe-rich clay preparations fired under oxidizing conditions at rather a high temperature. To get black colours under these firing conditions, Mn-rich iron minerals were added to the clay preparation, which resulted in the growth of jacobsite ($Mn^{2+}Fe^{3+}{}_2O_4$) a black-colour pigment in addition to hematite (Fig. 3).

Some of these slips, especially the ones containing K-rich illitic clay and a high rate of iron (10–20 % in oxide weight), can be easily vitrified during firing and give high-gloss coatings. Those types of surface finishes were especially developed during the Greek and Roman periods (Noble 1965; Tite et al. 1982). It is the basis of the manufacturing of famous Attic ceramics made in Athens and its region from 7th century BC until the late 3rd century BC. Roman craftsmen improved the making of high-gloss red coatings thanks to the focus on kilns permitting a better control of oxidizing conditions leading to the mass production of Terra Sigillata (Hartley 1971; Picon and Vernhet 2008; Sciau et al. 2006). These achievements and the nanostructure of these coatings are detailed in the next sections.

3 High Gloss Coatings of Greek and Roman Potteries

3.1 Outlines and Historical Framework

The first high-gloss coatings developed by Greek craftsmen were black and were used to produce beginning the 7th century BC the black-figure pottery painting, also called black-figure style or black-figure ceramic (Noble 1965). The decor was painted with a liquid fine clay preparation, which becomes black during the firing while the non-painted surface of vessel appears red. The end of the heating step was performed under reducing conditions (smoke) at a temperature high enough to glaze

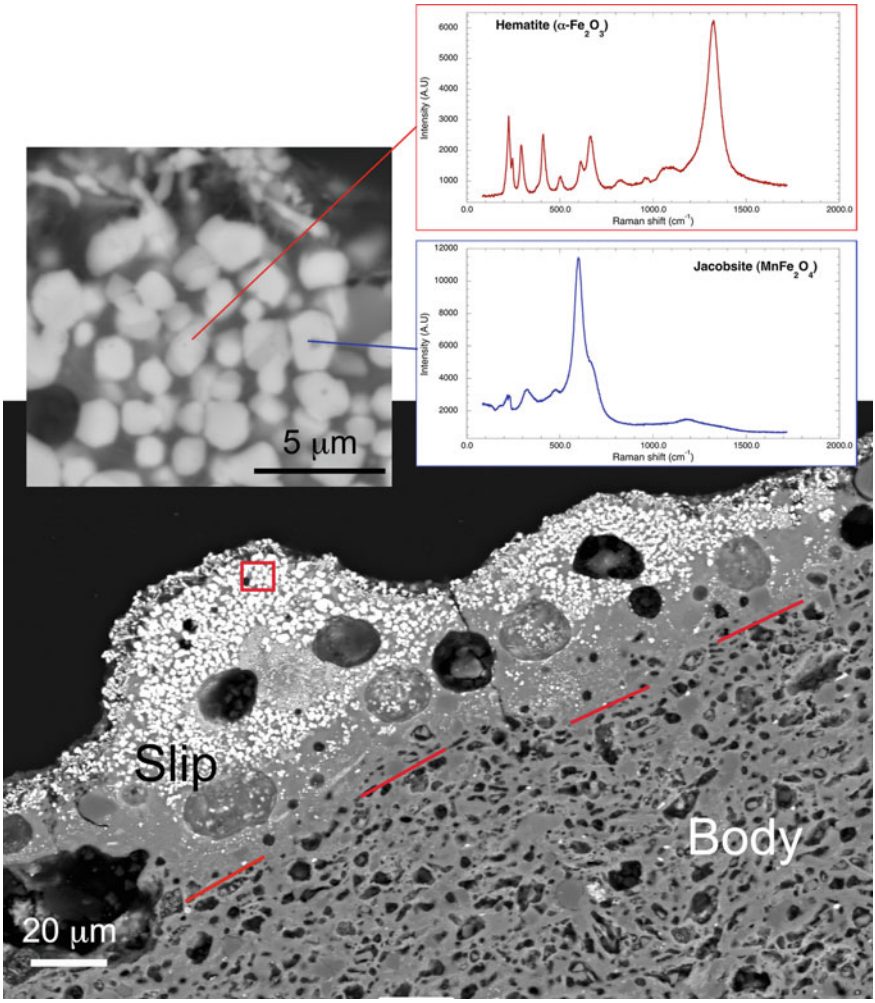

Fig. 3 Cross-section of a black decor of a Cucuteni ceramic containing both hematite and jacobsite crystals

the painted zones but not enough to glaze the non-painted zones. Then an oxidizing step at lower temperature was performed in order to oxidize the non-glassy zones. Around the last quarter of the 6th century BC, a new style appeared in Athens, which consisted of inverting the colours: the background is black while the figures are red (Fig. 4). To strengthen the red colour of non-glossy zones, fine clay preparations were sometime affixed to these zones. It is specially the case of Attic pottery with coral red slip (Walton et al. 2009). The achievement of such pottery requires a perfect mastery of firing protocol but also the use of two different clay preparations. The clay preparation used for the red zones must have a glassy

Fig. 4 Attic ceramic of the red figure type (5th c. BC) found in Lattes (France) and described in Chazalon (2010). (Micrograph, courtesy E. Gailledrat)

temperature higher than the one used for the black zones so that only the black zones are glassy during the reducing heating step. These two clay preparations can be obtained, or not, from the same raw clay material. Walton et al. showed that the clay preparations used for red parts had either a higher Ca rate or (and) a larger particle size, so that after the reducing heating step these zones have a higher porosity than the black zones and they can be re-oxidized during the next step.

However, a recent study concerning an attic vase of 5th century attributed to Berlin Painter revealed that this vessel was not obtained using the three phase firing protocol (Cianchetta et al. 2015). It presents a complicated layered architecture of black and red gloss, which seems to require multiple rounds of painting/firing to be achieved. The use of multiple firing was previously suggested on the basis of replication investigations (Walton et al. 2013). Studies are currently underway on the firing protocol of the Attic red-figure ceramics, which could have been more complex than considered until now. Although these potteries were made by civilizations where writing was commonly used, no details were found up to now in antique writings concerning their firings. They are only mentioned on a few drawings on terracotta slabs called “pinakes” and in only one poem (Jubier-Galinier et al. 2003; Lyons 2005; Sciau and Goudeau 2015).

Besides the red-figure ceramics, a lot of tableware was made without decorations and with only a high-gloss black coating. This tradition of black coating vessels was continuous during the Roman Republic period and gave the Campanian tableware, which archaeologists divided into 3 classes (A, B and C) based on the aspect, the period and the production zone. These potteries were produced in Italy (Campania, Etruria) and widely exported in the Mediterranean, in particular in The Gulf of Lion or along Balearic seacoasts. C type is of lower quality with coatings scarcely sintered and thicker (Mirti and Davit 2001). The clay preparations used for their coatings had generally a particle size lightly superior to the one used for Attic production and the firing temperatures were higher (Vendrell-Saz et al. 1991). From a recent study, a firing protocol including a heating step under reducing conditions (mainly at the end of the step) followed by oxidizing cooling allows for obtaining this type of production (Meirer et al. 2013).

Fig. 5 Terra Sigillata vessel (Drag. 29, 1st c. AD) found in La Graufesenque workshop. (Micrograph, courtesy A. Verhnet)

During the latter half of the first century BC, started in central Italy, tableware with a very high-gloss red coating, also called *Terra Sigillata* or *Samian ware*. Terra Sigillata pottery (Fig. 5) was the most famous tableware produced during the Roman period owing to the mass production of standardized shapes and the widespread distribution of the vessels (Hartley 1971). The beautiful ceramics were characterized by their reddish coloration, glossy coating, and the unique ornamentation created by the use of moulds and stamps (sigilla). The success of this pottery led to the rapid spreading of the technique outside the Italic peninsula and from the beginning of the first century AD, large production centres were set up in southern Gaul in such sites as La Graufesenque (Schaad 2007). From the latter half of the 1st century AD, workshops were developed in Spain maybe with the help of Gallic potters (Keay 1988). During the 2nd century AD, the production of southern Gallic workshops drops sharply and a new large workshop was established in central Gaul (Lezoux). Within 3rd and 4th centuries, the Gallic production of Terra Sigillata was moved to eastern Gaul but with a drop in quality. The coatings produced during the 4th century are very little vitrified and their red colours come mainly from a re-oxidation during the last step of firing process. Sigillata or related productions of lesser quality were manufactured in other zones of Roman Empire, mainly from the 2nd century AD.

3.2 Composition and Structure

As mentioned in the Sect. 3.1, the manufacturing of these high gloss coatings concerns both a wide time period and a large geographic area. Also, it is no question here to describe exhaustively the composition and structure of the different coatings produced but just to give some of their characteristics through a few examples (Table 1). Inside a type, significant differences appear among the various workshops

Table 1 Examples of the elemental composition ($\%_{mass}$) of coatings determined by electron microprobe (*Géosciences Environnement Toulouse* (GET) of Toulouse University)

	Na_2O	MgO	Al_2O_3	SiO_2	P_2O_5	K_2O	CaO	TiO_2	MnO	Fe_2O_3	BaO	Total
Attic (10)	0.51 (0.18)	2.05 (0.17)	27.83 (1.08)	45.28 (0.93)	0.19 (0.05)	5.75 (0.69)	0.45 (0.19)	0.65 (0.14)	0.08 (0.03)	16.35 (0.56)	0.01 (0.01)	99.2
Camp A (8)	2.09 (0.36)	1.68 (0.45)	28.29 (0.63)	44.97 (0.80)	0.16 (0.02)	4.67 (0.40)	0.93 (0.15)	0.60 (0.11)	0.17 (0.05)	15.91 (1.00)	0.08 (0.02)	99.6
Camp B (11)	0.71 (0.19)	2.26 (0.07)	27.92 (0.43)	46.47 (0.70)	0.15 (0.02)	6.59 (1.18)	0.79 (0.16)	0.48 (0.03)	0.10 (0.03)	14.27 (1.50)	0.07 (0.02)	99.8
TS Italic (39)	0.94 (0.37)	3.19 (0.45)	26.64 (0.60)	48.97 (0.77)	0.12 (0.02)	6.51 (0.90)	1.51 (0.90)	0.57 (0.08)	0.07 (0.02)	10.27 (0.61)	0.09 (0.02)	98.9
TS Gaul (72)	0.08 (0.06)	0.94 (0.22)	22.87 (2.37)	54.86 (2.79)	0.17 (0.04)	7.90 (0.85)	1.37 (0.87)	0.71 (0.10)	0.05 (0.01)	9.49 (1.00)	0.08 (0.02)	98.5

The standard deviations are given in brackets as well as the number of samples. The attic and Campanian ceramics were provided by the *laboratoire d'Archéologie des Sociétés Méditerranéennes* and come from the Lattes and Narbonne excavations respectively. The terra sigillata data were extracted from Leon's work (Leon et al. 2015)

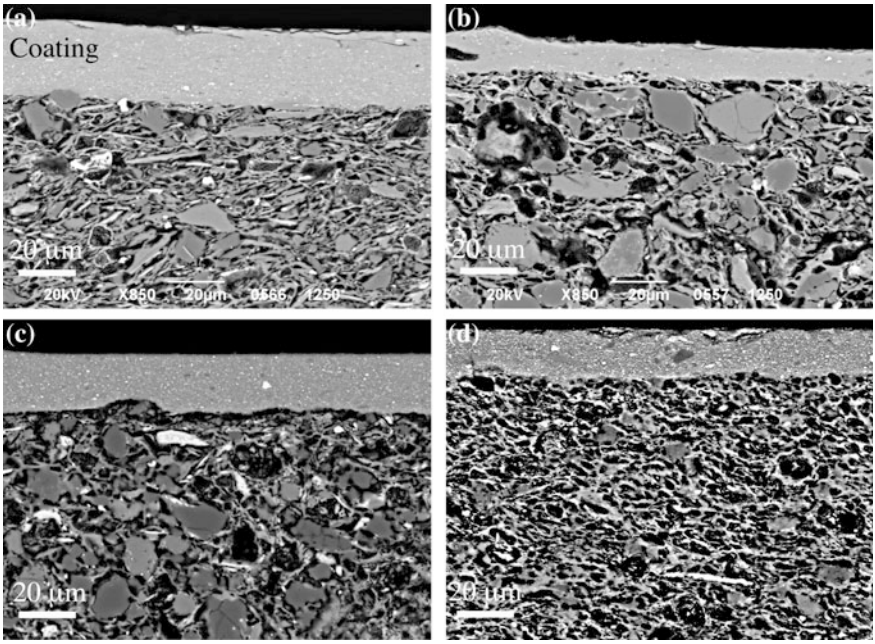

Fig. 6 Cross-sections of various ceramic types: **a** Attic, **b** Campanian B, **c** Italic Terra Sigillata and **d** Gallic Terra Sigillata

as one can observe comparing the elemental compositions of two main italic workshops (Arezzo, Pisa) of Terra Sigillata and the one (La Graufesenque) of the main southern Gallic workshops. In some cases, the discrimination can be finer and allows for separating the production of an individual pottery-making firm inside the same workshop. For example at Arezzo, the products of "Ateius" can be separated from the one of "Perrenius" on the basis of their element compositions (Leon et al. 2015). Of course, it is also the case for other ceramic types. However even if the Table 1 does not give an exhaustive view of coating compositions, some information can be retrieved (drawn). All these coatings present a low Ca rate (<2 %) and a high rate of Fe and K. The Al/Si ratio is also very similar. Only the coatings of Terra Sigillata made in Gaul contain more silicon oxide. These coatings were obtained from a less fine clay preparation containing a few more quartz crystals. The Fe amount is higher for the black coatings (Attic and Campanian) while the Ca rate is a little higher in the red coatings (Terra Sigillata). The slight deficiency in potassium of Campanian type A was already reported and is a characteristic of these products (Mirti and Davit 2001).

Observed in cross-section using a scanning electron microscope, these diverse ceramics show quite similar structure. The coating appears as a thin layer of a few tens of micrometres denser and much more homogeneous than the body (Fig. 6). The grain size difference between the materials used for the coating and the body is

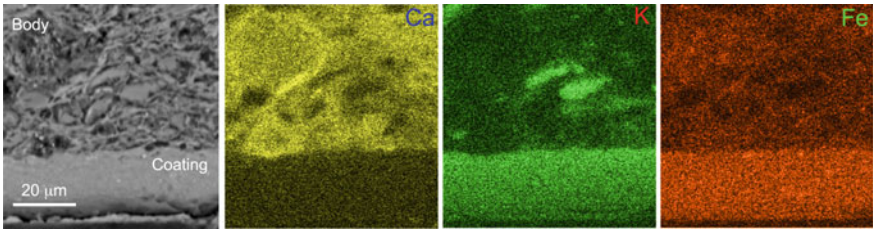

Fig. 7 Elemental maps recorded on a cross-section of an Attic ceramic. The coating contains more iron and potassium and less calcium than the body

evident. Large crystals of tempers ("non-plastic" phases, such as quartz, feldspars…) are observed in the bodies while only a few small quartz crystals are noticeable in the Gallic Terra Sigillata coatings. The differences in composition between the bodies and coatings are also clearly shown in the elemental maps (Fig. 7) obtained using energy-dispersive X-ray spectroscopy (SEM-EDX). All bodies of these diverse potteries were made from calcareous clay containing tempers of small grain size (a few tens microns).

3.3 Phase Transformations During Firing

During firing, only the concentration of atoms (H, C, O, Cl, S,…) of volatile elements (water, organic material, carbonate, chlorides, sulphites,…) is changed. The ratio of the other elements (Si, Al, Mg, Ca, Fe,…) is slightly or not modified by the firing process. By contrast, the structural organization (the nature of crystallographic phases) is greatly changed during the firing. The clay minerals (kaolinite, illite, smectite,…) begin to lose water with the elevation of temperature, leading then to structural disruptions. The decomposition produces various new crystalline (mullite, alumina, spinel…) or disordered (glass) phases depending on the nature of clay minerals (McConville and Lee 2005; Lee et al. 2008). Clay minerals can also react with other mineral phases such as hydro-oxides, oxides or carbonates present in the non-fired pottery, to form new phases such as pyroxene, plagioclase, iron oxide,… (Maggetti 1982). The chemical reactions taking place during the firing of a pottery are very diverse and depend, of course, on the chemical and crystallographic composition, but also on the size and spatial distribution of crystallites (heterogeneity) in the starting mixture. Firing atmosphere (reducing or oxidizing) has also a significant influence on the formation of the crystals containing transition metal elements such as the iron oxides. Many of these reactions are irreversible and this great diversity can be considered as an advantage, which can be used to obtain extensive information from the study of pottery fragments.

The firing conditions are seldom suitable for growing large crystals and then only nanometric or submicrometric crystallites are formed. It is particularly true for

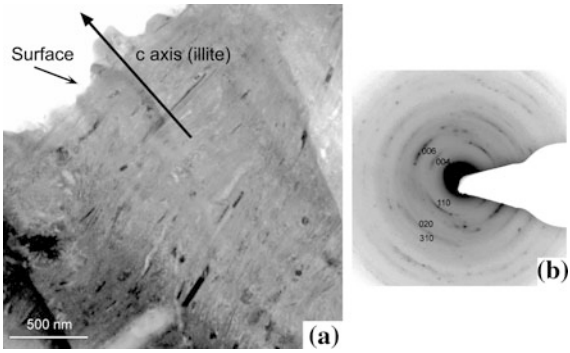

Fig. 8 Example of a non-glassy coating of the Roman period fired at a low temperature (<850 °C). **a** Bright field TEM image of a cross section showing the microstructure of oriented dehydrated-illite crystals. **b** SA electron diffraction pattern of the same area showing the orientation and also the badly crystallisation

the high gloss coatings. The clay preparations used were essentially composed of clay minerals and badly crystallized iron oxides and hydro-oxides. The SiO_2/Al_2O_3 ratios measured in the black coatings [Attic (1.6), Campanian A (1.6) and Campanian B (1.7)] are between those of kaolinite (1.2) and illite (2.2) values. This indicates that the mixtures used for their manufacturing contained mainly these two phases in addition to iron based phases. The ratios are higher in the Terra Sigillata red coating according to higher illite fraction. In contrast to kaolinite, illite contains potassium and the increase of K rate is also in agreement with an increasing account of illite. The high proportion of illite is also confirmed by the observation performed on badly fired ceramics (Fig. 8).

The temperature was not high enough to destroy all illite crystals. This type of image reveals also the organization of illite crystals before firing due to their plate-shape and the use of a liquid preparation in which the thin particles are in suspension and homogeneously distributed. This regular organization allows for obtaining a shiny appearance with only a partial vitrification. The clay crystals are distributed on the surface of the pottery somewhat like tiles on a roof and a beginning of vitrification is enough to make rather dense and not too rough coatings. Of course, the very shiny coating of high quality ceramics requires a further glazing but thanks to this particle organization, it can be obtained at quite low temperatures (850–1000 °C) depending on the composition (K, Na, Mg rates) and the atmosphere (oxidizing or reducing). Above 850 °C, the tetrahedral (SiO_4^{4-}) layers of illitic structure begin to create the glassy matrix while a part of octahedral (AlO_6^{9-}) layers contributes to the formation of various spinel structure types depending on the other elements (Fe, Mg) substituted to Al and/or present in surrounding particles such as iron oxides. For instance, the presence of Mg leads to $MgAl_2O_4$ spinel growth which in turn decreases the Al rate in destroyed illite cluster structure promoting then the glassy matrix (Sciau et al. 2008). Under reducing conditions a second process takes place. The iron oxides/hydroxides are transformed into FeO, which reacts with Al atoms of the illite decomposed structure to form hercynite spinel structure ($FeAl_2O_4$). Here again, the hercynite formation facilitates the formation of the glassy matrix. Since the Fe rate is much higher than the Mg rate, the second mechanism is more efficient and can also concern Al atoms

contained in metakaolin clusters. Above 600 °C, kaolinite has lost all constitutional OH groups and the dehydroxylated product is often referred to as metakaolin (Deer et al. 1992; Lee et al. 2008). Under oxidation conditions, iron oxides/hydroxides are transformed into Fe_2O_3, which is a stable form and does not react with Al. Only the formation of $MgAl_2O_4$ spinel can lower the vitrification temperature. In the absence of Mg atoms, the dehydration of K-rich illite leads to the formation of an intermediate potassium aluminium silicate phase (of $KAl_3Si_3O_{11}$ type) above 800 °C. For temperatures higher than 950 °C, this phase begins to lose its crystallographic long range order and gives between 1000–1100 °C a glassy matrix containing corundum (α-Al_2O_3) nanocrystals (Sciau et al. 2008).

3.4 *Nanocrystals and Physical Properties*

Observed in transmission electron microscopy, the high gloss coatings are constituted of a glassy matrix containing mainly nano and submicrometric crystals. A few micrometric quartz crystals can also be observed especially in Gallic Terra Sigillata coatings.

The nanometric crystals of black coatings are essentially hercynite (Fig. 9), which gives the colour of these coatings. X-ray diffraction and Raman spectroscopy revealed also the presence of magnetite, but mainly in the coating surface. The presence of maghemite (γ-Fe_2O_3) was also reported in the top layer of some Campanian B coatings and was attributed to a re-oxidation of the surface during the cooling phase. The density of hercynite crystals is sufficient to give a dark black colour and the presence of a few maghemite crystals in surface has no influence on the colour. In fact, the distribution of crystals containing Fe atoms is mostly useful to rebuild the firing process (Meirer et al. 2013).

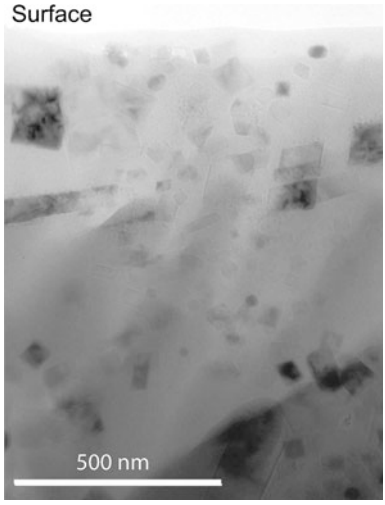

Fig. 9 Hercynite crystals observed by TEM in a high gloss coating of a Campanian of type B

The influence of crystal parameters (size, composition, spatial distribution) is more significant for red coatings. In these coatings, the colour is due to hematite but the crystal size, the composition and the homogeneity of repartition in the glassy matrix define the hue. Absorption of hematite in visible spectrum is high and the crystal size plays a major role on the colour hue. Micrometric crystal gives a dark colour while large crystals appear black with a metallic glint. The characteristic red colour of sigillata requires nanometric crystals. However investigations revealed that the hematite crystals grown in sigillata coating contain Al in substitution to Fe (Sciau et al. 2006). This substitution lowers the absorption and allows for obtaining the same colour with submicrometric crystals.

Gallic Terra Sigillata were fired at higher temperatures (around 1050 °C) than the Italic Terra Sigillata (950–1000 °C). This results in a slight increase of the average size of hematite crystals (30 → 50 nm), but this effect is balanced both by the lower crystal density (Fe rate is lower in Gallic Terra Sigillata) and a higher Al substitution (around 8–9 % in Gallic Terra Sigillata). Recent studies showed that the rate of substitution increases with the temperature and that the rate value was higher in Gallic productions than in Italic ones (Leon et al. 2010, 2015). One consequence is that the two types of production present similar colours. In contrast, their mechanical properties are quite different. The higher firing temperature of Gallic products leads to a partial vitrification of their body, which results in a better adherence of coatings. These coatings (Fig. 10) are almost free of spinel in agreement with their low Mg rate, but contain a lot of corundum (α-Al_2O_3) nanocrystals (average size 20 nm). X-ray diffraction and electron energy loss spectroscopy revealed that these crystals contained around 8–9 % Al in substitution to Fe [$(Al_{0.92}Fe_{0.08})_2O_3$, Fig. 11]. The presence of iron confers a yellowish colour to this phase, as can be found in the gemmological varieties of this mineral. However, the colour arises mainly from the iron atoms in octahedral coordination in the hematite structure. Actually, the main effect of corundum is to turn the slip into a mechanically strong coating (Sciau et al. 2006).

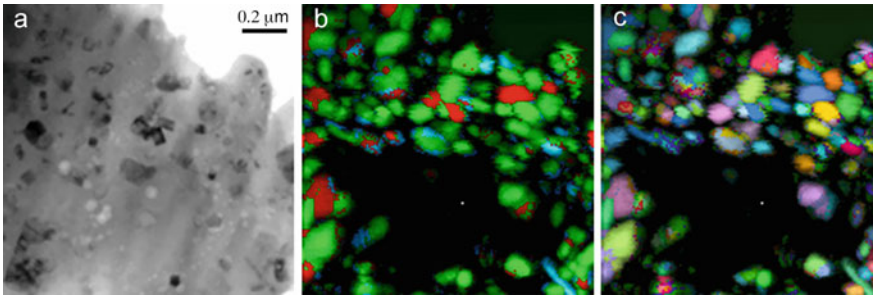

Fig. 10 Gallic terra sigillata coating observed in TEM. **a** Bright field image, ASTAR high resolution phase (**b**) and orientation (**c**). The coating **b** consists of hematite (in *red*), corundum (in *green*) and spinel (in *blue*) crystals in a glass matrix. There is no particular orientation of crystals (**c**)

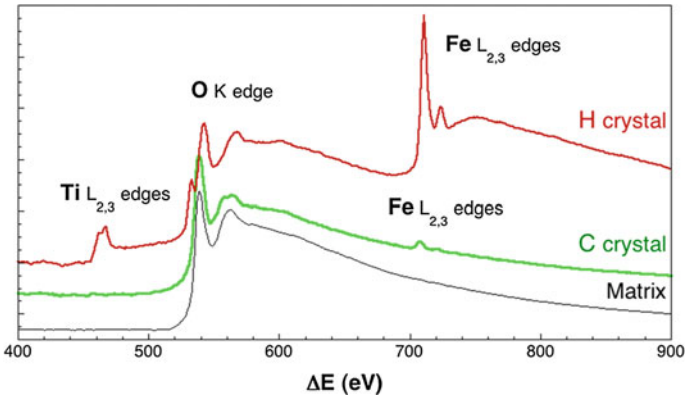

Fig. 11 EELS analysis of the matrix, hematite and corundum crystals in a Gallic terra sigillata coating

4 Iron Oxides in Black Glazed Chinese Ceramics

A rare and metastable ferric oxide polymorph (ε-Fe_2O_3) has just been discovered in ancient Chinese ceramics (Dejoie et al. 2014). Identified in 1934, this phase keenly interests the materials science community for its promising applications in the fields of electronic storage media and magnetic stripe cards. It exhibits a giant coercive field at room temperature, millimetre-wave ferromagnetic resonance, and magnetoelectric coupling (Gich et al. 2006; Tucek et al. 2010). It is the only single metal oxide to accumulate such magnetic/electric properties. Unfortunately, this phase is metastable and its crystal growth is very difficult to obtain. Up to now only nanoscale crystals (nanoparticles, nanowires, thin films) have been obtained (Tronc et al. 1998; Gich et al. 2010).

Black-glazed Jian ware of the Chinese Song dynasty (960–1279 AD) was known for its lustrous black, which could exhibit various coloured patterns. The variety called "hare's fur" was the most famous and common pattern (Li et al. 2008). Its shining black slip reveals fine radial rust-coloured streaks. Much less prevalent, the variety called "oil spot" was also sought for its silvery glints. Recently, one fragment of each variety was analysed using a set of characterization techniques including micro X-ray fluorescence and micro X-ray diffraction synchrotron, Raman spectroscopy and transmission electron microscopy (Dejoie et al. 2014). It was established that the coloured patterns were due to the crystallization of iron oxides in the glaze surface (Li et al. 2008), but without considering that the predominant form was ε-Fe_2O_3. In the "hare's fur" variety, the epsilon phase is associated with the alpha form (hematite) while at the surface of the "oil spot" sample, only ε-Fe_2O_3 phase was found. The sub-micrometric crystals are concentrated in the oil spots (bubbles arrive at the surface during the firing) and organized in dendritic networks. A majority of these networks are very regular and define quasi perfect 2D gratings (Fig. 12), which behave as dispersive elements leading to

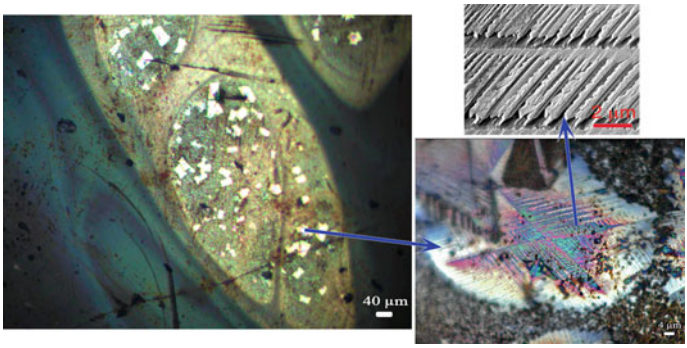

Fig. 12 Optical and SEM images of the ε-Fe_2O_3 crystals observed at the surface of a black-glazed Jian ware of the "oil spot" type (Song dynasty: 960–1279 AD)

the creation of structural colours through interference effects (Zuppiroli et al. 2003). These colours, which depend on angular lighting conditions, are very brilliant and iridescent with blue to red variations as shown in Fig. 12.

This organization of sub-micrometric crystals can be related to 2D photonic crystals (Joannopoulos et al. 1997) where a periodic array of nanoparticles affect the motion of photons (visible light) in the same way that a tri-periodic atom arrangement (standard crystal) affects X-rays. In fact, these dendritic networks are rather similar to the structure which can be found in nature in feathers of birds or scales of butterflies showing iridescent colours (Kinoshita and Yoshioka 2005).

5 Conclusion

In this chapter, we have shown that the nanoscale crystals present in the coatings of Greek and Roman potteries are responsible for their colour features and also contribute to their mechanical properties. For instance, the high hardness of Gallic sigillata coatings is due to nanocrystals of corundum homogeneously dispersed in the glassy matrix. Actually, nanocrystals and/or sub micrometric crystals play a significant role in the colour feature of several decorative layers of ancient potteries such as the copper crystals in the oxblood glaze or blue cobalt particles ($CoAl_2O_4$ spinel phase) in blue and white porcelains and other blue colours underglaze (Wang and Wang 2011; Figueiredo et al. 2012).

The study of nanocrystals present in ceramic coatings is also a powerful way to obtain relevant information concerning the manufacturing processes. Thus the different steps of the firing of some Greek and Roman ceramics were clarified from the study of Fe-based particles. It was shown that the Al/Fe substitution in hematite structure influences the tin colour and depends on the firing temperature. An ongoing study seems to indicate that the blue cobalt particles are also substituted in

blue decorations of Qinghua porcelains (Wang et al. 2016). Indeed, the majority of crystallographic phases formed during the firing of potteries are substituted. The nature and rate of the substitution depend both on the raw material composition and the firing conditions. An in depth study of these parameters could provide new significant information concerning manufacturing process. The current analytical facilities allow us to perform such studies on nanocrystals. Hopefully, these relevant data should be available in a near future.

Acknowledgments The author gratefully acknowledge Eric Gailledrat, Cécile Jubier-Galinier and Corinne Sanchez (laboratoire Archéologie des Sociétés Méditerranéennes, UMR 5140) and Dragomir Nicolae Popovici (National Museum of Romania's History) for the archaeological samples as well as Philippe de Parseval (GET, Toulouse University) for the elemental composition measurements, Christophe Deshayes (CEMES) for SEM investigations and Sébastien Joulié (CEMES) for TEM-ASTAR investigations. I would also like to thank Deborah Decamaret and Philippe Goudeau for their help. This article was partially funded by the ARCHIMEDE Labex programme: Investissement d'Avenir ANR-11-LABX-0032-01.

References

Angelini I, Artioli G, Bellintani P, Diella V, Gemmi M, Polla A, Rossi A (2004) Chemical analyses of bronze age glasses from Frattesina di Rovigo, northern Italy. J Archaeol Sci 31(8):1175–1184. doi:10.1016/j.jas.2004.02.015

Barber DJ, Freestone IC (1990) An investigation of the origin of the color of Lycurgus cup by analytical transmission electron-microscopy. Archaeometry 32:33–45

Brun N, Mazerolles L, Pernot M (1991) Microstructure of opaque red glass containing copper. J Mater Sci Lett 10(23):1418–1420. doi:10.1007/BF00735696

Bugoi R, Constantinescu B, Pantos E, Popovici D (2008) Investigation of Neolithic ceramic pigments using synchrotron radiation X-ray diffraction. Powder Diffr 23(3):195–199

Chazalon L (2010) Les céramiques attiques du Ve s. av n.è à Lattes. Première données sur le cinquième siécle avant notre ère dans la ville de Lattara, ADAL, Lattes (Lattara 21) 2:l.5, 618

Cianchetta I, Trentelman K, Maish J, Saunders D, Foran B, Walton M, Sciau P, Wang T, Pouyet E, Cotte M, Meirer F, Liu Y, Pianetta P (2015) Evidence for an unorthodox firing sequence employed by the Berlin painter: deciphering ancient ceramic firing conditions through high-resolution material characterization and replication. J Anal At Spectrom 30:666–676. doi:10.1039/C4JA00376D

Colomban P (2009) The use of metal nanoparticles to produce yellow, red and iridescent colour, from bronze age to present times in lustre pottery and glass: solid state chemistry, spectroscopy and nanostructure. J Nano Res 8:109–132

Colomban P, Liem NQ, Sagon G, Tinh HX, Hoanh TB (2003) Microstructure, composition and processing of 15th century Vietnamese porcelains and celadons. J Cult Herit 4(3):187–197. doi:10.1016/s1296-2074(03)00045-1

Deer WA, Howie RA, Zussman J (1992) An introduction to the rock-forming minerals. Pearson, Harlow

Dejoie C, Sciau P, Li WD, Noe L, Mehta A, Chen K, Luo HJ, Kunz M, Tamura N, Liu Z (2014) Learning from the past: rare epsilon-Fe_2O_3 in the ancient black-glazed Jian (Tenmoku) wares. Sci Rep 4:4941. doi:10.1038/srep04941

Figueiredo MO, Silva TP, Veiga JP (2012) A XANES study of cobalt speciation state in blue-and-white glazes from 16th to 17th century Chinese porcelains. J Electron Spectrosc Relat Phenom 185(3–4):97–102. doi:10.1016/j.elspec.2012.02.007

Freestone I, Meeks N, Sax M, Higgitt C (2007) The Lycurgus cup—a Roman nanotechnology. Gold Bull. 40(4):270–277

Garcia D, d' Anna A, Desbat A, Schmitt A, Verhaeghe F (2014) La Céramique: La poterie du Néolithique aux temps modernes. Editions Errance

Gich M, Frontera C, Roig A, Fontcuberta J, Molins E, Bellido N, Simon C, Fleta C (2006) Magnetoelectric coupling in epsilon-Fe_2O_3 nanoparticles. Nanotechnology 17(3):687–691. doi:10.1088/0957-4484/17/3/012

Gich M, Gazquez J, Roig A, Crespi A, Fontcuberta J, Idrobo JC, Pennycook SJ, Varela M, Skumryev V (2010) Epitaxial stabilization of epsilon-Fe_2O_3 (00l) thin films on $SrTiO_3$ (111). Appl Phys Lett 96(11):112508. doi:10.1063/1.3360217

Hartley BR (1971) Roman Samian Ware: Terra Sigillata. Herts Archaeol Soc

Joannopoulos JD, Villeneuve PR, Fan SH (1997) Photonic crystals: putting a new twist on light. Nature 386(6621):143–149. doi:10.1038/386143a0

Jubier-Galinier C, Laurens A-F, Tsingarida A (2003) Les atelier de potiers en attique. In: Rouillard P, Verbanck-Pierard A (eds) Le vase grec et ses destins. Biering and Brinkmann, Munich, pp 27–43

Keay SJ (1988) Roman Spain. University of California Press, California

Kinoshita S, Yoshioka S (2005) Structural colors in nature: the role of regularity and irregularity in the structure. Chem Phys Chem 6(8):1442–1459. doi:10.1002/cphc.200500007

Lee WE, Souza GP, McConville CJ, Tarvornpanich T, Iqbal Y (2008) Mullite formation in clays and clays-derived vitreous ceramics. J Eur Ceram Soc 28:465–471

Leon Y, Lofrumento C, Zoppi A, Carles R, Castellucci EM, Sciau P (2010) Micro-Raman investigations of terra sigillata slips: a comparative study of central italian and southern Gaul productions. J Raman Spectrosc 41(11):1550–1555

Leon Y, Sciau P, Passelac M, Sanchez C, Sablayrolles R, Goudeau P (2015) Evolution of terra sigillata technology from Italy to Gaul through a multi-technique approach. J Anal At Spectrom 30(3):658–665. doi:10.1039/C4JA00367E

Li WD, Luo HJ, Li JN, Li JZ, Guo JK (2008) Studies on the microstructure of the black-glazed bowl sherds excavated from the Jian kiln site of ancient China. Ceram Int 34(6):1473–1480. doi:10.1016/j.ceramint.2007.04.004

Lyons CL (2005) The Greek vase and its destinies. Am J Archaeol 109(1):113–114

Maggetti M (1982) Phase analysis and its significance for technology and origin. In: Olin JS, Franklin AD (eds) Archaeological ceramics. Smithsonian Institution Press, Washington DC, pp 121–133

McConville CJ, Lee WE (2005) Microstructural development on firing illite and smectite clays, compared with that in kaolinite. J Am Ceram Soc 88(8):2267–2276

Meirer F, Liu YJ, Pouyet E, Fayard B, Cotte M, Sanchez C, Andrews JC, Mehta A, Sciau P (2013) Full-field XANES analysis of Roman ceramics to estimate firing conditions—a novel probe to study hierarchical heterogeneous materials. J Anal At Spectrom 28(12):1870–1883

Mirti P, Davit P (2001) Technological characterization of Campanian pottery of type A, B and C and of regional products from ancient Calabria (southern Italy). Archaeometry 43:19–33. doi:10.1111/1475-4754.00002

Nakai I, Numako C, Hosono H, Yamasaki K (1999) Origin of the red color of satsuma copper-ruby glass as determined by EXAFS and optical absorption spectroscopy. J Am Ceram Soc 82(3):689–695

Noble JV (1965) The techniques of painted Attic pottery. Watson-Guptill edn, New York

Picon M, Vernhet A (2008) Les très grands fours à sigillées en Gaule, et notamment à la Graufesenque. SFECAG, actes du Congrès de L'Escala-Empuries, pp 553–566

Ricciardi P, Colomban P, Tournie A, Macchiarola M, Ayed N (2009) A non-invasive study of Roman Age mosaic glass tesserae by means of Raman spectroscopy. J Archaeol Sci 36 (11):2551–2559. doi:10.1016/j.jas.2009.07.008

Schaad D (2007) La Graufesenque (Millau, Aveyron), volume I; Condatomagos une agglomération de confluent en territoire rutène., vol I. La Graufesenque (Millau, Aveyron), Editions de la Fédération Aquitania

Sciau P (2012) Nanoparticles in ancient materials: the metallic lustre decoration of medieval ceramics. In: Hashim AA (ed) The delivery of nanoparticles. InTech, pp 525–540. doi:10.5772/34080

Sciau P, Goudeau P (2015) Ceramics in art and archaeology: a review of the materials science aspects. Eur Phys J B 88(5):1–11. doi:10.1140/epjb/e2015-60253-8

Sciau P, Relaix S, Roucau C, Kihn Y (2006) Microstructural and microchemical characterization of roman period terra sigillate slips from archeological sites in southern France. J Am Ceram Soc 89(3):1053–1058

Sciau P, Relaix S, Mirguet C, Goudeau P, Bell AMT, Jones RL, Pantos E (2008) Synchrotron X-ray diffraction study of phase transformations in illitic clays to extract information on sigillata manufacturing processes. Appl Phys A 90:61–66

Tite MS (2008) Ceramic production, provenance and use, a review. Archaeometry 50(2):216–231

Tite MS, Bimson M, Freestone IC (1982) An examination of the high gloss surface finishes on Greek Attic and Roman Samian wares. Archaeometry 24:117–126

Tronc E, Chaneac C, Jolivet JP (1998) Structural and magnetic characterization of epsilon-Fe_2O_3. J Solid State Chem 139(1):93–104. doi:10.1006/jssc.1998.7817

Tucek J, Zboril R, Namai A, Ohkoshi S (2010) Epsilon-Fe_2O_3: an advanced nanomaterial exhibiting giant coercive field, millimeter-wave ferromagnetic resonance, and magnetoelectric coupling. Chem Mater 22(24):6483–6505. doi:10.1021/cm101967h

Vendrell-Saz M, Pradell T, Molera J, Aliaga S (1991) Proto-campanian and A-campanian ceramics: characterization of the differences between the black coatings. Archaeometry 33(1):109–117

Walton MS, Doehne E, Trentelman K, Chiari G, Maish J, Buxbaum A (2009) Characterization of coral red slips on Greek Attic pottery. Archaeometry 51(3):383–396

Walton M, Trentelman K, Cummings M, Poretti G, Maish J, Saunders D, Foran B, Brodie M, Mehta A (2013) Material evidence for multiple firings of ancient athenian red-figure pottery. J Am Ceram Soc 96(7):2031–2035

Wang L, Wang C (2011) Co speciation in blue decorations of blue-and-white porcelains from Jingdezhen kiln by using XAFS spectroscopy. J Anal At Spectrom 26(9):1796–1801. doi:10.1039/c0ja00240b

Wang T, Sciau P, Feng ZY, Fayard B, Pouyet E, Cotte M, De Nolf W, Zhu TQ (2016) Synchrotron-based multi-analytical study of Chinese Qinghua porcelains (Ming dynasty): micro-composition and chromogenic mechanisms of blue decors. Anal Chem (to be published)

Wood N (1999) Chinese glazes, their origins, chemistry and recreation. University of Pennsylvania Press, Philadelphia

Zuppiroli L, Bussac M-N, Grimm C (2003) Traité des couleurs. Presses polytechniques et universitaires romandes, Lausanne

Natural Nanosized Raw Materials and Sol-Gel Technology: The Base of Pottery Since Millenniums

Philippe Colomban

Abstract The temperature required to achieve the densification of a pottery, an assembly of grains, depends on the grain size. Mother Nature offers a variety of nanosized materials that possess exceptional properties. For instance kaolin and clays were a base of pottery for at least 15,000 years because their nanometric size allowed controlling of the viscosity trough their interaction with water and of the sintering through their reactivity. Since millennia 'asbestos' ultrafine long fibres allowed—when mixed with clays—the preparing of the first ceramic fibre ceramic matrix (CMC) composite. This material presented exceptional mechanical properties. Metal nanoparticles are used to colour glass and enamel since at least two millenia. Thermal treatment of many hydrated/proton containing minerals and biomaterials is another way to obtain nanosized powder. After a brief overview of the technological history of pottery we will address the natural nanosized materials used by potters and glazemakers and the link between traditional preparation routes and advanced chemical methods to prepare complex ceramics.

1 Introduction

Pottery technology allows for the creation of containers, thus production of potteries is associated with the Palaeolithic/Neolithic transition when mankind left the nomadic hunting-gathering lifestyle and turned to sedentary agriculture. Indeed, well sintered pottery and glass objects which are waterproof permitted for the long

P. Colomban (✉)
De la Molécule aux Nano-Objets: Réactivité, Interactions et Spectroscopies (MONARIS), UPMC Univ Paris 06, Sorbonne Universités, 4 Place Jussieu, Paris 75005, France
e-mail: philippe.colomban@upmc.fr

P. Colomban
CNRS, IP2CT, UPMS, MONARIS UMR8233, 4 Place Jussieu, Paris 75005, France

P. Dillmann et al. (eds.), *Nanoscience and Cultural Heritage*,
DOI 10.2991/978-94-6239-198-7_3

term conservation of many products, a necessary step for sedentary life. There are two difficult tasks in ceramic and glass technologies: (i) the availability of fine, reactive powders in order to facilitate their reaction and consequent partial (pottery) or total (glass) melting, and the wettability between liquid and solid, and (ii) the firing and its control. However, the consolidation of an object made of an assembly of particulates requires the welding of the grains together, i.e. the sintering. Such a strengthening takes place at the point of contact between grains, and by the mean of two main phenomena: (i) if a liquid phase is formed by the effect of temperature heating, some dissolution of the grain tip occurs and new phase(s) precipitate(s) on cooling, forming a bridge in between adjacent grain, and (ii) some atoms diffuse in adjacent grains, forming a neck that enlarges with time. The scale of both mechanisms intensifies when the grain size decreases, because of the higher number of contacts and the shorter diffusion path. Typically, if the sintering temperature of a 5–10 μm grain assembly is achieved at 0.8 Tm (Tm, melting temperature), the sintering temperature of well-compacted artefact constituted of submicronic grains decreases to about 0.5 Tm (Bouquin et al. 1985).

Mother Nature offers a variety of nanosized materials that possess exceptional properties: clays, kaolin, talc, asbestos, etc. Consequently, these materials were a base of pottery for at least 15,000 years because their nanometric size allowed controlling of the viscosity after their mixing with water—that is at the green state through their interaction with water molecules—and of the sintering through their reactivity (Brongniart 1877; Colomban 1989; Haussone 1969): the reactivity of a material is directly linked to its surface area that increases drastically when the grain size become submicronic (Colomban et al. 2005). Grinding requires a lot of energy, which only really became available since the Industrial Revolution. In ancient times this difficulty was solved by thermal treatments: the heating of many water/proton containing minerals (flint/cherts, lime, etc.) and biomaterials (shells, bones, wood, stroh …) led to nanosized powder without grinding (and without any pollution). The temperature required to achieve densification depends on the grain size but also on the grains composition, and the variety of process reflects the variety of raw materials.

Advanced preparation of nanomaterials is old. Controlled reduction in the solid or viscous state (glazes and enamels) allowed the preparing of dispersions of copper nanoparticles to obtain red colour for millennia (Colomban et al. 2004a; Colomban 2009). The preparation of silver-containing yellow glasses dates back to the Middle-Ages and that of gold nanoparticles from the Renaissance (Colomban 2009). Since millennia, ‘asbestos’ ultrafine long fibres allowed—when mixed with clays—the preparing of the first ceramic fibre ceramic matrix (CMC) composite with outstanding mechanical properties (Colomban and Gouadec 2005; Mezzadri 1986).

We will review here the use of nanometric materials in ceramic/pottery (and glass/glaze) production.

2 Brief History of the Technology of Pottery and Glaze

The foundation of Chemistry is often related to the practices of ancient alchemists. However, the know-how required for the controlled transformation of the matter is much older. The mastery of fire, in other words Solid State Chemistry technology, is directly linked to the development of Mankind and its control over the environment (Colomban 2013). The first pottery obtained by shaping clay date back to the Neolithic/Palaeolithic transition, about 15,000 BCE (Cooper 2000; Kingery 1984, 1986a, b; McGovern et al. 1989). The main evidences were found in Africa, Siberia, and Japan. The manufacture of moulded clay objects is older; it dates back to the palaeolithic with for example the Venus of Dolni Vestonice (~25,000 BC, Czech Republic), even though the deliberateness of his 'cooking' remains debated (Vandiver et al. 1989).

The essence of modern Chemistry, can be found in two main practices (Colomban 2013): (i) the *Arts du feu*, i.e., the preparation of pottery, glass and metals artefacts (and associated techniques for the selection and preparation of the used raw materials: geology, mining,…)—in other words Inorganic and Solid State Chemistry—as well as in (ii) the preparation of remedy, alcohols and perfumes, pigments, dyes, and binding for frescoes, painting and textiles—in other words Organic and Liquid State Chemistry.

Through consolidating, the clay goes through a strong 'welding' between some of the grains in order to impart to the artefact a permanent form and mechanical resistance, chemical inertia, etc. This requires that at least one of the components of the 'earth mixture' makes a liquid phase which will forms a bridge—a weld—between adjacent grains: the liquid phase dissolved the solid once in contact, the composition of the liquid phase is modified and new phases precipitate (American Ceramic Society 1971). The reaction stops generally before the achievement of a homogeneous state. Ceramics are thus heterogeneous and their microstructures retain information about how they were prepared (Colomban 2012; Simsek et al. 2014, 2015a, b). On the other hand, the achievement of the molten state for glass (glaze, enamel) homogenizes the matter and information should only be found in traces elements and in the nanostructure (Caggiani et al. 2014; Simsek et al. 2015b).

If a temperature of 600 °C is sufficient to destroy the clay structure, formation of a liquid phase requires more than 700 °C, i.e. the typical temperature requested to have a liquid phase in the Na_2O–CaO–FeO–SiO_2 (Al_2O_3)–K_2O (–PbO)—based phase diagram (American Ceramic Society 1971). FeO promotes easier liquid phase than Fe_2O_3 and this is why the first ceramics were generally prepared with ferruginous clays, fired in a reducing environment (Cooper 2000). Addition of Bore or Lithium also promotes the formation of a liquid phase but their use was scarce before modern Times (Colomban 2013). A significant volume of liquid phase at the grain interface is required to be efficient. Only in porcelain a large part of the body volume reaches the viscous liquid state (~30–50 %) that permits the final optical translucency (Lee and Iqbal 2001). The soldering of two grains already in contact will even occur as fast as the diffusion of surface atoms and/or volume is promoted.

The phenomenon is even more effective when the grain size is small and the compaction maximal, because the distance—and the time requested for the diffusion—is minimal. The application of stress on clay paste (20–30 wt % water) e.g. by moulding or wheeling, promotes the organization of the clay particles and their sintering. The so-call "*paste memory*" can lead to a deformation of the object after firing if the stress application was irregular: it is assumed that the number of contact between clay particles is enhanced, increasing the sintering kinetics.

Glass paste and glazed artefacts date back to 3,000 BCE, in Mesopotamia and Egypt (Vandiver and Kingery 1986). The crude beads usually formed around a wire have blue (chromophore : Co^{2+} ion), green (chromophore : Cu^{2+} ion) and yellow (chromophore : Fe^{2+} ion) colours suggesting that they were used to evoke (semi)precious stones like lapis lazuli, turquoise, etc. True glass artefacts and glazed pottery date back to 1500–2000 BCE (Egypt, Phoenicia, Mesopotamia and Hindus Valley). Glasses were also used to coat stone (quartzite), and the first Egyptian faience may be considered as synthetic quartzite (Ellis and Newman 2005).

Glass and glaze first opacification was obtained with yellow lead, and white calcium antimonite (Colomban 2013). Heating above 900–1000 °C was required. At the same times, Chinese Shang and Shang-Zhou proto-porcelains (3500–1500 BCE) were already fired at much higher temperatures, from 950 to 1250 °C (Fukang 1984; Wood 1999). Actually, the progression of the firing technology was not linear and suffered from periods of wars accompanied by a trade disruption and loss of technologies.

Mass production was experimented very early: Roman potters produced *sigillata* (Leon et al. 2015), and Roman glassmakers glass ingots, in very limited places that can be considered as the first manufactures. Ingots were exported to many places where glassformers elaborated artefacts (Fontaine and Foy 2007). Due to the scarcity of some source of colouring agents, for instance cobalt, intense recycling of blue glass pieces was established in the Mediterranean area (Fontaine and Foy 2007).

Chinese Eastern Han to Sui potters (2nd BCE to 7th century CE) initiated the development of advanced kilns and fired at temperature up to 1250 °C, even above 1300 °C for Yue wares (Fukang 1984; Wood 1999), to form crystalline mullite—the base of hard paste porcelain—from the kaolin-rich paste. Mullite is a non-stoichiometric aluminosilicate (3 $Al_2O_3$2 SiO_2 to 2 $Al_2O_3SiO_2$) with high melting temperature (Martinon-Torres et al. 2008; Lee and Iqbal 2001), higher than that of silica. The 3:2 composition grows in long needles (mm) with nanometric section area, that form a 3D network retaining in, during the firing, the liquid silica-rich phase formed by the reaction between feldspar and kaolin (Fig. 1b). The latter phase gives a glassy aluminosilicate on cooling, at the origin of the porcelain translucency. Glazed white porcelain appeared during Sui and Tang Dynasties (7th–8th century CE).

At the same time, Islamic Abbasid potters took advantage of the very efficient opacification power of cassiterite tin oxide, a prior Roman/Byzantine innovation (Neri et al. 2016), which combined with a low temperature firing (<1000 °C) allowed them to compete at lower cost with high temperature fired Chinese

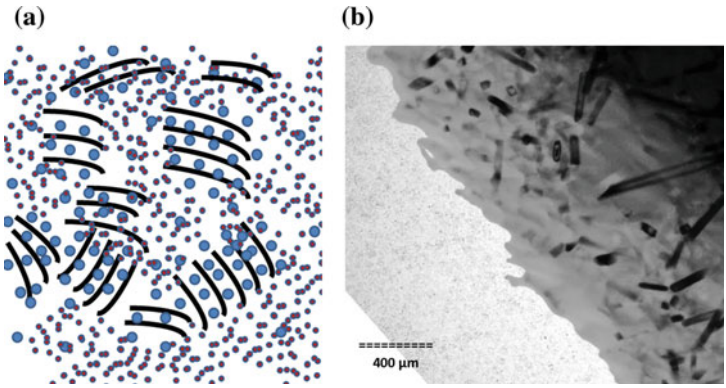

Fig. 1 Schematic of **a** a dispersion sol of clay particles in water (small dots: water molecules); *blue big dots* represents solvated cations in between clay slab; **b** TEM image of a porcelain body made of 3:2 mullite needles dispersed in the aluminosilicate glass (Courtesy of Ph. Sciau, CEMES CNRS)

porcelain, in producing artefacts with complex, multicoloured depictions (Colomban et al. 2004a; Colomban and Truong 2004). As we will discuss further, this innovation arises from the very small size of the Euphrates alluvium that allows preparing a fine grain body at low temperature. This characteristic arises from the very low down slope of the river along the Mesopotamia Valley which allows for a fine pottery—the first faience (Fig. 2)—with a medium porosity, intermediate between that of stoneware and porcelains (<3 %) and that of *terra cotta* (>20 %). This innovation resulted from the imitation of the Tang Dynasty porcelain wares with blue and green glaze (Kingery 1984, 1986a; Wood 1999). The reaction between the blue (or green) lead-based glaze of Abbasid artefact with the (earth) alkaline-based colourless glaze led to precipitation of white cassiterite (Colomban and Truong 2004), showing the interest of complex glaze compositions.

The technology of glazed pottery opacified with cassiterite spread out throughout Mediterranean Sea (Fig. 2a) with the extension of the Islamic World (Ifriqaya, 7th c., Al Andalous 8th c, Sicilia 9th c. and Italy 13th c.), where the technique was called *majolica* and was transmitted with Italian potters in France (15th–16th c.) and served as support in North part of Europe to imitate Chinese porcelain (e.g. Delft wares) (Colomban 2004). Attempts to imitate the Chinese porcelain were also conducted in Anatolia, but with a very different technology: Ottoman Iznik fritwares production peaks after 1450, and with the lack of white 'clay', the kaolin, they develop a white body by firing together sand quartz grains and lead-based frit, a low melting temperature glass (Atasoy and Raby 1989; Colomban et al. 2004a; Simsek and Geckinli 2012). Actually the Ottoman potters created a very innovative material by applying a slip made of crushed quartz grains that reflect the light, enamelled the slipped body with a colourless lead-based glaze and developed advanced pigments and chromophores, especially by the use of multifiring procedure, as experimented for enamelled glass masterpieces during

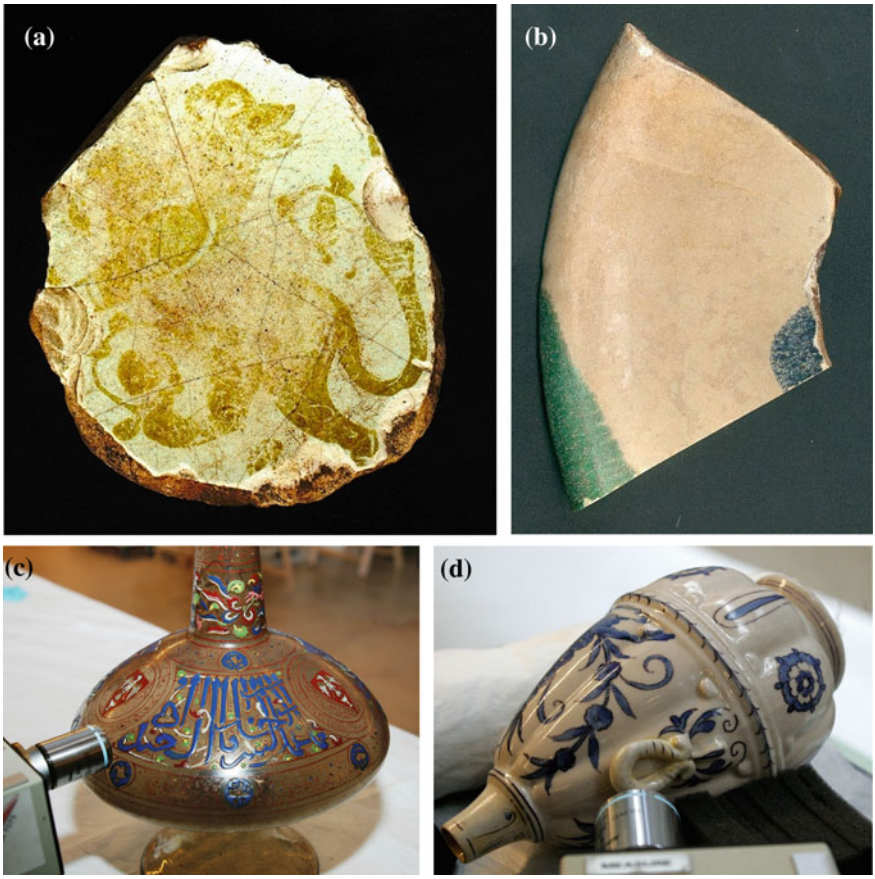

Fig. 2 Examples of objects made using nanosized materials: **a** the formation of a glaze layer opacified with cassiterite SnO_2 precipitation gives a white substrate to make sophisticated décors, i.e. a pantheir or griffon in this Fatimids lustre pottery where the '*gold*' colour arise from *silver* metal nanoparticles (Colomban 2004a); **b** this early Abbasids 3-colour pottery shows only SnO_2 opacification when the lead-rich Co-based *blue* or Cu-based *green* glazes react with the alkaline glaze covering the body (Colomban and Truong 2004); the very fine body is made from Euphrate nanosized alluvium; **c** the vivid *blue* of the Mameluk lamp [Louvre Museum (Caggiani et al. 2013)] is obtained with lapis lazuli grains; **d** the *blue* décor of the Medici porcelain (Limoges Museum) is obtained with cobalt-based compound. In both later artefacts the white opacification results from calcium phosphates nanoprecipitates obtained from bone ash dissolution within the glaze

Roman times (Caggiani et al. 2013). The use of a black non-stoichimetry phase (chromite and/or ferrite) to isolate glazed area lead to very sharp depicts. Furthermore the nonstoichiometric phase could trap diffusing ions, keeping thus the depict sharpness. At the same time the colour palette of Chinese production was enlarged. Part of the Chinese chromophore technology was very specific with for instance the use of barium derivatives to produce violet, blue and green colours

(Berke and Wiedeman 2000) with composition homologous with that of Egyptian blue and green (Bianchetti et al. 2000). Surprisingly, contemporary Japanese potters, inspirited by ancient (12–14th c.) Vietnamese and Chinese productions developed original pottery for the tea ceremony, characterized by simple, brut aspect (the *wabi sabi* style), now popularized under the term 'Raku'. Discovery of these productions in the middle of the 19th century by European connoisseurs is at the origin of Japonism and Craft Movements (Colomban 2004b).

Iznik fritware technology (Atasoy and Raby 1989; Colomban et al. 2004b; Colomban et al. 2004c; Simsek and Geckinli 2012) served as model for the first production of *Pâte Tendre* (Soft Paste) European porcelains in Rouen (∼1673), which then spread to the rest of France at Saint-Cloud (1695–1766), Mennecy (1737–1773), Chantilly (1725–1800), and Vincennes (1740–1753)/Sèvres (>1754-present) and in neighbouring countries: Tournai (1751–1800, Belgium), Burslem (1795-present, GB) … (d'Albis 1984; Colomban and Treppoz 2001; Colomban et al. 2004b) The firing of soft paste body was very difficult because the very short firing dwell (20–50 °C) below the porcelain-look was not achieved and above the artefact shape was distorted, or even molten! A second firing was needed for the décor (*Petit Feu*). The high lead-content of the glaze led to a material easily scratched by the knife, from which came the soft paste naming. During about 12 years (1575–1587) the Duke of Medici produced alumina-rich porcelain using an hybrid technology, intermediate between the fritware and the hard—paste Chinese technology, because the use of a white kaolin-containing earth from Vicenza (Colomban et al. 2004a).

The search of adequate raw materials in Saxony by E. von Tschirnhaus and J. F. Böttger and their research for the development of a kiln able to reach the high temperature (>1400 °C) needed to fire porcelain, led to the first European production of red (*boccaro* ware, ∼1708) and then white porcelain (>1710, Colomban et al. 2004a) with the discovery of kaolin. The discovery of kaolinized clay and kaolin in different places in Saxony (Okrilla, Aue, Meissen, Zwickau, etc.) and then in France (Saint-Yriex) and in other places in Europe allowed large production and technological developments, first in Meissen, then Vienna (1718), Strasbourg (1756), Sèvres (1766), etc. All these production were first limited and dedicated to European Courts. A revolution took place after 1750 with the development of fine faience and porcelain factories for the Bourgeoisie, especially during the 19th century.

Gilding décor also requires nanosized gold particles. First gilding décor were obtained through the physical bonding of the gold leaf on the corrugated ceramic surface (Simsek et al. 2015a, 2015b; Colomban et al. 2005) or by sandwiching a gold foil between two glass layers (Colomban et al. 2005). J.F. Böttger was one of the earliest recorded pioneers of gold decoration, which might be a result of the fact that he was a young alchemist before his attempts to produce porcelain. He experimented both with the Chinese/Vietnamese ancient technology of using gold leaf physically bound to the ceramic surface and also with the technique of applying liquid gold (i.e. nanometric gold powder applied in a medium, and successively fired). He prepared a mixture of gold powder with ferrous sulphate in *aqua regia* to produce "a very fine precipitate", according to the new technique experimented by Perrot, Kunkel and Cassius (Ricciardi et al. 2009).

With the development of chemistry and metal purification during the second part of 19th century, new body, pigment and glaze compositions were experimented (Colomban 2013). A second ceramic revolution occurred after the 2nd World War with the development of advanced ceramics, in particular dielectric passive components (capacitors, substrates, sockets, etc.), cutting tools, magnets, piezoelectric actuators and aerospace materials (thermal barrier coating, composites) using chemical routes also called coprecipitation, gel or sol-gel routes Colomban (1976, 1989; Johnson 1985; Klein 1988; Mazdiyasni 1982; Perthuis and Colomban 1984; Roy 1969; Sakka and Kamiya 1980; Snow 1973).

The development of the ceramic technology can be summarized by (i) an increase of the firing temperature and control with a concomitant reduction of the cycle duration; typically the firing cycle duration requires several days for kilns heated with wood, a few days (weeks) for kiln heated with coal, gas or electricity or a few hours or less for last generation of kilns where refractory bricks are replaced with felts made of ceramic fibres; and (ii) the availability of raw materials with reproducible composition (purification/blending). The latter two evolutions led to an increase of the sintering temperature and of the production cost.

Consequently two other actions were conducted; (i) the reduction of the grain size of the raw material by attrition grinding and then the use of chemical routes to mimic the traditional clay technology (Colomban 1989, 2011; Johnson 1985; Mazdiyasni 1982) and then the use of metal-organic precursors, (ii) the achievement of a high densification in the green state (sol-gel transition control, high pressure compaction). The two later actions aim to mimic the clay routes for non-silicate compositions.

3 Clay Structure, Water Content and Viscosity/Plasticity: A Control at the Nanoscale

Clay minerals are (lamellar) phyllo-aluminosilicates, which grain size is less than ~ 1 µm. Actually the particle thickness is much smaller and depends on the structure: the slab thickness is 0.7, 1 or 1.4 nm as a function of the number of octahedral and tetrahedral slab. Ionic cations (Na^+,K^+, H_3O^+) located in between the slab and more or less hydrated assure the electric charge compensation (Jouenne 2001). A clay particle is made of a small number of slabs and its sliding is very easy, which can modify the thickness. Phyllosilicates are classified as 1:1 or TO (the slab consists of one layer made of Si tetrahedra and one of Al octahedra), 2:1 or TOT (two tetrahedra with one octahedra interlayer) and 2:1:1 or TOTO (slab made of alternative tretraedra/octahedral stackings). The presence of water in between the slab lubricates the sliding of one slab against adjacent ones and is at the origin of the exceptional rheologic and ionic exchange properties of clays and their clay/water mixture (sol, gel) (Colomban 1989).

The most common clays used for pottery preparation are illites K-based 2:1 phylloaluminosilicate. Commonly Si atoms are substituted by Mg or Fe, giving red coloured clays. Kaolinite, the mineral of Kaolin rock, $Si_4Al_4O_{10}(OH)_8$ is not a clay *stricto sensu* but is often considered the model compound: the slab doesn't have permanent charge and no interlayer (solvated) cation are present. For these reasons the plasticity of kaolin is very poor and hand shaping of kaolin-based porcelain difficult. Pyrophillite and talc are other phyllosilicates without charge deficit and intercalated cation. On the contrary Montmorillonite slabs $(Al_{3.4}, Mg_{0.6})Si_8O_{20}(OH)_4$·exhibit a negative charge deficit compensated by solvated sodium cations $(Na)_{0.6}$ nH_2O and is very plastic.

Solvated slabs develop hydrogen bonds and electrostatic interactions with surrounding H_2O molecules (the Helmotz-Gouy layer) that structure the water. For instance addition of a few g of Bentonite, a smectite clay belonging to Montmorillonite group, transforms one liter of water into gel, a characteristic used to control drilling in oil industry. Increasing the water-to-clay ratio and the addition of electrolyte controlling the slab-water shell interaction allows the driving of the gel-sol transition and vice versa. The gel or the high viscous clay-water mixture/slurry (typically 20 wt% water should be added to obtain a plastic earth that can be hand shaped, 40 wt% water led to a fluid slurry) allows keeping homogeneous and stable the dispersion of inert (non-water interacting) grains such as sand or feldspar (Colomban 2009). The above clay characteristics, namely the nanosize of the particles and the easy viscosity/rheology control served as goal in the 80 to prepare new multicomponent oxides but also carbides and nitrides in the same way (Okamura and Bowen 1986; McGovern et al. 1989).

3.1 Drying, Firing and Densification

Pottery artefacts are shaped by hand, generally with the help of a wheel using a clay-sand or more complex mixture. To be fashionable the clay should be hydrated (20–30 wt% H_2O). The drying of the artefact with the elimination of the water will generate cracks. In order to avoid the formation of big cracks that could not be eliminated during the sintering step, potters add inert grains, sand, powdered rock or grog (powdered pieces of low quality pottery, not good for use). The presence of the inert grains will limit the crack size.

Modern studies demonstrate that fast sintering cycles are more efficient than low heating rate cycles. Typically the duration of ancient firing cycles extended to weeks (e.g. in Chinese Dragoon kilns). This very slow rate of heating doesn't favour a rapid densification but minimizes the crack formation and promotes the good coating of the glaze even if its viscosity remains high. This is at the origin of the quality of Celadon glaze, where the silky translucency arises from the dispersion of very small bubbles. The bubble growth and coalescence is hindered by the high viscosity of the glaze at the firing temperature.

Table 1 Natural precursors of nanosized powder by thermal treatment

Raw material	Final nanosized material
Limestone ($CaCO_3$)	$CaO/Ca(OH)_2$
Gypsum, albaster ($CaSO_4$ 0.5 H_2O)$^+$	”
Shell	”
Wood, plant ashes	(K_2O, Na_2O, P_2O_5, etc.)
Rice hulls	SiO_2
Flint, cherts	”
Bones	$CaPO_4$
PbS	PbO

4 Production of Nanosized Powder by Thermal Treatment

Grinding hard materials is a difficult task that takes a long time and requires a lot of energy. For instance, before being powdered, pebbles should be fragmented by chock. Moreover, a fine powder is needed for preparing the glaze slurry for the artefact's enamelling. And the final grinding was made by putting, often for days, the framented pieces with pebbles and water in a spinning barrel. Alternatively, another way to prepare a fine powder is thermal treatment (Table 1). This preparation route is efficient if the materials contain water or protonic species. On heating, the water content changes at the molecular scale and the unit volume of the phases increases which creates many cracks. The huge volume expansion due to the water gazification leads to a pressure increase inbetween the cracks. Consequently the matter crumbles while the phenomenon is enhanced with the temperature gradient. This technique was traditionnally used to powdered flint/chert pebbles that contain a few % of water.

The material formed by thermal treatment is generally very reactive and on cooling reacts with air humidity (hydrolysis) and CO_2 (carbonation) but keeps a very small grain size and a high reactivity.

Plants are made of water, cellulose and lignigne but they also contain a variable amount of oxides that can be recovered by burning (Colomban et al. 2010). The ashes have thus been used for millenia as chemicals. Their very small grain size is very well suited for the preparation of glass and glaze. However the ashes' composition depends on many factors: the taxon, the used part of the plant/tree (leaves, branch, stamm, roots), the seasons, the soil and the washing procedure.

5 Controlled Oxydo-Reduction and Metal Nanoparticle Formation in Glasses and Enamels

There are different methods to disperse the chromophores in a glassy matrix: the first one is to dissolve 3d transition metals (Fe^{2+}, Fe^{3+}, Co^{3+}, Mn^{5+}, Cu^{2+}, V^{5+}…) or 4f Rare Earth (Pr^{3+}) ions with electronic levels absorbing in the visible range; the

second one is to disperse pigment grains, a matter already containing the above mentioned ions (Colomban 2009). The latter method is the formation/precipitation of the colouring agent during the thermal treatment (generally when cooling). Each method has advantages and drawbacks: the first one is simple but hues are weak, the colours easily spread out thanks to the fast diffusion of small colouring ions, and reproducibility of the décor is difficult; the second requires sophisticated preparation (synthesis, grinding, flux addition).

Another technique is the controlled formation of a small quantity of metal nanoparticles of copper (red), silver (yellow to braun) and gold (red) in an optically clear matrix which gives rise to colourfull materials through the specific interaction of the light with the electron gas at the particle surface: the so-called plasmon resonance (Colomban 2009). This gives way to a narrow peak absorption and more complex features related to the particle composition, size and shape.

The controlled reduction of copper ions into metal nanoparticle is used to make red glasses. Originally a Celtic innovation for the preparation of enamel on metal, it was subsequently used for Roman red mosaic tessarae, middle-ages stained red glasses, some lustre pottery, Jun and *Flammés*, *Sang-de-Pigeon* etc. Chinese porcelains as well as *Satsuma* Japanese glass. The high tinting power of metal particles (Colomban 2009; Colomban et al. 2009) imposes the control of their number. The control is indirectly obtained through the atmosphere of the kiln: if hydrogen is produced by the combustion of wet wood, it diffuses in the glass to reduce $Cu^{2+/+}$, Ag^{+} or Au^{4+} ions; the diffusion of CO species is too slow and 'go-between' cations such as Sn^{4+}, Fe^{3+}, Sb^{5+}, … reduced at the glass surface are needed, they diffuse in the glass and then oxidizise at the contact of $Cu^{2+/+}$, Ag^{+} or Au^{4+} ions thus reducing them into metal nanoparticles. Because the huge light absorption of Cu nanoparticles, middle-age stained glass masters deposited alternations of thin red and colour less glass films (a few μm/tenths of μm thick) on a colourless subtrate (Colomban et al. 2009).

Yellow stained glasses are prepared by silver ion diffusion from one side of the glass surface ('cementation') and then in situ reduction into silver nanoparticles to obtain a coloration by the Ag plasmon light absorption. This preparation technique limits the formation of silver nanoparticles to the glass surface in contact with the mixture used as a silver ion source, the thermal treatment assuring the oxydo-reduction into silver nanoparticles. The technique was first described in a report from the middle-ages (Anonymous 1279; Cannela 2006).

Another way to obtain nice red or orange colours is the use of nanosized hematites or parent structures. The size reduction of particles to nanorange modifies the shape of electronic absorption bands and hence modifies the electronic gap, leading to a small colour change. This phenomenon is at the origin of Roman Sigillatta's (Leon et al. 2015) nice colours where the orange to red colour of the fired slip arise from the association of micronic haematite and/or hercynite grains. Rather similar fine microstructure are observed for Iznik red (Armenian bole) (Colomban et al. 2004; Simsek and Gecckinli 2012), red Meissen décor (Colomban and Milande 2006) and French faience red décor obtained using Thiviers sandstone as red pigment precursor.

6 Conclusion: Traditional Pottery, A Model for Advanced Ceramics

The traditional ceramic route experimented since millenia offers the following advantages (Colomban 2005):

(i) nanosized raw materials
(ii) transition from the sol (a dispersion in water with a very low viscosity) to a gel by the simple modification of the pH or pKa of the sol
(iii) easy control of the viscosity and of the plasticity by the water content control

The fantastic potential of clay-water mixtures was discovered very early on. Evidently, although the nanometric scale of clay particles has only been known for less than 1 century, potters have known and developped techniques aimed at selecting the thiner particles (selection of raw materials, levigation, storage and ageing to developp bacteria action, …) for millenias.

Roy demonstrated in the 1970's that similar properties can be obtained with a silica sol (Roy 1969) obtained from soda silicate liquid or from silica fume. The first application was the preparation of synthetics opals (Colomban 1989). The development of metalorganic chemistry showed that the controlled hydrolysis-polycondensation—with water (Snow 1973; Colomban 1976; Sakka and Kamiya 1980; Masdiyasni 1982; Perthuis and Colomban 1984; Klein 1988) or without [using polyiols (Touati et al. 2000)]—of alkoxides makes possible the preparation of a variety of compositions. The nanosized powder allows preparing high purity, optically clear complex ceramics (Snow 1973; Colomban 1976; Perthuis and Colomban 1984). Nowadays, developments of modern chemistry also makes the preparation of non-oxide compositions (carbures, nitrures) possible, demonstrating that imitation of Nature offers many sources for inspiration in order to further mankind's knowledge.

References

d'Albis A (1984) Steps in the manufacture of the soft paste porcelain of Vincennes, according to the book of Hellot. In: Kingery WD (ed) Ceramic and Civilization. In Ancient Technol. to Mod. Sci. Vol 1. The Am Ceram Soc, Columbus

American Ceramic Society (1971) Phase Diagrams for Ceramists. Vol. 10. Westerville, OH, USA

Anonymous (1279) El Lapidario del Rey Alphonso X, translation in spanish by king Alfonso in the year. In: Heaton N (ed) J British Society of Master Glass-Painters 1947:48 p 9

Atasoy N, Raby J (1989) In: Petsopoulos Y (ed) Iznik, the pottery of Ottoman Turkey. Alexandria Press, London, pp 50–73

Berke H, Wiedemann HG (2000) The chemistry and fabrication of anthropogenic pigments Chinese blue and purple in ancient China. EASTM 17:94–120

Bianchetti P, Talarico F, Vigliano MG, Fuad Ali M (2000) Production and characterization of Egyptian Blue and green frit. J. Cult Her 1(2):179–188

Bouquin O, Perthuis H, Colomban Ph (1985) Low temparature sintering and optimal physical properties: a challenge the NASICON ceramics case. J Mat Sci Lett 4:956–959

Brongniart A (1877) Traité des arts céramiques ou des poteries considérées dans leur histoire. In: Salvetat A. (ed) Leur pratique et leur théorie 3rd edn. Asselin–Libraire de la Faculté de Médecine. Vol 2. Paris

Caggiani MC, Colomban Ph, Mangone A, Valloteau C, Cambon P (2013) Mobile Raman spectroscopy analysis of ancient enamelled glass masterpieces. Anal Methods 5:4345–4354

Caggiani MC, Valloteau C, Colomban Ph (2014) Inside the glassmaker technology: search of Raman criteria to discriminate between Emile Gallé and Philippe-Joseph Brocard enamels and pigment signatures. J Raman Spectrosc 45(6):456–464

Cannela A-F (2006) Gemmes, verre coloré, Fausses pierres précieuses au moyen âge, Le quatrième livre du « Trésorier de Philosophie naturelle des pierres précieuses » de Jean d'Outremeuse. Bibliothèque de la Faculté de Philosophie et Lettres de l'Université de Liège-Fascicule. CCLXXXVIII. Librairie Droz, S.AGenève

Colomban Ph (1976) Frittage de céramiques transparentes PLZT. L'Industrie Céramique 697:531–535

Colomban Ph (1989) Gel technology in ceramics, glass-ceramics and ceramic-ceramic composites. Ceramics Int 15:23–50

Colomban Ph (2004a) Secrets retrouvés du Lustre Abbasside. La Revue de la Céramique et du Verre. 139: p 13–21. http://www.ladir.cnrs.fr/pages/colomban/Lustreceramique.pdf

Colomban Ph (2004b) Préface, in Grès et Raku du Japon–Techniques décoratives et critères d'appréciation. In: Colomban Ph (ed.) Taoci 3: pp 1–5 SFECO–Edn Findakly (ISSN 1624-4842 ISBN 2-86805-113-8)

Colomban Ph (2005) Nano/micro-structure and property control of single and multiphase materials, ch 12. In: Komarneni S, Lee B (eds.) Chemical Processing of Ceramics-2nd Edn: pp 303–339. CRC Press, Boca Raton

Colomban Ph (2009) The use of metal nanoparticles to produce yellow, red and iridescent colour, from bronze age to present times in lustre pottery and glass: solid state chemistry, spectroscopy and nanostructure. J. Nano Research 8:109–132

Colomban Ph (2011) SiC, from amorphous to nanosized materials, the example of SiC fibres issued of polymer precursors. INTECH http://www.intechopen.com/books/howtoreference/silicon-carbide-materials-processing-and-applications-in-electronic-devices/sic-from-amorphous-to-nanosized-materials-the-exemple-of-sic-fibres-issued-of-polymer-precursors October 2015

Colomban Ph (2012) Pottery, Glass and enamelled artefacts: how to extract information on their manufacture technology, origin and age? In: Howell HGM, Vandenabeele P (Eds.) Analytical Archaeometry Ch 8: pp 245–267 Royal Society of Chemistry, Cambridge (978-1-84973-162-1)

Colomban Ph (2013) The destructive/non-destructive identification of enamelled pottery and glass artifacts and associated pigments– A brief overview. Arts 2(3):111–123. doi:10.3390/arts2030111

Colomban Ph, Calligaro Th, Vibert-Guigue C, Nguyen QL, Edwards HGM (2005) Dorures des céramiques et tesselles anciennes: technologies et accrochage. Revue d'Archéométrie 29:7–20

Colomban Ph, Gouadec G (2005) The ideal ceramic fiber/ oxide matrix composite: how to conciliate antagonist physical and chemical requirements? Ann Chimie– Sci Matér. 30[6]: pp 673–688

Colomban Ph, Milande V (2006) On-site analysis of the earliest known Meissen porcelain and stoneware. J Raman Spectrosc 37(5):606–613

Colomban Ph, Milande V, Lucas H (2004a) On-site raman analysis of Medici porcelain. J Raman Spectrosc 35(1):68–72

Colomban Ph, Milande V, Le Bihan L (2004b) On-site raman analysis of Iznik pottery glazes and pigments. J Raman Spectrosc 35:527–535

Colomban Ph, Robert I, Roche C, Sagon G, Milande V (2004c) Identification des porcelains tendres du 18ème siècle par spectroscopie Raman: Saint-Cloud, Chantilly, Mennecy et Vincennes/Sèvres. Revue d'Archéométrie 28:153–167

Colomban Ph, Tournié A, Ricciardi P (2009) Raman spectroscopy of copper nanoparticles-containing glass matrix: the ancient red stained-glass windows. J Raman Spectrosc 40(12):1949–1955

Colomban Ph, Tournié A, Fr de Montmollin D, et al (2010) Vegetable ash as raw material in the production of glasses and enamels, for example the contemporary vegetable ashes from Burgundy, France, https://hal.archives-ouvertes.fr/hal-00542830/ 08 August 2015

Colomban Ph, Treppoz F (2001) Identification and differentiation of ancient and modern european porcelains by raman macro- and microspectroscopy. J Raman Spectrosc 32:93–102

Colomban Ph, Truong C (2004) A non-destructive raman study of the glazing technique in lustre potteries and faiences (9th–14th centuries): silver ions. Nanoclusters, Microstructure and Processing, J Raman Spectrosc 35:195–207

Cooper E (2000) Ten thousand years of pottery (4th ed) University of Pennsylvania Press: Philadelphia

Ellis L, Newman R (2005) The analyzis of glazed quartzite sculpture from Kerma, Capital of ancient Kush (Sudan). MRS Fall Meeting Proc. Vol 852: OO7.3 OO7.10

Fontaine SD, Foy D (2007) L'épave Ouest-Embiez, 1. Var. Le commerce maritime du verre brut et manufacturé en Méditerranée occidentale dans l'Antiquité. Rev. Archéologique de Narbonaise 40:235–265

Fukang Z (1984) The origin and development of traditional Chinese glazes and decorative ceramic colors. In: Kingery WD (ed) Ancient technology to modern science, ceramic and civilization, vol I. The Am Ceram Soc, Columbus

Haussone M (1969) Technologie Générale. Faïences, Grès, Porcelaines, Bibliothèque Professionnelle. J-B Baillère & Fils: Paris

Johnson DW Jr. (1985) Sol-Gel processing of ceramic and glass. Am Ceram Soc Bull 64:1587–1602

Jouenne C-A (2001) Traité de Céramique et Matériaux Minéraux. Editions Septima, Paris

Kingery WD (ed) (1984) Ancient technology to modern science, ceramic and civilization, vol I. The Am Ceram Soc, Columbus

Kingery WD (ed) (1986a) Technology and style, ceramic and civilization, vol II. The Am Ceram Soc, Columbus

Kingery WD (ed.) (1986b) High technology ceramics–past, present, and future. The Nature of Innovation and Change in Ceramic Technology. Ceramic and Civilization Vol III. The Am Ceram Soc, Westerville

Klein LC (ed) (1988) Sol-Gel Technology. NOYES Publications, Park Ridge, New-Jersey

Lee WE, Iqbal Y (2001) Influence of mixing on mullite formation in porcelain. J Eur Ceram Soc 21:2583–2586

Leon Y, Sciau P, Passelac M, Sanchez C, Sablayrolles R, Goudeau P, Tamura N (2015) Evolution of *terra sigillata* technology from Italy to Gaul through a multi-technique approach. J Anal Atom Spectr 30:658–665

Mazdiyasni KS (1982) Powder synthesis from metal-organic precursors. Ceram Int 8:42–56

Martinon-Torres M, Freestone IC, Hunt A, Rehren T (2008) Mass-produced mullite crucibles in medieval Europe: manufacture and material properties. J Am Ceram Soc 91(6):2071–2074

McGovern PE, Notis MD, Kingery WD (eds) (1989) Cross-craft and cross-cultural interactions in ceramics, ceramic and civilization, vol IV. The Am Ceram Soc, Westerville

Mezzadri B (1986) La Corse, poterie traditionnelle à l'amiante. Revue de la Céramique et du Verre 26:5–9

Neri E, Morvan C, Colomban Ph, et al (2016) Raman identification of opacifiers in late Roman and Byzantine (4th-8th c.) mosaic tesserae: continuity and discontinuity of Roman technology. Archaeometry

Okamura H, Bowen HK (1986) Preparation of alkoxide for the synthesis of ceramics. Ceramics Int 12:161–171

Perthuis H, Colomban Ph (1984) Well densified NASICON-type ceramics elaborated using sol-gel process and sintering at low temperatures. Mater Res Bull 19(5):621–631

Ricciardi P, Colomban Ph, Tournié A, Milande V (2009) Non-destructive on-site identification of ancient glasses: genuine artefacts, embellished pieces or forgeries? J Raman Spectrosc 40:604–617

Roy R (1969) Gel route to homogeneous glass preparation. J Am Ceram Soc 52:344–347

Sakka S, Kamiya K (1980) Glasses from metal alcoholates. J Non-Crystall Sol 42:403–422

Simsek G, Colomban Ph, Wong S, Zhao B, Rougeulle A, Liem NQ (2015a) Toward a fast non-destructive identification of pottery: the sourcing of 14th–16th century Vietnamese and Chinese ceramic shards. J Cult Her 16(2):159–172

Simsek S, Geckinli AE (2012) An assessment study of tiles from topkapi palace museum with energy-dispersive X-ray and Raman spectrometers. J Raman Spectrosc 43:917–927

Simsek G, Casadio F, Colomban Ph, Faber K, Bellot-Gurlet L, Zelleke G, Milande V, Moinet E (2014) On-site identification of earlier Meissen Böttger red stonewares using portable XRF: 1, body analysis. J. Am. Ceramic Society 97(9):2745–2754

Simsek G, Colomban Ph, Casadio F, Bellot-Gurlet L, Faber K, Zelleke G, Milande V, Tilliard L (2015b) On-site identification of early Böttger red stonewares using portable XRF/Raman instruments: 2 glaze and guilding analysis. J Am Ceram Soc 98(10):3006–3013

Snow G (1973) Fabrication of transparent electronic PLZT ceramics by atmosphere sintering. J Am Ceram Soc 56:91–96

Touati F, Gharbi N, Colomban Ph (2000) Structural evolution in polyolysed hybrid organic-inorganic alumina gels. J Mater Sci 35:1565–1570

Vandiver P, Kingery WD (1986) Egyptian faience: the first high-tech ceramic. In: Kingery WD (ed) High Technology Ceramics–Past, Present, and Future. The Nature of Innovation and Change in Ceramic Technology, Ed. Ceramic and Civilization Vol III. The Am Ceram Soc, Westerville, pp 19–34

Vandiver PB, Soffer O, Klina B, Svoboda J (1989) The origin of ceramic technology at dolni-vestonice czechoslovakia. Sci 246:1002–1008

Wood N (1999) Chinese glazes: their origins, chemistry and recreation. A & C Black Publishers Ltd, London

Informative Potential of Multiscale Observations in Archaeological Biominerals Down to Nanoscale

Ina Reiche and Aurélien Gourrier

Abstract Humans have intentionally used biological materials such as bone, ivory and shells since prehistoric times due to their particular physical and chemical properties. The composite nature of biological materials at the nanoscale combined with an important structural hierarchy up to the macroscopic level is responsible for these exceptional properties. In this chapter we discuss the relation of the structural features of different biological materials within their archaeological and historical contexts along with their anthropological use and function. Amid the wealth of biological materials of archaeological interest, a special attention is paid to carbonate–based materials such as corals and shells and phosphate-based ones, including bone, teeth, ivory and antler. The structural features of these archaeobiominerals at different length scales down to the nanoscopic scale are highlighted in this chapter as they allow drawing conclusions on ancient working techniques, the provision and circulation of raw materials, anthropological heat processes, and, last but not least, on diagenetic changes and authentication purposes. The informative potential of observations of archaeological biological materials at different length scales is finally illustrated by some case studies.

I. Reiche (✉)
CNRS, UMR 8220, Laboratoire d'Archéologie Moléculaire et Structurale (LAMS), Sorbonne Universités, UPMC Univ. Paris 06, 4 Place Jussieu, 75005, Paris, France
e-mail: i.reiche@smb.spk-berlin.de; ina.reiche@upmc.fr

I. Reiche
Rathgen-Forschungslabor, Staatliche Museen zu Berlin-Preußischer Kulturbesitz, Schloßstraße 1a, 14059 Berlin, Germany

A. Gourrier
Univ. Grenoble Alpes, LIPHY, 38000 Grenoble, France
e-mail: aurelien.gourrier@univ-grenoble-alpes.fr

A. Gourrier
CNRS, LIPHY, 38000 Grenoble, France

P. Dillmann et al. (eds.), *Nanoscience and Cultural Heritage*,
DOI 10.2991/978-94-6239-198-7_4

1 Introduction

Biological materials are key witnesses of past societies, when they are preserved, as they serve as important archives in the archaeological and geological record bearing a wealth of information on ways of life, climates, environments and age in their shape, structure as well as in their chemical, isotopic and genetic composition. They have also been used to produce art objects from prehistoric to contemporary times because of their availability as well as the symbolic and precious nature of these materials. As such, those works of art convey information about technological skills and cognitive capabilities of human societies through the way they have been produced in relation to their specific chemical composition and structure (Backwell and d'Errico 2008; Backwell et al. 2008; d'Errico and Henshilwood 2007; White and Schwarcz 1989; White 1995, 2006; Conard 2003, 2009). Tracing the geographical origin of the artefact's material can also reveal trading routes and societal organizations of ancient cultures. Finally, the genetic analysis of these biological remains and artifacts can also shed light on the phylogeny and phylogeography of the respective animals which body parts are witnesses of past events (Nogués-Bravo et al. 2008; Haile et al. 2009; Enk et al. 2011).

Besides morphological and micro-morphological studies currently used in archaeology to investigate archaeological biological materials, an increasing number of physicochemical studies are dedicated to elucidate their structural, chemical and isotopic features (Weiner et al. 1998; Bocherens et al. 2007; Buckley et al. 2008, 2010; Zazzo et al. 2006; Weiner and Bar-Yosef 1990; Bartsiokas and Middleton 1992). This adds a considerable amount of information contained in their hierarchical structure from the macro- down to the nanoscale. Up to the last two decades, biological materials were essentially studied using powdered samples, which, by destroying their hierarchical organization, resulted in a considerable loss of information. Therefore, many efforts were recently made to overcome this issue by improving the analytical procedures to obtain spatially resolved data on physical and virtual sections of these materials. At first, relatively small areas could be analyzed to establish elemental distribution profiles (e.g. Grime and Watt 1993; Reiche et al. 1999). Nowadays, two and sometimes three-dimensional (2D and 3D) elemental, molecular, structural and isotopic imaging of entire objects has becomes possible owing to recent technological developments of focused analytical probes used in scanning mode and detectors (e.g. Lebon et al. 2011a; Reiche et al. 2011a, 2003, 2010; Reiche and Chalmin 2008; Anne et al. 2014; Bergmann et al. 2010; Gueriau et al. 2014; Gourrier et al. 2007b, 2010).

However, archaeological biological materials and objects are rarely preserved in their initial state and more likely modified in their constitution over time due to bio-physicochemical alteration processes also called diagenetic or taphonomic processes. These processes are complex because they are multi-factorial, non-linear in time and operate in a heterogeneous way and at different structural levels (Hedges 2002; Budd et al. 2000; Kohn et al. 1999; Reiche et al. 2002a, 2003; Dauphin and Williams 2004; Geigl 2002; O'Connor et al. 2011; Godfrey et al. 2002; Albéric et al. 2014; Large et al. 2011; Baud and Tochon-Danguy 1985; Jans et al. 2004;

Nielsen-March and Hedges 1999; Nielsen-Marsh et al. 2007; Smith et al. 2007; Collins et al. 2002).

Diagenetic changes can bias the information yielded from archaeo-biominerals, such that it becomes important to distinguish features due to diagenetic changes from representative bio-physico-chemical markers of the past. This became particularly clear from palaeogenetic and palaeogenomic studies. Indeed, it is known that ancient DNA molecules are heavily fragmented and the nucleotide bases are chemically altered changing the genetic code (e.g. Pruvost et al. 2007, 2008; Llamas et al. 2012; Sawyer et al. 2012). For all those reasons, a precise evaluation of the informative potential of those archaeological witnesses of past societies remains a difficult challenge. However, much is yet to be gained from the study of objects made of biominerals, when considering carefully the morphological and biochemical signatures at the appropriate length scale with respect to diagenetic changes.

In this chapter, the informative potential of archaeological biominerals is discussed from a structural and morphological perspective at a very small length scale which forms what Steve Weiner introduced as "Microarchaeology", meaning, among other investigations, the study of the archeological information contained in the materials at the nano- and microscale which are not visible to the naked eye (Weiner 2010). For more in-depth discussions on biogeochemical signatures the reader is oriented towards other reviews and books such as "*Message d'os: archéométrie du squelette animal et humain*" (Balasse et al. 2015).

2 Structural and Chemical Characteristics of Some Biominerals of Archaeological Interest

The survival strategies of early human groups were based on exhaustive exploitation of surrounding materials. Beyond immediately available sources such as wood and stones, animals were also used extensively for their skins and fur as well as more rigid organs such as the skeletal parts and teeth.

Therefore, in the archaeological context, especially the prehistoric one, the following biological materials are of outmost importance aside from wood, when preserved: bone, teeth, ivory, antler, skin, leather, hair, feathers as well as corals and shells. From this short-list, it can clearly be seen that biominerals occupy a central role.

Biominerals from marine or terrestrial origin, in their present form, are the result of an evolutionary adaptation process, which has persisted for millions of years. These materials are therefore considered to be well adapted to their respective physical and chemical environment (Weiner and Wagner 1998; Fratzl and Weinkammer 2007). This results in an amazing diversity of designs and shapes with characteristic functions. However, most biominerals essentially fall in three broad classes in terms of chemical composition: calcium carbonates (e.g. shells, nacre), calcium phosphates (e.g. bone, teeth, woods) and silicates typically found in

certain plants. Additionally, those materials are generally composite and exhibit a high degree of structural hierarchy at more than one length scale down to the nanoscale (Currey 2005; Lakes 1993; Addadi and Weiner 2001; Lowenstam and Weiner 1989; Mann and Weiner 1999).

Biominerals are often structurally optimized to achieve outstanding mechanical properties. Bone or shells, for example, combine a high stiffness and toughness, which are difficult to combine for most engineered bulk materials. Generally, stiff materials, like ceramics, are not very tough and, tough materials, like polymers, are not stiff. The combination of both classes of materials, (bio)minerals and (bio) polymers associated in varying amounts at the nanoscale to form (bio)composites allows combining those properties. The key for this efficient combination of mechanical properties in biomineralized tissues is their hierarchical structure (Fratzl 2004).

2.1 Phosphate-Based Biominerals

The phosphate phase generally found in biominerals is poorly crystalline carbonated calcium hydroxyapatite (a hydrated calcium phosphate). It is found among others in bone, antler, teeth and tusks (ivory). It is a very stable mineral and can accommodate many chemical species in its structure, which make it an ideal mineral for biologically controlled mineralization. In biominerals the nanocrystals of calcium apatite are generally embedded in a collagen-matrix. The imbrication of both phases is the key for the exceptional properties of these biominerals, some of them of archaeological relevance are discussed in detail in the following paragraphs.

2.1.1 Bone

Bones are extremely complex and smart objects (Fig. 1). First, because they are multi-functional as they must ensure body integrity and structure through the skeleton, thus protecting the most exposed organs (brain, heart, lungs etc.) and allowing movement through the musculo-skeletal system. Secondly, they host the production of red blood cells in the marrow around which bones form a sophisticated barrier. Third, they act as a reservoir for calcium storage, which is fundamental to all cellular processes throughout the body. Thus, the shapes, structures and chemical compositions of various types of bone must be seen as a reasonable compromise to achieve those three functions simultaneously (which implies that the mechanical properties should not be overestimated). Implicitly, this assumes that the bone shape/structure dictates the function (biomechanics) and/or vice versa (mechanobiology), i.e. the structure defines the function. We, now, have a very

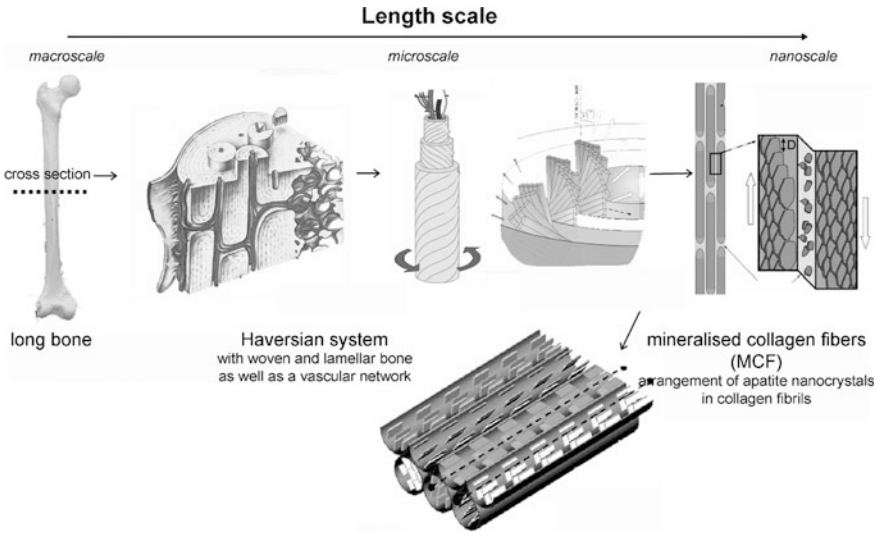

Fig. 1 Scheme of the structural hierarchy of bone. Adapted from Gupta et al. (2006), Rubin et al. (2005), Wagermaier et al. (2006)

reasonable understanding that this is, in fact, the case (Currey 1999, 2002; Rho et al. 1998; Klein-Nulend et al. 2005; Carter and Beaupré 2007; Weiner and Wagner 1998).

Although the primary shapes of bones are encoded genetically and are determined during the first stages of growth (with many associated pathologies), the diet plays an important role in tissue formation and remodelling. The characteristic structural features of bone at microscale are the Haversian systems, also called secondary osteons (Fig. 2). The quality of the collagen and calcium phosphate, which constitutes the tissue will depend on the availability of calcium or similar types of ions and on the amount of amino acids present.

Collagen molecules are known to form a rather large family of ubiquitous macromolecules, which plays an important structural role in many different types of tissues including cornea, skin, artery, tendons, bone (Wess 2008). Depending on the tissue type and, thus, function, collagen molecules can form diverse supramolecular arrangements, from dense and rigid nano-/microfibrils to extended branched elastic networks. However, all collagen types share common characteristics (Hulmes 2008): they consist of three polypeptide chains, each of which having at least one domain formed by a repeating -(Gly-X-Y)-$_n$ motif, n generally falling in the range 337–343. The Glycine residue provides flexibility to the chains such that the overall macromolecular conformation strongly relies on the nature of the two other amino acids and the extension of this domain. Ultimately, the presence of hydrophobic and hydrophilic residues results in a folding of the three chains in a right-handed triple helix, with the glycine residues positioned close to the central axis. In bone, collagen is of type I, and consists of $\sim$20 % proline and hydroxyproline. The cyclic ring of

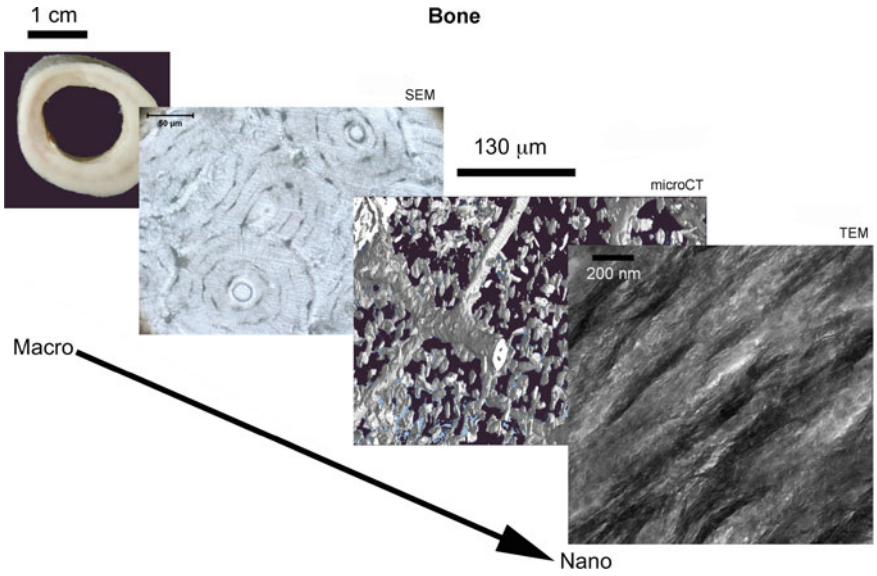

Fig. 2 Structural features of bone observed at different length scales using optical, electron microscopy (SEM and TEM) and micro-X-ray tomography

these residues considerably limits the number of accessible conformations and provides rigidity to the molecule. The triple helix extends to ~300 nm in length and 1.5 nm in diameter and pack densely due to affinity between domains of adjacent molecules. This favors the formation of nanofibrils of ~100 nm in diameter, which are known to organize in different ways at the tissue (supra-fibrillar) level, from highly disorganized in woven bone, to cholesteric type packing in osteons, similar to synthetic liquid crystals. From this, it can be qualitatively understood that the presence (or absence) of specific vitamins in the diet can influence the physical properties of bone tissue, as has clearly been demonstrated for vitamins B, D and E (Arjmandi et al. 2002; Bailey and Wijngaarden 2015).

The inorganic phase of bone (70 wt%) corresponds to a poorly crystalline carbonated hydroxyapatite with a chemical formula close to $Ca_{8.3}\square_{1.7}(PO_4)_{4.3}(HPO_4, CO_3)_{1.7}(OH)_{0.3}\square_{1.7}$ (carb. HAP) with a hexagonal crystal lattice ($P6_{3/m}$). In addition, bone contains about 10 wt% of water. Dietary factors can also affect the mineral composition in bone, which is generally found in the form of a carbonated hydroxyapatite (Posner 1969; Betts et al. 1981; Meneghini et al. 2003; Rey et al. 2009). It is, now, well known that bone mineral can accommodate various amounts of magnesium, sodium, fluorine, and even much heavier ions such as strontium or even uranium (Skinner 2013). Furthermore, a large number of crystal chemistry modifications can occur in bone, the most important one being carbonate to phosphate substitution. Such substitutions can have an important impact on the mineral crystal size, structure and organization at the nanoscale and can lead to

drastic consequences for macroscopic scale properties (e.g. Boivin et al. 1988; Roschger et al. 1997; Rubin et al. 2003; Gourrier et al. 2010). In addition, the specific trace elemental composition of the mineral phase can be used to classify groups of individual and derive valuable archaeological information (Molleson 1987). Of particular importance for studies based on the analysis of the mineral in bone artefacts is the isotope ratio composition, which has been shown to strongly relate to diet (Ambrose 1991; Balasse et al. 2001; Balasse and Tresset 2002; Bocherens et al. 1994, 2006; Ericson 1985; Iacumin et al. 1996; Lee-Thorp et al. 1997).

It is now well established that the mineral phase in bone forms as elongated thin platelet-shaped crystals with typical dimensions $3 \times 50 \times 100$ nm^3 (Weiner and Traub 1986; Weiner and Wagner 1998; Rubin et al. 2003; Landis et al. 1996; Fratzl et al. 2004). These dimensions are very unusual when compared with geological apatite of similar composition. Additionally, the crystallographic c-axis has been shown to coincide with the main axis of the collagen fibrils within a couple of degrees at most (Wagermaier et al. 2013).

As for other biominerals, these aspect can only be understood by taking into account the intimate relation between the two phases, the collagen fibrils serving as a template for mineral deposition and crystallization (Hodge and Petruska 1963; Landis et al. 1996; Traub et al. 1992; Weiner and Traub 1986; Ziv et al. 1996).

It is worthwhile emphasizing that any change from an average "reference" (healthy individual, animal) tissue structure should result in modifications of the collagen fibril/mineral nanocrystal structure and organization. In medicine, the nanoscale bone structure is currently investigated to evidence pathological modifications (e.g. Ruppel et al. 2008), while in archaeology and forensic sciences, this provides powerful markers of anthropological alterations or diagenetic processes (Chadefaux and Reiche 2009; Chadefaux et al. 2009b; Reiche et al. 2011a).

Given that the archaeological bone artefact represents a structure "frozen" at a given time of life and setting aside the diagenetic modifications, one should thus be able to retrieve information concerning diet, ways of life and health of the indiviual by the thorough investigations of bones at all structural scales.

Additionally and, possibly, more importantly than the sole tissue composition, it is now a relatively well established fact that the structure of bone can be (strongly) affected by external stimuli such as mechanical loads. Thus, any kind of physical activity of an individual will trigger a cascade of cellular events leading to what is described in the literature as bone remodelling (as opposed to modelling, i.e. bone formation) (Currey 2002). In brief, this implies resorption of damaged or unnecessary bone parts by osteoclasts and formation of new tissue by osteoblasts, e.g. to resorb micro-cracks, to better adapt to specific loading conditions etc. The magnitude of those cellular events is directly connected to the amount of external stimuli, i.e. an important physical activity will result in a higher remodelling. However, the remodelling activity can also be affected by various pathologies, osteoporosis being a well-known example.

2.1.2 Teeth

Teeth are specialized structures adapted for food mastication. Mammal's teeth present a wide range of morphologies depending of the phylogenetic groups, animal diets and functions (as for example in the case of proboscidian tusks). Teeth mainly consist of two parts: a crown and a root. The crown is generally coated with a hard layer called enamel, whereas the root, firmly fixed in the jaw, is coated with a tissue called cement. In many species, the crown enamel is also coated with cement. Underlying these surface layers, a resistant tissue called dentin forms the inner part and constitutes the "backbone" of the tooth. This dentin tissue is also the main constituent of tusks, where it is called ivory (because of its archaeological importance a special paragraph is dedicated to the description of ivory). Inside the tooth is the pulp, corresponding to a soft tissue including blood vessels and nerves.

Dentin of tooth and tusks is a composite material made up of an organic and inorganic fraction, which are intimately mixed on a nanometre scale. Dentin has basically the same composition as bone but differs in its tubular micromorphology due to a dentinogenesis starting by osteoblasts in the pulp.

The organic phase of dentin (20 wt%) is mainly composed of a collagen type I matrix. The inorganic phase (about 70 wt%) consists, like in bone, of a poorly crystalline carb. HAP. In addition, they contain about 10 wt% of water. The organic matrix is first formed by odontoblasts and then mineralised during dentinogenesis. The mineralization continues with ages. The characteristic dentinal tubules radiate outward through the dentin from the pulp to the exterior cementum or enamel border.

Enamel at the tooth surface is the most highly mineralized and hard tissue of mammal. It is composed at 96 wt% by well-crystallized carb. HAP. This higher crystallinity is particularly due to lower amount of substituted carbonate (about 3 wt %) than in bone and dentin (up to 6 wt%). Organic matter (non-collagenous protein) represent less than 1 wt% and the rest is water (3 %). The enamel crystals can reach up to 1 μm length and 50 nm in diameter. The crystals are packed in small bundles called prisms around 4–12 μm wide and extended from the Enamel Dentin Junction (EDJ) up to the surface of the crown. The long axis of prism is perpendicular thus to the EDJ (Hillson 2009).

Because of its interesting mechanical properties, human tooth dentin has been studied to understand better the structure-mechanical function relations of mineralized collagen tissue. Wang and Weiner (1998) have shown that HAP are aligned in three dimensions within in individual collagen fibril and are found as aggregates without any preferred orientation leading to a anisotropic material regarding the structure (Wang and Weiner 1998). By testing the micro-hardness in the three orthogonal planes, they found that dentin is a mechanically isotropic material regarding the micro-hardness. This paradoxical situation was attributed to the variable modes of crystal orientation. More recently, Tesch et al. 2001 determined local variations of the mechanical properties by nano-indentation from the bulk dentin to the DEJ as well as in the size of particles (determined by small-angle X-ray scattering (SAXS) measurements) and mineralization degree (qBEI) (Tesch et al. 2001).

The dentin layer close to the DEJ corresponds to a local minimum in hardness and modulus, which is known to stop crack propagation. This specific layer between enamel and bulk dentin has been characterized as a porous reticulate matrix of intertubular-dentin containing tubules with no peritubular dentin and presenting low stiffness. These specific properties are responsible for the durability of the whole tooth (Zaslansky et al. 2006).

2.1.3 Ivories

Ivory is generally associated with the dentin part of the exo-skeletal incisor teeth or tusks of several mammalian species, mainly elephant and mammoth *(Laxodonta africana, Elephas maximus, Mammuthus)* but also hippopotamus, warthog, walrus, sperm, killer and narwhal (Espinoza and Mann 1991). Teeth are specialized structures adapted for food mastication whereas tusks are mainly used for digging, foraging and as weapons. The study of the structure and composition of ivory is essential to understand the extraordinary mechanical properties required for the specific use of tusks.

From a macroscopic point of view, teeth and tusks have the same physical structures: the pulp cavity in the centre, surrounded by the dentin (main part), the cementum and a thin enamel layer at the outer surface.

Two special kinds of macroscopic pattern can be observed in the dentin on tusk cross sections only for *proboscidean ivory*: the growth lines and the Schreger patterns. The growth line sequence, exploited using an isotopic analysis approach on micro-milled samples across the tusk, allow the determination of climatic variations, palaeodietary reconstructions and an estimation of the animal age (Codron et al. 2012; Fox and Fisher 2004; Fox et al. 2007). The elemental composition also varies significantly from the central tusk cavity to the cement layer of the tusk and variations in trace element concentrations (Mn, Zn, Sr) have been correlated to the growth lines in order to derive from it information on the environmental conditions during life time (Prozesky et al. 1995; Müller and Reiche 2011).

The Schreger pattern, firstly described as intersecting lines radiating in spiral fashion forming the Schreger angles (Miles et al. 1960), has been studied to distinguish between mammoth and elephant ivory and even between Asiatic and African elephant (Espinoza and Mann 1991; Singh et al. 2006; Trapani and Fisher 2003). The microstructural origin of the Schreger pattern is still not totally understood.

Various microstructural models considering the arrangement, shape, distribution and orientation of dentinal tubules have been proposed. Considering the tubuli structure, the dentinal tubules are micro-canals that radiate outward through the dentin from the pulp cavity to the exterior cementum border. These canals are formed by odontoblasts that move centripetally in cytoplasmic filaments and depose dentin along their pathway. When the cytoplasmic filaments disappear they leave the dental tubules (between 0.8 and 2.2 μm in diameter) (Raubenheimer 1999). The 3D conformation of the dentinal tubules is under genetic control and therefore

characteristic for the respective types of ivory. According to Raubenheimer et al. 1998a, b), the Schreger pattern is the result of the sinusoidal and centripetal course followed by the dentinal tubule. However, Locke (2008) suggested that the tubules are not following a sinusoidal path but a straight one and the apparent sinusoidal curves are due to overlapping images in the helicoidal architecture (Locke 2008). Virag (2012) proposed a 3D model of the tubule organization for elephantoids introducing the "phase shift" model, which assumes a sinusoid undulation of the dentinal tubules in radial profile with different phases (Virag 2012). Recently, the work undertaken by Albéric et al. showed a helical tubule path combined with a phase shift (Albéric et al. accepted).

Finally, Su and Cui (1999) explained the Schreger patterns from the collagen point of view. Collagen fibrils in ivory are in two radially distributed planes and interweave forming a network comparable to the rotated plywood structure observed in lamellar bone. The collagen fibrils form 2 μm large fibrils bundles lying parallel to one another within one layer and rotating by about 90° from one layer to its neighbour (Su and Cui 1999).

At the nanoscale, the average size of apatite crystals was determined to $31 \times 20 \times 3$ nm^3. Jantou-Morris et al. (2010) published a "¼ stagger model" for mineralised collagen molecules analogously to the one proposed model for bones by Jäger and Fratzl (2000) (Jantou-Morris et al. 2010; Jäger and Fratzl 2000). The specific relationship between collagen fibrils and minerals give particular mechanical properties to the material.

Ivory dentin is rich in Mg in comparison to other tooth dentin (about 6 wt%) and the Mg, being a key component for the stabilization of amorphous carbonate, is supposed to play an important role in biomineralization. Hence, several studies have been focused on this subject (Finch and Allison 2007; Politi et al. 2010).

Tusks, mainly used for digging, foraging and as weapons, are subjected to important compression and shear forces and present strong macroscopic mechanical anisotropy. Dentin is known to be stiff because of its mineral part and tough because of its organic part (Baohua and Gao 2004). Cui et al. (1994) investigated the orientation dependence of indentation morphology and micro-hardness of ivory (Cui et al. 1994). Nothnagel et al. (1996) correlated the texture of hydroxyapatite and mechanical properties related to the function of the tusk (Nothnagel et al. 1996). The correlation between the orientation of the collagen fibers and the elastic properties was shown by Nalla et al. (2003) for elephant ivory and by Currey et al. (1994) for narwhal ivory (Nalla 2003; Currey et al. 1994).

2.1.4 Antler

Antlers are bony appendages which are developed pairwise externally onto the frontal bone of the skull in most members of the deer family (*Cervidae*). They are made solely of bone tissue unlike keratin-covered horns (Chapman 1981). Similar to other bones they are composed of protein (mainly collagen type I), mineral (carbonated hydroxyapatite) and water. Their apatite weight content, however, is

slightly less than that of bone which is why their elastic mechanical properties such as the Young's modulus and, hence, the stiffness is lower than in bone.

The basic structure of antlers is similar to long bones, comprised of an outer compact bone shell enclosing a core of spongy bone. Antlers, however, stand apart from other vertebrate biomineralized organs. They are totally regenerated annually at a rapid growth rate. Although they grow over a very short period of time (4–5 months), they can attain elaborate branched or palmate forms, huge sizes (>1 m), and weights of several kilograms. The microstructural arrangements that are important to such rapid and large-scale tissue growth and organization are, still, poorly known, although several studies of antler regeneration histogenesis have been performed (Banks 1974; Wislocki 1942; Kierdorf et al. 1995; Li et al. 2005). The characterization of the three-dimensional microstructural development in antler bone revealed that antler re-growth is a process of scaffold generation, replacement and then filling. The process begins with the building of a mineralized cartilage scaffold, composed of longitudinally oriented cartilaginous tubes of several millimetres in length. A lamellar bone scaffold, consisting of highly longitudinal oriented fenestrated bone tubes, then replaces the cartilaginous framework. In mature antler these bone tubes are then filled with primary osteons, leading to a pattern of less mineralized osteons situated within a more highly mineralized bone matrix (Krauss et al. 2011).

The most distinctive feature of antlers with respect to other bones is their remarkable toughness (Zioupos et al. 1994; Currey 1999; Launey et al. 2010; Rajaram and Ramanathan 1982). Structural toughening mechanisms at the micrometre scale such as microcracking, crack deflection, crack bridging, visco-plastic flow and combinations of these have been identified for bone (Launey et al. 2010; Zioupos et al. 1996; Nalla et al. 2003; Nalla 2005; Vashishth et al. 1997, 2000, 2003). Evidence was also found for a toughening mechanism at the nanoscale in antler compact bone. Results showed a heterogeneous response to load in antler after the onset of inelastic deformation. This was interpreted by the formation of isolated nanoscale defects, which clearly contribute to the antler's toughness (Krauss et al. 2009).

2.2 *Carbonate-Based Biominerals*

Calcium carbonate exists in three polymorphous forms: calcite, aragonite and vaterite, two of which namely aragonite and calcite are found to be the major phases in carbonate-based biominerals such as shells and corals. Calcite is the thermodynamically more stable phase under ambient conditions. It crystallizes in a rhombohedral lattice system and is pure of a whitish colour.

Aragonite is the more stable polymorph under high pressure and crystallzes in a orthorhombic lattice system. It is less frequent than calcite in nature and also shows a white colour.

2.2.1 Shells

Shells are the result of a biologically controlled process of shelled molluscs. Shelled molluscs can live in sea and in freshwater. The shell is formed by an anatomical part of the mollusc called mantle due to the super-saturation of calcium and bicarbonate. Therefore, it is generally a calcareous exoskeleton with an organic calcifying matrix composed of a complex mixture of proteins, glycoproteins, polysaccharides, acids and chitine, which protects the molluscs including snails, clams, tusk shells etc. The organic matrix is genetically encoded to execute the assemblage of the shell. In general the shell is constituted of at least three morphologically different layers from the external border to the internal one: the periostracum (organic layer), one chalk-like prismatic layer (calcerous prismes) and an inner pearly, nacreous layer composed of lamellar successive calcium carbonate layers with organic substances. In general the calcium carbonate fraction represents 95–99 wt% of the shell and the organic matrix the remaining part of 1–5 wt%.

2.2.2 Corals

Corals are sessile animals having a polyp as body unit. They live mostly in colonies that gradually develop from a small start. Corals can be divided in stony and soft corals. Stony corals, also called hard corals, are of interest in the archaeological context as they are used as jewellery. Their skeleton is composed of calcium carbonate that provides hardness, strength and protection to the organism. The polyps are situated in cup-shaped depressions in the skeleton known as corallites. Stony corals can have very variable appearances as a function of different types of habitat, light levels and water movement. Red coral, *Corallium rubrum*, is the most emblematic species used for jewellery and found in the Mediterranean Sea in depths ranging from 10 to 200 m. It is composed of a solid axial skeleton coated with living tissue. The cellular layer called ectoderm forms the external surface above a thick acellular layer composed of collagen (mesoglea). This mesoglae contains small granules of living tissue also called sclerites. The mineral phase of the axial skeletal structures and the sclerites is composed of Mg-rich calcite. This biological calcite also contain about 1.5 wt% of organic matter. The color of red corals is attibuted to the presence of conjugated hydrocarbon chains, whose structure and chain length is still the object of controversy. The crystals are arranged in submicrometer crystalline units. These units show different crystal sizes and shapes although platelet-like crystals are predominant. Their size varies between some tens to some hundreds of nanometers (Vielzeuf et al. 2008). Further transmission electron microscopy (TEM) observations revealed the presence 2–5 nm crystal domains in the submicrometer units that are actually composed of 50–100 nm crystalline superstructures. These formations have important implications for the mechanisms of crystal growth in the living organisms. Interestingly such nanocomposite structures are common to many biominerals. A long-range crystallographic order combined with interfaces at various scales might be responsible the various shapes observed of this kind of biominerals (Vielzeuf et al. 2010).

Fig. 3 Example of an archaeological object dating from the Iron Age bearing an altered red coral from the Celtic princely tomb of Asperg-Grafenbühl, Baden-Württemberg, Germany

The growth rings of corals are marked by a variation in the Mg and the organic matter content. These variations are anti-correlated and can be used for chronological issues as annual variations have been reported. All these features can be exploited for archaeological, environmental, climatic and geological issues.

There has been research on red corals for 130 years (Tischler 1886; Olhausen 1888), but there have been hardly any extensive studies on archaeological findings (Fig. 3) (Perrin 1996; Liverino 1989; Tescione 1965). One reason for this limited research is possibly that corals lose their intense red colour and shiny surface structure due to poorly understood ageing processes, which is why other light-coloured materials such as bone, ivory, chalk or shells are often mistaken for corals. It is therefore not surprising that attempts have repeatedly been made to identify these substances in archaeological contexts using different methods (Fürst et al. 2014).

3 Archaeological Implications of the Study of Biominerals

As already stated, biominerals are an important source of raw material used by former human societies. Therefore, these materials can be used as tracers for provenance and circulation studies of these materials, when their exact nature is well characterized. They can give insights as worked objects onto ancient working techniques of the material (bone, ivory, antler) to be used for tools and weapons as well as on production processes for art objects. In many cases these objects were heated, especially in prehistoric times. Information on former production techniques can also be inferred from the study of heat-induced transformations of these materials. As biological materials, these objects can be used for multiple dating purposes, diet reconstructions as well as environmental and climatic studies (Fig. 4). The latter types of information are generally inferred from stable or instable isotope analyses and not from structural features, except in the case of the study of microwears on teeth. Therefore these isotopic studies are not discussed in this chapter and the reader can find information on this elsewhere (Balasse et al. 2015; Bocherens et al. 2006;

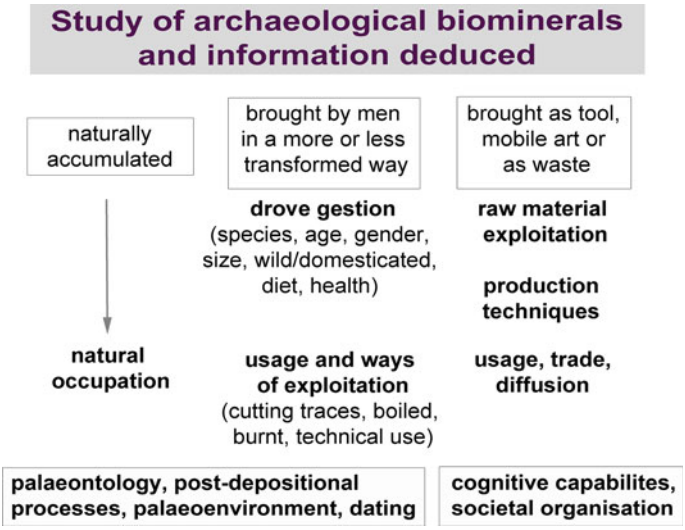

Fig. 4 Overview of the possible implications of the study of archaeological biominerals (pers. comm. M. Regert)

Dupont and Marchand 2008; Gillespie et al. 1984; Hameau et al. 2007; Hedges and Law 1989; Latham 1997; Millard and Pike 1999; Rink et al. 1996; Saliège et al. 1995).

3.1 Tracers of Provenance and Circulation

The study of the provenance and circulation of biominerals in the past is important because these materials have been widely used by ancient societies as tools and as art objects (e.g. body ornaments). The study of tools and art objects is not only interesting to get insights into working techniques, cognitive capabilities of the humans but also because they can be used as tracers of social and technological exchanges between civilisations.

Due to the wide distribution of archaeological biomineral finds, distinct types of social activities can be addressed. If an economically-oriented perspective is considered, three functionally and geographically distinct areas can be differentiated: (1) a production zone, (2) a trading zone and (3) a consumption zone.

A special attention concerning provenancing and circulation studies is paid to precious biominerals such as ivory and corals used to produce different kinds of art objects. As a prominent example, elephant ivory has been traded between Asia, Africa and Europe. As shown in ancient times the geographical areas, where the animals (elephants and mammoths) lived, and the cultural regions, where the material was used, do not necessarily coincide. Therefore, the study of the spread and

commercialization of ivory with respect to its biological origin can provide valuable information about exchanges in ancient societies (Caubet and Gaborit-Chopin 2004).

As another example, coral finds play a crucial role in the reconstruction of social structures, because they are present in many graves, wealthy or not, as well as in élite burials. The distribution of coral seems to show the coupling of coral redistribution with the local élites. In the late Hallstatt and early La Tène periods (620–250 av. Chr.), which are particularly rich in coral imports, they represent the most common Mediterranean find category. They are particularly well suited to understand the economic exchanges between Central Europe and Mediterranean cultures (Fürst et al. 2014).

Although there are legitimate doubts about the reliability of previous material interpretations, it can be assumed that a large number of objects have been incorrectly identified and the number of coral decorations actually present is much underestimated. Therefore, based on reliable materials identification, the informative potential of archaeological coral finds can be better exploited and their spread and trade studied in a more reliable way.

3.2 Working Techniques

Since Prehistoric times, the survival and acquisition strategies of human groups imply the use of animals in every respect. They provide nutritional resources and are an important source of raw material for the production of objects. The hard animal materials, above all osseous materials, were used to produce different kinds of equipment for "artistic" purposes such as statuettes and body ornaments as well for hunting such as projectile points. The different kinds of objects, their production techniques, functions and use are directly dependent on the specific morphological and mechanical properties of the different hard biological materials (Christensen 2004; Tejero et al. 2012; Christensen and Tejero 2015). The understanding and interpretation of these osseous objects therefore necessarily passes through the analyses of macro-, micro- and nanoscopic features of the used raw material in relation to the investigation of their mechanical properties to check the adequacy of the relationship between structure, function and use. Sometimes when the artefacts are heavily carved, the type of osseous material or the type of coral is difficult to be determined. In these cases physico-chemical analysis and morphological studies at different length scales are of outmost importance to identify the employed biological material. The size and morphology of biominerals—combined with other critical factors like mechanical properties, availability as well as a conceptual vision of each animal—have certainly influenced the choice of prehistoric and historic craftsmen in their quest for functionally adapted blanks to produce the artefacts. For example, bones with broad surface would be adequate to receive regular decorative feature such as the ribs of medium or large herbivores. Antlers of deer, because of their exceptional stiff- and toughness, provide the functional requirements necessary for a large part of prehistoric hunting equipment (projectile points).

Fig. 5 Phoenician ivory carving "Woman at the window" (Inv. No. AO 11459) from Arslan Tash site, Syria, 8th c. BC, kept in the collection of the *Département des Antiquités Orientales* of the Louvre museum, Paris

Ivory, a tough and durable material coming from the tusks of strong animals such as mammoths and elephants, adds a high symbolic value to this material within Prehistoric and historic societies. It can be related to wood as it is large enough to be carved and sculptured in different ways without inflicting, as other bone materials, its original macroscopic form. Ivory seems to be the preferred choice to produce art objects, statuettes and personal ornaments (Fig. 5). In later time, ivory was also used in combination with other valuable materials, such as gold and pigments (White 1995). Materials characteristics including their mechanical properties, colour, shape and use wear are important clues to confirm hypotheses about the use and symbolic function of valuable objects (Christensen and Tejero 2015).

3.3 Heat-Induced Transformations

Biominerals can be used as combustible because they contain organic substances. Indeed, traces of heating are often observed on bone fragments and artefacts in the form of color changes and increased mechanical fragility (Stiner et al. 1995; Shahack-Gross et al. 1997; Weiner et al. 1998; Reiche 2009b; Chadefaux et al. 2009b). The way of firing and the firing temperature can allow drawing conclusions on management of resources in former societies. In many cases, however, the effects on bone are difficult to distinguish from other diagenetic phenomena, which could induce similar changes (Bennett 1999; Reiche et al. 2000, 2002b). In some cases, they are identified as burned on the basis of the context in which they are found on the field (e.g. urns), despite of the absence of any colour changes.

This often leaves unanswered a number of questions relating to the identification, conservation and understanding of the accidental or intentional origins of the heating process (Koon et al. 2003, 2010).

3.4 Microwear Studies

Besides personal body ornaments, bones, teeth and even shells are important nutritional resources, providing indications of ways of life. They also represent important archives of information from their macroscopic and microscopic properties, up to their elemental or isotopic composition (Tütken and Vennemann 2011). Palaeontologists usually used teeth morphology or dental microwears to obtain palaeodietary information of animal or human extinct species. Enamel growth marks and other histological features can be used to reconstruct the life history of animal or human fossil specimens (e.g. timing of tooth development, weaning and feeding stresses). Teeth and bone morphology can be used to reconstruct phylogenetic relations between species, especially for human remains.

4 Diagenesis and Taphonomy of Biominerals

Diagenetic and taphonomoic processes of archaeological biominerals are very complex as they are multifactorial and non-linear in time (Fig. 6). They occur during burial time and depend, among others, on material properties (type of tissues, bone, teeth morphology, age of specimen, etc.). They are controlled by external factor such as microorganism development and physicochemical conditions in the burial environment (temperature, moisture, pH, redox condition) (Nielsen-Marsh et al. 2007; Smith et al. 2007; Hedges 2002; Collins et al. 2002).

Although osseous and shell remains constitute the most resistant skeletal remains, they can undergo significant modifications of their structure and morphology after the death of the individual. The most important processes are induced by climatic (weathering) and edaphic conditions, such as temperature and moisture variations which induce a fracturation, similarly to compaction in sediment (Hedges 2002; Denys and Patou-Methis 2014).

Different post-mortem processes can deeply affect histology, micro-structure, mineralogical properties and composition of these tissues. These processes occur even before burial, since microbial organism (bacteria and fungi) can colonize organic-containing tissues as soon as the first steps of flesh putrefaction. Microbial development results in alterations of histological micro-structures. Collagen loss in phosphate-based biominerals leads to an increase of porosity that, in turn, modifies the possibility of exchange between mineral phase and surrounding sedimentary environment during burial (Collins et al. 2002). Alteration processes can induce dissolution and/or recrystallization of the biomineral in more thermodynamically

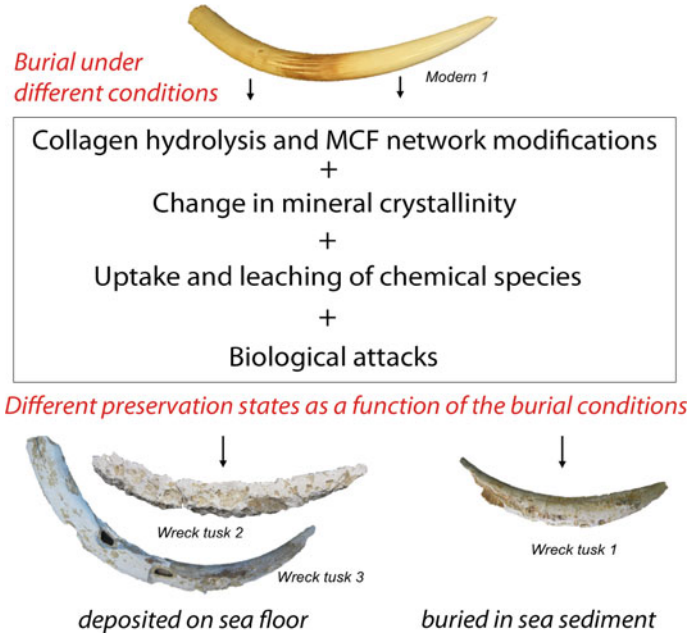

Fig. 6 Example of early diagenetic processes of elephant ivory from a marine site Les Poulins, Brittany, France. Adapted from Albéric et al. (2014)

stable phases (more stoichiometric carbonate apatite, HAP and finally fluroapatite for phosphate-based biominerals and in calcite for carbonate-based minerals) and the precipitation of authigenic minerals in porosities (Berna et al. 2004; Kohn et al. 1999). Dissolution-recrystallization processes or diffusion, absorption and ionic exchange processes can promote the incorporation of foreign ions in the crystal lattices.

Some of these alteration processes can lead to a preservation of biomolecular proxies or appearance of geochemical signals. Re-crystallization of biogenic biominerals during the first steps of diagenesis can encapsulate non-collagenous proteins or DNA fragments within crystal aggregates and preserve them to long-term alteration. Uranium uptake in dental, osseous and calcareous material and accumulation of electrons in paramagnetic centres of apatite crystal lattice over geological time can allow obtaining chronological data by Uranium-series and Electron Spin Resonance (ESR) dating methods (used separately or combined) (Grün et al. 2010; Falguères et al. 2010). However, the main part of diagenetic processes leads to a partial or complete modification of biogenic signal such as elemental or isotopic composition. Uptake of foreign ions such as Strontium, Fluorine, Rare Earth Elements etc. can occur in the first steps of diagenetic processes and continue over geological times (Trueman et al. 2004). The different tooth and bone tissues are more or less resistant to diagenetic alteration. Enamel is considered to be much less sensitive to diagenetic alteration than bone-like tissues

(dentin and cement) mainly due to higher crystal perfection and size of its mineral phase, and the very low amount of organic matter.

When the biomineral was transformed into an art object, the alteration phenomena can be different and represent a combination of use wear and diagenetic changes as a function of whether the object was buried or not. Naturally, alterations also occur when the material is extracted from the living tissue. During the life of the animal, the biomineral remains hydrated and this cycle is interrupted when producing the tool or the art object.

When the object, for instance an ivory sculpture, has never been buried, the main macroscopic alteration features are cracks induced by changes in humidity and discolorations due to the influence of light.

When the object was buried in stable humid soils, it can be quite well preserved until their excavation in the field. Therefore, the biggest issue of the conservation of buried biomineralised objects is during their excavation. The drying process must be as slow as possible and a high humidity should be maintained as long as possible to avoid bursting. Additionally and also observed on other biological tissues, the alteration features within an object might be variable depending on the environmental conditions and the advancement of alteration (Godfrey et al. 2002; Lafontaine and Wood 1982; Chadefaux and Reiche 2009; Large et al. 2011; Reiche 2011; Reiche et al. 2003, 2010).

Similarly to osseous biominerals, coloured corals and shells, especially red corals that have been used for the decoration of art objects, for instance in the Iron Age, are also subject to alteration processes. During long-term aging of red corals, the calcitic mineral phase is preserved, as it is the most stable calcium carbonate phase under ambient conditions. However, during their burial in the soil, a loss of its intense red colour and shiny surface structure is observed. The degradation processes leading to this fading is probably the degradation of the colorants, e.g. the polyenes that are responsible for the red colour. The altered coral can then be mixed up with other biological materials such as bone, ivory or shell that are light-coloured materials. The fact that corals and other (bio-)minerals were used as small honed studs or pearls (on average only 0.5–1 cm in diameter) makes it even more difficult because there are hardly any distinct surface characteristics of the raw material left. Because such coral decorations are often parts of metallic artefacts, some additional coloured corrosion products from the metal can stain the coral in red or green.

Until now, relatively few studies of the bio-physicochemical alterations have been performed taking into account the different hierarchical length scales of biominerals. Such multi-scale analytical approach combining different complementary methods was recently adapted to determine the preservation state of archaeological elephant ivories and bone. The investigation allowed characterizing both, the mineral and organic phase of ivory, with 2D and 3D structural information on the small samples at all length scales of the hierarchical tissue (Chadefaux and Reiche 2009; Large et al. 2011; Müller and Reiche 2011; Reiche 2009a, 2011; Reiche and Chadefaux 2009; Reiche et al. 2003, 2007, 2010, 2011a; Albéric et al. 2014).

5 Analytical Approaches at Different Length Scales

As mentioned before, structural features and composition of biominerals constitute valuable sources of information in current archaeological records. Many studies have therefore focused on these properties, and various analytical protocols were implemented and used for this purpose (Fig. 7).

Archaeological as well as reference materials modified through experimentation (archaeological reproductions) or by artificial aging are studied to understand the observed features and underlying processes at different length scales.

Morphological and micro-morphological characteristics of these different kinds of material have been explored by light and electron microscopy (Jans et al. 2002, 2004; Reiche 2009a; Reiche and Chadefaux 2009; Reiche et al. 2003; Turner-Walker and Jans 2008). The organic matter, its structure and content, has been studied by Mass Spectrometry (MS), Fourier Transform Infrared Spectroscopy (FTIR), Transmission Electron Microscopy (TEM), etc. (Buckley et al. 2008, 2010; Collins et al. 1995, 1999, 2002; Richter et al. 2011, 2011a; Chadefaux et al. 2009a; Chadefaux and Reiche 2009). Mineral matter composition and structure was investigated by means of X-Ray Diffraction (XRD), FTIR and Raman spectroscopy and various other techniques have been used to screen parameters such as crystallinity, carbonate content or uptake of foreign elements [Sr, F, rare earth elements (REE)] (Person et al. 1995, 1996a; Berna et al. 2004; Rogers and Daniels 2002; Edwards et al. 2006; Edwards and O'Connor 2012; Bartsiokas and Middleton 1992;

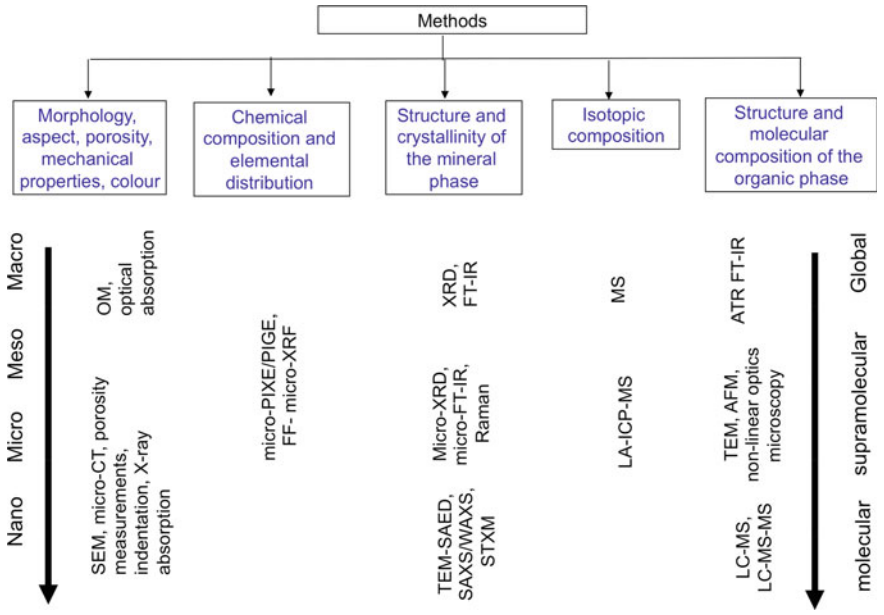

Fig. 7 Overview of the generally used analytical techniques for obtaining complementary information on the structure and composition at different length scales of biominerals

Trueman et al. 2004, 2008). Alteration processes enhance the original heterogeneity of these materials at all length scales, and if some parts are well preserved, other ones can be seriously altered. For a long time, most of the techniques were applied to bulk samples studying either the mineral matter or the organic matrix and only a limited amount of data was available on the spatial distribution of present phases in a more or less altered state within such hierarchically structured and composite tissues at different length scales. Since several years, and thanks to the development of new analytical devices with higher performances, site-selective micro- and nano-analyses become available, notably concerning elemental composition and structural features but to a lesser extent concerning isotopic composition (Goodwin et al. 2007; Schweitzer et al. 2008; Reiche et al. 1999; Gaschen et al. 2008; Duval 2011; Fischer et al. 1989). Variations of structural composition at histological scale was not explored until recently on archaeological material, excepted the works by micro- small-angle X-ray scattering (micro-SAXS) of Wess et al. (2001) on archaeological biological material. Recently, new analytical protocols were developed to investigate the composition and structural parameters at micro-and nanoscale by means of TEM on ultrathin sections, 2D FTIR and Raman micro-spectroscopy imaging, by quantitative scanning SAXS imaging (qsSAXSI) and by Full Field 2D chemical imaging using micro-XRF and PIXE (Reiche et al. 2010; Lebon et al. 2011a, b; Bertrand et al., submitted; Gourrier et al. 2007a, 2011b). These methods were developed on modern and experimentally altered (heated) bone samples, and applied to archaeological samples. Particularly, FTIR micro-spectroscopy imaging using synchrotron light was first performed on histological thin sections (<2 μm thick) in transmission mode to investigate qualitatively and quantitatively the mineral (mineral crystallinity, carbonate content, presence of authigenic minerals) and organic phases (collagen alteration state and content) in samples (Lebon et al. 2011a; Reiche et al. 2010). FTIR micro-spectroscopy in Attenuated Total Reflexion (ATR) mode was later applied to be able to analyse hard and brittle samples impossible to cut in very thin sections (Lebon et al. 2016). Quantitative sSAXSI applied on similar samples and TEM on ultrathin sections allows describing texture and crystal size distribution (Gourrier et al. 2011b).

Many of the currently used methods rely on laboratory instruments. One particular case requiring specific developments is the sSAXSI method for the measurement of mineral nanoparticles size, shape, crystal structure and organization. For archaeological bone or dentin for instance, in order to properly take into account the natural and diagenetic heterogeneity, one cannot rely only on traditional atomic or nanoscale sensitive instruments as they fail to provide a sufficient statistical data due to limited fields of view (typically 1–10 μm^2 of a thin section of $\sim$100 nm for TEM). It was recently shown that small- and wide-angle X-ray scattering (SAXS/WAXS), acquired using synchrotron radiation in scanning mode could provide a powerful solution to alleviate this problem in a unique way (Reiche et al. 2014).

The direct coupling of methods such as SAXS/WAXS and Raman, provides a powerful way to characterize archaeological samples since the information are obtained at similar sites and at the sample scale resolution.

The organic phase can be analysed on the supramolecular down to the molecular level. The principal organic phase of archaeological biominerals, collagen, can be analysed by FTIR by means of the detection of the amid absorption bands. These bands reflect amid polypeptide groups and the lateral chains of amino acids. The secondary protein structure can also be analysed. Micro-FTIR imaging on thin sections can be used to analyse the organic phase at a histological scale.

In addition, analysis of the state of preservation of the organic phase on the level of microscopic fibres can be performed using different kind of microscopies as TEM [50] and Scanning Transmission X-ray Microscopy (STXM) (Benzerara et al. 2006). The collagen content and distribution on thin sections can also be investigated using Time-Of-Flight Secondary Ion Mass Spectrometry (TOF-SIMS) (Eriksson et al. 2006).

Additionally, as new methodological developments for these purposes, confocal fluorescence and second harmonic generation mode (SHG) microscopies will be used for tubuli and collagen imaging, respectively (Chen et al. 2012; Strupler et al. 2007).

The characterisation of the mechanical properties of biological material is mainly based on indentation experiments. Indentation hardness is used to describe properties of materials such as resistance to penetration and scratching, and rebound resilience; it involves a complex combination of mechanical properties, such as elastic modulus, yield strength, and strain-hardening capacity.

It has been shown that microstructure of biological materials influences the indentation hardness and morphology (Cui et al. 1994). As the properties of biological materials presumably depend significantly on its material structure at the micro- and nanometer level, nano-indentation shall be used. Nano-indentation is used to measure small and thin samples. The advantage is that it allows the measure with μm resolution and a depth of penetration up to a few tens of nm.

6 Case Studies

Different case studies are discussed in the following section with the aim to illustrate the different archaeological implications of the study of archaeological biominerals at different hierarchical levels.

6.1 Tracers of Use, Provenance and Circulation of Biominerals in Past Societies

In the following section two examples highlight the approach and the informative potential of biominerals on the use, acquisition and circulation of them in past societies.

6.1.1 Antler Traces Revealed in Palaeolithic Pigments from Lascaux Cave

In numerous research works about a hundred of pigment samples taken in different Palaeolithic cave sites in France and Spain were analysed. Prestigious cave art such as paintings and drawings of Chauvet (30,000 BP), Arcy-sur-Cure (28,000 BP), Lascaux (16,000 BP) and Ekain (Spain) were analysed in order to evidence preparation techniques of painting matter (paint pots) and its way of application. Formula using mineral as "charge" in pigment were brought to the fore (Chalmin et al. 2003).

In some of the paint matter, phosphorus and calcium have been found as minor constituents. The presence of this couple of characteristic elements of hydroxylapatite has suggested that crushed bone or antler was used as "charge" to give thickness to painting matter. The use of osseous tools to work the colouring mixture was suggested too.

TEM micrographs (Fig. 8a, b) of two Lascaux pigment samples show, next to the Fe and Mn oxides, Ca and P bearing nanocrystals. The comparison of the crystal features at nanoscale of bone, antler, dentine and the mineral P-containing phase in the Lascaux pigments aims at identifying its nature in the pigment mixture.

For this reason, the crystallinity of archaeological and palaeontological bones, dentines and antler was compared by means of different techniques: XRD, FTIR, SEM-EDX and also with PIXE-PIGE and TEM-EDX (Reiche et al. 2002b;

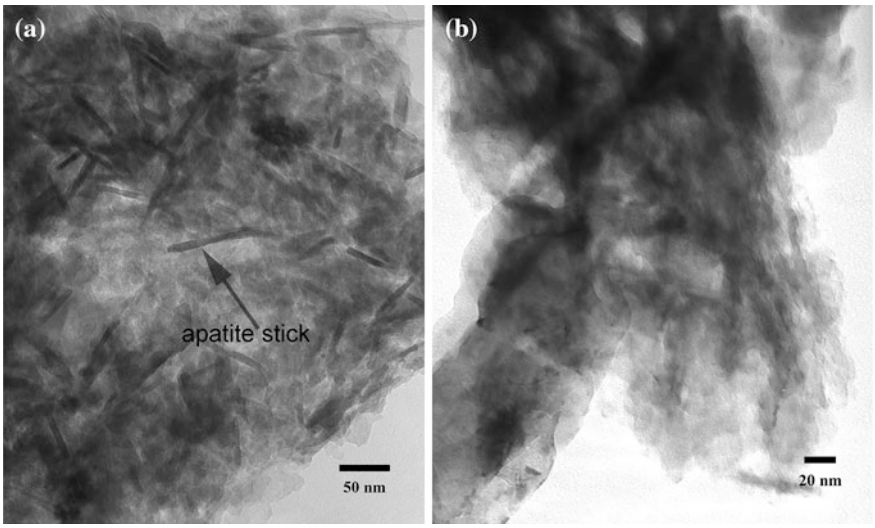

Fig. 8 Transmission electron micrographs of two pigment samples **a** GLAS 62 (brown horse from the "Salle des taureaux") and **b** 67 (red and black horse from the "Diverticule axial") from the Lascaux cave bearing some apatite sticks possibly originating from antler traces mixed to the pigments. Adapted from Chadefaux et al. (2008a, b)

Chadefaux et al. 2008a, b). TEM-EDX analysis of the nanocrystals was the method of choice. Besides the investigation of the crystal characteristics, TEM-EDX analysis permits differentiating bone apatite and mineral fluorapatite thanks to the identification of fluorine peak and to quantify the Ca/P ratio.

No significant difference in the chemical composition of altered archaeological bone, reindeer antler or dentine was found. However, crystallinity characterisation shows differences between the features of different archaeological osseous materials at nanoscale. These different features could be used to specify most likely archaeological reindeer antler traces in pigments from Lascaux cave (Chadefaux et al. 2008b). Indeed, sticks with a width of about 7 nm and a length of about 80 nm were observed that show the electron diffraction patterns of apatite. The crystal size is intermediate between modern and very altered reindeer antler found in the Magdalenian reindeer antler fragments.

These observations are consistent with the fact that tools made of reindeer antlers were found in the Lascaux cave (Leroi-Gourhan and Allain 1979). Indeed, the small quantity of calcium and phosphorus measured in the samples may be considered as a pollution, which comes from working the pigments with antler tools. In this case, the fact to find reindeer antler traces in the pigment would not be a deliberate addition by the prehistoric artist to prepare painting matter but more likely pollution. We can imagine that painting and sculpture on bone materials took place in neighbouring or common sites. Nevertheless, the presence of antler in several paint pots allows definiting a “chronological” marker of figures made in a similar period of time. With the absence of absolute dating of the prehistoric figures in the Lascaux cave, this fact give important new possibilities to distinguish the material used for different figures. These markers allow classifying different prehistoric representations and represent also relative chronological marker that can help to decide whether one or several hands painted them in the Lascaux cave.

6.1.2 Identification of the Raw Materials for the Production of Prehistoric Ornaments

The use of biominerals to produce ornaments is a distinctive human behavior that emerges in Europe in the early Upper Palaeolithic (Mellars 1989a, b; White 1995, 2006; Taborin 2004; Vanhaeren et al. 2006; Stiner et al. 2013; Christensen 2004; Christensen and Tejero 2015; Tejero et al. 2012). The exact identification of the raw material used for the manufacture of ancient objects, especially for prehistoric periods, is the basis to get insights into archaeological key questions as availability and circulation of materials, technological capabilities of man in ancient societies, as well as symbolic meanings of the objects. Even if the material identification can, often, easily be made on the basis of macro-morphological characteristics, the identification can be tricky, when the objects are very small or their surfaces have been heavily worked.

This is the case for a specific type of beads excavated from the Final Gravettian level (level 2) of the Abri Pataud (Dordogne, France). Some uncertainty remained about the raw material in which these small beads were made: mammoth ivory,

reindeer antler or bone. If ivory could be identified as raw material, the exceptional status of the beads found in Southern France would be emphasized, as ivory is rare among the findings and mammoths didn't live, to our knowledge, in this region at that time period. A large assemblage of body ornaments that consists essentially of 85 quite standardized rectangular beads was found there. Due to their association with the human remains of level 2, these rectangular beads could be considered, like other "extraordinary" objects, as mortuary deposits (Chiotti et al. 2009). Non-invasive methods were employed in order to determine the raw material: microbeam Proton Induced X-ray Emission analysis (micro-PIXE) as well as synchrotron and laboratory X-ray microtomography (micro-CT).

The chemical approach was based on chemical markers for ivory identification, defined thanks to a micro-PIXE database comprising about 150 objects (modern and archaeological ivory, bone and antler) (Müller and Reiche 2011). However, these chemical markers can be used for the determination of well-preserved objects but cannot be applied for clear identification of diagenetic altered archaeological objects. For this reason, the chemical distinction markers did not enable us to identify the raw material used for the manufacture of the Palaeolithic beads.

Assuming that micro-morphology is less sensitive to diagenetic changes, morphological characteristics for distinction purposes have been studied by means of micro-CT (Reiche et al. 2011b). The micro-CT study allowed establishing distinctive features of modern references of ivory, antler and bone. Tubular pores of about 1–2 µm in diameter are characteristic for ivory, whereas bone and antler show typical osteon structures ranging from 100–500 µm in diameter. Size and shape of the osteons differ between bone and antler and depend strongly on the original localization of the studied sample within the antler. In addition, micro-CT enables the comparison of inner and possibly less altered parts of the objects. By studying archaeological osseous samples from the permafrost as well as determined Palaeolithic fragments from the Abri Pataud, it could be shown that the observed micro-morphological characteristics were preserved even for Palaeolithic diagenetically altered osseous materials. The established parameters were applied on eight beads analysed by synchrotron micro-CT and allowed us to identify ivory for all of them except for one, which shows slightly different morphological features. The micro-CT analyses confirm that most rectangular beads are made of mammoth ivory. Given the fact that mammoth ivory is rare in level 2 of Abri Pataud, whereas bones and reindeer antler are very abundant, this study demonstrates the exceptional status of this type of beads not only because of their archaeological context, but also due to the choice of raw material for their manufacture (Vercoutère et al. 2011).

6.2 Working Techniques

As illustration of the possible insights that can be gained from studying phosphate-based biominerals, the study of Palaeolithic beads from three French

Gravettian key sites in South-western France is discussed here, besides the identification of the used raw material. It will be emphasized that there may be additionally a relationship between shape and function of these body ornaments. A second example of the study of working techniques concerns the study of surface traces of ivory carvings to understand ancient decoration technology.

6.2.1 Insights into the Relationship of the Employed Raw Material, the Shape and the Functon of Body Ornaments

The use of biominerals in the production of art and ornaments is a subject of much interest in studies of the Upper Palaeolithic. Material characteristics such as mechanical properties, colour, shape and use-wear are important clues to test hypotheses about the use and symbolic function of Palaeolithic ornaments.

Similar rectangular beads as those found at Abri Pataud (Vercoutère et al. 2011; Chiotti et al. 2014; Reiche et al. 2014) have been discovered in two additional French sites known for the Final Gravettian period: at the rock shelter of Les Peyrugues (Allard et al. 1997; Rodière 2011) and at the site of Le Blot (Chauvière and Fontana 2005). A closer look at these ornaments explains the difficulty of raw material identification and of the study of their use. All beads are relatively small and polished and most of them are varnished today for conservation purposes. The primary feature they share is the central circular perforation. Despite their similarity the beads do show some variation in shape and surface-features. The beads are sometimes rectangular and sometimes more or less oval in outline. They variably show convex and flat surfaces and the presence or absence of incisions next to the central circular perforation. Some of the beads seemed to be made of mammoth ivory, but we couldn't exclude the use of reindeer antler or/and bone, because these raw materials have been previously proposed for the beads found at Les Peyrugues (Allard et al. 1997) and Le Blot (Chauvière 2012; Chauvière and Fontana 2005).

Therefore, a study was devoted to investigate the relationship between the possible use, and status of beads from three key sites of the French Gravettian, through comparative analysis of the raw materials used and morphological characteristics of the beads. A selected set of beads was studied by micro-CT and SEM analysis (Reiche et al. 2014). This analytical approach was also combined with experimentation to simulate the production process.

Four steps of the *chaine opératoire* have been tested: (1) shaping, (2) perforation, (3) segmenting and (4) polishing (Rodière 2011).

Concerning the bead shapes and dimensions, it could be shown that besides a very high degree of standardisation two types of bead can be distinguished: beads with a central symmetric perforation and two convex sides as well as beads with one flat and one convex side presenting an asymmetric perforation combined with a concentric depression surrounding the perforation from the convex side and an incision on the flat side (Fig. 9).

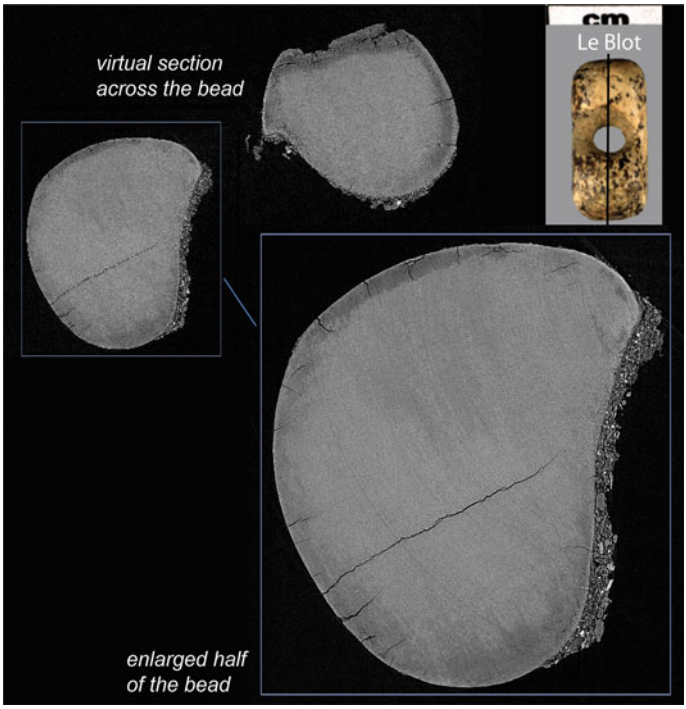

Fig. 9 Micro-X-ray CT virtual section of the Gravettian bead from Le Blot site, Dordogne, France

According to first experimental reproductions, the Abri Pataud and Le Blot beads (flat/convex beads) on the one hand have similar dimensions but are different in shape with respect to Les Peyrugues beads (two convex sides) on the other hand. The production process is slightly different although both processes start form a rod. The perforation is produced either symmetrically from both sides (two convex sides) or preferentially from one side (flat/convex beads). Flint tools have been tested and seemed appropriate. This surface could have been gouged out starting from the former shape and reducing its thickness. In both cases the perforation seems to be performed by semi-rotation of $\sim 120°$. After the delicate perforation step the beads were cut from the rod and polished, possibly with hematite powder.

The raw material identification performed by means of micro-CT at the BAM*line*, at the synchrotron source BESSY II (HZB Berlin, Germany) showed that the bead types defined as a function of their shape corresponds to the classification in terms of the used raw material. The beads with two convex sides are made of antler, possibly reindeer antler, whereas the beads with a convex and a flat side are made of ivory, in the context of mammoth ivory without any exception (Fig. 10). The type of biomineral could be identified thanks to the observation of internal micro-morphological features such as primary Haversian systems for antler and microtubular structure for ivory (Reiche et al. 2011b).

Fig. 10 Examples of two beads from Abri Pataud, Dordogne, France exemplifying the two types of Gravettian rectangular beads observed, *left* with one flat and one round-shaped side and a preferential perforation from the round shaped side and *right* with two round-shaped sides and a symmetric bi-perforation

It was, additionally, interesting to check if there may be a relationship between the type of the beads and their usage. If such a relationship was found, it could be indicative of a deliberate choice of raw material for the production of body ornaments with a specific status and function. On the basis of the above mentioned observations two different usages could be hypothesized: (1) the beads with two convex sides could be used for necklaces and (2) the other type with the incision in the flat side could be sewed on clothes. In those cases, antler would be used to produce beads for necklaces while ivory would rather be used for the production of ornaments that were sewed on clothes. Further investigations on more numerous beads including surface and use wear analyses as well as experimental reproductions are necessary in order to confirm these first hypotheses (Reiche et al., accepted).

6.2.2 Evidencing Traces of Gilding and Polychromy at the Surface of Phoenician Ivories from Northern Syria (8th c. BC, Syria)

A selection of Phoenician carved ivories excavated at Arslan Tash (Syria), a neo-Assyrian site dating from the 8th century BC, was studied to evaluate the preservation state and to identify the original polychromy. Analogously to neo-Assyrian stone objects, these ivories must have been very colourful (Veri et al. 2009). The objects have been altered due to diagenetic processes during burial, change of environmental conditions when excavated, display and storage in the museums as well as restoration treatments. Today, no visible traces of the original colours are left. The revealing of the original object's appearance is fundamental to better understand the manufacturing technique, the purpose of use for specific objects in order to place them properly in their historical context.

A total of 16 carved ivories of the Département des Antiquités orientales, Musée du Louvre (Paris, France), have been analysed by means of optical microscopy, UV photography, X-ray radiography and micro-PIXE imaging (Fontan and Reiche 2011; Albéric et al. 2015). Additionally, 13 objects kept in the Badische Landesmuseum (Karlsruhe, Germany) could be studied by Full Field Synchrotron micro X-Ray Fluorescence (FF-SR-μXRF) with a new 3D imaging X-ray detector, the Colour X-ray Camera (CXC) at the synchrotron facility ANKA

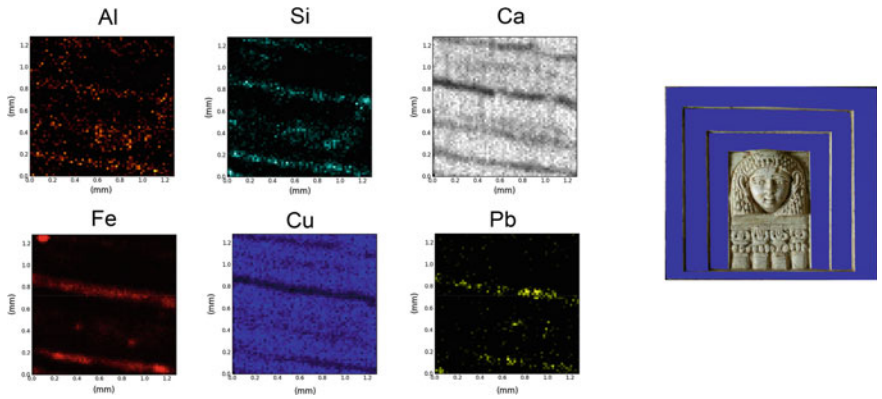

Fig. 11 Chemical maps of Al, Si, Ca, Fe, Cu and Pb indicating trace element distributions at the carving surface of the "Woman at the window" (DAO, Louvre museum, Inv. No. AO 11459) allowing the reconstruction of former polychrome decorations. Cu is possibly indicative of *blue* or *green* pigments such as Egyptian *blue* or *green*

(Karlsruhe, Germany). Full Field-SR-μXRF enabled us to record the elemental distribution of a large area (12.4 × 11.3 mm^2) in 2D elemental maps indicating zones of former coloration (Reiche et al. 2013). The objects are in general well preserved, apart from some cracks, purple stains, black spots correlated to the deposition of MnO_2. The enrichment of several other trace elements (Al, Si, Ti, Fe, Cu, Pb and Au) was detected in respective areas. Al, and Si come surely from sediment residues, but possibly also Ti and Fe. Ti can also refer to restoration treatments. Pb, Cu and Fe can be correlated to pigment residues. Generally, a homogenous distribution of the element ratios may indicate the presence of a former pigment. Over well-defined areas homogeneously distributed Fe and Cu traces in enhanced concentrations were observed and can be considered as pigment residues of the original polychromy (Fig. 11). Iron can presumably be associated to a red pigment (Fe_2O_3) and Cu is likely linked to a blue pigment, copper azurite $2CuCO_3$ as $Cu(OH)_2$ or Egyptian blue containing mainly cuprovivaïte ($CaCuSi_4O_{10}$). Several objects exhibit two different surface alteration states (well preserved and scratched or rugged surfaces). In all cases the altered area presents increased Cu amounts compared to the well-preserved area. It is thinkable that, the presence of the pigment (and binder) facilitated the deterioration of the ivory surface. The underlying processes remained unexplained so far.

The purple stains could be associated with Au traces, probably residues of original gildings. Gold could be identified in the form of nanoparticles (AuNPs). A detailed study of the possible chemical formation process of AuNPs showed that the collagen originating from the ivory or the glue used to fix the gold on the ivory surface supported the formation of these nanoparticles even at low temperatures through a mechanism implying the formation of hybrid collagen-AuNPs. The collagen stabilizes the dissolved Au ions that form colloids on the nanocrystalline

apatite mineral surface of altered ivory. Therefore, these purple stains are indicative of former gilded parts of the carved ivory surface. Additionally, the appearance of such purple stains can be used as a non-invasive authentication criterion, as this process is not yet completely understood and the ancient gilded ivory carvings must have, in principle, been buried for a relatively long time so that the purple stains are formed. Additionally, reproduction seems difficult (Spadavecchia et al. 2014).

6.3 Heat-Induced Transformations

Evidencing unambiguously traces of an intentional heat process is a very important issue in archaeology and prehistory. Therefore, the study of structural markers induced by heat-induced changes at different length scales of the biominerals is crucial for archaeological interpretations of human activities at a given time period. Because of the importance of these questions, the next section is devoted to two studies that highlight the potential information and the analytical difficulties linked with heat-induced transformations of biominerals.

6.3.1 Heat-Induced Changes of Archaeological Bone and Archaeological Implications on the Detection of Fire and Cooking

Traces of heating observed on bone remains and artefacts are often attributed to cremations, cooking, fuel use or naturally occurring fires (Gifford 1981; Weiner and Wagner 1998; Cain 2005; Pijoan et al. 2007; Asmussen 2009; Gonçalves et al. 2011). The determination of the heating temperature plays a key role in these studies because it can be related to the kind of heating process. A first (major) complication consists in distinguishing burnt bone from diagenetically altered remains (Nicholson 1996; Shahack-Gross et al. 1997). Secondly, it is important to distinguish intentional heating effects (e.g. due to cooking) from non-intentional ones, which may have occurred following burial (Bennett 1999) or other causes of fire (Asmussen 2009). This implies that even when the observations can unambiguously be attributed to anthropogenic heating effects, it can still be difficult to conclude whether or not the process was intentional. Finally, many subtle anthropological questions require more in-depth analysis, e.g. to distinguish between various modes of heating for cooking (Koon et al. 2003, 2010).

Several qualitative criteria have extensively been used to identify heating temperature and effects: the presence of colour modifications, mass or volume fluctuations and changes in mechanical properties (with respect to modern bone) as an increased brittleness, reduced hardness, presence of fractures (Correia 1996). However, taken individually, such criteria are often insufficient. More holistic approaches need to be considered, taking into account a broad collection of metrics (Thompson 2004). This lead to the derivation of four stages of heat-induced

damages roughly corresponding to somewhat overlapping heating temperature ranges (100–600, 300–800, 500–1100 and >700 °C), each stage being associated with specific changes of above mentioned properties (Castillo et al. 2013). From a materials science point of view, this only provides limited insight into the causes and mechanisms leading to bone degradation upon heating. The weakness of such approaches essentially lies in the delicate choice of the parameters used to characterize the heating effects included in the statistical analysis. Clearly, owing to the structural complexity of bone multi-scale analytical approaches from the macroscopic to the nanoscopic scale are required. Moreover, model systems generally need to be analysed in combination with archaeological material to account for possible concomitant diagenetic changes.

Many studies were thus undertaken to clarify this matter by analysing changes in bone structure and properties upon controlled (artificial) heating in, both, field or laboratory conditions using a wide range of characterization methods (Shipman et al. 1984; Holden et al. 1995; Person et al. 1996b; Rogers and Daniels 2002; Piga et al. 2013; Hiller and Wess 2006; Munro et al. 2007; Lebon et al. 2010). A detailed review of the changes observed is beyond the scope of this chapter (see, e.g. Ellingham et al. 2015b) as a wide variety of bones from different human/animal origin and anatomical sites were used. Also, whilst the temperature is always clearly indicated, the heating conditions (duration, heating rate, atmosphere) vary strongly. Nevertheless a series of rough indications can be derived for dense (cortical) defleshed (but still hydrated) bone samples typically collected from long bones (femur, tibia): the weight loss, mainly associated with the loss of water, increases following a quadratic trend from 5 $\%_w$ at 100 °C to 30 $\%_w$ at 300 °C and reaches a plateau of 35–40 $\%_w$ at 400 °C (Kalsbeek and Richter 2006). This is associated with a progressive denaturation of the collagen followed by degradation at $\sim$400 °C (Nielsen-Marsh et al. 2000; Bozec and Odlyha 2011) and, consequently, to a significant drop in hardness (Kalsbeek and Richter 2006) and fragility (Stiner et al. 1995). Interestingly, the macroscopic shape and sample histology is found to be relatively well conserved up to $\sim$400 °C, albeit with traces of contamination (ashes and carbon deposition) in the Haversian porosity (Hanson and Cain 2007). In the above mentioned samples, the duration of heating is approximately 1 h and the time necessary to reach the temperature is assumed to be in the order of seconds.

In addition to monitoring collagen changes upon heating at the nanoscale (e.g. using TEM, Richter 1986) and molecular levels [with FTIR spectroscopy (Ellingham et al. 2015a; Lebon et al. 2008; Shahack-Gross et al. 1997; Squires et al. 2011; Thompson et al. 2009, 2011)], many studies were devoted to assess changes in mineral nanocrystal organization (Wess et al. 2002; Hiller et al. 2003; Gourrier et al. 2011a) and crystallographic structure (Person et al. 1996b; Enzo et al. 2007; Rogers et al. 2010; Rogers and Daniels 2002; Piga et al. 2008, 2013). Oddly, while the collagen structure undergoes important denaturation processes before degrading at $\sim$400 °C, a vast majority of experiments point to the quasi-systematic absence of changes in the mineral properties below this temperature. Recently, an extensive combination of physico-chemical analysis showed that there were indeed significant structural changes at those temperatures, most of which occurring at the nanoscale

and, thus, difficult to detect (Chadefaux and Reiche 2009). Based on the TEM results, which indicated an increase in nanocrystal size, new measurements were conducted using Synchrotron Small-Angle X-ray Scattering (SAXS) and X-ray Diffraction (XRD) methods. Those new results revealed a two-fold increase in nanocrystal thickness at 300 °C for thin sample sections (100 µm) heated during 1 h (Gourrier et al. 2011a), which confirms previous TEM findings, but contradicts most XRD studies. This showed that SAXS was the most efficient tool to describe the nanocrystal increase in thickness and organization over statistically significant volumes at low heating temperatures (Fig. 12).

An important conclusion to be drawn from this case study: while SAXS had not originally been included in the structural measurement sequence, the multiscale approach adopted by Chadefaux et al. (Chadefaux and Reiche 2009) allowed identifying key markers of heating on bone at the nanoscale. From this global, statistical analysis of fundamental structural parameters (i.e. objective criteria), more appropriate tools were identified (in particular SAXS) to better characterize

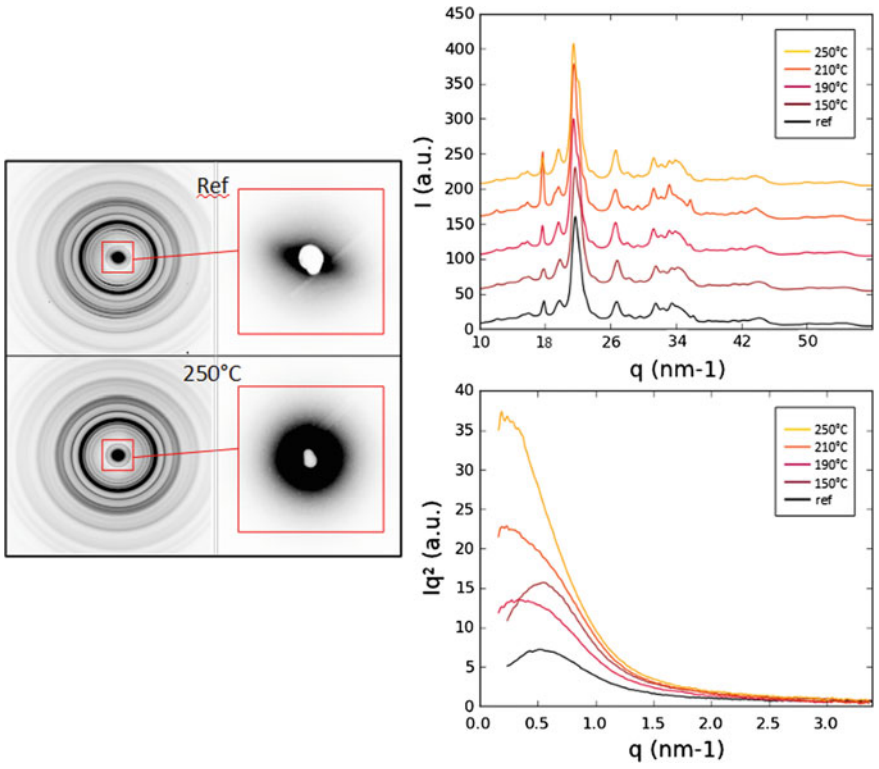

Fig. 12 2D XRD pattern (*left*) of unheated (*top*) and heated bone at 250 °C (*bottom*) with the SAXS region show by the corresponding *red insets*. 1D radial profile of the XRD (*center*) and SAXS (*right*) regions as a function of temperature

heat-induced changes at low temperatures. Since many cooking or tool manufacturing procedures could very well fall within this range, this strategy opens new possibilities for related archeological, paleontological and forensic studies.

6.3.2 Evidencing of Accidential or Intentional Heating for Special Techniques of Production of Body Ornaments Made of Shells

The Franchthi Cave is a key archaeological site in Greece with a unique continuous series of archaeological layers spanning from probably earlier than 20,000 years BC to ca 3000 years BC. The prehistoric site is located in the south-eastern Argolid, in a small bay next to the modern Greek village of Koilada, and yielded an exceptionally rich collection of personal ornaments, which belongs to the oldest known in Europe. Excavation at the site began in 1967 and ended in 1976. The deepest sounding in the cave is in Trench F/A (over 11 m of stratified living debris); the earliest homogeneous cultural deposits yet found (of the Upper Palaeolithic period) come from Trench H/H1 at a depth of 9 m.

The archaeological reassessment of this category of material culture at the site of Franchthi Cave A performed by Catherine Perlès and Marianne Vanhaeren showed that shells *Cyclope Neritea* were perforated and were used for the production of body ornaments in the Palaeolithic and Mesolithic period.

The gastropod *Cyclope Neritea* is a seashell very frequent in the Mediterranean and the Black sea. The shell is living in mudflat on lower cost level. The shell is of about 1 cm in diameter and presents on the dorsal face pastel colours ranging from brown, green to orange and in the ventral face, which is very polished an ivory colour. The composition of the carbonate phase of *Cyclope Neritea* shell is 98.4 wt % of aragonite with 1.6 % of calcite.

Besides naturally coloured beads, some of the beads showed a dark-brown colour in the archaeological record. This finding led to the hypothesis that one type of personal ornaments, i.e. marine shell beads belonging to the species *Cyclope neritea*, were intentionally heated to change their natural whitish colour to black. In order to identify possible diagnostic criteria for intentional heating, a small selection of archaeological beads as well as experimental beads were studied. The reference shells were modern *Cyclope neritea* shells, one of which unmodified, the other experimentally blackened through heating with additional organic material. The two archaeological specimens studied were one presenting a natural whitish colour and another black one. All these beads were submitted to complementary analytical methods: optical (OM) and SEM-EDX, FTIR and micro-Raman spectroscopy as well as Differential Scanning Calorimetry (DSC) in order to identify structural and composition differences of the beads as a function of aging and heat-induced modifications.

Results show that heated black shells can be differentiated based on their microstructure and chemical phases present from the unheated modern and archaeological shells. The modern and archaeological whitish shells are composed

of aragonite with some traces of colorant found for the modern white shell. The blackish experimental and archaeological shells in contrast are composed of calcite and present additionally a black C-based compound, namely a compound similar to black graphite as revealed by Raman spectroscopy (Fig. 13). This means that the black archaeological shell positively matches the modern shell blackened through heating. Heating tests showed that the temperatures needed to transform shell

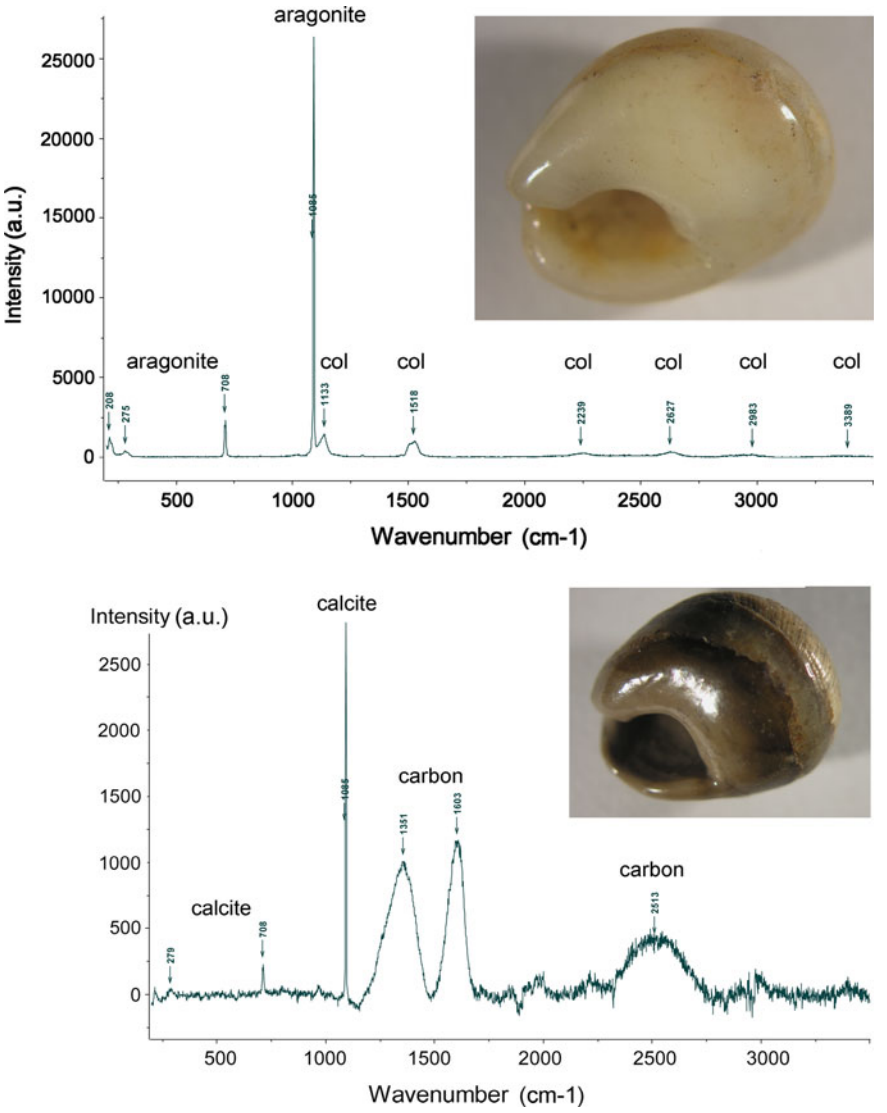

Fig. 13 Micro-Raman spectra of a *white* unburnt and a *black* burnt archaeological shell *Cyclope Neritea* from the site of Franchthi, Argolid, Greece

aragonite into calcite are relatively low in the range of 280 °C. Identification of the limited conditions meaning in the presence of a large amount of organic matter, in which blackening through heating occurs, further supports a special heat-treatment for *Cyclope neritea* shells at Franchthi Cave. Indeed reducing atmosphere is needed to produce black carbon remains during the heat process of the shells. The reducing conditions could be obtained by adding organic material such as tree leaves.

This discovery emphasized the fact that the black shells were intentionally heated because special heating conditions needed to be created in order to obtain the wished result of blackening of the shells. Accidental heating would more likely lead to shells with irregular blackening or even a completely whitish colour (Lange et al. 2008; Perlès and Vanhaeren 2010).

7 Conclusions and Perspectives

In this chapter the importance of biominerals as archaeological archives was highlighted. It also emphasized the relevance of considering these highly structured nanocomposite materials at different length scales. Much new information can be gained from their comprehensive study in this way. Particularly invaluable information on ancient working techniques, acquisition and circulation strategies, heating and boiling and in general on ancient ways of life can be obtained, if additionally diagenetic and taphonomic changes that can hamper the understanding of these processes, are properly taken into account.

We can benefit from these naturally altered biominerals and use them as a "natural laboratory" to study their durability over time. Such long-term experiments cannot be directly performed in the laboratory and their behaviour upon aging is, at best, approximated under relatively aggressive chemical and physical modifications (e.g. heating, light, atmospheric gases, cyclic loading etc.). In addition, in the case of archaeological materials, the interplay between the different aging factors is too complex to be analysed in a controlled manner. For the evaluation of the durability of the biominerals, models need to be established, which however never completely reflect the natural or biological conditions. Therefore, archaeological biominerals provide a unique opportunity to study alteration phenomena without applying artificial conditions.

Although archaeological biominerals are precious witnesses of our past, adequate conservation strategies are still lacking. Indeed, they may be sensitive to micro-cracking and powdering for very extreme degradation. As the open porosity of this material is generally very poor, it is very difficult to identify resin formula able to diffuse efficiently in the matrix. The main protocols currently available are usually limited to simple surface treatments. Therefore, there is a real need for designing new practical conservation measures for these materials. Key material features that are beneficial for a good preservation over time could be deduced from these spatially resolved studies and may allow designing new conservation

treatments of the archaeological objects as well as inspiring new concepts for modern materials design used in an "archaeo-mimetic" approach.

Indeed, the field of biomimetics studies the engineering of new bio-inspired materials based on the study of biological materials as bone, trees, seashells, sponges, spider silk (Fratzl 2004, 2007). As shown in this chapter nature has developed materials with remarkable properties albeit with a limited set of widely available constituents using different strategies. In a way to make the most of the remarkable properties of biominerals, structure-function relations are very interesting subjects to be studied in detail to be able to use the exceptional properties to design new bio-inspired materials (Fratzl 2007; Currey et al. 1994; Nalla 2003).

References

Addadi L, Weiner S (2001) Biomineralization: crystals, asymmetry and life. Nature 411:753–755

Albéric M, Dean MN, Gourrier A, Wagermaier W, Dunlop JWC, Staude A, Fratzl P, Reiche I (accepted) Relation between the macroscopic pattern of elephant ivory and its three-dimensionsal micro-tubutlar network. PLOS ONE

Albéric M, Gourrier A, Müller K, Zizak I, Wagermaier W, Fratzl P, Reiche I (2014) Early diagenesis of elephant tusks in marine environment. Palaeogeogr Palaeoclimatol Palaeoecol 416(1):120–132

Albéric M, Müller K, Pichon L, Lemasson Q, Moignard B, Pacheco C, Fontan E, Reiche I (2015) Non-invasive quantitative micro-PIXE-RBS/EBS imaging reveals the lost polychromy and gilding of the Neo-Assyrian ivories from the Louvre collection. Talanta 137:100–108

Allard M, Drieux M, Jarry M, Pomies MP, Rodière J (1997) Perles en bois de renne du niveau 18 des Peyrugues, à Orniac (Lot): hypothèse sur l'origine du protomagdalénien. Paléo 9:355–369

Ambrose SH (1991) Effects of diet, climate and physiology on nitrogen isotope abundances in terrestrial foodwebs. J Archaeol Sci 18:293–317

Anne J, Edwards NP, Wogelius RA, Tumarkin-Deratzian AR, Sellers WI, van Veelen A, Bergmann U, Sokaras D, Alonso-Mori R, Ignatyev K, Egerton VM, Manning PL (2014) Synchrotron imaging reveals bone healing and remodelling strategies in extinct and extant vertebrates. J R Soc Interface 11(96):20140277. doi:10.1098/rsif.2014.0277

Arjmandi BH, Juma S, Beharka A, Bapna MS, Akhter M, Meydani SN (2002) Vitamin E improves bone quality in the aged but not in young adult male mice. J Nutr Biochem 13(9):543–549

Asmussen B (2009) Intentional or incidental thermal modification? Analysing site occupation via burned bone. J Archaeol Sci 36(2):528–536

Backwell L, d'Errico F (2008) Early hominid bone tools from Drimolen, South Africa. J Archaeol Sci 35(11):2880–2894. doi:10.1016/j.jas.2008.05.017

Backwell L, d'Errico F, Wadley L (2008) Middle stone age bone tools from the Howiesons Poort layers, Sibudu Cave, South Africa. J Archaeol Sci 35(6):1566–1580. doi:10.1016/j.jas.2007.11.006

Bailey R, Wijngaarden Jv (2015) The role of B-vitamins in bone health and disease in older adults. Curr Osteoporos Rep 13(4):256–261

Balasse M, Tresset A (2002) Early weaning of Neolithic domestic cattle (Bercy, France) revealed by intra-tooth variation in Nitrogen isotopes ratios. J Archaeol Sci 29:853–859

Balasse M, Bocherens H, Mariotti A, Ambrose SH (2001) Detection of dietary changes by intra-tooth carbon and nitrogen isotopic analysis: an experimental study of dentine collagen of cattle (Bos taurus). J Archaeol Sci 28:235–245

Balasse M, Brugal J-P, Dauphin Y, Geigl E-M, Oberlin C, Reiche I (2015) Message d'os. Archéométrie du squelette animal et humain. Collection «Sciences Archéologiques». Editions des archives contemporaines, Paris

Banks WJ (1974) The ossification process of the developping antler in the white-tailed deer (Odocoileus virginianus). Calc Tiss Res 14:257–274

Baohua J, Gao XJ (2004) Mechanical properties of nanostructure of biological materials. J Mech Phys Solids 52(9):1963–1990

Bartsiokas A, Middleton AP (1992) Characterization and dating of recent and fossil bone by Xray diffraction. J Archaeol Sci 19:63–72

Baud CA, Tochon-Danguy HJ (1985) Les caractéristiques physico-chimiques de l'ivoire et leurs modifications par traitement thermique. Bulletin l'association pro Aventico 29:49–52

Bennett JL (1999) Thermal alteration of buried bone. J Archaol Sci 26:1–8

Benzerara K, Miller VM, Barell G, Kumar V, Miot J, Brown GE Jr, Lieske JC (2006) Search for microbial signatures within human and microbial calcifications using soft X-ray spectromicroscopy. J Investig Med 54(7):1–15

Bergmann U, Morton RW, Manning PL, Sellers WI, Farrar S, Huntley KG, Wogelius RA, Larson P (2010) Archaeopteryx feathers and bone chemistry fully revealed via synchrotron imaging. Proc Natl Acad Sci USA 107(20):9060–9065. doi:10.1073/pnas.1001569107

Berna F, Matthews A, Weiner S (2004) Solubilities of bone mineral from archaeological sites: the recrystallization window. J Archaeol Sci 31(7):867–882. doi:10.1016/j.jas.2003.12.003

Bertrand L, Bernard S, Marone F, Thoury M, Reiche I, Gourrier A, Sciau P, Bergmann U (submitted) Emerging approaches in synchrotron studies of materials from cultural and natural history collections. Top Curr Chem

Betts F, Blumenthal NC, Posner AS (1981) Bone mineralization. J Cryst Growth 53(1):63–73

Bocherens H, Fizet M, Mariotti A (1994) Diet, physiology and ecology of fossil mammals as inferred from stable carbon and nitrogen isotope biogeochemistry: implications for Pleistcene bears. Palaeogeogr Palaeoclimatol Palaeoecol 107:213–225

Bocherens H, Drucker DG, Billiou D, Geneste J-M, Jvd Plicht (2006) Bears and humans in Chauvet Cave (Vallon-Pont-d'Arc, Ardèche, France): insights from stable isotopes and radiocarbon dating of bone collagen. J Hum Evol 50(3):370–376. doi:10.1016/j.jhevol.2005.12.002

Bocherens H, Polet C, Toussaint M (2007) Palaeodiet of Mesolithic and Neolithic populations of Meuse Basin (Belgium): evidence from stable isotopes. J Archaeol Sci 34:10–27

Boivin G, Chapuy M-C, Baud CA, Meunier PJ (1988) Fluoride content in human iliac bone: results in controls, patients with fluorosis, and osteoporotic patients treated with fluoride. J Bone Miner Res 3(5):497–502

Bozec L, Odlyha M (2011) Thermal denaturation studies of collagen by microthermal analysis and atomic force microscopy. Biophys J 10(1):228–236

Buckley M, Walker A, Ho SY, Yang Y, Smith C, Ashton P, Oates JT, Cappellini E, Koon H, Penkman K, Elsworth B, Ashford D, Solazzo C, Andrews P, Strahler J, Shapiro B, Ostrom P, Gandhi H, Miller W, Raney B, Zylber MI, Gilbert MT, Prigodich RV, Ryan M, Rijsdijk KF, Janoo A, Collins MJ (2008) Comment on "Protein sequences from mastodon and Tyrannosaurus rex revealed by mass spectrometry". Science 319(5859):33; author reply 33. doi:10.1126/science.1147046

Buckley M, Whitcher Kansa S, Howard S, Campbell S, Thomas-Oates J, Collins M (2010) Distinguishing between archaeological sheep and goat bones using a single collagen peptide. J Archaeol Sci 37(1):13–20. doi:10.1016/j.jas.2009.08.020

Budd P, Montgomery J, Barreiro B, Thomas RG (2000) Differential diagenesis of strontium in archaeological human dental tissues. Appl Geochem 15:687–694

Cain CR (2005) Using burned animal bone to look at Middle Stone Age occupation and behavior. J Archaeol Sci 32(6):873–884

Carter DR, Beaupré GS (2007) Skeletal function and form. Mechanobiology of skeletal development, aging, and regeneration. Cambridge University Press, Cambridge

Castillo RF, Ubelaker DH, Acosta JAL, Rosa RJE, Garcia IG (2013) Effect of temperature on bone tissue: histological changes. J Forensic Sci 58(3):578–582

Caubet A, Gaborit-Chopin D (2004) Ivoires. Réunion des Musées Nationaux, Paris

Chadefaux C, Reiche I (2009) Archaeological bone from macro- to nanoscale. Heat-induced modifications at low temperatures. J NanoResearch 8:157–172

Chadefaux C, Vignaud C, Menu M, Reiche I (2008a) Effects and efficiency of consolidation treatments on Palaeolithic reindeer antler. Multi-analytical study by means of XRD, FT-IR microspectroscopy, SEM, TEM and μ-PIXE/PIGE analyses. Appl Phys A 92:171–177. doi:10.1007/s00339-008-4469-3

Chadefaux C, Vignaud C, Menu M, Reiche I (2008b) Multianalytical study of Palaeolithic reindeer antler. Discovery of antler traces in Lascaux pigments by TEM. Archaeometry 50:516–534

Chadefaux C, Le Hô A-S, Bellot-Gurlet L, Reiche I (2009a) Micro-ATR-FTIR studies combined with curve fitting of the amide I and II bands of type I collagen in archaeological bone materials. epreservation Science 6:129–137

Chadefaux C, Vignaud C, Chalmin E, Robles-Camacho J, Aarroyo-Cabrales J, Johnson E, Reiche aI (2009b) Color origin and heat evidence of paleontological bones: case study of blue and gray bones from San Josecito Cave, Mexico. Am Mineral 94:27–33

Chalmin E, Menu M, Vignaud C (2003) Analysis of rock art painting and the technology of Palaeolithic painters. Meas Sci Technol 14:1590–1597

Chapman DI (1981) Antler structure and function—a hypothesis. J Biomech 14(3):195–197

Chauvière F-X (2012) Objets d'ici et d'ailleurs: les industries osseuses du Paléolithique supérieur du Blot (Cerzat, Haute-Loire). Bulletin Préhistorique du Sud-Ouest 20(1):55–77

Chauvière F-X, Fontana L (2005) Modalités d'exploitation des rennes dans le Protomagdalénien du Blot (Haute-Loire, France): entre subsistance, technique et symbolique. In: Industrie osseuse et parures du Solutréen au Magdalénien en Europe—table ronde sur la paléolithique supérieur récent, Angoulême (Charente). Société Préhistorique Française, pp 137–147

Chen X, Nadiarynkh O, Plotnikov S, Campagnola PJ (2012) Second harmonic generation microscopy for quantitative analysis of collagen fibrillar structure. Nat Protoc 7(4):654–669

Chiotti L, Nespoulet R, Henry-Gambier D, Morala A, Vercoutère C, Agsous S, Lenoble A, Marquer L, Grimaud-Hervé D (2009) Statut des objets "extra-ordinaires" du Gravettien final de l'abri Pataud (Les Eyzies, Dordogne): objets abandonnés dans l'habitat ou dépôt intentionnel? In: Bonnardin S, Hamon C, Lauwers M, Quilliec B (eds) Du matériel au spirituel. Réalités archéologiques et historiques des "dépots" de la Préhistoire à nos jours. XXIXèmes rencontres internationales d'archéologie et d'histoire d'Antibes, Juan-les-Pins, 16–18 Oct 2008. éditions APDCA, pp 29–46

Chiotti L, Nespoulet R, Henry-Gambier D, Vercoutère C, Crépin L, Lebon M, Beck L, Müller K, Reiche I (2014) Un comportement funéraire original au Gravettien final. Bilan des analyses et études 2005–2011 de la couche 2 de l'abri Pataud (Les Eyzies-de-Tayac, Dordogne, France). In: Paillet P (ed) Les arts de la Préhistoire: microanalyses, mises en contextes et conservation. Actes du colloque "micro-analyses et datations de l'art préhistorique dans son contexte archéologique" MADAPCA, Paris, 2014. Paléo

Christensen M (2004) Fiche caractères morphologiques, histologiques et mécaniques des matières dures d'origin animales. In: Collectif DR (ed) Matières et techniques, Industrie de l'os préhistorique. Cahier XI. Société Préhistorique Française, Paris, pp 17–27

Christensen M, Tejero J-M (2015) La fabrication d'objets en matières dures animales. In: Balasse M, Brugal J-P, Dauphin Y, Geigl E-M, Oberlin C, Reiche I (eds) Messages d'os. Archives contemporaines, Paris

Codron J, Codron D, Sponheimer M, Kirkman K, Duffy KJ, Raubenheimer EJ, Melice JL, Grant R, Clauss M, Lee-Thorp JA (2012) Stable isotope series from elephant ivory reveal lifetime histories of a true dietary generalist. Proc Biol Sci 279(1737):2433–2441. doi:10.1098/rspb.2011.2472

Collins MJ, Riley MS, Child AM, Turner-Walker G (1995) A basic mathematical simulation of the chemical degradation of ancient collagen. J Archaeol Sci 22:175–183

Collins MJ, Waite ER, Van Duin ACT (1999) Predicting protein decomposition: the case of aspartic-acid racemization kinetics. Phil Trans R Soc Lond B 354:51–64
Collins MJ, Nielsen-Marsh CM, Hiller J, Smith CI, Roberts JP, Prigodich RV, Wess TJ, Csapo J, Millard AR, Turner-Walker G (2002) The survival of organic matter in bone: a review. Archaeometry 44(3):383–394
Conard N (2003) Palaeolithic ivory sculptures from southwestern Germany and the origins of figurative art. Nature 426:830–832
Conard NJ (2009) A female figurine from the basal Aurignacian of Hohle Fels Cave in southwestern Germany. Nature 459(7244):248–252. doi:10.1038/nature07995
Correia PM (1996) Fire modification of bone: a review of the literature. In: Haglund WDS, Sorg MH (eds) Forensic taphonomy. CRC Press, Boca Raton
Cui FZ, Wen HB, Zhang HB, Ma CL, Li HD (1994) Nanophase hydroxyapatite-like crystallites in natural ivory. J Mate Sci Lett 13:1042–1044
Currey JD (1999) The design of mineralised tissues for their mechanical functions. J Exp Biol 202:3285–3294
Currey JD (2002) Bones - Structure and Mechanics. Princeton
Currey JD (2005) Hierarchies in biomineral structures. Science 309:253–254
Currey JD, Brear K, Zioupos P (1994) Dependence of mechanical properties on fibre angle in narwhal tusk, a highly oriented biological composite. J Biomech 27:885–897
d'Errico F, Henshilwood CS (2007) Additional evidence for bone technology in the southern African Middle Stone Age. J Hum Evol 52(2):142–163. doi:10.1016/j.jhevol.2006.08.003
Dauphin Y, Williams CT (2004) Diagenetic trends of detnal tissues. C R Palevol 3:583–590
Denys C, Patou-Methis M (2014) Manuel de taphonomie. Collections archéologiques. Editions Errance, Paris
Dupont C, Marchand G (2008) Coastal exploitation in the Mesolithic of western France: la Pointe Saint-Gildas (Préfailles). Environ Archaeol 13(2):143–152. doi:10.1179/174963108X343263
Duval M (2011) High resolution LA-ICP-MS mapping of U and Th isotopes in an early Pleistocene equid tooth from Fuente Nueva-3 (Orce, Andalusia, Spain). Quat Geochronol 6 (5):458–467
Edwards HGM, O'Connor S (2012) Archaeological ivory: a challenge for analytical Raman spectroscopy. In: Edwards HGM, Vandenabeele P (eds) Analytical archaeometry. The Royal Society of Chemistry, Cambridge, pp 449–467
Edwards HGM, Brody RH, Nick Hassan NF, Farwell DW, O'Connor S (2006) Identification of archaeological ivories using FT-Raman spectroscopy. Anal Chim Acta 559:64–72
Ellingham ST, Thompson TJ, Islam M (2015a) The effect of soft tissue on temperature estimation from burnt bone using Fourier Transform Infrared Spectroscopy. J Forensic Sci 61:153–159
Ellingham ST, Thompson TJ, Islam M, Taylor G (2015b) Estimating temperature exposure of burnt bone: a methodological review. Sci Justice 55(3):181–188
Enk J, Devault A, Debruyne R, King CE, Treangen T, O'Rourke D, Salzberg SL, Fisher D, MacPhee R, Poinar H (2011) Complete Columbian mammoth mitogenome suggests interbreeding with woolly mammoths. Genome Biol 12(5):R51
Enzo S, Bazzoni M, Mazzarello V, Piga G, Bandiera P, Melis P (2007) A study of thermal treatment and X-ray powder diffraction on burnt fragmented bones from tomb II, IV and IX belonging to the hypogeic necropolis of "Sa Figu" near Ittiri, Sassari (Sardinia, Italy). J Archaeol Sci 34:1731–1737
Ericson JE (1985) Strontium isotope characterization in the study of prehistoric human ecology. J Hum Evol 14:503–514
Eriksson C, Börner K, Nygren H, Ohlson K, Bexell U, Billerdahl N, Johansson M (2006) Studies by imaging TOF-SIMS of bone mineralization on porous titanium implants after 1 week in bone. Appl Surf Sci 25:6757–6760
Espinoza EO, Mann M-J (1991) Guide d'identification de l'ivoire et de ses substituts. World Wildlife Fund and Conservation Foundation, New York

Falguères C, Bahain J-J, Duval M, Shao Q, Han F, Lebon M, Mercier N, Perez-Gonzalez A, Dolo J-M, Garcia T (2010) A 300–600 ka ESR/U-series chronology of Acheulian sites in Western Europe. Quatern Int 223–224:293–298. doi:10.1016/j.quaint.2009.10.008

Finch AA, Allison N (2007) Coordination of Sr and Mg in calcite and aragonite. Mineral Mag 71(5):539–552. doi:10.1180/minmag.2007.071.5.539

Fischer PM, Lodding ARE, Noren JG (1989) Trace elements and dating studies of teeth by secondary ion mass spectrometry (SIMS). In: Maniatis Y (ed) Archaeometry. Elsevier Science Publishers B. V, Amsterdam-Oxford-NY-Tokyo, pp 109–119

Fontan E, Reiche I (2011) Les ivoires d'Arslan Tash (Syrie) d'après une etude de la collection du Musée du Louvre: mise en oeuvre du matériau, traces de polychromie et de dorure, état de conservation. ArcheoSciences 35:283–295

Fox DL, Fisher DC (2004) Dietary reconstruction of Miocene Gomphotherium (Mammalia, Proboscidea) from the Great Plains region, USA, based on the carbon isotope composition of tusk and molar enamel. Palaeogeogr Palaeoclimatol Palaeoecol 206(3–4):311–335. doi:10.1016/j.palaeo.2004.01.010

Fox DL, Fisher DC, Vartanyan S, Tikhonov AN, Mol D, Buigues B (2007) Paleoclimatic implications of oxygen isotopic variation in late Pleistocene and Holocene tusks of Mammuthus primigenius from northern Eurasia. Quatern Int 169–170:154–165. doi:10.1016/j.quaint.2006.09.001

Fratzl P (2004) Hierarchical structure and mechanical adaptation of biological materials. In: Weiner RLRS (ed) Learning from nature how to design new implantable biomaterials: from biomineralisation fundamentals to biomimetic materials and processing routes. Kluwer Academic Publishers, Berlin, pp 15–34

Fratzl P (2007) Biomimetic materials research: what can we really learn from nature's structural materials? J R Soc Interface 4(15):637–642. doi:10.1098/rsif.2007.0218

Fratzl P, Weinkammer R (2007) Nature's hierarchical materials. Prog Mater Sci 52(8):271–298

Fratzl P, Gupta HS, Paschalis EP, Roschger P (2004) Structure and mechanical quality of the collagen–mineral nano-composite in bone. J Mater Chem 14:2115–2123

Fürst S, Müller K, Paris C, Bellot-Gurlet L, Pare C, Reiche I (2014) Neue Identifizierungsstrategie eisenzeitlicher Korallen anhand optischer und Raman-spektroskopischer Charakteristiken. Berliner Beiträge zur Archäometrie, Kunsttechnologie und Konservierungswissenschaft 22:25–35

Gaschen AA-M, Krähenbühl U, Döbeli M, Markwitz A, Barry B, Ulrich-Bochsler S (2008) Fluorine age dating of archaeological bones: fluorine depth profiling as a function of environmentally induced bone degradation. J Archaeol Sci 35:535–552

Geigl E-M (2002) Why ancient DNA research needs taphonomy. In: O'Connor T (ed) 9th Conference of the International Council of Archaeozoology, Durham, UK, 2004. Oxford, Oxbow Books, pp 78–85

Gifford DP (1981) Taphonomy and paleoecology: a critical review of archaeology's sister disciplines. In: Advances in archaeological method and theory, vol 4. Springer, Berlin, pp 365–438

Gillespie R, Hedges REM, Wand JO (1984) Radiocarbon dating of bone by accelerator mass spectrometry. J Archaeol Sci 11:165–170

Godfrey IM, Ghisalberti EL, Beng EW, Byrne LT, Richardson GW (2002) The analysis of ivory from a marine environment. ICC 47:1–29

Gonçalves D, Thompson T, Cunha E (2011) Implications of heat-induced changes in bone on the interpretation of funerary behaviour and practice. J Archaeol Sci 38(6):1308–1313

Goodwin MB, Grant PG, Bench G, Holroyd PA (2007) Elemental composition and diagenetic alteration of dinosaur bone: distinguishing micron-scale spatial and compositional heterogeneity using PIXE. Palaeogeogr Palaeoclimatol Palaeoecol 253:458–476

Gourrier A, Wagermaier W, Burghammer M, Lammie D, Gupta HS, Fratzl P, Riekel C, Wess TJ, Paris O (2007a) Scanning X-ray imaging with small-angle scattering contrast. J Appl Crystallogr 40(Supplement):s78–s82

Gourrier A, Wagermaier W, Burghammer M, Lammie D, Gupta HS, Fratzl P, Riekel C, Wess TJ, Paris O (2007b) Scanning X-ray imaging with small-angle scattering contrast. J Appl Crystallogr 40(Supplement):s78–s82

Gourrier A, Li C, Siegel S, Paris O, Roschger P, Klaushofer K, Fratzl P (2010) Scanning small-angle X-ray scattering analysis of the size and organization of the mineral nanoparticles in fluorotic bone using a stack of cards model. J Appl Crystallogr 43:1385–1392

Gourrier A, Bunk O, Müller K, Reiche I (2011a) Artificially heated bone at low temperatures: a quantitative scanning small-angle X-ray scattering imaging study of the mineral particle size. ArcheoSciences 35:191–199

Gourrier A, Bunk O, Müller K, Reiche I (2011b) Artificially heated bone at low temperatures: a quantitative scanning small angle X-ray scattering imaging study of the mineral particle size. ArcheoSciences 35:191–199

Grime G, Watt F (1993) A survey of recent PIXE applications in archaeometry and environmental sciences using the Oxford scanning proton microphobe facility. Nucl Instrum Methods Phys Res B75:495–503

Grün R, Aubert M, Hellstrom J, Duval M (2010) The challenge of direct dating old human fossils. Quatern Int 223–224:87–93. doi:10.1016/j.quaint.2009.10.005

Gueriau P, Mocuta C, Dutheil DB, Cohen SX, Thiaudiere D, Charbonnier S, Clement G, Bertrand L (2014) Trace elemental imaging of rare earth elements discriminates tissues at microscale in flat fossils. PLoS One 9(1):e86946. doi:10.1371/journal.pone.0086946

Gupta HS, Seto J, Wagermaier W, Zalansky P, Boesecke P, Fratzl P (2006) Cooperative deformation of mineral and collagen in bone at the nanoscale. PNAS 103 (47):17741–17746

Haile J, Froese DG, MacPhee RDE, Roberts RG, Arnold LJ, Reyes AV, Rasmussen M, Nielsen R, Brook BW, Robinson S, Demuro M, Gilbert MT, Munch K, Austin JJ, Cooper A, Barnes I, Möller P, Willerslev E (2009) Ancient DNA reveals late survival of mammoth and horse in interior Alaska. Proc Natl Acad Sci USA 106(52):22352–22357

Hameau S, Falguères C, Bahain JJ, Sémah F, Sémah AM, Dolo JM (2007) ESR dating in song terus cave (East Java, Indonesia). Quat Geochronol 2(1–4):398–402

Hanson M, Cain CR (2007) Examining histology to identify burned bone. J Archaeol Sci 34(11):1902–1913

Hedges REM (2002) Bone diagenesis: an overview of processes. Archaeometry 44(3):319–328

Hedges REM, Law IA (1989) The radiocarbon dating of bone. Appl Geochem 4:249

Hiller JC, Wess TJ (2006) The use of small-angle X-ray scattering to study archaeological and experimentally altered bone. J Archaeol Sci 33:560–572

Hiller JC, Thomson TJU, Evison MP, Chamberlain AT, Wess TJ (2003) Bone mineral change during experimental heating: an X-ray scattering investigation. Biomaterials 24:5091–5097

Hillson S (2009) Teeth. Cambridge manuals in archaeology. Cambridge University Press, New York

Hodge AJ, Petruska JA (1963) Recent studies with the electron microscope on ordered aggregats of the tropocollagen molecule. In: Narayana RG (ed) Aspects of protein structure. Academic Press, New York, pp 289–300

Holden J, Phakey P, Clement J (1995) Scanning electron microscope observations of heat-treated human bone. Forensic Sci Int 74(1–2):29–45

Hulmes D (2008) Collagen diversity, synthesis and assembly. In: Fratzl P (ed) Collagen. Springer US, New York, pp 15–47

Iacumin P, Bocherens H, Mariotti A, Longinelli A (1996) Oxygen isotope analyses of co-existing carbonate and phosphate in biogenic apatite: a way to monitor diagenetic alteration of bone phosphate? Earth Planet Sci Lett 142:1–6

Jäger I, Fratzl P (2000) Mineralized collagen fibrils: a mechanical model with a staggered arrangement of mineral particles. Biophys J 79:1737–1746

Jans MME, Kars H, Nielsen-Marsh CM, Smith CI, Nord AG, Arthur P, Earl E (2002) In situ preservation of archaeological bone: a histological study within a multidisciplinary approach. Archaeometry 44:343–352

Jans MME, Nielsen-Marsh CM, Smith CI, Collins MJ, Kars H (2004) Characterisation of microbial attack on archaeological bone. J Archaeol Sci 31:87–95

Jantou-Morris V, Horton MA, McComb DW (2010) The nano-morphological relationships between apatite crystals and collagen fibrils in ivory dentine. Biomaterials 31(19):5275–5286. doi:10.1016/j.biomaterials.2010.03.025

Kalsbeek N, Richter J (2006) Preservation of burned bones: an investigation of the effects of temperature and pH on hardness. Stud Conserv 51(2):123–138

Kierdorf H, Kierdorf U, Szuwart T, Clemen G (1995) A light microscopic study of primary antler develoment in fallow deer (*Dama dama*). Ann Anat 177:525–532

Klein-Nulend J, Bacabac R, Mullender M (2005) Mechanobiology of bone tissue. Pathol Biol 53 (10):576–580

Kohn MJ, Schoeninger MJ, Barker WW (1999) Altered states: effects of diagenesis on fossil tooth chemistry. Geochim Cosmochim Acta 63(18):2737–2747

Koon HEC, Nicholson RA, Collins MJ (2003) A practical approach to the identification of low temperature heated bone using TEM. J Archaeol Sci 30:1393–1399

Koon HEC, O'Connor TP, Collins MJ (2010) Sorting the butchered from the boiled. J Archaeol Sci 37:62–69

Krauss S, Fratzl P, Seto J, Currey JD, Estevez JA, Funari SS, Gupta HS (2009) Inhomogeneous fibril stretching in antler starts after macroscopic yielding: indication for a nanoscale toughening mechanism. Bone 44(6):1105–1110. doi:10.1016/j.bone.2009.02.009

Krauss S, Wagermaier W, Estevez JA, Currey JD, Fratzl P (2011) Tubular frameworks guiding orderly bone formation in the antler of the red deer (Cervus elaphus). J Struct Biol 175(3): 457–464. doi:10.1016/j.jsb.2011.06.005

Lafontaine RH, Wood PA (1982) The stabilization of ivory against relative humidity fluctuations. Stud Conserv 27:109–117

Lakes R (1993) Materials with structural hierarchy. Nature 361:511–515

Landis WJ, Hodgens KJ, Arena J, Song MJ, McEwen BF (1996) Structural relations between collagen and mineral in bone as determined by high voltage electron licroscopic tomography. Microsc Res Tech 33:192–202

Lange K, Perlès C, Vanhaeren M, Reiche I (2008) Heat-induced modification of marine shells used as personal ornaments at the prehistoric site of Franchthi cave, Greece: first results of a multi-analytical approach. In: Rabin I, Weiner S (eds) art'2008. Jerusalem, Israel

Large D, Müller K, Reiche I (2011) Approche analytique pour l'étude des ivoires archéologiques. ArcheoSciences 35:167–177

Latham AG (1997) Uranium-series dating of bone by gamma-ray spectrometry: comment. Archaeometry 39(1):217–219

Launey ME, Chen P-Y, McKittrick J, Ritchie RO (2010) Mechanistic aspects of the fracture toughness of elk antler bone. Acta Biomater 6:1505–1514

Lebon M, Reiche I, Gallet X, Bellot-Gurlet L, Zazzo A (2016) Rapid quantification of preserved bone collagen content by ATR-FTIR spectroscopy. Radiocarbon (in press)

Lebon M, Reiche I, Fröhlich F, Bahain J-J, Falguères C (2008) Characterization of archaeological burnt bones: contribution of a new analytical protocol based on derivative FTIR spectroscopy and curve fitting of the ν1ν3 PO4 domain. Anal Bioanal Chem 392(7–8):1479–1488

Lebon M, Reiche I, Bahain J-J, Chadefaux C, Moigne A-M, Fröhlich F, Sémah F, Schwarcz HP, Falguères C (2010) New parameters for the characterization of diagenetic alterations and heat-induced changes of fossil bone mineral using Fourier transform infrared spectrometry. J Archaeol Sci 37:2265–2276

Lebon M, Müller K, Bahain J-J, Fröhlich F, Falguères C, Bertrand L, Sandt C, Reiche I (2011a) Imaging fossil bone alterations at the microscale by SR-FTIR microspectroscopy. J Anal At Spectrom 26(5):922. doi:10.1039/c0ja00250j

Lebon M, Müller K, Bellot-Gurlet L, Paris C, Reiche I (2011b) Application des micro-spectrométries Infrarouge et Raman à l'étude des processus diagénétiques altérant les ossements Paléolithiques. ArcheoSciences 35:179–190

Lee-Thorp J, Manning L, Sponheimer M (1997) Problems and prospects for carbon isotope analysis of very small samples of fossil tooth enamel. Bulletin de la Société géologique de France 168(6):767–773
Leroi-Gourhan A, Allain J (1979) Lascaux inconnu. Editions du CNRS edn
Li C, Suttie JM, Clark DE (2005) Histological examination of antler regeneration in red deer (*Cervus Elaphus*). Anat Rec Part A 282A:163–174
Liverino B (1989) Red coral. In: Jewel of the Sea. Bologna
Llamas B, Holland ML, Chen K, Cropley JE, Cooper A, Suter CM (2012) High-resolution analysis of cytosine methylation in ancient DNA. PLoS One 7(1):e30226
Locke M (2008) Structure of ivory. J Morphol 269(4):423–450. doi:10.1002/jmor.10585
Lowenstam HA, Weiner S (1989) On biomineralization, 1st edn. Oxford University Press, New York Oxford
Mann S, Weiner S (1999) Biomineralization: structural questions at all length scales. J Struct Biol 126:179–181
Mellars P (1989a) Major issues in the origin of modern humans. Curr Anthropol 30:349–385
Mellars P (1989b) Technological changes across the Middle-Upper Paleolithic transition: economic, social, and cognitive perspectives. In: Mellars P, Stringer C (eds) The human revolution: behavioral and biological perspectives on the origins of modern humans. Edinburgh University Press, Edinburgh, pp 338–365
Meneghini C, Dalconi MC, Nuzzo S, Mobilio S, Wenk RH (2003) Rietveld refinement on X-ray diffraction patterns of bioapatite in human fetal bones. Biophys J 84(3):2021–2029
Miles AEW, F.D.S., L.R.C.P., M.R.C.S., J.W.White, L.D.S., R.C.S (1960) Ivory. In: Meeting at the Royal College of Surgeons Lincoln's Inn Fields, London. Section of Odontology, Royal Society of Medicine, pp 775–780
Millard AR, Pike AWG (1999) Uranium-series dating of the Tabun Neanderthal: a cautionary note. J Hum Evol 36:581–585
Molleson T (1987) Trace elements in human teeth. In: Grupe G, Herrmann B (eds) Trace elements in environmental history, Göttingen. Springer-Verlag Berlin Heidelberg New York, pp 67–82
Müller K, Reiche I (2011) Differentiation of archaeological ivory and bone materials by micro-PIXE/PIGE with emphasis on two Upper Palaeolithic key sites: Abri Pataud and Isturitz, France. J Archaeol Sci 38:3234–3243
Munro LE, Longstaffe FJ, White CD (2007) Burning and boiling of modern deer bone: effects on crystallinity and oxygen isotope composition of bioapatite phosphate. Palaeogeogr Palaeoclimatol Palaeoecol 249:90–1002
Nalla R (2003) Effect of orientation on the in vitro fracture toughness of dentin: the role of toughening mechanisms. Biomaterials 24(22):3955–3968. doi:10.1016/s0142-9612(03)00278-3
Nalla RK (2005) Fracture in human cortical bone: local fracture criteria and toughness mechanism. J Biomech 38(7):1517–1525. doi:10.1016/s0142-9612(03)00278-3
Nalla RK, Kinney JH, Ritchie RO (2003) Mechanistic fracture criteria for the failure of human cortical bone. Nat Mater 2(3):164–168
Nicholson RA (1996) Bone degradation, burial medium and species representation: debunking the myths, an experiment-based approach. J Archaeol Sci 23(4):513–533
Nielsen-March CM, Hedges REM (1999) Bone porosity and the use of mercury intrusion porosimetry in bone diagenesis studies. Archaeometry 41(1):165–174
Nielsen-Marsh CM, Hedges REM, Mann T, Collins MJ (2000) A preliminary investigation of the application of differential scanning calorimetry to the study of collagen degradation in archaeological bone. Thermochim Acta 365:129–139
Nielsen-Marsh CM, Smith CI, Jans MME, Nord A, Kars H, Collins MJ (2007) Bone diagenesis in the European Holocene II: taphonomic and environmental considerations. J Archaeol Sci 34:1523–1531
Nogués-Bravo D, Rodríguez J, Hortal J, Batra P, Araújo MB (2008) Climate change, humans, and the extinction of the woolly mammoth? PLoS Biol 6(4):e79
Nothnagel G, Le Roux SD, Grotepass WP (1996) Correlation between texture of hydroxyapatite and mechanical anisootropy in Loxodonta Africana ivory. Textures Microstruct 26–27:579–583

O'Connor S, Edwards HGM, Ali E (2011) An interim investigation of the potential of vibrational spectroscopy for the dating of cultural objects in ivory. ArcheoSciences 35:159–165
Olhausen O (1888) Über die farbigen Einlagen einer Bronzefibel von Schwabsburg in Rheinhessen. Kr. Mainz. Verhandlungen Berliner Ges Anthrop Ethnol u Urgesch XX:140–151
Perlès C, Vanhaeren M (2010) Black cyclope neritea marine shell in the Upper Palaeolithic and Mesolithic of Franchthi (Argolid, Greece). Arguments for an intentionnal heat treatment. J Field Archaeol 35(3):314–325
Perrin F (1996) Technologie et économie du corail de Méditerranée en Gaule du VIe au 1er siècle avant J.-C., Lyon
Person A, Bocherens H, Saliège J-F, Paris F, Zeitoun V, Gérard M (1995) Early diagenetic evolution of bone phosphate: an X-ray diffractometry analysis. J Archaeol Sci 22:211–221
Person A, Bocherens H, Mariotti A, Renard M (1996a) Diagenetic Evolution and experimental heating of Bone Phosphate. Palaeogeogr Palaeoclimatol Palaeoecol 126:135–149
Person A, Bochérens H, Mariotti A, Renard M (1996b) Diagenetic Evolution and experimental heating of Bone Phosphate. Palaeogeogr Palaeoclimatol Palaeoecol 126:135–149
Piga G, Malgosa A, Thompson T, Enzo S (2008) A new calibration of the XRD technique for the study of archaeological burned human remains. J Archaeol Sci 35:2171–2178
Piga G, Solinas G, Thompson T, Brunetti A, Malgosa A, Enzo S (2013) Is X-ray diffraction able to distinguish between animal and human bones? J Archaeol Sci 40(1):778–785
Pijoan CM, Mansilla J, Leboreiro I, Lara VH, Bosch P (2007) Thermal alterations in archaeological bones. Archaeometry 49:713–727
Politi Y, Batchelor DR, Zaslansky P, Chmelka BF, Weaver JC, Sagi I, Weiner S, Addadi L (2010) Role of magnesium ion in the stabilization of biogenic amorphous calcium carbonate: a structure-function investigation. Chem Mater 22:161–166. doi:10.1021/cm902674h; 10.1029/2008GL033543
Posner AS (1969) Crystal chemistry of bone mineral. Physiol Rev 49(4):760–792
Prozesky VM, Raubenheimer EJ, Heerden WFPV, Grotepass WP, Przybylowicz WJ, Pineda CA, Swart R (1995) Trace element concentration and distribution in ivory. Nucl Instrum Meth B 104:638–644
Pruvost M, Schwartz R, Correia VB, Champlot S, Braguier S, Morel N, Fernandez-Jalvo Y, Grange T, Geigl E-M (2007) Freshly excavated fossil bones are best for amplification of ancient DNA. PNAS 104(3):739–744
Pruvost M, Schwarz Bessa Correia, Champlot Grange T, Geigl E-M (2008) DNA diagenesis and palaeogenetic analysis: critical assessment and methodological progress. Palaeogeogr Palaeoclimatol Palaeoecol 266(3–4):211–219
Rajaram A, Ramanathan N (1982) Tensile properties of antler bone. Calcif Tissue Int 34(3):301–305
Raubenheimer EJ (1999) Morphological aspects and composition of African elephant (Loxodonta africana) ivory. Koedoe—African Protected Area Conserv Sci 42(2):57–64
Raubenheimer EJ, Biosman MC, Vorster R, Noffke CE (1998a) Histogenesis of the chequered pattern of ivory of the African elephant (*Loxodonta Africana*). Arch Oral Biol 43:969–977
Raubenheimer EJ, Brown JMM, Rama DBK, Dreyer MJ, Smith PD, Dauth J (1998b) Geographic variations in the composition of ivory of the african elephant (*Loxodonta africana*). Arch Oral Biol 43:641–647
Reiche I (2009a) Heating and diagenesis-induced heterogeneiteis in the chemical composition and structure of archaeological bones from the Neolithic site of Chalain 10 (Jura, France). Pal@thnologie 2:129–144
Reiche I (2009b) Hétérogénéité de la composition chimique et de la structure des ossements archéologiques provenant du site néolithique de Chalain 19 (Jura, France) indute par la chauffe et la diagenèse. Pal@thnologie 2
Reiche I (ed) (2011) dossier thématique: the international ArBoCo workshop. Towards a better understanding and preservation of ancient bone materials, vol 35. ArcheoSciences. PUR Rennes

Reiche I, Chalmin E (2008) Synchrotron radiation and cultural heritage: combined XANES/XRF study at Mn K-edge of blue, grey or black coloured palaeontological and archaeological bone material. J Anal At Spectrom 23:799–806

Reiche I, Chadefaux C (2009) Fluorine uptake in archaeological bone—study from macro- to nanoscale Chemistry Today N° special. Focus Fluorine Chem 27(3):48–51

Reiche I, Müller K, Rodière J, Allard M, Staude A, Riesemeier H, Chiotti L, Nespoulet R, Vercoutère C, Schwab C, Cleyet-Merle J-J (accepted) Relation between raw material, shape and function of Gravettian ornaments from three key sites in Southern France (Abri Pataud, Le Blot, Les Peyrugues). Paléo

Reiche I, Favre-Quattropani L, Calligaro T, Salomon J, Bocherens H, Charlet L, Menu M (1999) Trace element composition of archaeological bones and post-mortem alteration in the burial environment. Nucl Instr Meth Phys Res B 150:656–662

Reiche I, Vignaud C, Menu M (2000) Heat induced transformation of fossil mastodon ivory into turquoise "odontolite". Structural and elemental characterisation. Solid State Sci 2:625–636

Reiche I, Morin G, Brouder C, Sole VA, Petit P-E, Vignaud C, Calligaro T, Menu M (2002a) Manganese accomodation in fossilised mastodon ivory and heat-induced colour transformation: Evidence by EXAFS. Eur J Mineral 14(6):1069–1073

Reiche I, Vignaud C, Menu M (2002b) The crystallinity of ancient bone and dentine: new insights by transmission electron microscopy. Archaeometry 44(3):447–459

Reiche I, Favre-Quattropani L, Vignaud C, Bocherens H, Charlet L, Menu M (2003) A multi-analytical study of bone diagenesis: the Neolithic site of Bercy (Paris, France). Measur Sci Technol 14:1608–1619

Reiche I, Chadefaux C, Vignaud C, Menu M (2007) Les matériaux osseux archéologiques Des biomatériaux nanocomposites complexes. l'actualité chimique 312–313:86–92

Reiche I, Lebon M, Chadefaux C, Müller K, Le Hô A-S, Gensch M, Schade U (2010) Microscale imaging of the preservation state of 5,000-year-old archaeological bones by synchrotron infrared microspectroscopy. Anal Bioanal Chem 397:2491–2499

Reiche I, Chadefaux C, Müller K, Gourrier A (2011a) Towards a better understanding of alteration phenomena of archaeological bone by a closer look at the organic/mineral association at microscale. Preliminary results on Neolithic samples from Chalain lake site 19, Jura, France. ArcheoSciences 35:143–158

Reiche I, Müller K, Staude A, Goebbels J, Riesemeier H (2011b) Synchrotron radiation and laboratory micro X-ray computed tomography—useful tools for the material's identification of prehistoric objects made of ivory, bone or antler. J Anal At Spectrosc 26:1802–1812. doi:10.1039/c0ja00246a

Reiche I, Muller K, Alberic M, Scharf OU, Wahning A, Bjeoumikhov A, Radtke M, Simon R (2013) Discovering vanished paints and naturally formed gold nanoparticles on 2800 years old Phoenician ivories using SR-FF-microXRF with the Color X-ray Camera. Anal Chem 85 (12):5857–5866. doi:10.1021/ac4006167

Reiche I, Müller K, Vercoutère C, Nespoulet R, Chiotti L, Staude A, Riesemeier H (2014) Nouvelles méthodes de laboratoire et de synchrotron pour l'identification de la matière dure d'origine animale. L'étude des perles du Gravettien final de l'abri Pataud (Les Eyzies-de-Tayac-Sireuil, Dordogne, France). In: Paillet P (ed) Les arts de la Préhistoire: microanalyses, mises en contextes et conservation. Actes du colloque "Micro-analyses et datations de l'art préhistorique dans son contexte archéologique" MADAPCA, Paris. PALEO, numéro spécial:75–83

Rey C, Combes C, Drouet C, Glimcher M (2009) Bone mineral: update on chemical composition and structure. Osteoporos Int 20(6):1013–1021

Rho JY, Kuhn-Spearing L, Zioupos P (1998) Mechanical properties and the hierarchical structure of bone. Med Eng Phys 20:92–102

Richter J (1986) Experimental study of heat induced morphological changes in fish bone collagen. J Archaeol Sci 13:477–481

Richter KK, Wilson J, Jones AKG, Buckley M, van Doorn N, Collins MJ (2011) Fish'n chips: ZooMS peptide mass fingerprinting in a 96 well plate format to identify fish bone fragments. J Archaeol Sci 38(7):1502–1510. doi:10.1016/j.jas.2011.02.014

Rink WJ, Schwarcz HP, Lee HK, Valdés VC, Quiros FBd, Hoyos M (1996) ESR dating of tooth enamel: comparison with AMS ^{14}C at El Castillo Cave, Spain. J Archaeol Sci 23:945–951

Rodière J (2011) Etude tracéologique de la perforation. Application aux perles rectangulaires de l'abri Pataud, du Blot, des Peyrugues. ArchéoSciences 35:273–281

Rogers KD, Daniels P (2002) An X-ray diffraction study of the effects of heat treatment on bone mineral structure. Biomaterials 23:2577–2585

Rogers K, Beckett S, Kuhn S, Chamberlain A, Clement J (2010) Contrasting the crystallinity indicators of heated and diagenetically altered bone mineral. Palaeogeogr Palaeoclimatol Palaeoecol 296(1–2):125–129

Roschger P, Fratzl P, Klaushofer K, Rodan G (1997) Mineralization of cancellous bone after alendronate and sodium fluoride treatment: a quantitative backscattered electron imaging study on minipig ribs. Bone 20(5):393–397

Rubin MA, Jasiuk I, Taylor J, Rubin J, Ganey T, Apkarian RP (2003) TEM analysis of the nanostructure of normal and osteoporotic human trabecular bone. Bone 33:270–282

Rubin MA, Jasiuk I (2005) The TEM characterization of the lamellar structure of osteoporotic human trabecular bone. Micron 36:653–664

Ruppel ME, Miller LM, Burr DB (2008) The effect of the microscopic and nanoscale structure on bone fragility. Osteoporos Int 19(9):1251–1265

Saliège JF, Person A, Paris F (1995) Preservation of $^{13}C/^{12}C$ original ratio and ^{14}C dating of the mineral fraction of human bones from Saharan tombs, Niger. J Archaeol Sci 22:301–312

Sawyer S, Krause J, Guschanski K, Savolainen V, Pääbo S (2012) Temporal patterns of nucleotide misincorporations and DNA fragmentation in ancient DNA. PLoS One 7(3):e34131

Schweitzer MH, Avci R, Collier T, Goodwin MB (2008) Microscopic, chemical and molecular methods for examining fossil preservation. CR Palevol. doi:10.1016/j.crpv.2008.02.005

Shahack-Gross R, Bar-Yosef O, Weiner S (1997) Black-coloured bones in Hayonim Cave, Israel: differentiating between burning and oxide staining. J Archaeol Sci 24:439–446

Shipman P, Foster G, Schoeninger M (1984) Burnt bones and teeth: an experimental study of color, morpholgy, crystal strucure and shrinkage. J Archaeol Sci 11:307–325

Singh RR, Goyal SP, Khanna PP, Mukherjee PK, Sukumar R (2006) Using morphometric and analytical techniques to characterize elephant ivory. Forensic Sci Int 162(1–3):144–151. doi:10.1016/j.forsciint.2006.06.028

Skinner H (2013) Mineralogy of bones essentials of medical geology. Springer, Netherlands

Smith CI, Nielsen-Marsh CM, Jans MME, Collins MJ (2007) Bone diagenesis in the European Holocene I: patterns and mechanisms. J Archaeol Sci 34(2007):1485–1493

Spadavecchia J, Apchain E, Alberic M, Fontan E, Reiche I (2014) One step synthesis of collagen hybrid gold nanoparticles and formation on egyptian-like gold-plated archaeological ivory. Angew Chem Int Ed 53:8363–8366. doi:10.1002/anie.201403567

Squires KE, Thompson TJ, Islam M, Chamberlain A (2011) The application of histomorphometry and Fourier Transform Infrared Spectroscopy to the analysis of early Anglo-Saxon burned bone. J Archaeol Sci 38(9):2399–2409

Stiner MC, Kuhn SL, Weiner S, Bar-Yosef O (1995) Differential burning, recrystallisation, and fragmentation of archaeological bone. J Archaeol Sci 22:223–237

Stiner MC, Kuhn SL, Gulec E (2013) Early upper paleolithic shell beads at Ucagizli Cave I (Turkey): technology and the socioeconomic context of ornament life-histories. J Hum Evol 64 (5):380–398. doi:10.1016/j.jhevol.2013.01.008

Strupler M, Pena A-M, Hernest M, Tharaux P-L, Martin J-L, Beaurepaire E, Schanne-Klein M-C (2007) Second harmonic imaging and scoring of collagen in fibrotic tissues. Opt Express 15:4057–4065

Su XW, Cui FZ (1999) Hierarchical structure of ivory: from nanometer to centimeter. Mater Sci Eng C7:19–29

Taborin Y (2004) Language sans parole. La parure aux temps préhistoriques. La maison des roches, Paris, France
Tejero J-M, Christensen M, Bodu P (2012) Red deer antler technology and early modern humans in Southeast Europe: an experimental study. J Archaeol Sci 39:332–346
Tesch W, Eidelman N, Roschger P, Goldenberg F, Klaushofer K, Fratzl P (2001) Graded microstructure and mechanical properties of human crown dentin. Calcif Tissue Int 69(3):147–157. doi:10.1007/s00223-001-2012-z
Tescione G (1965) Il corallo nella storia e nell'arte. Neapel
Thompson T (2004) Recent advances in the study of burned bone and their implications for forensic anthropology. Forensic Sci Int 146(Supplement):S203–S205
Thompson T, Gauthier M, Islam M (2009) The application of a new method of Fourier Transform Infrared Spectroscopy to the analysis of burned bone. J Archaeol Sci 36(3):910–914
Thompson T, Islam M, Piduru K, Marcel A (2011) An investigation into the internal and external variables acting on crystallinity index using Fourier Transform Infrared Spectroscopy on unaltered and burned bone. Palaeogeogr Palaeoclimatol Palaeoecol 299(1–2):168–174
Tischler O (1886) Abriss der Geschichte des Emails. Schriften der Physikalisch-Ökonomischen Gesellschaft 27:39–59
Trapani J, Fisher DC (2003) Discriminating proboscidean taxa using features of the Schreger pattern in tusk dentin. J Archaeol Sci 30:429–438
Traub W, Arad T, Weiner S (1992) Origin of mineral crystal growth in collagen fibrils. Matrix, Depart Struct Biol 12(4):251–255
Trueman NG, Behrensmeyer AK, Tuross N, Weiner S (2004) Mineralogical and compositional changes in bones exposed on soil surfaces in Amboseli National Park, Kenya: diagenetic mechanisms and the role of sediment pore fluids. J Archaeol Sci 31:721–739
Trueman CN, Palmer MR, Field J, Privat K, Ludgate N, Chavagnac V, Eberth DA, Cifelli R, Rogers RR (2008) Comparing rates of recrystallisation and the potential for preservation of biomolecules from the distribution of trace elements in fossil bones. CR Palevol 7:145–158
Turner-Walker G, Jans M (2008) Reconstructing taphonomic histories using histological analysis. Palaeogeogr Palaeoclimatol Palaeoecol 266:227–235
Tütken T, Vennemann TW (2011) Fossil bones and teeth: Preservation or alteration of biogenic compositions? Palaeogeogr Palaeoclimatol Palaeoecol 310(1–2):1–8
Vanhaeren M, d'Errico F, Stringer C, James SL, Todd JA, Mienis HK (2006) Middle Palaeolithic shell beads in Israel and Algeria. Science 312:1785–1788
Vashishth D, Behiri JC, Bonfield W (1997) Crack growth resistance in cortical bone: concept of microcracking toughening. J Biomech 30(8):763–769
Vashishth D, Tanner KE, Bonfield W (2000) Contribution, development and morphology of microcracking in cortical bone during crack propagation. J Biomech 33(9):1169–1174
Vashishth D, Tanner KE, Bonfield W (2003) Experimental validation of a microcracking-based toughening mechanism for cortical bone. J Biomech 36(1):121–124
Vercoutère C, Müller K, Chiotti L, Nespoulet R, Staude A, Riesemeier H, Reiche I (2011) Rectangular beads from the final gravettian level of the abri Pataud: raw material identification and its archaeological implications. ArcheoSciences 35:259–271
Veri G, Collins P, Ambers J, Sweek T, Simpson SJ (2009) Assyrian colours: pigments on a neo-Assyrian relief of a parade horse. Tech Res Bull 3:57–62
Vielzeuf D, Garrabou J, Baronnet A, Grauby O, Marschal C (2008) Nano to macroscale biomineral archtitecture of red coral *(Corallium rubrum)*. Am Mineral 93:1799–1815
Vielzeuf D, Floquet N, Chatain D, Bonneté F, Ferry D, Garrabou J, Stolper EM (2010) Multilevel modular mesocrystalline organization in red coral. Am Mineral 95:242–248
Virag A (2012) Histogenesis of the unique morphology of proboscidean ivory. J Morphol 273 (12):1406–1423. doi:10.1002/jmor.20069
Wagermaier W, Gupta HS, Gourrier A, Burghammer M, Roschger P, Fratzl P (2006) Spiral twisting of fiber orientation inside bone lamellae. Biointerphases 1(1):1–5

Wagermaier W, Gourrier A, Aichmayer B (2013) Understanding hierarchy and functions of bone using scanning X-ray scattering methods In: Materials design inspired by nature: function through inner architecture. The Royal Society of Chemistry, pp 46–73
Wang R, Weiner S (1998) Human root dentin: structural anisotropy and Vickers microhardness isotropy. Connect Tissue Res 39:269–279
Weiner S (2010) Microarchaeology, beyond the visible archaeological record. Cambridge University Press, Cambridge
Weiner S, Traub W (1986) Organization of hydroxyapatite crystals within collagen fibrils. FEBS Lett 206(2):262–266
Weiner S, Bar-Yosef O (1990) States of preservation of bones from prehistoric sites in the Near East: a survey. J Archaeol Sci 17:187–196
Weiner S, Wagner H (1998) The material bone: structure-mechanical function relations. Annu Rev Mater Sci 28(1):271–298
Weiner S, Quinqi X, Goldberg P, Liu J, Bar-Yosef O (1998) Evidence for the use of fire at Zhoukoudian, China. Science 281:251–253
Wess T (2008) Collagen fibrillar structure and hierarchies. In: Fratzl Pe (ed) Collagen. Springer, Berlin, pp 49–80
Wess TJ, Drakoopoulos M, Snigirev A, Wouters J, Paris O, Fratzl P, Collins M, Hiller J, Nielsen K (2001) The use of small angle X-ray diffraction studies for the analysis of structural features in archaeological samples. Archaeometry 43(1):117–129
Wess T, Alberts I, Hiller J, Drakopoulos M, Chamberlain A, Collins M (2002) Microfocus small angle X-ray scattering reveals structural features in archaeological bone samples; detection of changes in bone mineral habit and size. Calcif Tissue Int 70(2):103–110
White R (1995) Ivory personal ornaments of Aurignacian Age: technological, social and symbolic perspectives. In: Travail et usages de l'ivoire au Paléolithique supérieur, Ravello. Centre universario europeo, pp 29–62
White R (2006) The women of brassempouy: a century of research and interpretation. J Archaeol Method Theor 13(4):250–303. doi:10.1007/s10816-006-9023-z
White CD, Schwarcz HP (1989) Ancient Maya diet: as inferred from isotopic and elemental analysis of human bone. J Archaeol Sci 16:451–474
Wislocki GB (1942) Studies of the growth of deer antlers. 1. The structure and histogenesis of the antlers of the Viginia Deer (*Odocoileus virginianus borealis*). Am J Anat 71:371–415
Zaslansky P, Friesem AA, Weiner S (2006) Structure and mechanical properties of the soft zone separating bulk dentin and enamel in crowns of human teeth: insight into tooth function. J Struct Biol 153(2):188–199. doi:10.1016/j.jsb.2005.10.010
Zazzo A, Balasse M, Patterson WP (2006) The reconstruction of mammal individual history: refining high-resolution isotope record in bovine tooth dentine. J Archaeol Sci 33(8): 1177–1187
Zioupos P, Currey JD, Sedman AJ (1994) An examination of the micromechanics of failure of bone and antler by acoustic emission tests and laser scanning confocal microscopy. Med Eng Phys 16:203–212
Zioupos P, Wang XT, Currey JD (1996) Experimental and theoretical quantification of the development of damage in fatigue tests of bone and antler. J Biomech 29(8):989–1002
Ziv V, Sabanay I, Arad T, Traub W, Weiner S (1996) Transitional structures in lamellar bone. Microsc Res Tech 33(2):203–213

Some Science Behind the Daguerreotype: Nanometer and Sub-micrometer Realities On and Beneath the Surface

Patrick Ravines, Lingjia Li, Lisa Chan and Rob McElroy

Abstract The daguerreotype, the first viable imaging process invented and developed by Louis-Jacques-Mande Daguerre in Paris in 1839 gave birth to photography and started the imaging revolution. This chapter will briefly introduce the daguerreotype, its enthusiastic worldwide acceptance as the first commercially viable form of photography, its short yet productive two decades of existence, and its legacy. The following sections will describe the historical daguerreotype process as practiced today by artists, professional photographers and aficionados. The process has been examined in detail at each of its many steps with scanning and transmission electron microscopies, optical microscopies and vibrational spectroscopies to reveal nanometer and sub-micrometer features at the surface and sub/meso-surface that are involved in and part of the image making process. Knowing more of this wondrous photochemical/physical process increases our appreciation for the object itself and the complexities related to their preservation.

P. Ravines (✉)
Art Conservation Department, State University of New York College at Buffalo, 1300 Elmwood Avenue—Rockwell Hall 230, Buffalo, NY 14222, USA
e-mail: ravinepc@buffalostate.edu

L. Li · L. Chan
TESCAN USA Inc., 765 Commonwealth Drive, Suite 101, Warrendale, PA 15086, USA
e-mail: lilingjia@gmail.com

L. Chan
e-mail: lchan@tescan-usa.com

R. McElroy
Archive Studio, 347 Franklin St., Buffalo, NY 14202, USA
e-mail: idag@pce.net

P. Dillmann et al. (eds.), *Nanoscience and Cultural Heritage*,
DOI 10.2991/978-94-6239-198-7_5

1 Introduction

The daguerreotype was the earliest form of practical photography and was invented by Louis-Jacques-Mandé Daguerre (1787–1851) in Paris and he presented his invention to the world in 1839. This photographic phenomenon spread rapidly throughout the world and to England and America. During its heyday period between 1839 and 1860 millions of daguerreotypes were produced. This first imaging system realized the full potential of the photograph with its remarkable resolution and dynamic range. Because each plate is a unique object that is labor intensive and technically complicated to make, its dominant period was short-lived as it was replaced by other competing photographic systems that produced multiple images and were less expensive. Today the historical daguerreotype is increasingly treasured for its fine art, artefactual as well as its documentary value. Additionally, in the past few decades daguerreotypy has been revived as an artistic photographic medium. A few images spanning the historical and contemporary nature of the daguerreotype are represented in Figs. 1 and 2. Figure 1a is of the man we can thank for initiating the imaging/photographic revolution, Louis Jacques Mande Daguerre taken by Sabatier Blot in 1844. Figure 1b is a beautiful example of a

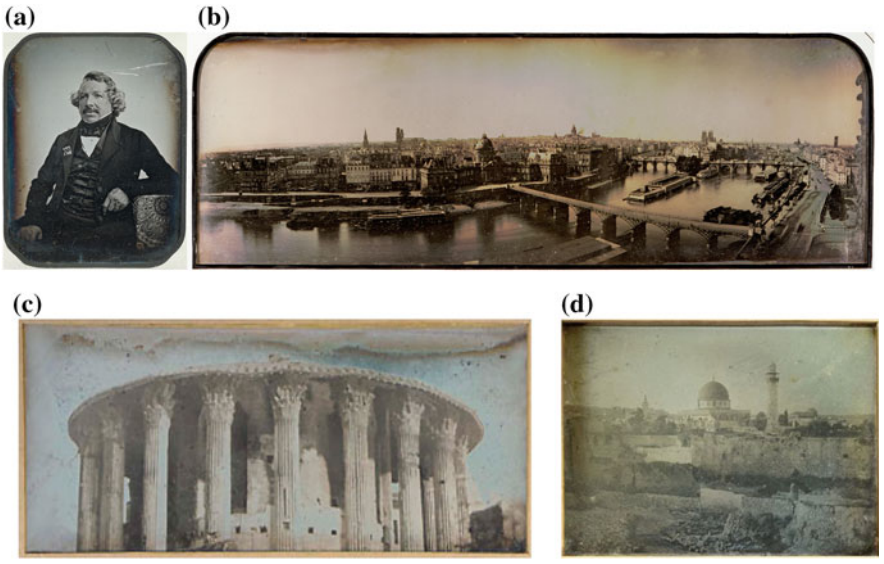

Fig. 1 **a** Portrait of Louis Jacques Mandé Daguerre in 1844 by Jean-Baptiste Sabatier-Blot (French, 1801–1881). Image: 9.1 x 6.9 cm (3 9/16 x 2 11/16 in.); overall: 17.2 x 13.6 cm (6 3/4 x 5 3/8 in.). George Eastman Museum, gift of Eastman Kodak Company, ex-collection Gabriel Cromer. Public domain. 1976.0168.0043; **b** a beautiful panoramic view of Paris, Quais de la Seine pris de la terrasse du Louvre, au toit du Salon carré , ca. 1845, Attributed to Friedrich von Martens (French, b. Germany, 1809–1875). Image: 10.5 x 37.6 cm; frame: 25 x 49 cm. George Eastman Museum, gift of Eastman Kodak Company, ex-collection Gabriel Cromer. Public domain. 1976.0168.0136; **c** the Temple of Vesta in Rome, 1842 by Joseph-Philibert Girault de Prangey. Public domain; **d** is southern view of the Dome of the Rock, Jerusalem, 1844, by Girault de Prangey. Public domain

Fig. 2 **a** Portrait of an unidentified bride, ca. 1850, Southworth & Hawes (American, active 1843–1863), Whole plate; 21.5 x 16.5 cm. George Eastman Museum, gift of Alden Scott Boyer. Public domain. 1974.0193.0251; **b** Portrait of an unidentified Child, ca. 1850, Southworth & Hawes (American, active 1843–1863), daguerreotype with applied color, Whole plate; 21.6 x 16.5 cm. George Eastman Museum, museum accession. Public domain. 1974.0193.0022; **c** contemporary daguerreotype by Rob McElroy, Cone Flower No.1, 2009, 10.16 x 12.7 cm/4 x 5 inches. Photo credit: © R. McElroy.; **d** contemporary daguerreotype by Adam Fuss, from the series "My Ghost", 2002, 35.6 x 27.9 cm/14 x 11 inches. Photo credit: © Adam Fuss. Courtesy Cheim & Read, New York

panoramic view, an uncommon format, of Paris showcasing the Seine and two if its bridges, the Louvre palace and Notre Dame de Paris cathedral photographed by Friedrich von Martens in the 1850s. Figure 1c, d show early, probably the first, images taken outside of France by Joseph-Philibert Girault de Prangey: 1c is the Temple of Vesta in Rome, 1842, and 1d is a view from the south of the Dome of the Rock in Jerusalem, 1844. As the daguerreotype process matured, it was able to capture portraits and Fig. 2a shows a full-length portrait of a bridesmaid in her flowing wedding gown circa 1850, and Fig. 2b shows the portrait of a seated and smiling young child circa 1850, both taken by the studio of Southworth and Hawes, two famous Boston daguerreotypists active from 1845 to 1861. Finally, two images from modern daguerreotypists/photographers and artists Rob McElroy, Fig. 2c shows a coneflower in full bloom, and Adam Fuss, Fig. 2d, shows a butterfly on a blue solarized background from his "My Ghost" series.

The daguerreotype is unique among photographic systems and presents a significant preservation challenge to museums, libraries and archives. The chemistry, physics and material science of the daguerreotype, the precise make-up of the fine structure of the image, and image-altering deterioration mechanisms is an area of active research (Centeno et al. 2008, 2011; Marquis et al. 2015; Ravines et al. 2008, 2010, 2016).

In the early days of photography, there is evidence that the daguerreotype image was changing and being damaged by spots and/or an obscuring film of corrosion/tarnish. The delicate image structure was being adversely affected and damaged by environmental conditions, contaminants and pollutants, and physical interactions. From their inception, various interventive approaches and chemically based restorative treatments have been applied to regenerate the daguerreotype image. However, little scientific evaluation of the effects of these treatments has been carried out.

This study presents the results of having used a modern variety of instrumental techniques such as Raman spectroscopy, and optical and electron imaging technologies such as confocal microscopy, high-resolution scanning electron microscopy, energy dispersive spectroscopy, focused ion beam scanning electron microscopy and transmission electron microscopy to examine every surface and beneath the surface through cross sections at each step in the process of making modern daguerreotypes using similar techniques to those used by 19th century daguerreotypists to reveal submicron and nano-metric features at the surface and sub/meso-surface that are involved in and part of the complex image making process.

The nature of our perception of the appearance of an image is the result of the complex interaction of surrounding illumination, surface optics (reflective properties) and surface geometry/topography (Motoyoshi et al. 2007). The daguerreotype image is an assemblage of minute nanometer to sub-micrometer-sized image particles dispersed over a highly polished silver plate interacting with light. Particle creation and distribution is directly related to light levels where the sensitized plate is exposed in the camera and then to mercury vapor development. This implies that highlights and white looking areas have high concentrations of image particles to scatter light, and dark/shadow areas have few to none (Barger et al. 1984). Barger and White (1991) have described the interaction of light with the daguerreotype surface.

Tarnishing of daguerreotypes made in the first two years, 1839–1841, before Armand Hippolyte Louis Fizeau (1819–1896) introduced gilding is understandable as the image was composed of silver and silver mercury amalgam (Fizeau 1841). After gilding with gold became part of the practice, daguerreotypes still tarnished, exhibiting colors ranging from light brown-yellows to browns to dark blue blacks. It would be expected that tarnishing should not be occurring or be minimal if the surface has been electrochemically coated with a thin film of gold, a noble metal.

The earliest scanning electron microscopy studies explain how light interacts with the daguerreotype surface to reveal an image, image particle composition, estimates of gold film thickness, chemical composition of tarnish, and removal approaches (Swan et al. 1979; Barger and White 1991).

The distinctively characteristic process by which the daguerreotype image—background surface and image particles—is generated is examined at every stage of the daguerreotype making process.

2 The Daguerreotype Process

The photographic process presented in 1839 by Daguerre involved the following steps (Daguerre 1839):

1. A silver plated or clad copper plate is polished to a mirror finish.
2. The plate is fumed with iodine vapors (I_2) to produce a light-sensitive silver iodide (AgI) layer.
3. The sensitized plate is placed in a camera and exposed to an image.
4. The image is developed by exposing it to heated mercury (Hg) vapors.
5. The remaining un-reacted silver iodide (AgI) is "fixed" and removed with "hypo" (sodium thiosulfate, $Na_2S_2O_3$).

At this point, the daguerreotype's dark and shadow areas are bare polished-and-etched silver plate. The areas ranging from dark grey through light grey to dull white to bright highlights are composed of silver-mercury amalgam image particles "resting" on the surface and are directly proportional to the reduced silver of the latent image. This delicate surface arrangement of image particles could easily be physically disturbed. "Gilding" was introduced by Armand Hippolyte Louis Fizeau in 1840: the electrochemical deposition of gold on the silver surface from a gold-chloride-thiosulfate solution, which is often locally heated. The claim was that gilding affixed the silver-mercury amalgam image particles to the surface, and increased contrast by making the highlights appears whiter and the shadow areas seem darker (Fizeau 1841). These two image-enhancing features of gilding ensured its inclusion as the final essential step in the daguerreotype making process.

The daguerreotype process can be divided into two distinct categories: the first set of steps involves the physical/mechanical polishing to a mirror finish, and the second group comprises the many chemical and photochemical steps to generate an image. Polishing a silver plate to a mirror finish is both labor intensive and time consuming and, if not done

properly, will affect the overall quality of the final image, hence, much attention and care was taken when polishing. This chapter examines the nature of the surface and sub-surface that have been generated at every stage of the daguerreotype making process and in some instances some steps have been further divided into sub-steps.

3 Physical/Mechanical Processing of the Silvered Copper Plates

3.1 As-Received Surface

The modern daguerreotype process used for this study is based on the original version developed by Daguerre with slight modifications introduced by Rob McElroy. The silver electroplated copper plates used were commercially prepared by Zapffe Silversmiths, Seattle, Washington http://www.zapffesilversmiths.com. Pure silver (99.99 %) with an average thickness of 12.7 μm (0.5 mil) was electrodeposited onto pre-polished 18 gauge copper plates. The "as received" silvered copper plate was examined before starting the steps to a mirror-finish polish (Fig. 3). The silver surface was not prepared in any way—no gold or carbon coatings were applied, and no plasma cleaning was done, in order to examine, as best as possible, the true nature of the surface at each stage in the process. Figure 3a shows the surface to be textured and rough with a large scratch on the top left quadrant and many large and deep pits. Figure 3b, clearly shows the surface silver grains ranging in size from 100 to 1000 nm.

The surface topography/geometry measurements confirm the visual observations of roughness. The average "root mean square roughness" (Sq) equals 38.6 ± 5.1 nm from 6 measurements in Table 1.

3.2 Polishing and Buffing to a Mirror Finish

Small square plates of 6.35 × 6.35 cm size were cut to fit Hasselblad medium-format cut-film holders from large silver-plates. These smaller pieces were individually polished with alumina (Al_2O_3) with a particle size range of 5–7 μm, and then buffed with a combination of two buffing compounds: jeweler's rouge [iron (III) oxide; Fe_2O_3, >99.9 % purity from Grobet USA® with a particle size range from 3.5 to 5.0 μm] and a black carbon-based powder (>99.9 % purity Rublev Lampblack from Natural Pigments®).

The historical polishing material used to first treat the surface would have been "rottenstone", a powdered mixture of decomposed limestone ($CaCO_3$) with amorphous or crystalline silica (SiO_2). The rottenstone would have had a particle size smaller than 37 μm. When rottenstone is used for polishing it readily breaks down into smaller particles (Humphrey 1858). The alumina particle size range we used is smaller than the polishing material used in the 19th century: 5–7 μm versus an average particle size of 37 μm.

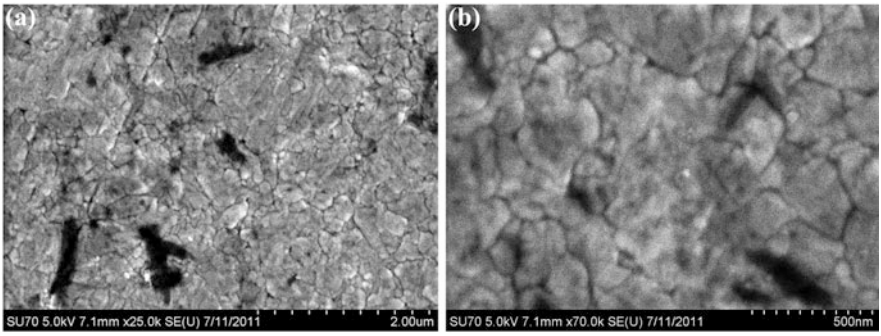

Fig. 3 The surface of the silver plate as it was received from Zapffe Silversmiths (electroplaters, Seattle, Washington) from secondary electron (SE) micrographs from a field emission scanning electron microscope (FE-SEM) taken at an accelerating voltage of 5 keV **a**, the textured surface shown at a magnification of ×25k with a scale bar of 2 μm, and **b** the surface shown at ×70k magnification with a 500 nm scale bar showing various sized silver grains

Table 1 Surface metrology of polishing steps: root mean square average roughness, Sq, values

Plate processing step	Sq ± Std. dev. (nm)	Number of areas sampled
"As is"	38.6 ± 5.1	6
After alumina (Al_2O_3) hand polishing	23.7 ± 2.4	7
After rouge (Fe_2O_3) and lampblack (C) buffing	12.6 ± 5.9	9

The intention of this step is to "clean" the surface of any silver plate maker's debris and/or surface contamination. The cleaning action observed is plate abrasion and, simultaneously, a homogenization of the surface. The surface metrology height parameters shows that the average root mean square (Sq) equals 23.7 ± 2.4 nm (8 measurements), which is a decrease of about one third compared to the "as is" plate (see Table 1). The electron micrograph of the surface shown in Fig. 4 shows large scratches on the silver surface caused by the hand rubbed alumina, and it also shows that the surface grain pattern that was visible has been obliterated.

The surface metrology values and electron micrographs show that the alumina abrasive has modified the surface as was intended.

The next step was to apply buffing compounds onto the roughened silver surface. Historically, jeweler's rouge and a black carbon dust/powder were used independently or together. Orr (1856) mentions use of both rouge and lampblack and Humphrey's (1858) used only rouge and felt strongly that it alone was sufficient.

The buffing and polishing powders have a wide range of hardness's; lampblack Mohs hardness is 1.5 at 20 °C and much softer than rouge with a hardness of 5.5–6.5 at 20 °C. The Mohs hardness for silver ranges from 2.5 to 3.0 and is exactly in between the values of the two buffing compounds. Once the buffing compounds were sprinkled onto the surface, in the 19th century the plate would have been hand

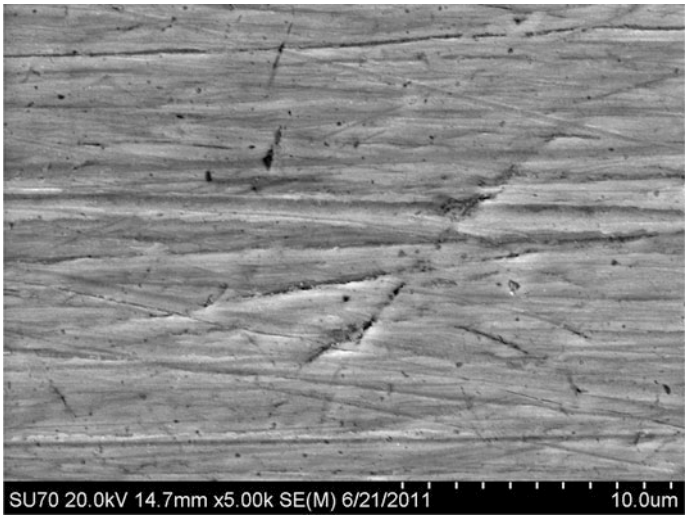

Fig. 4 SE electron micrograph of the *horizontal striations* or *scratch marks* of the silver plated surface caused by polishing with alumina (Al_2O_3 with particle size range of 5–7 μm; SEM conditions: accelerating voltage of 20 keV, magnification of ×5k.)

polished using buffing paddles covered with cotton velvet or machine polished on a rotary polishing wheel. In the preparation of our plates, random orbital sanders were used. Their advantage is that they sand by simultaneously spinning the sanding disk and moving it in an ellipse, thereby ensuring that no single part of the abrasive powder travels the same path twice, thereby minimizing scratches. This step is repeated several times until the highest quality mirror finish is achieved. The mirror finish is determined visually by checking for the absence of any scratches remaining from electroplating, deep scratches from earlier alumina polishing and/or fine elliptical or swirl patterns left by the random orbital sander during buffing. Additionally, two extra buffing steps were included with two random orbital sanders with clean cotton flannel pads with the expectation that both these extra buffing steps will remove as much of the rouge as possible. They serve the same function as the second polishing paddle step did during the 19th century.

Figure 5 shows the results of buffing with combined rouge and carbon powders. All four images in Fig. 5a show lots of grey and dark grey smaller particles embedded in the light grey silver surface. The embedded rouge particles sizes are well below 200 nm and based on the initial rouge particle size range of 3–5 μm, these smaller sized particles are the result of the physical breakdown of the larger rouge particles during buffing with the random orbital sander. The embedded carbon particles are close to and below the original average particle size of 95 nm. These images show the mirror-finished surface to be extremely smooth, no topography is observed except for the large diagonal scratch, and surface grain features are faintly visible.

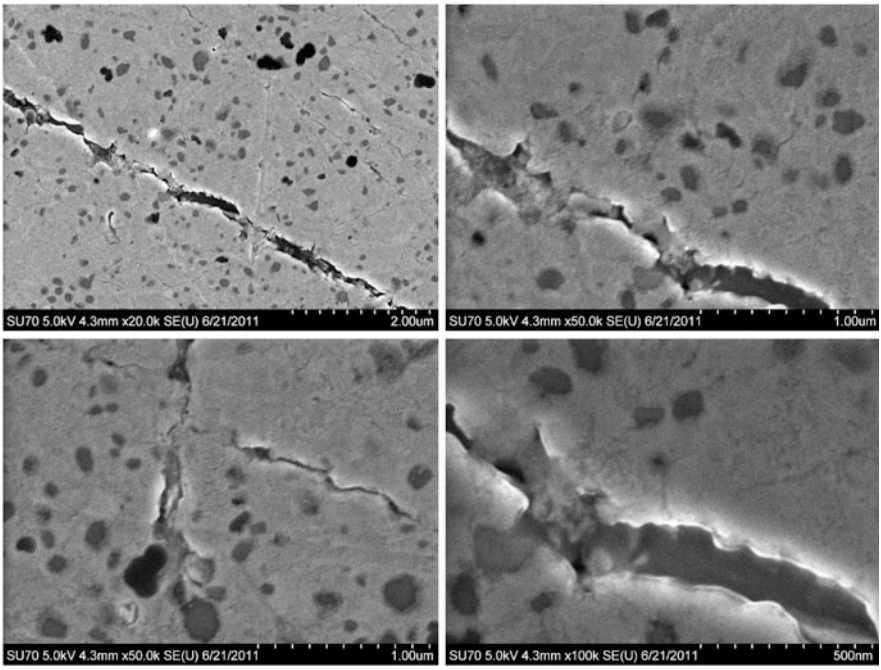

Fig. 5 Shows SE micrographs of the silver surface embedded with particles at increasing magnifications (×20k, ×50k and ×100k) after buffing with rouge (Fe_2O_3, particle size range 3.5–5 um; >99.9 % purity from Grobet USA; Mohs hardness 5.5–6 at 20 °C) and carbon black (average particle size 95 nm; >99.9 % purity Rublev lampblack from Natural Pigments; Mohs hardness 1.5 at 20 °C)

The EDX map and spectrum (Fig. 6) clearly identify the embedded particles as mostly rouge with some carbon and a small amount of alumina. Interestingly, all three different embedded particles have about the same size distribution. The alumina particles are small bits that broke when hand polishing in the first step and then embedded when hand polishing and/or in the second buffing step with the random orbital sander. At this stage in the process, the resulting mirror finish has additional polishing materials embedded in the surface.

We observed that buffing with rouge has had the effect of imparting an extremely faint reddish or pinkish coloration to the silver. The embedded lamp black may have a greater effect in the coloration of the plate by counteracting the reddishness imparted by the rouge rather than acting as a polishing agent because of its softer nature, Mohs hardness of 1.5 at 20 °C. This may be its only function since it is so much softer than silver that it may not serve the buffing process at all.

The two focused ion beam cross sections (Fig. 7) show how well the rouge/iron oxide and lamp black carbon nano-particles have embedded themselves into the silver surface and are below 200 nm in size. These particles decrease the overall silver surface and the areas they occupy are unavailable for photographic activity.

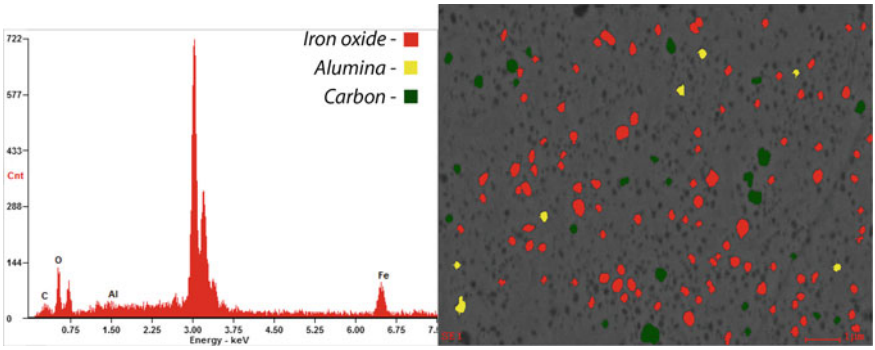

Fig. 6 Backscattered electron (BE) image of the surface and corresponding EDX map and spectrum showing buffing elements

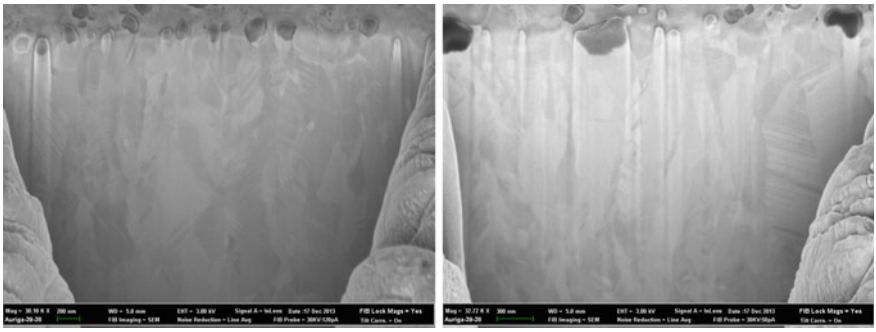

Fig. 7 SE micrographs of focused ion beam cross sections of two different areas of the buffed plate showing embedded particles (energy of gallium focused ion beam: 20–30 kV, currents from 240 to 600 pA, SEM conditions: 2–5 kV at magnifications of ×30k and ×33k)

The topography of the mirror finish, as would be expected, has decreased considerably with the low average root mean square roughness (Sq) value of 12.6 ± 5.9 nm (Table 1). This is a drop of about half from the alumina treated plate and two thirds from the "as is" plate. The decrease in the height parameter measurement of Sq at these three stages of polishing and buffing from 38.6 to 23.7 to 12.6 nm is not as impressive as the visual effect of the mirror-like finish.

Figure 8 showing the three Raman spectra corroborates the surface embedded nanometer-sized particles of alumina, carbon and rouge in Fig. 7. The spectrum of the silver plate as received (bottom) shows little Raman activity with a broad peak at 1300 cm^{-1} that likely comes from surface impurities from the electroplating process and handling. The middle spectrum shows alumina to be part of the surface with a strong peak at 224 cm^{-1}, which is representative of the transitional delta and theta phases of alumina (δ-, θ-Al_2O_3) (Weber 2000). The top spectrum clearly shows that to achieve the much desired mirror finish using all three polishing and buffing materials that they have been incorporated into the surface. The peak at

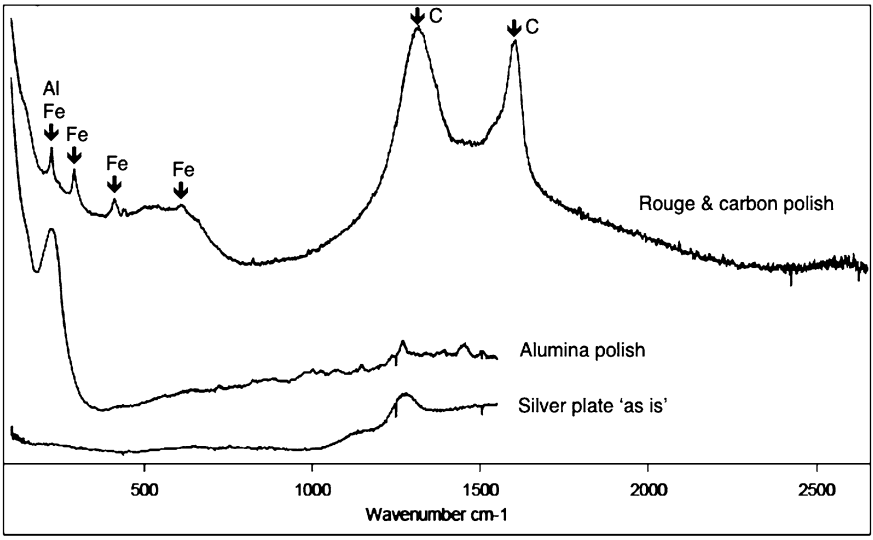

Fig. 8 Raman spectra of the silver plate as received (*bottom spectrum*), after polishing with alumina (*middle*) and buffing with rouge and carbon black (*top*). (Spectra acquired with a Bruker Senterra FT-Raman microscope spectrometer, 50× LWD objective, multiple laser wavelengths and power settings used)

225 cm^{-1} is likely to have contributions from both alumina and rouge. Since rouge is present on the surface in greater concentrations than alumina and carbon, and the peak shape is like that of the other rouge peaks, the majority of the Raman activity should be coming from rouge, Fe_2O_3. The carbon from lampblack has two extremely intense peaks that dwarf the others. The three peaks at 290, 411 and 609 cm^{-1} are from rouge (Legodi and de Waal 2007), and the two intense peaks at 1315 and 1604 cm^{-1} are from carbon of the lampblack (Tomasini et al. 2012; Bell et al. 1997; Burgio and Clark 2001). In light of the strong Raman signals, especially from carbon, it is likely that all three polishing materials are exhibiting surface enhancement due to both their nanoparticle size and being in a silver substrate.

Achieving the mirror finish has been accomplished; this concludes the physical preparation portion of the daguerreotype making process. Another step practiced in the 19th century, as well as by some of today's daguerreotypists, was to electroplate or "galvanize" (19th century term) the mirror-finished silver plate that would then be buffed with a soft cloth like velvet. This additional step was advantageous in that it would deposit a thin film of pure silver over all embedded polishing and buffing particles. In this study, the plates were not electroplated/galvanized a second time after buffing.

3.3 *Chemical Processing of the Mirror-Finish Silvered Copper Plates*

The first step in the chemical process is to prepare a light sensitive silver halide surface.

3.3.1 Preparing a Light Sensitive Silver Halide Plate

During Daguerre's first years silvered plates were exposed only to iodine gas (I_2) to yield a light sensitive "film" of silver iodide (AgI). Exposing silver to iodine gas over a period of time results in a predictable color change on the plate which begins with a light yellow color which changes to orange, then a pinkish rose and ends with violet, after which the color returns to yellow and starts the color changes over again with continued time in the iodine gas environment. Early daguerreotypists empirically determined that this first pinkish yellow color was the best for yielding high quality daguerreotypes. The temperature and relative humidity in the iodine chamber and preparation room/lab affect the time required to reach the desired color. According to Pobboravsky (1971), the color of the silver iodide film is due to interference and scattering, and an indication of the silver iodide film thickness. Pobboravsky writes that the ideal silver iodide film thickness for use in imaging/photography in the 19th century and based on the film's pinkish yellow coloration would have been

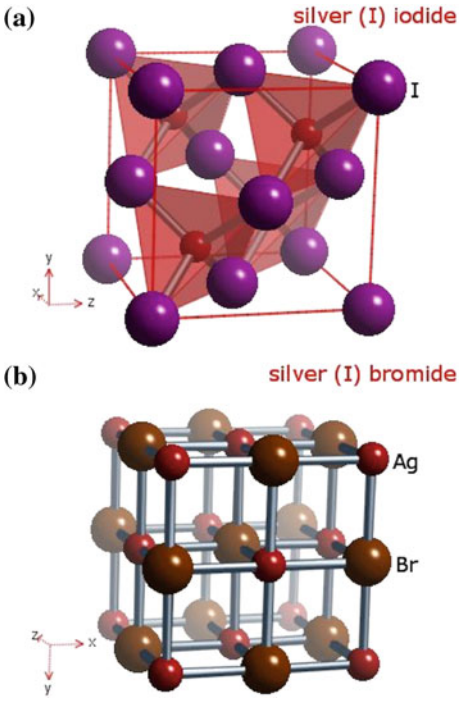

Fig. 9 Crystal structures for **a** silver (I) iodide (http://butulok.blogspot.com/2014/11/giant-structures.html); **b** silver (I) bromide (https://elfordchemistry.wikispaces.com/13+States+of+Matter)

Table 2 Silver iodide (AgI) and silver bromide (AgBr) physical characteristics and features

Compound	Crystal	Structure	Lattice, a/Å
AgI	β-phase	Wurtzite	–
AgBr, Bromargyrite	fcc	Rock-salt, NaCl	5.7745

approximate thickness of 16–30 nm. Equation 1 describes the chemical reaction between iodine gas and silver metal yielding silver iodide:

$$2Ag_{(s)} + I_{2(g)} \rightarrow 2AgI \tag{1}$$

The resulting silver iodide crystals have temperature dependent structures, the stable β-phase, with a wurtzite structure exists from room temperature (293 K, 20 °C) to 420 K (147 °C). In this wurtzite arrangement the silver iodide unit cells have the silver and iodide centers tetrahedrally coordinated, as shown in Fig. 9a (Binner et al. 2006). The wurtzite structured silver iodide salt grains nucleate heterogeneously at grain boundaries, dislocations and other locations of the silver surface.

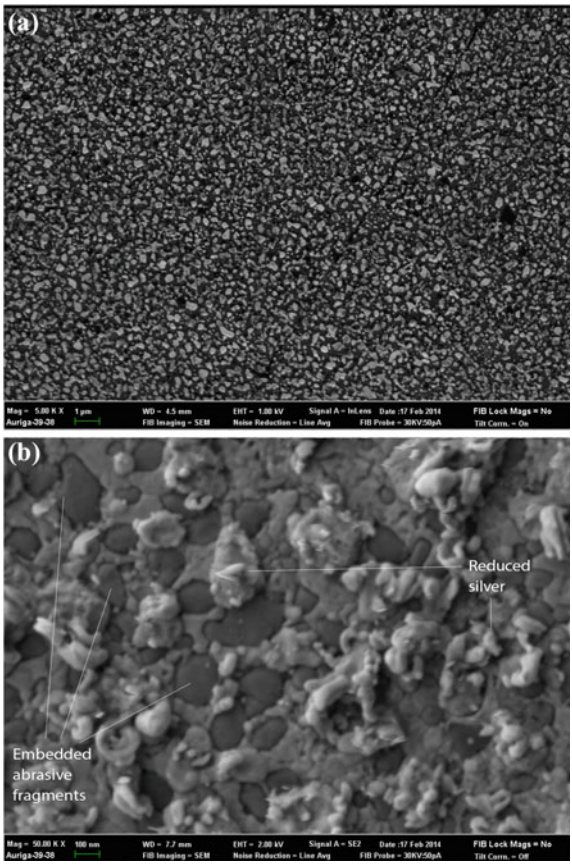

Fig. 10 Shows individual light grey colored β-phase silver iodide crystals on a blackish silver surface **a** at ×5000 magnification, SE in line/ttl detector; **b** at ×50k magnification shows that silver iodide crystals have reacted to the electron beam, the iodide crystals show reduced silver metal extending outward. The silver iodide grains do not form a continuous film, SE in line/ttl detector

The silver iodide "film" generated is composed of small wurtzite structured crystals that are not perfect and have point and line defects. It is these defects that are the active and sensitive sites to ultraviolet radiation and visible light (Eachus et al. 1999). Table 2 lists some basic physical characteristics of silver iodide.

Figure 10a shows the surface at ×5000 magnification that is well covered with individual light grey colored β-phase silver iodide crystals on a blackish silver surface. Figure 10b at ×50,000 magnification shows many interesting features not observed at lower magnifications. Firstly, the silver iodide reacted to the electron beam and the silver iodide crystals show that silver metal is reducing and jutting outward from the silver iodide crystals. This image also confirms that the silver iodide grains are individual isolated crystal units not necessarily in contact with other crystals, and, therefore, do not form a continuous AgI layer or film. Because of this the background is visible and consists of the polished silver and of the embedded polishing and buffing compounds of alumina, rouge/iron oxide and lampblack (carbon) mentioned earlier. The iron oxide and lampblack show up as darker grey rounded particles at the surface level. The areas where polishing and buffing material is found have not reacted with the iodine gas; they are inert to the iodine gas.

The focused ion beam cross section shown in Fig. 11, corroborates Fig. 10b and, again, demonstrates the discontinuous nature of the silver iodide surface "film" in that the silver iodide crystals are separate entities. This thickness range was also observed in other cross sections. These images of the silver iodide surface and cross sections corroborate Pobboravsky's suggestion that the silver iodide surface film was discontinuous and thicker than what was reported in 1971 (Pobboravsky 1971).

Video 1 is a short video clip that shows the reactivity between the electron beam and silver iodide at ×50,000 magnification. This is as close as we can get to directly

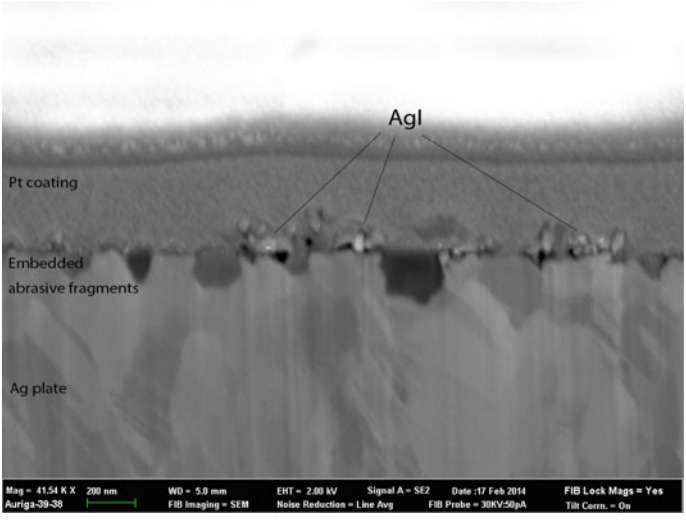

Fig. 11 The SE image of a focused ion beam cross-section shows silver iodide crystals are separate entities

witnessing the in situ effect of electrons on light sensitive silver halides (only available in electronic version).

Bromine gas was introduced and incorporated as an integral part of the daguerreotype process in 1841. Its effect, daguerreotypists claimed, was a marked increase in the sensitivity of the silver iodide/silver bromide film to light, thus increasing the "speed" of the plate.

The sensitization sequence using iodine and bromine gases was to first expose the mirrored silver plate to iodine gas until the surface coloration was yellow with a pinkish tinge, then to bromine gas for a about 5 s, and then a final exposure of iodine gas for a final 3–5 s.

Equations 1 and 2 describe the chemical nature of the reactions taking place:

$$2Ag_{(s)} + Br_{2(g)} \rightarrow 2AgBr \tag{2}$$

The silver halide chemistry is straightforward and it is likely that this reaction is occurring where there is exposed silver not affected by the initial exposure to iodine gas and with the existing silver iodide. Silver bromide has a face-centered cubic (fcc) rock-salt (NaCl) lattice structure, see Table 2 and Fig. 9b. The surface is now likely to be populated by individual silver iodide crystals, individual silver bromide crystals, and a crystal combination of silver iodide/silver bromide. The occurrence of silver halide crystal mix brings about the greater sensitivity to light and, thereby, increases the "film" speed (Mitchell 1957). 19th century daguerreotypists favored and used this mixture (Brewster 1847) but did not realize that it was the increase of the point and line defect imperfections in the silver halide grains that caused this favorable change.

Imperfections in silver halide crystals are needed for the imaging process. Imperfections such as defects, point and line dislocations, and kinks result in traps, charged regions in the crystal. For example, in defects a missing silver lattice ion will create a negative region at the resulting hole and an interstitial silver ion will create a positively charged region. Line dislocations, a sliding of a crystal plane, can cause similar conditions to defects where each ion is not surrounded by six ions of opposite charge, resulting in a positively or negatively charged region. If these dislocations occur at the crystal surface a negatively charged region can attract interstitial silver ions to the surface and a positively charged region can attract liberated electrons to the silver ions. These types of crystal imperfections occur in pure silver iodide and silver bromide crystals and are greatly increased when different crystals lattice structures such as the β-phase silver iodide and fcc silver bromide crystal systems are combined on the surface of a daguerreotype plate (Mitchell 1957; Eachus et al. 1999).

Figure 12 shows two electron micrographs of the light sensitive surface of silver iodide and silver bromide at two magnifications of ×6000 and ×22,000. Figure 12a, shows a white silver halide film with small black flecks/spots; and Fig. 12b shows white and bright areas of silver halide, and dark grey and black areas that are embedded polishing materials of rouge (Fe_2O_3), carbon and alumina, which are not sensitive to iodine or bromine gases. Interestingly, the iodine-bromine-iodine sensitization has increased the silver halide content on the surface when compared to silver

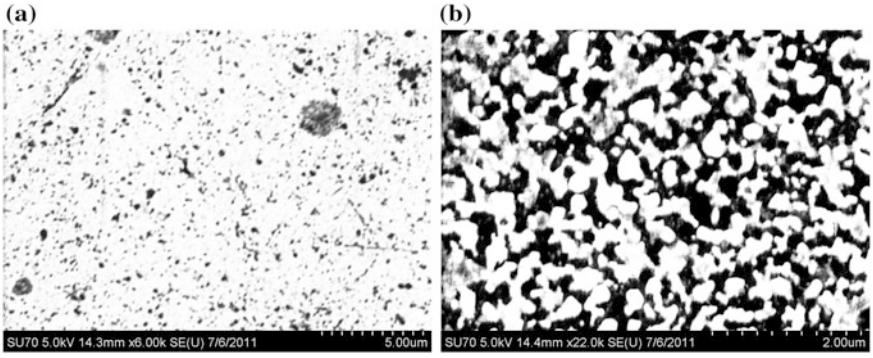

Fig. 12 **a** The SE image of silver iodide and silver bromide surface at ×6k magnification (acc. voltage of 5 kV); **b** SE image of silver iodide and silver bromide surface at ×22k magnification (5 kV). In both images the *white* represents the silver halide crystals and the *dark grey* background is unreacted silver metal and/or embedded polishing and buffing particles

iodide alone (Fig. 10), and in Fig. 12b the ratio of light to dark areas appears to be approximately 1 to 1.

One step in the preparation of the silver mirror surface practiced by 19th century and modern daguerreotypists is that of electroplating, refered to as galvanizing in the 19th century, after polishing and buffing. This extra step would likely have ensured as close as one can get to a 100 % silver surface for the greatest reactivity with the halogen gases.

At this stage the sensitized silver halide plate is ready to be placed in a camera to capture an image.

3.4 Imaging

3.4.1 Exposing the Sensitized Silver Halide Plate to Light

The sensitized plate is loaded onto a holder, inserted into a camera and exposed to a subject—person portrait, cityscape, nature scene or other. Exposure of the sensitized plate to light—daylight or artificial light, sets up a series of surface reactions that over the course of an exposure time of five to fifteen seconds yields a "latent image."

Latent image formation and the possible shapes it could take

The issue of latent image formation is still a question of interest to the world of silver based photography (Belous and Kuskovsky 2007). Discoveries in allied fields of chemical physics may offer new insight into the nature of the silver clusters formed when light interacts with silver halides.

Research into the structures of transition metal clusters formed in rare gas matrices have shown that stable cluster conformations can be attained.

Several groups have prepared silver clusters by sputtering a silver target with an Ar^+ ion beam and probed with Raman spectroscopy have shown that there are many silver clusters, $Ag_{n,}$ where n = 2, 3, 5, 7 and 9 (Harbich et al. 1990; Haslett et al. 1998, 1999; Bosnick et al. 1999).

Establishing the lowest energy form of these clusters prepared by Argon ion beam plasmas has been complicated and not many of these structures have been fully determined (Lombardi and Davis 2002). For example, the structure of the Ag_3 cluster has been determined to be a distorted triangle (Haslett et al. 1999); the Ag_5 cluster a planar trapezoid (Haslett et al. 1998), and Ag_7 a tri-capped tetrahedron (Haslett et al. 1999).

These intriguing results provide an interesting direction of study that may yield more information on the photo-physico-chemical changes taking place at the surface of silver halides when light impinges on them yielding latent image clusters or particles to determine if these and/or other multi-atom silver clusters are the ones formed at this initial stage in the photographic process.

The silver photographic chemistry process involving the interaction of light and silver halides is described by Eq. 3.

$$10AgI/AgBr_{(s)} + h\nu \leftrightarrow 4Ag_{(5)} + 5I_2/Br_2 \tag{3}$$

Equation 3 is reversible when the silver clusters formed are less than five atoms. When the critical size of five reduced silver atoms has been reached, the equation will not revert and the resulting formation of a series of stable clusters are distributed where light shone and constitute the "latent image" (Mott and Gurney 1940; Seitz 1951; Mitchell 1981; Hailstone and Hamilton 1985; Hamilton 1988; Belloni 2002). A recent review by Tani (1998) claims that the minimum number of silver atoms to form a cluster ranges from 2 to 5.

Once the latent image has been formed, the remaining light sensitive silver halide salts surround the reduced clusters of five or more silver atoms. The full formation of the photographic image requires that the latent image be developed.

3.4.2 Developing the Latent Image—Mercury Development and Surface Phenomena, Part 1

The predominant 19th century developing method was to expose the freshly captured latent image to mercury vapors as soon as possible. In this step the plate is placed face down in a chamber so that it is exposed to mercury gas that has been generated from a small warmed pool of mercury located at the bottom of the chamber. The process of silver and mercury amalgamation is based on the negatively charged silver clusters reacting with warm - heated to between 50 and 90 °C, (Swan et al. 1979) and positively charged gaseous mercury droplets (Brodie and Thackray 1984) to form a stable amalgam.

Ravines and coworkers (2016) have proposed that the amalgamation process between the latent image surface silver clusters and the mercury gas is a two-stage reaction in the formation of the final silver mercury amalgam image particles. The initial and first reaction in the development process is only between the surface silver clusters and mercury gas. The bulk of background silver is unaffected by the mercury gas since the unreacted silver halides cover the majority of the plate surface and, thereby, protect the silver from reacting with gaseous mercury. It is possible that some exposed areas of silver plate exist and may react with the mercury to form an amalgam. These exposed silver regions are where silver halides salts did not form during the sensitization stage.

The first set of reactions occurring at the surface between positively charged gaseous mercury with the negatively charged latent image silver clusters (Ag_5 or greater) on the surface could potentially yield many different types of initial silver-mercury amalgam seed particles. To date, two types of image particles claimed to have been found on daguerreotypes are the zeta (ζ) phase amalgam, $Ag_{11}Hg_9$, also known as the mineral Schachnerite, with a closed packed hexagonal (cph) unit cell structure in the *P6₃/mmc* space group (Baren 1992) that was visually identified by Barger and White (1991) and also observed by others (Ravines et al. 2010); and Swan and coworkers (1979) first observed the gamma (γ) phase amalgam, Ag_3Hg_4, with a body centered cubic (bcc) unit cell structure in the *I23* space group (Swan et al. 1979). Earlier studies in 1970s and 1980s visually examined top view secondary emission scanning electron micrographs of moderate magnification (×2000 to ×10,000) to determine these two types of surface silver mercury amalgam image particles present. The first reactions using these two amalgams are described in Eqs. 4 and 5 and they both yield two different silver-mercury amalgam seed image particles.

$$11Ag_5 + 45Hg_{(g)} \rightarrow 5Ag_{11}Hg_9 \tag{4}$$

(seeds of Schachnerite, zeta (ζ) phase, cph)

$$3Ag_5 + 20Hg_{(g)} \rightarrow 5Ag_3Hg_4 \tag{5}$$

(seeds of gamma (γ) phase, bcc)

The stability of the amalgams is a likely driving force in the formation of the seed image particles. These two seeds are on the surface and still surrounded by unreacted silver halide salts (Ravines et al. 2016).

Figure 13 shows two views of the surface of a new ungilded daguerreotype. Figure 13a shows some hexagonal and what appears to be cubic shaped image particles. The angled image of the same zone at a lower magnification (Fig. 13b) shows that there are many more shapes on the surface than can be identified from the top view. The three-dimensional solids range from trapezoidal to many-sided columnar to the expected hexagonal shapes and all are in the sub-micrometer and low micrometer size range. This image also highlights the nano-roughness of background plate surface texture. Figure 13b makes it clear that the visual inspection of SE SEM images is not enough to identify the nature and type of silver-mercury amalgam image particles on the

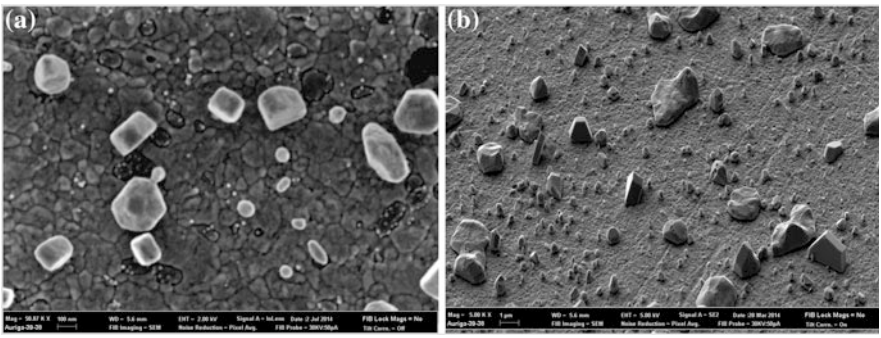

Fig. 13 Shows two SE micrograph views of the surface of a new ungilded daguerreotype, **a** SE image taken from the top, as is customary at 2 kV and ×50k magnification; **b** the same surface taken at an angle at 5 kV and ×5k magnification

daguerreotype surface. Studies of the surface image particles using diffraction techniques should elucidate the nature of all of the three dimensional shapes and their corresponding species (Ravines et al. 2016).

3.4.3 Developing the Latent Image—Mercury Development and Meso/Sub-surface Phenomena, Part 2

The second step in the development of the image particle is a seamless uninterrupted continuation of the amalgamation reactions after the newly constituted seeds have been formed from the surface silver clusters with mercury gas. More silver is needed to react with the gaseous mercury for the growth of the amalgam seeds into fully developed image particles. The fully developed image particles need to be large enough to make up the daguerreotype image as shown in Eqs. 6 for Schachnerite/zeta (ζ) phase and 7 for gamma (γ) phase amalgams.

Silver mercury amalgams: An overview

The establishment of clear definitions and corresponding structures for silver-mercury amalgams is in transition.

Regarding the $Ag_{11}Hg_9$ amalgam: In Barger and White's 1984 study (Barger et al. 1984) they observed hexagonal-shaped image particles on their modern/new daguerreotypes and referred to these as ε (epsilon) amalgam.

In the past, the $Ag_{11}Hg_9$ amalgam has been referred to as beta, and epsilon (Hansen and Anderko 1958) and now zeta (Mitchell 1981, Baren 1992).

The American Society for Metals' silver-mercury equilibrium phase diagram shows only the zeta (ζ) phase and the gamma (γ) phase amalgams (Baren 1992). Baren's 1996 review of the silver-mercury amalgam system uncovered that debates still exist regarding the exact nature and composition of gamma (γ) phase silver-mercury amalgam, Ag_3Hg_4 (Baren 1996).

Interestingly, natural amalgams found in nature are:

- Schachnerite also known as zeta (ζ) phase with a close packed hexagonal unit cell ($Ag_{11}Hg_9$) (Joint Committee for Powder Diffraction Standards (JCPDS): PDF# 00-027-0618 & 01-088-1737; Wikipedia non-silicates 2014)
- Paraschachnerite (Ag_3Hg_2) (JCPDS: PDF#-00-027-0617; Wikipedia non-silicates 2014)
- Gamma (γ) phase with a body centered cubic unit cell (Ag_3Hg_4) (Baren 1996)
- Moschellandsbergite (Ag_2Hg_3)(JCPDS: PDF# 01-071-0529, 01-072-5091 & 01-072-8408; Berman and Harcourt 1938; Wikipedia non-silicates 2014)
- Arquerite/Luanhite (Ag_3Hg) (Wikipedia arquerite 2014)
- Eugenite (Ag_9Hg_2) (JCPDS: PDF#-00-058-0450; Wikipedia non-silicates 2014)

Only two, Schachnerite and gamma phase are represented in Baren's phase diagram.

In a recent review of the silver mercury amalgam by Predel in 2006 the $Ag_{11}Hg_9$ amalgam is referred to as the epsilon (ε) phase (Predel 2006). Predel is directly quoting Hansen's 1958 work. Baren's (1992 and 1996) older yet more definitive review and research describing this amalgam as the zeta (ζ) phase is not mentioned by Predel.

This demonstrates that further research is required to clarify the formula and composition of the gamma silver-mercury amalgam system, and to characterize the other naturally occurring amalgams.

$$\begin{aligned} &m\mathrm{Ag}_{11}\mathrm{Hg}_9\ (\text{seed}) + 9n\mathrm{Hg}_{(g)} + 11n\mathrm{Ag}\ (\text{sub/meso-surface}) \\ &\quad \rightarrow (m+n)\mathrm{Ag}_{11}\mathrm{Hg}_9 \end{aligned} \tag{6}$$

(fully formed ζ(zeta) phase image particle)

$$\begin{aligned} &m\mathrm{Ag}_3\mathrm{Hg}_4\ (\text{seed}) + 4n\mathrm{Hg}_{(g)} + 3n\mathrm{Ag}\ (\text{sub/meso-surface}) \\ &\quad \rightarrow (m+n)\mathrm{Ag}_3\mathrm{Hg}_4 \end{aligned} \tag{7}$$

(fully formed γ(gamma) phase image particle)

The silver in this second step needs to come from somewhere close to the amalgam seeds. In this case, the silver appears to come from two regions in the vicinity of the seed amalgam image particles: from the meso/sub-surface and the top surface. The amalgamation reactions proceed and the fully formed image particles are generated because silver is made available through the physical process of atomic/mass transfer. The first source of silver to be transported to the surface seems to originate from the meso/sub-surface region, that narrow transitional region immediately below the surface. The evidence for this are the voids observed in both modern and historical daguerreotypes that are located directly beneath or close to

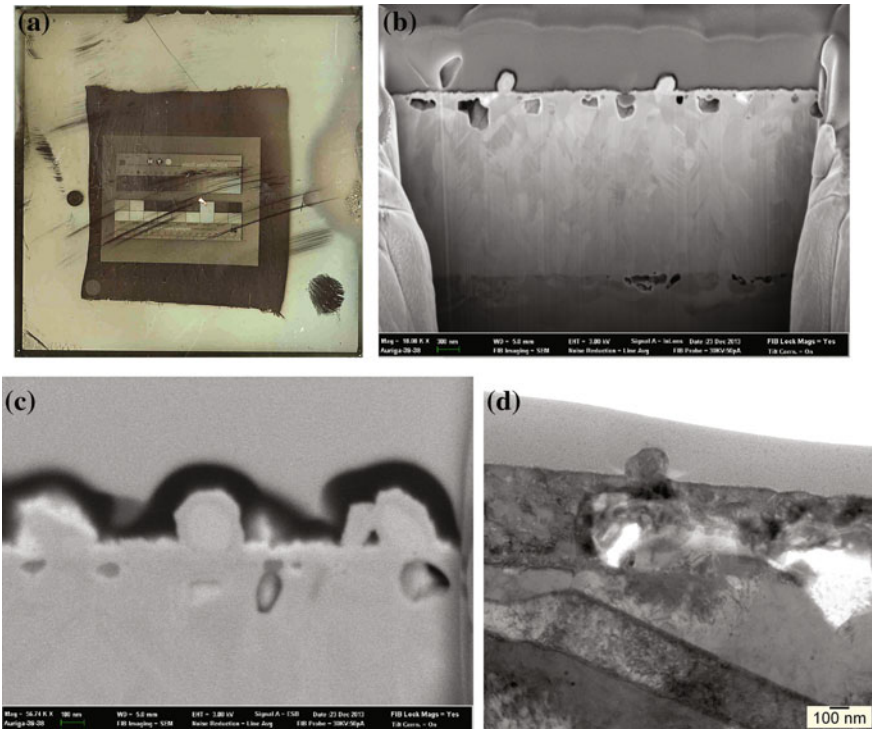

Fig. 14 Cross sections prepared using dual-beam focused ion beam scanning electron microscopes on two modern daguerreotypes, **a** a test daguerreotype made in 2011 where the *arrow* shows the region of image particles examined, **b** SE cross section, at 3 keV and ×57k magnification, **c** SE cross section at 3 keV and ×71k magnification, and **d** a TEM thin section of a 2008 daguerreotype

the image particles. And it appears that this meso/sub-surface region is the predominant region contributing silver.

Figure 14 shows cross sections prepared using dual-beam focused ion beam scanning electron microscopes on a modern (2011) daguerreotype where remaining silver halides have been removed using sodium thiosulfate, "hypo" ($Na_2S_2O_3$), and was gilded. Figure 14b shows an entire cross section view of approximately 6 μm with two large image particles and six voids. The two image particles sit over solid silver plate and are near the voids; approximately 300 nm from the particles to the voids. Neighboring grain surfaces and boundaries are seen in most of the voids, especially those on the left side. Figure 14c shows a void directly beneath an image particle on the right. The distance between the particle bottom and void top is below 100 nm. Figure 14d is a thin section of a modern daguerreotype prepared in 2008 where silver was fused to copper, polished and buffed, and then electroplated and buffed. The two silver strata—bottom fused and top electroplated silver, have distinctly different physical features. The lower third of the image shows the fused silver's large and elongated silver grains, characteristic of fusing, and the top of this fused layer, the interface between fused and electroplated layers, shows a

cold-worked structure due to extensive polishing to provide the mirror finish. The top electroplated silver stratum shows much smaller silver grains. The two voids in this example are at the interface of fused and electroplated silver. The image particle is directly above its void and the distance between the bottom of image particle to top of void is over 200 nm.

Video 2 (only available in electronic version) is a short video of a series of cross sections being milled on the modern daguerreotype shown in Fig. 15a. Note the image particles and their corresponding voids. This video further substantiates the new observations outlined above, showing the relationship between image particles and sub/meso-surface voids.

To achieve a better understanding of the relationship between the image particles and the meso/sub-surface, a study was designed to employ the use of 3D reconstruction of a series SEM images from FIB sectioning slices to examine an area rich in image particles of a modern daguerreotype prepared in 2011. A full series of 444

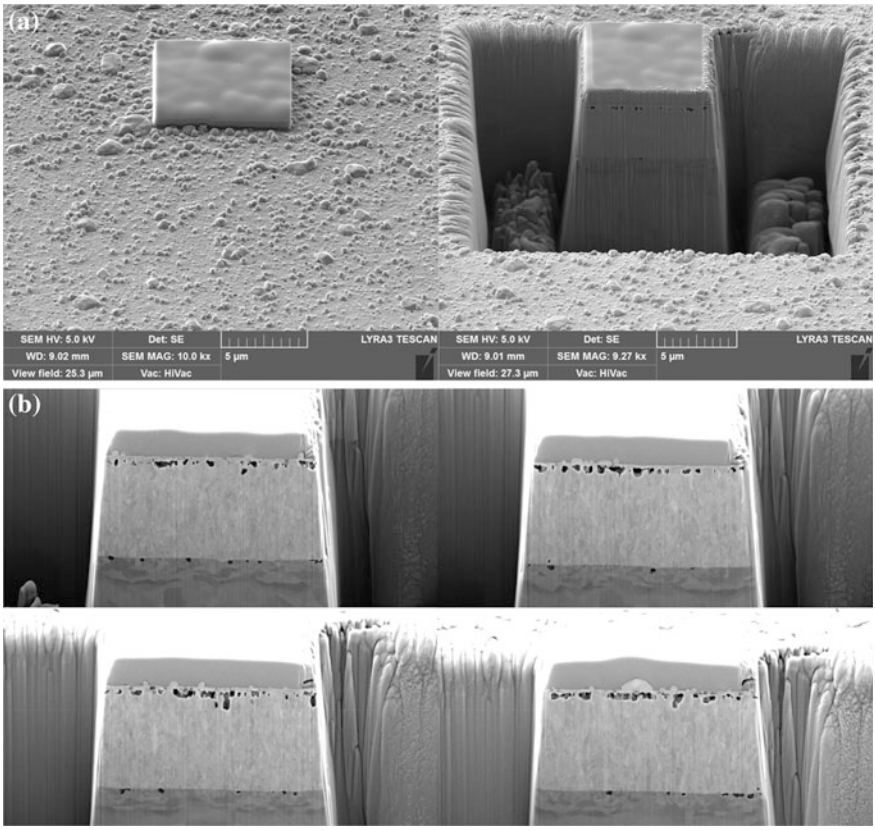

Fig. 15 The 3D reconstruction of a modern daguerreotype (2011) from a series SEM images from FIB sectioning slices **a** *left image* neatly placed surface coat of a protective platinum layer, and the preparatory trenching and clearing out beyond the area of interest, **b** four examples of the 444 slices taken

slices of 16.5 nm thickness were imaged and processed using Image J software. This allowed for qualitative 3D reconstruction and rendering of a volume with approximate dimensions of 6 × 6 × 7 µm. This approach has strengthened our hypothesis on the direct relationship between the surface and meso/sub-surface as seen in the images in Fig. 16 showing the volumetric relationship between image particles and meso/sub-surface voids. Figure 15b shows four examples of the 444 slices taken, which were used to reconstruct and render the 3D nature of surface particles and meso/sub-surface voids. Figure 16c shows two horizontal/lateral reconstructed virtual solid slices: the left slice is through image particles shown in a green color, and the right slice is through meso/sub-surface voids shown in blue. Finally, Fig. 16d shows the 3D volumetric renditions. These 3D renditions clearly show voids immediately beneath the image particles and that more voids exist beyond the area beneath the image particles. Because the image particles continue to grow after the initial amalgamation seed phase, there is a great need for a continuous source of silver, and that silver is being beckoned and transported from areas directly beneath the surface and beyond the image particle locations (Ravines et al. 2016).

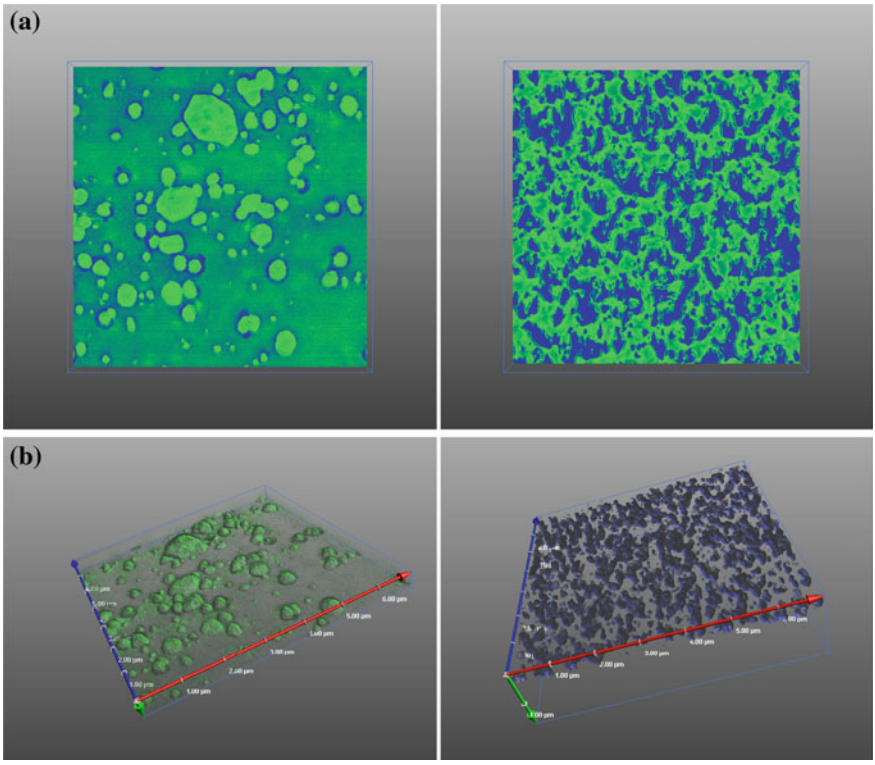

Fig. 16 **a** Horizontal/lateral reconstructed virtual solid slices, *left slice* through image particles shown in a *green color*, and the *right slice* is through meso/sub-surface voids shown in *blue*, and **b** 3D volumetric renditions of image particles (*left*), and meso/sub-surface voids (*right*). (All done with Image J—http://imagej.nih.gov/ij/)

Silver also appears to be supplied from surface grains. This second region of silver supply has been observed in a few modern (2011) daguerreotypes, and not in any of the historical daguerreotypes examined. The cross section shown in Fig. 17 shows the surface depressions and no meso/sub-surface voids.

The source of silver, whether it is from the meso/sub-surface or from surface depressions, is transported to the reactive site of image particle formation via the process of atomic/mass transfer. This is a sound physico-chemical step to invoke for these amalgamation reactions and the daguerreotype imaging process.

Our initial explorations of daguerreotypes with electron microscopy begun in 2006 revealed the sub/meso-surface voids. A review of the available literature on daguerreotypes regarding this newfound phenomenon did not find any observations of this type. Swan's 1979 paper shows the first ever daguerreotype cross section and the only cross section of the paper that depicts a particle with small dark areas beneath the surface under the particle, and the layers of silver and copper as seen in Fig. 18 (a reproduction of Swan's). No mention or description of these small dark areas is made. Given the above, we believe these to be the first publication of voids that were unnoticed by Swan and coworkers.

More recently, Whitmore and coworkers observed silver diffusion and void formation in their silver nanoparticle-sensor experiments (Whitmore 2014).

The driving force for the chemical reactions of amalgamation is likely to be the stable nature of the silver mercury amalgams being formed on the surface and the energetically active meso/sub-surface sites generated from cold working the silver.

In the past 30 years, with the advent of the miniaturization of electronic components of all types, the electronics and semiconductor industry have experienced

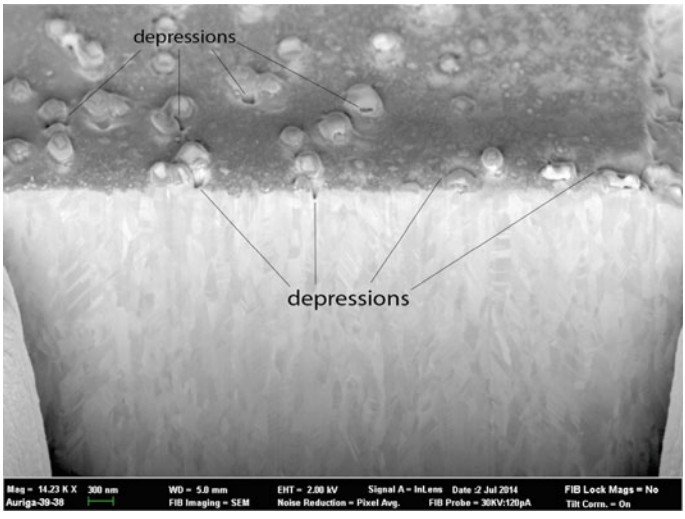

Fig. 17 A modern daguerreotype (2011) SE image showing depressions next to image particles at the cross section edge and throughout the surface

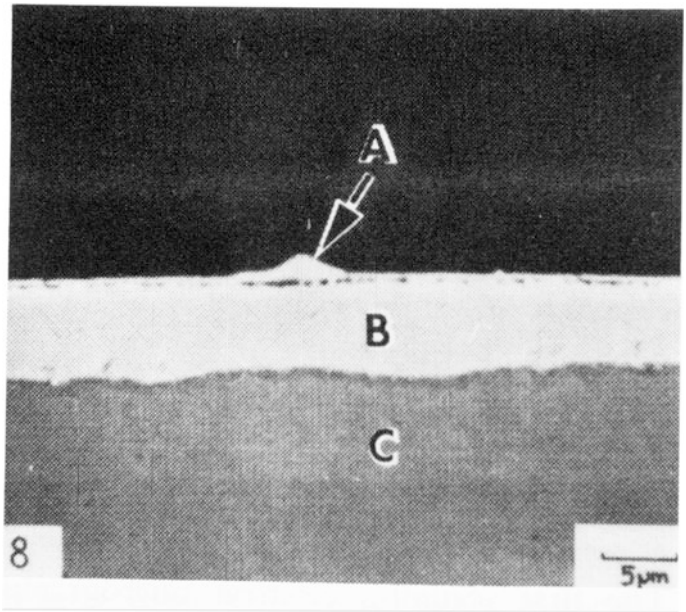

Fig. 18 The first daguerreotype cross section from Swan et al. (1979) (Reprinted from Swan et al. 1979, © 1979, with permission from SEM.)

the interesting damaging phenomenon of stress-induced void formation in metals used in the manufacture of critical electronic/semiconductor parts. Stress-induced voiding is not yet fully understood and is a multi-faceted problem involving grain structures, structural defects such as discontinuities, interfaces, and atomic transport processes (Suo 2003; Flinn et al. 1993). This is an active area of research and these findings could shed light on the daguerreotype observations presented herein.

Stress-induced voiding may provide a partial explanation for the voids observed in the meso/sub-surface of daguerreotypes. The daguerreotype has similar features of grain structures, structural defects, interfaces, and atomic transport processes seen in electronic/semiconductor systems yet these daguerreotype features are larger by an order of magnitude. In this case, the cold working of the surface from polishing and buffing to achieve the mirror-like finish required is likely to be causing enough nanometer and micrometer structural changes on the surface and meso/sub-surface grain structures resulting in a higher density of dislocations and sub-grain boundaries. Silver diffusion is likely to occur from all areas such as grain boundaries and dislocations, and from bulk silver grain. At this stage, the meso/sub-surface region is primed for action. The next step is the light-initiated formation of silver cluster latent image particles from the interaction of light with surface silver halides. This is then subjected to mercury development to form the initial silver-mercury amalgam seed image particles, a unique and separate step. It is followed by further development, the second portion of continued growth, through further exposure to gaseous mercury. At this second step in the development stage

the atomic/mass transfer of silver from the meso/sub-surface regions is invoked. The great mobility of silver from the meso/sub-surface is likely to occur by all diffusion modes—interstitial, substitutional and vacancy exchange, and is an area requiring further study to determine which of these is most prevalent. The higher density of grain defects could be considered to be part of the stressed condition as shown in Figs. 14, 15 and 16, the direct relationship between image particles and voids. Figure 14 shows that the voids are a total clearing out of an entire grain or grains and the void's walls are those of the neighboring and presumably more stable silver grains. The surface image particles are the reactive sites that in combination with the grain defects and instabilities are likely to jointly be providing the driving force for the atomic/mass transport of meso/sub-surface silver (Ravines et al. 2015).

This is what Daguerre offered the world and was how daguerreotypy was practiced for the first two years. Gilding was introduced in the 1840s and was quickly accepted by all daguerreotypists and became the final step in this first photographic process.

3.5 Gilding/Coating with Gold (Fizeau)

The entire gilding operation is a set of electrochemical reactions that result in the eventual formation of an overall thin gold film on the silver-mercury amalgam image particles and on the background silver surface. This electroless deposition of gold is an auto-catalytic plating process: a non-electrolytic process of depositing metals and alloys (Okinaka and Kato 2010). The electrochemically deposited thin film has its own physical properties and these properties depend on the solutions of the electroless deposition process.

The gold chloride solution is mixed with a sodium thiosulfate solution to readily form a stable gold thiosulfate complex. The chemical reaction describing the preparation of the gilding solution is:

$$AuCl_4^- + S_2O_3^{2-} + 3Na^+ \rightarrow \left[Au(S_2O_3)_2\right]^{3-} + 3Na^+ \quad (8)$$

The gold is being reduced from Au(III) to Au(I) and this happens readily in solution. The gold half reaction is: $Au^{3+} + 2e^- \rightarrow Au^+$, and its standard reduction potential ($E°_{red}$) = 1.401 V (Vanysek 2002). In this case, the thiosulfate remains unchanged and replaces the chlorides as ligands to form a stable linear gold coordinated complex (Bryce et al. 2003). Soon after the gold (I) thiosulfate solution is prepared, it is used to gild the daguerreotype.

The gilding of the daguerreotype was performed in a few ways. Some practitioners fully immersed the daguerreotype in a gold (I) thiosulfate solution bath and heated the daguerreotype in the bath. Others would pour the solution directly on the plate all the way to the edges so that the solution completely covered the top of the daguerreotype surface. It was then heated with a Bunsen burner from beneath. The heat applied to the bottom of the daguerreotype accelerated the gilding reactions.

The reactions taking place simultaneously are those of the gold (I) thiosulfate reacting with the silver-mercury amalgam image particles and with the silver background.

$$\left[Au(S_2O_3)_2\right]^{3-} + Ag_{(surface)} \rightarrow Au_{(surface)} + \left[Ag(S_2O_3)_2\right]^{3-} \quad (9)$$

In this set of reactions between the silver surface and the gold (I) thiosulfate solution, the gold is readily reduced from Au(I) to Au(0): the standard reduction potential (E°_{cell}) of this set of reactions is 0.14 (Abbruzzese et al. 1995). The half reactions occurring at the surface are:

$$\left[Au(S_2O_3)_2\right]^{3-} + e^- \rightarrow Au(surface) + 2S_2O_3^{2-} \quad E^\circ_{red} = 0.15 \quad (10)$$

$$Ag_{(surface)} + 2S_2O_3^{2-} \rightarrow \left[Ag(S_2O_3)_2\right]^{3-} + e^- \quad -\left(E^\circ_{red} = 0.01\right) \quad (11)$$

The reactions for silver taking place at the surfaces of the silver-mercury amalgam image particles are likely to be the same reactions for surface silver discussed above. Similarly, the reactions for mercury at the surfaces of the silver-mercury amalgam image particles are also simultaneously replaced with gold. The deposition reactions occur on the surface of the image particles yet we are unable to describe the mercury and gold (I) thiosulfate reactions in detail since these have not yet been fully studied (Oraby et al. 2010).

The standard reduction potentials for the half reactions of gold and mercury were chosen as representative to assist in the description of the overall electroless chemical reactions for mercury oxidation from mercury(0) to mercury(II) and gold reduction from gold (I) to gold (0) occurring at the surface of the image particle. The standard reduction potentials of half reactions for gold reduction, Eq. 12, and mercury oxidation, Eq. 13 (Vanysek 2002) are:

$$2Au^+ + 2e^- \rightarrow 2Au_{(surface)} \quad E^\circ_{red} = 1.692 \quad (12)$$

$$Hg_{(surface\ image\ particle\ amalgam)} \rightarrow Hg^{2+} + 2e^- \quad -\left(E^\circ_{red} = 0.851\right) \quad (13)$$

According to Eqs. 12 and 13, the overall reaction will occur spontaneously since the overall cell potential is positive, $E_{cell} = 0.841$, as was the case with the gold and silver thiosulfate system. Oraby and co-researchers (2010) investigated the stability constants for the formation of two mercury thiosulfate species: $[Hg(S_2O_3)_2]^{2-}$ with $\log k_2 = 29.23$, and $[Hg(S_2O_3)_3]^{4-}$ with $\log k_3 = 30.6$ (Oraby et al. 2010). The reactions that could occur to yield these and other stable mercury thiosulfate complexes in solution have yet to be investigated.

Both electroless gold deposition reactions involving silver and mercury occur readily and simultaneously, and result in a thin gold film on the silver background surface and on the silver-mercury amalgam image particles. The thin gold films were investigated with FIB SEM, STEM/TEM and electron backscattered diffraction (EBSD). FIB SEM results clearly show that a thin film was deposited. The gold

covers the entire surface; it completely envelops all silver background and silver mercury amalgam image particle surfaces. The embedded polishing materials—rouge, carbon black and alumina in the contemporary daguerreotypes—do not react with gold thiosulfate solution and, therefore, are not covered by gold. These uncovered locations appear as small pits on the gold surface. Figure 19 shows several views of the gilded surface of a modern surrogate daguerreotype. Figure 19b shows nature of the gilded surface film to be composed of nano-sized

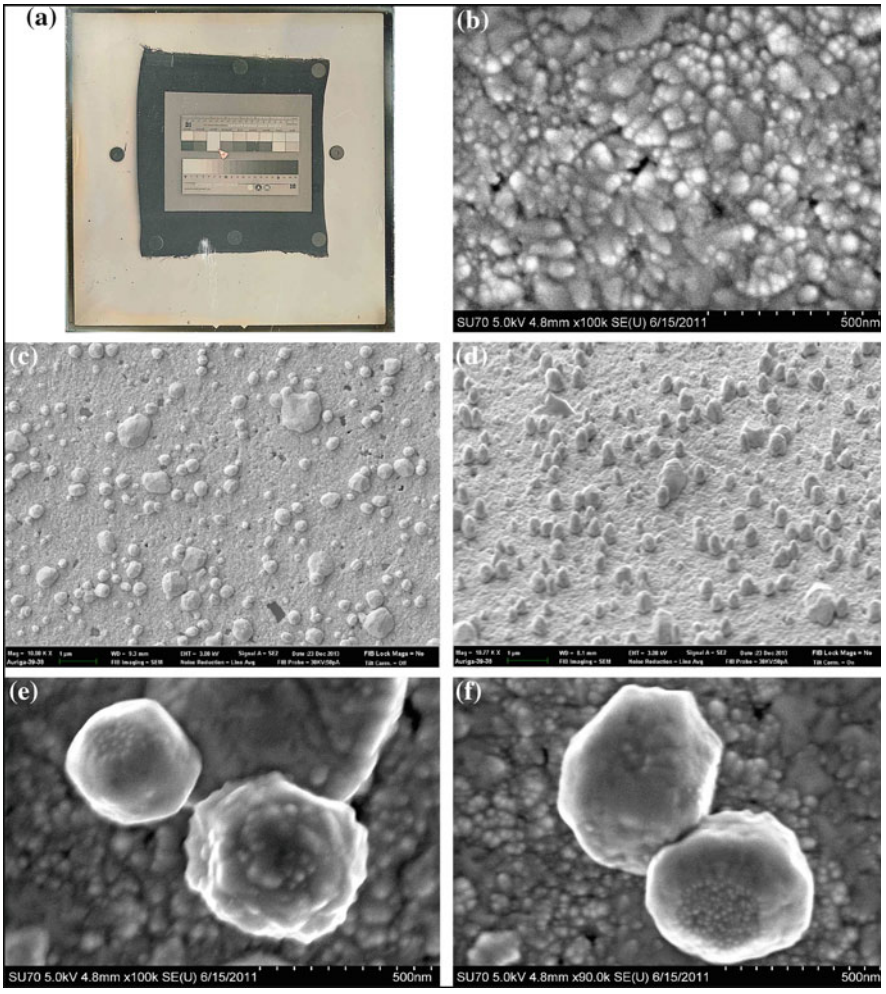

Fig. 19 SE electron micrographs of the gilded surface of a modern daguerreotype (2011), **a** general view with *arrow* showing area examined, **b** SEM-FEG, SE image of textured background surface, 5 kV and ×100k magnification, **c** top view of the surface, 3 kV and ×10k magnification, **d** angled view of the surface, 3 kV and ×11k magnification, **e** and **f** SE images of nano textured image particles both at 5 kV and ×100k and ×90k magnifications

gold grains. The angled view of Fig. 19d showcases what appears to be a more nano-textured film on the background surface and on the image particles. Figure 19e and f show the nano-texture acquired by the image particles as well, when compared with the sharp angled image particles before gilding as seen in Fig. 13b. The nano-gold film grains appear to be below 100 nm in lateral (x–y) size and hover in the 50 nm range.

Figure 19d shows the gilded background surface and it appears that this surface is more textured when compared to the un-gilded surface in Fig. 13b.

Table 3 lists the average root mean square roughness, Sq, values of the background of the un-gilded and gilded daguerreotypes. These values show an increase of about 10 % in the Sq of the background surface. Interestingly, this is pushing the limits of the spinning disc confocal microscope, and the Sq difference between un-gilded and gilded is not a large numerical difference but it seems that this is sufficient to considerably change the appearance and visual properties of the daguerreotype. It is also likely that other optical-physico-chemical aspects are involved with the overall appearance and the viewer's perception.

The various images in Fig. 20 show several cross sections of a modern surrogate daguerreotypes and a 19th century daguerreotype demonstrating the thinness of the gold film in both. Figure 20a, b and c are backscattered electron (BSE, BE) images of modern daguerreotypes, and Fig. 20d is an SE image of an historic daguerreotype. All cross sections demonstrate the thinness of the gold film. In general, it appears that the thickness is below 100 nm, and it seems that the gold nano-grains have similar dimensions in all axes, as seen above in Fig. 19b. The thin film of gold around the image particles in this example is thinner, approximately in the 20 nm range as shown in Fig. 15c. Figure 20d is a 19th century daguerreotype that has been cross-sectioned and shows the gold thickness to be over 100 nm. The thickness of the 19th century plate is slightly greater than that of the modern daguerreotypes examined.

Figure 21 shows cross sections of a different modern daguerreotype, Fig. 21a, b and c are TEM images. Figure 21b and c show a thin film that is less than 100 nm in thickness enveloping the image particles. This further confirms the FIB SEM cross sections of Fig. 20. Figure 21a and b are interesting in that they show cross sections of columnar image particles as shown earlier in the tilted or angled views of the ungilded and gilded plates of Figs. 14b and 19d.

Electron backscatter diffraction (EBSD) patterns can be obtained in the scanning electron microscope by focusing a stationary electron beam onto a crystalline sample that is tilted approximately 70° from the horizontal. When EBSD patterns are automatically collected at each point on a regular grid on the sample, it is

Table 3 Surface metrology of un-gilded and gilded daguerreotypes: root mean square average roughness, Sq, values

Plate processing step	Sq ± Std. dev. (nm)	Number of areas sampled
Un-gilded	70.5 ± 12.4	10
Gilded	77.9 ± 19.7	10

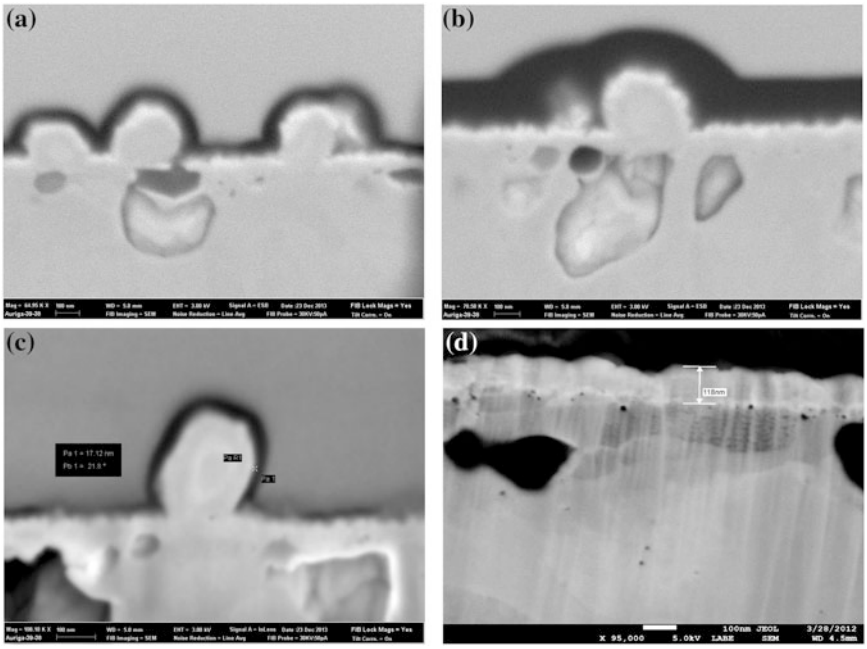

Fig. 20 BE electron micrographs of cross sections of modern and a 19th century daguerreotype, **a–c** BE images of a modern daguerreotype, all at 3 kV, and ×65k, ×71k and ×108k magnifications, **d** SE image of a 19th century daguerreotype, 5 kV, and ×95k magnification

possible to produce EBSD maps that fully characterize the grain orientations and grain boundary misorientations that are present within the microstructure.

In this portion of the investigation, EBSD maps were acquired on both a historic 19th century and a modern daguerreotype. Due to the delicate nature of the daguerreotypes' surfaces, no modifications were made to the daguerreotypes, i.e. no mechanical nor chemical polishing were performed, which is highly uncommon for EBSD analyses. The areas investigated contained the darkest shadow and/or the blackest areas to avoid any images particles that are protruding from the surface.

Figure 22 show the [001] inverse pole figure (IPF) maps acquired from the 19th century and modern daguerreotypes. The [001] inverse pole figure maps show the crystal direction that is parallel with the surface normal direction of the daguerreotypes and are colored according to the unit triangle shown below the maps. In Fig. 22a, the high fraction of blue-colored grains in the IPF map is an indication that there is a high preference for the crystal <111> direction to be aligned with the surface normal of the 19th century daguerreotype. A quick visual comparison shows that this preference is much stronger in the 19th century daguerreotype when compared to the modern daguerreotype.

Since crystal orientations are acquired at each point in the analyzed area, groups of similarly oriented points can be identified as individual grains. Grain size can

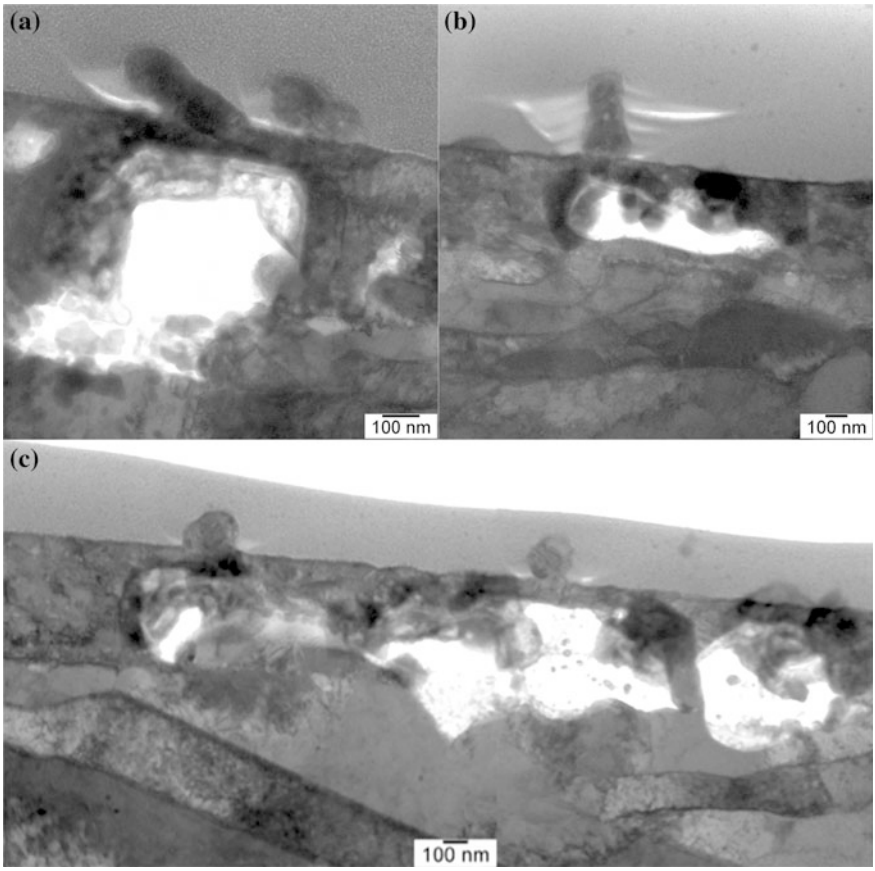

Fig. 21 Cross section images of a modern daguerreotype (**a**–**c**) with the transmission electron microscope (TEM), accelerating voltage 200 kV at several magnifications

then be calculated as the circle equivalent diameter after summing the number of data points contained within a grain into an area. A twin grain refers to a grain that is bounded by one or two twin boundaries, and typically has a long and narrow morphology in two dimensions. When twins are included in the grain size evaluation, the overall grain size distribution becomes biased towards the smaller grains (Wright and Larsen 2002).

The grain size distribution without twins for the 19th century and modern daguerreotypes are shown in Fig. 23. The average grain size is 70 and 77 nm for the 19th century and modern daguerreotypes respectively. Despite all efforts to reproduce daguerreotypes using the various methods precisely, it is unclear as to why the 19th century daguerreotypes have smaller average grain sizes and a more preferential alignment of the <111> crystal direction with the surface normal direction.

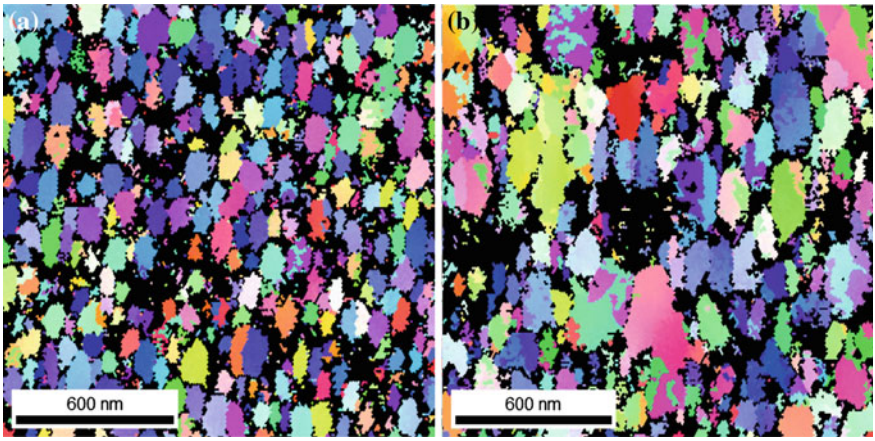

Fig. 22 Inverse pole figure (IPF) [001] maps from **a** the 19th century and **b** modern daguerreotypes

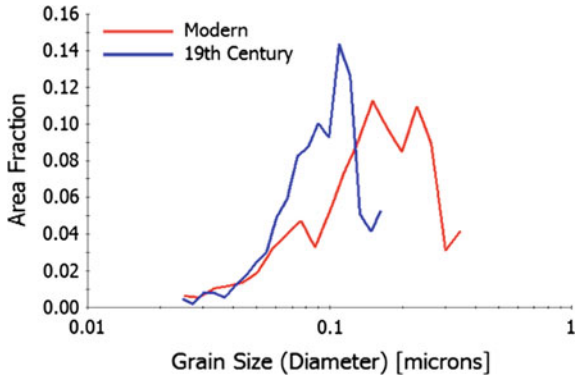

Fig. 23 Grain size distribution without twins for the 19th century and modern daguerreotypes

4 Conclusions

Although daguerreotypes have existed since 1839, this study at nanometer and sub-micrometer scales using the various instrumental techniques of confocal microscopy, Raman spectroscopy, HR SEM, FIB SEM, TEM/STEM and EBSD further contributes to the early research conducted by Swann et al. (1979) and Barger and White (1991), and provides a new overview of the many complex chemical, physical and material science concepts involved at the surface and meso-surface in each step of this intricate nano-structured image making process. In addition to shedding more light on some aspects of the complex photo-physicochemical reactions in this process, it has also, as is prone to happen, lead to other interesting observations that require further investigation.

At the physical processing steps of polishing and buffing it was observed that a significant amount of inert polishing materials (alumina, iron oxide and carbon) are embedded in the silver surface. These embedded nano-sized fragments decrease the overall silver surface available to react with halogen gases to provide the light sensitive surface required for imaging. This polishing material interference still allows for capturing images of high quality and resolution. Yet it is possible that even better quality and higher resolution images could be achieved if the polishing/buffing materials left less or no embedded material in the silver surface. This is a challenge for the modern daguerreotypist.

The exciting arena of transition metals cluster science could further clarify and significantly add to the photographic concept of the latent image. The relationship between the formation of plasma-generated clusters from silver metal could be akin to that of light activated silver clusters on silver halides.

The tilted electron micrograph images (Figs. 14b and 19d) show a large number of image particle shapes indicating the possible presence of many more amalgam types on the surface than has previously been reported in the literature. The presence of these multiple crystal formations is a good indication that complex physico-chemical nucleation reactions are occurring at the surface during the initial stages of mercury development. It is at this initial nucleation step of silver clusters amalgamating with mercury where the formation of an amalgam type is possibly determined. X-ray diffraction studies could elucidate this aspect.

Amalgam seeds grow into fully formed image particles and this appears to preferentially invoke silver from the meso-surface. This interesting mass transport phenomenon of "mining" silver from beneath the surface is creating a network of meso-surface voids and requires further study as well.

The end result of this entire complex set of physico-chemical reactions and the creation of nano-textured surfaces and nanometer and sub-micrometer image particles that were initiated by light interacting with silver halides is the formation of the photographic image that is, again, the resulting interplay of light with the surface through scattering and other plasmon effects.

The variety of electron microscopical techniques available nowadays, and used in this study has enabled us to peer into and gain a better understanding of the complexity of the image making process of the daguerreotype. These new insights should be useful in the long-term preservation and conservation efforts of the smaller and standard sized historical daguerreotypes as well as the larger mammoth sized contemporary daguerreotypes.

The complex physico-chemical nature of this nanometer and sub-micrometer scale photographic system is not necessarily unique. The nature and dimensional scale of other 19th century silver and non-silver based photographic processes is likely to be similar to that of the daguerreotype, and, perhaps, can also be found in other cultural heritage systems.

Acknowledgments The authors acknowledge the help and support of many colleagues and friends: Peter Bush, South Campus Instrumentation Center, SUNY Buffalo, SCIC, B1 Squire Hall, South Campus, Buffalo, New York, USA, pjbush@buffalo.edu. John Minter, Robledo Rodriguez

and Steve Stoker, Corporate Engineering & Analytical Science, Eastman Kodak Company, 1999 Lake Avenue, Rochester, New York, 14650-2104 USA, jrminter@gmail.com, rob.gutierrez@kodak.com. Anne West, Eastman Kodak Company (retired), 1999 Lake Avenue, Rochester, New York, USA 14650-2104, annewest78@gmail.com. Natasha Erdman, Product Manager, JEOL USA Inc., 11 Dearborn Road, Peabody, Massachusetts 01960 USA, erdman@jeol.com. Yueling Qin, Senior Research Support Specialist Department, Integrated Nanostructured Systems Initiative, SUNY Buffalo, 114 Davis Hall, UB North Campus, Buffalo, New York, USA, yqin@buffalo.edu. Richard Hailstone, Associate Professor, Chester F. Carlson Center for Imaging Science, Rochester Institute of Technology, 54 Lomb Memorial Drive, Rochester, NY 14623, USA, hailstone@cis.rit.edu.

References

Abbruzzese C, Fomari P, Massidda R, Veglio F, Ubaldini S (1995) Thiosulphate leaching for gold hydrometallurgy. Hydrometallurgy 39:265–276

Baren MR (1992) Silver mercury amalgam phase diagram. In: Baker H (ed) Alloy phase diagrams, vol 3, ASM handbook, 10th edn. ASM International, Materials Park, Ohio

Baren MR (1996) The Ag-Hg (Silver-Mercury) system. J Phase Equilib 17(2):122–128

Barger S, White W (1991) The daguerreotype: 19th century and modern science. Smithsonian Institution Press, John Hopkins University Press, Washington, D.C., pp 117–134

Barger S, Messier R, White W (1984) Nondestructive assessment of daguerreotype image quality by diffuse reflectance spectroscopy. Stud Conserv 29(2):84–86

Bell IM, Clark RJH, Gibbs PJ (1997) Raman spectroscopic library of natural and synthetic pigments (pre-approximately 1850 AD). Spectrochim Acta Part A Mol Biomol Spectros 53:2159–2179

Belloni J (2002) The role of silver clusters in photography. CR Phys 3:1–10

Belous VM, Kuskovsky IL (2007) On differences in photoluminescence and photographic characteristic of AgBr (100) and AgBr (111) microcrystals I: unsensitized and reduction sensitized emulsions. JIST 51(6):530–539

Berman H, Harcourt GA (1938) Natural amalgams. Am Min 23:761–764

Binner JGP, Dimitrakis G, Price DM, Reading M, Vaidhyanathan B (2006) Hysteresis in the—phase transition in silver iodide (PDF). J Therm Anal Calorim 84(2):409–412. doi:10.1007/s10973-005-7154-1

Bosnick KA et al (1999) Tricapped tetrahedral Ag_7: a structural determination by resonance Raman spectroscopy and density functional theory. J Chem Phys 111(19):8867–8870

Brewster D (1847) History of discoveries in photography. In: WH Bidwell (eds) Eclectic magazine of foreign literature, science and art, p 239

Brodie I, Thackray M (1984) Photocharging of thin films of silver iodide and its relevance to the Daguerrodiere photographic process. Nature 312:744–746

Bryce RA, Charnock JM, Pattrick RA, Lennie AR (2003) EXAFS and density functional study of gold thiosulfate complex in aqueous solution. J Phys Chem A 107:2516–2523

Burgio L, Clark RJH (2001) Library of FT-Raman spectra of pigments, minerals, pigment media and varnishes, and supplement to existing library of Raman spectra of pigments with visible excitation. Spectrochimica Acta Part A: Mol Biomol Spectros 57:1491–1521

Centeno SA, Meller T, Knnedy N, Wypyski M (2008) The daguerreotype surface as a SERS substrate: characterization of image deterioration in plates from the 19th century studio of Southworth & Hawes. J Raman Spectrosc 39:914–921. doi:10.1002/jrs.1934

Centeno SA, Schulte F, Kennedy NW, Schrott AG (2011) The formation of chlorine-induced alterations in daguerreotype image particles: a high resolution SEM-EDS study. Appl Phys A 105(1):55–63 (October 2011). doi:10.1007/s00339-011-6570-2

Daguerre L (1839) History and practice of the photogenic drawing on the true principles of the daguerreotype with the new method of dioramic painting. Stewart and Murray, London
Eachus RS, Marchetti AP, Muenter AA (1999) The photophysics of silver halide imaging materials. Annu Rev Phys Chem 50:117–144
Fizeau AHL (1841) Notes sur un moyen de fixer les images photographiques. Comptes Rendus hebdomadaires des séances de l'academie des sciences 11:237–238
Flinn PA, Flinn PA, Mack AS, Besser PR, Marieb TN (1993) Stress-induced void formation in metal lines. MRS Bull 18(12):26–35
Hailstone RK, Hamilton JF (1985) Determination of the minimum size of the latent image. J Imaging Science 29:125–131 and references therein
Hamilton JF (1988) The silver halide photographic process. Adv Phys 37(4):359–441
Hansen M, Anderko K (1958) Constitution of binary alloys. McGraw Hill, New York
Harbich W, Fedrigo S, Meyer F, Lindsay DM, Lignieres J, Rivoal JC, Kreisle D (1990) Deposition of mass selected silver clusters in rare gas matrices. J Chem Phys 93(12):8536–8543
Haslett TL, Bosnick A, Moskovits M (1998) Ag_5 is a planar trapezoidal molecule. J Chem Phys 108(9):3453–3457
Haslett TL et al (1999) Resonance Raman spectroscopy of matrix-isolated mass-selected Fe_3 and Ag_3. J Chem Phys V111(14):6456–6461
Humphrey SD (1858) American Hand Book of the Daguerreotype, 5th edn, New York, p 59
Legodi MA, de Waal D (2007) Preparation of magnetite, goethite, hematite of pigment quality from mill scale iron. Dyes Pigm 74:161–168
Lombardi JR, Davis B (2002) Periodic properties of force constants of small transition-metal and lanthanide clusters. Chem Rev 102:2431–2460
Marquis EA, C Y, Kohanek Julia, Dong Y, Centeno SA (2015) Exposing the sub-surface of historical daguerreotypes and the effects of sulfur-induced corrosion. Corros Sci 94:438–444
Mitchell JW (1957) Photographic sensitivity. Rep Prog Phys 20(1):433
Mitchell JW (1981) The formation of the latent image in photographic emulsion grains. Photographic Sci Eng 25:170–188
Motoyoshi I, Nishida S, Sharan L, Adelson EH (2007) Image statistics and the perception of surface qualities. Nature 447:206–209
Mott NF, Gurney RW (1940) Electronic processes in ionic crystals. Clarendon press, Oxford pp 227–248
Okinaka T, Kato M (2010) Electroless deposition of gold. In: Modern electroplating, 5th ed. Wiley, NY pp 483–498
Oraby EA, Jeffrey MI, Browner RE (2010) The deportment of mercury during thiosulfate leaching and resin-in-pulp recovery of gold from ores. Miner Metall Process 27(4):184–189
Orr WS (1856) Orr's circle of the sciences: a series of treatises on the principles of science with their application to practical pursuits, practical chemistry. Houlston and Stoneman, London, pp 260–261
Pobboravsky I (1971) Study of iodized daguerreotype plates. MS thesis, Rochester Institute of Technology, p 9
Predel B (2006) Ag-Hg (Silver-Mercury), This document is part of subvolume 12A 'Ac-Ag … Au-Zr, supplement to subvolume IV/5A' of volume 12 'phase equilibria, crystallographic and thermodynamic data of binary alloys' of Landolt-Börnstein—Group IV…—B. Predel in Ac-Ag … Au-Zr
Ravines P, Wiegandt R, Wichern CM (2008) Surface characterisation of daguerreotypes with the optical metrological technique of confocal microscopy. Surf Eng 24(2):139–146
Ravines P, West A, Minter J, Gutierrez RO (2010) The daguerreotype under high magnification: an ultra-high resolution SEM study of a 19th century daguerreotype's surface nanostructure. In: Ruvalcaba Sil JL, Reyes Trujeque J, Arenas Alatorre JA, Velázquez Castro A (eds) 2nd Latin–American symposium on physical and chemical methods in archaeology, art and cultural heritage conservation: selected papers. Symposium on archaeological and arts issues in material science (LASMAC & IMRC 2009, Cancun, Mexico). Universidad Nacional Autonoma de Mexico (UNAM), Mexico City, pp 99–109)

Ravines P, Lingjia Li, McElroy R (2016) An electron microscopy study of the image making process of the daguerreotype, the 19th century's first commercially viable photographic process. J Imaging Sci Technol 60(3):030504-1-030504-10

Seitz F (1951) Speculations on the properties of the silver halide crystals. Rev Mod Phys 23 (4):328–352

Suo Z (2003) Reliability of interconnect structures. In: Gerberich W, Yang W (eds) Interfacial and nanoscale failure, vol 8. In: Milne I, Ritchie RO, Karihaloo B (eds) Comprehensive structural integrity. Elsevier, Amsterdam, pp 265–324

Swan A, Fiori CE, Heinrich KJ (1979) Daguerreotypes: a study of the plates and the process. Scan Electron Microsc 1:411–423

Tani T (1998) Progress and future prospects of silver halide photography compared with digital imaging. J Imaging Sci Technol 42(1):1–13

Tomasini EP et al (2012) Micro-Raman spectroscopy of carbon-based black pigments. J Raman Spectrosc 43:1671–1675

Vanysek P (2002) Electrochemical series, chapter 8, pp 21–31. In: CRC handbook of chemistry and physics, 83rd edn

Weber WH (2000) Raman applications in catalysis for exhaust-gas treatment (pp 236–237, Chapter 6). In: Willes WH, Merlin R (eds) Raman scattering in materials science. Springer Science & Business Media, Aug 24, 2000, 492 p

Whitmore P (2014) Personal communication and a spin-off observation related to research. In: Chen R, Nuhfer NT, Moussa L, Morris HR, Whitmore PM (2008) Silver sulfide nanoparticle assembly obtained by reacting an assembled silver nanoparticle template with hydrogen sulfide gas. Nanotechnology 19:455604

Wikipedia, Classification of non-silicate minerals website, native elements http://en.wikipedia.org/wiki/Classification_of_non-silicate_minerals. Accessed Aug 2014

Wikipedia, Arquerite website, http://en.wikipedia.org/wiki/Arquerite. Accessed Aug 2014

Wright SI, Larsen RJ (2002) Extracting twins from orientation imaging microscopy scan data. J Microsc 205:245–252

Part II
Nanotechnologies and Analytical Strategies to Characterise Cultural Heritage

Surface-Enhanced Raman Spectroscopy: Using Nanoparticles to Detect Trace Amounts of Colorants in Works of Art

Federica Pozzi, Stephanie Zaleski, Francesca Casadio, Marco Leona, John R. Lombardi and Richard P. Van Duyne

Abstract In recent years, powerful physical processes occurring in the vicinity of nanoscale metal surfaces have been exploited in the art world for the detection of trace amounts of colorants with surface-enhanced Raman spectroscopy (SERS). With this technique, naturally occurring and man-made organic molecules used as dyes and pigments in objects from antiquity to the present day are being detected with high molecular specificity and unprecedented sensitivity. This chapter reviews the broad spectrum of SERS analytical methodologies and instrumental improvements that have been developed over the years in the field of cultural heritage science, and discusses significant case studies within different types of works of art and archaeological artifacts.

F. Pozzi (✉)
Department of Conservation, Solomon R. Guggenheim Museum, 1071 Fifth Ave, New York, NY 10128, USA
e-mail: fpozzi@guggenheim.org

S. Zaleski · R.P. Van Duyne
Department of Chemistry, Northwestern University, 2145 Sheridan Rd., Evanston, IL 60208, USA
e-mail: szaleski@u.northwestern.edu

R.P. Van Duyne
e-mail: vanduyne@northwestern.edu

F. Casadio
Department of Conservation, Art Institute of Chicago, 111 South Michigan Ave, Chicago 60603, USA
e-mail: fcasadio@artic.edu

M. Leona
Department of Scientific Research, Metropolitan Museum of Art, 1000 Fifth Avenue, New York, NY 10028, USA
e-mail: marco.leona@metmuseum.org

J.R. Lombardi
Department of Chemistry, City College of New York, 160 Convent Ave, New York, NY 10031, USA
e-mail: lombardi@sci.ccny.cuny.edu

P. Dillmann et al. (eds.), *Nanoscience and Cultural Heritage*,
DOI 10.2991/978-94-6239-198-7_6

1 Introduction

Since the dawn of time, color has been used by humanity to beautify the world and convey thoughts and feelings through various means of artistic expression.

Among the colored materials employed since antiquity, pigments and colorants have played a key role in the dyeing of fabrics and creation of artworks, to embellish individuals, decorate objects of everyday use, and as a sign of hierarchical status. The term "pigment" is used to describe insoluble materials, organic or inorganic, which are ground to fine powder and suspended in a binder to form paint. On the other hand, the terms "dye" and "colorant" generally refer to organic substances that are soluble in the medium and show affinity for a substrate either inherently or through the action of additives. In textile dyeing, colorants may be applied to fiber substrates directly (direct dyes), after being solubilized with a reducing agent (vat dyes), or with the aid of bridging metal ions called mordants (mordant dyes). In painting, dyestuffs were typically precipitated onto an inert, insoluble, inorganic substrate to produce lake pigments with significantly improved lightfastness properties compared to the primary fugitive dyes.

Prior to the introduction of synthetic colorants in the second half of the 19th century, dyes were derived from a variety of natural sources ranging from roots, berries, bark and leaves to different types of organisms such as lichens, insects and shellfish (Mills and White 1987; Hofenk de Graaff et al. 2004; Cardon 2007). Most natural red dyes owe their color to anthraquinone chromophores and can be extracted from insects, as in the case of cochineal, kermes and lac dye, or plants, among which madder and brazilwood are numbered. Several blue and purple colorants, including indigo and Tyrian purple, consist of a mixture of indigotin-related substances obtained from plants or sea snails, while other dyes of similar shades, like orchil, are derived from different sources, such as lichens. As far as yellow colorants are concerned, flavonoids—occurring as glycosides in a great variety of botanical species—are their main chromophores, although a number of other molecules such as carotenoids, curcuminoids, naphthoquinones and gallotannins may be found as well. Besides reds, blues and yellows, other hues could be produced by using two or more dyes in combination: green shades, for instance, were traditionally obtained as mixtures of a blue and a yellow colorant. For this reason, historic tapestries that have been extensively exposed to light often show blue foliage as a result of the fading of the more fugitive yellow component of the mixture.

The fortuitous discovery of mauveine, the first synthetic dye, by William Perkin in 1856 prompted extensive chemical experimentation that led both to the synthesis of molecules previously derived from natural sources, such as alizarin and indigotin, and to the introduction of several improved artificial colors that have no counterparts in nature, thus initiating a rapid decline in the dominance of natural dyes in world markets. In addition to their use in textiles and artworks, those synthetic colorants that could be tested as safe have found wide application as

printing and pen inks, paint components, dyes for food, plastic and rubber, and cosmetic constituents (Mills and White 1987; Lewis 1988).

Scientific analysis of objects of artistic, historic and archaeological significance is key to reconstructing their story and elucidating the circumstances in which they have been created and, in some cases, have travelled through the centuries prior to ending up in the inquiring hands of conservators and scientists for in-depth technical examination. In particular, the identification of natural and synthetic colorants may help to clarify attribution, provenance and dating, technology of fabrication, trade routes and commercial transactions that may have allowed the usage of certain dyes far away from their native locations. Moreover, investigating the origin, nature and chemical behavior of the colored materials employed in the production of artworks and historical artifacts may shed new light on their original color and appearance, thus offering insight into the artist's actual intentions and choices, the techniques used, and the dates *ante quem* and *post quem* the object was created, possibly even leading to the uncovering of falsifications and forgeries. Most importantly, a clear understanding of the materials used is essential to enable the object's long-term preservation and to inform conservation treatments, as well as museum display and lending policies.

The identification of colorants from artworks and objects of archaeological, anthropological or historical value poses a whole set of analytical challenges. Recent advances in macro-X-ray fluorescence (macro-XRF) mapping (Dik et al. 2008; Alfeld et al. 2013a, b) and infrared (IR), ultraviolet/visible (UV/vis), and hyperspectral imaging (Delaney et al. 2010, 2014; Ricciardi et al. 2012; Dooley et al. 2013; Rosi et al. 2013) have opened up exciting opportunities to track the distribution of pigments over the entire surface of a painted object. However, X-ray techniques are most successful at mapping inorganic pigments and are not able to map organic compounds, with the notable exception of eosin (tetrabromofluorescein, also known as geranium lake, a pigment extensively used by Vincent van Gogh). In hyperspectral imaging, the signal from dyes is invariably compounded with the spectral contributions of the binding medium and other paint components, so the identification of the organic colorant is possible only in rare cases. At the micro-scale, although recent research has been aiming at detecting and identifying dyes non-invasively in situ, to date the greatest chances of success still rely on the removal of one or more samples from the object under study. To complicate the analysis even further, the extraordinary tinting strength of many organic colorants caused them to be used in minute amounts in both historical textiles and works of art, where they are typically found in complex chemical environments, bound to cloth fibers by means of metal ions or embedded in paint layers in the form of lake pigments. As a result, the application of intensive sample pretreatment procedures often becomes a necessary step to isolate the colorants from their matrixes and achieve selective molecular identification. An additional obstacle is posed by the lack of permanence and susceptibility to deterioration of several colored organic materials that, upon exposure to air and light, undergo a number of chemical degradation processes leading to the formation of colorless species with a different molecular structure compared to the primary dye (Grosjean et al. 1988; Saunders

and Kirby 1994; Ferreira et al. 2001; Yoshizumi and Crews 2003; Ahn and Obendorf 2004, 2007; Cooksey and Sinclair 2005; Colombini et al. 2007; Clementi et al. 2007; Koperska et al. 2011; Manhita et al. 2011, 2013; Degano et al. 2011; Ramesova et al. 2012). Therefore, the amount of colorant available for analysis is often infinitesimal, challenging the limits of detection of many analytical techniques.

The analysis of organic colorants, made possible by the introduction of chromatographic and spectroscopic techniques, greatly benefited, in the past few decades, from both the improvement of pre-existing analytical procedures and the development of new cutting-edge instrumental methods. Initial attempts at detecting and identifying dyes in historical artifacts involved the use of absorbance UV/vis spectrophotometry (Taylor 1983; Wouters 1985) and thin-layer chromatography (TLC) (Masschelein-Kleiner and Heylen 1968; Schweppe 1993). However, in both cases, a sizable amount of colorant needs to be removed from the sample and brought into solution for analysis, thus requiring that the sample itself be of significant dimensions or deeply colored. Alternative non-invasive approaches by means of reflectance UV/vis spectrophotometry (Bacci et al. 1991; Montagner et al. 2011; Gulmini et al. 2013) and fluorimetry (Claro et al. 2008, 2010; Degano et al. 2009; Melo and Claro 2010; Romani et al. 2010; Clementi et al. 2014; Amat et al. 2015) have been also evaluated, occasionally leading to the successful characterization of pigments and colorants from medieval illuminations, paint cross sections, ancient textiles and wall paintings. Yet, electronic methods typically provide broad, featureless spectra that often appear to be nearly identical for distinct compounds of similar molecular classes and, in some cases, even for totally unrelated chemical groups. This, along with the ubiquitous additional contribution of binding media, fillers, additives, and all other sample components to the spectra, makes the interpretation extremely challenging. High-performance liquid chromatography (HPLC) remains the technique of choice for the characterization of organic colorants, allowing researchers to separate and identify dyes even in complex mixtures (Wouters 1985; Wouters and Verhecken 1989; Koren 1994; Halpine 1996; van Bommel et al. 2007). However, in this case, too, the amount of sample required for analysis may sometimes be prohibitive when dealing with museum objects for which permission to sample cannot be granted due to value, condition, or policy. While enabling the non-destructive characterization of colorants in minute samples or whole objects, vibrational methods such as Fourier-transform infrared (FTIR) (Gillard et al. 1994) and Raman/FT-Raman (Bell et al. 1997; de Oliveira et al. 2002; Edwards et al. 2003; Scherrer et al. 2009) spectroscopies were proven more suitable for the analysis of inorganic pigments and synthetic dyes. Raman spectroscopy, in particular, suffers from inherently weak signals and strong molecular fluorescence from natural dyestuffs that often obscures the Raman scattering signal even when using near-infrared (NIR) and IR excitation wavelengths to avoid fluorescence, such as 785 nm and above. Furthermore, because only sub-nanogram levels of dyes are needed to achieve intense coloration, Raman spectroscopy is often not sensitive enough to probe these materials, especially when they are embedded in complex matrixes such as textile fibers or artist's paints.

Among the less sample-intensive techniques, surface-enhanced Raman spectroscopy (SERS) has allowed researchers to overcome many of the drawbacks described above, enabling successful detection and identification of colorants from artworks and historical artifacts with high molecular specificity, unparalleled sensitivity, and the lowest known limits of detection (Chen et al. 2007; Wustholz et al. 2009; Casadio et al. 2010). In SERS, organic molecules are adsorbed on noble metal nanostructures and can thus be probed due to the exceptional Raman scattering enhancement and fluorescence quenching provided by the substrate via chemical and electromagnetic effects (Fig. 1) (Lombardi and Birke 2009, 2012). It has been demonstrated that the SERS signal of ensemble-averaged molecules exhibits enhancements up to eight orders of magnitude over the normal Raman cross section. Since the initial discovery of SERS (Fleischmann et al. 1974) and the explanation of the observed phenomenon in the 1970s (Albrecht and Creighton 1977; Jeanmaire and Vanduyne 1977), the field has grown enormously and has been enriched by a wealth of experimental studies. In particular, in the past ten years, the potential of SERS for dyestuff identification in various art and archaeological applications has been increasingly harnessed, with a significant growth in the number of publications in this area.

Initially, the greatest effort in the field of SERS for art and archaeology aimed at the characterization of reference materials, with special attention being paid to natural red colorants: alizarin, purpurin, carminic and laccaic acids, and related anthraquinones have been the subject of several studies in the scientific literature (Shadi et al. 2004; Cañamares et al. 2004, 2006a; Chen et al. 2006; Cañamares and Leona 2007; Baran et al. 2009; Rambaldi et al. 2015). Articles about the detection of flavonoids (Jurasekova et al. 2006, 2008, 2012; Wang et al. 2007; Teslova et al. 2007; Cañamares et al. 2009; Corredor et al. 2009; Mayhew et al. 2013), indigoids (Bruni et al. 2010; Oakley et al. 2012), and dyes belonging to other molecular classes (Leona and Lombardi 2007; Cañamares et al. 2008a, b, 2010, 2014;

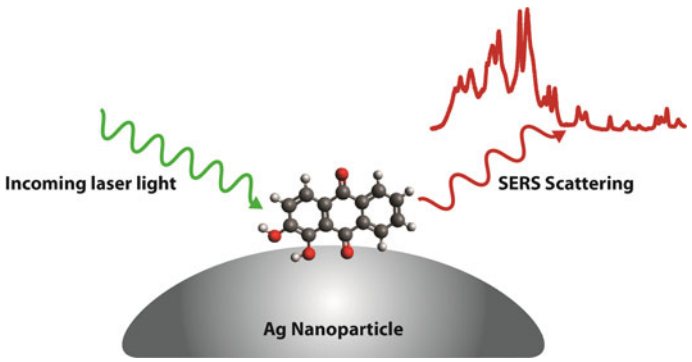

Fig. 1 Schematic of the surface-enhanced Raman scattering process. The molecule of interest, alizarin, is adsorbed onto an Ag nanoparticle substrate. The substrate is then irradiated with laser light (*green*), and the enhanced Raman scattering (*red*) is detected

Geiman et al. 2009; Chang et al. 2009; Xie et al. 2012; Bruni et al. 2011a; Mayhew et al. 2013; Benedetti et al. 2014; Greeneltch et al. 2012; Doherty et al. 2014; Cañamares and Lombardi 2015; Zaffino et al. 2015) can also be found in the literature. In addition to providing valuable reference spectra for identification purposes, these works have explored aspects such as the influence of pH on the resulting spectral patterns, and the binding geometry and relative orientation of the molecules examined with respect to the metal surface. Computational methods such as density functional theory (DFT) have also been used to calculate theoretical spectra and assign the normal modes of vibration to the Raman bands, thus supporting the interpretation of SERS data.

At the same time, extensive research has focused on the improvement and optimization of the technique as an analytical tool to be used for the detection and identification of dyes in samples of artistic and historical value that may be very complex, altered or degraded. In this context, identifying faded colorants in artworks, and investigating the nature and causes of the corresponding degradation processes is essential to implement measures to slow down or altogether prevent future fading and to shed new light on how certain artifacts might have looked like right after completion. SERS has offered insight into important examples of such processes, such as the fading of madder- and cochineal-based purples and reds in watercolors by the American painter Winslow Homer (1836–1910) (Brosseau et al. 2011) and in masterpieces by the French Impressionist Pierre-Auguste Renoir (1841–1919) (Collins et al. 2014; Pozzi et al. 2014a) and post-Impressionist Vincent van Gogh (1853–1890) (Vellekoop et al. 2013). In all these cases, the detection and identification of faded dyes with SERS allowed researchers to confirm that the current colorless or severely discolored appearance of the artworks is the result of a fading process, and to put forward hypotheses on how the masterpieces might have looked like right after the artists painted them.

Recent advancements in the SERS technique that will be discussed in this chapter include the comparison of various metal substrates, such as silver colloids and silver films over nanospheres (AgFONs), and evaluation of their performances; the development of non-invasive approaches involving the use of SERS-active removable substrates; the adaptation of pre-existing methodologies of sample treatment and analysis, such as laser ablation and tip-enhanced Raman spectroscopy (TERS), to the specific needs of the cultural heritage field; and the combination of SERS with separation techniques, such as TLC and microfluidics, to resolve dye mixtures.

Complemented by case studies drawn from important collections in the United States, this chapter will demonstrate the tremendous advances and high applicability of SERS, as well as outline areas of future development for a technique that is now solidly established as a powerful means of colorants' investigation in the field of art and archaeology.

2 SERS Substrates and Analytical Methodologies

Since the discovery of the surface-enhanced Raman effect in the 1970s, metal substrates of different types and forms have been developed for various SERS applications, beginning with roughened silver electrodes, then moving onto colloidal nanoparticles and solid surfaces with tailored thickness and nanostructured features. Accurate choice of the metal substrate is of utmost importance to ensure adequate measurement efficiency and high reproducibility of the spectra collected. While several metals including gold, copper, platinum, palladium and aluminum have been tested over the years, the best performances are expected from silver owing to its dielectric function and localized surface plasmon resonance (LSPR) spanning from the UV to the NIR/IR regions, i.e. the range of wavelengths typically used in SERS experiments for analyte excitation. Although incessant exploration in the field of high enhancing metal surfaces has provided practitioners with a continuously growing number of choices, substrates used in cultural heritage applied research must meet additional requirements of quick preparation, relatively low cost and straightforward use, as few museum laboratories have the extensive sample preparation capabilities of university-based facilities. Additionally, researchers are also striving to develop SERS substrates that could be used to identify colorants in situ without the need of removing even the smallest of samples: this would be crucial, for instance, in the case of works on paper or modern and contemporary art, from which sampling is normally more problematic.

The substrates and methodological approaches that have been used over the years for SERS analysis of art objects and archaeological artifacts are described in the following.

2.1 Colloidal Nanoparticles

Colloidal silver nanoparticles are by far the most widely used SERS substrate for art applications. The most popular method to synthesize silver colloids is by chemical reduction of a silver salt, typically silver nitrate, with trisodium citrate at boiling temperature (Lee and Meisel 1982). The Lee and Meisel method usually generates silver nanoparticles, mostly nanospheres and nanorods, in the 3–80 nm diameter range with a fairly broad visible absorption near 430 nm. Particle size, shape, and resulting plasmonic properties can be fine-tuned by suitable choice of the metal, reducing agent and stabilizer, chemicals concentration, addition rate, and temperature. In addition to testing alternative reducing agents, such as hydroxylamine (Leopold and Lendl 2003) and borohydride (Creighton et al. 1979), research groups all over the world have evaluated how different aggregants—including potassium nitrate (Cañamares et al. 2004), poly-L-lysine (Shadi et al. 2004), sodium chloride (Cañamares et al. 2008b) and perchlorate (Bruni et al. 2011a)—may promote the association of nanoparticles in clusters of various dimensions, where localized

regions of intense electromagnetic fields, the so-called hot spots, are responsible for a giant enhancement of the Raman signal (Ringe et al. 2013). An alternative to Lee-Meisel colloids involves a synthetic protocol based on the glucose-assisted reduction of silver sulfate in the presence of sodium citrate as a capping agent (Leona 2009). In this case, the use of a microwave oven equipped with pressure and temperature control has afforded silver colloids with a significantly narrower particle size range (3–10 nm) and absorption band, leading to increased stability of the substrate itself and more reproducible SERS performances.

The main drawback of citrate-capped silver nanoparticles lies in the occasional occurrence of spurious bands in SERS spectra that are due to competitive adsorption of citrate ions and related oxidation products onto the metal surface (Leona et al. 2006; Brosseau et al. 2009a; Bruni et al. 2010). This issue may be circumvented by adopting alternative techniques for the production of colloids, such as laser ablation and photoreduction. More popular than the first, based on the extraction of metallic nanoparticles from a silver plate induced by high intensity laser pulses (Cañamares et al. 2008c), is the fabrication of Ag substrates by laser photoreduction of a silver nitrate solution (Cañamares et al. 2007; Jurasekova et al. 2008, 2010; Retko et al. 2014). In both approaches, the absence of reducing or capping agents prevents disruptive interference (Cañamares et al. 2008c); however, the prolonged in situ irradiation required may raise concerns when these methods are applied to the analysis of samples from actual artworks due to the risk of thermal degradation and formation of carbon-rich phases.

In order to increase the applicability of SERS-active colloids to the analysis of complex samples from works of art, a useful pretreatment step has also been introduced involving a gas-solid hydrolysis performed by exposing microscopic samples to hydrofluoric acid (HF) vapor for 5 min in a closed polyethylene microchamber (Fig. 2). Specifically developed for mordant dyes and lake pigments, such pretreatment aims at hydrolyzing the chemical bond that the organic colorant forms with the fabric or inorganic portion of the lake through bridging metal ions. Compared to previously common extraction approaches based on the use of heated acids or alkali (Wouters 1985; Tiedemann and Yang 1995), the HF hydrolysis exploits milder experimental conditions and may be considered extractionless in that it does not involve physical detachment of the target dye from the sample under study. Simply, a small amount of colorant is released, in situ, from the surface of the dyed object becoming available for coupling to the silver nanoparticles. This methodology has proven critical to attain highly reproducible, conclusive dye identification in many instances, and has delivered superior results for the analysis of paints and glaze layers (Pozzi et al. 2012a, 2014a; Zaffino et al. 2014).

An alternative approach involves the use of colloidal pastes produced by centrifugation and concentration of nanoparticle suspensions. These pastes have been successfully used, in some cases, for the direct, extractionless, non-hydrolysis detection and characterization of organic colorants from textile fibers, pastels and watercolors (Brosseau et al. 2009a, b, 2011; Idone et al. 2013).

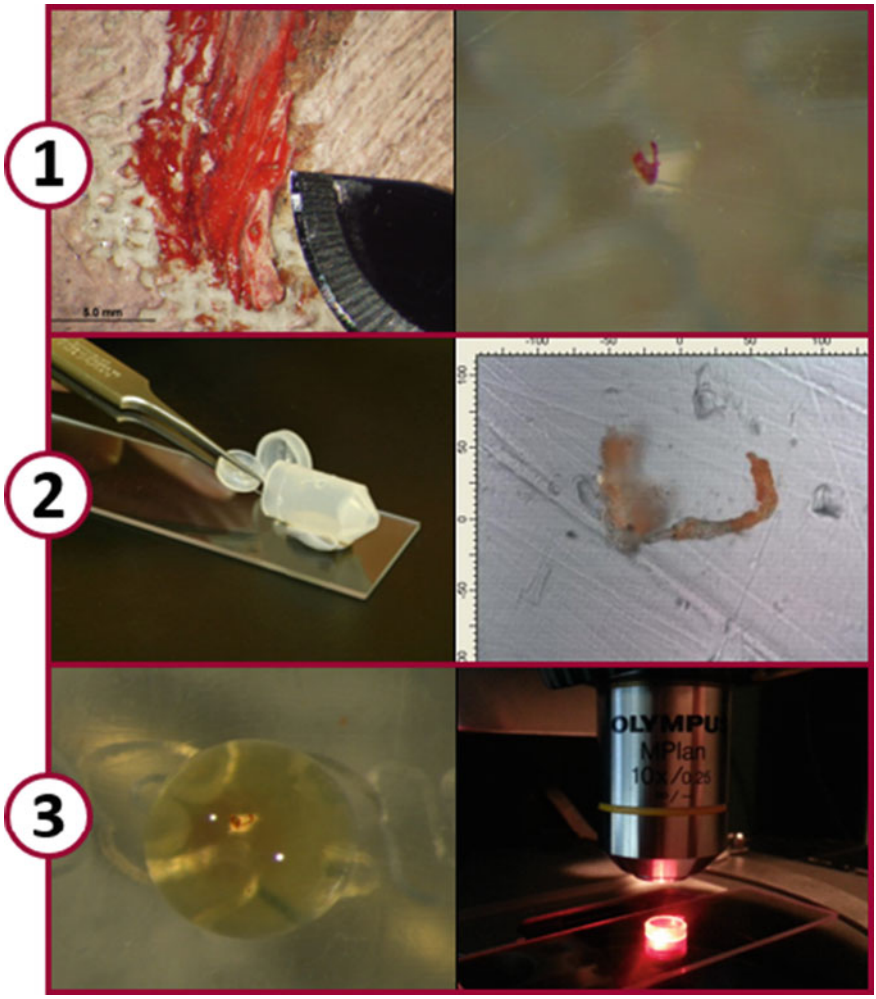

Fig. 2 SERS analysis of a red lake oil paint sample with Ag colloids upon HF hydrolysis treatment. Step (*1*) a microscopic paint specimen is removed from a painting by means of a scalpel blade and placed on a polyethylene holder; step (*2*) the sample is exposed to HF vapor at room temperature for 5 min in a closed polyethylene microchamber; step (*3*) 0.8 μL of Ag colloids and 0.1 μL of aggregant, typically 0.5 M KNO_3, are deposited onto the sample and SERS analysis is performed before evaporation of the droplet

Although most of the studies mentioned so far have been carried out on loose samples removed from works of art, a limited number of proof-of-concept works recently published in the literature have also reported initial attempts at applying colloids directly on cross sections from paintings, with the goal of obtaining spatially-resolved data (Idone et al. 2014; Retko et al. 2014; Frano et al. 2014).

2.2 *Solid-State SERS Substrates: Silver Films Over Nanospheres (AgFONs)*

The second most common SERS substrate aside from colloidal nanoparticles consists of lithographically fabricated metal surfaces. A variety of lithographic fabrication methods exist, such as electron beam lithography (EBL), focused ion beam (FIB) milling, and nanosphere lithography (NSL) (Fan et al. 2011). However, most of these techniques require costly equipment, which can be difficult to access in a museum setting, and have therefore seen limited use in the field. NSL is a cost-efficient and facile method of fabricating SERS substrates. NSL masks are obtained by dropcasting commercial polystyrene or silica microspheres onto a cleaned glass coverslip and allowed to dry in a hexagonal close packed array. A 200-nm layer of metal, typically Ag or Au, is then deposited through thermal vapor deposition on the microsphere mask to create the SERS substrate, commonly known as a film over nanospheres (FON) (Fig. 3). FONs have been shown to have high uniformity over a large area and their LSPR, readily tunable by changing the microsphere size, can be easily matched with the laser excitation wavelength (Sharma et al. 2013). When optimized, FONs have enhancement factors (EFs) on the order of 10^6–10^8.

The ease of fabrication, tunability, and high EFs of FONs make them ideal substrates for the identification of artists' materials with SERS. The first use of AgFONs in cultural heritage science was to identify and characterize the red dyestuffs alizarin, purpurin, lac, cochineal and their mixtures (Whitney et al. 2006). In this work, AgFONs were optimized in three excitation wavelength regimes relative to the electronic resonance of the dyes: pre-resonant (632.8 nm), resonant

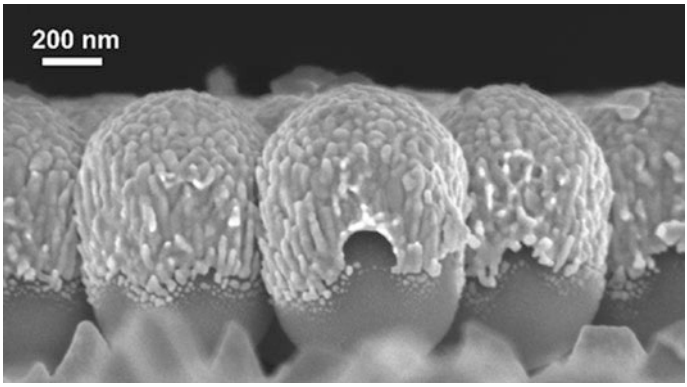

Fig. 3 Representative scanning electron microscopy (SEM) image of a FON. A 200-nm Ag layer is deposited on the surface of hexagonal close packed silica microspheres. The high enhancement from the FON originates from the formation of nanopillar-like structures on the deposited metal surface, which leads a high number of SERS hot spots on the Ag surface (SEM image courtesy of Dr. Anne-Isabelle Henry, Van Duyne group, Northwestern University)

(532 nm) and non-resonant (785 nm). It was found that the SERS signal was two orders of magnitude higher in the resonant regime compared to the non-resonant wavelength range, highlighting the importance of the resonance contribution to the SERS enhancement and the usefulness of a tunable SERS substrate. Additionally, the authors successfully resolved various binary dye mixtures in the pre-resonant wavelength regime. Whitney et al. (2007) demonstrated that exciting on electronic resonance with the dye in question can yield greater SERS signal, but it can also lead to photodegradation and possible fluorescence from binding media. Recent work examined the EFs of AgFONs optimized for NIR and IR wavelengths and Ag colloidal nanoparticles to identify eosin Y, an early modern synthetic dye, which was extensively used by Vincent van Gogh and sold under the name of geranium lake (Greeneltch et al. 2012). The use of NIR and IR laser excitation is beneficial for analyzing cultural heritage samples as compared to visible excitation because it minimizes photodegradation and interfering fluorescence. The authors observed that AgFONs EF using 1064 nm excitation was 20 times greater than that using 785 nm excitation. In addition, when compared to Lee and Meisel Ag colloidal nanoparticles, FONs were found to provide EFs greater by two orders of magnitude and more uniform signal.

Notwithstanding their ease of fabrication, high enhancement, uniformity, and tunability, AgFONs have been only occasionally used for practical applications of SERS to the identification of artists' colorants. One of the main hurdles in their widespread use may be that the dyestuff needs to be brought into solution by extraction from the sample, while colloids and colloidal pastes can be applied directly onto a solid sample with or without HF pretreatment.

3 Innovative SERS Approaches

A significant portion of the recent research in the field of SERS for cultural heritage has focused on the development of new methods that can be deployed in situ or approaches that are endowed with enhanced spatial resolution. The most promising methodological developments to date are reported in the following.

3.1 Laser Ablation (LA)—SERS

A substantial drawback of most approaches to SERS for analyzing cultural heritage samples is their lack of spatial resolution. Samples smaller than 50–100 μm are difficult to extract in a controlled and precisely localized way, and, in the case in which drops of colloid are deposited directly on the sample by hand (Idone et al. 2013) the spatial resolution is ultimately limited by the size of the drop, i.e. about

0.5–1 mm in diameter with the most common pipettes. Even when using inkjet devices to deliver the colloidal nanoparticles (Benedetti et al. 2014) the spatial resolution does not go below 50–80 μm. Londero et al. improved the applicability of SERS analysis towards complex organic samples, while simultaneously reaching high spatial resolution, by combining laser ablation microsampling with SERS detection on a silver nanoisland film in a vacuum chamber (Londero et al. 2013). They successfully demonstrated spatial resolution of 5 μm and sensitivity down to 120 attomol on a test sample created by vacuum depositing a film of copper phthalocyanine on a quartz disc. In their setup, a visible laser pulse from an optical parametric oscillator (OPO) is focused on a target inside a vacuum chamber with sufficient intensity to ionize the sample and produce a plasma. The plasma heats the ionized region via an inverse Bremsstrahlung process and causes the material to explode outward as a plume of vapor. The vapor deposits onto a SERS active substrate, the silver nanoisland-coated bottom surface of the chamber window, where it can be interrogated by a read laser (Fig. 4).

Laser ablation has another advantage over the use of colloids besides spatial resolution: as it relies on vapor deposition rather than diffusion through water for the analyte to adsorb on the plasmonic substrate, it can be used on water insoluble pigments with excellent results. In their work, Londero et al. (2013) showed this on the pigments quinacridone and quinacridone quinone, and their mixture Pigment Orange 48.

An improved version of the ablation setup (Cesaratto et al. 2014) features UV ablation. By ablating in the UV, specifically at 355 nm, i.e. at a wavelength where virtually all organic materials are highly absorbing, vaporization is confined to approximately 1-μm depth. Even with extremely simple UV optics, Cesaratto and coworkers were able to show significant advantages over visible ablation. A cross section taken from the red area of a 16th-century decorated dish shows that two separate red paint layers exist on the plate (Fig. 5). The top layer is composed of sparse carbon particle embedded in a red glaze, while the bottom one is a lighter red glaze. The cross section was ablated in three different areas, with a minimum spot size about 13-μm wide (as determined by atomic force microscopy after the analysis). The two different layers could be characterized separately and without contamination one from the other, and the red colorant in the very top thin layer could be easily distinguished from the carbon particles. This is particularly critical given graphite's ability to displace colorants on the SERS substrate, which can result in it being the only detectable component. The bottom layer was identified as a madder-based lake, while the upper one gave a SERS spectrum compatible with an unidentified synthetic organic colorant. The results reinforced suspicions of a modern addition raised from previous visual inspection of the object. This kind of work would not have been possible with the conventional approaches to SERS because of the complexity of the layering structure, or indeed, with any alternative technique, given that samples suitable for HPLC or liquid chromatography/mass spectrometry (LC/MS) could not have been obtained from such thin layers.

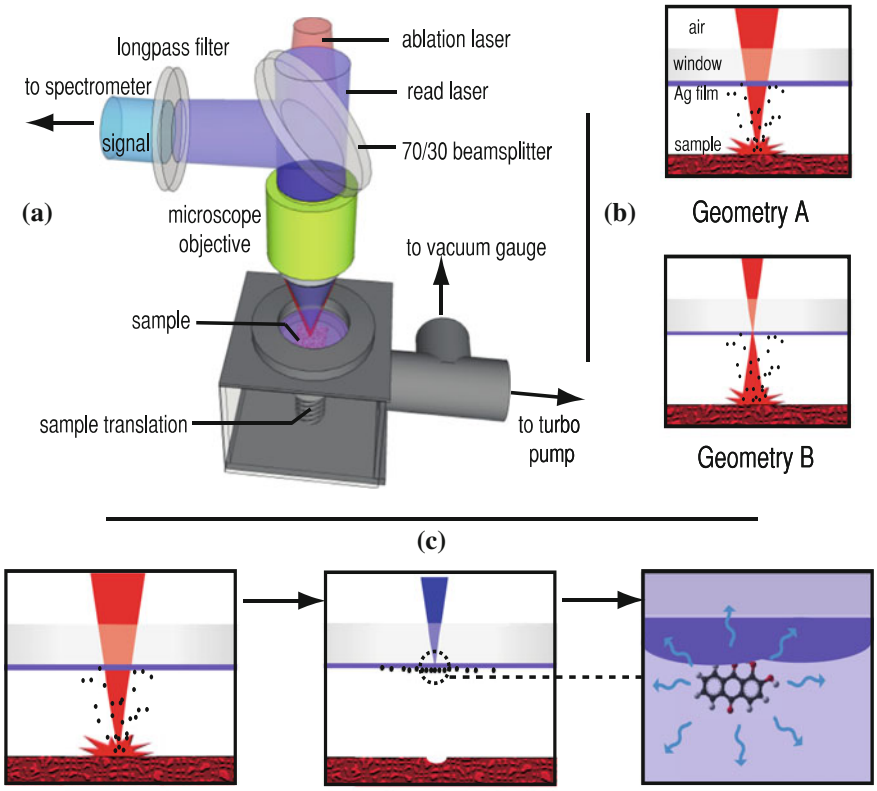

Fig. 4 Experimental setup for LA-SERS. **a** The sample is placed on a holder within a vacuum chamber and is elevated to 200–300 μm from the SERS active quartz window. The ablation and read lasers are imaged onto the sample and SERS film, respectively, by the microscope objective. The signal generated from the read laser is collected by the same objective and filtered from any backscattered laser light by the longpass filter, after which a spectrum is recorded. **b** Illustration of the two ablation geometries that can be utilized: geometry A optimizes spatial resolution, while geometry B increases the ablated surface area for situations such as representative sampling of granular mixtures. **c** Steps for a typical measurement: the sample is ablated in one of the two possible ablation geometries and then collected on the SERS-active film, where it is excited by the read laser

3.2 Inkjet Nanoparticle Delivery SERS

An interesting alternative to traditional approaches that involves removing a sample and treating it with a colloid in a separate stage was presented by Benedetti et al. (2014). Using inkjet technology to reproducibly deliver microdroplets of silver nanoparticles either on the specimen to be analyzed by SERS or on a work of art,

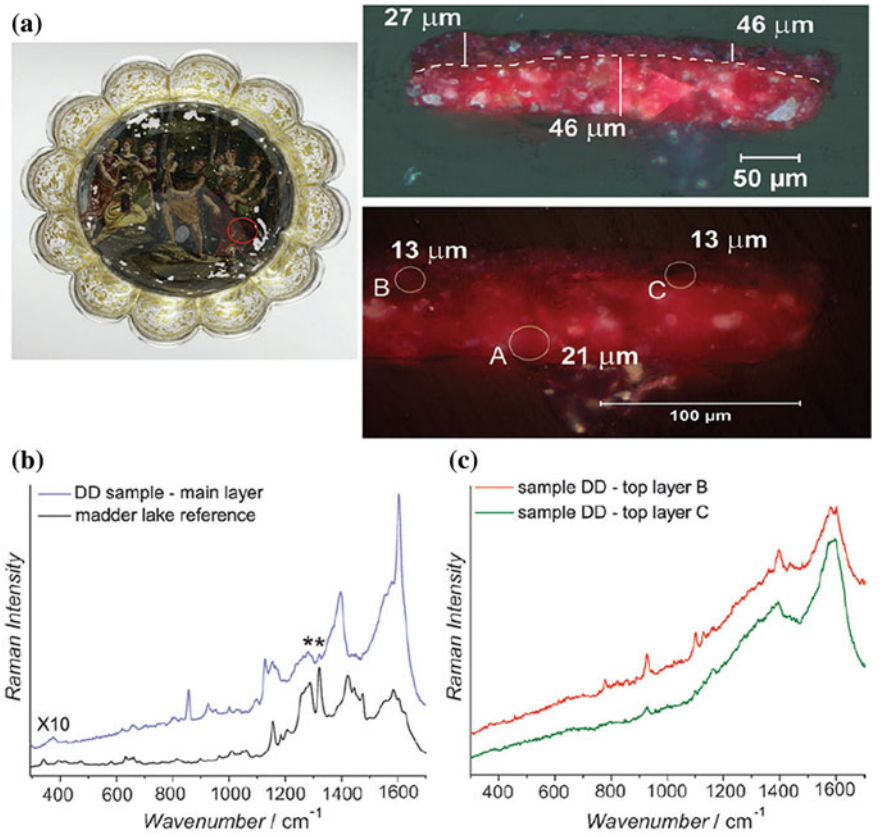

Fig. 5 **a** A 16th-century decorated dish and microscope images of a cross section from the decoration (sample DD), with the ablated craters A, B and C. **b** SERS spectrum of the UV-ablated crater A in the main layer. Signals of reference madder lake were detected at 1283 and 1321 cm^{-1}, highlighted in the graph with an asterisk. **c** SERS spectra of the UV-ablated craters B and C in the top layer

the authors of this work were able to demonstrate quasi non-destructive analytical capabilities. Droplets of approximately 50–80 µm were deposited directly onto a Japanese woodblock print with a piezoelectric inkjet head mounted on the Raman microscope and aimed at the focal point of the microscope objective. The suitability of either thermal or inkjet printing heads to deliver silver colloids for SERS analysis was demonstrated as well (Leona and Tague 2010). Although the droplets of silver nanoparticles cannot be removed from the substrate when dry, they are of such small diameter that they are nearly invisible to the naked eye.

3.3 Detachable SERS Substrates

While SERS analysis, unlike ordinary Raman, cannot be carried out in an entirely non-invasive way, several researchers have investigated quasi non-invasive analytical approaches based on the use of gels. Gels have been used for years in conservation to remove surface contamination from works of art in a localized and selective way. A gel confines the action of a solvent or cleaning agent to the area of the object with which it is in contact, preventing the spread of any material—either the cleaning agents or the materials targeted for removal—through and across the artwork (Carretti et al. 2010; Baglioni et al. 2015). For SERS applications, a gel could substitute the colloid drop traditionally used as the medium for the target dye and the plasmonic nanoparticles to interact; alternatively, a gel loaded with appropriate reagents could be used to perform a mild extraction of the target analyte from its substrate, for subsequent analysis with a silver colloid deposited on the gel.

Gel-based colloidal substrates for SERS analysis were first explored by Bell and Spence (2001) and by Farquharson and Maksymiuk (2003) without, however, a specific focus on quasi non-invasive sampling of works of art. The first application of gels to SERS analysis of artworks is due to Leona, who used cross-linked hydroxyacrylate gels for non-destructive dye extraction from paper and textiles (Leona 2008; Leona et al. 2011). The cross-linked gels were effectively used as solid-phase microextraction substrates, and SERS analysis was performed by depositing silver colloids on the gels after removal from the work of art. The method was tested on the Metropolitan Museum's *Unicorn Tapestries* (1495–1505), enabling the identification of madder, and on a 19th-century Japanese woodblock print, where methyl violet was detected (Fig. 6).

A different approach was followed by Doherty et al. (2011) using methyl cellulose as the gel medium and Lofrumento et al. (2013), Platania et al. (2015) using

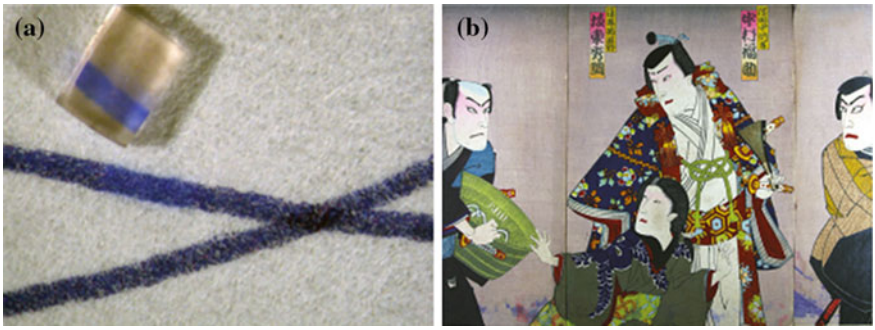

Fig. 6 **a** Use of hydroxygels to extract minute amounts of ink from a ball point pen tracing on paper. The region of extraction is barely distinguishable from the area from which no extraction takes place. **b** *Sekigahara Homare no Gaika* (*A poem about the battle of Sekigahara*) by Toyoharu Kunichika, 1892. Woodblock print on paper, triptych, each sheet originally oban size (27 × 39 cm), slightly trimmed. Private collection

agar. Both groups incorporated the silver colloid directly in the gel substrate to be put in contact with the work of art. The agar gel approach was further refined by Platania et al. (2014) by adding ethylenediaminetetraacetic acid (EDTA)—a chelating agent—to the gel, thus improving the extraction of a variety of dyes from substrates such as oil paints, printed and dyed textiles. The agar gel seems to be one of the most promising approaches because, due to its shrinking upon drying, it causes the nanoparticles to come into close contact, inducing the occurrence of SERS active hot spots. Additionally, agar gels are increasingly used for conservation treatments and are, therefore, widely accepted in the field.

3.4 Tip-Enhanced Raman Spectroscopy (TERS)

Tip-enhanced Raman spectroscopy (TERS) is a promising non-destructive analog to SERS, which combines the nanometer spatial resolution of scanning probe microscopy (SPM) and the chemical sensitivity of SERS. A TERS experiment can be performed using one of two variants of SPM: scanning tunneling microscopy (STM) and atomic force microscopy (AFM). In an STM experiment, a voltage is applied to the scanning probe tip that comes in tunneling contact with the sample. An STM image is produced by measuring the changes in the tunneling current as a function of tip position across the sample. Despite its sub-nanometer scale spatial resolution, STM is sample-limited due to the requirement that the substrate of interest must be conductive and therefore cannot be used to analyze most materials from works of art. Alternatively, in an AFM experiment, the scanning probe tip is on a cantilever which makes contact with the surface of interest; changes in tip height due to local surface topography are measured to produce an AFM image. While the AFM tip does make contact with the sample, the tip can be readily removed from the sample surface, which is advantageous when analyzing sensitive cultural heritage samples. The surface generality of AFM is an advantage over STM and has been used to probe a wide range of surfaces such as DNA strands, amyloid fibrils, cell membranes and polymer films, as highlighted in a recent review (Schmid et al. 2013). Moreover, the surface generality of AFM makes it amenable to analyze surfaces relevant to cultural heritage such as cross sections, paint films, works on paper including watercolors, and textile fragments.

The scanning probe tip is at the heart of a TERS experiment, as it is both the source of the nanometer scale spatial resolution as well as the plasmonic enhancing surface. A TERS-active scanning probe is fabricated by electrochemical etching of Ag or Au wire for STM, or by thermal deposition of an Ag or Au metal film onto a commercial Si cantilever for AFM.

The methodology of a TERS experiment is illustrated in Fig. 7. First, the plasmonic tip is brought in close contact with the sample surface of interest. Laser light is then directed towards and focused onto the tip-sample junction. Low laser powers on the order of microwatts are often used in TERS experiments because of the tight focusing of the laser at the probe tip apex, which can be a beneficial feature

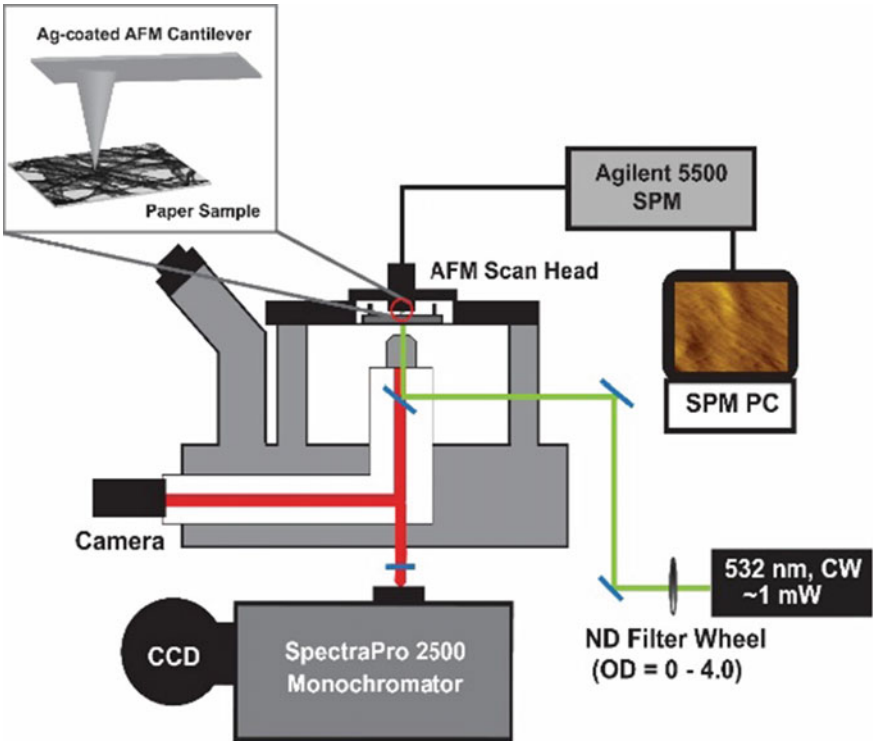

Fig. 7 Schematic of an experimental setup for AFM-TERS. The sample of interest is placed underneath the AFM scan head (inset). After the sample is put in contact with the AFM tip, the laser light is brought up through a microscope objective and focused at the apex of the Ag-coated AFM cantilever tip, and a TERS approached signal is acquired. The sample is then withdrawn from the tip and spectra are collected to ensure that no normal Raman or SERS signal is present or any tip contamination occurred

when analyzing artworks prone to thermal and photodegradation. The illumination of the tip induces an enhanced electromagnetic field around the probe tip apex, and only molecules directly beneath the tip experience Raman scattering enhancement. Then, the probe can either remain stationary in a single location while TERS spectra are acquired, or it can scan across the surface of interest. The intensity of a specific Raman band as a function of tip position on the surface can be used to produce a TER spectral map. Lastly, in order to ensure the TERS signal acquired is not due to contamination of the scanning tip or normal Raman or SERS of the substrate, a 'withdrawn' or 'retracted' spectrum is typically acquired with the plasmonic tip far from the surface of interest.

The first proof-of-principle AFM-TERS study for the non-invasive identification of dyestuffs of significance for the art field was recently reported (Kurouski et al. 2014). In this work, the authors analyzed a reference sample consisting of Kinwashi paper dyed with indigo, and were able to successfully acquire TERS spectra of the

blue colorant on the paper support. When the dyed paper spectra were compared to a reference of indigo on an Au film, they observed missing vibrational bands and band shifts in the dyed paper spectral patterns, likely indicating the occurring of complex dye-substrate interactions. It was also found that signature peaks of cellulose and glucose, two major constituents of paper, were present in the TERS spectra. In order to demonstrate the feasibility of TERS for analysis of artworks, TERS spectra were obtained from a historic 19th-century manuscript fragment with iron gall ink and compared to that of Kinwashi paper freshly dyed with iron gall ink. The authors found that some vibrational modes of gallic acid, a primary component of iron gall ink, were only observed in either Kinwashi paper or the manuscript, which was attributed to the complex chemical composition of the ink and paper and to the interaction of gallic acid with the paper substrate. This work demonstrates the feasibility and strong future potential for TERS to non-invasively probe artworks with the high sensitivity of SERS. At present, the main limitations of the technique are that it is highly specialized and mostly available in university research labs (although commercial instruments have started to appear on the market in the past 5 years); in addition, when used in transmission mode, samples need to be semi-transparent to be able to be analyzed and they have to be limited in size to what the sample chamber can accommodate. These drawbacks can be overcome by working in reflectance mode, but to date no applications to cultural heritage materials have been described in the literature.

4 Resolving Dye Mixtures

Although SERS has successfully reduced the sample size requirements with respect to HPLC, it is still limited by its inability to physically separate dye mixtures. An immediate consequence of this is that, in the case of dye mixtures, only the signals of the main component are typically detected due to discrepancies in resonance, solubility, affinity for the metal surface, SERS cross section, or a combination of two or more of these factors (Shadi et al. 2004). This represents a real limitation, as it is well known from documentary sources that, throughout history, dyes were often used in combination to achieve particular color shades both in painting and textile dyeing (Cardon 2007). Several studies describing applications of the SERS technique to the analysis of artworks and historical textiles have described instances in which, while the presence of multiple colorants had been assessed by HPLC, only one could be detected by SERS (Leona and Lombardi 2007; Pozzi et al. 2012b). On the other hand, recent contributions to the scientific literature have offered proof of the simultaneous SERS detection of binary mixtures of dyes in multiple-component commercial pigments (Londero et al. 2013), fibers from historical textiles (Idone et al. 2013), and oil paint samples (Pozzi et al. 2014a). This has prompted researchers to pursue an extensive investigation of the capabilities of

SERS to concurrently detect and identify several dyes in combination and, at the same time, has encouraged alternative, more efficient ways to accomplish analysis of mixtures of organic colorants by SERS upon physical separation of the individual constituents.

4.1 Binary Mixtures in Solutions

While a detailed evaluation of the SERS technique's ability to detect single dyes has been the subject of comprehensive studies in the past decade, to date very little work has focused specifically on the identification of individual components of dye mixtures. Thus far, spectra of binary combinations of reference alizarin, purpurin and lac dye have been presented within very preliminary studies (Whitney et al. 2007; Van Elslande et al. 2008; Jurasekova et al. 2010), some of which have offered an initial assessment of suitable metal substrates and ideal experimental conditions, along with summary considerations on marker bands, adsorption geometries, and relative detection limits of the colorants examined. These early studies have been significantly expanded by a more systematic work recently carried out at the Art Institute of Chicago. This work aims to determine the capabilities of SERS in terms of distinguishing a wider number of dyes, including alizarin, purpurin, carminic acid, laccaic acid and brazilein, in series of historically relevant mixtures, both for reference solutions and in actual samples such as mock-up red lake oil paints. First, SERS spectra of binary mixtures of the commercial colorants in various relative proportions and concentration comparable to that observed in museum objects were recorded on two different SERS substrates, i.e. Lee-Meisel citrate-reduced silver colloids and AgFONs. This aimed to qualitatively establish relative detection limits for each dye when present in solution alongside another colorant, and to gain a deeper understanding of how different metal substrates and analytical methodologies may affect dye identification. Second, binary mixtures of madder, cochineal and brazilwood were analyzed with SERS in red lake oil paint reconstructions prepared according to 19th-century historical recipes. For this set of samples, analysis was performed after hydrolysis with HF and only employed Lee-Meisel silver colloids as SERS-active substrate. Preliminary results from experiments on reference solutions have shown that, in many cases, the spectral contribution of the second dye in the mixture remains undetected unless it is present in high relative proportions (usually 1:1). A typical example, in this regard, is offered by mixtures of alizarin and carminic acid: for both colloids and FONs, the latter component becomes detectable in the 1:1 mixture, while the contribution of alizarin is predominant even in the 1:10 solution, i.e. in cases where the relative amounts of carminic acid are 10 times as high as those of alizarin. In addition, remarkable differences were observed between the two substrates both in terms of contribution of each dye in the mixture to the SERS spectrum and, in some cases, for what concerns the position and relative intensities of bands. This is likely due to the experiments' different incubation times, enhancing in the case of colloidal

nanoparticles the preferential adsorption of one of the two dyes possibly due to the factors listed above as well as to differences in the surface chemistry of the metal substrates used. Overall, these new results underscore the need for more extensive experimentation in the area of hyphenated techniques that may enable the combined separation of colorants (e.g. via TLC or microfluidics) and their SERS detection in artworks.

4.2 Thin-Layer Chromatography (TLC)—SERS

Combining efficient separation with the fingerprinting ability typical of vibrational spectroscopies, the coupling of SERS with chromatographic techniques such as TLC or HPLC provides an obvious means toward effective discrimination of multiple dye components in complex mixtures. In particular, TLC-SERS, whose first application was reported by Henzel in 1977 (Henzel 1977), has been used for a series of preliminary proof-of-concept studies recently undertaken in the cultural heritage field thanks to its ability to significantly reduce the amount of material, sophisticated equipment and time needed for analysis. The first example of use of TLC-SERS for the characterization of several organic colorants in combination was demonstrated by Brosseau et al. (2009b). In this work, the authors were able to discriminate single anthraquinoid dyes in a binary mixture in both reference solutions and extracts from a dyed wool fiber. In the same year, a second work published by a different research group described the separation and identification of dye components in ballpoint pen inks by TLC-SERS, highlighting the great potential of this technique in the field of forensics (Geiman et al. 2009). After these initial studies, applications of TLC-SERS were then extended to the analysis of mixtures of the main β-carboline alkaloids from the seeds of the Syrian rue plant (*Peganum harmala*), i.e. harmalol, harmaline, harmane and harmine, which are relevant as historical dyes and as drugs (Pozzi et al. 2013a), and to the separation and identification of the structurally related components of mauve, the first synthetic organic dyestuff (Cañamares et al. 2014). All these works share a common analytical procedure, in which solution aliquots of the dye extract or commercial material of interest were deposited onto a silica gel TLC plate using a glass capillary and eluted in a glass developing chamber by means of an appropriate solvent mixture. Then, the eluted spots were visualized and marked under ultraviolet light. SERS analysis was subsequently performed directly on the silica gel plate, upon deposition of a few microliters of Ag colloid with or without aggregant, after drying of the droplet or while the spots were still wet. In these approaches, the sometimes inefficient dye separation provided by the silica gel was compensated for by its chemical and vibrational inactivity compared to other substrates. Initial attempts to make the entire TLC plate SERS-active by both pre- and post-treatment with silver colloids resulted either in poor separation of the dyes and difficult spot identification, or in an uneven distribution of the nanoparticles on the plate surface. New avenues for methodological improvement include the application of AgI and other

silver halides onto gold-coated slides to form a new generation of SERS-active TLC substrates that have shown great promise thanks to their tunable structure, as well as superionic, optical, and complexing properties (Sciutto et al. 2015).

4.3 Microfluidics—SERS

An alternative method to simultaneously separate, detect and identify multiple analytes is offered by the development of a microfluidic-SERS platform. In this approach, the channels of the microfluidic-SERS device are functionalized with alkanethiol self-assembled monolayers (SAMs), all which have different functionalities. The polarity of the tail group can be adjusted to attract different classes of dyes, analogous to adjusting the mobile phase solvent polarity in chromatography. A microfluidic-SERS approach is not only tailorable, but also requires a small sample; the micrometer scale of the device channels typically involve sample volumes on the order of 100 μL to flow solution through the entire device. This is beneficial when working with samples that are limited in size or volume, which is often an issue in cultural heritage science. Previous work has shown that microfluidic-SERS devices can detect analytes with a concentration as low as 3 nM (Kim et al. 2014).

A microfluidic-SERS device developed by the Van Duyne group at Northwestern University consists of a SERS-active substrate, i.e. metal FONs, and a polydimethylsiloxane (PDMS) patterned channel mold. Device fabrication is illustrated in Fig. 8. First, the microfluidic devices are produced by lithographically patterning the channel design onto the AuFON SERS substrate with UV light cured photoresist. Next, the photoresist is removed, leaving behind the channel pattern directly on the SERS substrate. The patterned SERS-active substrate and the cured PDMS mold are exposed to oxygen plasma and fused together. Holes are punched in the PDMS to create the inlets and outlets for the channels, where solutions can be injected in a controlled manner via an infusion pump. Each individual channel is then functionalized with the alkanethiol of interest, and the channels are rinsed to remove excess or unbound reagent. Lastly, the target analyte is flown through the entire device and SERS measurements are taken on an inverted microscope setup by focusing the laser light at the plasmonic substrate surface.

In proof-of-principle experiments, the Van Duyne group has successfully fabricated microfluidic-SERS devices and explored the separation capability of alkanethiol SAMs on a SERS substrate. First, SERS spectra of a 100 μM alizarin solution in both a non-functionalized device and a SAM-functionalized device channel were acquired, and the characteristic SERS spectrum of the dye was successfully detected in both devices. Additionally, it was found that the PDMS has a unique Raman spectrum, which can be subtracted out from the SERS spectra to avoid interference. Non-microfluidic device FONs were then prepared in order to explore the capability of different terminated alkanethiol SAMs to separate different classes of dyestuffs. Two FONs were functionalized with a $–CH_3$ and –OH

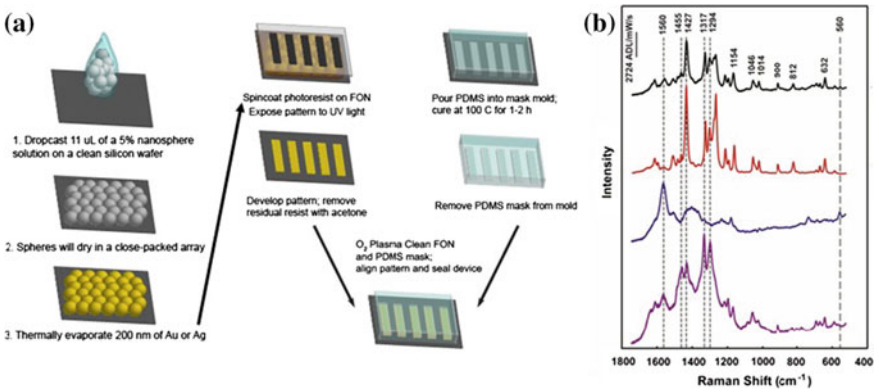

Fig. 8 **a** Schematic of FON fabrication (*left*) and microfluidic-SERS device fabrication (*right*). **b** SERS on various alkanethiol SAM-functionalized FONs. Only alizarin was detected with HS–$(CH_2)_5$–CH_3 SAM (*red*), while both brazilein and alizarin were identified with HS–$(CH_2)_6$–OH SAM (*black*), as compared to SERS of alizarin (*purple*) and brazilein (*blue*) on a non-functionalized FON. Experimental parameters for SERS measurements: excitation wavelength = 633 nm; acquisition time = 4 s; power at the sample ≈ 360 μW

terminated alkanethiol SAMs, HS–$(CH_2)_5$–CH_3 and HS–$(CH_2)_6$–OH. After thorough rinsing, the FONs were incubated in a 1:1 ratio mixture of dyes alizarin, an anthraquinone dye, and brazilein, a neoflavonoid dye. As shown in Fig. 8, the –CH_3 terminated SAM only shows SERS of alizarin, but the –OH SAM displays SERS signal characteristic of the mixture of alizarin and brazilein. The two proof-of-principle experiments demonstrate that alkanethiol SAM-functionalized microfluidic-SERS devices can be designed to selectively separate and detect different classes of dyes in mixtures.

5 Case Studies

Almost three decades after the first reported use of SERS for the analysis of art samples using a roughened silver electrode (Guineau and Guichard 1987), and particularly after the last decade of renewed and sustained interest in the technique, SERS has become an established and increasingly used method for the identification of organic colorants in art and archaeology. Following demonstration of the reproducibility of the results obtained on reference dyes, colored fibers, and lake pigments (Pozzi et al. 2013b), and upon publication of significant collections of reference spectra of anthraquinoids, flavonoids, carotenoids, and other classes of colorants widely encountered when analyzing art (Leona et al. 2006; Cañamares et al. 2006a, 2008b; Whitney et al. 2006; Cañamares and Leona 2007; Bruni et al.

2011a), SERS has become a powerful technique in the analyst's toolbox to advance the knowledge and support the preservation of a wide range of art objects, as demonstrated in the following sections.

5.1 Textiles

Dyers and craftsmen have harnessed the coloring power of various insects and plants to dye textiles since the beginning of human history. Hence, it is natural that the first applications of SERS as a less sample-intensive alternative to HPLC for the analysis of colorants in art have been directed to the analysis of textiles. As early as 1987, Guineau and Guichard identified madder on a woolen thread after extraction with hydrochloric acid (HCl) and acetone using a roughened silver electrode (Guineau and Guichard 1987). Borrowing from the sample preparation approaches developed for HPLC, the most commonly followed analytical procedures to analyze historical textiles initially involved pretreatment of the sampled threads with a hot solution of HCl and methanol (MeOH) in water. Such pretreatment aimed to release the dyestuff from the complex with the metal cation that acts as a linker between the colorant and the fiber. This type of hydrolysis, however, is rather aggressive and may affect the proteinaceous or glycosidic structure of the fiber itself, bringing in solution much more than just the free dye. While not much of a concern for separation techniques such as HPLC, this is an impediment to efficient SERS analysis of colorants due to interfering components being included in the analysis. Thus, very early on researchers started to experiment with milder extraction methods (Leona et al. 2006) for textile fibers, such as treatment with 1:1 dimethylformamide and water with 1 % EDTA, as originally proposed by Tiedemann and Yang (1995). An extraction procedure based on immersion of the fiber in 4 M HF, coupled with SERS on $NaClO_4$-aggregated silver colloids, allowed the identification of a yellow dye derived from the dried fruit rinds of pomegranate in archaeological woolen threads from the Libyan Sahara, a result confirmed by parallel analysis with gas chromatography/mass spectrometry (GC/MS) and HPLC (Bruni et al. 2011b). Moreover, Bruni and coworkers identified madder on a red woolen thread from the same burial site and Tyrian purple on an ancient bone from a 4th-century tomb in the basilica of S. Ambrose in Milan, where the colorant had likely transferred from the textile used to wrap the body. While it was not possible, in the first case, to identify madder upon HCl:MeOH extraction due to interference of the peptide residues from the hydrolyzed wool protein, a milder method based on immersion in HF led to the successful identification of the red anthraquinone colorant with SERS (Bruni et al. 2010).

Researchers have also been able to circumvent the issue of extraction of the dyestuff from colored fibers with a variety of alternative methodological approaches. Jurasekova et al. (2010) used laser photoreduction of an aqueous solution of silver nitrate to perform in situ SERS identification of alizarin and carminic acid on reference wool and linen fibers dyed with madder and cochineal. In the same work,

colorants belonging to the flavonoid family have also been identified in fibers dyed with dyer's greenweed (*Genista tinctoria* L.), onionskin (*Allium cepa*), chilca (*Baccharis* sp.) and old fustic (*Clorophora tinctoria* L.) following traditional pre-Columbian recipes. This approach was also successfully applied to the identification of alizarin in an archaeological Coptic textile from Egypt dated to the 6th–8th century. Although the authors were able to detect Al-complexes of the dyestuffs, in many cases the spectra reported appear on top of the bands of carbonaceous material between 1300 and 1600 cm^{-1}, likely formed because of the laser's thermal energy (dwelling for up to 20 min on the analyzed spot) and conductive silver nanoparticles.

A milder, in situ, extractionless SERS method relies on the use of Ag nanoparticle pastes obtained by centrifugation of Lee-Meisel colloids that are deposited directly on textile fibers. These colloidal pastes were first described by Cañamares (Cañamares et al. 2006b). A few years later, Brosseau et al. applied them directly to reference wool fibers dyed with purpurin, carminic acid, madder, Cape Jasmine, as well as to samples from historical textiles (Brosseau et al. 2009a). Thus, they were able to identify purpurin on a silk thread from a 17th-century cover from Italy; cochineal in the red and pink silk fibers from a long shawl from France dated to the 19th century; and lac, native of India, on a wool thread from a Turkish carpet dated to the late 16th/early 17th century. Brosseau and coworkers also demonstrated the validity of this methodological approach by identifying curcumin in reference silk yarns dyed with turmeric, though a certain degree of photodegradation was observed in this case, as evidenced by the broad carbon bands on which diagnostic signals for the dyestuff were superimposed.

Interesting studies of alizarin, purpurin and madder include the work of Wustholz et al. (2009), who used pastes of silver colloids applied directly on a minute fragment of a Peruvian textile (800–1350 A.D.) to identify alizarin, likely derived from the native plant *Galium corymbosum* L. Rambaldi et al. (2015) used silver colloids with and without HF pretreatment to record SERS spectra of wool threads tinted with various species of madder (*Oldenlandia umbellata* L. and *Rubia tinctorum* L.), which led to the preferential detection of alizarin or pseudopurpurin —a minor component of the dyestuff mixture present in madder—depending on the specific botanical species employed for dyeing. Additionally, the silver-doped agar gel micro-extraction procedure described above was successfully applied by Lofrumento and coworkers on a pre-Columbian textile to detect alizarin after training the method on laboratory-dyed textiles treated with alum and purpurin, alizarin and caminic acid (Lofrumento et al. 2013). In an effort to identify areas with the highest metal coverage by monitoring the morphology and distribution of the applied silver nanoparticles, Prikhodko et al. (2015) recently developed a hyphenated SEM-Raman system to conduct SERS analysis on reference samples dyed with cochineal and madder.

A few works also concern themselves with lesser studied compounds. For example, in situ applications of silver colloids were exploited to characterize the colorants of wool threads dyed with materials traditionally used in Mexico, such as carminic acid from cochineal (*Dactylopius coccus*), achiote (*Bixa orellana*), muitle

(*Justicia spicigera*), zacatlaxcalli (*Cuscuta* sp.), brazilwood (*Caesalpinia echinata*), and cempazuchitl (*Tagetes erecta*) (Casanova-González et al. 2012). Doherty et al. successfully employed SERS to identify different orchil species, i.e. *Roccella tinctoria* and *Lasalia pustulata*, on wool fibers both on reference samples and on a 16th-century purple dyed tapestry from Brussels. In this work, Lee-Meisel colloids aggregated with magnesium sulfate were directly deposited onto the threads, without any pretreatment (Doherty et al. 2014).

Early approaches availing themselves of an in situ hydrolysis pretreatment step include Leona and Lombardi's demonstration of the use of HCl vapor to enhance detection of berberine on a small thread from a faded and weathered 17th-century silk textile from China, which had been previously analyzed with HPLC to reveal a mixture of berberine and safflower (Leona and Lombardi 2007).

The in situ, non-extractive hydrolysis with HF described above for the analysis of red lakes in paints (Fig. 1) has also been demonstrated to be of value for the analysis of textile samples, a first example of this being the identification of berberine on a Byzantine textile dated to the 11th century (Leona et al. 2006). The HF pretreatment has proven to be highly effective for the analysis of textile samples, with the notable exception of silk fibers (Pozzi et al. 2012a). These were found to undergo a significant degree of hydrolysis resulting in the release of proteinaceous by-products in the analyte solution, which interfere with the analysis by preferential adsorption on the silver nanoparticles. Despite the challenges encountered in the examination of silk fibers, the HF hydrolysis was still successfully applied to the analysis of both reference and historic silk samples. For example, a reference silk fiber dyed with weld, from the *Reseda luteola* dried plant, was treated with HF vapors and then analyzed with concentrated Ag colloids by Corredor et al. (2009), revealing the presence of luteolin. This method was also applied to the identification of reference silk dyed with extracts of Persian berries, demonstrating the identification of some diagnostic bands for quercetin, probably mixed with other flavonoids such as rhamnetin and kaempferol (Teslova et al. 2007). Other examples include the examination of reference samples of unmordanted and mordanted silk, as well as mordanted wool fibers dyed with Cape Jasmine, leading to the SERS identification of the main chromophores of this dye, the carotenoids crocetin and crocin (Cañamares et al. 2010). The authors noted, though, that in this case SERS analysis allowed the detection of the diagnostic bands for the dyestuffs even without the HF hydrolysis pretreatment step, likely because the two colorants identified also display a strong normal Raman spectrum.

Zaffino et al. (2014) extended the SERS analysis of colorants in textiles to NIR excitation, comparing HF pretreatment and non-hydrolysis procedures on a large set of reference dyes and dyed fibers, as well as historical samples from Chinese Ningxia (18th and 19th century) and Caucasian Kaitag (17th and 18th century) textiles. This work included the first instance of FT-SERS spectrum of an iron-gall dye on a sample from the latter (Zaffino et al. 2014). In one of the most extensive applications of the combined HF pretreatment and silver colloid SERS, Pozzi et al. examined an important corpus of Navajo blankets in the collection of the Art Institute of Chicago (Pozzi et al. 2014b), allowing the identification of the colorants

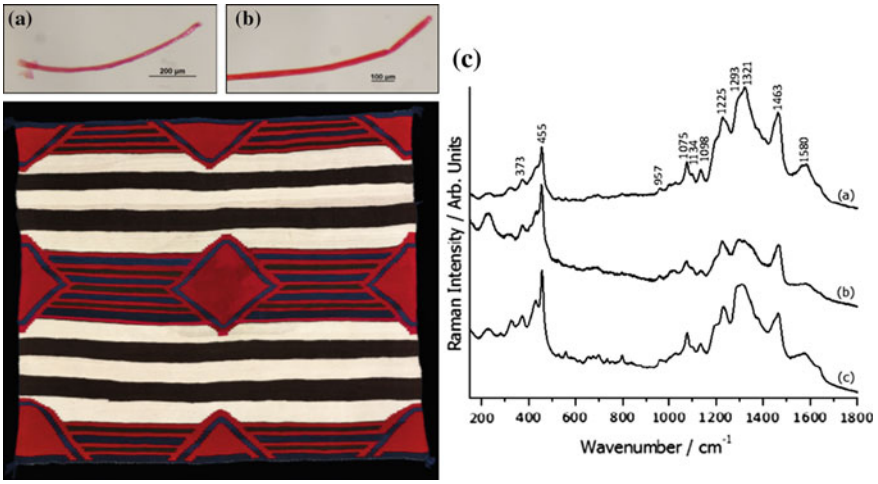

Fig. 9 *Chief Blanket* (Third Phase), 1865/80. Navajo; northern New Mexico or Arizona, United States. Wool, single interlocking tapestry weave; twined edges; corner tassels; two selvages present; 149.6 × 173.9 cm (58 7/8 × 68 1/2 in.). Collins et al. (2001). The SERS spectra of two red fibers removed from the blanket (*a*, *b*) are in accordance with that obtained from a reference wool sample dyed with cochineal (*c*)

in their various red woolen yarns in a selection of 8 19th-century blankets. While the presence of carminic acid was positively confirmed by SERS for fibers dyed with natural dyes, synthetic organic colorants were identified by normal Raman spectroscopy with 785 nm excitation, highlighting the use of Ponceau 4R and two beta-naphthol dyes. Results from this study had a major impact on the dating of some of the blankets examined, that had been given an earlier date based on stylistic grounds only (Fig. 9).

In many cases, it is advantageous to combine SERS with complementary methods of colorant identification and materials characterization. This multi-technique approach was followed, for example, in the analysis of Kaitag textiles from Russia (Pozzi et al. 2012b), where SERS was used in association with SEM/energy dispersive X-ray (EDX) analysis, visible reflectance spectroscopy, HPLC, and XRF spectrometry for a complete characterization of the textile fibers, with special focus on their colorants and deterioration products. The two dozen textiles analyzed, dating from the 17th to 18th century, were primarily made of cotton with silk embroideries and showed a variety of colorants. Of those, SERS identified madder for red; indigo for dark and light blue; weld (or another luteolin-based dye) for yellow; the same luteolin-based dye, or sometimes a different yellow one, in combination with indigo for green; tannins mordanted with iron for dark brown; again tannins, sometimes with the addition of indigo, for black. In this particular case study, the main limitation of SERS emerged during examination of those threads that were shown through the multi-technique analytical approach to be dyed with more than one dyestuffs, as only one component was detected by SERS.

To date, only a handful of examples have been reported on the successful SERS detection of multiple dyestuffs on a single textile fiber. One of these accounts was provided by Idone and coworkers, who performed direct, extractionless identification of both cochineal carmine and brazilwood on animal and vegetable fibers using colloidal pastes (Idone et al. 2013). The study focused on the much admired textiles produced in Italy in the early 20th century by artist Mariano Fortuny y de Madrazo (Granada, Spain, 1871—Venice, Italy, 1949). The samples dyed with both carmine and brazilwood, as identified by SERS, included two red cotton panels produced by the *Società Anonima Fortuny* and a silk thread of a red velvet panel made at the Palazzo Pesara-Orfei in Venice, the latter also displaying a *Mariano Fortuny Deposé* stamp.

5.2 Paintings

Although many of the technical and methodological improvements in the field of SERS for cultural heritage have only been tested on mock-up paint layers (Doherty et al. 2011, 2014; Platania et al. 2014; Retko et al. 2014), SERS is becoming increasingly popular in real-world case studies to detect and identify red dyes and lake pigments in samples from actual paintings. The first application in this context, reported in 2009, concerns the analysis of a 50-µm red glaze sample from *St. John the Baptist Bearing Witness* (ca. 1506–07), a painting from the workshop of Italian artist Francesco Granacci (Leona 2009). In this case, SERS analysis was performed on glucose-reduced citrate-capped silver nanoparticles with HF hydrolysis pretreatment of the sample, proving the effectiveness of this combined methodology for the ultra-sensitive analysis of medium-rich paint samples such as colorants dispersed in oil glazes. Remarkably, the identification of kermes in the specimen examined is consistent with this anthraquinoid dye being deemed as the main colorant for red glazes in Europe before the introduction of cochineal from the New World in the second decade of the 16th century. This analytical procedure, progressively grown into a standard protocol at the Metropolitan Museum of Art and other institutions, has then proven successful in various routine applications, including the characterization of madder lake in oil paint samples from *The Card Players* (1623–24) by the Dutch painter Jan Lievens and from an homonymous painting (1890–92) by Paul Cézanne (Pozzi et al. 2013b).

The first extractionless non-hydrolysis study of organic dyes in oil paintings was reported by Oakley et al. (2011), who employed colloidal pastes to examine red colorants in oil glazes from works belonging to the Colonial Williamsburg Foundation collection, i.e. *Portrait of William Nelson* (1748–50) by the earliest native-born American artist of European descent, Robert Feke, and *Portrait of Isaac Barré* (1766) by Sir Joshua Reynolds, a founder of the Royal Academy of Arts. In this case, in addition to providing a probe of local environment by means of correlated fluorescence measurements, the authors identified carmine lake in

samples from the two paintings, albeit showing poor reproducibility due to unevenness of the silver nanoparticle coating.

A systematic work comparing SERS spectra of anthraquinoid red dyes from a wide variety of substrates obtained with or without HF hydrolysis confirmed how, in many cases, highly reproducible, conclusive dye identification in lake-containing glazes can only be achieved upon HF hydrolysis (Pozzi et al. 2012a). The high effectiveness of the HF treatment for SERS analysis of oil paints has been initially demonstrated on the aforementioned samples from Cézanne's *The Card Players*, as well as paints from Henri Matisse's *The Young Sailor* (1906), and Rembrandt's *Aristotle With a Bust of Homer* (1653). Further proof of the efficacy of the HF treatment is offered in another article by Pozzi et al. (2014a), which examines a wide selection of red lake oil paint reconstructions prepared according to 19th-century historical recipes, proving that successful dye identification can be accomplished upon HF hydrolysis even when inorganic pigments, extenders, ground materials or binding media are associated with the red lake in the sample analyzed. This comprehensive work on reference materials was then extended, in the same paper, to the systematic analysis of samples from 19th-century French Impressionist and post-Impressionist paintings in the collection of the Art Institute of Chicago, including works by Manet, Pissarro, Renoir, Monet and Gauguin. This study demonstrated the pervasive use of mostly two types of red lakes by these artists: cochineal and madder. In the case of Renoir's *Chrysanthemums* (1881–82), microscopic examination of the painting revealed the presence of a very thin, purple-colored overpaint on top of the original red lake. The two paint layers could be analyzed individually upon careful separation by means of a scalpel, revealing the use of cochineal as the original lake and Pigment Red 48:3 for the $\sim$20-μm thick retouching (Fig. 10).

The first evidence of SERS identification of binary mixtures of red lakes in painting layers was offered in two instances, i.e. Renoir's *Woman at the Piano* (1875–76) and Édouard Manet's *Woman Reading* (1879–80). In the first case, a few particles with an orange fluorescence emission were spotted within a non-fluorescing red lake paint layer in a cross section sample removed from the painting. The identity of the two types of lake pigments could be determined by SERS: while the signals observed right after sample preparation were consistent with madder, after a few minutes the spectrum of carminic acid was recorded from the same sample. This observation most likely indicates that the alizarin and purpurin molecules originating from the fluorescing madder particles, which have a higher affinity for the silver substrate (Cañamares et al. 2006a), were adsorbed first on the nanoparticle surface. As aggregation proceeded, carminic acid from cochineal—present in significantly higher amounts in the sample within the non-fluorescing layer—then occupied the remaining surface sites, resulting in the carminic acid signals becoming predominant in the SERS spectrum. As to Manet's *Woman Reading*, while the SERS data acquired from the corresponding samples did not match the individual reference spectra of commercial madder or cochineal lakes, a perfect correspondence was found with the spectrum of a red lake paint

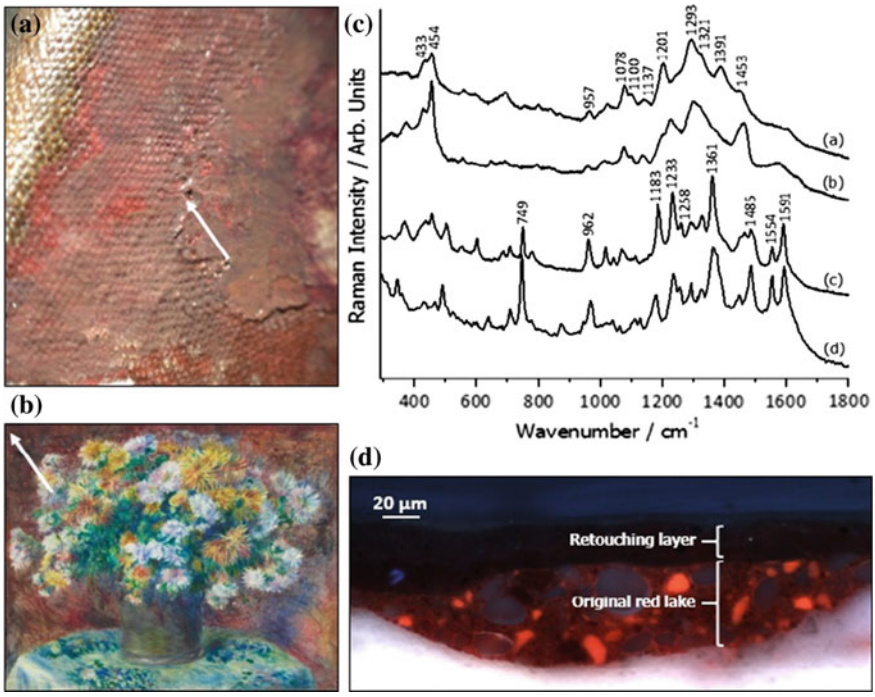

Fig. 10 Pierre-Auguste Renoir's *Chrysanthemums*, 1881/82 (Mr. and Mrs. Martin A. Ryerson Collection, The Art Institute of Chicago 1933.1173), where sampling site is indicated by an *arrow* in the painting image and micrograph. The UV-induced fluorescence image (500×) of a sample mounted as a cross section shows the presence of a thin varnish application and a purplish retouching layer on top of the original paint. The SERS spectrum of the Renoir's original red lake (*a*) is in accordance with those obtained from carmine oil paint historical reconstructions (*b*), while the spectral pattern of the retouching material (*c*) matches reference Pigment Red 48:3 (*d*)

reconstruction prepared as a mixture of cochineal and Kopp's purpurin (a purpurin-rich extract of the madder lake) on aluminum sulfate (Pozzi et al. 2014a).

Beside successfully detecting red lakes in combination in a few cases, SERS was used by Oakley et al. (2012) upon treatment with sulfuric acid to probe mixtures of blue inorganic pigments and organic colorants, i.e. Prussian blue and indigo, in a single sample from the early 18th-century oil painting *Portrait of Evelyn Byrd* (1725–26).

Most recently, the applicability of SERS to the analysis of oil paints and lake glazes has been further expanded to include the examination of paint layers in cross section samples. Idone et al. (2014) used an extractionless non-hydrolysis approach to characterize highly fluorescing red lake pigments in a cross section from a 16th-century mural painting of *Sant'Anna Metterza*. Although the experiment was successful, the authors emphasized the need to repeat the experiment on a number of different areas in order to find suitable spots where clusters of aggregated nanoparticles give rise to a significantly improved signal enhancement. Frano et al.

(2014) identified carmine and madder lakes in cross sections of 18th- and 19th-century paintings by direct deposition of colloidal pastes. Although more complex and equipment-intensive, the coupling of UV laser ablation sampling with SERS detection on a vapor-deposited silver nanoisland film, described above, has recently led to the successful identification of kermes in samples from *The Incredulity of Saint Thomas* by Venetian master Luca Signorelli and *Adoration of the Shepherds* by Giorgione, both dated to the 15th century (Cesaratto et al. 2014).

5.3 Works of Art on Paper

Applications of SERS to the analysis of colorants used in works of art on paper are still rare. In graphic works, the pigment particles are typically bound with small quantities of aqueous media such as glue or gums, and mixtures of compounds tend to be simpler than for pigments used in paintings. Therefore, reported uses of SERS in this area have involved the direct deposition of colloidal pastes on small pigment particles removed from the artworks. To date, various authors have successfully performed SERS analysis on watercolors and pastels from the 19th century, illuminated manuscripts, and Japanese screens and woodblock prints.

Brosseau et al. (2009b) analyzed the colorants of late 19th-century pastel sticks that belonged to artist Mary Cassatt (1844–1926), ranging in color from pale pink to dark purple, and found dyestuffs that were also encountered on a pastel drawing by the artist in the collection of the Art Institute of Chicago. Analysis was performed with citrate-reduced Lee-Meisel colloids concentrated into a paste and deposited directly on individual pigment grains. Interestingly, the materials identified show the coexistence of traditional dyes with some newly introduced synthetic organic colorants in the palette of the artist, including carmine lake, madder, rhodamine B and 6G, and a beta-naphthol or monoazo dye.

Regarding the watercolor medium, Pozzi et al. (2013c) used the HF pretreatment to analyze reference historical lake pigments in series of watercolor washes included in historical catalogs of the famed English colorman Winsor and Newton, and reported identification of madder on a sample removed from *Silver Ball, Barge and Trees* (1930), a watercolor by Arthur Dove made with gouache, ink and charcoal (Pozzi et al. 2013b). SERS analysis of a sample taken from an extremely faded area of the sky of Winslow Homer's watercolor *For to Be a Farmer's Boy* (1887) found cochineal, Indian purple (a precipitate of cochineal carmine on copper substrate) and purple madder by comparison with reference spectra taken on a Winsor and Newton antique book showing swatches of original, unfaded watercolor samples (Brosseau et al. 2011). In Homer's work, the red lakes were found to be mixed with vermilion and chrome yellow, which led to conclude that the sky must once have depicted a sunset or dawn scene. Based on this newly found

evidence, a decision was made to digitally recolorize an image of the work of art to offer scholars and the public the opportunity to view the work as the artist originally intended.

Several researchers have recently added SERS to the toolbox of analytical methods deployed to investigate illuminated manuscripts, artifacts that are generally studied mostly non-invasively and for which miniaturization of the samples analyzed is of paramount importance in light of the rarity of the illuminations and extremely thin layers of colored media. Castro et al. (2014) combined minimally invasive SERS with non-invasive microspectrofluorimetry to identify, upon HF hydrolysis, lac dye reds in 12th–13th-century medieval illuminations from Portugal. Aceto et al. (2015) successfully combined SERS and other micro-invasive techniques (such as matrix assisted laser desorption ionization-time of flight-mass spectrometry, and inductively coupled plasma-mass spectrometry) with FTIR, FT-Raman, fiber optic reflectance spectrophotometry, spectrofluorimetry, and XRF spectrometry to identify folium and orchil on various reference samples including dyed parchment—a mock up of the exceedingly rare purple codices. The authors claim that SERS was effective at identifying the colorants on the dyed parchment samples with and without extraction with formic acid, and report the first SERS spectrum of folium. El Bakkali et al. (2014) used UV/vis reflectance and fluorescence spectroscopies alongside SERS to identify carminic acid in red and pink inks on 19th-century manuscripts from Morocco. In a work by Leona and coworkers (featured in Sgamellotti et al. 2014), SERS on silver colloids was used to identify lac dye in the center of the iris petals in Ogata Kōrin's masterpiece *Irises at Yatsuhashi* (1709 or later), a pair of Japanese screens from the early 18th century in the collection of the Metropolitan Museum of Art. The identification of a triarylmethane dye, either methyl violet or crystal violet (the two dyes cannot be differentiated by SERS) on a Japanese print from 1892, *Sekigahara Homare no Gaika* (*A poem about the battle of Sekigahara*) by Toyoharu Kunichika, was also reported by Leona et al. as an example of both gel-sampling SERS and inkjet colloid delivery SERS.

Additional work on Japanese woodblock prints of the Meiji period (1868–1912) is being conducted at the Metropolitan Museum of Art. The two-step SERS protocol developed by Pozzi et al. (2012a) has been used to detect what are probably some of the earliest uses of magenta, cochineal, and eosine in Japan (Fig. 11) (Leona et al. 2015).

Of relevance to the analysis of graphic documents are the recent applications of SERS to study historical inks. Roldán et al. (2014) combined SERS and other analytical techniques to identify inks made with bistre. Among historic inks, sepia can be challenging to identify in old and aged samples because of the similarity of its spectral pattern with the profiles of carbon-based blacks. Centeno, Roldán, and respective coworkers (Centeno and Shamir 2008; Roldán et al. 2014) have studied this subject extensively and combined SERS with complementary analytical techniques to successfully characterize the synthetic chromophore in both reference and historical materials.

Fig. 11 *Hiroshige III, View of Benten on Nakanoshima in Shinobazu Pond, Ueno Park*, 1881. Woodblock print triptych on paper. The *violet* is methyl *violet*, the lighter *red* on the robes is cochineal, and the *pink* of the *cherry* blossoms is eosine

5.4 Other Applications

The ability to detect minute amounts of colorants makes SERS an ideal technique for the investigation of archaeological samples, which often contain only very small remnants of the original material and are heavily affected by contamination and aging. Hence, SERS may sometimes be the only analytical method that can be used to obtain dye information from these very ancient and often fragmentary artifacts. The first application of SERS to archaeological material was demonstrated by Van Elslande et al. (2008), who detected purpurin in Roman cosmetics. Subsequently, Leona (2009) described the earliest identification of madder dye in a 4000 years old Egyptian leather fragment. The identification of madder in archaeological samples including pink pigments from an excavation at Corinth (2nd century B.C.) and a statue of Caligula (Virginia Museum of Fine Art, 1st century A.D.) were reported by Pozzi et al. (2013b). Londero et al. (2013) also identified madder in a fragment from the trappings of an ancient Egyptian chariot of Amenhotep III (New Kingdom, 1390–1352 B.C.) pretreated with HF and analyzed with LA-SERS.

Few studies exist in the literature in relation to lake pigments used to decorate polychrome sculpture and furniture. Some notable examples include studies of red glazes in medieval polychrome sculpture at the Metropolitan Museum of Art, i.e. the detection of lac dye in a Spanish crucifix dating to 1150–1200, which is thought to be the earliest example of the use of lac dye in European sculpture (Pozzi et al. 2013b). From a slightly later date, ca. 1175–1200, the French Romanesque sculpture of a *Virgin and Child in Majesty*, made in Auvergne, France, is the earliest documented example of lac dye use in France (Leona 2009). These findings document trade from India, where the colorant originates from, in medieval times

and are of great historical importance. Daher et al. (2014) also used non-hydrolysis SERS on Ag colloids to identify carmine and madder lake in pink layers from French decorative arts objects such as a weaving shuttle and a commode dating from the 18th century.

Introduced in the mid-19th century as the first form of recording a photographic image on a plate, daguerreotypes by their very nature owe to the image-forming process the presence of silver/mercury nanoparticles on their surface. Hence, Centeno et al. (2008) exploited this structural and compositional property of the medium to diagnose the nature of a white degradation haze forming on daguerreotypes originating from the famed Southworth and Hawes studio. Silver chloride compounds and substituted aromatic compounds were identified by simply focusing a 785 nm laser onto the naturally nanostructured silver surface of the daguerreotypes, giving rise to the SERS effect. Because metallic silver can be redeposited when silver chlorides are exposed to UV/vis illumination, ultimately obfuscating the original image, the SERS data was instrumental to inform exhibition policies for the collection.

5.5 The Interface with Forensics: Modern Inks

The examination of questioned documents is an active area of interest for the application of Raman spectroscopy and SERS, which are considered of value in identifying and comparing the inks of questioned entries. Since it represents a relatively non-destructive technique, Raman spectroscopy promotes the identification of pigments and dyes, which often represent the most intense contributors to the Raman signal. While several reviews on the analysis of questioned documents discuss most of the recent literature concerning normal Raman spectroscopy (Braz et al. 2013; Calcerrada and Garcia-Ruiz 2015), the special contributions of SERS studies are presented here.

In recent years, the focus of forensic research on the characterization of pen inks has turned to ball point and gel inks. These are especially amenable to SERS studies since the dyes typically display a strong SERS enhancement, and the fluorescence interference that usually hampers normal Raman spectroscopy is readily suppressed by adsorption of the analyte on a metal substrate. A recent study on synthetic dyes compared systematically the discrimination capabilities of SERS with various excitation wavelengths (Geiman et al. 2009). Ten dyes representing classes commonly found in ink formulations were selected for the study: Acid Blue 1, Acid Orange 10, Acid Red 52, Aniline Blue, Crystal Violet, Methyl Violet, Pararosaniline, Rhodamine B, Sudan Black B, and Victoria Blue B. These dyes were studied at several excitation wavelengths, i.e. 633, 785 nm (with and without SERS), as well as FT-Raman 1064 nm. Among normal Raman techniques, only the FT-Raman produced spectra with fairly good signal intensity and signal-to-noise ratios, while 633 and 785 nm laser excitation caused high levels of fluorescence overwhelming the dye signals. SERS spectra were obtained using dilute solutions

of the dye molecules with silver colloids, and although some differences were encountered between SERS and the normal Raman spectra, presumably due to differences in the selection rules, a considerable net increase in signal intensity was observed. In a related study, Seifar et al. reported that methyl violet exhibited a strong resonance effect (SERS) at 514.5 and 457.9 nm, while other dyes were most easily observed with 785 nm excitation (Seifar et al. 2001). Bell and Spence (2001) have compared the discriminant advantages of SERS using in situ deposition of silver colloids and normal Raman spectroscopy combined with other analytical techniques commonly employed in document examination. Compared with various extraction methods such as TLC, they found that Raman techniques provided an equivalent and sometimes better discrimination, while being both rapid and non-destructive. SERS ensured an increased differentiation when compared with normal Raman spectroscopic techniques, but problems of reproducibility were obtained in several samples. Luo et al. (2013) employed gold nanoparticles as a SERS active substrate in order to analyze pens and printers/copiers inks in situ at 633 nm. Raza and Saha employed silver-doped agarose gel disks as SERS substrate for examining ballpoint inks, carrying out analysis at 785 and 514 nm excitation. The gel disks have been shown to extract the ink on small sections of the pen strokes. The dyes extracted into the gel medium were found to be stable for more than thirty days and were furthermore examined by attenuated total reflection (ATR)-FTIR in sequence (Raza and Saha 2013). White (2003) reported an interesting SERS experiment on a three year old bank check that was coated with silver colloid. Finally, Wagner and Clement (2001) described the use of SERS (silver colloid, 633 nm) on ballpoint inks as well as fluid inks of varying colors. A comparison of the discrimination power of normal Raman spectroscopy and SERS showed significant enhancement of the Raman signal using SERS. However, black ballpoint inks apparently lack characteristic features. They are most likely composed entirely of graphite, which usually displays only several broad peaks in normal Raman spectroscopy, and are difficult to characterize using SERS.

Only few reports have focused on ink jet/toner printers as analyzed by SERS. Rodger et al. have obtained SERS on a set of four different ink jet dyes on five different papers on silver colloid, at 514 and 633 nm, as well as FT-Raman at 1064 nm (Rodger et al. 2000). SERS was shown to be successful for identifying the dyes, while FT-Raman produced interference from the paper and filler as well. This was explained as due to the increased size of the area sampled, which most likely included some of the paper. Additionally, SERS is relatively insensitive to the ingredients in paper. Luo et al. (2013) have examined a gold colloid formulation on ink from printers and copiers as well as pen inks, although no information on the samples were provided.

Beside the popularity of pen and printers inks, security inks have a special forensic interest. They are largely used on banknotes (either as the ink used in the banknote itself or as an added stain during robberies), various official documents, and checks, by doping the material of interest with pigments or nanoparticles that exhibit unique optical properties such as fluorescence. Historically, security inks were formulated using materials doped with rare earth lanthanides elements such as

europium, terbium, ytterbium, thulium or erbium. These rare earths have unique spectral features when added to a normal ink, which can be clearly discriminated from any other attempted forgery or counterfeit. In recent years different patents have been issued which utilize SERS taggants or SERS active sols in security inks. SERS nanotags consist of a nanoparticle coated with a unique "reporter" molecule, which is then encapsulated by an inert silica or polymer layer. The outermost layer ensures nanoparticle stability over time and protection from environmental conditions, so that the taggants can be analyzed even after many years.

6 Conclusions and Future Outlook

It has taken the science of SERS over thirty years since inception for it to become a mature field of study. This is testament to the wide variety and applicability of its scope, as well as the potential for numerous applications covering a wide variety of disciplines. Furthermore, the theoretical underpinnings have engendered lively controversy, and have also led to connections to numerous other areas of scientific concern. Ultimately, the potent combination of high sensitivity and high resolution afforded by SERS makes it unique as an analytical tool, and provides numerous pathways for potential applications. In this chapter, we have reviewed the application of SERS to cultural heritage objects and, due to the similarity of analytical techniques and materials, to systems of interest to forensic science. It may be fairly said that even the above compilation is likely incomplete, and subject to augmentation in the near future.

Researchers have reached the hallmark of a robust field, which should be celebrated. However, this brings up the question as to where the field goes next. Certainly, some of the techniques discussed above are still in their infancy, such as TERS, laser ablation—SERS, and microfluidics—SERS. Therefore, considerable intensification of effort and progress should be expected in these areas. More common hybrid techniques such a TLC-SERS have the promise to allow SERS to become more multidimensional in its approach. More well-developed areas, such as substrate development or extraction methodology, have been of considerable interest for some time, and may not see such rapid change in the future. In any case, the exciting aspect of recent developments is that there is an increasing variety of new locales in which SERS is applied to cultural heritage and forensic science. This proliferation confirms that the applications described here are becoming more widely accepted, and of interest to a wider scientific community for routine-based use. We hope that this review will become a springboard for new researchers interested in advancing the field through their own ideas and unique applications.

Acknowledgments SZ, FC and RPVD would like to acknowledge the National Science Foundation (MRSEC NSF DMR-1121262, NSF CHE-1152547, and NSF CHE-1041812) and the Northwestern University/Art Institute of Chicago Center for Scientific Studies in the Arts (NU-ACCESS) for their support. Additionally, this work made use of the EPIC facility (NUANCE

Center-Northwestern University), which has received support from the MRSEC program (NSF DMR-1121262) at the Materials Research Center; the International Institute for Nanotechnology (IIN); and the State of Illinois, through the IIN. JL and ML thank the National Science Foundation (CHE-1402750) for funding. FC and FP are indebted to the Andrew W. Mellon Foundation for funding a postdoctoral research position and providing support for Conservation Science at the Art Institute of Chicago.

References

Aceto M, Arrais A, Marsano F, Agostino A, Fenoglio G, Idone A, Gulmini M (2015) A diagnostic study on folium and orchil dyes with non-invasive and micro-destructive methods. Spectrochim Acta Part A Mol Biomol Spectrosc 142:159–168. doi:10.1016/j.saa.2015.02.001

Ahn C, Obendorf SK (2004) Dyes on archaeological textiles: analyzing alizarin and its degradation products. Text Res J 74:949–954. doi:10.1177/004051750407401102

Ahn C, Obendorf SK (2007) GGMS analysis of curcumin dye after selective degradation treatment. Fibers Polym 8:278–283. doi:10.1007/BF02877270

Albrecht M, Creighton J (1977) Anomalously Intense Raman-Spectra of Pyridine at a Silver Electrode. J Am Chem Soc 99:5215–5217. doi:10.1021/ja00457a071

Alfeld M, De Nolf W, Cagno S, Appel K, Siddons DP, Kuczewski A, Janssens K, Dik J, Trentelman K, Walton M, Sartorius A (2013a) Revealing hidden paint layers in oil paintings by means of scanning macro-XRF: a mock-up study based on Rembrandt's "An old man in military costume". J Anal At Spectrom 28:40–51. doi:10.1039/c2ja30119a

Alfeld M, Pedroso JV, van Eikema Hommes M, Van der Snickt G, Tauber G, Blaas J, Haschke M, Erler K, Dik J, Janssens K (2013b) A mobile instrument for in situ scanning macro-XRF investigation of historical paintings. J Anal At Spectrom 28:760–767. doi:10.1039/c3ja30341a

Amat A, Miliani C, Romani A, Fantacci S (2015) DFT/TDDFT investigation on the UV-vis absorption and fluorescence properties of alizarin dye. Phys Chem Chem Phys 17:6374–6382. doi:10.1039/c4cp04728a

Bacci M, Baldini F, Carla R, Linari R (1991) A color analysis of the Brancacci Chapel frescoes. Appl Spectrosc 45:26–31. doi:10.1366/0003702914337713

Baglioni P, Carretti E, Chelazzi D (2015) Nanomaterials in art conservation. Nat Nanotechnol 10:287–290. doi:10.1038/nnano.2015.38

Baran A, Wrzosek B, Bukowska J, Proniewicz LM, Baranska M (2009) Analysis of alizarin by surface-enhanced and FT-Raman spectroscopy. J Raman Spectrosc 40:436–441. doi:10.1002/jrs.2147

Bell SEJ, Spence SJ (2001) Disposable, stable media for reproducible surface-enhanced Raman spectroscopy. Analyst 126:1–3. doi:10.1039/b009519m

Bell IM, Clark RJH, Gibbs PJ (1997) Raman spectroscopic library of natural and synthetic pigments (pre- ≈ 1850 AD). Spectrochim Acta Part A Mol Biomol Spectrosc 53:2159–2179. doi:10.1016/S1386-1425(97)00140-6

Benedetti DP, Zhang J, Tague TJ, Lombardi JR, Leona M (2014) In situ microanalysis of organic colorants by inkjet colloid deposition surface-enhanced Raman scattering. J Raman Spectrosc 45:123–127. doi:10.1002/jrs.4424

Braz A, Lopez-Lopez M, Garcia-Ruiz C (2013) Raman spectroscopy for forensic analysis of inks in questioned documents. Forensic Sci Int 232:206–212. doi:10.1016/j.forsciint.2013.07.017

Brosseau CL, Gambardella A, Casadio F, Grzywacz CM, Wouters J, Van Duyne RP (2009a) Ad-hoc surface-enhanced Raman spectroscopy methodologies for the detection of artist dyestuffs: thin layer chromatography-surface enhanced Raman spectroscopy and in situ on the fiber analysis. Anal Chem 81:3056–3062. doi:10.1021/ac802761v

Brosseau CL, Rayner KS, Casadio F, Grzywacz CM, van Duyne RP (2009b) Surface-enhanced Raman spectroscopy: a direct method to identity colorants in various artist media. Anal Chem 81:7443–7447. doi:10.1021/ac901219m

Brosseau CL, Casadio F, Van Duyne RP (2011) Revealing the invisible: using surface-enhanced Raman spectroscopy to identify minute remnants of color in Winslow Homer's colorless skies. J Raman Spectrosc 42:1305–1310. doi:10.1002/jrs.2877

Bruni S, Guglielmi V, Pozzi F (2010) Surface-enhanced Raman spectroscopy (SERS) on silver colloids for the identification of ancient textile dyes: tyrian purple and madder. J Raman Spectrosc 41:175–180. doi:10.1002/jrs.2456

Bruni S, Guglielmi V, Pozzi F (2011a) Historical organic dyes: a surface-enhanced Raman scattering (SERS) spectral database on Ag Lee-Meisel colloids aggregated by $NaClO_4$. J Raman Spectrosc 42:1267–1281. doi:10.1002/jrs.2872

Bruni S, Guglielmi V, Pozzi F, Mercuri AM (2011b) Surface-enhanced Raman spectroscopy (SERS) on silver colloids for the identification of ancient textile dyes. Part II: pomegranate and sumac. J Raman Spectrosc 42:465–473. doi:10.1002/jrs.2736

Calcerrada M, Garcia-Ruiz C (2015) Analysis of questioned documents: a review. Anal Chim Acta 853:143–166. doi:10.1016/j.aca.2014.10.057

Cañamares MV, Leona M (2007) Surface-enhanced Raman scattering study of the red dye laccaic acid. J Raman Spectrosc 38:1259–1266. doi:10.1002/jrs.1761

Cañamares MV, Lombardi JR (2015) Raman, SERS, and DFT of Mauve Dye: adsorption on Ag nanoparticles. J Phys Chem C 119:14297–14303. doi:10.1021/acs.jpcc.5b02619

Cañamares MV, Garcia-Ramos JV, Domingo C, Sanchez-Cortes S (2004) Surface-enhanced Raman scattering study of the adsorption of the anthraquinone pigment alizarin on Ag nanoparticles. J Raman Spectrosc 35:921–927. doi:10.1002/jrs.1228

Cañamares MV, Garcia-Ramos JV, Domingo C, Sanchez-Cortes S (2006a) Surface-enhanced Raman scattering study of the anthraquinone red pigment carminic acid. Vib Spectrosc 40:161–167. doi:10.1016/j.vibspec.2005.08.002

Cañamares MV, Sanchez-Cortes S, Garcia-Ramos JV (2006b) In: IRUG7 proceedings, New York, 28–31 Mar 2006. Museum of Modern Art, p 19

Cañamares MV, Garcia-Ramos JV, Gomez-Varga JD, Domingo C, Sanchez-Cortes S (2007) Ag nanoparticles prepared by laser photoreduction as substrates for in situ surface-enhanced raman scattering analysis of dyes. Langmuir 23:5210–5215. doi:10.1021/la063445v

Cañamares MV, Chenal C, Birke RL, Lombardi JR (2008a) DFT, SERS, and single-molecule SERS of crystal violet. J Phys Chem C 112:20295–20300. doi:10.1021/jp807807j

Cañamares MV, Lombardi JR, Leona M (2008b) Surface-enhanced Raman scattering of protoberberine alkaloids. J Raman Spectrosc 39:1907–1914. doi:10.1002/jrs.2057

Cañamares MV, Garcia-Ramos JV, Sanchez-Cortes S, Castillejo M, Oujja M (2008c) Comparative SERS effectiveness of silver nanoparticles prepared by different methods: a study of the enhancement factor and the interfacial properties. J Colloid Interface Sci 326:103–109. doi:10.1016/j.jcis.2008.06.052

Cañamares MV, Lombardi J, Leona M (2009) Raman and surface enhanced Raman spectra of 7-hydroxyflavone and 3′,4′-dihydroxyflavone. E-PS, pp 81–88

Cañamares MV, Leona M, Bouchard M, Grzywacz CM, Wouters J, Trentelman K (2010) Evaluation of Raman and SERS analytical protocols in the analysis of Cape Jasmine dye (*Gardenia augusta* L.). J Raman Spectrosc 41:391–397. doi:10.1002/jrs.2462

Cañamares MV, Reagan DA, Lombardi JR, Leona M (2014) TLC-SERS of mauve, the first synthetic dye. J Raman Spectrosc 45:1147–1152. doi:10.1002/jrs.4508

Cardon D (2007) Natural dyes: sources, tradition, technology and science. Archetype, London

Carretti E, Bonini M, Dei L, Berrie BH, Angelova LV, Baglioni P, Weiss RG (2010) New Frontiers in materials science for art conservation: responsive gels and beyond Acc Chem Res 43:751–760. doi:10.1021/ar900282h

Casadio F, Leona M, Lombardi JR, Van Duyne R (2010) Identification of organic colorants in fibers, paints, and glazes by surface enhanced Raman spectroscopy. Acc Chem Res 43:782–791. doi:10.1021/ar100019q

Casanova-González E, García-Bucio A, Ruvalcaba-Sil JL, Santos-Vasquez V, Esquivel B, Falcón T, Arroyo E, Zetina S, Roldán ML, Domingo C (2012) Surface-enhanced Raman spectroscopy spectra of Mexican dyestuffs. J Raman Spectrosc 43:1551–1559. doi:10.1002/jrs.4086

Castro R, Pozzi F, Leona M, Melo MJ (2014) Combining SERS and microspectrofluorimetry with historically accurate reconstructions for the characterization of lac dye paints in medieval manuscript illuminations. J Raman Spectrosc 45:1172–1179. doi:10.1002/jrs.4608

Centeno SA, Shamir J (2008) Surface enhanced Raman scattering (SERS) and FTIR characterization of the sepia melanin pigment used in works of art. J Mol Struct 873:149–159. doi:10.1016/j.molstruc.2007.03.026

Centeno SA, Meller T, Kennedy N, Wypyski M (2008) The daguerreotype surface as a SERS substrate: characterization of image deterioration in plates from the 19th century studio of Southworth & Hawes. J Raman Spectrosc 39:914–921. doi:10.1002/jrs.1934

Cesaratto A, Leona M, Lombardi JR, Comelli D, Nevin A, Londero P (2014) Detection of organic colorants in historical painting layers using UV laser ablation surface-enhanced Raman microspectroscopy. Angew Chem Int Ed 53:14373–14377. doi:10.1002/anie.201408016

Chang J, Cañamares MV, Aydin M, Vetter W, Schreiner M, Xu W, Lombardi JR (2009) Surface-enhanced Raman spectroscopy of indanthrone and flavanthrone. J Raman Spectrosc 40:1557–1563. doi:10.1002/jrs.2298

Chen K, Leona M, Vo-Dinh KC, Yan F, Wabuyele MB, Vo-Dinh T (2006) Application of surface-enhanced Raman scattering (SERS) for the identification of anthraquinone dyes used in works of art. J Raman Spectrosc 37:520–527. doi:10.1002/jrs.1426

Chen K, Leona M, Vo-Dinh T (2007) Surface-enhanced Raman scattering for identification of organic pigments and dyes in works of art and cultural heritage material. Sens Rev 27:109–120. doi:10.1108/02602280710731678

Claro A, Melo MJ, Schafer S, de Melo JSS, Pina F, van den Berg KJ, Burnstock A (2008) The use of microspectrofluorimetry for the characterization of lake pigments. Talanta 74:922–929. doi:10.1016/j.talanta.2007.07.036

Claro A, Melo MJ, Seixas de Melo JS, van den Berg KJ, Burnstock A, Montague M, Newman R (2010) Identification of red colorants in van Gogh paintings and ancient Andean textiles by microspectrofluorimetry. J Cult Herit 11:27–34. doi:10.1016/j.culher.2009.03.006

Clementi C, Nowik W, Romani A, Cibin F, Favaro G (2007) A spectrometric and chromatographic approach to the study of ageing of madder (*Rubia tinctorum* L.) dyestuff on wool. Anal Chim Acta 596:46–54. doi:10.1016/j.aca.2007.05.036

Clementi C, Basconi G, Pellegrino R, Romani A (2014) *Carthamus tinctorius* L.: a photophysical study of the main coloured species for artwork diagnostic purposes. Dyes Pigm 103:127–137. doi:10.1016/j.dyepig.2013.12.002

Collins D, Groom G, Ireson N, Keegan K, Shaw J, Nichols K (2014) Renoir paintings and drawings at the Art Institute of Chicago. Art Institute of Chicago, Chicago, USA

Colombini MP, Andreotti A, Baraldi C, Degano I, Lucejko JJ (2007) Colour fading in textiles: a model study on the decomposition of natural dyes. Microchem J 85:174–182. doi:10.1016/j.microc.2006.04.002

Cooksey C, Sinclair RS (2005) Colour variations in tyrian purple dyeing. Dyes Hist Archaeol 20:127

Corredor C, Teslova T, Cañamares MV, Chen Z, Zhang J, Lombardi JR, Leona M (2009) Raman and surface-enhanced Raman spectra of chrysin, apigenin and luteolin. Vib Spectrosc 49:190–195. doi:10.1016/j.vibspec.2008.07.012

Creighton J, Blatchford C, Albrecht M (1979) Plasma resonance enhancement of Raman-scattering by pyridine adsorbed on silver or gold sol particles of size comparable to the excitation wavelength. J Chem Soc, Faraday Trans 75:790–798. doi:10.1039/f29797500790

Daher C, Drieu L, Bellot-Gurlet L, Percot A, Paris C, Le Hô A-S (2014) Combined approach of FT-Raman, SERS and IR micro-ATR spectroscopies to enlighten ancient technologies of painted and varnished works of art. J Raman Spectrosc 45:1207–1214. doi:10.1002/jrs.4565

de Oliveira LFC, Edwards HGM, Velozo ES, Nesbitt M (2002) Vibrational spectroscopic study of brazilin and brazilein, the main constituents of brazilwood from Brazil. Vib Spectrosc 28:243–249. doi:10.1016/S0924-2031(01)00138-2

Degano I, Ribechini E, Modugno F, Colombini MP (2009) Analytical methods for the characterization of organic dyes in artworks and in historical textiles. Appl Spectrosc Rev 44:363–410. doi:10.1080/05704920902937876

Degano I, Biesaga M, Colombini MP, Trojanowicz M (2011) Historical and archaeological textiles: An insight on degradation products of wool and silk yarns. J Chromatogr A 1218:5837–5847. doi:10.1016/j.chroma.2011.06.095

Delaney JK, Zeibel JG, Thoury M, Littleton R, Palmer M, Morales KM, de la Rie ER, Hoenigswald A (2010) Visible and infrared imaging spectroscopy of Picasso's Harlequin musician: mapping and identification of artist materials in situ. Appl Spectrosc 64:584–594

Delaney JK, Ricciardi P, Glinsman LD, Facini M, Thoury M, Palmer M, de la Rie ER (2014) Use of imaging spectroscopy, fiber optic reflectance spectroscopy, and X-ray fluorescence to map and identify pigments in illuminated manuscripts. Stud Conserv 59:91–101. doi:10.1179/2047058412Y.0000000078

Dik J, Janssens K, Van der Snickt G, van der Loeff L, Rickers K, Cotte M (2008) Visualization of a lost painting by Vincent van Gogh using synchrotron radiation based X-ray fluorescence elemental mapping. Anal Chem 80:6436–6442. doi:10.1021/ac800965g

Doherty B, Brunetti BG, Sgamellotti A, Miliani C (2011) A detachable SERS active cellulose film: a minimally invasive approach to the study of painting lakes. J Raman Spectrosc 42:1932–1938. doi:10.1002/jrs.2942

Doherty B, Gabrieli F, Clementi C, Cardon D, Sgamellotti A, Brunetti B, Miliani C (2014) Surface enhanced Raman spectroscopic investigation of orchil dyed wool from *Roccella tinctoria* and *Lasallia pustulata*. J Raman Spectrosc 45:723–729. doi:10.1002/jrs.4543

Dooley KA, Lomax S, Zeibel JG, Miliani C, Ricciardi P, Hoenigswald A, Loew M, Delaney JK (2013) Mapping of egg yolk and animal skin glue paint binders in Early Renaissance paintings using near infrared reflectance imaging spectroscopy. Analyst 138:4838–4848. doi:10.1039/c3an00926b

Edwards HGM, de Oliveira LFC, Nesbitt M (2003) Fourier-transform Raman characterization of brazilwood trees and substitutes. Analyst 128:82–87. doi:10.1039/b209052j

El Bakkali A, Lamhasni T, Lyazidi SA, Haddad M, Rosi F, Miliani C, Sanchez-Cortes S, El Rhaiti M (2014) Assessment of a multi-technical non-invasive approach for the typology of inks, dyes and pigments in two 19th century's ancient manuscripts of Morocco. Vib Spectrosc 74:47–56. doi:10.1016/j.vibspec.2014.07.008

Fan M, Andrade GFS, Brolo AG (2011) A review on the fabrication of substrates for surface enhanced Raman spectroscopy and their applications in analytical chemistry. Anal Chim Acta 693:7–25. doi:10.1016/j.aca.2011.03.002

Farquharson S, Maksymiuk P (2003) Simultaneous chemical separation and surface-enhanced Raman spectral detection using silver-doped sol-gels. Appl Spectrosc 57:479–482. doi:10.1366/00037020360626041

Ferreira ESB, Quye A, McNab H, Hulme AN, Wouters J, Boon JJ (2001) Development of analytical techniques for the study of natural yellow dyes in historical textiles. Dyes Hist Archaeol 16(17):179–186

Fleischmann M, Hendra P, Mcquilla AJ (1974) Raman-spectra of pyridine adsorbed at a silver electrode. Chem Phys Lett 26:163–166. doi:10.1016/0009-2614(74)85388-1

Frano KA, Mayhew HE, Svoboda SA, Wustholz KL (2014) Combined SERS and Raman analysis for the identification of red pigments in cross-sections from historic oil paintings. Analyst 139:6450–6455. doi:10.1039/c4an01581a

Geiman I, Leona M, Lombardi JR (2009) Application of Raman spectroscopy and surface-enhanced Raman scattering to the analysis of synthetic dyes found in ballpoint pen inks. J Forensic Sci 54:947–952. doi:10.1111/j.1556-4029.2009.01058.x

Gillard RD, Hardman SM, Thomas RG, Watkinson DE (1994) The detection of dyes by FTIR microscopy. Stud Conserv 39:187–192. doi:10.2307/1506597

Greeneltch NG, Davis AS, Valley NA, Casadio F, Schatz GC, Van Duyne RP, Shah NC (2012) Near-infrared surface-enhanced Raman spectroscopy (NIR-SERS) for the identification of Eosin Y: theoretical calculations and evaluation of two different nanoplasmonic substrates. J Phys Chem A 116:11863–11869. doi:10.1021/jp3081035

Grosjean D, Whitmore P, Demoor C, Cass G, Druzik J (1988) Ozone fading of organic colorants—products and mechanism of the reaction of ozone with curcumin. Environ Sci Technol 22:1357–1361. doi:10.1021/es00176a017

Guineau B, Guichard V (1987) Identification des colorants organiques naturels par microspectrometrie Raman de resonance et par effet Raman exalte de surface (SERS). The Getty Conservation Institute, Sydney, pp 659–666

Gulmini M, Idone A, Diana E, Gastaldi D, Vaudan D, Aceto M (2013) Identification of dyestuffs in historical textiles: Strong and weak points of a non-invasive approach. Dyes Pigm 98:136–145. doi:10.1016/j.dyepig.2013.02.010

Halpine SM (1996) An improved dye and lake pigment analysis method for high-performance liquid chromatography and diode-array detector. Stud Conserv 41:76–94. doi:10.2307/1506519

Henzel (1977) Journal of chromatography library. Elsevier, Amsterdam

Hofenk de Graaff JH, Roelofs WGT, Van Bommel MR (2004) The colourful past: origins, chemistry and identification of natural dyestuffs. Archetype Publications, London ; Abegg-Stiftung, Riggisberg, Switzerland

Idone A, Gulmini M, Henry A-I, Casadio F, Chang L, Appolonia L, Van Duyne RP, Shah NC (2013) Silver colloidal pastes for dye analysis of reference and historical textile fibers using direct, extractionless, non-hydrolysis surface-enhanced Raman spectroscopy. Analyst 138:5895–5903. doi:10.1039/c3an00788j

Idone A, Aceto M, Diana E, Appolonia L, Gulmini M (2014) Surface-enhanced Raman scattering for the analysis of red lake pigments in painting layers mounted in cross sections. J Raman Spectrosc 45:1127–1132. doi:10.1002/jrs.4491

Jeanmaire D, Vanduyne R (1977) Surface Raman spectroelectrochemistry. 1. Heterocyclic, aromatic, and aliphatic-amines adsorbed on anodized silver electrode. J Electroanal Chem 84:1–20. doi:10.1016/S0022-0728(77)80224-6

Jurasekova Z, Garcia-Ramos JV, Domingo C, Sanchez-Cortes S (2006) Surface-enhanced Raman scattering of flavonoids. J Raman Spectrosc 37:1239–1241. doi:10.1002/jrs.1634

Jurasekova Z, Domingo C, Garcia-Ramos JV, Sanchez-Cortes S (2008) In situ detection of flavonoids in weld-dyed wool and silk textiles by surface-enhanced Raman scattering. J Raman Spectrosc 39:1309–1312. doi:10.1002/jrs.2053

Jurasekova Z, del Puerto E, Bruno G, Garcia-Ramos JV, Sanchez-Cortes S, Domingo C (2010) Extractionless non-hydrolysis surface-enhanced Raman spectroscopic detection of historical mordant dyes on textile fibers. J Raman Spectrosc 41:1455–1461. doi:10.1002/jrs.2651

Jurasekova Z, Domingo C, Garcia-Ramos JV, Sanchez-Cortes S (2012) Adsorption and catalysis of flavonoid quercetin on different plasmonic metal nanoparticles monitored by SERS. J Raman Spectrosc 43:1913–1919. doi:10.1002/jrs.4114

Kim D, Campos AR, Datt A, Gao Z, Rycenga M, Burrows ND, Greeneltch NG, Mirkin CA, Murphy CJ, Van Duyne RP, Haynes CL (2014) Microfluidic-SERS devices for one shot limit-of-detection. Analyst 139:3227–3234. doi:10.1039/c4an00357h

Koperska M, Lojewski T, Lojewska J (2011) Vibrational spectroscopy to study degradation of natural dyes. Assessment of oxygen-free cassette for safe exposition of artefacts. Anal Bioanal Chem 399:3271–3283. doi:10.1007/s00216-010-4460-7

Koren Z (1994) HPLC analysis of the natural scale insect, madder and indigoid dyes. J Soc Dye Colour 110:273–277. doi: 10.1111/j.1478-4408.1994.tb01656.x

Kurouski D, Zaleski S, Casadio F, Van Duyne RP, Shah NC (2014) Tip-enhanced Raman spectroscopy (TERS) for in situ identification of indigo and iron gall ink on paper. J Am Chem Soc 136:8677–8684. doi:10.1021/ja5027612

Lee PC, Meisel D (1982) Adsorption and surface-enhanced Raman of dyes on silver and gold sols. J Phys Chem 86:3391–3395. doi:10.1021/j100214a025

Leona M (2008) Non-invasive identification of fluorescent dyes in historic textiles by matrix transfer-surface enhanced Raman scattering. United States Patent and Trademark Office; 7,362,431 B2. Filed 9 Aug 2006; awarded 22 Apr 2008

Leona M (2009) Microanalysis of organic pigments and glazes in polychrome works of art by surface-enhanced resonance Raman scattering. Proc Natl Acad Sci USA 106:14757–14762. doi:10.1073/pnas.0906995106

Leona M, Lombardi JR (2007) Identification of berberine in ancient and historical textiles by surface-enhanced Raman scattering. J Raman Spectrosc 38:853–858. doi:10.1002/jrs.1726

Leona M, Tague T (2010) Method and apparatus for in situ measurement of material properties by surface enhanced raman spectroscopy. United States Patent and Trademark Office; US 7,787,117 B1. Filed 24 June 2008; awarded 31 Aug 2010

Leona M, Stenger J, Ferloni E (2006) Application of surface-enhanced Raman scattering techniques to the ultrasensitive identification of natural dyes in works of art. J Raman Spectrosc 37:981–992. doi:10.1002/jrs.1582

Leona M, Decuzzi P, Kubic TA, Gates G, Lombardi JR (2011) Nondestructive identification of natural and synthetic organic colorants in works of art by surface enhanced Raman scattering. Anal Chem 83:3990–3993. doi:10.1021/ac2007015

Leona M, Smith HD II, Cesaratto A, Luo YB (2015) Synthetic dyes in the woodblock prints of Meiji Japan. In: Technart 2015, non-destructive and microanalytical techniques in art and cultural heritage, Catania, 27–30 Apr 2015

Leopold N, Lendl B (2003) A new method for fast preparation of highly surface-enhanced Raman scattering (SERS) active silver colloids at room temperature by reduction of silver nitrate with hydroxylamine hydrochloride. J Phys Chem B 107:5723–5727. doi:10.1021/jp027460u

Lewis PA (1988) Organic pigments. Federation of Societies for Coatings Technology, Philadelphia, PA, USA (1315 Walnut St., Philadelphia 19107)

Lofrumento C, Ricci M, Platania E, Becucci M, Castellucci E (2013) SERS detection of red organic dyes in Ag-agar gel. J Raman Spectrosc 44:47–54. doi:10.1002/jrs.4162

Lombardi JR, Birke RL (2009) A unified view of surface-enhanced Raman scattering. Acc Chem Res 42:734–742. doi:10.1021/ar800249y

Lombardi JR, Birke RL (2012) The theory of surface-enhanced Raman scattering. J Chem Phys 136:144704. doi:10.1063/1.3698292

Londero PS, Lombardi JR, Leona M (2013) Laser ablation surface-enhanced Raman microspectroscopy. Anal Chem 85:5463–5467. doi:10.1021/ac400440c

Luo Z, Smith JC, Goff TM, Adair JH, Castleman AW (2013) Gold cluster coatings enhancing Raman scattering from surfaces: Ink analysis and document identification. Chem Phys 423:73–78. doi:10.1016/j.chemphys.2013.06.021

Manhita A, Ferreira V, Vargas H, Ribeiro I, Candeias A, Teixeira D, Ferreira T, Dias CB (2011) Enlightening the influence of mordant, dyeing technique and photodegradation on the colour hue of textiles dyed with madder—a chromatographic and spectrometric approach. Microchem J 98:82–90. doi:10.1016/j.microc.2010.12.002

Manhita A, Santos V, Vargas H, Candeias A, Ferreira T, Dias CB (2013) Ageing of brazilwood dye in wool—a chromatographic and spectrometric study. J Cult Herit 14:471–479. doi:10.1016/j.culher.2012.10.016

Masschelein-Kleiner L, Heylen JB (1968) Analyse des laques rouges anciennes. Stud Conserv 13:87–97

Mayhew HE, Fabian DM, Svoboda SA, Wustholz KL (2013) Surface-enhanced Raman spectroscopy studies of yellow organic dyestuffs and lake pigments in oil paint. Analyst 138:4493–4499. doi:10.1039/C3AN00611E

Melo MJ, Claro A (2010) Bright light: microspectrofluorimetry for the characterization of lake pigments and dyes in works of art. Acc Chem Res 43:857–866. doi:10.1021/ar9001894

Mills JS, White R (1987) The organic chemistry of museum objects. Butterworths, London

Montagner C, Bacci M, Bracci S, Freeman R, Picollo M (2011) Library of UV-Vis-NIR reflectance spectra of modern organic dyes from historic pattern-card coloured papers. Spectrochim Acta Part A Mol Biomol Spectrosc 79:1669–1680. doi:10.1016/j.saa.2011.05.033

Oakley LH, Dinehart SA, Svoboda SA, Wustholz KL (2011) Identification of organic materials in historic oil paintings using correlated extractionless surface-enhanced Raman scattering and fluorescence microscopy. Anal Chem 83:3986–3989. doi:10.1021/ac200698q

Oakley LH, Fabian DM, Mayhew HE, Svoboda SA, Wustholz KL (2012) Pretreatment strategies for sers analysis of indigo and prussian blue in aged painted surfaces. Anal Chem 84:8006–8012. doi:10.1021/ac301814e

Platania E, Lombardi JR, Leona M, Shibayama N, Lofrumento C, Ricci M, Becucci M, Castellucci E (2014) Suitability of Ag-agar gel for the micro-extraction of organic dyes on different substrates: the case study of wool, silk, printed cotton and a panel painting mock-up. J Raman Spectrosc 45:1133–1139. doi:10.1002/jrs.4531

Platania E, Lofrumento C, Lottini E, Azzaro E, Ricci M, Becucci M (2015) Tailored micro-extraction method for Raman/SERS detection of indigoids in ancient textiles. Anal Bioanal Chem 407:6505–6514. doi:10.1007/s00216-015-8816-x

Pozzi F, Lombardi JR, Bruni S, Leona M (2012a) Sample treatment considerations in the analysis of organic colorants by surface-enhanced Raman scattering. Anal Chem 84:3751–3757. doi:10.1021/ac300380c

Pozzi F, Poldi G, Bruni S, De Luca E, Guglielmi V (2012b) Multi-technique characterization of dyes in ancient Kaitag textiles from Caucasus. Archaeol Anthropol Sci 4:185–197. doi:10.1007/s12520-012-0092-5

Pozzi F, Shibayama N, Leona M, Lombardi JR (2013a) TLC-SERS study of Syrian rue (*Peganum harmala*) and its main alkaloid constituents. J Raman Spectrosc 44:102–107. doi:10.1002/jrs.4140

Pozzi F, Porcinai S, Lombardi JR, Leona M (2013b) Statistical methods and library search approaches for fast and reliable identification of dyes using surface-enhanced Raman spectroscopy (SERS). Anal Methods 5:4205–4212. doi:10.1039/C3AY40673C

Pozzi F, Lombardi JR, Leona M (2013c) Winsor & Newton original handbooks: a surface-enhanced Raman scattering (SERS) and Raman spectral database of dyes from modern watercolor pigments. Heritage Sci 1(23):1–8. doi:10.1186/2050-7445-1-23

Pozzi F, van den Berg KJ, Fiedler I, Casadio F (2014a) A systematic analysis of red lake pigments in French Impressionist and Post-Impressionist paintings by surface-enhanced Raman spectroscopy (SERS). J Raman Spectrosc 45(11–12):1119–1126. doi:10.1002/jrs.4483

Pozzi F, Chang LK, Casadio F (2014b) The Navajo blankets from the Art Institute of Chicago collection: technical analysis of yarn and weavings coupled with dye identification by normal Raman and surface-enhanced Raman spectroscopy (SERS). In: BridglandJ (ed) ICOM-CC 17th triennial conference preprints, Melbourne, 15–19 Sept 2014, art. 1808, 8pp. International Council of Museums, Paris (ISBN 978-92-9012-410-8)

Prikhodko SV, Rambaldi DC, King A, Burr E, Muros V, Kakoulli I (2015) New advancements in SERS dye detection using interfaced SEM and Raman spectromicroscopy (μRS). J Raman Spectrosc 46:632–635. doi:10.1002/jrs.4710

Rambaldi DC, Pozzi F, Shibayama N, Leona M, Preusser FD (2015) Surface-enhanced Raman spectroscopy of various madder species on wool fibers: the role of pseudopurpurin in the interpretation of the spectra. J Raman Spectrosc 46(11):1073–1081. doi:10.1002/jrs.4726

Ramesova S, Sokolova R, Degano I, Bulickova J, Zabka J, Gal M (2012) On the stability of the bioactive flavonoids quercetin and luteolin under oxygen-free conditions. Anal Bioanal Chem 402:975–982. doi:10.1007/s00216-011-5504-3

Raza A, Saha B (2013) Silver nanoparticles doped agarose disk: highly sensitive surface-enhanced Raman scattering substrate for in situ analysis of ink dyes. Forensic Sci Int 233:21–27. doi:10.1016/j.forsciint.2013.08.004

Retko K, Ropret P, Korosec RC (2014) Surface-enhanced Raman spectroscopy (SERS) analysis of organic colourants utilising a new UV-photoreduced substrate. J Raman Spectrosc 45:1140–1146. doi:10.1002/jrs.4533

Ricciardi P, Delaney JK, Facini M, Zeibel JG, Picollo M, Lomax S, Loew M (2012) Near infrared reflectance imaging spectroscopy to map paint binders in situ on illuminated manuscripts. Angew Chem Int Ed 51:5607–5610. doi:10.1002/anie.201200840

Ringe E, Sharma B, Henry A-I, Marks LD, Van Duyne RP (2013) Single nanoparticle plasmonics. Phys Chem Chem Phys 15:4110–4129. doi:10.1039/c3cp44574g

Rodger C, Dent G, Watkinson J, Smith WE (2000) Surface-enhanced resonance Raman scattering and near-infrared Fourier transform Raman scattering as in situ probes of ink jet dyes printed on paper. Appl Spectrosc 54:1567–1576. doi:10.1366/0003702001948817

Roldán ML, Centeno SA, Rizzo A (2014) An improved methodology for the characterization and identification of sepia in works of art by normal Raman and SERS, complemented by FTIR, Py-GC/MS, and XRF. J Raman Spectrosc 45:1160–1171. doi:10.1002/jrs.4620

Romani A, Clementi C, Miliani C, Favaro G (2010) Fluorescence spectroscopy: a powerful technique for the noninvasive characterization of artwork. Acc Chem Res 43:837–846. doi:10.1021/ar900291y

Rosi F, Miliani C, Braun R, Harig R, Sali D, Brunetti BG, Sgamellotti A (2013) Noninvasive analysis of paintings by mid-infrared hyperspectral imaging. Angew Chem Int Ed 52:5258–5261. doi:10.1002/anie.201209929

Saunders D, Kirby J (1994) Light-induced colour changes in red and yellow lake pigments. Natl Gallery Tech Bull 15:79–97

Scherrer NC, Stefan Z, Francoise D, Annette F, Renate K (2009) Synthetic organic pigments of the 20th and 21st century relevant to artist's paints: Raman spectra reference collection. Spectrochim Acta Part A Mol Biomol Spectrosc 73:505–524. doi:10.1016/j.saa.2008.11.029

Schmid T, Opilik L, Blum C, Zenobi R (2013) Nanoscale chemical imaging using tip-enhanced Raman spectroscopy: a critical review. Angew Chem-Int Ed 52:5940–5954. doi:10.1002/anie.201203849

Schweppe H (1993) Handbuch der Naturfarbstoffe: Vorkommen, Verwendung, Nachweis. Nikol-Verl.-Ges, Hamburg

Sciutto G, Prati S, Bonacini I, Litti L, Meneghetti M, Mazzeo R (2015) In Technart 2015, non-destructive and microanalytical techniques in art and cultural heritage, Catania, 27–30 Apr 2015

Seifar RM, Verheul JM, Ariese F, Brinkman Ua T, Gooijer C (2001) Applicability of surface-enhanced resonance Raman scattering for the direct discrimination of ballpoint pen inks. Analyst 126:1418–1422. doi:10.1039/b103042f

Sgamellotti A, Brunetti B, Miliani C (2014) Science and art: the painted surface. The Royal Society of Chemistry, Cambridge

Shadi QT, Chowdhry BZ, Snowden MJ, Withnall R (2004) Semi-quantitative analysis of alizarin and purpurin by surface-enhanced resonance Raman spectroscopy (SERRS) using silver colloids. J Raman Spectrosc 35:800–807. doi:10.1002/jrs.1199

Sharma B, Cardinal MF, Kleinman SL, Greeneltch NG, Frontiera RR, Blaber MG, Schatz GC, Van Duyne RP (2013) High-performance SERS substrates: advances and challenges. MRS Bull 38:615–624. doi:10.1557/mrs.2013.161

Taylor GW (1983) Detection and identiflcation of dyes on Anglo-Scandinavian textiles. Stud Conserv 28:153–160

Teslova T, Corredor C, Livingstone R, Spataru T, Birke RL, Lombardi JR, Cañamares MV, Leona M (2007) Raman and surface-enhanced Raman spectra of flavone and several hydroxy derivatives. J Raman Spectrosc 38:802–818. doi:10.1002/jrs.1695

Tiedemann EJ, Yang Y (1995) Fiber-safe extraction of red mordant dyes from hair fibers. J Am Inst Conserv 34:195–206. doi:10.1179/019713695806124657

van Bommel MR, Berghe IV, Wallert AM, Boitelle R, Wouters J (2007) High-performance liquid chromatography and non-destructive three-dimensional fluorescence analysis of early synthetic dyes. J Chromatogr A 1157:260–272. doi:10.1016/j.chroma.2007.05.017

Van Elslande E, Lecomte S, Le Ho A-S (2008) Micro-Raman spectroscopy (MRS) and surface-enhanced Raman scattering (SERS) on organic colourants in archaeological pigments. J Raman Spectrosc 39:1001–1006. doi:10.1002/jrs.1994

Vellekoop M, Bakker N, van Dijk M, Geldof M, Hendriks E, Reissland B, Holberton P, Alkins T, Hoyle M, Jackson B, van Gogh V, Van Gogh Museum A (2013) Van Gogh at work

Wagner E, Clement S (2001) Surface enhanced resonance Raman scattering (Serrs) spectroscopy —study on inks. Probl Forensic Sci 46:437–441

Wang M, Teslova T, Xu F, Spataru T, Lombardi JR, Birke RL, Leona M (2007) Raman and surface enhanced Raman scattering of 3-hydroxyflavone. J Phys Chem C 111:3038–3043. doi:10.1021/jp062100i

White PC (2003) In situ surface enhanced resonance Raman scattering (SERRS) spectroscopy of biro inks—long term stability of colloid treated samples. Sci Justice 43:149–152. doi:10.1016/S1355-0306(03)71762-6

Whitney AV, Van Duyne RP, Casadio F (2006) An innovative surface-enhanced Raman spectroscopy (SERS) method for the identification of six historical red lakes and dyestuffs. J Raman Spectrosc 37:993–1002. doi:10.1002/jrs.1576

Whitney AV, Casadio F, Van Duyne RP (2007) Identification and characterization of artists' red dyes and their mixtures by surface-enhanced Raman spectroscopy. Appl Spectrosc 61:994–1000. doi:0003-7028/07/6109-0994$2.00/0

Wouters J (1985) High performance liquid chromatography of anthraquinones: analysis of plant and insect extracts and dyed textiles. Stud Conserv 30:119–128. doi:10.2307/1505927

Wouters J, Verhecken A (1989) The coccid insect dyes: HPLC and computerized diode-array analysis of dyed yarns. Stud Conserv 34:189–200. doi:10.2307/1506286

Wustholz KL, Brosseau CL, Casadio F, Van Duyne RP (2009) Surface-enhanced Raman spectroscopy of dyes: from single molecules to the artists' canvas. Phys Chem Chem Phys 11:7350–7359. doi:10.1039/b904733f

Xie Y, Li Y, Sun Y, Wang H, Qian H, Yao W (2012) Theoretical calculation (DFT), Raman and surface-enhanced Raman scattering (SERS) study of ponceau 4R. Spectrochim Acta Part A Mol Biomol Spectrosc 96:600–604. doi:10.1016/j.saa.2012.06.055

Yoshizumi K, Crews PC (2003) Characteristics of fading of wool cloth dyed with selected natural dyestuffs on the basis of solar radiant energy. Dyes Pigm 58:197–204. doi:10.1016/S0143-7208(03)00065-2

Zaffino C, Bruni S, Guglielmi V, De Luca E (2014) Fourier-transform surface-enhanced Raman spectroscopy (FT-SERS) applied to the identification of natural dyes in textile fibers: an extractionless approach to the analysis. J Raman Spectrosc 45:211–218. doi:10.1002/jrs.4443

Zaffino C, Russo B, Bruni S (2015) Surface-enhanced Raman scattering (SERS) study of anthocyanidins. Spectrochim Acta A Mol Biomol Spectrosc 149:41–47. doi:10.1016/j.saa.2015.04.039

From Archaeological Sites to Nanoscale: The Quest of Tailored Analytical Strategy and Modelling

Ludovic Bellot-Gurlet, Philippe Dillmann and Delphine Neff

Abstract Last developments of nano probes allows scientists of Cultural Heritage to assess a new kind of information that is crucial in the different topics concerned by the field: determining ancient manufacturing processes, studying use and provenance of ancient artefacts, revealing the degradation processes and developing adapted cleaning and conservation treatments. Nevertheless to be useful, these nanoscale approaches must be integrated in a tailored multi-step analysis. The final aim of these approaches will be to reach understanding and/or reliable modelling of the behaviours of the ancient systems. A first part of this chapter will review the issues in Cultural Heritage and the nature of the physico-chemical data that can be collected on the systems. In a second part, a selection of examples dealing with nano characterisation in Cultural Heritage will allow us to present several up to date techniques and methodologies employed in Cultural Heritage science. Then, the third part of the chapter will review some of the different modelling attempts that where already made in the domain of Cultural Heritage, and that were based on the use of physico-chemical descriptions at different scales. The challenge for the next future will be, for different kind of materials and environments, to propose multi-scale models from nano to functional scale. Some key steps to face these challenges bridging the gap between multiscale descriptive characterisation and numerical modelling are reviewed here.

L. Bellot-Gurlet
MONARIS "de la Molécule aux Nano-objets: Réactivité, Interactions et Spectroscopies", UMR 8233, UPMC-CNRS, Sorbonne Universités, UPMC Université Paris 6, 75252 Paris Cedex 05, France
e-mail: ludovic.bellot-gurlet@upmc.fr

P. Dillmann (✉) · D. Neff
LAPA-IRAMAT, NIMBE, CEA, CNRS, Université Paris-Saclay, CEA Saclay, 91191 Gif-sur-Yvette, France
e-mail: philippe.dillmann@cea.fr

D. Neff
e-mail: delphine.neff@cea.fr

P. Dillmann et al. (eds.), *Nanoscience and Cultural Heritage*,
DOI 10.2991/978-94-6239-198-7_7

1 Introduction

The different chapters of this book demonstrated on the one hand the pertinence of looking at physico-chemical systems of Cultural Heritage at the nanometre scale, on the other hand the fact that, despite the absence of measurement tools to observe them at nanometre scale, ancient craftsmen's mastered the control of nano-particules and nano-structuration for some marvel of ancient technical realisation (metallic lustres, ceramics, etc.). For studying such nano-structures or understanding the properties originating from the nano-scale, the development of nanoprobes or nano-investigation techniques is called to increase in heritage studies. Nevertheless, an investigation at the nano-scale alone does not allow an expert of heritage science to understand the system under investigation and to answer to the scientific question asked. Therefore this is only by integrating this nanometer scale approach in a tailored multi-step and multi-scale scientific and analytical methodology that the "nanometer scale will make sense".

Thus, today challenges and breakthrough are double:

- to develop the use of accurate and efficient nanoprobes or nanometre scale investigation techniques in multistep methodologies,
- to bridge the gap between the different scales, concerning the understanding of Cultural Heritage systems and/or the modelling of their behaviour.

The first aspect is, still today, linked by a limited access to the nanometre scale investigation methods. This is chiefly due to financial reasons limiting the widespread of devices and associated analytical know-how. Moreover most of the time experiments at nanoscale are costly and time consuming. This is an additional reason to integrate them in a step by step analytical strategy, beginning with reliable macroscopic investigation methods and a careful selection of the representative sample at a given scale. Then, at the end of the process, only the most representative sample should be submitted to nanometre observation, avoiding waste of time and means. To that purpose, and to help scientist of Cultural Heritage to develop right analytical strategies, the first part of this chapter will present a brief review of the various aspects of physico-chemical issues, at different scales of investigation, linked to the systems of Cultural Heritage.

To select the most adapted nanoscale investigation method it is necessary, for the conservation scientist or the scientist practicing archaeometry who will implement it in close collaboration with the specialist of the method, to have in mind the potentiality of the different available methods and the nature of the information they can deliver. This is the aim of the second part of this chapter that will give a tentative overview, through selected and concrete examples, of the cutting edge techniques used in the field of heritage but also in some related domains of research that have comparable scientific and analytical concerns.

The second aspect, aiming to bridge the gap between the different scales, may seem to be trivial but is not. This issue is not restricted to Cultural Heritage materials, but it is a crucial issue in other domains of science dealing also with

heterogeneous materials in which a nanometre scale process can be (or not) at the origin of a macroscopic behaviour at the functional scale (earth sciences, environmental science, material science, etc.). The synergy of different potential mechanisms and processes happening at different scales renders the interpretation and the evaluation of the dominant parameter or mechanism (if there is one) very difficult. To reach that goal, we believe that a very important, challenging and promising research direction is linked to the multiscale modelling of such systems. This modelling, even by being only descriptive (and not predictive) will allow one to better understand the role of the different parameters and their respective influence on the macroscopic behaviour. In the most favourable case they could be able to predict the future of Cultural Heritage systems, being a wonderful tool for our societies that have the duty to transmit the Cultural Heritage and its knowledge to the next generations. These aspects will be detailed in the third and last part of the present chapter, reviewing the modelling attempts in the domain of Cultural Heritage research and pointing the challenges for the forthcoming researches that will try to develop multiscale models.

2 Issues Dealing with "Heritage Systems"

Listing or reviewing all the studies dealing with "material aspects" and Heritage is not straightforward. According to the review or book aim, author background or specialities, it will focus on, or highlight, various aspects of the numerous facets of heritage systems or studies (for examples: Pollard and Heron 2008; Colombini and Modugno 2009; Casadio and Van Duyne 2013; Creagh and Bradley 2006, 2007; Edwards and Vandenabeele 2012; Madariaga 2015; Dillmann and Bellot-Gurlet 2014).

For issues dealing with analytical studies, then focusing on objects or materials, one could try to depict the Heritage problematics through a simplified object life pathway (Fig. 1). All objects start from some raw material, which could be manufactured only by shaping, grinding (or any transformations without chemical changes), or through techniques/processes, which will transform the constituents to obtain some new materials. Societies and their knowledge could be studied through their ability of knowing their environment/resources, the ways for exploiting resources, the abilities for procurement and distribution of goods, and the techniques to manufacture objects or materials for specific uses or purposes. All these aspects are describing a technical (and even sometimes technological) level and relations between societies and their natural environment. During history a wide dynamic exists, according to places, cultures, their interactions and evolutions. Many studies in the field of Cultural Heritage aim to reconstruct the history of some materials' use, some techniques or some technical gesture. This especially thanks to the information that analytical methods deliver to identify raw materials, their geographic origin or reveal ancient techniques. All these clues are linked to physico-chemical features of the constituent of the materials/artefacts.

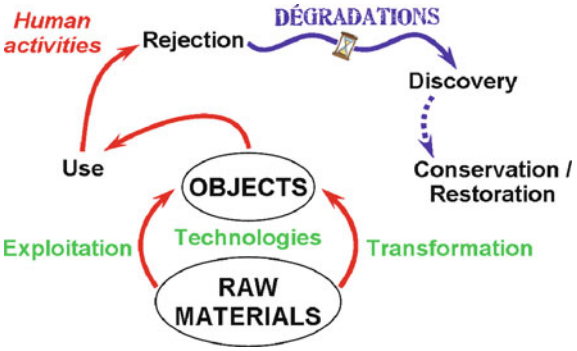

Fig. 1 Illustration of the life cycle of Heritage objects

After being manufactured objects were used, and according to some use wear or residues the human activities related to objects could be clarified (as stone tools (Astruc et al. 2011) or ceramics contents (Evershed 2008)). An important aspect is also the recycling practices that can be investigated by analytical approaches.

Before being transmitted to the present, objects and masterpieces could remain "in use" (as buildings, mural or canvas paintings, etc.) or buried by constituting the archaeological sites. Along time, with multisecular duration, degradation mechanisms modified the objects leading sometimes to their complete change (according to their nature and their environment). For heritage studies, first the effects of these degradations need to be understood for being able to differentiate them from information related to previous object life. Second, if this testimony of past societies is decided to be conserved for future generations, one must understand the running degradation mechanisms in order to be able to diagnose the stability of the object and recommend some conservation policies, strategies or treatments. On the other hand, in order to be presented to a public, an object should be "easily understood" and thus some adapted restoration treatments need to be developed and undertaken in compliance with existing guidelines (as UNESCO, International Council of Museums-Committee for Conservation (ICOM-CC)[1] and the International Centre for the Study of the Preservation and Restoration of Cultural Property[2]).

Dealing with "heritage systems", requires to apprehend all the scales/systems that constitute it: from a small artefact/object, to a building and a whole site and its environment. Just taking into account the system studied, problems are multi-scaled, with interactions between the scales or parts of objects/systems. Addressing these challenges requires the development of adapted analytical strategies and concepts to make the links between on the one hand, measures and scales, and on the other hand, studied systems and problematics. Such challenges are the daily work of scientists and Cultural Heritage experts.

[1] http://www.icom-cc.org/.

[2] http://www.iccrom.org/.

Thus, for each of these stages of the life (and vanishing) of heritage systems, and for their protection and conservation, different issues arise, linked to historical, cultural or conservation purposes. These issues can be expressed in terms of scientific concepts or questions. Then, to answer these questions, specific physico-chemical parameters must be measured on the systems. These measurements must be made at different scales, from the nanometre to the functional scale, in order to determine the synergies between these scales and pertinent (dominant) processes. These scientific questions and parameters are summed up in Table 1.

Concerning the manufacturing processes (from transformation of raw materials to secondary and final elaboration of artefacts), the key issues are linked to the determining of the raw materials (nature and origin) and the nature (temperature, chemical conditions, duration, efficiency, etc.) of the processes.

The first issue linked to historical aspects is the determination of supply network of goods and raw materials in ancient societies. This is linked to the crucial question of provenance and circulation of materials and artefacts. Determining the chemical compositions of the trace elements (Leroy et al. 2012) and/or the isotopic composition (Brauns et al. 2013) can approach this. Because ancient systems and artefacts are per nature heterogeneous at different scales, and because these trace elements and isotopes are heterogeneously distributed in the material, investigation at different scales must here also be implemented.

The raw material selection is also involved in the manufacturing processes, as technologies are linked to the composition of the materials, but besides to the properties and reactivity of the constituents. This information can be reached by knowing the chemical composition (mainly of major or minor elements) but also and chiefly by the nature of the phases in relation to their thermodynamic properties. The sizes of the different precipitates and aggregates in the systems are also crucial parameters to be determined. Lastly, linked to the duration and the efficiencies of the processes, transport phenomena, depending on temperatures, nature of media, phases and involved species are key parameters that need to be understood. Transport mechanisms could be assessed by measuring the porosity of the system if they are porous (gaseous state transport), by the sizes of particles (implying active surfaces available) or by the nature of the phases in which solid state transport could happen (mostly at high temperatures).

If one considers now the use and the functions of the artefacts (tools, utensils, weapons, buildings, etc.) other questions must be considered. Beyond than their shapes, uses and functions are on the one hand linked to the aesthetical aspect of the materials (surface state, colour, …), sometimes due to surface treatments, and on the other hand to the mechanical resistance and behaviour. To understand the first of these aspects, the nature (chemical and physical/optical) of the former surface layer —called limit of the initial surface by the conservation scientists (Bertholon 2001)— must be investigated. This implies to determine local composition and structural changes (including sizes of nanophases) at the location of the initial surface. The mechanical behaviour can be estimated with the nature of the material (composition) but also by its texture down to the micro and nano-structure (nature and organisation of phases and precipitates, linked to the move of dislocation for example).

Table 1 Topic, historical, cultural and conservation issues, scientific questions and associated physico-chemical parameters to be determined at different scale on the Cultural Heritage systems

Topic	Historical, cultural and conservation issues	Scientific questions	Physico-chemical information to be gathered
Manufacturing	• Initial raw materials used • Provenance and diffusion networks • Nature of the processes	• Composition, texture and structure of the bulk material or coatings/surfaces • Thermodynamic properties of phases, Partitioning of elements during processes • Reactivity linked to several parameters (temperature, oxido-reduction, …) • Transport of species (solid and gaseous states)	• Chemical composition: major/minor/trace elements • Isotopic ratio of some elements • Valence/oxidation state/local structure • Nature of the phases (structure) • Size of the particles, precipitates and aggregates • Nature and size of porosities
Use	• Aesthetical aspect (surface state, layer, color) • Mechanical behaviour • Provenance and diffusion networks	• Nature and properties of surface layer • Evolution of surface treatments • Optical behaviour • Study of use wear	• Local composition and structural changes at the (limit of the original) surface • Nature and size of local precipitates • Chemical (trace elements) and isotopic (major elements) local and bulk composition
Degradation	• Nature of the processes and interaction with environments • Degradation rate • Stability of the system	• Thermodynamic properties of the phases/compounds • Chemical reactivity of the layers/products • Transport of species in the layers (liquid/solid state)	• Chemical nature of the phases/compounds (composition and structure) • Physical behaviour (conductivity, density, hardness, local young modulus, etc.) • Porosity (variability, size and nature)

(continued)

Table 1 (continued)

Topic	Historical, cultural and conservation issues	Scientific questions	Physico-chemical information to be gathered
Cleaning/protection/restoration	• Efficiency of the protection treatment • Durability • Reversibility • Integrity of the heritage system	• Chemical reactivity of the phases of the system with the treatment • Transport of the treatment in the system • Stability/evolution of the products used for the treatment	• Nature of the new formed phases (composition and structure) • Localisation of the new formed phase in the system • Porosities, mechanical properties • Chemical and structural evolution of the phases in function of the environmental stress (relative humidity, light, temperature, composition)

As far as degradation processes are involved, the challenges are here to determine the nature of the processes and the degradation rates linked to the stability of the systems in regards to their environments. This requires to assess to the thermodynamic properties of the phases but also their chemical and sometimes electrochemical reactivity and transport inside the alteration layers. These scientific questions need to determine here again the chemical and structural nature of the alteration layers at different scales, but also the chemical and physical properties (as reactivity, conductivity, hardness, density, etc.). Transport phenomena of species, the most of the time in porosities saturated in hydrous fluids and sometimes in solid state (vacancies, ions) in nanolayers, must also be considered.

Lastly, a crucial issue dealing with heritage is the setting up and the use of adapted cleaning, restoration and protection treatments. This topic needs to consider on the one hand the efficiency and durability of treatments but, also on the other hand the influence of this treatment on the integrity of the heritage system (modification of appearance, reversibility). This implies to characterise the nature (including chemical composition, structure and thermodynamic properties) of the new formed phases after interaction with the treatments, or the treatment product itself, but also to locate these compounds in the system and especially in the degradation system. Here again, in addition to the reactivity, the transport in the system (characterisation of porosities) is crucial. Lastly, the evolution under different environmental conditions of the new-formed phases (chemistry and structure) or the products used are key parameters to determine. Because the treated objects must be stable for the longest period, considering this behaviour requires a fine understanding of their durability properties over periods not mandatory for everyday life contexts.

3 Analytical Techniques

3.1 From Macro to Nano Scales

Analyses of Cultural Heritage materials and systems need specific protocols adapted to each context. The constraints on the sampling as well as the fragility of the artefacts can orientate the drawing of the analytical procedure. For that, the analytical set-up can be adapted to the potential various sample dimensions (from millimetre to decametre). As said before, characteristic of the samples are various and numerous and deals with the determination of their physical properties (among them: hardness, porosity, morphology of particles, conductivity), and their chemical properties mainly connected to their chemical composition and the nature and crystallinity of phases in presence. The choice of the most appropriate analytical technique to assess them is crucial to get the desired information.

Most of the studies dealing with the nanoscale, namely the characteristics and properties of the material at the nanoscale, start with a multiscale analysis. Indeed,

apart the difficulty to access to nanoprobe equipment (due to their high cost, then rare occurrence, especially in Cultural Heritage laboratories), answering scientific issues concerned by nanoscale properties often starts at first by surveys and studies at lower scales (i.e. macro and microscopic scales). This process needs a first analytical chain composed of classical devices and setups used in material sciences and described in details in previous publications (as Edwards and Vandenabeele 2012). It is not in the scope of this chapter to describe it exhaustively. Yet it is important to insist on the fact that macro to microscale characterization prior to nanoscale analyses is unavoidable to ensure satisfying data acquisition and treatment. Actually the nanoscale analyses could be realized to the detriment of the representativeness regarding the totality and complexity of the studied artefacts. That is why the characterisation at the lower magnifications is required. First observations can be realized thanks to optical microscopy, especially when samples are prepared on sections which enlighten their heterogeneities. This provides information on the morphology and texture of the sample and allows one to locate the zones of interest for further analyses, by screening large surfaces and various samples. Additional observations can be obtained thanks to Scanning Electron Microscopy (SEM). This analytical tool is the ultimate multiscale device thanks to its wide range of magnification. Particularly Field Emission Gun (FEG) SEM capable to work down to few nanometers resolution is a preferred technique to correlate information between micro and nanoscales.

In the following paragraph the different instruments working at the nanoscale are briefly presented, through selected examples. The aim is to illustrate the possibilities offered by these nanoscale techniques. Selected presented studies are mostly dealing with Cultural Heritage, and the authors hope that this overview will help new actors of the Cultural Heritage to enlarge the spectra of the techniques they can potentially use.

3.2 Analyses at Nanometer Scale

High Resolution X-ray Diffraction (HR-XRD) analyses can provide information on the sizes of nanocristallites present in the sampled materials, by using the Scherrer formula. For example Bayle (2015) measured the crystallite sizes of akaganeite powders by XRD under synchrotron radiation to determine the effect of a dechlorination treatment on the progressive transformation of this chlorinated phase present in the corrosion layers of archaeological iron artefacts. Helary et al. (2003) measured the crystallite size of silver particles to understand the technology used in the medieval period for the production of metallic lustre ceramics. Another example, Ungár et al. (2002) studied by XRD under synchrotron radiation the crystallite size of black make-up of Ancient Egypt. Last a recent study used XRD under synchrotron to determine particle sizes on a range from the micrometric to the nanometric scale on various ancient materials like Roman *terra sigillata*, Neolithic flint (Fig. 2) or Roman iron nails (Dejoie et al. 2015). This was achieved thanks to a

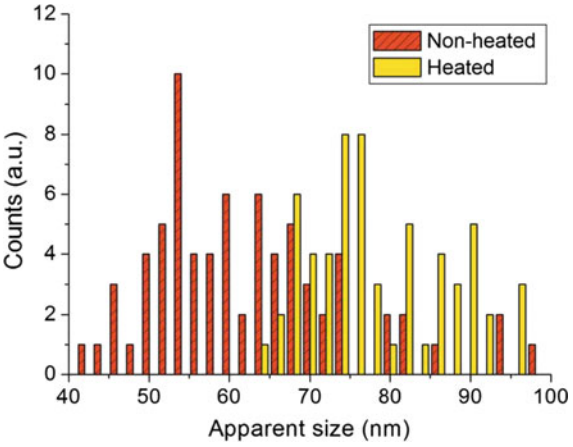

Fig. 2 Histogram of the apparent size of the coherently diffracting domains obtained after refinement of the powder data, showing a slight increase after the heating process of natural flints (Dejoie et al. 2015). Such analysis is used to prove the performing of a heat treatment by the ancient men to improve the flint knapping behaviour's

micrometric and monochromatic beam combined to the exploitation of Laue diffraction.

For surface analyses, Atomic Force Microscope (AFM) is one of the techniques used by few studies (Crina Anca Sandu et al. 2011), mainly dealing with the understanding of coatings like gilding or the assessment of protection properties for coatings protective treatments. This technique presents a lateral resolution, depending on the apex chosen for the surface probing, of about 10 nm. For example Ambrosi et al. (2001) studied the efficiency of the solvation of $Ca(OH)_2$ in various organic solvent by AFM. The $Ca(OH)_2$ is used to reinforce the wall paintings and the carbonic stones in the field of Cultural Heritage. The interest of AFM is to observe the dispersions of the nanoparticles in their solvents and to measure the sizes of the aggregates formed (Fig. 3).

Dal Bianco and Bertoncello (2008) worked on mosaics recovered by a golden leaf. Initially the golden leaf was coated by a thin overlaying glass layer called *cartellina* but its weathering leave the golden leaf tessera unprotected. That is why they studied a protection treatment of this type of artefacts thanks to various sol-gel silica coatings. This latter was applied on model sample and the roughness of their surfaces was studied thanks to AFM. In the same way Manoudis et al. (2009) studied the effect of siloxane based coatings on the enhancement of hydrophobic properties of stones. AFM was a complementary technique showing that the addition of SiO_2 nanoparticles in the coatings conducts to the formation of nano-aggregates on the stone surface that impacts its colour. This consequence conducts the authors to recommend against adding nanoparticles in the coatings to respect the aesthetical aspect of the stone.

Concerning the direct studies at the nanometric scale up to now the most used technique is the Transmission Electronic Microscope (TEM). This technique provides imaging with a resolution of less than 0.1 nm when a suitable preparation of the sample is realised. The electron beam is focused on the sample and images are recorded in transmission. In addition the electronic diffraction can provide structural

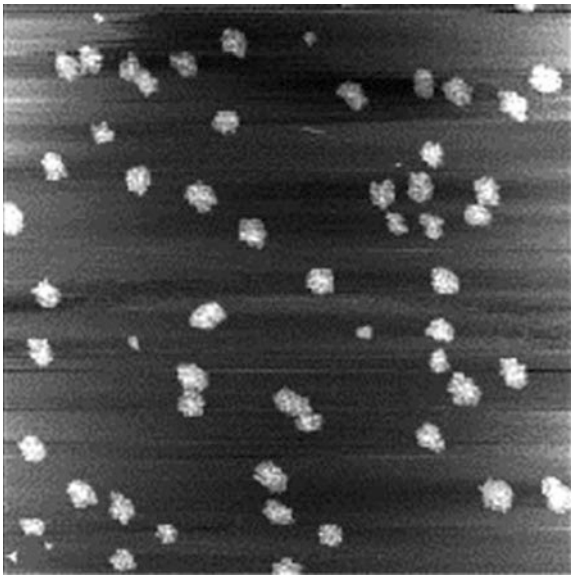

Fig. 3 Atomic Force image taken in a liquid phase (1-propanol) of the $Ca(OH)_2$ nanoparticles obtained at 60 °C: image dimensions 3.3 μm × 3.3 μm, (Ambrosi et al. 2001)

analyses on the compounds observed. Moreover the interaction between the atoms of the sample and the electrons provokes the emission of X-rays providing qualitative and semi-quantitative information about the elementary composition of the samples thanks to the Energy Dispersive Spectroscopy (EDS). Last, the Electron Energy Loss Spectroscopy (EELS), although more delicate to interpret, can be used to provide information on the speciation of chemical elements present in the samples.

Complementary to AFM studies, the TEM imaging is used to determine the aggregates size used for the consolidation of stones (Baglioni et al. 2013). For example Chelazzi et al. (2013) and Baglioni et al. in this book, determined the aggregate size of $Ca(OH)_2$, $Mg(OH)_2$ or $Ba(OH)_2$ dispersed in propanol. Yet, the control of the particle sizes and the polydispersity should be of the same range than the porosity of the treated surfaces. TEM is involved in this study to tailor these particles by varying the synthesis parameters. One other interesting example of TEM concerns the study of pigments sampled in ornamented prehistoric caves. In their studies Pomiès et al. and Chalmin et al. (Pomiès et al. 1998; Chalmin et al. 2004, 2006) have shown that many information can be obtained from a very low amount of pigments collected on the wall and deposited on a copper grid (Fig. 4).

Particularly in the case of the Lascaux cave different mineral phases have been identified depending on the colour: hematite (α-Fe_2O_3) for the red, goethite (α-FeOOH) for the yellow and mix of manganese oxides (MnOOH, MnO_2, Mn_2O_3, Mn_3O_4) for the black pigments. Moreover the particle morphology indicates their crystallinity degree. Specifically for the hematite various class of low crystallinity or high crystallinity pigments have been established. Furthermore TEM imaging can document the pigment heating treatment as it revealed that the presence of porosity

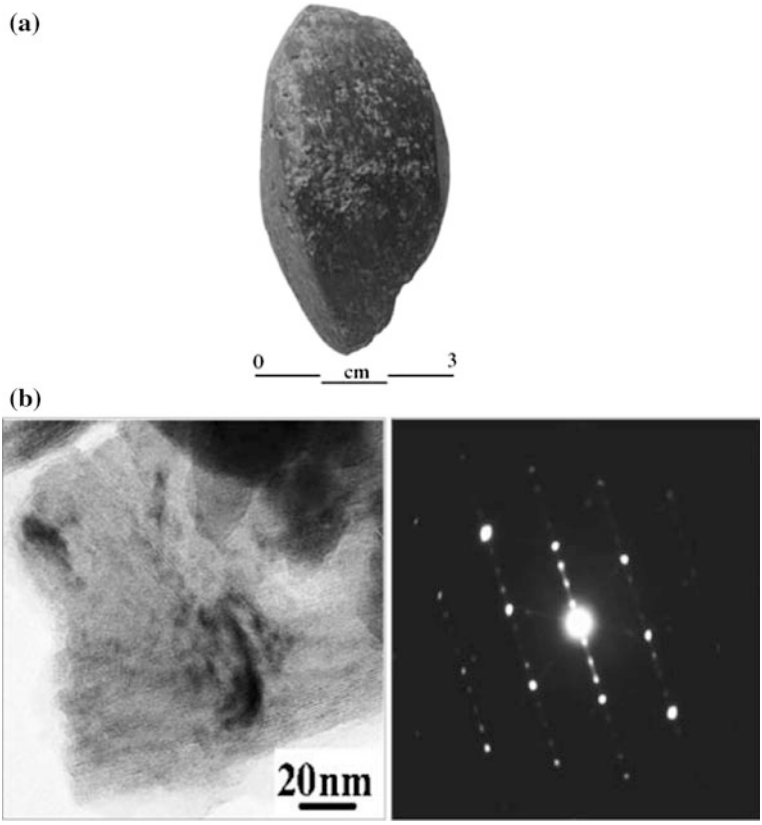

Fig. 4 **a** Black "crayon" of Combe Saunière, the only faceted block Marcillaud J.G. **b** G17C20 block of Combe Saunière: TEM micrograph of todorokite crystals identified by electron microdiffraction pattern ([001] zone axis single crystal), (Chalmin et al. 2006)

on hematite pigments is due to the dehydration of a goethite (α-FeOOH) when heated to obtain hematite (Pomiès et al. 1998). These nano-scale experiments provide indication of the mastering of heating treatment, highlighting the use of firing techniques for pigment preparation to produce red hematite from yellow goethite. Moreover TEM-EDS analyses indicate the presence of various minor elements that allows one to discriminate several pigments of the same mineral class, showing the possible correlation between different paintings panels and the paintings pots excavated in the cave. A last example of TEM is given by Leon et al. (Leon et al. 2015) with the observation of samples of *terra sigillata*, ceramics of the Roman period, which provides information about the technological transfer between Italy and Gaul. Indeed thanks to the complementarity with microXRD under synchrotron radiation, Raman spectroscopy, SEM and TEM, it has been evidenced that the technology of production has evolved between Italy where the production started and Gaul where this production was implemented. In this study TEM delivered

information on the ceramic production process, particularly by showing the shape of the particles originated from the clay used for the production. In this case the shape and composition of particles were related to the firing temperature and the materials chosen to produce the *terra sigillata*.

Thanks to the development of synchrotron facilities, specific experiments are developed that allow one to obtain nanometer range beam (Sakdinawat and Attwood 2010). Among them another technique is getting involved in the characterisation of Cultural Heritage artefacts, the Scanning Transmission X-ray Microscopy (STXM). This microscopy is provided under synchrotron light source and consists in scanning a thin sample by a tuneable light to obtain a chemical image (or map). The energy chosen depends on the elemental composition of the sample. Through the scanning in energy around the absorption edge of an element (K, L depending on the element), the XANES (X-ray Absorption Near Edge Structure) spectra can be reconstituted. The principal advantage of this technique is to deliver hyperspectral images that allow to preserve the information about the location on the samples of the extracted XANES spectra.

XANES provide structural data about the crystalline environment/speciation of a chemical element. Thus, it can help to determine the crystalline or amorphous nature of a phase as well as the oxidation degree of an element. STXM delivers a beam size of 25 × 25 nm^2 and is applied on thin samples of various thicknesses, depending on the composition of the sample and the chemical element that is studied. STXM is mostly used in material, geosciences or Natural Heritage as for example on fossils (Bernard et al. 2010; Galvez et al. 2009). One example of application on archaeological samples is given by Leon et al. (2014). The aim of the study is to understand the corrosion mechanisms of ancient nails corroded in an anoxic soil. The sample of 100 nm thickness has been prepared by Focused Ion Beam (FIB-see below). This study showed that an iron oxide layer of few hundred nanometers has precipitated at the interface with the metal. The whole corrosion layer of several hundred micrometer thickness is composed of an iron +II carbonate while this interfacial oxide layer presents a mixed iron +II/+III oxidation degree (Fig. 5). This specificity could confer to this thin layer specific conductive property that could play a major role in the control of the iron corrosion kinetics.

Synchrotron facilities also afford high resolution tomographic setups (Sakdinawat and Attwood 2010). For organic or light materials the spatial resolution of a voxel can reach 150 nm. For example fossils of arthropods embryo dated from 520 million year old can now be studied in 3D, avoiding any invasive sampling. Their analyses reveal the presence of mouth, teeth and gut on a few hundred micrometer sample size. Some examples of X-ray fluorescence synchrotron nano-tomography (SR-TOMO) are also provided by the planetary sciences that analysed stardust (Silversmit et al. 2009). This technique enables to analyse non-destructively the chemical composition of small samples.

Back to laboratory, high spatial resolution facilities are nowadays developed. The Focused Ion Beam (FIB) is one of them. This technique is based on the sample sputtering by a fine focused ion beam, generally gallium, allowing an efficient

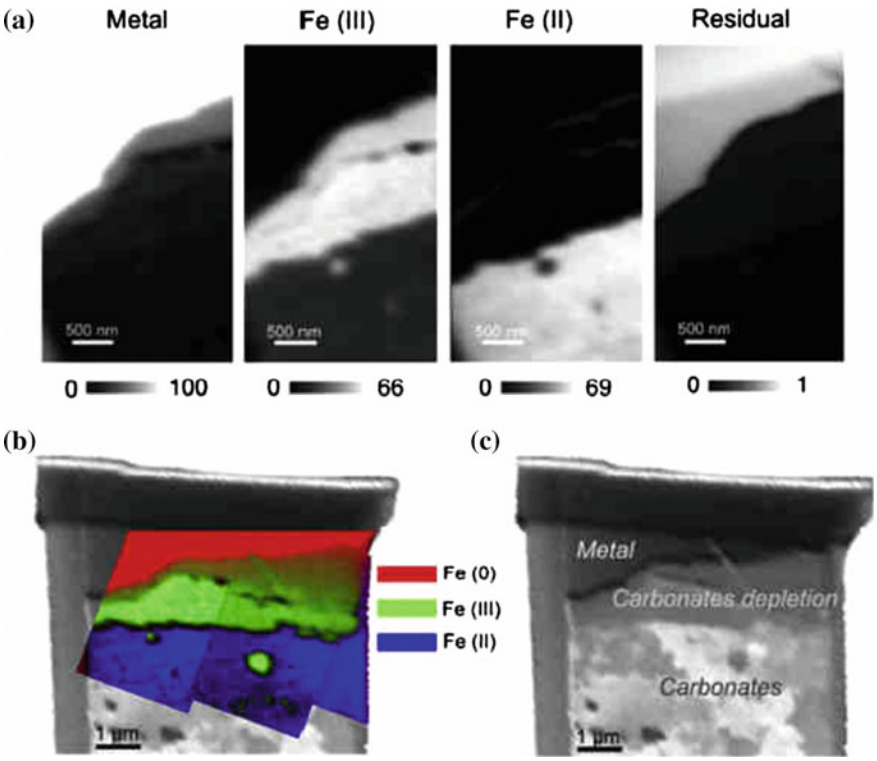

Fig. 5 STXM investigations of the sample thin film GL10-03: **a** SDV component maps of the Fe (III), Fe(II) and Fe(0) species obtained with the siderite, maghemite and metal reference spectra. Grey scales for Fe(II), Fe(III) and Fe(0) maps: equivalent thickness (nm), for the residual map: optical density. **b** Overlay of the color-coded Fe(0), Fe(II) and Fe(III) component maps **c** C K-edge difference map (290–280 eV) of the thin film, (Leon et al. 2014)

thin sample preparation for TEM or SEM. An additional interest is the coupling to a Scanning Electron Microscope (SEM). The specific interest of such dual-beam Focused Ion Beam Scanning Electron Microscopy (FIB-SEM) is to collect images during the milling, so that a volume of the sample can be 3D-imaged with a few tenth nanometers resolution. The first study in Cultural Heritage using the combination of FIB and SEM is illustrated by Giachi et al. (2014). The authors observed archaeological waterlogged wood impregnated with colophony (Fig. 6). The milling of local surfaces allowed to observe with a high resolution the wood cell walls, showing that they were totally filled confirming the deposition of the colophony at least on the surface of the cells. A second example of preparation of sample thanks to FIB is given by Villanueva-Amadoz et al. (2012). In their study these authors worked on the characterisation of palaeopalynological remains. Slice spores and pollen grains were sectioned by FIB-SEM for reconstructing their ornamentation and wall-ultrastructure, providing information on their internal structure. King et al.

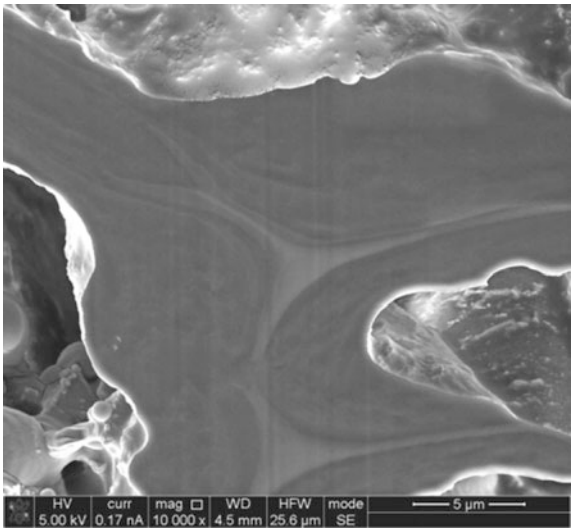

Fig. 6 FIB/SEM image of the cell wall of pine treated with colophony, Giachi et. al. (2014)

(2014) used 3D reconstruction by FIB-SEM to investigate the formation of cohesive calcium oxalate layers on marble surfaces for the conservation of stone. They used FIB-SEM complementary to SEM analyses to determine the 3D porosity network at a sub-micrometric scale showing that nanopores are partially connected inside a treated marble cube.

Various spectroscopies can now reach nanometric scales. In the UV-Visible spectroscopy with a synchrotron light source the analysed volume can be of a few hundred micrometers. Thoury et al. (2011) illustrated this technique on samples of ancient varnish of a musical instrument and on painting pigments containing ZnO. The authors obtained mapping of the organic materials present in the varnish at the submicrometer scale. They also visualized the heterogeneities of the semiconductor pigment material. Tip Enhanced Raman Spectroscopy (TERS) thanks to the Near-field Scanning Optical Microscopy (NSOM) allows now the acquisition of Raman spectra with a nanometric resolution (Fleischer 2012). Few examples mostly related to the analyses of dyes are available in the literature. Kurouski et al. (2014) analysed in situ indigo and iron gall ink on historical documents of the 19th century. These techniques allowed the authors to identify pigments even at low concentration on the papers. Last, X-ray Photoelectron Spectroscopy (XPS) is a sensitive surface technique that provides chemical information on the few first hundred nanometers in the depth of materials but the lateral resolution is in the micrometric range. Nowadays, thanks to the coupling with synchrotron, X-ray Photoelectron Emission Spectroscopy (XPEEM) can deliver lateral resolution of about 10 nm. Among the few examples available in the Cultural Heritage field, De Stasio et al. (2001) tested the surface of Roman silver coins. and conclude on the presence of fluorine that can avoid the tarnishing of the studied silver coins.

The principle of Secondary Ion Mass Spectrometry (SIMS) has been developed for various facilities that are able to deliver submicronic beams. Among them is the ToF-SIMS (Time of Flight SIMS) that can provide a 200 nm lateral resolution in specific acquisition modes. Complementary to this technique the nano-SIMS provides a beam of about 50 nm of lateral resolution. Both ToF and nano-SIMS allow one to analyse the chemical and isotopic composition of thin surface of the samples. They also work in mapping mode preserving the information on the location of the analyses. The principle of these techniques is to sputter ions on the sample surface, collect and analyse the masses of the ejected secondary ions. The mass/charge ratio is analysed thanks to a mass spectrometer that delivers the elemental and isotopic composition of the samples. ToF-SIMS (Fig. 7) has been used to analyse painting pigments (Richardin et al. 2011) or human skin remains (Cersoy et al. 2012). Concerning nano-SIMS, this technique is mostly used in the geoscience field (see for example Hoppe et al. 2013). One study dealing with the understanding of iron corrosion mechanisms focused on an archaeological nail of the 16th century. In order to determine the transport properties inside the corrosion layer, it was immersed in deuterated water during 3 months (Leon et al. 2014). The nail was cut and prepared on transverse section. Thanks to the deuterium mapping at the interface with the metal, the authors showed that a micrometric interfacial layer was not porous, blocking the deuterated water penetration.

Figure 8 sums up in a simplified way the scales reached by the quoted nano-techniques and the nature of information they bring. It has to be stressed that, in this simplified view, the techniques at the micrometer are not taken into account, nor the possible requested sample preparation treatment (thin film, etc.) that can render the use of a given technique very tricky. Nevertheless, this short review demonstrates

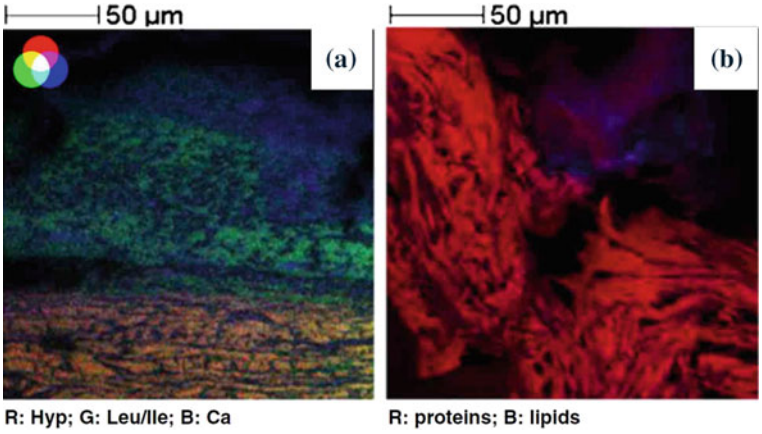

Fig. 7 High spatial resolution ion images (ToF-SIMS) of the skin cross section **a** Three color overlay between ion images (HYP: hydroxyproline fragment in *red* (R), leucine or isoleucine fragment in *green* (G) and calcium ion in *blue* (B)). **b** Hypodermis area, two color overlay between ion images (protein backbone in *red* (R) and fatty acids in *blue* (B). Field of view 200 × 200 mm^2; 512 × 512 pixels, pixel size 390 nm (Cersoy et al. 2012)

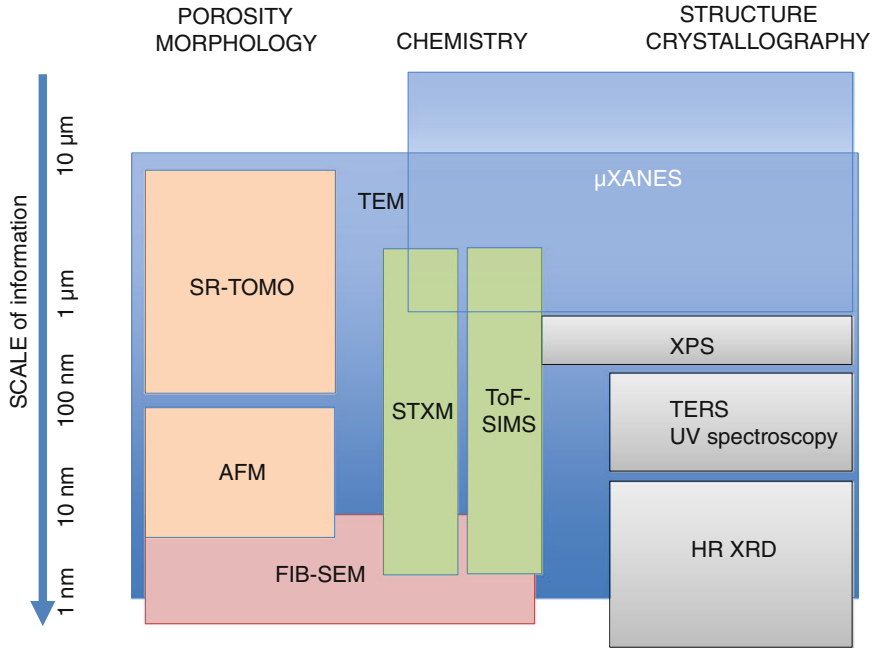

Fig. 8 Summary of the nanoscale techniques used in Cultural Heritage (SR-TOMO: X-ray tomography under synchrotron radiation, *AFM* Atomic Force Microscopy, *FIB-SEM* Focused Ion Beam Scanning Electron Microscopy, *HR XRD* High Resolution X-ray Diffraction, *STXM* Scanning Transmission X-ray Microscopy, *TEM* Transmission Electron Microscopy, *TERS* Tip Enhanced Raman Spectroscopy, *ToF-SIMS* Time of Flight Secondary Ion Mass Spectrometry, *XAS* X-ray Absorption Spectroscopy, *XPS* X-ray Photoelectron Spectroscopy

clearly that nanoscale techniques can provide unique information about the chemical composition and structure of ancient materials. Unfortunately, almost all of these techniques imply the sampling of heritage artefacts, not always allowed regarding conservation policies. Nevertheless, the constant improvement and development of new probes and micro-sampling solutions will facilitate their use on fragile or rare materials and thus improve their access for Heritage Science samples.

4 From Description at Nanoscale to Multiscale Modelling: A New Challenge for Cultural Heritage

The first parts of the present chapter and the other chapters of this book, show important examples of nano and, more generally, multiscale descriptions and analytical methods of systems linked to Cultural Heritage and ancient materials.

These studies are more and more developed and tailored to assess crucial information on dimensioning parameters and to propose pertinent chemical mechanisms or processes. At the contrary very few attempts have been made, using these parameters, to model the behaviour of "heritage systems". A model can have different aims. A first one is, for example, a descriptive approach, allowing one to better understand the influence of each parameter on the global behaviour of the system. This, naturally conducts to an explanatory stage where the past and present behaviour laws of the system are understood. Lastly a predictive model can be built, in order to predict the behaviour of the system for the forthcoming years and centuries. Actually these different sorts of models can be combined to describe the complexity of a given system, as for example "multi-agent" approaches. They also can be based on analytical and empirical or phenomenological considerations.

Each of these approaches can concern the so-called "heritage systems", which behaviours have to be modelled and predicted to propose scenarii for the past evolution of the societies and their environments (historical purpose), or the becoming of human achievements (conservation purpose). These studied systems could be ancient societies or human groups, archaeological landscapes and sites, ancient materials and of course, artefacts and structures that have to be protected and conserved for the future generations.

Models have been used for a long time, for example to understand the properties of materials during their manufacture, as for example glass viscosity (Bingham and Jackson 2008), or thermodynamic phase predominance domains in metallurgy or corrosion. Nevertheless, one of the most exciting challenge for the modelling of "heritage systems" is to link properties and behaviours at different scales. For example, the modelling of the corrosion behaviour of a heritage artefact made of metal needs to understand the nanometer scale properties of the layers formed on the metallic surfaces, but also the climatic evolution of the area where the artefact is stored or exposed. The need of a multiscale approach is actually not a specificity of conservation science or Cultural Heritage approaches, but is a demand in several domains and fields of science and engineering (Yang and Marquardt 2009). In chemical engineering, because of the need to go from a laboratory scaled production to the industrial one, this multiscale approach is relatively popular for several ten years as detailed by Vlachos (2005). In ecology and environmental sciences, some efforts have been made to perform multi-scale approaches to evaluate structures of landscapes (Burnett and Blaschke 2003). For "Heritage systems" as buildings, multiscale modelling combining micro and macro approaches allows to understand ancient building techniques in order to better diagnose the seismic risks (Mele et al. 2003; Abruzzese et al. 2009), or understanding the influence of use of some materials (wooden beams reinforcement) for resistance to earthquakes (Kouris and Kappos 2012). In the same area of Cultural Heritage, multiscale data are often used for 3D modelling (Remondino et al. 2009; De Luca 2014), but also for the modelling of large and complex archaeological areas (Guidi et al. 2009). Nevertheless, these approaches do not include as large scales gap than the ones that must be involved for other domain of Heritage science as conservation or even multidisciplinary Archaeological sciences. For example, to model the use of

resources or materials by ancient societies, to apprehend the qualities of raw materials or artefacts and consequently their technical and economical values, it is necessary to perform analytical studies (referring to Archaeometry or Archaeological science) to assess the nanometric and microscopic composition or structure of the ancient artefacts/archaeological materials found during excavations (see other chapters of this book). This data can then be included in wider databases, containing information on the different archaeological sites and on the link between the different sites. This holistic analysis of these different kinds of data, collected at different scales (from the nanometre for the chemical composition of the artefacts, to the kilometre scale for the archaeological sites), would allow one, in the future, to model the technico-economical developments of ancient societies, based on the use of the data collected on "Heritage systems". Another crucial issue is linked to Cultural Heritage conservation. The aim here, is to make reliable diagnosis to help the restoration decision (Kim et al. 2010; Cacciotti et al. 2015). This implies a multidisciplinary interpretation and a comprehensive knowledge based system in which modelling and predicting alteration processes are crucial steps. Here again, both nanometre (molecular interactions) and kilometre (climate) scales must be understood and integrated in a comprehensive multiscale interactive system. Let us develop in the following the different concepts linked with the prediction of the degradation of materials of Cultural Heritage, which is one of the most important challenges for the protection and transmission of Cultural Heritage.

Dealing with corrosion, several holistic multiscale models have been developed linking the behaviour of a given structure to the one of the surfaces involved in the corrosion processes (Cole et al. 2011; Cole and Hughes 2014). Inspired from these approaches, models dealing with different kinds of alteration processes could try to describe and predict the behaviour of materials encountered in Cultural Heritage. To that purpose we must identify the processes involved at the different ranges of scales. Inspired by the ones proposed by Cole et al. (2003) for atmospheric corrosion, it is possible to propose seven scales to model processes (Fig. 9):

- Macro: linked to gross meteorological conditions (polar, tropical, continental, etc.).
- Meso: meteorological parameters concerning regions of about 100 km^2 (marine, urban, rural, etc.).
- Local: immediate vicinity of the artefact, the building or the site.
- Micro: absolute proximity of the surface material.
- Surface: physical response of the surface (deposition and retention of pollutants, condensation, evaporation), radiation (sun, lights).
- Micron: interaction within interfaces in the material (material/electrolyte), charge and mass transfer and transport phenomena (in electrolyte).
- Nanometer: chemical reactions, charge and mass transfers, transport phenomena (in the solid).

Different sub-models could then be defined, linked to each of their scale. Concerning the macro and meso-stage, to our knowledge, no model was directly developed in the field of conservation science, except the one developed by Tidblad

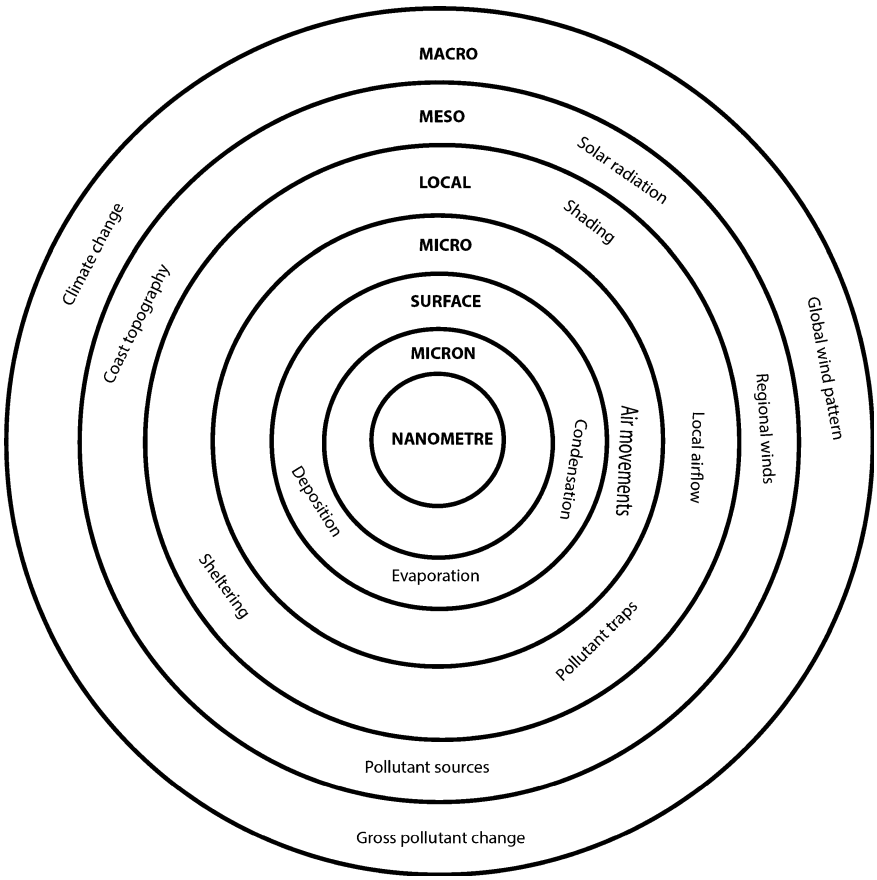

Fig. 9 Framework for an holistic model of alteration of Cultural Heritage underlining the various scales and the related phenomena (inspired from Cole et al. 2003)

(2013) to predict the effect of climatic change on corrosion of metals. Nevertheless, already existing ones could be used in a forthcoming holistic approach. For example some modules developed by Cole et al. (2003) can be used for metals but probably also for a wide range of other materials. Up to now, models already developed in the domain of conservation of Cultural Heritage deals only with a single stage and the largest scale is the one corresponding to local conditions.

For example, de la Fuente et al. (2011), aims to assess and predict the effect of different pollutants on materials and object of the Cultural Heritage. Depending on the variation of concentration of different pollutants (SO_2, NO_2, O_3 and PM10-Particulate Matter with size bellow 10 μm) and the alteration rate observed on different kinds of materials (bronze, limestone, …), dose response functions were empirically established. They allowed one to propose maps corresponding to different scenarii of pollutions and damages.

At the "micro" scale, the 3D models on buildings, as the one developed by Stefani et al. (2014) on the Chambord Castle, can be helpful to locate the different degradation patterns by efficient alteration mapping and to link them to local environmental variations. This is the first step to build models at the "micro" and "surface" stages of the Cole's scale. Then, the local variations can be linked for modelling the variations of outdoor or indoor atmospheres. Considering indoor atmosphere of buildings and museums, some attempt has been made to model the evolution of heat and moisture using meteorological data, building properties and users behaviour and a combination of a hydrothermal simulation and finite element approach (Huijbregts et al. 2015). Another example linked to that scale of interest is the modelling of the temperature and humidity distribution by computational fluid dynamic based on finite volumes methods in the Hall of the Domus Aurea in Rome (Albero et al. 2004). At the "surface" levels, three dimensional computational fluid dynamics model were used to understand the influence of thermohygrometric parameters and airflow patterns responsible for salt recrystallization in the stones of the Crypt of the Lecce Cathedral in South Italy (D'Agostino et al. 2014). At the "micron" scale, several models dealing with local chemical processes have been developed. For example, to understand the reaction of sulphur dioxide from the atmosphere with calcareous porous stones (found for example in statuary) the models consider reactivity and diffusion of species to give a behaviour law and a quantitative description of the processes by 3D simulation (Giavarini et al. 2008). Parameters as crucial as diffusion coefficient of some species were collected and are used to serve modelling of processes at this stage. For example this was performed in a study of bronze corrosion in sulphate medium in order to understand the influence of tin content on corrosion processes (Muller et al. 2013). An analytical model of the long term corrosion of iron reinforcement embedded in hydraulic binders using parameters directly measured on archaeological artefacts was proposed by Chitty et al. (2008a, b). This model considers the kinetic of oxygen diffusion through the system and its consumptions at the metal/corrosion product interface. Also dealing with corrosion of iron from Cultural Heritage buildings, Monnier et al. (2010) proposed a phenomenological model based on the establishment of a reactivity index of the constitutive phases of the corrosion layers formed on the artefacts. Several models involving the nanoscale have been proposed to describe long term corrosion of iron. They are constructed by taking into account a limiting step, for example the presence of a corrosion layer or nanopores hindering transport at this level (Hoerlé et al. 2004; Bataillon et al. 2010). Another phenomenological model for long term prediction at "micron" and "nano" scales was also developed for glasses in the context of the deep storage of nuclear wastes (Verney-Carron et al. 2010). This latter one involves nanometer scale phenomenology to understand and predict the formation of a protective gel at the surface of the glass depending on the solution of the water of the surrounding medium (clay). These three latter models were developed after analytical and

parametric studies on archaeological and heritage metallic/glassy artefacts despite their application domains are not directly linked to the conservation of Cultural Heritage. Thus, they can perfectly be transposed back to "heritage systems" with the advantage to directly address "realistic" materials and conditions by directly exploiting the formalisms of the developed models.

This short review clearly shows that, by combining all these different scales, from global climatic changes to nano properties of the heritage systems, it would be possible in the next future, at least for several kinds of these systems, to propose such an holistic model. This new challenge could be a wonderful mean to federate research teams around a global interdisciplinary project for conservation of Cultural Heritage.

Nevertheless, these kinds of holistic models could only be achievable by using consolidated databases containing heterogeneous data. Thus, one of the next forthcoming challenge, dealing with all sort of data (from climatic change to nanoscale measurements), is to construct perennial and interoperable databases. Several research teams are now on that path but this objective can only be achievable with a coordination at a national or European level for example.

Last but not least, any model has to be validated. Considering predictive models aiming to predict the behaviour of heritage systems on several 10 years or even centuries, this validation could be a real breakthrough. One solution could be a retroactive approach, considering the behaviour of the system in the past, studying "analogues", for benchmarking. This challenge linked with long term prediction is also one of the most exciting one for researches in the future.

This multistep and multiscale approach for predictive modelling will have to face several challenges to reach the goal. First it has to be stressed that the link between the fine characterisation of mechanisms and the properties of the system and the numerical modelling must constantly be preserved by regular come and go between all the concerned disciplines. This could be implemented in the future in the frame of global interdisciplinary projects dealing with one kind of material (metal, stone, etc.) in a given environment. This kind of project have a sense for example at the European scale and must gather all the specialists from laboratories skilled in fine and multiscale characterisation to teams specialised in numerical modelling. We believe that it is only in that frame that the synergies between all disciplines will be found. Another crucial aspect, we can think that in the future these new models for predicting the evolution of heritage systems with environment and climate can be considered as a new kind of immaterial Cultural Heritage, in the same way that the digitalised museums or libraries collections. This new "digitalised" Cultural Heritage resource, allowing future generation of scientist to develop and use predictive models will be based on the mastering of international and multi-source databases. This other aspect constitutes also an exciting challenge for future generations that could be faced at the European scale by gathering research and engineering teams using European facilities for data storage and treatment.

References

Abruzzese D, Miccoli L, Yuan J (2009) Mechanical behavior of leaning masonry Huzhu Pagoda. J Cult Heritage 10:480–486. doi:10.1016/j.culher.2009.02.004

Albero S, Giavarini C, Santarelli ML, Vodret A (2004) CFD modeling for the conservation of the Gilded Vault Hall in the Domus Aurea. J Cult Heritage 5:197–203. doi:10.1016/j.culher.2003.08.001

Ambrosi M, Dei L, Giorgi R, Neto C, Baglioni P (2001) Colloidal particles of $Ca(OH)_2$: properties and applications to restoration of frescoes. Langmuir 17(14):4251–4255. doi:10.1021/la010269b

Astruc L, Vargiolu R, Tkaya MB, Balkan-Atlı N, Özbaşaran M, Zahouani H (2011) Multi-scale tribological analysis of the technique of manufacture of an obsidian bracelet from Aşıklı Höyük (Aceramic Neolithic, Central Anatolia). J Archaeol Sci 38(12):3415–3424

Baglioni P, Chelazzi D, Giorgi R, Poggi G (2013) Colloid and materials science for the conservation of cultural heritage: cleaning, consolidation, and deacidification. Langmuir 29(17):5110–5122. doi:10.1021/la304456n

Bataillon C, Bouchon F, Chainais-Hillairet C, Desgranges C, Hoarau E, Martin F, Perrin S, Tupin M, Talandier J (2010) Corrosion modelling of iron based alloy in nuclear waste repository. Electrochim Acta 55(15):4451–4467. doi:10.1016/j.electacta.2010.02.087

Bayle M (2015) Déchloruration des objets archéologiques ferreux par le processus de stabilisation subcritique - Caractérisations physico-chimiques des systèmes transformés. Pierre et Marie Curie University, Ph.D. thesis

Bernard S, Benzerara K, Beyssac O, Brown GE (2010) Multiscale characterization of pyritized plant tissues in blueschist facies metamorphic rocks. Geochim Cosmochim Acta 74(17):5054–5068. doi:10.1016/j.gca.2010.06.011

Bertholon R (2001) The original surface of corroded metallic archaeological objects: characterization and location. La Revue de Métallurgie 9:817–823. doi:10.1051/metal:2001128

Bingham PA, Jackson CM (2008) Roman blue-green bottle glass: chemical–optical analysis and high temperature viscosity modelling. J Archaeol Sci 35:302–309. doi:10.1016/j.jas.2007.03.011

Brauns M, Schwab R, Gassmann G, Wieland G, Pernicka E (2013) Provenance of iron age iron in southern Germany: a new approach. J Archaeol Sci 40(2):841–849. doi:10.1016/j.jas.2012.08.044

Burnett C, Blaschke T (2003) A multi-scale segmentation/object relationship modelling methodology for landscape analysis. Ecol Model 168:233–249. doi:10.1016/S0304-3800(03)00139-X

Cacciotti R, Blaško M, Valach J (2015) A diagnostic ontological model for damages to historical constructions. J Cult Heritage 16:40–48. doi:10.1016/j.culher.2014.02.002

Casadio F, Van Duyne RP (2013) Molecular analysis for art, archaeometry and conservation. Analyst 138(24):7276–7278. doi:10.1039/C3AN90096G

Cersoy S, Richardin P, Walter P, Brunelle A (2012) Cluster TOF-SIMS imaging of human skin remains: analysis of a South-Andean mummy sample. J Mass Spectrom 47(3):338–346. doi:10.1002/jms.2979

Chalmin E, Menu M, Pomiès M-P, Vignaud C, Aujoulat N, Geneste J-M (2004) Les blasons de Lascaux. L'Anthropologie 108(5):571–592. doi:10.1016/j.anthro.2004.12.001

Chalmin E, Vignaud C, Salomon H, Farges F, Susini J, Menu M (2006) Minerals discovered in paleolithic black pigments by transmission electron microscopy and micro-X-ray absorption near-edge structure. Appl Phys A 83(2):213–218. doi:10.1007/s00339-006-3510-7

Chelazzi D, Poggi G, Jaidar Y, Toccafondi N, Giorgi R, Baglioni P (2013) Hydroxide nanoparticles for cultural heritage: consolidation and protection of wall paintings and carbonate materials. J Colloid Interface Sci 392:42–49. doi:10.1016/j.jcis.2012.09.069

Chitty W-J, Berger P, Dillmann P, L'Hostis V (2008a) Long-term corrosion of rebars embedded in aerial and hydraulic binders—mechanisms and crucial physico-chemical parameters. Corros Sci 50(8):2117–2123. doi:10.1016/j.corsci.2008.03.017

Chitty W-J, Dillmann P, L'Hostis V, Millard A (2008b) Long-term corrosion of rebars embedded in aerial and hydraulic binders—parametric study and first step of modelling. Corros Sci 50 (11):3047–3065. doi:10.1016/j.corsci.2008.08.010

Cole IS, Hughes AE (2014) Designing molecular protection: new paradigm for developing corrosion resistant materials uniting high throughput studies, multiscale modelling and self-repair. Corros Eng Sci Technol 49:109–115. doi:10.1179/1743278213Y.0000000119

Cole IS, Paterson DA, Ganther WD (2003) Holistic model for atmospheric corrosion Part 1—theoretical framework for production, transportation and deposition of marine salts. Corros Eng, Sci Technol 38:129–134. doi:10.1179/147842203767789203

Cole IS, Muster TH, Azmat NS, Venkatraman MS, Cook A (2011) Multiscale modelling of the corrosion of metals under atmospheric corrosion. Electrochim Acta 56:1856–1865. doi:10.1016/j.electacta.2010.10.025

Colombini MP, Modugno F (2009) Organic materials in art and archaeology. In: Colombini MP, Modugno F (eds) Organic mass spectrometry in art and archaeology. Wiley, New York, pp 1–36

Creagh D, Bradley D (2006) Physical techniques in the study of art. In: Archaeology and Cultural Heritage, vol 1. Elsevier

Creagh D, Bradley D (2007) Physical techniques in the study of art, archaeology and cultural heritage, vol 2. Elsevier

Crina Anca Sandu I, de Sá MH, Pereira MC (2011) Ancient 'gilded' art objects from European cultural heritage: a review on different scales of characterization. Surf Interface Anal 43 (8):1134–1151. doi:10.1002/sia.3740

D'Agostino D, Congedo PM, Cataldo R (2014) Computational fluid dynamics (CFD) modeling of microclimate for salts crystallization control and artworks conservation. J Cult Heritage 15:448–457. doi:10.1016/j.culher.2013.10.002

Dal Bianco B, Bertoncello R (2008) Sol–gel silica coatings for the protection of cultural heritage glass. Nucl Instrum Methods Phys Res, Sect B 266(10):2358–2362. doi:10.1016/j.nimb.2008.03.014

de la Fuente D, Díaz I, Simancas J, Chico B, Morcillo M (2011) Long-term atmospheric corrosion of mild steel. Corros Sci 53(2):604–617. doi:10.1016/j.corsci.2010.10.007

De Luca L (2014) Methods, formalisms and tools for the semantic-based surveying and representation of architectural heritage. Appl Geomatics 6:115–139. doi:10.1007/s12518-011-0076-7

De Stasio G, Gilbert B, Frazer BH, Nealson KH, Conrad PG, Livi V, Labrenz M, Banfield JF (2001) The multidisciplinarity of spectromicroscopy: from geomicrobiology to archaeology. J Electron Spectrosc Relat Phenom 114–116:997–1003. doi:10.1016/S0368-2048(00)00369-8

Dejoie C, Tamura N, Kunz M, Goudeau P, Sciau P (2015) Complementary use of monochromatic and white-beam X-ray micro-diffraction for the investigation of ancient materials. J Appl Crystallogr 48(5):1522–1533. doi:10.1107/S1600576715014983

Dillmann P, Bellot-Gurlet L (2014) Circulation et provenance des matériaux dans les sociétés anciennes. Sciences Archéologiques. Editions Archives Contemporaines Paris

Edwards H, Vandenabeele P (2012) Analytical archaeometry: selected topics. Royal Society of Chemistry, Cambridge

Evershed RP (2008) Organic residue analysis in archaeology: the archaeological biomarker revolution. Archaeometry 50(6):895–924. doi:10.1111/j.1475-4754.2008.00446.x

Fleischer M (2012) Near-field scanning optical microscopy nanoprobes. Nanotechnology Reviews 1. doi:10.1515/ntrev-2012-0027.

Galvez ME, Benzerara K, Beyssac O, Bernard S (2009) Chemical and structural imaging of fossilized tissues at the nanoscale and assessment of their taphonomy. Geochim Cosmochim Acta 73(13):A408

Giachi G, Bugani S, Łucejko J, Modugno F, Tatti F (2014) Different techniques (SR-μCT, SEM, FIB/SEM) for the evaluation of the deposition of impregnating substances into waterlogged archaeological wood, woodcutter.com

Giavarini C, Santarelli ML, Natalini R, Freddi F (2008) A non-linear model of sulphation of porous stones: numerical simulations and preliminary laboratory assessments. J Cult Heritage 9:14–22. doi:10.1016/j.culher.2007.12.001

Guidi G, Remondino F, Russo M, Menna F, Rizzi A, Ercoli S (2009) A multi-resolution methodology for the 3d modeling of large and complex archeological areas. Int J Archit Comput 7:39–55. doi:10.1260/147807709788549439

Hélary D, Darque-Ceretti E, Bouquillon A, Aucouturier M, Monge G (2003) Contribution de la diffraction de rayons X sous incidence rasante à l'étude de céramiques lustrées. Revue d'Archéométrie, 115–122. doi:10.3406/arsci.2003.1047

Hoerlé S, Mazaudier F, Dillmann P, Santarini G (2004) Advances in understanding atmospheric corrosion of iron II—mechanistic modelling of wet-dry cycles. Corrosion Sci 46(6):1431–1465. doi:10.1016/j.corsci.2003.09.028

Hoppe P, Cohen S, Meibom A (2013) NanoSIMS: technical aspects and applications in cosmochemistry and biological geochemistry. Geostand Geoanal Res 37(2):111–154. doi:10.1111/j.1751-908X.2013.00239.x

Huijbregts Z, Schellen H, Jv Schijndel, Ankersmit B (2015) Modelling of heat and moisture induced strain to assess the impact of present and historical indoor climate conditions on mechanical degradation of a wooden cabinet. J Cult Heritage 16:419–427. doi:10.1016/j.culher.2014.11.001

Kim C-J, Yoo WS, Lee U-K, Song K-J, Kang K-I, Cho H (2010) An experience curve-based decision support model for prioritizing restoration needs of cultural heritage. J Cult Heritage 11:430–437. doi:10.1016/j.culher.2010.03.004

King HE, Mattner DC, Plümper O, Geisler T, Putnis A (2014) Forming cohesive calcium oxalate layers on marble surfaces for stone conservation. Cryst Growth Des 14(8):3910–3917. doi:10.1021/cg500495a

Kouris LAS, Kappos AJ (2012) Detailed and simplified non-linear models for timber-framed masonry structures. J Cult Heritage 13:47–58. doi:10.1016/j.culher.2011.05.009

Kurouski D, Zaleski S, Casadio F, Van Duyne RP, Shah NC (2014) Tip-enhanced raman spectroscopy (TERS) for in situ identification of indigo and iron gall ink on paper. J Am Chem Soc 136(24):8677–8684. doi:10.1021/ja5027612

Leon Y, Saheb M, Drouet E, Neff D, Foy E, Leroy E, Dynes JJ, Dillmann P (2014) Interfacial layer on archaeological mild steel corroded in carbonated anoxic environments studied with coupled micro and nano probes. Corros Sci 88:23–35. doi:10.1016/j.corsci.2014.07.005

Leon Y, Sciau P, Passelac M, Sanchez C, Sablayrolles R, Goudeau P, Tamura N (2015) Evolution of terra sigillata technology from Italy to Gaul through a multi-technique approach. J Anal At Spectrom 30(3):658–665. doi:10.1039/C4JA00367E

Leroy S, Cohen SX, Verna C, Gratuze B, Téreygeol F, Fluzin P, Bertrand L, Dillmann P (2012) The medieval iron market in Ariège (France). Multidisciplinary analytical approach and multivariate analyses. J Archaeol Sci 39(4):1080–1093. doi:10.1016/j.jas.2011.11.025

Madariaga JM (2015) Analytical chemistry in the field of cultural heritage. Anal Methods 7 (12):4848–4876. doi:10.1039/C5AY00072F

Manoudis PN, Karapanagiotis I, Tsakalof A, Zuburtikudis I, Kolinkeová B, Panayiotou C (2009) Superhydrophobic films for the protection of outdoor cultural heritage assets. Appl Phys A 97 (2):351–360. doi:10.1007/s00339-009-5233-z

Mele E, Luca AD, Giordano A (2003) Modelling and analysis of a basilica under earthquake loading. J Cult Heritage 4:355–367. doi:10.1016/j.culher.2003.03.002

Monnier J, Dillmann P, Legrand L, Guillot I (2010) Corrosion of iron from heritage buildings: proposal for degradation indexes based on rust layer composition and electrochemical reactivity. Corros Eng, Sci Technol 4 (5):375–80.10.1179/147842210X12779093813740

Muller J, Laïk B, Guillot I (2013) α-CuSn bronzes in sulphate medium: Influence of the tin content on corrosion processes. Corros Sci 77:46–51. doi:10.1016/j.corsci.2013.07.025

Pollard AM, Heron C (2008) Archaeological chemistry. Royal Society of Chemistry, UK
Pomiès MP, Menu M, Vignaud C (1999) TEM observations of goethite dehydratation: application to archaeological samples. J Eur Ceram Soc 19:1605–1614. doi:10.1016/S0955-2219(98)00254-4
Remondino F, Girardi S, Rizzi A, Gonzo L (2009) 3D Modeling of complex and detailed cultural heritage using multi-resolution data. J Comput Cult Herit 2:2:1–2:20. doi:10.1145/1551676.1551678
Richardin P, Mazel V, Walter P, Laprévote O, Brunelle A (2011) Identification of different copper green pigments in renaissance paintings by cluster-TOF-SIMS imaging analysis. J Am Soc Mass Spectrom 22(10):1729–1736. doi:10.1007/s13361-011-0171-3
Sakdinawat A, Attwood D (2010) Nanoscale X-ray imaging. Nat Photon 4(12):840–848. doi:10.1038/nphoton.2010.267
Silversmit G, Vekemans B, Brenker FE, Schmitz S, Burghammer M, Riekel C, Vincze L (2009) X-ray fluorescence nanotomography on cometary matter from comet 81P/Wild2 returned by stardust. Anal Chem 81(15):6107–6112. doi:10.1021/ac900507x
Stefani C, Brunetaud X, Janvier-Badosa S, Beck K, Luca LD, Al-Mukhtar M (2014) Developing a toolkit for mapping and displaying stone alteration on a web-based documentation platform. J Cult Heritage 15:1–9. doi:10.1016/j.culher.2013.01.011
Thoury M, Echard J-P, Réfrégiers M, Berrie B, Nevin A, Jamme F, Bertrand L (2011) Synchrotron UV—visible multispectral luminescence micro imaging of historical samples. Anal Chem 83(5):1737–1745. doi:10.1021/ac102986h
Tidblad J (2013) Atmospheric corrosion of heritage metallic artefacts: processes and prevention. Corrosion and conservation of cultural heritage metallic artefacts. EFC series. Woodhead Publishing, Oxford, pp 37–52
Ungár T, Martinetto P, Ribárik G, Dooryhée E, Walter P, Anne M (2002) Revealing the powdering methods of black makeup in Ancient Egypt by fitting microstructure based Fourier coefficients to the whole x-ray diffraction profiles of galena. J Appl Phys 91(4):2455–2465. doi:10.1063/1.1429792
Verney-Carron A, Gin S, Frugier P, Libourel G (2010) Long-term modeling of alteration-transport coupling: application to a fractured Roman glass. Geochim Cosmochim Acta 74(8):2291–2315. doi:10.1016/j.gca.2010.01.001
Villanueva-Amadoz U, Benedetti A, Méndez J, Sender LM, Diez JB (2012) Focused ion beam nano-sectioning and imaging: a new method in characterisation of palaeopalynological remains. Grana 51(1):1–9. doi:10.1080/00173134.2011.641579
Vlachos DG (2005) A review of multiscale analysis: examples from systems biology, materials engineering, and other fluid–surface interacting systems. In: Marin GB (ed) Advances in chemical engineering multiscale analysis. Advances in Chemical Engineering, vol 30. Academic Press, pp 1–61
Yang A, Marquardt W (2009) An ontological conceptualization of multiscale models. Computers & Chemical Engineering, 822–837. doi:10.1016/j.compchemeng.2008.11.015

Part III
Conserve and Protect the Cultural Heritage using Nanomaterials and Nanoscience

Nanoscale Aspects of Corrosion on Cultural Heritage Metals

Philippe Dillmann

Abstract Metallic artefacts are an important part of the cultural heritage and must be protected for the future generations. Unfortunately, classical metal protection methods used for example in industry, can in most of cases not be used in the context of the conservation of cultural heritage because artefacts must not be aesthetically modified and any protection treatment must be potentially removable without any damage to the artefact. For that reason, to set up efficient conservation strategies, it is necessary to understand and model the long term corrosion mechanisms. In addition to environmental monitoring and empirical approaches, the fine understanding of the corrosion systems, based on the use of multiscale characterisation techniques and methodologies is a key issue to understand the mechanisms and evaluate the degradation rates. This chapter reviews the cases for which investigations at nano scales are necessary to understand and model in a reliable way the corrosion behaviour of different metals (ferrous alloys and bronzes). Nanoscale investigation, also allows scientists to understand the way intentional patinas were made on ancient bronzes. Lastly, an example of the use of nanotechnology to set up an adapted and innovative protective treatment is given.

1 Introduction

Metallic cultural heritage cannot be protected by usual industrial anticorrosion methods as painting or inhibiting agents that will cause changes of the external appearence of the artefacts. In this context, the protection of metallic artefacts is a key issue and necessitates sometimes costly and hazardous choices for curators, because they don't know the potential future evolution of their systems, especially with environmental and climatic changes. Besides, at a moment of budget lowering for states and institutions in charge of the cultural heritage protection, it is of primary

P. Dillmann (✉)
LAPA-IRAMAT, NIMBE, Université de Paris Saclay,
91191 Gif Sur Yvette Cedex, France
e-mail: philippe.dillmann@cea.fr

P. Dillmann et al. (eds.), *Nanoscience and Cultural Heritage*,
DOI 10.2991/978-94-6239-198-7_8

interest to take the relevant decisions on conservation or restoration processes. For these reasons and for basic preventive conservation purposes, the degradation processes must be managed in advance on the basis of scientific long-term prediction of risks of damage. This implies a fine knowledge of the corrosion mechanisms involved in the degradation of the metals of the cultural heritage.

During their life and after their abandonment and sometime their burial, metallic artefacts of cultural heritage are submitted to long term corrosion processes, associated with the progressive modification of their surfaces and their covering of corrosion products. The nature of these corrosion products depends on the one hand on the kind of metal that is corroded and, on the other hand, on the kind of environment (soil, atmosphere, marine water…) presenting a specific chemical composition. The understanding of the corrosion processes and their modelling (see Sect. 2.2. in the present book) is a crucial issue for conservation and restoration purposes (Scott and Eggert 2009; Dillmann et al. 2013). In that context, the exact role of the corrosion products in these mechanisms must be understood, because in most of times it controls the corrosion kinetics. Actually the electrochemical reactivity of the involved phases and transport phenomena are critical aspects. From the functional scale of the considered artefacts to the nanoscale, these points must be considered and, actually, several studies demonstrated that, in addition to environmental key parameters and microscale processes, nanoscale phenomenon as the presence of barrier layers or typical reactive products potentially plays a dominant role on the macroscopic behaviour of the artefacts.

Thus, the aim of the first part of this chapter is not to review all the numerous corrosion studies dedicated to cultural heritage that are already published, but to give an overview of the cases where the nanometre scale is crucial to the understanding of the corrosion mechanisms and processes. Another interesting aspect of metals of cultural heritage, especially bronzes, is that some of them were submitted in ancient times, to intentional treatments to form artificial patinas, aiming to modify their aesthetic aspects. Researches are conducted to decipher the nature of the treatments performed by ancient craftsmen and, again, this involves investigations at the nanoscale to decipher the technical gestures. The chapter will present some studies dealing with the analytical strategies and the comprehension of phenomenon in that particular frame. Lastly, a third part, will illustrate the way nanotechnology is involved to set up protection treatments for metallic artefacts of the cultural heritage.

2 Corrosion Mechanisms

For most of metals, the stable thermodynamic states in natural conditions are under the form of oxides, sulphurs, chlorides and carbonates. That is the reason why artefacts of cultural heritage are submitted to corrosion processes of various natures in contact with their environment. In most of cases this occurs in presence of water (electrolyte) and other oxidant species, the most frequent one, being oxygen.

Corrosion is an electrochemical process, implying an electron transfer at different interfaces. Nevertheless, because of the presence of precipitated corrosion products, the corrosion processes cannot be considered as simple interactions between the surface of the metal and an electrolyte. The corrosion product layers are more or less passivating or inhibiting, provoking a lowering of the corrosion rates. The thermodynamic aspects of this protective effect was considered by Pourbaix (1977) who expressed the predominance domains of the constitutive phases of the corrosion products in potential-pH diagrams, depending of the activity (concentration) of the different species in the electrolyte. These potential-pH diagrams are fundamental in corrosion studies because they give an estimation of the nature of the formed corrosion products in function of the environmental conditions but the approach is limited to thermodynamic and static considerations. Moreover this approach considers only a macroscopic scale, and an homogenous composition of the electrolyte in contact with the metal. This is definitively not the case for artefacts corroded during very long periods (centuries), on which thick corrosion layers formed, sometimes of several 100 μm or even millimetre in thickness for very corrosive conditions (Dillmann et al. 2013). These thick corrosion layers control the local chemical and electrochemical conditions in the porous network they form and these conditions could drastically change at the micro and nano-scales from the metal corrosion product interface to the outer zone of these corrosion products. That is the reason why, to be understood, these ancient systems must absolutely be investigated at different scales. Moreover, the presence at nanometre scale of specific phases or layer, can control the macroscopic processes. Some examples will be given in the following.

2.1 Ferrous Alloys

A non negligible part of artefacts of the cultural heritage made of iron or iron alloys is submitted to atmospheric corrosion. In museum exhibition showcases, it is possible to control the exposure conditions and to keep the artefacts at a low relative humidity. Nevertheless, in most of cases (including outdoor exposure, but also some storage rooms) it is not possible to control these conditions. For example, reinforcing iron elements in Gothic mediaeval cathedrals (see for example Fig. 1), that were put in the monuments during their building (Leroy et al. 2015), are today considered as a integral part of the historic monument and must be protected in the same way than stone. Here, it is obviously not possible to control the environmental conditions and corrosion mechanisms must be understood and monitored to predict the behaviour of the metal and take the right conservation decisions. Corrosion of ferrous alloys under atmospheric conditions during very long periods conducts to the formation of thick layers (about several 100 μm) made of a mix of oxyhydroxides as goethite (α-FeOOH), lepidocrocite (γ-FeOOH), ferroxihyte (δ-FeOOH) and more or less hydrated oxides as magnetite (Fe_3O_4), maghemite (γ-Fe_2O_3) or ferrihydrite ($5Fe_2O_3.9H_2O$). In case of the presence of pollutants in the atmosphere, some specific phases as akaganeite

Fig. 1 **a** View of the triforium of the Amiens Cathedral, **b** close view of the reinforcing chain of the triforium

(β-FeOOH), a Cl containing phase, can also constitute the corrosion layer (Dillmann et al. 2004; Monnier et al. 2010a, b; Bouchar et al. 2013). It has been demonstrated that the atmospheric corrosion processes of iron alloys are driven by the so called wet/dry cycle, during which a water electrolyte of several monolayers cyclically deposit and evaporate on the material (Stratmann 1987; Stratmann et al. 1990; Stratmann and Streckel 1990). A very important aspect of this mechanism is that, during the wetting phase, it is not the oxygen of the atmosphere that is the oxidant specie causing the cathodic reaction, but Fe-containing phases, constituting the corrosion layers. It was demonstrated that Fe(III) phases, if they are physically connected to the metallic substrate can be electrochemically reactive and provoke, by their reduction into Fe(II) species, the oxidation of the Fe(0) substrate. The electrochemical behaviour of the different phases constituting the corrosion layer was studied by many authors (Antony et al. 2004, 2005, 2007) and a reactivity index was provided to express the potential corrosive effect of the layer (Kashima et al. 2001; Dillmann et al. 2004; Monnier et al. 2010a, 2013). It was also demonstrated that the grain size of the considered phase, highly influence the reactivity and well crystallised nano grains are much less reactive (Monnier et al. 2010b). For that reason, in a general corrosion study on the reinforcing

iron chain of triforium of the Amiens cathedral, put there in 1498 to avoid the collapse of the cathedral (Dillmann 2011), the grain size of the corrosion products formed was observed and measured (Monnier et al. 2010b). High Resolution TEM and electron energy loss spectroscopy (EELS) in high resolution mode on 130 crystallites of goethite enable to determine that the grain size of this phase varies between 10 and 70 nm (Fig. 2). This low crystallite size was associated to a relatively low electrochemical reactivity of the rust that could be considered as relatively protective (Monnier et al. 2013). These kinds of approaches are now more and more integrated to corrosion studies dealing with metal of heritage artefacts and are a mean to understand better the evolution of electrochemical reactivity in function of some specific parameters of the constitutive phase of the corrosion layers.

Another important part of the iron based metallic cultural heritage comes from archaeological excavations. Some of these archaeological sites are situated on fields made of specific soils saturated with water. This is for example the case of numerous sites situated in wetland in North of Europe, but also of sites situated under dams, retaining water until their abandon. On some of these sites, in situ conservation

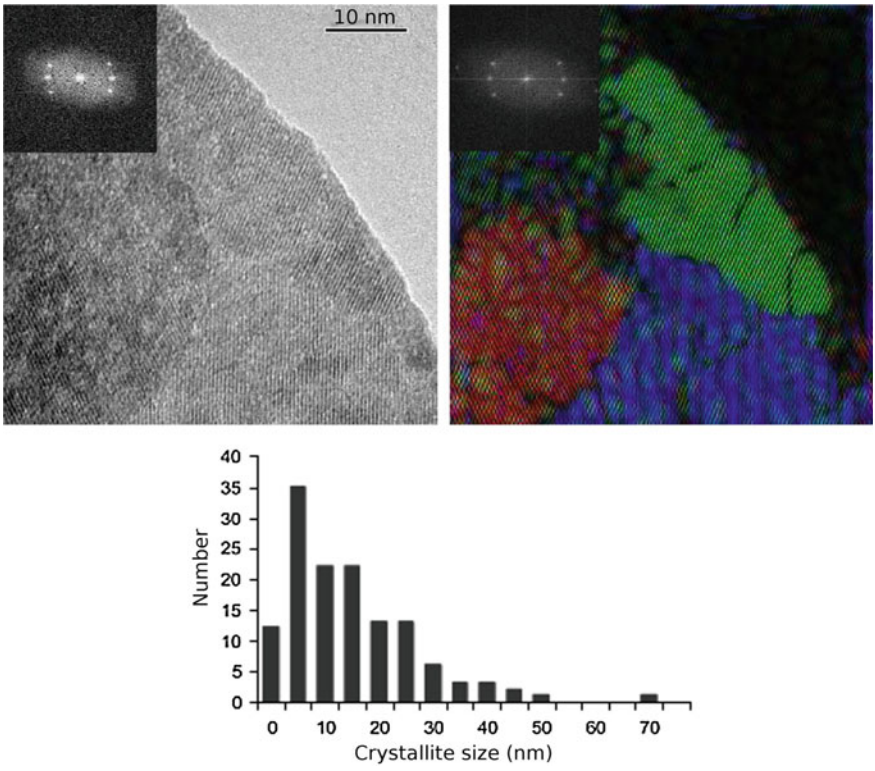

Fig. 2 HR-TEM images of goethite from the corrosion products taken on the reinforcing chain of the triforium of the Amiens cathedral (15th c.), corresponding Fourier transformed image and crystallite sizes (Monnier et al. 2010b)

is performed. The principle here is to conserve the artefacts buried in the archaeological soil and to monitor and model the environmental conditions and the artefacts behaviour to be sure that these latter are maintained in undisturbed and stable conditions (Corfield 1996; Matthiesen et al. 2004a; Corfield and Williams 2011). As stated by several authors, this can be achieved only by a good and reliable environmental monitoring (Matthiesen et al. 2004a) but also by understanding the degradation mechanisms of the metallic artefacts. Waterlogged soils are characterised by a low oxygen level below a certain depth. This lead corrosionnists to consider in details the very long term corrosion of iron in anoxic conditions. This was recently performed on two archaeological sites on which the corrosion mechanisms were studied. The first one is the site of Nydam Mose in Denmark, dated from the Danish Iron Age and situated in a water meadow. Nydam was a lake in which sacrificial offerings were deposited between 200 and 500 AD (Matthiesen et al. 2004b). All kind of weapons and artefacts made of iron alloys can be found on the site (swords, arrows, spears, etc.). The excavations, that began in the middle of the 19th c. were stopped in 1997 to investigate the feasibility of in situ conservation. The second site is an iron production site dated from the 15th c. AD and situated in Normandy in France. Because of the use of hydraulic power during the middle age to produce iron, a water dam remains on the site (Arribet-Deroin 2001; Dillmann et al. 2003), causing a complete saturation of the soil with water after its abandon and during the burial of the artefacts. On both of these sites, carbonated anoxic conditions were evidenced (Matthiesen et al. 2004a; Saheb et al. 2010a). It has to be stressed here that these conditions of corrosion are interesting to be studied for conservation reasons but also in another completely different frame, the one of the prediction of long term corrosion of steel for the design of over containers for the storage of nuclear wastes (Dillmann et al. 2014). In this latter context, the archaeological artefacts are considered as analogues and bring useful and unique data for modelling and simulating the century-long corrosion processes.

On both of these sites some artefacts (mainly nails) could be analysed using adapted investigations methods of material sciences. It was observed that the corrosion systems were constituted of carbonates as siderite ($FeCO_3$) and hydroxicarbonates as chukanovite ($Fe_2(OH)_2CO_3$) precipitated on the metallic substrate (Saheb et al. 2010b), and forming layers of about 100 µm. The average corrosion rates deduced from mass balance of the analysed corrosion products and from the initial shape of the artefacts (Matthiesen et al. 2004b; Neff et al. 2005) were very low (i.e. several µm/year) and in good agreement with short term corrosion experiments made in laboratory to simulate the corrosion mechanisms (Schlegel et al. 2008, 2014). Besides, electrochemical measurements made by impedance spectroscopy during short term laboratory experiments suggested that the mere presence of the carbonate thick layer was not sufficient to explain the low corrosion rates (because of their relatively high porosity), but that a dense and barrier layer should be present at the interface between the metal and the carbonated corrosion products (Rangel et al. 1986; Castro et al. 1991; Bataillon et al. 2001; Han et al. 2009). To verify this assertion the metal/corrosion product interface of some archaeological artefacts was studied at the nanometric scale by a combination of TEM and Scanning Transmission X ray Microscope (STXM) observations

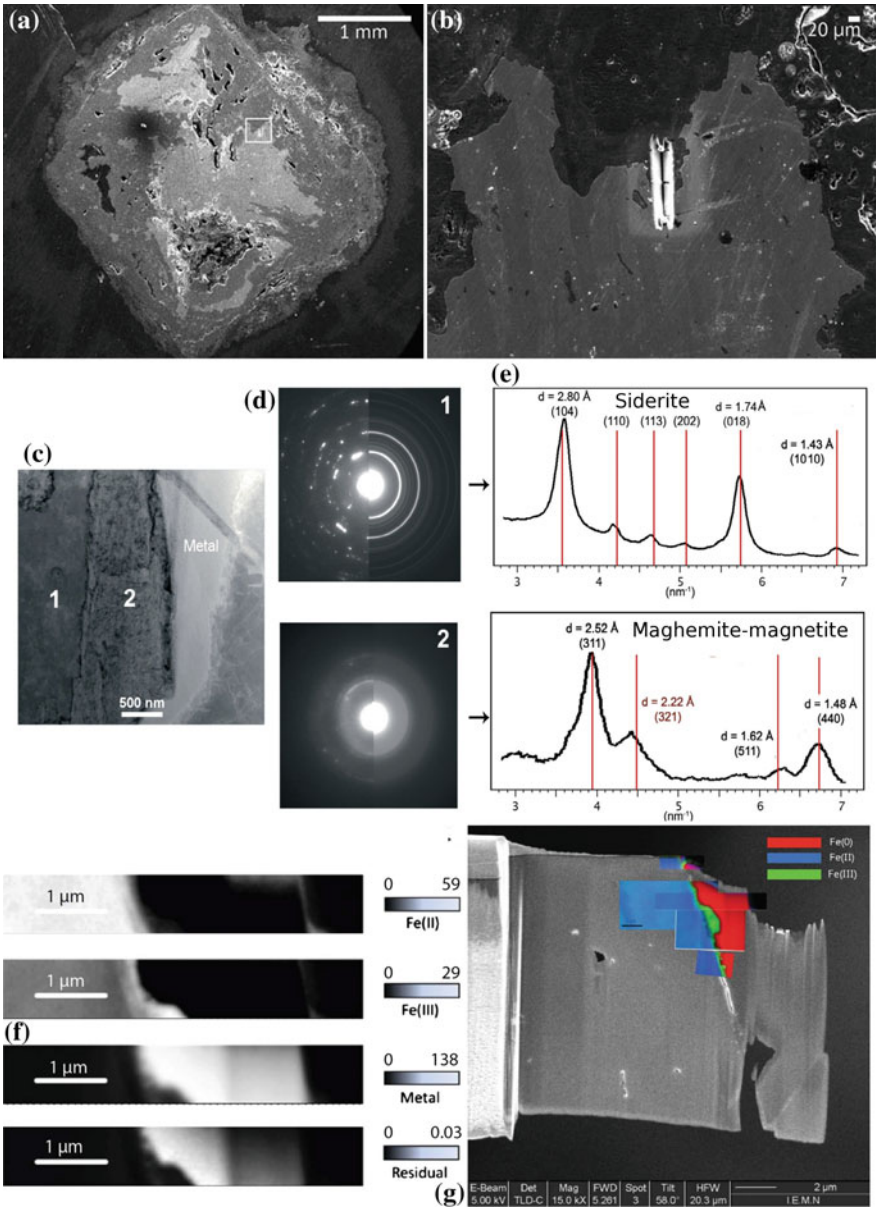

Fig. 3 **a** SEM image of the cross section of an archaeological iron nail corroded since the 15th c. in an anoxic carbonated environment. **b** Location of the thin film sample at the metal/corrosion product interface, **c** TEM image and associated (**d**, **e**) electron diffraction patterns. (**f**, **g**) STXM maps obtained at the Fe L edge. Repartition of Fe(0), Fe(II) and Fe(III) valences (Michelin et al. 2013; Leon et al. 2014)

performed on a thin film sample obtained by Focused Ion Beam (FIB) at the metal/corrosion product interface. It was clearly demonstrated that, in addition to the layer of carbonates, an interface nanometric layer varying from 50 to several 100 nm in thickness was present on the artefacts (Michelin et al. 2013; Leon et al. 2014). This layer is made of a mix of iron oxides (maghemite and magnetite see Fig. 3).

The porosity and protectiveness of the layer were studied by another specific experiment. Another archaeological nail was immersed before any cutting or sampling, in a D_2O solution reproducing the archaeological pore water of the soil, during 3 month. Then, a transverse section of the nail was examined by nano-SIMS in order to map ^{16}O, D and H distribution (Leon et al. 2014). On Fig. 4, the ^{16}O distribution allows one to distinguish the corrosion products from the metal. The D/H map, clearly indicates a D depletion at the metal oxide interface, revealing the hindering role for the transport of water to the metallic interface of the barrier layer made of magnetite and maghemite identified by TEM and STXM at this location. The formation of this nanometric interface layer is explained by some authors by a local acidification at the metal/corrosion product interface due to water hydrolysis during the iron oxidation process (Han et al. 2009). This important observation corroborates the potential protective role of the interfacial layer in the corrosion process, and its influence on the kinetics evoked by some authors (Bataillon et al. 2010). This is now taken into account in further modelling of iron and steel long term corrosion, both for conservation and long term prediction purposes. It is also a good example of a nanometric process controlling a macroscopic corrosion kinetic.

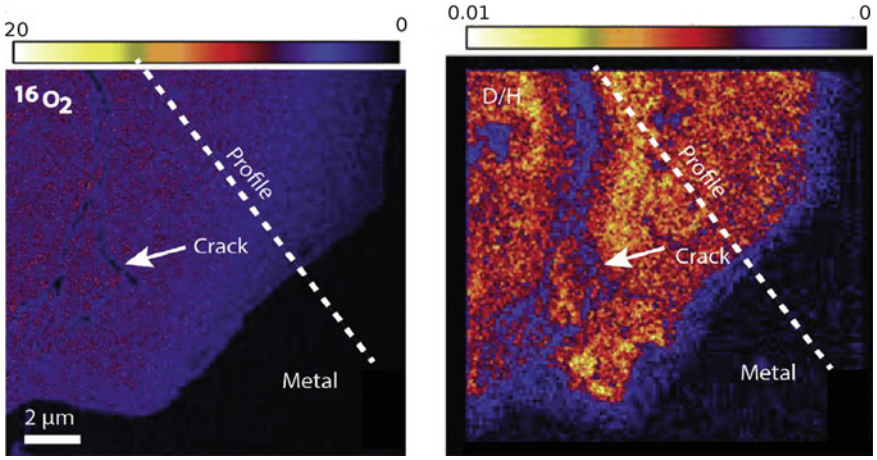

Fig. 4 Nano-SIMS maps of $^{16}O_2$ and D/H ratio obtained at the Metal/Corrosion products interface of an archaeological nail from the 15th c. put 3 month in a D_2O solution (Leon et al. 2014)

2.2 *Non-ferrous Alloys*

The outdoor corrosion of ancient "bronzes" (Cu-Sn alloys with sometimes significant quantities of Zn and Pb), conducts to the formation of a protective patina of about 20–50 µm of thickness. An important number of studies was dedicated to understand the nature of these patinas that have similarity with the behaviour of pure copper but differs from it because of the presence of alloying elements (Selwyn et al. 1996; Robbiola et al. 1998; Spoto et al. 2000; Ingo et al. 2006; Chiavari et al. 2007). Patina can contain both Cu-rich and Sn rich compounds, mainly cuprite (Cu_2O) or cassiterite (SnO_2). Moreover, in rainfall conditions, cyclic processes can occur, based on the successive dissolution and leaching phenomenon. In that context it is of primary importance to understand the physico-chemical nature of the patina on the one hand and its electrochemical reactivity on the other hand. This latter information can be obtained by performing cyclic voltammetry or electrochemical impedance spectrometry (EIS) using a cavity electrode, allowing to test small quantities of scrapped powders (Chiavari et al. 2007; Bernard and Joiret 2009). Concerning physico-chemical investigations at low scales, several studies demonstrate the important role of nanocrystalline areas with a specific behaviour in the patina. For example, Chiavari et al. (2007) by High Resolution Transmission Electronic Microscopy investigations coupled with EDS on powder scrapped on a French outdoor Bronze monument (Monument to Francis Garnier 1898, Fig. 5), confirms the presence of nanocrystals in the pale green external patina that is depleted in copper and enriched in tin, probably constituted of oxide or hydroxide compounds (Fig. 6). This kind of nanoparticles was also evidenced in the corrosion

Fig. 5 Monument to Charles Garnier, Paris (Chiavari et al. 2007)

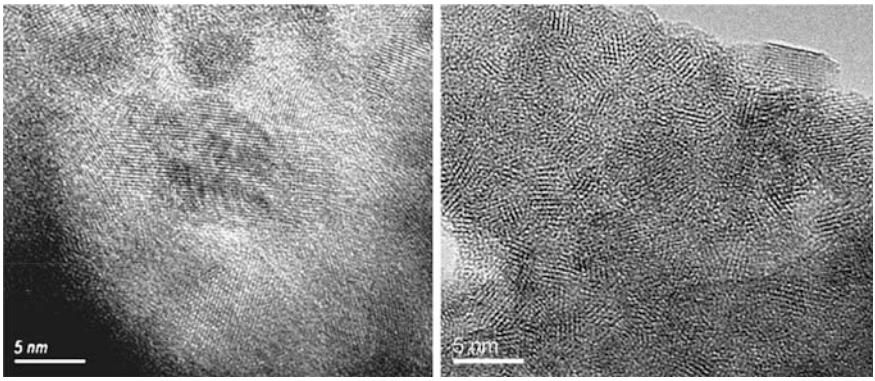

Fig. 6 HR-TEM lattice images of pale green patina from an outdoor bronze monument. Presence of 5 nm nanocrystals (Chiavari et al. 2007)

products of ancient Chinese mirrors. Several studies were interested into the fine characterisation of the SnO_2 nanometric particles that formed during the corrosion process of black mirrors, made of a Cu-Sn alloy because, they potentially influence the corrosion resistance of the artefact. Wang et al. (1995), combining TEM (using Selected Area Electron Diffraction) and XAS, manage to index the structure of cassiterite (SnO_2), attributed to an hypothetical compounds of $Sn_{1-x}(CuFePbSi)_xO_2$.

Ancient mirrors were made of tin amalgam (Hadsund 1993). These kinds of mirrors were used from the 16th c. to the beginning of the 20th c. To obtain these mirrors, first, a 100 μm film of Sn is laid on a flat plate of marble. Then, mercury is poured onto the tin film. Finally a polished glass is put on the amalgam. The process is detailed in (Herrera et al. 2009). The obtained amalgam after 24 h is made of a two phase system: tin mercury compounds surrounded by a mercury rich liquid phase (Herrera et al. 2008a). The corrosion of this amalgam causes the final formation of SnO_2 after an initial precipitation of thermodynamically unstable SnO particles (Duran et al. 2008; Herrera et al. 2008b). Because mercury is volatile, after the ageing processes the final altered layer is made of divided SnO_2 particles. Herrera et al. (2009) studied in details the nature of these particles on an Andalusian baroque mirror, comparing an altered and an non-altered zone, by performing SEM, XRD and TEM. The very large peaks obtained by XRD on the surface of the altered zones of the mirrors indicate the presence of small size particles (estimated size by Sherrer law: 4–5 nm). TEM images were acquired on the SnO_2 particles and Selected Area Electron Diffraction (SEAD) was performed confirming the presence of 5 nm particles and aggregates (Fig. 7). Authors proposed that this layer of nanocrystalline corrosion products protects the metal very efficiently because nanometric crystals seems to have a lower surface activity and, consequently forms a more protective layer.

The nature of the tin containing phases developed after corrosion processes of bronzes is also an issue for archaeological artefacts corroded in soil. Robbiola et al. (1998) proposed a mechanism based on selective dissolution on copper. Two types

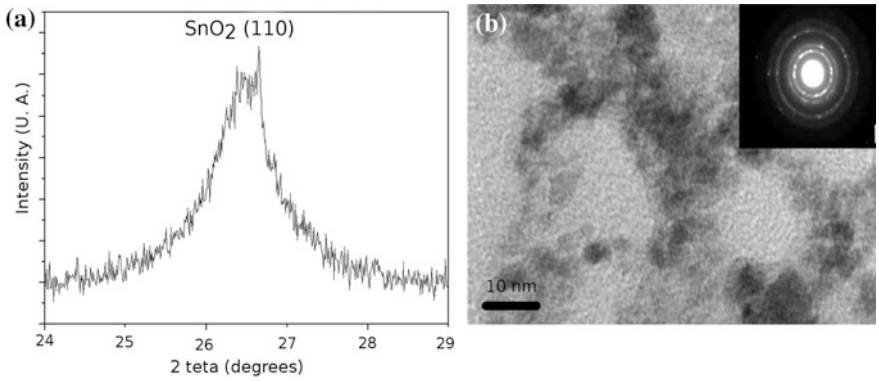

Fig. 7 **a** XRD at incidence angle $\gamma = 5^{o}$ of SnO_2 powder separated from the surface of a corroded Andalusian baroque mirror by the sonication method **b** TEM image and electron diffraction patterns from SnO_2 particles from the surface of a corroded mirror (Herrera et al. 2009)

of corrosion profiles are evidenced on archaeological artefacts depending on the nature and aggressiveness of the environment. In the type I, formed in a low aggressive environment, a protective barrier enriched in tin forms on the metal. In the case of more aggressive environment, for example containing chloride, accumulating at the metal/corrosion layer interface, localised corrosion phenomena are observed (type II patterns). In these processes, the nature of the tin layer and the way it protects the metal was a long time in discussion. To enlighten that point, Muller et al. (Muller et al. 2010, 2013) performed a study on coupons simulating the type I pattern after corrosion in sulphate aqueous solution. Different kind of bronzes were tested (α-Cu(Sn) and $CuSn_7$). The tin enriched phases where tested after anodic polarisation simulating the aging by electrochemical methods, X-ray spectroscopy (XPS), Auger Electron Spectroscopy (AES) and TEM. STEM and XPS investigations reveal that the formed passivating layer is of about 15 nm thick.

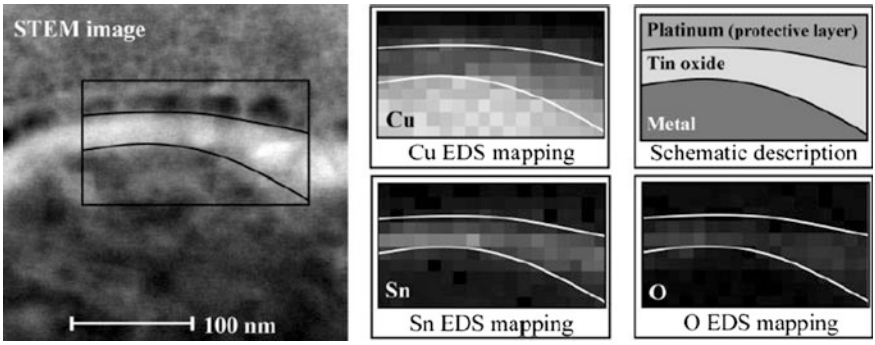

Fig. 8 STEM image and EDS maps of the passive Sn containing passivating layer on a bronze coupon simulating corrosion in a low aggressive environment (soil) (Muller et al. 2010)

It is made of a mix at this scale of SnO_2 (cassiterite) and Cu_2O (cuprite), despite an external layer of pure cuprite can not be excluded (Fig. 8).

3 Artificial Patinas and Ancient Surface Treatments on Bronzes

As for ceramic or glasses (see other chapters of this book), the knowledge of the technical development of ancient societies needs to understand the technical gestures applied by ancient craftsmen to form and decorate metals. In several cases processes took place at nanometre scale. To modify the external aspect of bronzes, and especially their colour, different kind of artificial treatments (chemical or physic-chemical) were applied on the alloys, in order to form a specific patina with different colours (reddish and dark brown, or black). The exact chemical structure and formation mechanisms of these artificial patina were in debate until the recent use, combined to classical characterisation techniques, of fine surface analysis techniques allowing one to investigate the patinas at lower scales.

For example, in different regions of the world and at different periods (Egypt 2nd millenary BC, Roman Empire 1st c. AD, China 4th c. AD or Japan 14th c. AD), a typical chemical treatment was applied on bronzes or coppers to obtain what is called "Black bronzes" or "Black coppers". These treatments, giving a black or velvet colour to the surface of the artefact, were applied on specific copper alloys containing gold (1–8 wt%) and silver (1–4 wt%). Combined to micro-scale investigations (micro-Raman spectroscopy, SEM, ICP-AES…) in a tailored step by step analytical strategy, a comprehensive study performed these last years on several pieces from the Louvre Museum (Aucouturier et al. 2010), used an Ion Beam Analysis approach by Rutherford Back Scattering (RBS) to decipher the nature of the layer with a resolution of about 100 nm. It was demonstrated that small amounts of Au and Ag inside Cu_2O layer allowed to change the colour and to obtain the desired one.

Artificial patinas on bronzes could be obtained by hot (heat colouring, torch techniques) or cold treatments. Hot treatments were performed by successive cycles consisting of a first oxidation of the metal generating a thin layer of oxides, followed by the application of a solution on the oxidized area. These successive cycles allowed the craftsman to build progressively the desired colour. The obtained colour is the result of a complex combination of cycles, temperature and composition of the applied chemical solution (Hiorns 1911; Hughes and Rowe 1982). The fact that this treatment is performed by cycles, generates a thin patina with compositional and structural heterogeneities lower than the μm in thickness. Thus, to understand their formation processes, chemical and structural profiles must be performed with a nanoscale resolution. For that reason, Balta et al. (2009), to better understand the reddish brown, dark brown and black patinas obtained on bronzes and coppers by torch techniques based on ferric chloride, ferric nitrate and

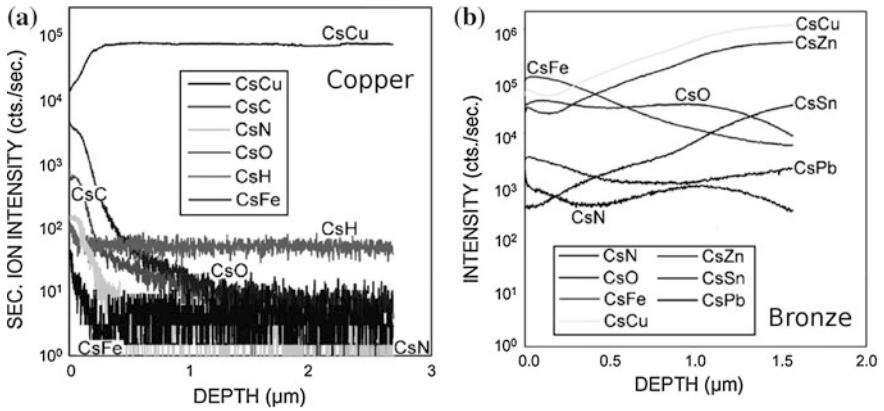

Fig. 9 **a** Normalised D-SIMS depth profile on a copper sample after presenting a 200 nm reddish brown nitrate solution patina, **b** Normalised D-SIMS depth profile on a bronze sample after presenting a 1600 nm reddish brown nitrate solution patina (Balta et al. 2009)

potassium sulphide solutions, performed Secondary Ion Mass Spectrometry (SIMS) and XPS on artificially treated coupons presenting the most common composition of 19th c. bronzes. XPS allowed to study the oxidation states of the different components and D-SIMS revealed the depth of penetration of different exogenous elements coming from the solution (O, C, H, Cl, Fe, K). The results (Fig. 9) demonstrate the heterogeneous distribution of exogenous elements in the thickness of the patina, leading to different colouring effects. A selective dissolution of the different elements of the bronze alloy (Cu, Zn, Sn and Pb) is also evidenced. It was also observed that the colour and the texture of patinas are influenced by nature and concentration of the solutions applied. Last but not least, the successive cycles of application of the patination solutions were tracked and found in the elemental depth profile.

4 Nano Coatings Against Corrosion

The protection of metallic artefacts of the cultural heritage against further corrosion degradation is a key issue. A way to reach that goal is to store the artefacts in controlled environment with low RH, free of pollutants and of aggressive gases. Nevertheless, this is not always possible, due to economical or practical considerations. For that reason, another solution would be to apply a protective coating on the artefacts to separate it from the environment. Nevertheless, for cultural heritage metal, the treatment must not alter the aesthetic aspect of the object and must be removable. Most of the treatments that are applied today as waxes (Degrigny 2010; Shashoua and Matthiesen 2010) or carboxylate (Hollner et al. 2010), deal with layers with thickness of several micron or tenth of microns, susceptible to modify

the external aspect after applying. Moreover, the durability of the efficiency of these treatment is questioned. Concerning the specific case of silver, submitted to a tarnishing effect in several environment, some successful attempts were made by using nanotechnology to develop a nanometre scale protective layer (Marquardt et al. 2015). For this metal, nitrocellulose treatments, manually applied are usually used. They are unfortunately non uniform, and their efficiency on long time period is limited. Particularly this compounds is well know to degrade and yellow under UV exposure, causing an undesirable colour on the artefact with time (Baše et al. 2010). At the contrary, to our knowledge, Atomic Layer Deposited (ALD) thin film of metal oxide does not present this limitation. As explained by Marquandt et al., ALD is a thermally activated gas phase process for synthesizing thin solid films by sequentially exposing an object to a series of two or more gaseous reactants, each of which undergoes self-limiting chemisorption surface reactions (Leskelä and Ritala 2002; Puurunen 2005). The artefacts to be covered is placed in the vacuum chamber where the process take place, in which a metal organic precursor and an oxiding co-reactant are pulsed. For example, in order to depose an alumina (Al_2O_3) coating, the metal-organic compound is trimethylaluminium (TMA) and the co-reactant, water. The precursor only reacts with the hydroxyl groups already present on the surface of the metal. Once all hydroxyl sites have reacted, additional exposure to the precursor will not results in an additional grow and thus, only a monolayer of coating is formed on the metallic surface. The co reactant is then introduced in a second stage to form the final Al_2O_3 monolayer. The obtained surface of the Al_2O_3 is also hydroxyl terminated, so the process can be repeated to obtain the final desired Al_2O_3 coated layer (Fig. 10). The self limiting nature of the process is the guaranty of the formation of a dense conformal and compact protecting film forming a very effective diffusion barrier against corrosion (Matero et al. 1999; Abdulagatov et al. 2011; Díaz et al. 2011a, b; Carcia et al. 2011). For cultural heritage applications, the thickness of the coating layer must be sufficiently thick to be an effective diffusion barrier for corrosion processes and sufficiently thin to be

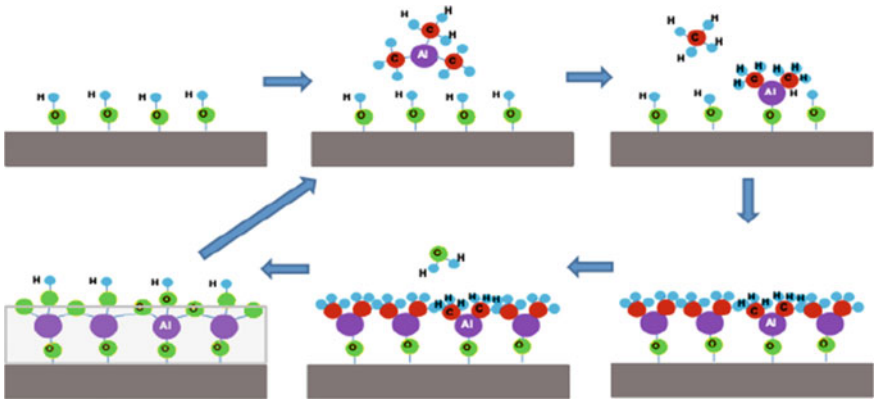

Fig. 10 Different stages of ALD for an Al_2O_3 coating (Marquardt et al. 2015)

optically transparent. Recent studies demonstrate that this optimal layer is about 20–100 nm (Paussa et al. 2011; Marquardt et al. 2015). As ALD is a non directional technique (contrary to spray based technique for example), all surfaces of even a complex artefact can be coated uniformly. Recently, specific systems working at low temperature (and consequently not disturbing the structure of the metallic surface) and atmospheric pressure have been developed and are especially adapted to the case of heritage artefacts.

Another promising method for protecting cultural heritage metals against corrosion is the deposit of a nano layer of silicon containing organic compounds (organosilicons) by Plasma Enhanced Chemical Vapor deposition (PECVD) (Angelini et al. 2004; d'Agostino et al. 2005). This method is highly versatile and allows one to test different deposition conditions and, thus, thin films characteristics (D'Agostino et al. 1997; Fracassi et al. 2003).

The protectiveness of the treatment was tested on different kind of metallic substrates as silver and copper alloys (Angelini et al. 2004, 2006). The SiO_2-like coatings are characterized by high chemical and thermal stability, good dielectric properties, low gas permeability, etc. The surface quality of a thin film deposited under different conditions on reference copper alloys presenting different roughness was evaluated by AFM observations (Fig. 11) by Angelini et al. (2006).

The high degree of adaptability to different kind of surfaces is a key factor for the protection of cultural heritage artefacts, which sometimes present complex shapes. Another very interesting feature of plasma polymerisation processes is that they can be preceded in the same chamber by a first cleaning stage or passivating treatment. During this etching stage the surface ion bombardment can be carefully controlled in order to avoid any damage at nanoscale.

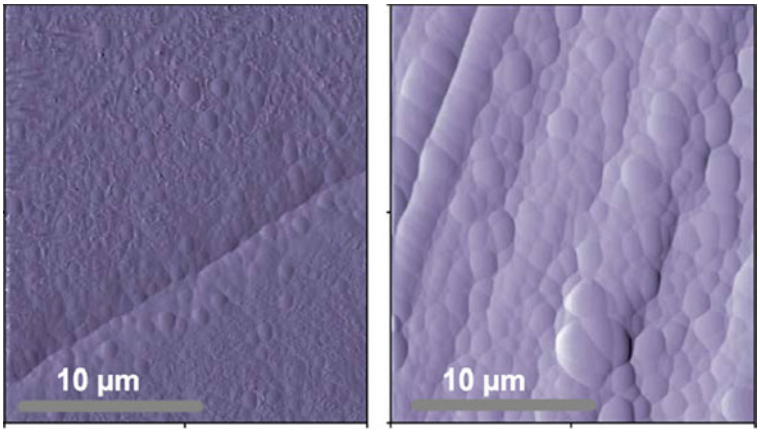

Fig. 11 AFM images of SIO_2-like films deposited by PECVD on copper based reference alloys of different roughness, representative of metals of cultural heritage (Angelini et al. 2006)

5 Conclusion

This short review aimed to show how it is crucial, in order to completely understand a corrosion mechanism and its dynamic over centuries in a given environment, to study the system at different scales, including the nanometre one. It has been shown that, on iron based metals, even if corrosion layers of several hundred micrometers are observed, in some cases, mechanisms at the nanometer scale control the kinetics or the electrochemical reactivity of the considered systems. The same for ancient bronzes on which the formation of tin containing phases and their protective ability can not be understood without an investigation at the nanoscale. Concerning patinas naturally or artificially formed on ancient bronzes, the use of surface investigation techniques, allowing one to model the valence and the chemistry of corrosion layers with a thickness lower than 1 μm and in which nanometric composition variation can be linked to ancient technical gestures, is a key approach. Last but not least, the use of nanotechnology to set up protection treatment adapted to the particular case of conservation of heritage artefacts will be to our opinion an important option for future approaches, for metallic artefacts as for other materials (see Sects. 3.2 and 3.3 in the present book) as demonstrated here for silver. Thus, it is no doubt that nano-characterisation techniques, nanotechnologies and nanosciences, will be more and more integrated in the various approaches linked to corrosion and protection of metals of the cultural heritage.

References

Abdulagatov AI, Yan Y, Cooper JR, Zhang Y, Gibbs ZM, Cavanagh AS, Yang RG, Lee YC, George SM (2011) Al_2O_3 and TiO_2 atomic layer deposition on copper for water corrosion resistance. ACS Appl Mater Interfaces 3:4593–4601. doi:10.1021/am2009579

Angelini E, Fracassi F, D'Agostino R, Grassini S, Rosalbino F (2004) PECVD of organosilicon thin films for corrosion protection of metals. In: Trends in electrochemistry and corrosion at the beginning of the 21st century, p 20

Angelini E, Grassini S, Solorzano G, Campos GD, De Caro T (2006) Integrated approach to the characterization and conservation of artefacts of the Brazilian colonial period. Appl Phys A-Mater Sci Process 83:485–491. doi:10.1007/s00339-006-3544-x

Antony H, Peulon S, Legrand L, Chaussé A (2004) Electrochemical synthesis of lepidocrocite thin films on gold substrate—EQCM, IRRAS, SEM and XRD study. Electrochim Acta 50:1015–1021

Antony H, Legrand L, Maréchal L, Perrin S, Dillmann P, Chaussé A (2005) Study of lepidocrocite electrochemical reduction in neutral and slightly alkaline solutions at 25 °C. Electrochim Acta 51:745–753

Antony H, Perrin S, Dillmann P, Legrand L, Chaussé A (2007) Electrochemical study of indoor atmospheric corrosion layers formed on ancient iron artefacts. Electrochim Acta 52:7754–7759

Arribet-Deroin D (2001) Fondre le fer en gueuses au XVIe siècle. Le haut fourneau de Glinet en pays de Bray (Normandie). Paris I Sorbonne, Paris

Aucouturier M, Mathis F, Robcis D, Castaing J, Salomon J, Pichon L, Delange E, Descamps S (2010) Intentional patina of metal archaeological artefacts: non-destructive investigation of

Egyptian and Roman museum treasures. Corros Eng Sci Technol 45:314–321. doi:10.1179/147842210x12710800383567

Balta IZ, Pederzoli S, Iacob E, Bersani M (2009) Dynamic secondary ion mass spectrometry and X-ray photoelectron spectroscopy on artistic bronze and copper artificial patinas. Appl Surf Sci 255:6378–6385. doi:10.1016/j.apsusc.2009.02.020

Baše T, Bastl Z, Havránek V, Lang K, Bould J, Londesborough MGS, Macháček J, Plešek J (2010) Carborane–thiol–silver interactions. A comparative study of the molecular protection of silver surfaces. Surf Coat Technol 204:2639–2646. doi:10.1016/j.surfcoat.2010.02.019

Bataillon C, Musy C, Roy M (2001) Corrosion des surconteneurs de déchets, cas d'un surconteneur en acier faiblement allié. J Phys IV France 267–274

Bataillon C, Bouchon F, Chainais-Hillairet C, Desgranges C, Hoarau E, Martin F, Perrin S, Tupin M, Talandier J (2010) Corrosion modelling of iron based alloy in nuclear waste repository. Electrochim Acta 55:4451–4467

Bernard MC, Joiret S (2009) Understanding corrosion of ancient metals for the conservation of cultural heritage. Electrochim Acta 54:5199–5205. doi:10.1016/j.electacta.2009.01.036

Bouchar M, Foy E, Neff D, Dillmann P (2013) The complex corrosion system of a medieval iron rebar from the Bourges' Cathedral. Characterization and reactivity studies. Corros Sci 76:361–372. doi:10.1016/j.corsci.2013.07.007

Carcia PF, Mclean RS, Sauer BB, Reilly MH (2011) Atomic layer deposition ultra-barriers for electronic applications, strategies and implementation. J Nanosci Nanotechnol 11:7994–7998. doi:10.1166/jnn.2011.5075

Castro EB, Vilche JR, Arvia AJ (1991) Iron dissolution and passivation in K_2CO_3-$KHCO_3$ solutions. rotating ring disc electrode and XPS studies. Corros Sci 32:37–50. doi:10.1016/0010-938X(91)90062-T

Chiavari C, Rahmouni K, Takenouti H, Joiret S, Vermaut P, Robbiola L (2007) Composition and electrochemical properties of natural patinas of outdoor bronze monuments. Electrochim Acta 52:7760–7769

Corfield M (1996) Preventive conservation for archaeological sites. In: Archaeological conservation and its consequences preprints of the contributions to the copenhagen congress, 26–30 August 1996. London, pp 32–37

Corfield M, Williams J (2011) Review of "Preservation of archaeological remains in situ (PARIS 4)." e-conservation magazine 24–29

D'Agostino R, Fracassi F, Favia P (1997) Plasma processing of polymers. Kluwer Academic Publishers, Berlin

d'Agostino R, Fracassi F, Palumbo F, Angelini E, Grassini S, Rosalbino F (2005) Protection of silver-based alloys from tarnishing by means of plasma-enhanced chemical vapor deposition. Plasma Proc Polym 2:91–96. doi:10.1002/ppap.200400031

Degrigny C (2010) Use of artificial metal coupons to test new protection systems on cultural heritage objects: manufacturing and validation. Corros Eng Sci Technol 45:367–374. doi:10.1179/147842210X12754747500649

Díaz B, Härkönen E, Światowska J, Maurice V, Seyeux A, Marcus P, Ritala M (2011a) Low-temperature atomic layer deposition of Al_2O_3 thin coatings for corrosion protection of steel: surface and electrochemical analysis. Corros Sci 53:2168–2175. doi:10.1016/j.corsci.2011.02.036

Díaz B, Światowska J, Maurice V, Seyeux A, Normand B, Härkönen E, Ritala M, Marcus P (2011b) Electrochemical and time-of-flight secondary ion mass spectrometry analysis of ultra-thin metal oxide (Al_2O_3 and Ta_2O_5) coatings deposited by atomic layer deposition on stainless steel. Electrochim Acta 56:10516–10523. doi:10.1016/j.electacta.2011.02.074

Dillmann P (2011) From Soissons to Beauvais : the use of iron in some French cathedrals. In: Hosek J, Cleere H, Lubomir Mihok (eds) The archaeometallurgy of iron—recent developments in archaeological and scientific research. Prague, pp 173–196

Dillmann P, Arribet-Deroin D, Vega E, Benoit P (2003) Early modern cast iron and iron at Glinet. In: Jensen I-MP, Ohman U (eds). Jernkontorets Bergshistorika Utskott, pp 99–106

Dillmann P, Mazaudier F, Hoerle S (2004) Advances in understanding atmospheric corrosion of iron I—rust characterisation of ancient ferrous artefacts exposed to indoor atmospheric corrosion. Corros Sci 46:1401–1429

Dillmann P, Watkinson D, Angelini E, Adriens A (2013) Corrosion and conservation of cultural heritage metallic artefacts. Woodhead publishing, Oxford

Dillmann P, Neff D, Féron D (2014) Archaeological analogues and corrosion prediction: from past to future. A review. Corros Eng Sci Technol 49:567–576. doi:10.1179/1743278214Y.0000000214

Duran A, Herrera LK, de Haro MCJ, Justo A, Perez-Rodriguez JL (2008) Non-destructive analysis of cultural heritage artefacts from Andalusia, Spain, by X-ray diffraction with Göbel mirrors. Talanta 76:183–188. doi:10.1016/j.talanta.2008.02.025

Fracassi F, d'Agostino R, Palumbo F, Angelini E, Grassini S, Rosalbino F (2003) Application of plasma deposited organosilicon thin films for the corrosion protection of metals. Surf Coat Technol 174–175:107–111. doi:http://dx.doi.org/10.1016/S0257-8972(03)00422-5

Hadsund P (1993) The tin-mercury mirror: its manufacturing technique and deterioration processes. Stud Conserv 38:3–16. doi:10.1179/sic.1993.38.1.3

Han J, Young D, Colijn H, Tripathi A, Nešić S (2009) Chemistry and structure of the passive film on mild steel in CO_2 corrosion environments. Ind Eng Chem Res 48:6296–6302. doi:10.1021/ie801819y

Herrera LK, Duran A, Franquelo M, Gonzales-Elipe A, Espinos J, Rubio-Zuazo J, Castro G, Justo A, Perez-Rodriguez JL (2008a) Study by grazing incident diffraction and surface spectroscopy of amalgams from ancient mirrors. Open Chemistry 7:47–53

Herrera LK, Duran A, Franquelo ML, de Haro MCJ, Erbez AJ, Perez-Rodriguez JL (2008b) Studies of deterioration of the tin–mercury alloy within ancient Spanish mirrors. J Cult Heritage 9(Supplement):e41–e46. doi:10.1016/j.culher.2008.06.007

Herrera LK, Justo A, Perez-Rodriguez JL (2009) Study of nanocrystalline SnO_2 particles formed during the corrosion processes of ancient amalgam mirrors. J Nano Res 8:99–107

Hiorns AH (1911) Metal-colouring and bronzing. MacMillan & Co, London

Hollner S, Mirambet F, Rocca E, Reguer S (2010) Evaluation of new non-toxic corrosion inhibitors for conservation of iron artefacts. Corros Eng Sci Technol 45:362–366. doi:10.1179/147842210x12732285051311

Hughes R, Rowe M (1982) The colouring, bronzing and patination of metals. Crafts Council, London

Ingo GM, De Caro T, Riccucci C, Angelini E, Grassini S, Balbi S, Bernardini P, Salvi D, Bousselmi L, Cilingiroglu A, Gener M, Gouda VK, Al Jarrah O, Khosroff S, Mahdjoub Z, Al Saad Z, El-Saddik W, Vassiliou P (2006) Large scale investigation of chemical composition, structure and corrosion mechanism of bronze archeological artefacts from Mediterranean basin. Appl Phys A-Mater Sci Process 83:513–520. doi:10.1007/s00339-006-3550-z

Kashima K, Hara S, Kishikawa H, Miyuki H (2001) Evaluation of protective ability of rust layers on weathering steels by potential measurement. Corros Eng 49:25–37

Leon Y, Saheb M, Drouet E, Neff D, Foy E, Leroy E, Dynes JJ, Dillmann P (2014) Interfacial layer on archaeological mild steel corroded in carbonated anoxic environments studied with coupled micro and nano probes. Corros Sci 88:23–35. doi:10.1016/j.corsci.2014.07.005

Leroy S, L'Héritier M, Delqué-Kolic E, Dumoulin J-P, Moreau C, Dillmann P (2015) Consolidation or initial design? Radiocarbon dating of ancient iron alloys sheds light on the reinforcements of French Gothic Cathedrals. J Archaeol Sci 53:190–201. doi:10.1016/j.jas.2014.10.016

Leskelä M, Ritala M (2002) Atomic layer deposition (ALD): from precursors to thin film structures. Thin Solid Films 409:138–146. doi:10.1016/S0040-6090(02)00117-7

Marquardt AE, Breitung EM, Drayman-Weisser T, Gates G, Phaneuf RJ (2015) Protecting silver cultural heritage objects with atomic layer deposited corrosion barriers. Heritage Sci 3:1–12. doi:10.1186/s40494-015-0066-x

Matero R, Ritala M, Leskelä M, Salo T, Aromaa J, Forsén O (1999) Atomic layer deposited thin films for corrosion protection. J Phys IV France 09:Pr8–493–Pr8–499. doi:10.1051/jp4:1999862

Matthiesen H, Gregory D, Jensen P, Sørensen B (2004a) Environmental monitoring at Nydam, a waterlogged site with weapon sacrifices from the Danish Iron age. I: a comparison of methods used and results from undisturbed conditions. J Wetland Archaeol 4:55–74

Matthiesen H, Salomonsen E, Sørensen B (2004b) The use of radiography and GIS to assess the deterioration of archaeological iron objects from a water logged environment. J Archaeol Sci 31:1451–1461

Michelin A, Drouet E, Foy E, Dynes JJ, Neff D, Dillmann P (2013) Investigation at the nanometer scale on the corrosion mechanisms of the archaeological ferrous artifacts by STXM. J Anal At Spectrom 28:59–66

Monnier J, Dillmann P, Legrand L, Guillot I (2010a) Corrosion of iron from heritage buildings: proposal for degradation indexes based on rust layer composition and electrochemical reactivity. Corros Eng Sci Technol 45:375–380

Monnier J, Neff D, Réguer S, Dillmann P, Bellot-Gurlet L, Leroy E, Foy E, Legrand L, Guillot I (2010b) A corrosion study of the ferrous medieval reinforcement of the Amiens cathedral. Phase characterisation and localisation by various microprobes techniques. Corros Sci 52:695–710

Monnier J, Guillot I, Legrand L, Dillmann P (2013) Reactivity studies of atmospheric corrosion of heritage iron artefacts. In: Dillmann P, Watkinson D, Angelini E, Adriens A (eds) Corrosion and conservation of cultural heritage metallic artefacts. Woodhead Publishing, Oxford, pp 285–310

Muller J, Lorang G, Leroy E, Laik B, Guillot I (2010) Electrochemically synthesised bronze patina: characterisation and application to the cultural heritage. Corros Eng Sci Technol 45:322–326. doi:10.1179/147842210X12692706339265

Muller J, Laïk B, Guillot I (2013) α-CuSn bronzes in sulphate medium: influence of the tin content on corrosion processes. Corros Sci 77:46–51. doi:10.1016/j.corsci.2013.07.025

Neff D, Dillmann P, Bellot-Gurlet L, Beranger G (2005) Corrosion of iron archaeological artefacts in soil: characterisation of the corrosion system. Corros Sci 47:515–535. doi:10.1016/j.corsci.2004.05.029

Paussa L, Guzman L, Marin E, Isomaki N, Fedrizzi L (2011) Protection of silver surfaces against tarnishing by means of alumina/titania-nanolayers. Surf Coat Technol 206:976–980. doi:10.1016/j.surfcoat.2011.03.101

Pourbaix M (1977) Electrochemical corrosion and reduction. Corrosion and metal artifatcs : a dialogue between conservators and archaeologists 1–16

Puurunen RL (2005) Surface chemistry of atomic layer deposition: a case study for the trimethylaluminum/water process. J Appl Phys. doi:10.1063/1.1940727

Rangel CM, Fonseca IT, Leitão RA (1986) Some aspects of the electrochemical behaviour of mild steel in carbonate/bicarbonate solutions. Electrochim Acta 31:1659–1662. doi:10.1016/0013-4686(86)87089-X

Robbiola L, Blengino J-M, Fiaud C (1998) Morphology and mechanisms of formation of natural patinas on archaeological Cu–Sn alloys. Corros Sci 40:2083–2111. doi:10.1016/S0010-938X(98)00096-1

Saheb M, Descostes M, Neff D, Matthiesen H, Michelin A, Dillmann P (2010a) Iron corrosion in an anoxic soil: comparison between thermodynamic modelling and ferrous archaeological artefacts characterised along with the local in situ geochemical conditions. Appl Geochem 25:1937–1948. doi:10.1016/j.apgeochem.2010.10.010

Saheb M, Neff D, Demory J, Foy E, Dillmann P (2010b) Characterisation of corrosion layers formed on ferrous artefacts buried in anoxic media. Corros Eng Sci Technol 45:381–387

Schlegel ML, Bataillon C, Benhamida K, Blanc C, Menut D, Lacour J-L (2008) Metal corrosion and argillite transformation at the water-saturated, high-temperature iron–clay interface: a microscopic-scale study. Appl Geochem 23:2619–2633

Schlegel ML, Bataillon C, Brucker F, Blanc C, Prêt D, Foy E, Chorro M (2014) Corrosion of metal iron in contact with anoxic clay at 90 °C: characterization of the corrosion products after two years of interaction. Appl Geochem 51:1–14

Scott D, Eggert G (2009) Iron and steel in art: corrosion, colorants, conservation. Archetype Publications Ltd, Plymouth

Selwyn LS, Binnie NE, Poitras J, Laver ME, Downham DA (1996) Outdoor bronze statues: analysis of metal and surface samples. Stud Conserv 41:205–228. doi:10.1179/sic.1996.41.4.205

Shashoua Y, Matthiesen H (2010) Protection of iron and steel in large outdoor industrial heritage objects. Corros Eng Sci Technol 45:357–361. doi:10.1179/147842210X12710800383648

Spoto G, Ciliberto E, Allen GC, Younes CM, Piccardo P, Pinasco MR, Stagno E, Ienco MG, Maggi R (2000) Chemical and structural properties of ancient metallic artefacts: multitechnique approach to study of early bronzes. Br Corros J 35:43–47

Stratmann M (1987) The investigation of the corrosion properties of metals, covered with adsorbed electrolyte layers—a new experimental technique. Corros Sci 27:869–872

Stratmann M, Streckel H (1990) On the atmospheric corrosion of metals which are covered with thin electrolyte layers—II. Experimental results. Corros Sci 30:697–714

Stratmann M, Streckel H, Kim KT, Crockett S (1990) On the atmospheric corrosion of metals which are covered with thin electrolyte layers—III. The measurement of polarisation curves on metal surfaces which are covered by thin electrolyte layers. Corros Sci 30:715–734

Wang C, Lu B, Zuo J, Zhang S, Tan S, Suzuki M, Chase WT (1995) Structural and elemental analysis on the nanocrystalline SnO_2 in the surface of ancient Chinese black mirrors. Nanostruct Mater 5:489–496. doi:10.1016/0965-9773(95)002

Alkaline Nanoparticles for the Deacidification and pH Control of Books and Manuscripts

Piero Baglioni, David Chelazzi, Rodorico Giorgi, Huiping Xing and Giovanna Poggi

Abstract Manuscripts and books are susceptible to fast degradation owing to the presence of detrimental components used in the papermaking techniques, and to the action of environmental pollutants. As a result, the acidity of documents increases, promoting the acid-catalyzed depolymerization of cellulose. The latter process strongly reduces the mechanical properties of paper, reducing its long-term resistance to natural aging. The presence of inks concurs to degradation, making the conservation of manuscripts particularly demanding. In this chapter, the use of dispersions of alkaline earth metal hydroxide nanoparticles will be discussed as a method for counteracting the degradation of paper. These systems have proven efficient for the deacidification of cellulose-based artifacts, providing a mild alkaline buffer and maintaining a stable neutral environment. The palette of formulations nowadays available to conservators includes systems designed for the treatment of manuscripts featuring metal gall inks and modern industrial inks.

1 Introduction

This chapter provides an overview on the use of nanomaterials, in particular dispersions of alkaline nanoparticles in non aqueous media, for the preservation of cellulose-based artifacts, such as those commonly found in archives, libraries, museums and private collections. First, a brief introduction will be given on cellulose chemistry and on degradation mechanisms both in acidic and in alkaline environments. We will focus on factors that influence the aging of books and manuscripts, in particular the presence of iron gall inks and their detrimental action on paper. Then the traditional conservation treatments will be discussed before describing the advantages of the methodologies developed in the framework of Colloids and Nanosciences. The syntheses, stabilization, and characterization of

P. Baglioni (✉) · D. Chelazzi · R. Giorgi · H. Xing · G. Poggi
Department of Chemistry and CSGI, University of Florence,
via della Lastruccia 3, 50019 Florence, Italy
e-mail: baglioni@csgi.unifi.it

P. Dillmann et al. (eds.), *Nanoscience and Cultural Heritage*,
DOI 10.2991/978-94-6239-198-7_9

alkaline nanoparticles dispersions will be outlined, and applicative aspects will be illustrated in the Case Studies Sect. (5.4).

2 Chemistry and Degradation of Cellulose-Based Material

Cellulose based-materials are largely present in the cultural patrimony of all civilizations. Paper, canvas, and wood objects constitute a significant amount of the documentary, historical, and artistic heritage that needs to be preserved and transferred to future generations. Authors belonging to different countries worldwide have brought this issue to the attention of the scientific and conservation communities (Dobrodskaya et al. 2004; Strlič and Kolar 2005; Wouters 2008; Yanjuan et al. 2013; Afsharpour and Hadadi 2014). Before discussing the use of nanomaterials for the conservation of cellulose-based artifacts, a brief introduction on the properties and degradation pathways of cellulose will be given.

2.1 Cellulose Chemistry

Cellulose is a linear polymer naturally found in the walls of plants cells and plays a fundamental role in determining the mechanical properties of vegetal tissues. Cellobiose, which is the repeating unit of cellulose, consists of two molecules of D-glucose, linked through a β-1,4-glycosidic bond formed upon condensation. One of the most important parameters in evaluating the conservation status of cellulose-based artifacts is the degree of polymerization (DP), which is defined as the average number of monomer units for cellulose chain. The degree of polymerization of native cellulose depends upon the vegetal species, ranging between 9000 and 15,000 (Fengel and Wegener 1984). Typically, the manufacturing process of cellulose, i.e. its extraction from wood, significantly reduces the original DP. It is worth noting that the mechanical properties of the polymer are related to the average chain length; for instance, if DP decreases down to 300, which is a possible value for aged cellulose in historical objects, the resistance is dramatically reduced resulting in mechanical failure (crumbling, rupture).

The supramolecular structure of cellulose is due to hydrogen bonds formed between hydroxyl groups either of the same chain (intramolecular bonds) or of different chains (intermolecular bonds). Hydroxyl groups can also give hydrogen bonds to water molecules, accounting for the hygroscopicity of cellulose, whose average water content is 6–7 % (w/w) at standard conditions. Hydrophobic interactions also contribute to the network of bonds and their importance in determining the solubility of cellulose has been recently discussed (Medronho et al. 2012; Glasser et al. 2012). Overall, the polymer chains are organized into a hierarchical

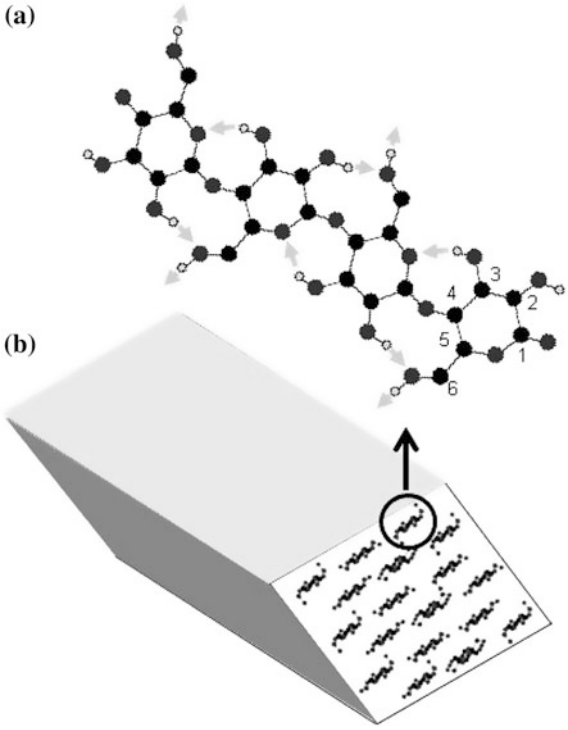

Fig. 1 **a** Structure of a single cellulose chain. *Gray arrows* indicate the hydrogen bonds **b** a cellulose Iβ microfibril, composed by single cellulose chains. (Reprinted from Altaner et al. (2014)

structure. The chain network exhibits both amorphous and crystalline regions (Nisizawa 1973). Elementary fibrils are formed by a succession of highly crystalline sites (crystallites) and amorphous zones. The elementary fibrils are in turn bound to form microfibrils (see Fig. 1). The latter are arranged into fibrils and fibers, to create the cellulose network of paper, canvas and wood.

Degradation via hydrolysis and oxidation is known to affect amorphous regions first, as the crystallites are less accessible to degradation agents. As a matter of fact, the acid-catalyzed hydrolysis of β-1,4-glycosidic bonds can proceed up to complete depolymerization of the amorphous zones, leaving the crystallites to set a lower DP limit, known as Levelling-off Degree of Polymerization (LODP) (Calvini 2005), which can be seen as a watershed between amorphous and crystalline regions of cellulose (Calvini 2014).

The crystalline structure of cellulose has been widely studied starting from the second half of the 20th century (Wilkie 1961). The structure established by von Nägeli in 1858 was confirmed by Meyer and Misch through X-ray crystallography (Meyer and Misch 1937). Four different crystalline allomorphs have been identified (Cellulose I–IV), cellulose I being the most abundant in nature. It is well known (Atalla and Vanderhart 1984) that the crystalline structure of cellulose I is composed of celluloses Iα (triclinic) and Iβ (monoclinic), whose relative amount depends on the original source. Cellulose crystallites are usually about 5 nm in

width. The relative amount of crystalline portions is defined by the crystallinity index (CI), and typically ranges from 50 to 90 %, depending on the cellulose source and on the measurement method (Park et al. 2010).

2.2 Reactions in Acidic Medium

The main reaction that takes place in acidic media is the acid-catalyzed hydrolysis of β-1,4-glycosidic bonds, leading to the depolymerization of cellulose and, macroscopically, to the loss of mechanical properties of the polymer. Beside the concentration of hydrogen ions, several factors concur to speed up the reaction, including temperature, and relative humidity. It is worth noting that the scission of glycosidic bonds occurs even at room temperature, posing a threat to the conservation of any cellulose-based artworks. The acid-catalyzed hydrolysis (see Fig. 2) can be described as a three-step process where (i) a hydrogen ion interacts with a glycosidic oxygen, forming a conjugate acid; (ii) the glycosidic bond is cleaved (a water molecule is required) and a cyclic carbocation is formed; (iii) the electron couple of the water molecule flips to the carbocation and a new hydrogen ion is available for further reaction (Harris 1975; Banait and Jencks 1991; Zhang et al. 1994; Lundgaard et al. 2004).

Degradation in acidic environments is also due to oxidation, which is interconnected to acid-catalyzed hydrolysis. Oxidized groups on cellulose chains are

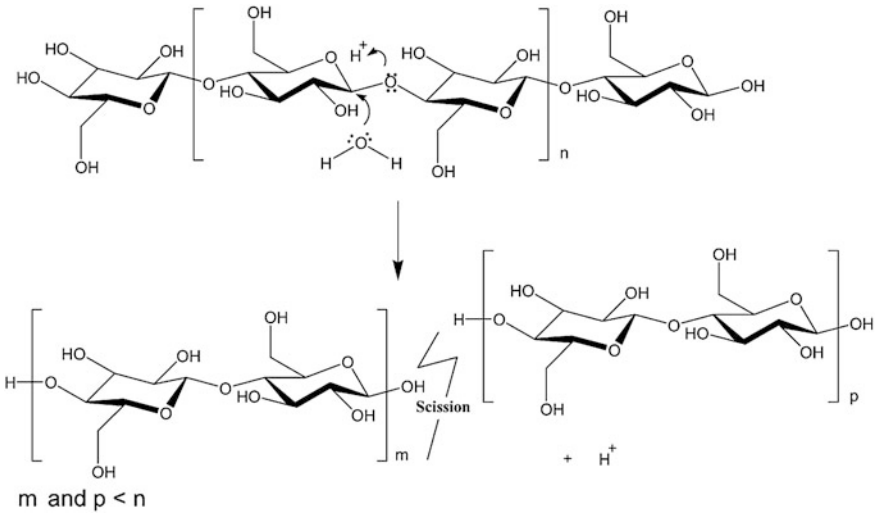

Fig. 2 Acid-catalyzed hydrolysis of β(1-4)-glycosidic bonds in cellulose. (Reproduced from Sequeira et al. (2006). Copyright © 2006 Elsevier Masson SAS. All rights reserved)

unstable in acidic conditions, favoring scission of bonds even at room temperature (Calvini et al. 2008). Oxidation of cellulose chains can also result in the production of acids, including glucuronic, glucaric, uronic and aldaric acids that promote hydrolysis in the so-called *spiraling effect* (Shanani and Harrison 2002). Conjugated carbonyl and carboxyl compounds formed during degradation are chromophores responsible for browning of aged paper (Bronzato et al. 2013).

Volatile acids are developed during the aging of cellulose-based material and, if not removed, result in an autocatalytic degradation process (Calvini et al. 2008). This can be the case in sealed environments, for instance when books are tightly packed in shelves (Carter et al. 2000). Instead, the removal of volatile acids leads to an auto retardant degradation process (Calvini et al. 2008).

2.3 Reactions in Alkaline Medium

Polysaccharides are affected by concentrated alkaline solutions at high temperature, the main steps being: (i) dissolution of polysaccharides; (ii) peeling of end-groups; (iii) alkaline hydrolysis of acetyl groups and glycosidic bonds; (iv) degradation of dissolved polysaccharides and peeled monosaccharides (Rydholm 1965; Sjostrom 1977).

Through the well-known β-alkoxy elimination mechanism, an alkali attacks a hydrogen atom in position α to carbonyl groups and, as a result, the group in position β is eliminated, leading to the peeling of the cellulose chain (Strlič et al. 1998; Santucci and Zappalà 2001). On undegraded cellulose, only carbonyls at the end of each chain are affected by this mechanism, with no dramatic consequences in terms of DP decrease. On the other hand, oxidized cellulose is very sensitive to alkaline solutions even at room temperature (Calvini et al. 1988), and the β-alkoxy elimination causes the random cleavage of polymeric chains (see Fig. 3).

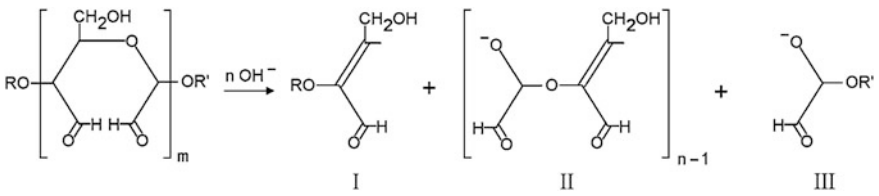

Fig. 3 Fragmentation of oxidized cellulose due to β-alkoxy elimination. (Reprinted with kind permission from Springer Science + Business Media. Calvini and Gorassini (2012), Fig. 1)

3 Factors Affecting Books and Manuscripts Degradation

The degradation of archival material is due to several factors that are either internal, i.e. related to the presence of detrimental compounds from making processes, original components or even past conservation treatments, or external, i.e. environmental factors.

3.1 External Factors

There are many environmental factors that can affect paper stability. Merely day light, in combination with temperature and oxygen, plays a fundamental role in the degradation of cellulose (McKellar and Allen 1979; Feller 1994; Zervos 2010). In particular, the interaction between light and cellulose leads to the oxidation of functional groups and to the formation of oxidized compounds, as described above. At the macroscopic scale, these phenomena result in the typical browning of paper. Air pollutants such as sulfur and nitrogen oxides hydrate in moisture within cellulose fibers and form acids that promote hydrolysis (Carter 1989). The migration of degrading compounds from packing materials, cardboard as well as furniture, cabinet, and cases, in particular if treated with poly vinyl acetate based coatings, is another factor to be taken into account (Tétreault and Stamatopoulou 1997; Carter et al. 2000; Tétreault 2003). In fact, it has been shown that detrimental organic compounds can also be found inside microclimate frames (Lopez-Aparicio et al. 2010; Grøntoft et al. 2010). Environmental factors also include the attack of cellulose by fungi and bacteria, both aerobic and anaerobic, for instance through the use of hydrolytic enzymes (Coughlan 1991).

3.2 Internal Factors

The internal factors affecting paper stability include the quality of raw materials, as well as the presence of compounds introduced during the manufacturing processes. For instance, the purity and crystallinity of cellulose are important parameters in determining its resistance to degradation, as mentioned above. Up to 19th century, papers were obtained from cotton and linen rags, which are mainly composed of cellulose. On the other hand, the onset of the large-scale production of paper gradually imposed the use of wood as a raw material. This involves several conservation issues: (i) both lignin oxidation products and residual chemicals from the pulping and bleaching processes can increase the intrinsic acidity of paper; (ii) paper sheets made from chemical and mechanical pulp, containing considerable amount of lignin, tend to absorb more SO_2 from polluted atmosphere than lignin-free paper (Bégin et al. 1998; Tse et al. 2002).

Regarding the manufacturing processes, it must be considered that, from the beginning of the 19th century until the mid 20th, papermaking used alum and rosin for the sizing of paper sheets. Both materials are major sources of acidity, and Chamberlain (2007) showed that the reactivity of aluminum salts in catalyzing the degradation of cellulose can be predicted with reference to the aqueous chemistry of aluminum ions. In fact, it is interesting to note that gelatin, historically used in combination with alum, has anionic groups capable of interacting with aluminum cations, and this could hinder the degrading action of alum on paper (Dupont 2002).

3.2.1 Iron Gall Ink

Iron gall inks have been widely used since the 5th century up to the 20th, when organic dyes and pigments replaced them. Throughout the centuries, a number of recipes have been used to prepare these inks, the main components being: (i) gall nuts, from which tannic acid was extracted; (ii) iron or copper sulfate; (iii) vinegar or wine; (iv) water; (v) arabic gum as a binder (Lucarelli and Mandò 1996; Neevel et al. 1999). Metal gall inks, which include formulations with iron and copper, contain several compounds that are detrimental to cellulose. Gallic acid, coming from hydrolization of tannic acid, reacts with iron(II) sulfate to form sulfuric acid and iron(III) pyrogallate complex that provides color to the ink (Neevel et al. 1999). Sulfuric acid catalyzes the hydrolysis of cellulose and causes its oxidation. Iron sulfate was used in excess in traditional recipes, and the iron ions that are not involved in the formation of the coloring complex promote the formation of hydrogen peroxide in acidic environment:

$$\begin{aligned} &Fe^{2+} + O_2 + H^+ \rightarrow Fe^{3+} + HOO^{\cdot} \\ &Fe^{2+} + HOO^{\cdot} + H^+ \rightarrow Fe^{3+} + H_2O_2 \end{aligned}$$ Formation of peroxides in acidic environment

Moreover, free iron ions are also involved in the formation of hydroxyl radicals through a mechanism known as Fenton reaction, which requires the presence of hydrogen peroxide:

$$Fe^{2+} + H_2O_2 \rightarrow Fe^{3+} + OH^- + OH^{\cdot} \quad \text{Fenton reaction}$$

Both hydroxyl radicals and hydrogen peroxide oxidize cellulose. A similar reaction, called Fenton-like, describe the production of hydroxyl radicals in the presence of copper ions:

$$Cu^+ + H_2O_2 \rightarrow Cu^{2+} + OH^- + OH^{\cdot} \quad \text{Fenton-like reaction}$$

Iron and copper ions are transition metal that can easily change their oxidation state by reacting, for instance, with cellulose reducing groups, creating a cyclic process. It is worth noting that Šelih et al. (2007) showed that copper ions are far more active than other transition metals in the oxidative degradation of cellulose.

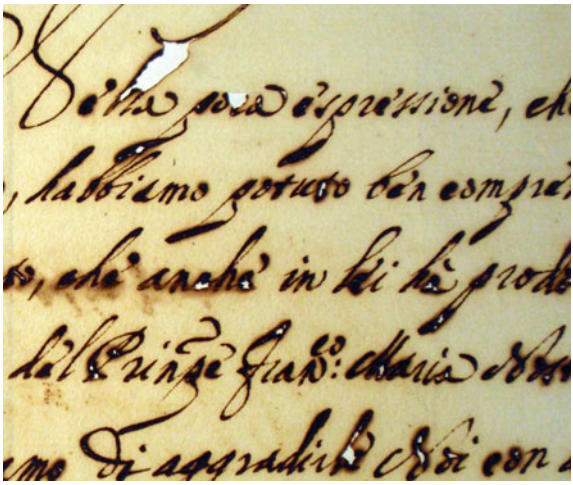

Fig. 4 18th century manuscript featuring iron gall ink. Corrosion of paper due to the writing fluid is evident. (Reprinted with permission from Poggi et al. (2010). Copyright © (2010) American Chemical Society)

Not surprisingly, documents featuring metal gall inks typically show severe degradation in the form of cellulose corrosion, and paper perforation, in particular in correspondence to the inked areas (see Fig. 4).

4 State-of-the-Art Methods for the Conservation of Cellulose-Based Artworks

Besides preventive measurements, such as the choice of appropriate display materials and storage conditions, several conservation strategies have been developed for counteracting cellulose oxidation and hydrolysis. These include deacidification treatments and antioxidants, even if there is a strong interest in finding a single method capable of hindering both degradation mechanisms in one step.

4.1 Deacidification Treatments

There is a long tradition on deacidification in the conservation practice, and conservation scientists have developed and proposed many methodologies throughout the last decades (Baty et al. 2010). Neutralization of acidity needs to be achieved because in neutral conditions both the random cleavage of cellulose chains catalyzed by acids and the oxidation reactions favored by an acidic environment proceed at a much slower pace. Hydroxides, applied directly or formed in situ, are used to neutralize acidity on the substrates. Sometimes, carbonates or bicarbonates are directly used as milder neutralizing agents. Deacidification methods should use solvents that are neither toxic to the operator nor dangerous for the environment.

Moreover, the deacidification treatment must be physically and chemically compatible with the substrate and its components, i.e. sizing, fillers, inks etc., which means that the treatment must not produce any undesired alteration of the substrate's original characteristics. To this end, it is important to carry out preliminary tests to evaluate the compatibility between the neutralizing system and the object to be treated. The cost of a deacidification treatment is a crucial factor in most conservation scenarios. For instance, when entire library or archival collections need to be neutralized, interventions on single paper sheets are simply not feasible. Therefore mass deacidification methodologies were developed in order to keep the costs low and increase the number of books deacidified with a single intervention. Mass deacidification methods are typically based on non-aqueous solvents that produce fewer undesired effects than water. In the next sections we will briefly introduce the most important and common deacidification methods in conservation practice.

4.1.1 Aqueous Treatments

During aqueous deacidification treatments, paper sheets (separated from the binding) are either immersed into the neutralizing solution or sprayed with it (Barrow and Sproull 1959); aqueous solutions of calcium (or magnesium) bicarbonate and calcium hydroxide are commonly used. Neutralization of cellulose-based material by aqueous alkaline treatments is very effective because of the high mobility of the hydroxide ions.

Moreover, aqueous treatments can improve the visual aspect of samples owing to direct washing of hydro-soluble dirt and of sizing compounds usually involved in the browning of paper (Sequeira et al. 2006); in fact, a resizing bath is usually needed after aqueous treatments (Giorgi et al. 2005).

On the other hand, aqueous treatments also show severe drawbacks.

Any excess of free hydroxide ions will readily interact with cellulose, which might be depolymerized and degraded in highly alkaline aqueous environments as described in the previous sections. Besides, both the aqueous medium and the alkaline environment can lead to the removal of original material (inks, sizing), and in some cases to ink discoloration due to the decomposition of the ink complex (Kolar 1997; Neevel 2000; Malesič et al. 2002; Sequeira et al. 2006; Stefanis and Panayiotou 2007).

4.1.2 Non Aqueous Treatments

Non-aqueous wet treatments are based on neutralizing agents dispersed or dissolved in solvents that are less polar than water, in order to limit or completely avoid ink bleeding or solubilization of sizing and other hydrophilic paper components (Sequeira et al. 2006). The most inert solvents are usually employed in mass deacidification methods.

The Bookkeeper

The Bookkeeper (Preservation Technologies, L.P.) is a commercial dispersion of micron-sized particles of MgO (concentration of about 4 g/L) in a blend of perfluoroalkanes. Fluorinated solvents are completely inert to paper components, including modern inks. However, the stabilization of magnesium oxide microparticles in the dispersing media requires several additives, including surfactants, probably either a perfluorinated Mg-soap, a perfluoropolyether derivative or a non-ionic fluorinated acyl ester (Zumbühl and Wuelfert 2001).

After the application, magnesium oxide is converted into hydroxide in contact with moisture; the hydroxide neutralizes acidity and, if in excess, forms a carbonate buffer against recurring acidity.

The Bookkeeper is available for single sheet deacidification, i.e. spray products, or for mass deacidification. The latter has been used in the National Congress Library of Washington, D.C., since its development in 1992.

Although it presents several advantages over conventional deacidification methods, Bookkeeper also shows some drawbacks: for instance, its application is discouraged on low porosity material, on highly calendered paper, and on black and dark colored substrates due to the fact that the micro-particles do not penetrate easily through the fiber network, resulting in light whitening of the documents surface (Pauk 1996; Boone et al. 1998), see for instance Fig. 5.

The influence of surfactants on the neutralization process has been studied by Zumbühl and Wuelfert (2001) that showed how the presence of a hydrophobic coating hampers the reactivity of magnesium oxide. Slow conversion of magnesium hydroxide into carbonate might create a too alkaline environment that could be

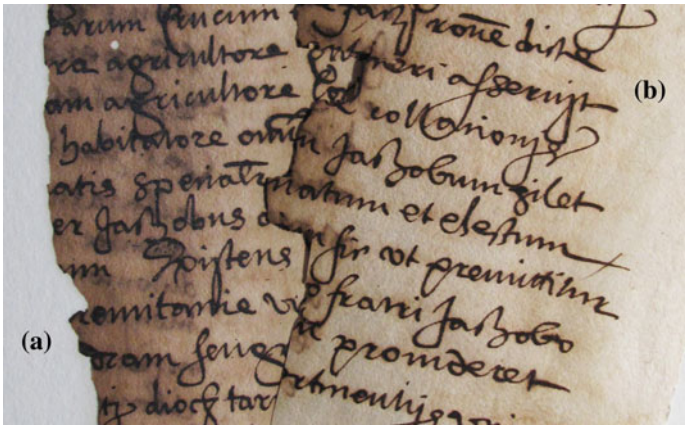

Fig. 5 **a** Bookkeeper application on a 16th century manuscripts. A white haze is visible where MgO microparticles were sprayed. **b** The same sample treated with $Ca(OH)_2$ nanoparticles, showing no white haze. [Printed with the kind permission of SELIDO (at IPCE, Instituto del Patrimonio Cultural de España, Madrid)]

risky for the cellulose fibers. Despite these drawbacks, Bookkeeper is widely used and it is one of the best non-aqueous mass deacidification treatments available.

The Battelle or Papersave Process

The National German Library, back in 1987, asked the Battelle Ingenieurtechnik GmbH to investigate different deacidification methods and to develop an innovative system. In 1994, the Battelle process was tested and approved by the Library; the treatment was based on a combination of magnesium ethoxide and titanium alkoxides in hexadimethyl disiloxane (HMDO), a colorless organic silicon compound. The complex formulation is referred to as METE (Magnesium Ethoxide Titanium Ethoxide). Some authors also reported that a surfactant is added to the system to improve paper impregnation (Dufour and Havermans 2001). Magnesium ethoxide reacts with moisture to form magnesium hydroxide that neutralizes cellulose acidity and, if present in excess, is transformed into carbonate by reaction with carbon dioxide. Titanium ethoxide, on the other hand, hydrates to form titanium oxide and water, thus not contributing to the deacidification process (Blüher and Grossenbacher 2006). In fact, the role of titanium alcoholate is to increase the solubility of magnesium ethoxide in HMDO. This method is also known as Papersave and is currently being developed by the German company ZFB. Finally, the Ink save process targets ink corrosion through the use of neutralizing agents (calcium and magnesium alkoxides) in conjunction with quaternary ammonium halides as antioxidants (Baty et al. 2010).

4.2 Anti-oxidants

In the field of conservation science, only a limited number of reducing agents, namely mild agents, can be applied on paper in order to preserve the status of the fibers. In this regard, borane amine complexes, where the high boron reactivity is reduced by complexation with nitrogen, are thought to reduce oxidized groups. In particular, the borane tert-butylamine complex in a non-aqueous solvent, has been widely used in the ICRCPAL Laboratories of Rome (previously known as ICPL) as a reducing agent for carbonyl functionalities (Bicchieri and Brusa 1997; Bicchieri et al. 1999, 2000). More recently, its capability of neutralizing carboxyl groups has been evaluated (Sanna et al. 2009) with the aim of developing a single treatment for inhibiting acid-catalyzed hydrolysis and oxidation of paper. Further data are needed to confirm these interesting preliminary results (Sanna et al. 2009).

Alternatively, J. Neevel proposed the usage of phytates as metal deactivators capable of inhibiting metal gall ink corrosion, back in 1995 (Neevel 1995). Phytate is the commonly used term to indicate myo-inositol hexaphosphate that is the salt of myo-inositol hexaphosphoric acid, a substance present in various food of plant

origin. Being a metal deactivator, phytate reduces the oxidizing potential of iron(II) ions, inhibiting its oxidation to iron(III), hence hampering the Fenton reaction.

The method has become popular among conservators and many scientific papers have been published on the subject (Neevel 2000; Botti et al. 2005; Kolar et al. 2005; Zappalà and Stefani 2005; Henniges et al. 2008; Potthast et al. 2008). More recently, J. Kolar proposed the usage of magnesium phytate (Kolar et al. 2007), which can be completely dissolved at standard working conditions, avoiding the risk of forming surface deposits.

According to Kolar et al. (2003), the chelating action of phytate is specific to iron ions, which could hinder the effectiveness of the method in the presence of metal gall inks containing substantial amount of copper ions. However, some authors reported that phytate copper ions complexes are very stable between pH 5 and 7 (Persson et al. 1998). In fact, the phytate treatment increased the resistance to aging of paper featuring metal gall inks with both copper and iron ions (Henniges et al. 2008). Treatment with phytate does not hamper acid-catalyzed hydrolysis of cellulose, therefore, a subsequent deacidification treatment is carried out commonly using calcium hydrogen carbonate aqueous solutions.

In recent years, Kolar et al. proposed the application of quaternary ammonium halides that are specifically designed for the inhibition of cellulose oxidation induced by metal gall inks. Halides are known to act as antioxidants, as they are catalytic peroxide decomposers; therefore they can limit the degradation of paper that contains metal gall inks, regardless of the transition metal ions contained in the inks. The first new antioxidant proposed was tetrabutylammonium bromide (TBABr) (Kolar et al. 2003). In 2005, experimental data acquired on several quaternary ammonium halides showed that the efficiency of the treatment is related to the size of the associated cation. In particular, halides with large counter ions were demonstrated to be more efficient in hampering cellulose degradation; among the tested quaternary ammonium halides, TBABr and TBACl (tetrabutylammonium chloride), in water and dichloromethane, resulted the best systems for the preservation of inked paper (Malešič et al. 2005a, b). More recently, the usage of alkylimidazolium halides and alkaline compounds (i.e. magnesium and calcium ethoxide in ethanol) has been proposed (Kolar et al. 2008). This method is interesting as it combines deacidification with antioxidants in a low-polar system.

5 Alkaline Nanoparticles for pH Control

As highlighted in the previous sections, the ideal deacidification treatment must fulfill several requirements in terms of effectiveness, physico-chemical compatibility with the artifacts, feasibility, and low impact both on the operator and the environment. In this sense, a significant contribution to the development of advanced solutions has come from colloids and nanoscience. The first works date back to the early 2000s, and introduced the use of nanoparticles of alkaline earth metal hydroxides as neutralizing agents for paper and canvas (Giorgi et al. 2002a, b, 2005).

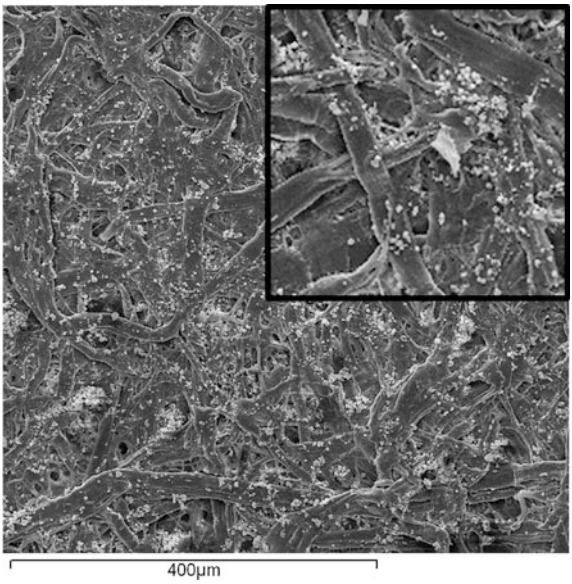

Fig. 6 SEM image of calcium hydroxide nanoparticles adhering to cellulose fibers; the panel in the right upper corner is an enlargement (2-fold). (Adapted with permission from Baglioni et al. (2013). Copyright © (2013) American Chemical Society)

In fact, using these hydroxides as nanoparticles dispersed in carrier solvents (e.g. short chain alcohols or less polar solvents) avoids the limitations typically involved in the state-of-the-art deacidification methods. First, the possibility of dispersing solid particles stably in a solvent allows for overcoming the solubility limit of hydroxides and carbonates commonly applied for neutralizing acidity in aqueous treatments. Moreover, hydroxide ions are released more gradually and have less mobility in nanoparticles dispersions as opposed to aqueous solutions, where free and highly mobile OH^- ions in excess are immediately disposable for interaction with alkali-sensitive cellulose (Calvini et al. 1988). The size of the particles plays a fundamental role: for instance, the surface area of a spherical microparticle (diameter of 1 µm) can be increased by a factor 10 dividing the same mass into spherical nanoparticles (diameter of 100 nm). A higher surface area grants higher reactivity to acids and carbon dioxide. The latter transforms the excess of hydroxides in carbonates, which are milder deacidifying agents that remain as a buffer against reoccurring acidity. Reducing the size of particles also allows obtaining stable dispersions in several solvents without using stabilizers (e.g. surfactants). Finally the reduced size favors penetration of the particles and limits the formation of surface deposit, such as white veils. The particles distribute homogeneously and adhere to cellulose fibers (see Fig. 6), possibly favored by the interaction between the positively charged surface of the particles and hydroxyl groups on cellulose (Giorgi et al. 2002a).

For what concerns the solvents, short chain alcohols were initially selected (and are still used) as dispersing media because they exhibit several advantages: (i) they exhibit good wetting properties; (ii) they favor the dispersion of nanoparticles, probably due to the presence of a hydrophobic layer on the surface of the particles;

this layer is formed upon physisorption of the alcohol hydroxyl group on the surface of particles (Ambrosi et al. 2001), resulting in inhibition of the particles face-to-face sticking (Fratini et al. 2007).

In the next sections, we will illustrate the main synthetic routes of nanoparticles dispersions, as well as the characterization of these systems and their application to deacidification of works of art throughout the last 15 years.

5.1 Synthesis of Alkaline Nanoparticles Dispersions

Several different strategies can be used to prepare inorganic particles. Synthetic methods are usually divided into top-down and bottom-up, based respectively on breaking particles down to the nanoscale, or on building up nanoparticles atom by atom (or molecule by molecule). A detailed description of the methods for the preparation of inorganic nanoparticles is beyond the scope of this chapter. Therefore, in this section, we will focus on the synthetic routes of alkaline nanoparticles for the pH control of cellulose-based artworks.

A bottom-up synthesis of calcium hydroxide nanoparticles from aqueous homogenous phase was the first method used for the preparation of an alkaline system to be used on paper and canvas artifacts (Giorgi et al. 2002a). Particles were obtained by adding an aqueous solution of sodium hydroxide to an aqueous solution of calcium chloride, both kept at 90 °C. The supersaturation degree (S) of the resulting solution was kept high, S being defined as:

$$S = \frac{\left[Ca^{2+}\right]}{\left[Ca^{2+}\right]_{sat}}$$

where $[Ca^{2+}]_{sat}$ is the concentration of Ca^{2+} ions in the $Ca(OH)_2$ saturated solution. High values of S promote the nucleation of particles rather than their growth, leading to the formation of nanoparticles. After sedimentation, the particles are separated from the supernatant, and washed with lime water to remove sodium chloride, a byproduct of the reaction. The usage of lime water is necessary to avoid the growth of particles due to Ostwald ripening (Sugimoto 1978; Marqusee and Ross 1983). Calcium hydroxide nanoparticles obtained from these synthetic procedures show an average diameter of about 260 nm. Dispersions were prepared by mixing 10 g of particles with 1 L of 2-propanol, and used to control the pH of paper dating from the 14th, 17th, 19th and 20th century, which is representative of documents usually found in archives.

A completely different synthetic strategy for the preparation of calcium hydroxide nanoparticles was recently proposed (Poggi et al. 2014), based on a solvothermal reaction. The main advantage of this process relies in the possible future up-scale of the method, with great benefits in terms of costs. The use of

dispersions obtained by the solvothermal process to hinder the degradation of cellulose-based materials will be discussed in Sect. 5.4.

As previously discussed, several state-of-the-art deacidification methods (e.g., Bookkeeper and PaperSave) are based on the usage of magnesium compounds as precursors for magnesium hydroxide, which then acts as the neutralizing agent. Alternatively, a coprecipitation reaction in aqueous solutions was achieved in 2005 (Giorgi et al. 2005) with the aim of synthesizing $Mg(OH)_2$ nanoparticles to be dispersed in alcohols and directly applied on cellulose-based materials. Aqueous solutions of sodium hydroxide were added to solutions of different magnesium salts, such as sulfate, chloride, nitrate and perchlorate. The size of the obtained $Mg(OH)_2$ particles range from ca. 50 to 200 nm, and was shown to be dependent on the counterions, following the Hofmeister anion series. Magnesium hydroxide nanoparticles were then dispersed in 2-propanol and applied by brushing on paper samples. The resistance of paper to photo-oxidative and hydrothermal aging was evaluated in terms of percentage of broken bonds in cellulose and tensile strength, showing that the nanoparticles dispersion is more efficient than the other state-of-the-art methods in preventing degradation.

A modified procedure to synthesize magnesium hydroxide nanoparticles has been recently proposed, where the removal of residual water (by drying) from particles before dispersion in propanol was demonstrated a key factor in further reducing the particles' size. Particles obtained with this method were used to control the pH of paper containing metal-gall inks (see Sect. 5.4; Poggi et al. 2010).

5.2 *Stabilization of Alkaline Nanoparticles Dispersions*

To be applied for deacidification purposes, nanoparticles are typically dispersed in solvents. As previously indicated, solvents should be neither toxic to the operator nor dangerous for the environment; in addition to that, their compatibility with the original materials found in artifacts should be checked prior to application. The preparation of stable dispersions of solid particles in liquids can be achieved in several ways, commonly including the usage of stabilizers, mechanical stirring and sonication by ultrasound. It is worth noting that in the framework of works of art conservation, the usage of electrolytes and additives should be avoided, as it might result in the presence of salt efflorescence or residues on the treated artifacts. Therefore, ultrahomogenizer and ultrasonic treatments are preferred to improve the stability of particles in organic solvents. In some cases, for instance in solvothermal synthetic routes, the synthesis directly yields dispersed particles that exhibit good stability, e.g. several weeks. For what concerns nanoparticles obtained from a co-precipitation reaction (see previous section), it has been shown that the stability of dispersions depends on the presence of residual water from the synthesis, which interacts with hydroxide particles through hydrogen bonds, leading to particles' aggregation (Fratini et al. 2007). Vacuum-drying of particles prior to their dispersion decreases crystal size (Poggi et al. 2010), thus enhancing the stability of

dispersions. Besides particles' size, stability is governed by different kinds of interactions, such as Van der Waals interactions, Coulombic interactions, steric interactions, hydrophobic forces and solvation forces (Luckham 2004). Coulombic interactions play a fundamental role in particular when nanoparticles of ionic solids (e.g. hydroxides) are considered, as these typically exhibit surface charges already after their preparation. When particles are dispersed in polar media, the particles surface charge influences the distribution of nearby ions. Some counterions are located close to the particles surface, defining the Stern layer, and the remainder is broadly distributed in the diffuse layer (see Fig. 7). The potential difference between the Stern plane and the diffuse layer is called the zeta-potential (Hunter 1981). Both the zeta potential and the thickness of the diffuse layer should not be too small, in order to favor repulsion between particles and increase the stability of the dispersions. When the concentration of ions in the solvent is high, both the thickness and the potential decrease, the repulsion between the particles is reduced, and stability is lowered.

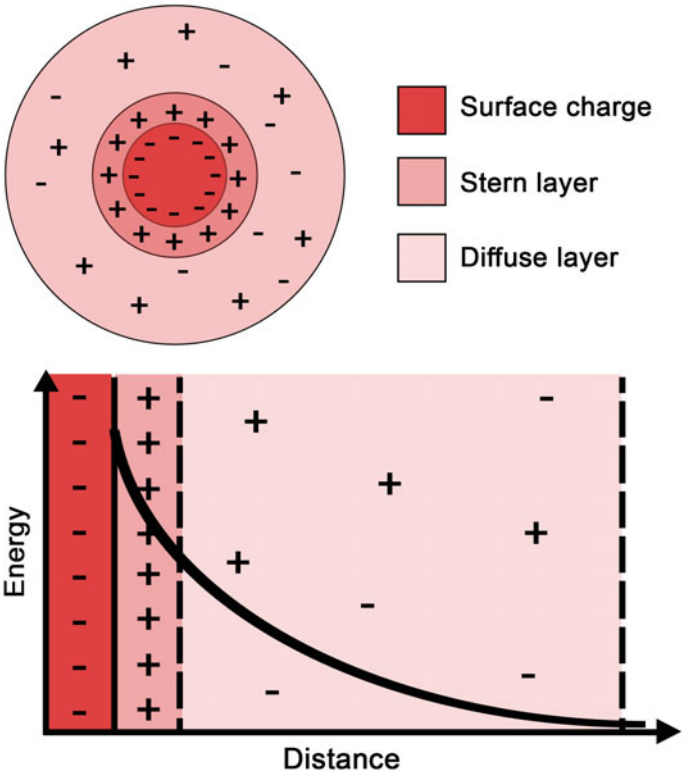

Fig. 7 Negatively charged particles in a polar solvent. The Stern and diffuse double layer are indicated

Depending on the synthetic routes, the stability of the dispersions commonly used for deacidification purposes may range from several hours to months. It is worth noting that the stability of dispersions should be at least on the same time-scale as the application onto artifacts, which normally requires from some minutes up to few hours. Another important factor is the reversibility of particles sedimentation. In many cases, after settling calcium and magnesium hydroxide nanoparticles can be easily re-dispersed again by gently shaking the container. After long storage time, sonication of dispersions might be used to favor the re-dispersion of settled nanoparticles in the organic solvent.

5.3 Characterization of Alkaline Nanoparticles Dispersions

Size, shape, polydispersity, specific area, superficial charge, composition and crystallinity, all are fundamental properties of the nanoparticles, which have to be characterized before application for conservation purposes. For what concerns solid particles, the crystallinity grade is usually assessed by XRD (X-Ray Diffractometry), while chemical composition and purity grade are commonly checked by Fourier-Transform InfraRed Spectroscopy (FTIR). Gas-porosimetry and Z-potential are used to measure the specific area of particles and their superficial charge distribution, respectively.

Microscopy techniques, such as Scanning Electron Microscopy (SEM), Atomic Force Microscopy (AFM) and Transmission Electron Microscopy (TEM) are widely used for the morphological investigation of particles. Besides information about morphology, surface texture, and roughness, SEM and TEM analysis can also be used for compositional analysis (SEM-EDS) and crystal structure determination (HR-TEM). It is worth noting that TEM provides a unique tool that allows direct visualization of particles (see Fig. 8) and can be used for obtaining size distribution and polydispersity of nanoparticles, even if the method requires careful considerations about the statistical significance of the obtained results (Pyrz and Buttrey 2008). In this respect, Dynamic Light Scattering (DLS) is to be considered the most important tool for the analysis of colloidal systems. In fact, this technique provides accurate particles size distribution and polydispersity, in a wide range of size, in a fast and simple way (Gabrowsky and Morrison 1983; Hassan et al. 2015).

5.4 Application of Alkaline Nanoparticles Dispersions

Brushing or spraying dispersions of alkaline nanoparticles onto the surface of the cellulose-based artifacts are two methods commonly used to carry out a deacidification intervention (see Fig. 9).

When manuscripts and documents are treated, both sides of the paper sheets (*recto* and *verso*) should be treated if possible. Artworks can also be immersed in

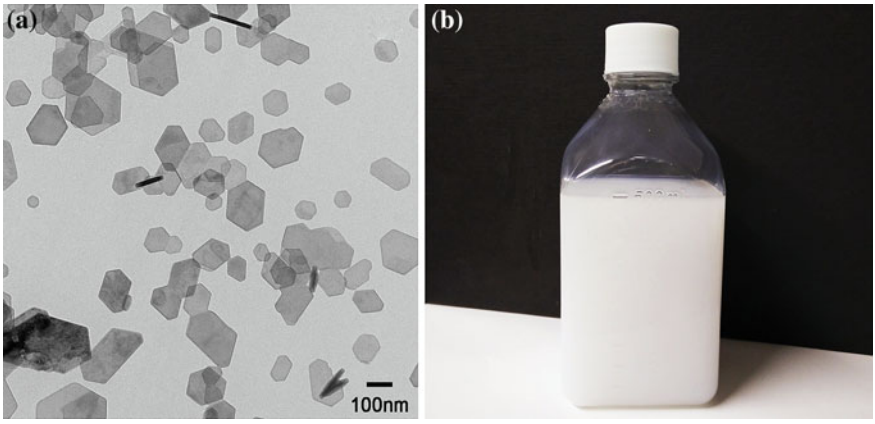

Fig. 8 **a** TEM image of calcium hydroxide nanoparticles obtained from a solvothermal reaction in ethanol. (Reprinted with kind permission from Springer Science + Business Media. Poggi et al. (2010). Figure 1) **b** Calcium hydroxide nanoparticles obtained from a solvothermal reaction, dispersed in ethanol at 10 g/L

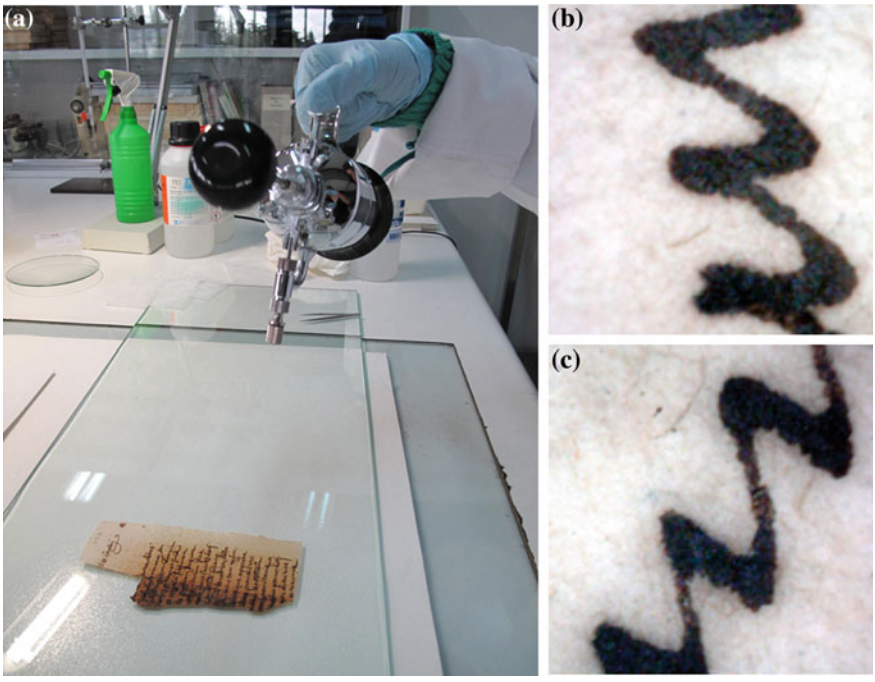

Fig. 9 **a** Application (spraying) of calcium hydroxide nanoparticles dispersed in ethanol on a 16th century manuscript. **b** Optical microscope picture (magnification = 10×) of an *inked area*, before treatment with nanoparticles. **c** Optical microscope picture (magnification = 10×) of an *inked area* of the same manuscript, after treatment with calcium hydroxide nanoparticles dispersed in ethanol. [Printed with the kind permission of SELIDO (at IPCE, Instituto del Patrimonio Cultural de España, Madrid)]

the dispersion. The choice of the most appropriate application procedure is usually made by conservators. As previously indicated, before any deacidification treatment, compatibility tests should be carried out, to check solvent interactions with the original components of artworks.

For the deacidification of cellulose-based artifacts, a concentration of 2.5 g/L usually grants the neutralization of present acidity and, at the same time, avoids the formation of white veils on the surface. The use of less concentrated nanoparticles dispersions is advisable when low porosity substrates, e.g. calendered paper, need to be treated.

Before applying the nanoparticles, pH measurements should be carried out on the artifacts. Several methods are commonly used to measure pH, including standardized procedures such as cold extraction (ASTM D788-97 2002; TAPPI T 509 Om-02 2002) and surface determination (TAPPI T 529 Om-04 2004). If pH is below 5.5, a deacidification intervention is advisable.

As previously indicated, hydroxide nanoparticles react with artworks acidity and, if in excess, turn into carbonate, which acts as a mild alkaline buffer against reoccurring acidity. The amount of particles applied can be tuned so to obtain a final pH of 7.0–8.0 after carbonation, as checked with pH measurements. This value is optimal for counteracting acidity and avoiding excessive alkalinity on cellulose fibers. More detailed information has been recently provided by Baglioni et al. (2015) regarding application procedures and examples of quantities typically applied in paper deacidification.

Finally, it must be noticed that the carbonation of hydroxide nanoparticles depends upon several factors including temperature, relative humidity and carbon dioxide concentration. In standard conditions (room temperature, RH = 60 %), full carbonation requires approximately two weeks.

5.5 *Case Studies*

In this section we will discuss some recent case studies on the use of nanomaterials for the pH control of cellulose-based artifacts.

As previously stated, the corrosion of documents featuring metal gall inks is due to the concomitant action of sulfuric acid and free metal ions, which pose a threat to the preservation of manuscripts and archival material. In 2010, Poggi et al. proposed the synthesis and use of magnesium hydroxide nanoparticles dispersed in 2-propanol for the inhibition of both mechanisms involved in cellulose corrosion due to iron gall inks (Poggi et al. 2010). The rationale for the treatment is the following: alkaline nanoparticles readily react with sulfuric acid and, if in excess, turn into carbonate that is milder to alkali-sensitive cellulose fibers. In fact, the quantity of applied nanoparticles can be feasibly tuned to obtain a final pH of 7–8, which hinders acid-catalyzed hydrolysis of cellulose. A pH value around neutrality is also fundamental in hindering the oxidation of cellulose induced by iron and

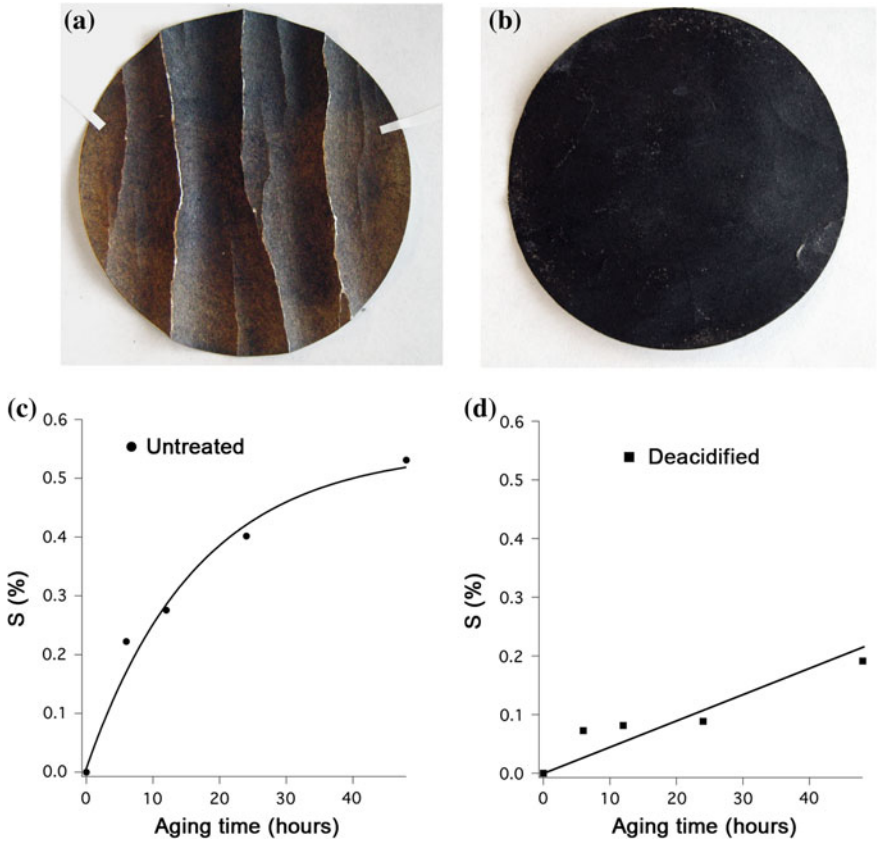

Fig. 10 **a**, **b** Whatman filter paper featuring metal gall ink after 48 h of artificial aging. While the untreated sample is fragile and cannot be manipulated (**a**), paper deacidified prior to aging using magnesium hydroxide nanoparticles retains the original mechanical resistance (**b**). Degradation curves showing the percentage of glycosidic bonds scissored (S) upon aging on untreated sample (**c**) and deacidified sample (**d**). The visual aspect reflects the difference in degradation curves. (Adapted with permission from Poggi et al. (2010). Copyright © (2010) American Chemical Society)

copper ions, whose catalytic activity is minimal when pH is around 7–7.5 (Strlič et al. 2003). $Mg(OH)_2$ nanoparticles in alcohol were applied on Whatman filter paper samples that had been brushed with metal and iron gall inks. Both deacidified and untreated inked samples were aged under severe hydrothermal conditions (RH = 75 % and T = 90 °C) for up to 48 h. When inked paper is not protected with the nanoparticles, this aging protocol causes a degradation of cellulose in terms of scissored glycosidic bonds that is representative of that found in historical samples (final DP lower than 300). On the other hand, the number of scissored glycosidic bonds over time was drastically reduced when the neutralizing dispersions are applied prior to aging of the samples (Fig. 10).

Macroscopically, at the end of the aging the deacidified samples retained their original mechanical resistance, while untreated samples showed dramatic discoloration and severe mechanical failure. Overall this showed that an enduring stabilization of pH around neutrality is effective in preventing cellulose fibers degradation in manuscripts that feature metal and iron gall inks.

One of the recent upgrades of this methodology is the investigation of hybrid systems where the nanoparticles dispersions are mixed to gelatin and applied onto paper that already exhibits reduced mechanical properties. In fact, hydroalcoholic solutions of gelatin are commonly used in paper conservation for the lamination of manuscripts fragments, carried out by gluing Japanese paper tissue to the degraded paper sheets. The mechanical resistance of degraded manuscript is thus increased. In order to prevent the degradation of the laminated manuscript, nanoparticles can be easily added to the hydroalcoholic solutions of gelatin, creating a combined treatment that allows mechanical strengthening and hampering of cellulose degradation. Preliminary test conducted on mockups samples and on 16th and 18th century manuscripts showed that the combined method may improve on the traditional conservation method, prolonging the useful life of historical manuscripts and granting, at the same time, their manipulation (Poggi et al. 2015).

As mentioned in the previous section, dispersions of calcium hydroxide nanoparticles have been recently obtained using a two-step solvothermal process (Poggi et al. 2014). The first step of the reaction consists in the oxidation of calcium metal by short chain alcohol, such as ethanol and 1-propanol, resulting in the formation of the corresponding alkoxide. Addition of water to the reaction bulk induces the precipitation of colloidal calcium hydroxide, meaning that these nanoparticles can be synthesized as dispersed in alcohol and directly applied without any further processing. Another interesting feature of this synthetic route is the possibility of obtaining highly concentrated dispersions (about 35 g/L), which in turn is essential for the upscale of the production, with great benefits in terms of cost. Nanoparticles obtained via solvothermal reaction consisted of highly crystalline platelets of Portandite, having an average diameter below 300 nm for the system dispersed in 1-propanol and 80 nm for the system in ethanol, and a thickness of about 20–30 nm (Fig. 11).

These calcium hydroxide nanoparticles were applied on artificially acidified Whatman paper samples, which were then subjected to severe hydrothermal conditions. In acidic samples, the increase of bonds scissions in cellulose chains during aging has an initial linear shape that is followed by a deceleration toward a horizontal asymptote, corresponding to the reaching of the LODP (see Sect. 2.1). This pattern is typically showed by autocatalytic degradation mechanisms (Calvini et al. 2007, 2008). Instead, the degradation plots over time obtained for deacidified paper samples, highlight that the treatment with $Ca(OH)_2$ nanoparticles increases the resistance of samples to aging (see Fig. 12). Paper samples were also analyzed using Differential Thermo Gravimetry (DTG), which allows determining the pyrolysis temperature of cellulose (Tp), used as an indicator of the paper's conservation status (Soares et al. 1995; Franceschi et al. 2001; Sandu et al. 2003).

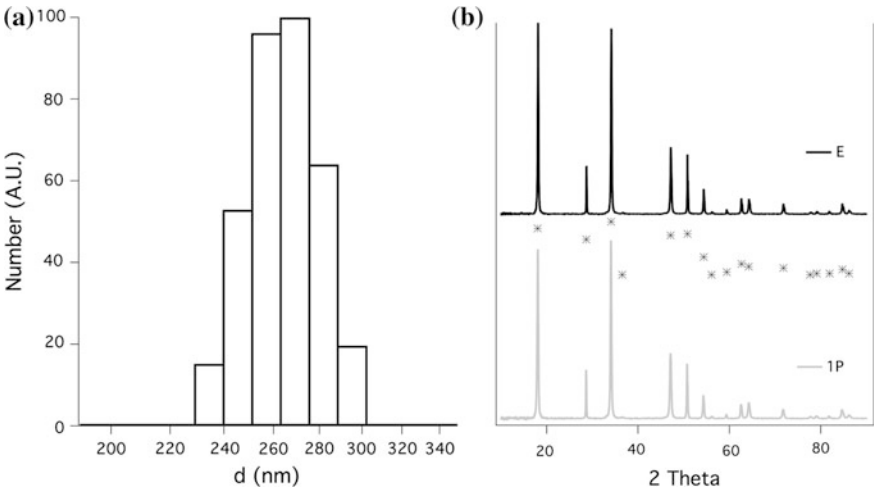

Fig. 11 **a** Size distribution of calcium hydroxide nanoparticles dispersed in 1-propanol obtained by DLS. **b** XRPD of calcium hydroxide nanoparticles synthesized in ethanol (*black line*) and in 1-propanol (*grey line*). *Stars* correspond to the peaks of Portlandite, used as a reference. (Reprinted with kind permission from Springer Science + Business Media. Poggi et al. (2014), Figs. 3 and 4)

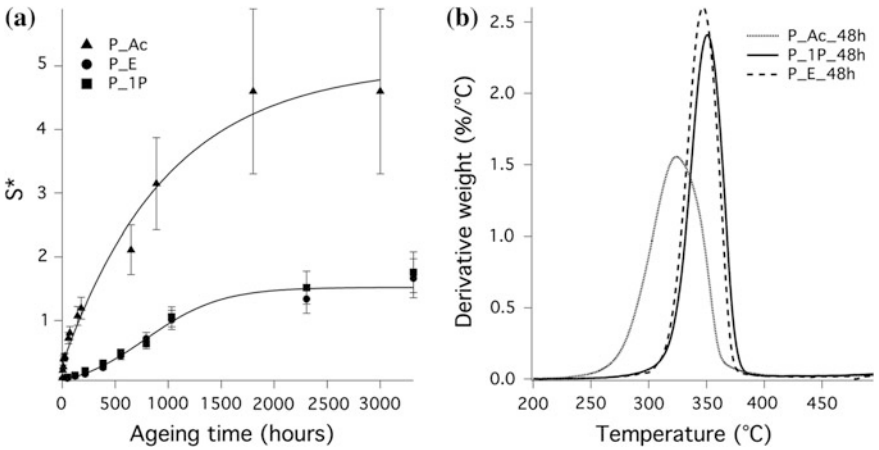

Fig. 12 **a** Degradation curves showing the scissions per initial cellulose chain (S^*) occurred upon aging of acidified paper sample (P_Ac), and of acidified paper neutralized with calcium hydroxide nanoparticles in ethanol and in 1-propanol (respectively, P_E and P_1P). The *lines* show the trends for each system. **b** Thermal analyses on paper samples: comparison after 48 h of aging between acidified paper (P_Ac) and acidified paper neutralized with calcium hydroxide nanoparticles in ethanol and in 1-propanol (P_E and P_1P). (Reprinted with kind permission from Springer Science + Business Media. Poggi et al. (2014), Figs. 6 and 7)

Acidification of Whatman paper lowered cellulose Tp of about 35 °C as compared to pristine samples. As can be seen in Fig. 12, treatment of acidic paper with nanoparticles (either dispersed in ethanol or propanol) kept cellulose Tp 20 °C higher than that of non-protected acidic samples throughout 48 h of aging. As a matter of fact, neutralization of acidity inhibits the dehydration of cellulose, which is the first step of the thermal degradation process (Fengel and Wegener 1984). In addition to that, it has been hypothesized that bivalent calcium ions are capable of interacting with cellulose carboxylate groups (formed upon neutralization of carboxylic groups). These interactions could create a network between the deacidified cellulose chains, increasing both paper resistance to thermal degradation (Bukovský 2000; Baglioni et al. 2012) and to folding, which has been observed during tests on treated paper samples.

As previously discussed, manuscripts featuring iron and metal gall inks exhibit good compatibility with alcohols, and can be successfully treated using formulations of calcium and magnesium nanoparticles both in ethanol and in 2-propanol. On the contrary, only few available treatments can be safely used on contemporary drawings or contemporary artworks on paper. As a matter of fact, during the 20th century, the notion of drawing underwent great changes. The use of paper changed from a simple support for studies or sketches to form the basis for autonomous work, at times torn, burnt, folded, perforated, twisted or scraped. At the same time a large number of new media, such as acrylic and vinyl resins, pressure sensitive adhesives, ballpoint and felt-tip pens and markers, entered the world of art. All of these media are rarely compatible with traditional restoration procedures. This makes the conservation and restoration of of contemporary drawings a widely unexplored field.

Calcium hydroxide nanoparticles obtained by the solvothermal process exhibit another interesting feature, i.e. their dispersibility in apolar solvents such as alkanes. A good candidate is cyclohexane, which is a colorless, volatile, nonpolar liquid. Due to its high volatility, the spraying of the solvent guarantees a fast and simple application. Moreover, owing to its nonpolar character, cyclohexane does not affect cellulose fibers and does not cause solubilization of several modern inks (see, for instance, Fig. 13).

Therefore, even in the case of creased or folded paper, such as Simon Schubert, Kiki Smith or Stefano Arienti artworks, the treatment will not cause any changes in the original visual aspect of the object. Promising results obtained on preliminary laboratory tests led to the application of this innovative formulation on contemporary drawings from a private collection, potentially paving the way for the treatment of a significant portion of contemporary artworks.

To conclude, dispersions of nanoparticles in non aqueous solvents have proven in the last fifteen years as feasible and effective tools for the preservation of cellulose-based artifacts. As a matter of fact, these systems are able to counteract the main degradation mechanisms affecting cellulose (acid-catalyzed hydrolysis and oxidation), and represent valid alternatives to traditional conservation treatments.

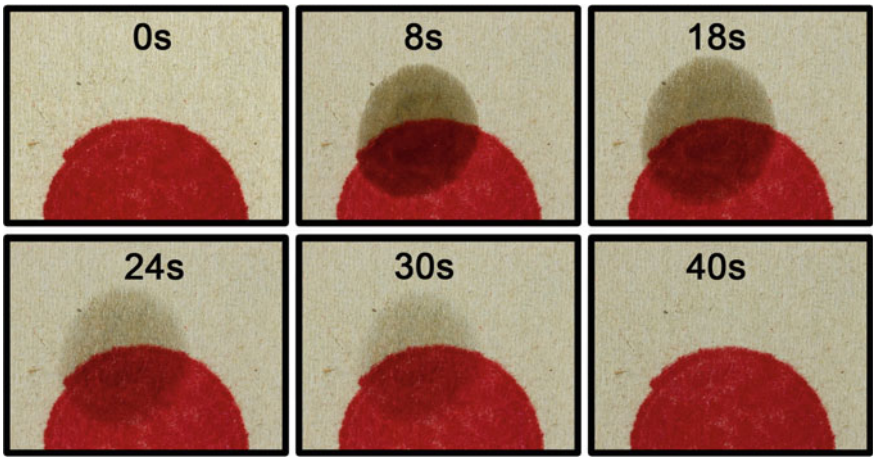

Fig. 13 Application of calcium hydroxide nanoparticles dispersed in cyclohexane on paper inked with a red felt-tip pen. The use of cyclohexane prevents bleeding or leaching of the ink; moreover, no white veil is observed after the evaporation of the solvent

Moreover, the potential applications of nanomaterials in this field have been recently expanded, with new perspectives opened by the preparation of nanoparticles-polymer hybrid systems and by the dispersion of nanoparticles in inert solvents.

Acknowledgments This work was partly funded by NANOFORART – Nano-materials for the conservation and preservation of movable and immovable artworks, FP7-NMP European project, (http://www.nanoforart.eu); and by NANORESTART, NANO materials for the REStoration of works of ART, H2020-NMP-2014 project (http://www.nanorestart.eu).

References

Afsharpour M, Hadadi M (2014) Titanium dioxide thin film: environmental control for preservation of paper-art-works. J Cult Herit 15:569–574. doi:10.1016/j.culher.2013.10.008

Altaner CM, Thomas LH, Fernandes AN, Jarvis MC (2014) How cellulose stretches: synergism between covalent and hydrogen bonding. Biomacromolecules 15:791–798. http://pubs.acs.org/doi/pdf/10.1021/bm401616n)

Ambrosi M, Dei L, Giorgi R, Neto C, Baglioni P (2001) Stable dispersions of $Ca(OH)_2$ in aliphatic alcohols: properties and application in cultural heritage conservation. In: Koutsoukos PG (ed) Trends in colloid and interface science XV. Springer, Berlin, pp 68–72

ASTM D788-97 (2002) Standard test methods for hydrogen ion concentration (pH) of paper extracts (hot-extraction and cold-extraction procedures)

Atalla RH, Vanderhart DL (1984) Native cellulose: a composite of two distinct crystalline forms. Science 223:283–285. doi:10.1126/science.223.4633.283

Baglioni P, Chelazzi D, Giorgi R, Poggi G (2012) Nanoparticles for the conservation of cultural heritage: paper and wood. In: Somasundaran P (ed) Encyclopedia of surface and colloid science, 2nd edn. Taylor & Francis, New York, pp 1–16

Baglioni P, Chelazzi D, Giorgi R, Poggi G (2013) Colloid and materials science for the conservation of cultural heritage: cleaning, consolidation, and deacidification. Langmuir 29:5110–5122

Baglioni P, Chelazzi D, Giorgi R (2015) Nanotechnologies in the conservation of cultural heritage—a compendium of materials and techniques

Banait NS, Jencks WP (1991) Reactions of anionic nucleophiles with alpha-D-glucopyranosyl fluoride in aqueous solution through a concerted, ANDN (SN2) mechanism. J Am Chem Soc 113:7951–7958. doi:10.1021/ja00021a021

Barrow WJ, Sproull RC (1959) Permanence in book papers: investigation of deterioration in modern papers suggests a practical basis for remedy. Science 80–129:1075–1084. doi:10.1126/science.129.3356.1075

Baty JW, Maitland CL, Minter W, Hubbe MA, Jordan-Mowery SK (2010) Deacidification for the conservation and preservation of paper-based works: a review. BioResources 5:1955–2023

Bégin P, Deschâtelets S, Grattan D, Gurnagul N, Iraci J, Kaminska E, Woods D, Zou X (1998) The impact of Lignin on paper permanence. A comprehensive study of the ageing behaviour of handsheets and commercial paper samples. Restaurator 19:135–154. doi:10.1515/rest.1998.19.3.135

Bicchieri M, Brusa P (1997) The bleaching of paper by reduction with the borane tert-butylamine complex. Restaurator 18:1–11. doi:10.1515/rest.1997.18.1.1

Bicchieri M, Bella M, Semetilli F (1999) A quantitative measure of borane tert-butylamine complex effectiveness in carbonyl reduction of aged papers. Restaurator 20:22–29. doi:10.1515/rest.1999.20.1.22

Bicchieri M, Sementilli FM, Sodo A (2000) Application of seven borane complexes in paper conservation. Restaurator 21:213–228. doi:10.1515/REST.2000.213

Blüher A, Grossenbacher G (eds) (2006) Save paper! mass deacidification, today's experiences, tomorrow's perspectives: paper given at the international conference, 15–17 Feb 2006. Swiss National Library, Bern

Boone T, Kidder L, Russick S (1998) Bookkeeper® for spray use in single item treatments, 17

Botti L, Mantovani O, Ruggiero D (2005) Calcium Phytate in the Treatment of Corrosion Caused by Iron Gall Inks: Effects on Paper. Restaurator 26:44–62. doi: 10.1515/REST.2005.44

Bronzato M, Calvini P, Federici C, Bogialli S, Favaro G, Meneghetti M, Mba M, Brustolon M, Zoleo A (2013) Degradation products from naturally aged paper leaves of a 16th-century-printed book: a spectrochemical study. Chemistry 19:9569–9577. doi:10.1002/chem.201300756

Bukovský V (2000) The influence of light on ageing of newsprint paper. Restaurator 21:55–76. doi:10.1515/REST.2000.55

Calvini P (2005) The influence of levelling-off degree of polymerisation on the kinetics of cellulose degradation. Cellulose 12:445–447. doi:10.1007/s10570-005-2206-z

Calvini P (2014) On the meaning of the Emsley, Ding & Wang and Calvini equations applied to the degradation of cellulose. Cellulose 21:1127–1134. doi:10.1007/s10570-014-0224-4

Calvini P, Gorassini G (2012) Surface and bulk reactions of cellulose oxidation by periodate. A simple kinetic model. Cellulose 19:1107–1114

Calvini P, Grosso V, Hey M, Rossi L, Santucci L (1988) Deacidification of paper—a More fundamental approach. Pap Conserv 12:35–39. doi:10.1080/03094227.1988.9638560

Calvini P, Gorassini A, Merlani AL (2007) Autocatalytic degradation of cellulose paper in sealed vessels. Restaurator 28:47–54

Calvini P, Gorassini A, Merlani AL (2008) On the kinetics of cellulose degradation: looking beyond the pseudo zero order rate equation. Cellulose 15:193–203. doi:10.1007/s10570-007-9162-8

Carter HA (1989) Chemistry in the comics: part 3. The acidity of paper. J Chem Educ 66:883. doi:10.1021/ed066p883

Carter H, Bégin P, Grattan D (2000) Migration of volatile compounds through stacked sheets of paper during accelerated ageing—part 1: acid migration at 90°. C Restaurator. doi:10.1515/REST.2000.77

Chamberlain D (2007) Anion mediation of aluminium-catalysed degradation of paper. Polym Degrad Stab 92:1417–1420. doi:10.1016/j.polymdegradstab.2007.04.006

Coughlan MP (1991) Mechanisms of cellulose degradation by fungi and bacteria. Anim Feed Sci Technol 32:77–100. doi:10.1016/0377-8401(91)90012-H

Dobrodskaya TV, Egoyants PA, Ikonnikov VK, Romashenkova ND, Sirotin SA, Dobrusina SA, Podgornaya NI (2004) Treatment of paper with basic agents in alcohols and supercritical carbon dioxide to neutralize acid and prolong storage time. Russ J Appl Chem 77:2017–2021. doi:10.1007/s11167-005-0211-5

Dufour J, Havermans JBGA (2001) Study of the photo-oxidation of mass-deacidified papers. Restaurator. doi:10.1515/REST.2001.20

Dupont (2002) The role of gelatine/alum sizing in the degradation of paper: a study by size exclusion chromatography in lithium chloride/*N*,*N*-dimethylacetamide using multiangle light scattering detection. In: Daniels V, Donnithorne A, Smith P (eds) Preprint of IIC Baltimore congress 2002, works of art on paper, books, documents and photographs: techniques and conservation. International Institute for Conservation, Baltimore, pp 59–64

Feller (1994) Accelerated ageing in conservation science. Getty Conservation Institute, Los Angeles

Fengel D, Wegener G (1984) Wood: chemistry, ultrastructure, reactions. Walter De Gruyter, Berlin

Franceschi E, Palazzi D, Pedemonte E (2001) Thermoanalytical contribution to the study on paper degradation. characterisation of oxidised paper. J Therm Anal Calorim 66:349–358

Fratini E, Page MG, Giorgi R, Cölfen H, Baglioni P, Demé B, Zemb T (2007) Competitive surface adsorption of solvent molecules and compactness of agglomeration in calcium hydroxide nanoparticles. Langmuir 23:2330–2338. doi:10.1021/la062023i

Gabrowsky E, Morrison I (1983) Particle size distributions from analysis of quasi-elastic light scattering data. In: Dahneke BE (ed) Wiley-Interscience, New York

Giorgi R, Dei L, Ceccato M, Schettino C, Baglioni P (2002a) Nanotechnologies for conservation of cultural heritage: paper and canvas deacidification. Langmuir 18:8198–8203. doi:10.1021/la025964d

Giorgi R, Dei L, Schettino C, Baglioni P (2002b) A new method for paper deacidification based on calcium hydroxide dispersed in nonaqueous media. In: Daniels V, Donnithorne A, Smith P (eds) Preprint of IIC Baltimore congress 2002, works of art on paper, books, documents and photographs: techniques and conservation. International Institute for Conservation, Baltimore, pp 69–73

Giorgi R, Bozzi C, Dei L, Gabbiani C, Ninham BW, Baglioni P (2005) Nanoparticles of $Mg(OH)_2$: synthesis and application to paper conservation. Langmuir 21:8495–8501. doi:10.1021/la050564m

Glasser WG, Atalla RH, Blackwell J, Malcolm Brown R, Burchard W, French AD, Klemm DO, Nishiyama Y (2012) About the structure of cellulose: debating the Lindman hypothesis. Cellulose 19:589–598. doi:10.1007/s10570-012-9691-7

Grøntoft T, Odlyha M, Mottner P, Dahlin E, Lopez-Aparicio S, Jakiela S, Scharff M, Andrade G, Obarzanowski M, Ryhl-Svendsen M, Thickett D, Hackney S, Wadum J (2010) Pollution monitoring by dosimetry and passive diffusion sampling for evaluation of environmental conditions for paintings in microclimate frames. J Cult Herit 11:411–419. doi:10.1016/j.culher.2010.02.004

Harris JF (1975) Acid hydrolysis and dehydration reactions for utilizing plant carbohydrates. Appl Polym Symp 28:131

Hassan PA, Rana S, Verma G (2015) Making sense of brownian motion: colloid characterization by dynamic light scattering. Langmuir 31:3–12. doi:10.1021/la501789z

Henniges U, Reibke R, Banik G, Huhsmann E, Hähner U, Prohaska T, Potthast A (2008) Iron gall ink-induced corrosion of cellulose: aging, degradation and stabilization. Part 2: application on historic sample material. Cellulose 15:861–870. doi:10.1007/s10570-008-9238-0

Hunter RJ (1981) Zeta Potential in Colloid Science. Elsevier, London

Kolar J (1997) Mechanism of autoxidative degradation of cellulose. Restaurator 18:163–176. doi:10.1515/rest.1997.18.4.163

Kolar J, Strlič M, Budnar M, Malesič J, Šelih VS, Simčič J (2003) Stabilisation of corrosive iron gall inks. Acta Chim Slov 50:763–770

Kolar J, Šala M, Strlič M, Šelih VS (2005) Stabilisation of Paper Containing Iron-Gall Ink with Current Aqueous Processes. Restaurator 26:181–189. doi: 10.1515/rest.2005.26.3.181

Kolar J, Možir A, Strlič M, de Bruin G, Pihlar B, Steemers T (2007) Stabilisation of iron gall ink: aqueous treatment with magnesium phytate. e-Preservation Sci 4:19–24

Kolar J, Možir A, Balažic A, Strlič M, Ceres G, Conte V, Mirruzzo V, Steemers T, de Bruin G (2008) New antioxidants for treatment of transition metal containing inks and pigments. Restaurator 29:184–198. doi:10.1515/rest.2008.013

Lopez-Aparicio S, Grøntoft T, Odlyha M, Dahlin E, Mottner P, Thickett D, Ryhl-Svendsen M, Schmidbauer N, Scharff M (2010) Measurement of organic and inorganic pollutants in microclimate frames for paintings. e-Preservation Sci 7:59–70

Lucarelli F, Mandò PA (1996) Recent applications to the study of ancient inks with the Florence external-PIXE facility. Nucl Instruments Methods Phys Res Sect B Beam Interact with Mater Atoms 109–110:644–652. doi:10.1016/0168-583X(95)00985-X

Luckham PF (2004) Manipulating forces between surfaces: applications in colloid science and biophysics. Adv Colloid Interface Sci 111:29–47. doi:10.1016/j.cis.2004.07.008

Lundgaard LE, Hansen W, Linhjell D, Painter TJ (2004) Aging of oil-impregnated paper in power transformers. Power Deliv IEEE Trans 19:230–239

Malesič J, Kolar J, Strlič M (2002) Effect of pH and carbonyls on the degradation of alkaline paper factors affecting ageing of alkaline paper. Restaurator 23:145–153. doi:10.1515/REST.2002.145

Malešič J, Strlič M, Kolar J, Polanc S (2005a) The influence of halide and pseudo-halide antioxidants in Fenton-like reaction systems containing copper(II) ions. J Mol Catal A: Chem 241:126–132. doi:10.1016/j.molcata.2005.06.047

Malešič J, Kolar J, Strlič M, Polanc S (2005b) The use of halides for stabilisation of iron gall ink containing paper—the pronounced effect of cation. e-Preservation Sci 2:13–18

Marqusee JA, Ross J (1983) Kinetics of phase transitions: theory of Ostwald ripening. J Chem Phys 79:373–378. doi:10.1063/1.445532

McKellar JF, Allen NS (1979) Photochemistry of man-made polymers. Elsevier, London

Medronho B, Romano A, Miguel MG, Stigsson L, Lindman B (2012) Rationalizing cellulose (in)solubility: reviewing basic physicochemical aspects and role of hydrophobic interactions. Cellulose 19:581–587. doi:10.1007/s10570-011-9644-6

Meyer KH, Misch L (1937) Positions des atomes dans le nouveau modele spatial de la cellulose. Helv Chim Acta 20:232–244. doi:10.1002/hlca.19370200134

Neevel JG (1995) Phytate: a potential conservation agent for the treatment of ink corrosion caused by Irongall Inks. Restaurator 16:143–160. doi:10.1515/rest.1995.16.3.143

Neevel JG (2000) (Im)possibilities of the phytate treatment. In: Brown JE (ed) Newcastle upon Tyne. The University of Northumbria, pp 127–134

Neevel JG, Mensch CTJ, Cornelis TJ (1999) The behaviour of iron and sulphuric acid during iron gall ink corrosion. In: Bridgland J (ed) ICOM committee for conservation triennial meeting. James and James, London, pp 528–533

Nisizawa K (1973) Mode of action of cellulases. J Ferment Technol 51:267–304

Park S, Baker JO, Himmel ME, Parilla PA, Johnson DK (2010) Cellulose crystallinity index: measurement techniques and their impact on interpreting cellulase performance. Biotechnol Biofuels 3:10. doi:10.1186/1754-6834-3-10

Pauk S (1996) Bookkeeper mass deacidification process—some effects on 20th-century library material. Abbey Newsl 20:50–53

Persson H, Türk M, Nyman M, Sandberg A-S (1998) Binding of Cu2+, Zn2+, and Cd2+ to Inositol Tri-, Tetra-, Penta-, and Hexaphosphates. J Agric Food Chem 46:3194–3200. doi: 10.1021/jf971055w

Poggi G, Giorgi R, Toccafondi N, Katzur V, Baglioni P (2010) Hydroxide nanoparticles for deacidification and concomitant inhibition of iron-gall ink corrosion of paper. Langmuir 26:19084–19090. doi:10.1021/la1030944

Poggi G, Toccafondi N, Melita LN, Knowles JC, Bozec L, Giorgi R, Baglioni P (2014) Calcium hydroxide nanoparticles for the conservation of cultural heritage: new formulations for the deacidification of cellulose-based artifacts. Appl Phys A 114:685–693. doi:10.1007/s00339-013-8172-7

Poggi G, Sistach MC, Marin E, Garcia JF, Giorgi R, Baglioni P (2015) The GEOLNAN, a combined deacidification and reinforcement treatment for metal gall ink manuscripts

Potthast A, Henniges U, Banik G (2008) Iron gall ink-induced corrosion of cellulose: aging, degradation and stabilization. Part 1: model paper studies. Cellulose 15:849–859. doi: 10.1007/s10570-008-9237-1

Pyrz WD, Buttrey DJ (2008) Particle size determination using TEM: a discussion of image acquisition and analysis for the novice microscopist. Langmuir 24:11350–11360. doi:10.1021/la801367j

Rydholm S (1965) Pulping processes. Interscience Publisher, New York

Sandu ICA, Brebu M, Luca C, Sandu I, Vasile C (2003) Thermogravimetric study on the ageing of lime wood supports of old paintings. Polym Degrad Stab 80:83–91. doi:10.1016/S0141-3910(02)00386-5

Sanna C, Sodo A, Laguzzi G, Mancini G, Bicchieri M (2009) Tert-butyl amine borane complex: an unusual application of a reducing agent on model molecules of cellulose based materials. J Cult Herit 10:356–361. doi:10.1016/j.culher.2008.10.008

Santucci L, Zappalà MP (2001) Cellulose viscometric oxidometry. Restaurator 22:51–65. doi:10.1515/REST.2001.51

Šelih VS, Strlič M, Kolar J, Pihlar B (2007) The role of transition metals in oxidative degradation of cellulose. Polym Degrad Stab 92:1476–1481. doi:10.1016/j.polymdegradstab.2007.05.006

Sequeira S, Casanova C, Cabrita EJ (2006) Deacidification of paper using dispersions of $Ca(OH)_2$ nanoparticles in isopropanol. Study of efficiency. J Cult Herit 7:264–272. doi:10.1016/j.culher.2006.04.004

Shanani CJ, Harrison G (2002) Spontaneous formation of acids in the natural aging of paper. In: Daniels V, Donnithorne A, Smith P (eds) Works of art on paper: books, documents and photographs. International Institute for Conservation of Historic and Artistic Works, London, pp 189–192

Sjostrom E (1977) TAPPI J 60:151

Soares S, Camino G, Levchik S (1995) Comparative study of the thermal decomposition of pure cellulose and pulp paper. Polym Degrad Stab 49:275–283. doi:10.1016/0141-3910(95)87009-1

Stefanis E, Panayiotou C (2007) Protection of lignocellulosic and cellulosic paper by deacidification with dispersions of micro- and nano-particles of $Ca(OH)_2$ and $Mg(OH)_2$ in alcohols. Restaurator 28:185–200. doi:10.1515/REST.2007.185

Strlič M, Kolar J (eds) (2005) Ageing and stabilization of paper. National and University Library, Ljubljana

Strlič M, Kolar J, Žigon M, Pihlar B (1998) Evaluation of size-exclusion chromatography and viscometry for the determination of molecular masses of oxidised cellulose. J Chromatogr A 805:93–99. doi:10.1016/S0021-9673(98)00008-9

Strlič M, Kolar J, Šelih VS, Kocar D, Pihlar B (2003) A comparative study of several transition metals in Fenton-like reaction system at circumneutral. Acta Chim Slov 50:619–632

Sugimoto T (1978) General kinetics of Ostwald ripening of precipitates. J Colloid Interface Sci 63:16–26. doi:10.1016/0021-9797(78)90030-9

TAPPI T 509 Om-02 (2002) Hydrogen ion concentration (pH) of paper extracts (cold extraction method)

TAPPI T 529 Om-04 (2004) Surface pH measurement of paper

Tétreault J (2003) Airborne pollutants in museums, galleries and archives: risk assessment, control strategies and preservation management. Canadian Conservation Institute, Ottawa

Tétreault J, Stamatopoulou E (1997) Determination of concentrations of acetic acid emitted from wood coatings in enclosures. Stud Conserv 42:141–156. doi:10.2307/1506710

Tse S, Bégin P, Kaminska E (2002) Highlights of paper research at the Canadian Conservation Institute. International Institution for Conservation of Historic and Artistic Works, London, pp 193–198

Wilkie JS (1961) Carl Nägeli and the fine structure of living matter. Nature 190:1145–1150. doi:10.1038/1901145a0

Wouters J (2008) Coming soon to a library near you? Science 80–322:1196–1198. doi:10.1126/science.1164991

Yanjuan W, Yanxiong F, Wei T, Chunying L (2013) Preservation of aged paper using borax in alcohols and the supercritical carbon dioxide system. J Cult Herit 14:16–22. doi:10.1016/j.culher.2012.02.010

Zappalà A, Stefani C De (2005) Evaluation of the Effectiveness of Stabilization Methods. Treatments by Deacidification, Trehalose, Phytates on Iron Gall Inks. Restaurator 26:36–43. doi: 10.1515/REST.2005.36

Zervos S (2010) Natural and accelerated ageing of cellulose and paper: a literature review. In: Lejeune A, Deprez T (eds) Cellulose: structure and properties, derivatives and industrial uses. Nova Science Publishers Inc, New York

Zhang Y, Bommuswamy J, Sinnott ML (1994) Kinetic isotope effect study of transition states for the hydrolyses of alpha- and beta-glucopyranosyl fluorides. J Am Chem Soc 116:7557–7563. doi:10.1021/ja00096a012

Zumbühl S, Wuelfert S (2001) Chemical aspects of the bookkeeper deacidification of cellulosic materials: the influence of surfactants. Stud Conserv 46:169–180. doi:10.2307/1506808

Confined Aqueous Media for the Cleaning of Cultural Heritage: Innovative Gels and Amphiphile-Based Nanofluids

Nicole Bonelli, David Chelazzi, Michele Baglioni, Rodorico Giorgi and Piero Baglioni

Abstract This chapter presents the applicative potentialities of gels for the cleaning of artworks surfaces. In particular, innovative physical and chemical gels, with high water retention capability, high responsiveness to external stimuli, and suitable mechanical properties, are described. The high solvent retention capability and the specific mechanical properties of these gels allow the safe cleaning of artifacts, even including water-sensitive substrates. In fact, the cleaning action is limited to the contact surface, and the complete removal of soil is achieved while avoiding solvent spreading and absorption within the substrate. In particular, the use of gels based on semi-interpenetrating (IPN) polymer networks provides great advantages because these gels are able to load water-based detergent systems, such as micellar solutions and microemulsions, which are effective in removing synthetic adhesives and highly hydrophobic detrimental materials. The combination of semi-IPN polymer networks with these detergents allows the cleaning of sensitive substrates such as canvas paintings and manuscripts.

1 Introduction

Restoration of works of art typically consists in three main operations: cleaning, consolidation and protection. Among these, cleaning probably is the most common and one of the most complex and delicate tasks to undertake on a work of art, due to the large amount of variables that conservators may have to deal with in everyday practice. Many different materials can be found on a work of art, aged or unaged,

Michele Baglioni, Piero Baglioni: No kinship exists among these authors

N. Bonelli · D. Chelazzi · M. Baglioni · R. Giorgi · P. Baglioni (✉)
Department of Chemistry and CSGI, University of Florence,
via della Lastruccia 3, 50019 Florence, Italy
e-mail: baglioni@csgi.unifi.it

P. Dillmann et al. (eds.), *Nanoscience and Cultural Heritage*,
DOI 10.2991/978-94-6239-198-7_10

originally present or altered, lately applied by other conservators or accidentally deposited on its surface, etc. Since the second half of the 20th century, the criterion of *reversibility* of a restoration treatment was considered as a "golden rule", due to impossibility to predict, in the short and long term, the behavior and the possible side effects triggered by the addition of new materials to the work of art during restoration process. With the term "cleaning" we generally refer to the removal of one or more undesired substances from the surface of a work of art. These can range from common dirt (greasy and oily compounds, dust, particulate pollution), to aged materials that were originally applied by the artist (varnishes—i.e. resins, siccative oils, protein or polysaccharide coatings—, synthetic polymers), aged or detrimental materials (varnishes, adhesives, synthetic materials), or even materials coming from extraordinary events (floods, fires, microbial attack).

Everyday practice and tradition provided conservators with several products and strategies to be used during cleaning operations, however conservation scientists are constantly searching for innovative, safer and more effective solutions.

Common cleaning procedures nowadays involve the use of water, several organic solvents, thickeners and supportants, surfactants, chelating agents, enzymes and instruments for laser or mechanical ablation. Among these tools, non-confined neat solvents (including both organic solvents and water) are presently the most common cleaning tools in restoration practice. Owing to ease of handling, reasonable low cost and usually fair effectiveness, they often are the first choice of conservators. However, both scientific studies (Burnstock et al. 1992; Khandekar et al. 1994; Phenix and Sutherland 2001) and daily practice have shown that the use of non-confined solvents entails two main drawbacks: insufficient specificity or selectivity and a poor controllability of solving action and penetration within the layered structure of the artwork. Possible undesired side effects, that may arise as a consequence of this general lack in control during cleaning process, are swelling and leaching of the binding media, pigment alteration, surface erosion, transport and re-deposition of the dissolved matter through the porous matrices, over-cleaning (removal of original *patinas* and pigment loss), or mechanical stress for the painting support. Furthermore, the increasing awareness on health and safety of workers, results in seeking alternatives to the use of free organic solvents, since most of these compounds possess not-negligible toxicity issues, especially in this context, where conservators often are forced to work in poorly ventilated environments and/or without the due precautions.

In order to find a solution to the aforementioned issues, since the introduction of organic solvents in conservation of cultural heritage, pastes and poultices composed by wax and solvents mixtures were proposed (Stulik et al. 2004). In this case, the wax prevented the solvent from migrating to the areas surrounding the target of the cleaning, besides reducing its evaporation rate. However, waxy mixtures were not easy to prepare and to be used, and the significant presence of wax residues on the treated surface was a major drawback of this methodology. Yet, this concept has

been further developed by the use of thickened liquids. Cellulose derivatives, such as methyl cellulose, ethyl cellulose, hydroxymethyl cellulose or carboxymethyl cellulose, were used to thicken and support several organic solvents. The resulting systems showed great versatility and they became fairly popular in the field of conservation of cultural heritage (Goldberg 1989).

Since then, several polymers have been used by conservators for the formulation of gels and viscous polymeric dispersions either with organic solvents or water-based cleaning systems. The confinement of a given cleaning fluid (e.g. water, organic solvent, enzymes solutions, chelating agents, etc.) permits a slow and controlled release on the artistic surface reducing spreading and penetration of the fluid itself within the porous matrix of the treated object. Moreover, the reduction in solvent evaporation and penetration rates permits to increase (when needed) the contact time between the cleaning system and the material to be removed, resulting in a more effective and safer cleaning action, with minimized environmental impact and toxicity.

The main disadvantage of traditional gel systems (i.e. solvent gels or physical gels in general) resides in the fact that their formulation includes non-volatile substances (mainly polymers, used as thickeners, or surfactants), which may remain as residues on a treated surface. This means that even using traditional gels it is possible to increase *control* and *selectivity* of the cleaning action, while solving the *residues issue* becomes the real challenge for conservation scientists. What is the amount of these residues? How can they be completely cleared off? Can we expect dangerous interactions between gels' residues and the materials of a given work of art? These are some of the questions, which scientists and conservators are currently trying to answer. A possible answer is the use of a different class of gels. In fact, with the growing contribution of nanoscience to the field of conservation of cultural heritage, several innovative materials were proposed, which possess interesting properties, such as responsiveness to external stimuli (e.g. magnetic fields, pH), peculiar rheological behavior, or covalently bound tridimensional polymeric networks (chemical gels). Parallel to the evolution of gels and thickened formulations, also cleaning fluids benefitted from the fundamentals of nanoscience and colloid science, which were used to set up nanostructured fluids (hereafter, shortly, "nanofluids", i.e. micelles and microemulsions), generally composed by water, organic solvents and surfactants, having excellent cleaning properties, low environmental impact and high versatility. Most recently, gels and nanofluids were combined together with the aim of obtaining innovative nanomaterials having useful properties.

This chapter is devoted to the description of the most interesting cleaning tools (gels, nanofluids, or combined systems) proposed in the recent years, presenting their main feature and some case studies. In the following paragraphs, a concise overview on the fundamentals and the theoretical background that lies behind these classes of materials is reported.

2 Theoretical Background

2.1 Gels

2.1.1 What Is a Gel? Some Definitions

Despite the vast amount of publications and the conspicuous literature available on the topic, giving a precise and universally valid definition of the gel-state is still not an easy task. This ambiguity is mainly due to both, the intrinsic complexity of the system and variability of its characteristics, and to the numerous fields of application, which results in different approaches depending on the theoretical background.

Presently, the international Union of Pure and Applied Chemistry (IUPAC), defines a gel as a "*non-fluid colloidal network or polymer network that is expanded throughout its whole volume by a fluid*" (Alemán et al. 2007). In other words, gels can be described as soft materials made-up by colloidal particles (continuous entities with a dimension ranging from 1 to 100 nm, i.e. the typical size for colloidal systems) or interconnected polymer chains that build a tridimensional network throughout the whole volume of a given fluid. The result is a system displaying physical properties that are in-between those of a liquid and a solid.

In making considerations on the gel-state, in the mid-1920s, J. Lloyd suggests that a gel is "*easier to recognize than to define*" (Lloyd 1926). Moreover, he observed that gels are "*build up of two components, one of which must be a liquid, and the other of which, the gelling substance proper, often spoken as the gelator, is a solid*" and that "*the gel itself has the mechanical properties of a solid, i.e. it can maintain its form under the stress of its own weight, and under any mechanical stress it shows the phenomenon of strain*". In 1949, P.H. Hermans introduced the concept of bi-continuity of the two phases, stating that "*both, the dispersed component and the dispersion medium extend themselves continuously through the whole system*" (Hermans 1949). P.J. Flory and W.H. Stockmayer set important milestones for a better understanding of the gelation process proposing a theory for non-linear polymerization and cross-linking of linear polymer chains (Stockmayer 1944; Flory 1953). The "gelation theory" has been further extended by D. Stauffer and R. Zallen with the formulation of the "percolation model" (Stauffer et al. 1982; Zallen 1983).

To satisfy the need for a precise and measurable parameter indicating that a material can be considered a gel, in 1993 Almdal et al. proposed a definition based on the rheological properties of gels (Almdal et al. 1993). According to Almdal theory, in order to be considered a gel, a material must fulfill the following criteria: (i) it must consist of two or more components, one of which must be liquid and present in substantial quantity and (ii) it must be a soft, solid or solid-like material. Referring to point (ii), the definition of the solid-like characteristics is given in terms of the dynamic mechanical properties and is based on the observation that "true" gels display a plateau in the storage modulus $G'(\omega)$, which is higher than the

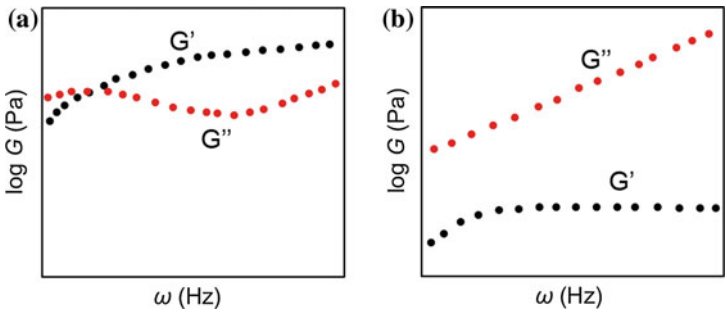

Fig. 1 Examples of typical log-log plots of storage modulus, $G'(\omega)$, and loss modulus, $G''(\omega)$ for polymeric dispersions. Panel **a** shows the behavior of a polymeric dispersion that is considered a gel since $G'(\omega)$ exhibits a plateau and is much higher than $G''(\omega)$ over a wide range of frequencies. In panel **b**, although $G'(\omega)$ exhibits a plateau, $G'(\omega) < G''(\omega)$ in the plateau region, thus, the polymeric dispersion cannot be classified as a gel

loss modulus $G''(\omega)$ over a wide range of frequencies, and which confers their characteristic resilience on gel systems. Figure 1a, b shows the typical rheological behavior of a system that according to Almdal is classified as a gel (Fig. 1a) and of a diluted system which might possess a gel-like behavior (i.e. a polymeric dispersion), but cannot be classified as a gel: although the storage modulus $G'(\omega)$ exhibits a plateau, $G'(\omega) < G''(\omega)$ in the plateau region (Fig. 1b).

However, it is important that even this definition, which is based on a more analytical approach, excludes some systems that are currently classified as gels, i.e. aerogels, xerogels or undiluted systems (e.g. cross-linked polymer melts) (Hermans 1949; Flory 1953).

According to this definition, in the following sections a distinction will be made between gels and gel-like systems (i.e. viscous polymeric dispersions), such as *solvent gels* and PVA-borax systems.

2.1.2 Classification of Gels

As well as for gel definition, also identifying a unique classification criterion with universal validity is not trivial. Depending on the theoretical background and the field of interest, gels may be classified according to different parameters, i.e. the source or the nature of the gellant, the preparation method, the medium, the thermal behavior, functional groups, etc. (Kopeček and Yang 2007).

In this section only the classification criteria will be recalled, which are useful for a better understanding of the application properties of the different gel systems used in conservation of cultural heritage.

In this context, gels are mainly used as a vehicle for the cleaning fluid. Therefore, a first classification divides the gelled systems in two classes, whether the liquid phase is an organic solvent or water: organogels and hydrogels. In

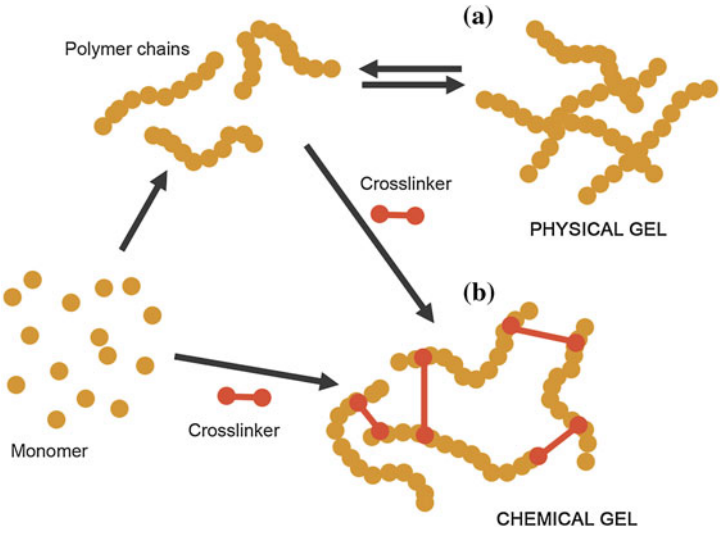

Fig. 2 Schematic representation of **a** a physical gel formed by association of macromolecular chains and **b** a chemical gel formed through a polymerization and crosslinking reaction

organogels a hydrophobic polymer usually forms the structural network and they are used for the removal of apolar water-insoluble materials. On the other hand, a network build up by a hydrophilic polymer is able to retain polar solvents. When the solvent is water, the gel is called a hydrogel. Hydrogels are used to support water, water-based cleaning systems (enzymes or salts solutions, chelating agents, etc.) or polar solvents (pure or blended).

One of the most useful classifications considers the nature of interactions occurring in the 3D structural network of gels. If the gelation process occurs owing to hydrophobic, electrostatic, van der Waals or hydrogen bond interactions, the system is named a "physical gel". If connections between different polymer chains are due to covalent bonds, the gel is referred to as a "chemical gel" (see Fig. 2).

The nature of the cross-links responsible for gel formation has considerable practical consequences on the application features of the final gel system. This is mainly due to the different energies involved in bond formation: physical interactions are characterized by energies approximately in the 1–120 kJ mol^{-1} range, while the energies involved in a covalent bond formation are much higher, typically spanning from ca. 200 to 650 kJ mol^{-1}. Owing to the low energies involved in gel formation, physical gels are usually thermoreversible, that is, the system reverts to the solution ("sol") state upon heating, due to melting of the supramolecular structure. Cooling back the solution results in a new sol-gel transition and the original gel is obtained. For instance, mixtures of water and natural polymers such as polysaccharides or proteins yield physical gels: the polymer is typically dissolved in water by heating the mixture (60–80 °C) and gelation occurs upon cooling the obtained solution to room temperature. On the other hand, when

Table 1 Overview on the principal differences between physical and chemical gels

	Physical gel	Chemical gel
Cross-linking	Weak interactions	Covalent bond
Thermal behavior	Reversible	Irreversible
Solvent dilution	Eventually solubilizes	Swells but not solubilizes
Shape	Mechanically adjustable	Fixed
Elastic modulus	Intermediate values	High values

cross-linking is due to covalent bonds, increasing the temperature over a critical value will break these bonds, but this is an irreversible process and the system will not be able to restore its original form. Chemical gels are typically obtained through polymerization and cross-linking reactions. For instance, in the 60s, the first soft contact lenses were obtained through the polymerization of hydroxyethyl methacrylate cross-linked with ethyleneglycol dimethacrylate (HEMA/EGDMA) (Wichterle and Lím 1960).

The physico-chemical structural differences between physical and chemical gels determine a completely different behavior in cleaning operations. In particular, physical gels grant a homogenous cleaning action even on rough surface, because they can be easily forced to adhere to non-flat areas. However, owing to fact that cohesion forces (between different parts of the gel) and adhesion forces (between the gel and the surface) are of the same order of magnitude, physical gels are likely to leave residues on the treated surface. For the clearance of gel residues, one is forced to use again non-confined neat solvents, arising those very issues described in previous paragraphs, which were the motivation for the introduction of gels in conservation of cultural heritage: even with appropriate solvents, this action may be damaging and stressful for the artifacts original materials. This is why the residues issue is the main controversy of the use of gels for cleaning purposes. On the other hand, the presence of covalent bonds in chemical gels makes them similar to a solid, also in mechanical behavior: being characterized by strong cohesion forces, their use ensures a residue-free treatment. As it will be further detailed in next paragraphs, the formulation of chemical gels specifically tailored for cleaning purposes were a breakthrough in conservation of cultural heritage. Table 1 reports the main differences between physical and chemical gels.

2.2 Nanofluids

The peculiar properties of nanofluids (i.e. micelles and microemulsions) are intrinsically related to those of surfactants, a wide class of chemicals that possess an extremely interesting behavior.

2.2.1 Surfactants

The term "surfactant" comes from the contraction of "surface active agent", which refers to the most prominent property of this class of compounds. In fact, surfactants are peculiar molecules composed by two different portions, having opposite affinity towards water: the first is commonly called "head" and is hydrophilic, while the other is called "tail" and is hydrophobic. Due to this "double affinity", surfactants are also called "amphiphiles" (from the greek words *amphi*, which means "both", and *philia*, which means "love", "friendship", "affinity") and they tend to distribute at the interfaces between two substances, usually lowering their interfacial energy.

Surfactants are grouped, according to their molecular structure, in four classes: (i) anionics, i.e. in water they ionize giving a negatively charged molecule (alkyl sulfates or sulfonates, alkyl carboxylates, alkyl phosphates); (ii) cationics, i.e. in water they ionize giving a positively charged molecule (quaternary ammonium salts, which one or more long alkyl chains are attached to); (iii) zwitterionics, i.e. molecules that possess two moieties having opposite charge (phospholipides, etc.); (iv) nonionics, i.e. uncharged molecular structures that do not ionize in water (polyethylene oxides, ortho esters, etc.).

2.2.2 Micelles

The main properties of surfactants are related to their ability of giving self-assembly. This feature, mainly observable in aqueous solutions (but not only), is due to attractive interaction, such as Van der Waals forces or effects related to the variation of interfacial free energy (Evans and Wennerström 1999; Holmberg et al. 2002; Cosgrove 2010). Depending on the chemical nature, concentration, and several other variables, surfactant molecules can aggregate from small oligomers to much more complex structures composed by 50–200 units and a size in the 2–200 nm range. Such aggregates are generally defined as "micelles" and they form when surfactant concentration is above a critic value called CMC, i.e. *critical micelle concentration* (see Fig. 3).

A micelle that forms in an aqueous environment is composed of a hydrophobic core, separated from the water bulk phase by a hydrophilic shell.

Micelles are able to solubilize small apolar molecules in the hydrophobic core, which are nearly to completely immiscible with water. This property has important applicative significance in that surfactant solutions with concentration higher than the CMC may be used for cleaning purposes. In fact micelles or surfactants are able to remove greasy organic matter adhered to a surface, following one of the mechanisms described by the classical theory of detergency (see Fig. 4) (Holmberg et al. 2002).

Roll-up: This mechanism is mainly related to fabric wetting, i.e. the surfactant-fabric interaction is decisive. Good soil release is usually obtained when

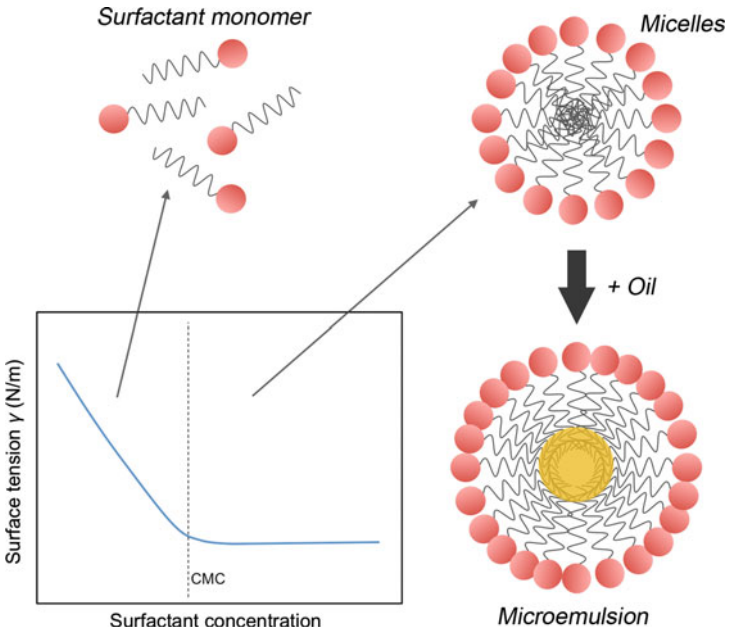

Fig. 3 The figure shows how surface tension of a surfactant aqueous solution changes as a function of surfactant concentration. Above the CMC micelles form. If an oil is added in the right amount a microemulsion may form, where droplets of oil are confined in the hydrophobic core of micelles

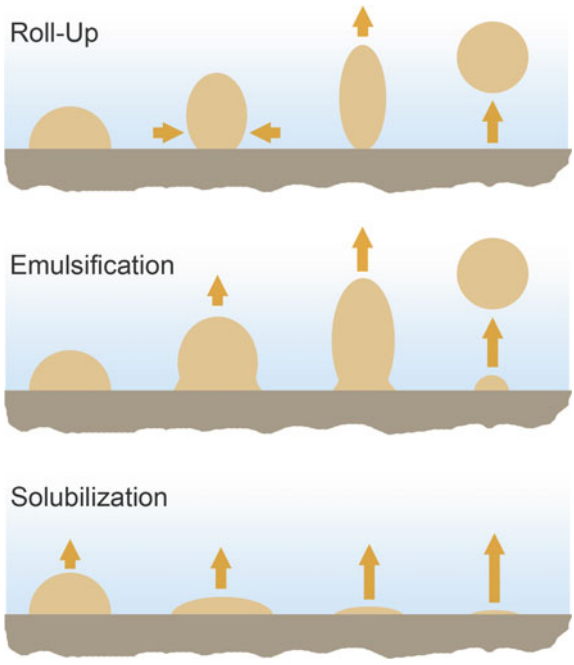

Fig. 4 The three mechanism for soil removal described by the classical detergency theory

contact angle is larger than 90°. This is typically the case of apolar oily soils on polar fibers, such as cotton.

Emulsification: This mechanism only involves surfactant/oil interaction, thus it is independent of the nature of the substrate. Low interfacial tension is needed in this process.

Solubilization: The oily soil is solubilized into a "microemulsion" (see next section) that forms in situ. Thus, in this process ultra-low interfacial tension between oil and the surfactant solution is needed. Also this mechanism is independent of the nature of the surface.

The last of the three mechanisms described by the classical detergency theory introduces the concept of "microemulsion", which is a further complex nanofluid possessing extremely interesting properties. As just said above, in this case the surfactant role is to provide ultra-low interfacial tension.

2.2.3 Microemulsions

As for gels, the rigorous definition of a microemulsion is not straightforward. Here we report two of the most accepted definitions available in literature:

> "A microemulsion is defined as a system of water, oil and amphiphile, which is a single optically isotropic and thermodynamically stable liquid solution" (Danielsson and Lindman 1981), and "We […] use the term microemulsion to mean a thermodynamically stable dispersion of large oil and surfactant or water and surfactant aggregates" (Mitchell and Ninham 1981).

According to these definitions, microemulsions possess some peculiar properties: they are macroscopically homogeneous and optically transparent fluids, while on the nanoscale, they are dispersed and non-continuous systems.

There can be oil-in-water (o/w) or water-in-oil (w/o) microemulsions, depending on the dispersed phase respectively being oil or water. Moreover, waterless or oil-in-oil (o/o) microemulsions exist, which possess valuable scientific interest, such as fluorinated compounds (LoNostro et al. 1999), or ionic liquids-based systems (Qiu and Texter 2008).

Differently from common oil/water emulsions, which are thermodynamically unstable (or meta-stable), microemulsions are considered as thermodynamically stable systems and are stable for very long time. This is due to the presence of one or more surfactants, which lower the surface tension at the water/oil interface to such an extent that spontaneous emulsification takes place. As said in the previous paragraph, ultra-low interfacial tension is needed for the formation of microemulsions, depending on the surfactant nature. A single surfactant might not be able to lower the interfacial tension to such low values, so that a co-surfactant, e.g. a medium length chain alcohol, is often needed to form microemulsions. This is the reason why macro-emulsions are more commonly encountered than microemulsions in everyday practice, even when water and oil are mixed together with a surfactant (Langevin 1988).

Moreover, droplets size in microemulsions and miniemulsions is comprised in the 10 to 8–100 nm range, thus sensibly smaller than visible radiation wavelength, and this is why they appear as optically transparent, while common emulsions are usually cloudy or milky, due to the presence of larger aggregates, usually in the micrometric range.

Due to their interesting properties, microemulsions can be used for a lot of purposes, ranging from enhanced oil recovery (Holmberg et al. 2002) to cosmetics and detergency (Stubenrauch 2008), from the synthesis of nanoparticles or latex paints to farmceutics and drug delivery (Fanun 2008). Recently, they were successfully proposed as cleaning systems in the field of conservation of cultural heritage. The detergent power of a generic microemulsion is given by the combination of several factors: detergency properties of micelles and surfactants solutions, solving power of the organic solvents included in the formulation and the huge interfacial surface of the system create a synergy that make these systems extremely effective and versatile in the removal of several organic compounds from the surface of works of art.

A more detailed description of surfactants, micelles and microemulsions is beyond the aim of this chapter; however, readers interested in having further information, may refer to this selected literature (Zana 1987; Langevin 1988; Laughlin 1994; Evans and Wennerström 1999; Holmberg et al. 2002; Robinson 2003; Stubenrauch 2008; Fanun 2008; Cosgrove 2010).

3 Gels and Nanofluids in Art Conservation

3.1 Traditional Gels

Before introducing to the most commonly used and to some innovative gelled systems for the cleaning of artistic surfaces, it is worth noting that not all described systems can be strictly defined as "gels" according to the mechanical definition (which is recalled in previous sections) formulated by Almdal et al. (1993). However, for simplicity and owing to their macroscopic appearance, which is very close to that of "real" gels, we will refer to these systems as gel-like systems.

One important class of materials traditionally used as a thickening agent to obtain gel-like systems consist of cellulose derivatives such as cellulose ethers (e.g. Klucel®, hydroxypropyl cellulose; Tylose®, methyl hydroxyethyl cellulose), which are common materials in pharmaceutical, cosmetic and food industry. In restoration practice cellulose ethers are mainly used as thickeners for water and polar solvents (e.g. alcohols). The dispersion of the polymer in the liquid phase yields a pasty system (see Fig. 5), whose viscosity depends on concentration, polymer degree of polymerization (DP) and the type of solvent.

These gel-like systems have many characteristics in common with physical gels. In fact, owing to their weak cohesion forces and adhesive properties they are prone

Fig. 5 Application of a 4 % w/w Klucel gel in an ethanol/acetone/isooctane mixture [printed with the kind permission of SELIDO (at IPCE, Instituto del Patrimonio Cultural de España, Madrid)]

to leave residues on the surface after treatment. Achieving a complete removal of the solid residue might be difficult, even after an accurate rinsing procedure (Casoli et al. 2014). Depending on the degree of substitution of the polymeric backbone, cellulose ethers are subjected to biological degradation; thus, the presence of residues might increase the risk of microbial proliferation.

The so-called "solvent gels" (see Fig. 6) represent another class of gel-like systems commonly used in restoration procedures. It is worth noting that here the term "gel" is used for these systems even if they are not *actual* gels according to their rheological behavior, rather they are simply thickened viscous systems. The use of this term is therefore improper from a strictly scientific standpoint, but justified by its use by conservators. Solvent gels were proposed by R. Wolbers at the end of the 80s (Wolbers et al. 1988; Wolbers 2000), and are based on the use of

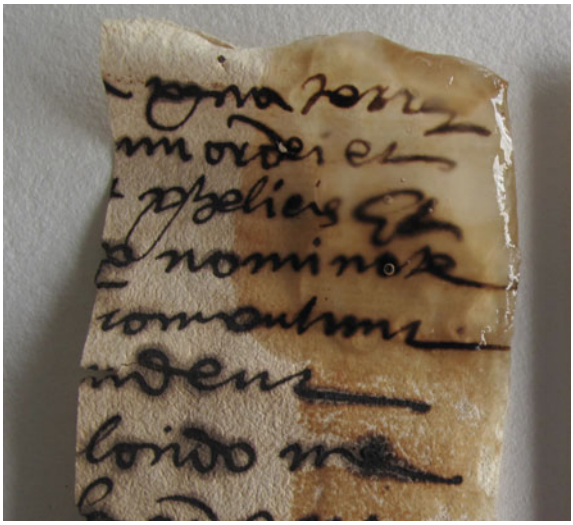

Fig. 6 Application of a *solvent gel* formulation on paper [printed with the kind permission of SELIDO (IPCE, Instituto del Patrimonio Cultural de España, Madrid)]

polyacrylic acid as the gellant (e.g. Carbopol®, Pemulens®). Their preparation involves the dispersion of the polymer in a solvent and further addition of a weakly basic nonionic surfactant (Ethomeen®), together with a small amount of water, whose alkalinity causes deprotonation of the carboxylic functions of the polyacrylic acid. The consequent unfolding of the polymer chains and their association into a 3D network yields a viscous system able to thicken the solvent. The choice of surfactants having different polarities permits solvent gel systems being able to thicken several organic solvents (Ethomeen C12 is used for low-polarity solvents, while Ethomeen C25 is used to gel highly polar solvents).

Owing to this considerable versatility, the fair effectiveness and relatively ease of preparation, solvent gels are one of the most diffused thickened cleaning systems nowadays used among restorers.

Thus, their use must always be combined with the formulation of an adequate rinsing procedure. The residues consist in the non-volatile components of the solvent-gel, that is both, the gellant polymer and the surfactant. In an extensive study carried out by Kieslich and Burnstock in 1996 through gas-chromatography/mass spectroscopy (GC-MS) and scanning electron microscope (SEM), Ethomeen residues were detected on the surface even after clearance of the treated area using swabs or solvent mixtures (Burnstock and Kieslich 1996). Furthermore, as suggested by the SEM investigations, the surface changes caused by the clearance solvents are close to those observed after cleaning using non-confined solvents.

The stability and nature of Ethomeen degradation products were extensively studied (Burnstock and White 2000; Stulik et al. 2004). Although the long-term effects of their interactions with the original materials are not completely understood, some concerns emerged, especially for prolonged contact with oil/resin paint media (Burnstock and White 2000).

Some natural polysaccharide-based hydrogels such as agar and gellan gum, were recently introduced for the cleaning of artistic substrates. These materials are widely used in pharmacological, biomedical and food industry. They are non-toxic (they are used as thickeners for food preparations) and can be attacked by bacteria and other microorganisms (in fact they are used as growth media in biological applications). On the market they are available as powders, with a moderate cost. For gel preparation they are typically dissolved in water (by heating at ca. 80 °C) in concentrations ranging from 1 to 5 %. Gel formation occurs similarly for both materials: at 80 °C the system is a *sol* and polysaccharide chains exist as random coils which rearrange upon cooling (typically below 40 °C) assuming a double-helix conformation. The thermoreversible 3D network of the gel finally consists in double-helix chains, linked together through secondary bonds such as hydrogen or van der Waals interactions (Arnott et al. 1974; Takahashi et al. 1999; Djabourov et al. 2013). For cleaning purposes, polysaccharide-based systems can be used as both, a viscous solution or after gelation has occurred. In fact, after cooling of the solution, these systems maintain the shape of the container where they are casted, for which reason they are also known as “rigid gels”. The “rigid” nature of these gels permits the cleaning of surfaces minimizing left residues after treatment (Cremonesi 2006; Mazzuca et al. 2014).

Agar-agar (e.g. AgarArt) consists in a mixture of agarose and agaropectin, two polysaccharides extracted from the cell walls of some red *algae* (mostly *Gelidium*, *Euchema* and *Gracilaria* genera). The gel porosity, which affects the water retention features of the hydrogel, depends on agarose concentration. Agar gels are stable in a relatively extended pH range and can be loaded with water-based cleaning system (enzymes, chelating agents, surfactant solutions). More recently, their use in association with nanostructured cleaning fluids (microemulsions) has also been assessed (Gorel 2010). The use of agar gels is generally proposed for paper artifacts (Banik et al. 2003), but in-door and out-door applications on immovable artworks are also reported in literature (Marchiafava et al. 2014; Gulotta et al. 2014).

Gellan gum (e.g. Phytagel®, Kelocogel®) is a linear heteropolysaccharide produced by the bacteria Pseudomonas elodea. It consists of (1,3)-β-D-glucose, (1,4)-β-D-glucuronic acid, (1,4)-β-D-glucose and (1,4)-α-L-rhamnose units. In respect to agar gels, gellan gum gels are more transparent and smaller concentrations (1–2 %) are needed to obtain similar gel strengths. The presence of cations (e.g. Ca^{2+} added as calcium acetate solution) contributes to stabilization of the structure, enhancing gel strength and elasticity (Mao et al. 2001). The ability of gellan gum hydrogels to perform a safer cleaning action on paper artifacts was compared to those of a traditional water bath by Micheli et al. (2014). Mazzuca et al. (2014) used gellan gum gels in association with enzymes for the removal of starch paste from paper and assessed the absence of residues with chromatographic techniques.

Although water retention features of polysaccharide-based hydrogels are considerably higher than those of other physical gels (e.g. Klucel®), in the presence of water-sensitive materials (e.g. water-soluble binders or inks on paintings or manuscripts) are not sufficient, causing the alteration of the original materials (Domingues et al. 2013).

3.2 Contributes from Colloid Science: Innovative Gels

As highlighted above, the use traditional gels and gel-like systems might present some limitations related to residues or not sufficient retention properties. Recent colloid and surface science research was focused on the formulation of alternative and advanced systems able to overcome these limitations. In particular, innovative gel systems were proposed (Baglioni and Chelazzi 2013; Baglioni et al. 2014b). More recently, the most promising formulations developed at CSGI were registered under the trademark "Nanorestore Gel®", and are available to restorers (www.csgi.unifi.it/products/products.html).

3.2.1 Rheoreversible Gels

Rheoreversible gels can be obtained starting from polyamines (i.e. polyallylamine, PAA and polyethyleneimine, PEI) (Carretti et al. 2003b, 2004, 2005, 2008, 2010a). Bubbling CO_2 through a PAA solution yields a gel whose 3-D network is build up by the strong inter-chain interactions established between the newly formed polyammonium carbamate (PAA·CO_2) chains. The formed gel can be directly applied on the surface to be cleaned. After the cleaning action, gel removal is obtained through conversion of the viscoelastic system in a free-flowing liquid, which can be cleared by means of a cotton swab. The sol-gel transition of these rheoreversible gels is obtained through decarboxylation of the PAA·CO_2 that occurs by simply adding a small amount (a few drops) of a weak (0.05 M) acetic acid solution (see Fig. 7).

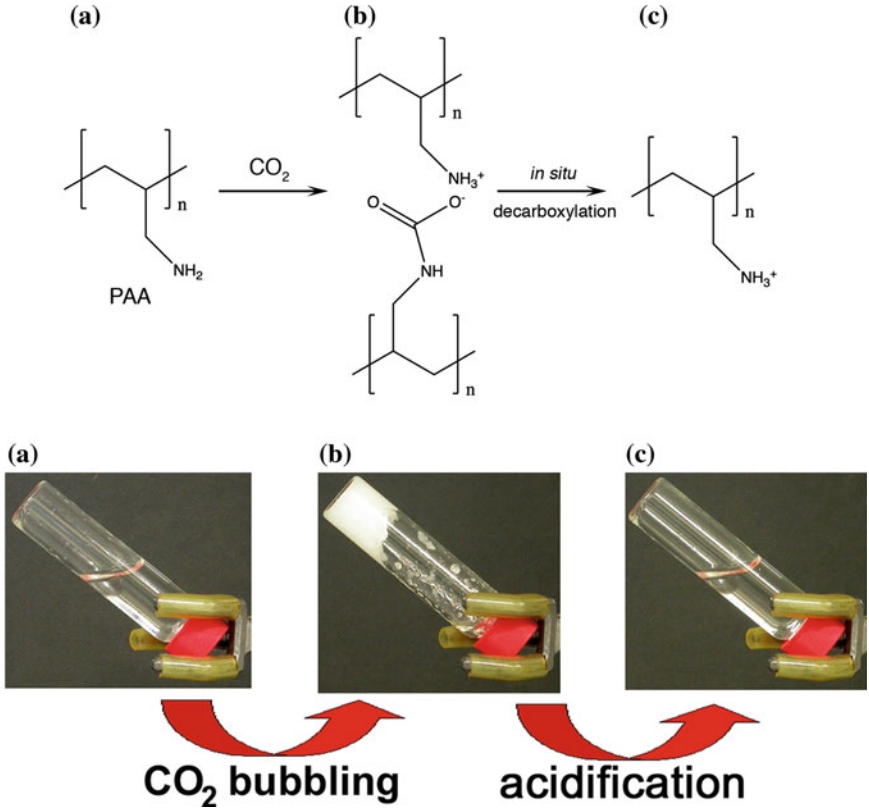

Fig. 7 Mechanism of formation of a polyallylamine rheoreversible gel: bubbling CO_2 into solution leads to gel formation, while acidification converts the gel back to a free-flowing system. (Reprinted with permission from Carretti et al. (2004). Copyright (2004) American Chemical Society)

3.2.2 Acrylamide-Based Nanosponges

The association of a gel network with magnetic nanoparticles, thus permitting the gel to be responsive to an applied magnetic field, represents a further approach, useful for the cleaning of surfaces that are sensitive to mechanical stress. Magnetic ferrite nanoparticles were synthesized and characterized by Bonini et al. (2007, 2008). Nanoparticles were functionalized and associated to an acrylamide-based hydrogel. Acrylamide-based hydrogels are chemical gels characterized by good mechanical properties, which permit an easy handling, and micrometric pores, which permit a slow and controlled release of the cleaning fluid on the artistic surface. When functionalized with magnetic nanoparticles, these nanomagnetic sponges can be removed from the surface without any direct handling, simply using a permanent magnet (see Fig. 8).

The complete gel removal and the absence of nanoparticle residues on the surface after treatment was confirmed by Fourier transform infrared analysis (FT-IR) and investigations trough Scanning Electron Microscope coupled with Energy dispersive X-ray spectroscopy (SEM-EDX) (Bonini et al. 2007). Moreover, gels can be freeze-dried yielding a magnetic xerogel (i.e. a gel after the complete loss of the fluid phase) that can be reverted to its original swollen state after rehydration.

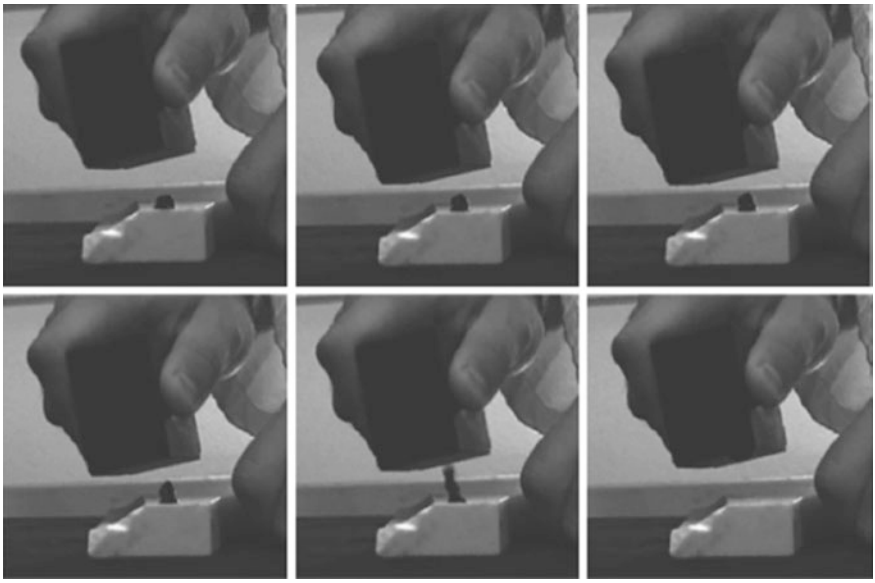

Fig. 8 When functionalized with magnetic nanoparticles the acrylamide-based hydrogel can be removed without any direct handling by using a permanent magnet. (Reprinted with permission from Bonini et al. (2007). Copyright (2007) American Chemical Society)

3.2.3 PVA-Borax Highly Viscous Polymeric Dispersions

One of the most appealing, recently developed cleaning tools, is represented by gel-like systems based on a 3D poly(vinyl alcohol) (PVA)-borax network (Carretti et al. 2009, 2010a, b; Natali et al. 2011). The macroscopic appearance of these systems is that of a gel, but since they cannot be classified as gels from a strict rheological point of view, they are referred to as Highly Viscous Polymeric Dispersions (HVPDs). Cross-linking of the PVA [or partially hydrolyzed poly(vinyl acetate) (PVAc)] is achieved through a condensation reaction between the PVA hydroxyl groups and borax, which results in a highly viscoelastic system. As reported in literature, parameters as pH, temperature, composition of the fluid phase and relative amounts of reagents, affect the nature of the cross-links. As a consequence, the final mechanical properties of the system can be tuned and adapted to specific needs. In fact thanks to viscoelastic properties, PVA-borax HVPDs are easily shaped and modeled, thus maximizing contact to the surface they are put in contact with. Moreover, the high elastic modulus is responsible for a further important application feature: after application, the system can be easily removed from the surface through a one-step peeling action (e.g. using tweezers) (see Fig. 9). As investigated by Carretti et al. (2010b) through FT-IR measurements, no detectable residues are present on the treated surface after "peeling" of the HVPD.

The choice of the gellant (PVA or partially hydrolyzed PVAc) permits to tune the solubilizing power of these versatile systems. In fact, significant amounts of organic co-solvents (up to 75 % w/w of the total liquid portion of the system, depending on the nature of both, the gellant and loaded solvent), including 1-propanol, 2-propanol, *N*-methyl-2-pyrrolidone, acetone, cyclohexanone and propylene carbonate, can be loaded in PVA-borax formulations making them suitable for the removal of a wide range of different materials (Angelova et al. 2011; Natali et al. 2011).

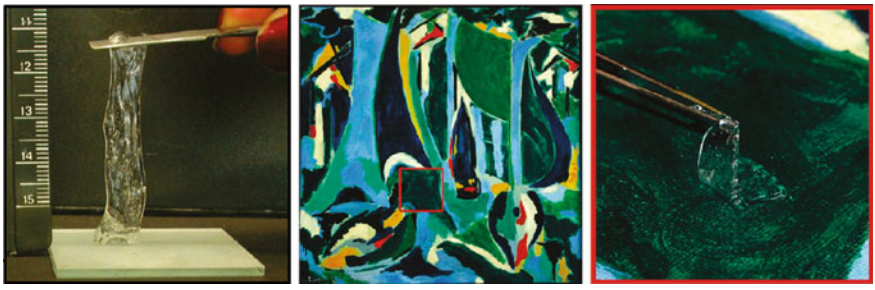

Fig. 9 Removal by peeling of a PVA-Borax HVPD (*left*). A PVA-Borax HVPD is applied on the oil on canvas painting, "Le Voiles" by Marcel Burtin (1902–1979) and removed by means of tweezers. (Readapted with permission from Natali et al. (2011). Copyright (2011) American Chemical Society)

3.2.4 Cleaning Water-Sensitive Surfaces: Highly Retentive Chemical Hydrogels

In the last two decades restorers were encouraged by the scientific community to limit the use of free organic solvents due to lack in control and selectivity and to issues related to the safety of the working environment. For these reasons, several alternative water-based cleaning systems were proposed, including the use of enzymes, surfactants, chelating agents (Wolbers 2000; Stavroudis et al. 2005), and, more recently, nanostructured fluids (Baglioni and Chelazzi 2013; Baglioni et al. 2014b).

However, the majority of artistic surfaces are water-sensitive (e.g. canvas, paper, water-soluble binders and inks), thus the interaction with water may cause mechanical stress (swelling) or unwanted solubilization of the original materials. Confining the water-based system in a gel permits a safer cleaning action by controlling the penetration within the porous structure of the artifact.

On the other hand, chemical gels are very attractive materials for applications as cleaning tools of artistic surfaces. In fact, a 3D network built up by covalent bonds represents a guarantee towards concerns on gel residues after treatment. In fact, thanks to strong cohesion forces of the network, no potentially harmful rinsing strategies using free solvent mixtures nor mechanical action to remove the gel is needed after the cleaning process has been performed.

In order to face the excessive penetration of the water-based cleaning fluid and the residue issues, highly retentive chemical hydrogels were recently developed by CSGI (Domingues et al. 2013). The proposed formulation is based on a semi-interpenetrating network (semi-IPN), obtained embedding free chains of poly (vinyl pyrrolidone)—PVP—in a network of poly(2-hydroxyethyl methacrylate)—p (HEMA) (see Fig. 10). In fact, PVP chains are entangled and physically bound to the pHEMA 3D network. The semi-interpenetrated structure of the network permits

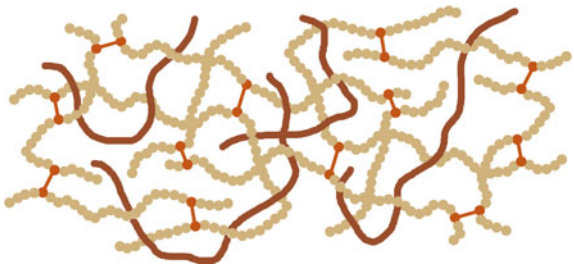

Fig. 10 Schematic representation of a semi-IPN network. While the polymeric chains obtained through the polyaddition reaction are crosslinked creating a tridimensional network, the interpenetrating polymer (i.e. PVP in the present case) interacts via physical reactions. However, the embedding/entanglement of PVP macromolecules, which takes place during the gelling reaction, is so efficient that, once the gel has been washed to remove unreacted chemicals, it behaves like a "true" chemical gel, leaving no residues on treated surfaces

Table 2 Water release (mg/cm^2) for three different semi-IPN formulations and for two polysaccharide-based physical gels (agar and gellan gum, both 3 % w/w)

	Water release (mg/cm^2)
p(HEMA)/PVP 50 % H_2O	8
p(HEMA)/PVP 58 % H_2O	15
p(HEMA)/PVP 65 % H_2O	16
Agar (3 % w/w)	30
Gellan gum (35 w/w)	33

Readapted with kind permission from Springer Science + Business Media, Domingues et al. (2014) Table 1

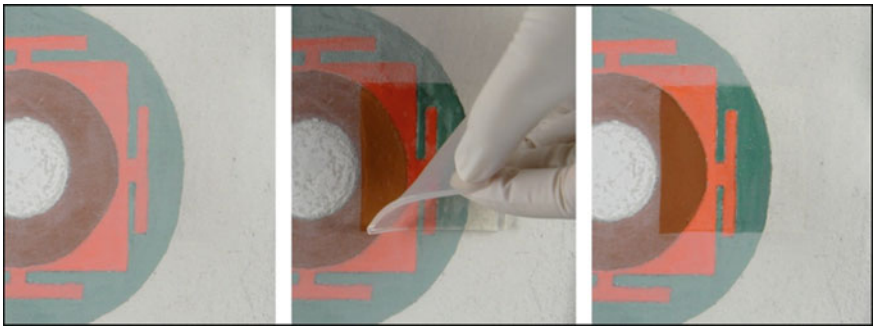

Fig. 11 Application and removal of a water loaded p(HEMA)/PVP hydrogel for the cleaning of water-soluble grime from a painted surface. (Reprinted with permission from Domingues et al. (2013). Copyright (2013) American Chemical Society)

to benefit from both, the mechanical stability of the p(HEMA) network and the high hydrophilicity of PVP.

Hydrogels are soft and transparent and can hold high water content (see Table 2). Moreover, the good mechanical properties permit an easy handling and gel preparation as foils (ca. 2–3 mm thickness) that can be directly applied on the surface to be treated. Hydrogels can be used with neat water (for the removal of water soluble grime), water-based cleaning fluids, but also associated to some polar solvents (e.g. glycols, alcohols, among others) (Domingues et al. 2014). Due to their cohesion, after application they can be easily removed (see Fig. 11) without leaving detectable residues.

The final properties of the hydrogel mainly depend on the p(HEMA)/PVP ratio and the amount of water used during gel preparation. In fact, changes in the compositional ratios permit to tune hydrogels properties (i.e. hydrophilicity of the network, pore size distribution, mechanical properties) for specific application needs.

Literature reports three different formulations, having different water content, that were deeply investigated (Domingues et al. 2013). The study showed that macropores size ranges from 5 to 35 μm, while the mesh, that intrinsically gives a measure of nano-sized pores, ranges from 2.5 to 3.1 nm (see Fig. 12).

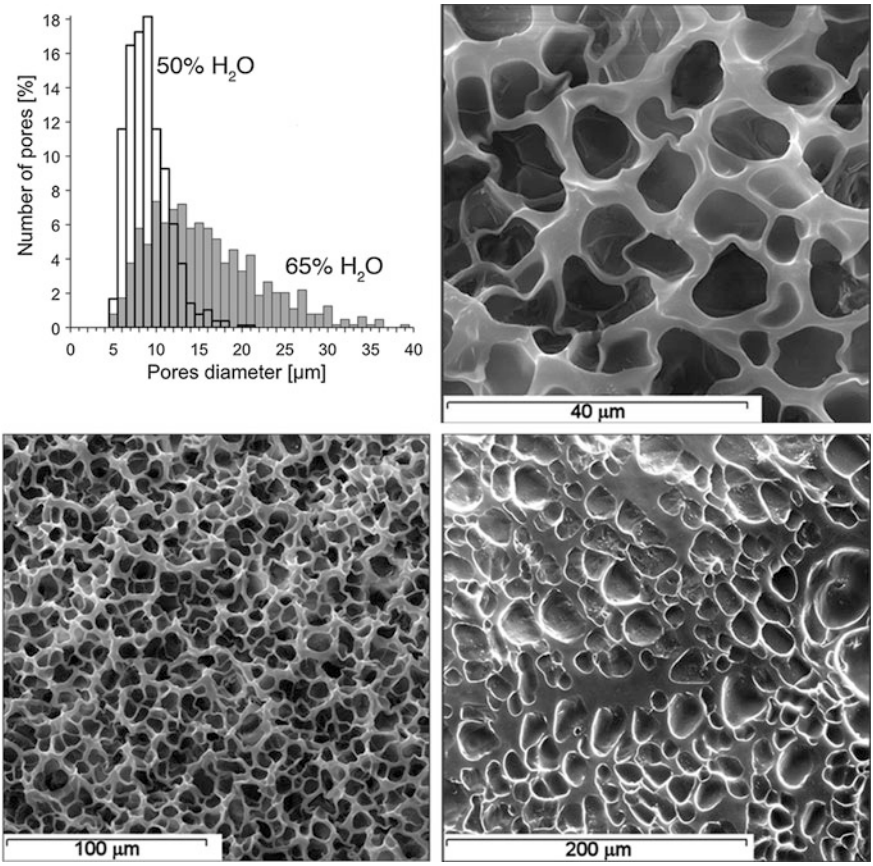

Fig. 12 Scanning electron microscope images of p(HEMA)/PVP different hydrogel formulations and relative pore size distribution. (Readapted with permission from Domingues et al. (2013). Copyright (2013) American Chemical Society)

The mechanical properties affect the ability of the gel to adhere to different surfaces, while hydrophilicity of the network and porosity have a direct influence on retention/release ability of the embedded fluid.

Chemical p(HEMA)/PVP hydrogels have proven to be highly retentive and permit to control the action of water even on highly-sensitive substrates. The water release of the three p(HEMA)/PVP formulations, along with those of agar and gellan gum gels (3 % w/w), are reported in Table 2, showing that the fluid (water) is more effectively confined in the chemical gel formulations. Figure 13 shows the application of a p(HEMA)/PVP formulation and a 3 % w/w AgarArt® hydrogel on a water-soluble ink on paper. The effect of the excessive wetting of the surface using AgarArt® is evidenced by the migration of the ink, that is completely avoided using the p(HEMA)/PVP formulation.

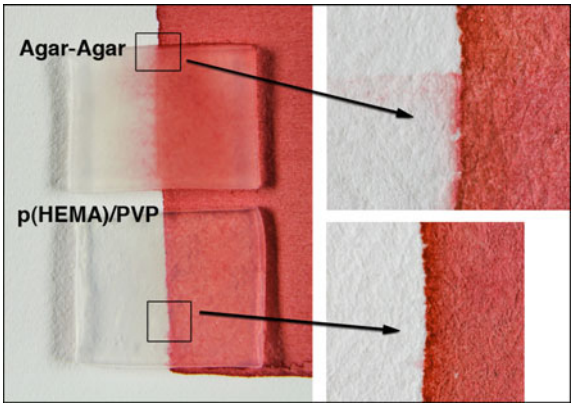

Fig. 13 Five minutes application of a 3 % agar and a p(HEMA)/PVP hydrogel on paper colored with a water soluble ink (brazilwood). (Reprinted with permission from Domingues et al. (2013). Copyright (2013) American Chemical Society)

One of the most remarkable features of p(HEMA)/PVP hydrogels is that their application field can be further expanded through the synergic association with nanofluids, such as micellar solutions or microemulsions. In fact, nanofluids-loaded semi-IPNs hydrogels are being successfully used for the removal of unwanted hydrophobic coatings (i.e. aged adhesives, varnishes or protective agents) from water-sensitive substrates, such as canvas and paper. The following paragraphs will highlight the benefits related to the use of the above-mentioned cleaning fluids and the advantages arising by merging these two advanced technologies.

3.3 Nanofluids in the Cleaning of Cultural Heritage

Before entering the details on the properties of nanofluid-loaded hydrogels, it is worth spending a few lines describing the role of micelles and microemulsions in conservation of cultural heritage.

The introduction of nanofluids in the field of conservation of cultural heritage is relatively recent. The first use of a microemulsion for the cleaning of works of art dates back to the end of the 80s of last century, during the restoration of the frescoes by Masaccio and Masolino in the Brancacci Chapel, Florence (Borgioli et al. 1995; Baglioni and Chelazzi 2013). The paintings were covered by several stains and wax spots, due to the many votive candles that were kept close to the walls for centuries. In order to remove the hydrophobic contaminants from the wall matrix it was necessary to intervene with a system capable of solubilizing wax without spreading it inside the pores of the mortar. It was thus decided to use a dodecane-in-water microemulsion, so that waxy compounds could be solubilized by the alkane and dispersed in the micelles' core in an aqueous environment. The excellent outcome of this first application led the way to the use of nanofluids in conservation of cultural heritage.

Nanofluids nowadays are the most interesting alternative to the use of non-confined neat organic solvents. Using such systems it is possible to obtain a more controlled and (often) selective cleaning action. Moreover, the low amount of the organic phase and the aqueous nature of nanofluids make them low-environmental impact and low-toxicity systems, besides reducing the risk of redeposition of the removed matter in the porous substrate of the work of art, since it is swollen and detached rather than completely dissolved, as it occurs for traditional neat organic solvents.

After the excellent results obtained in the workshop of Brancacci Chapel, the research on nanofluids for the cleaning of works of art was carried on by CSGI researchers at the University of Florence with the aim of finding more and more effective systems able to answer to complex conservative issues. Since the end of the 90s of last century, several formulations were proposed, which were used worldwide for the removal of polymeric coating from wall paintings, becoming useful tools for conservators and restorers. Several important case studies exist, where different issues were addressed, spanning from the removal of a thick polymer coating that was irreversibly damaging the mural decoration of the Annunciation Church in Nazareth, Israel, to the removal of acrylic/vinyl copolymeric coatings from Mesoamerican wall paintings conserved in the archaeological sites of Cholula and Mayapan (Mexico), or Uaxactun (Guatemala), going through tests in several Italian contexts, such as the cases of Siena, Arezzo, Milan and others. The formulations proposed to intervene in the aforementioned case studies include ionic, nonionic or zwitterionic surfactants, and a wide palette of organic solvents, i.e. alkanes, alcohols, ketons, esters, aromatic compounds, selected depending on the nature of the given material that has to be removed, e.g. acrylic, vinyl, acrylic/vinyl, acrylate/styrene, siliconic resins or alkyd polymers and copolymers (Carretti et al. 2001, 2003a, 2007; Grassi et al. 2009; Baglioni et al. 2010, 2012, 2014a, b, 2015; Giorgi et al. 2010; Baglioni and Chelazzi 2013).

3.4 Nanofluids-Loaded Hydrogels

As reported in previous paragraphs, chemical hydrogels, such as acrylamide-based gels or p(HEMA)/PVP can be regarded as containers for aqueous cleaning systems. These include aqueous nanofluids, which can be loaded into the hydrogels simply immersing the gels in the fluids and letting the composite system equilibrating. In fact the porosity of these hydrogels has a sufficient size to permit the supramolecular aggregates of nanofluids to migrate from the bulk aqueous phase to the gel core. Small-angle X-ray scattering techniques were used to confirm that both, the gel and the nanostructured cleaning fluid keep their structure upon being associated (Pizzorusso et al. 2012), which is essential to provide maximum cleaning effectiveness.

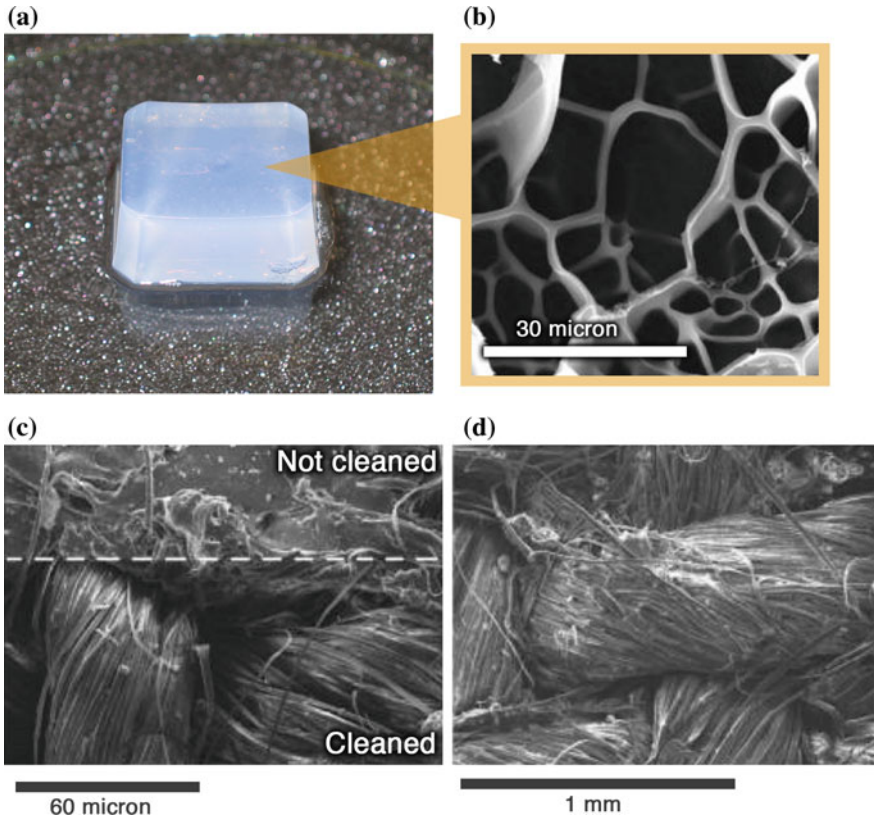

Fig. 14 **a** An acrylamide-based hydrogel is shown together with its structure (**b**), investigated through SEM imaging. In **c**, **d** SEM micrographs the removal of a relining adhesive from the back of a canvas is shown. **c** Here the boundary between a cleaned area and the untreated surroundings is reported. **d** The final appearance of cleaned canvas fibers. (Readapted with permission from Pizzorusso et al. (2012). Copyright (2012) American Chemical Society)

Acrylamide-based hydrogels loaded with microemulsions were successfully used for the removal of aged adhesives (e.g. Mowilith DM5®, a commercial adhesive based on vinyl acetate and *n*-butyl acrylate) as for instance from lined canvases (Chevalier et al. 2008; Pizzorusso et al. 2012). The application demonstrated that the gels permit a good wettability of the surface, while avoiding penetration through the substrate or spreading along the canvas surface. After treatment with the gel, the swollen adhesive was removed through gentle mechanical action and no alteration (i.e. swelling) of the fibers was observed (see Fig. 14).

More recently the combination of p(HEMA)/PVP hydrogels with several nanofluids created a new class of detergent systems, which are quickly attracting a significant interest by the conservators' community.

Mechanical properties of these semi-IPNs can be easily tuned by changing the amount of water in the formulation and their handling is safe and convenient. Loading of the cleaning agent, i.e. the nanofluid, is simple and doesn't requires particular equipment, so that can be also performed in situ, during restoration workshops, prior to their use. Gel sheets can be shaped at will, simply by cutting them with a blade or with a spatula, and can be used both on horizontal and vertical surfaces, due to their adhesion properties. In addition to the excellent properties of the gels, the nanofluid, i.e. the actual cleaning agent of the formulation, permit the removal of water-insoluble organic matter, with the use of a system mainly composed by water, which is safe, non-toxic and easily controllable.

All these features make the nanofluids-loaded p(HEMA)/PVP hydrogels one of the most interesting innovation in the field of cleaning of works of art.

3.5 Cleaning of Contemporary Paintings—A Case Study

Here we report on a cleaning test performed on contemporary painting by the Italian artist Enrico Castellani. The work of art belongs to series of the "*Superfici Bianche*" ("*White Surfaces*"), which are unframed canvases totally painted in white by the artist. The peculiarity of this paintings is that, while the canvas is completely monochromatic, its surface planarity was modified by the artist by means of nails and supports, in order to create volumetric and lighting effects without using other colors. The painting that we had the opportunity to test belongs to a private collection and was being restored by Studio Restauri Formica s.r.l.

Over time, the white paint used by the artist had yellowed; therefore a delicate cleaning intervention was needed aimed to remove the most superficial altered layers of the paint, in order to revert back to the original white. In other words, the pictorial layer had to be thinned by an extremely controlled cleaning action to avoid any overcleaning.

It was then decided to test a nanofluid-loaded hydrogel, which could guarantee an effective swelling of the external layers of the paint, together with a good control on the cleaning action.

In order to select the right nanofluid to load into the gel, the organic binder of the paint was identified, by means of FT-IR investigation, as poly(vinyl acetate). Thus, a nanofluid originally formulated for the removal of vinyl coatings from Mesoamerican wall paintings was chosen for the cleaning test, which is based on an anionic surfactant, ethyl acetate and propylene carbonate (Baglioni et al. 2010; Giorgi et al. 2010). The nanofluid was loaded into a p(HEMA)/PVP hydrogel, simply by keeping the gel immersed in the cleaning fluid overnight. Then a small square of gel was cut, having a size of about 2 cm × 2.5 cm and a thickness of 2 mm. The gel was gently applied over the yellowed painted surface for 30 s to 1 min. After gel removal the surface appeared just slightly wet, indicating that the surface layers of the paint were swollen, but no halo nor deformation of the canvas was observed after the treatment. The treated area was then gently cleared by

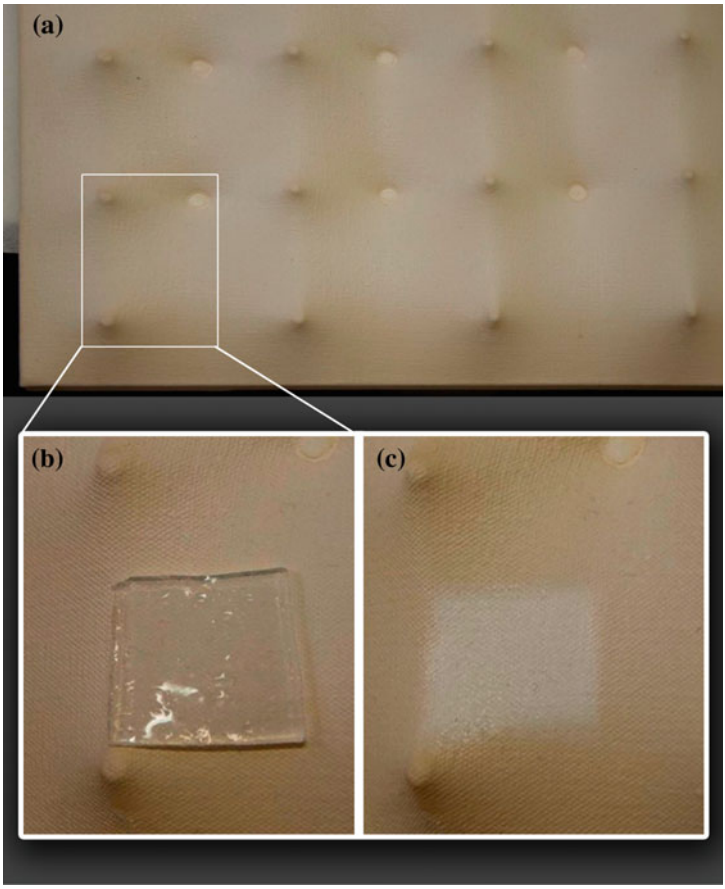

Fig. 15 **a** A portion of the painting "Superficie Bianca" by E. Castellani. Nails and supports that modify the canvas planarity are clearly visible. **b** In the detail-box, the nanofluid-loaded hydrogel is applied over the yellowed surface of the painting. **c** After gel removal, the surface is gently cleared with a dry cotton swab; the treated area is clearly whiter than the surrounding surface, indicating that the aged superficial layers have been successfully removed by the action of the combined cleaning system

carefully rolling a dry cotton swab over the swollen paint. The result of the cleaning test is shown in Fig. 15, where the recovery of the original white color is evident.

As shown in this example, cleaning is a very delicate and crucial part of the restoration of a work of art. Thus, conservation scientists are continuously searching for innovative tools that restorers can benefit from. The introduction of gels and organic solvents in this field opened up new perspectives, but the growing contribution of nanoscience and surface science was particularly important in view of the innovative materials that were proposed in the recent years. Among these, confined-aqueous cleaning media, such as hydrogels and nanofluids represent a

series of tools, which is attracting increasing interest in the community of conservators. Finally, the combined cleaning systems obtained loading nanofluids into hydrogels are one of the most promising innovations in the field of conservation science.

Acknowledgments Aurelia Chevalier is acknowledged for her help in the assessment of acrylamide-based hydrogels for the removal of polymeric coatings from relining canvases. Florence Gorel is acknowledged for the preparation of samples for the assessment of p(HEMA)/PVP hydrogels. Vittoria Castoldi and Luciano Formica (Studio Restauri Formica s.r.l.) are gratefully acknowledged for giving us the opportunity to test the nanofluid-loaded hydrogels on an extremely interesting conservation case. Patrizia Buratti (Studio Restauri Formica s.r.l.) is acknowledged for the assistance during the cleaning test on the painting by E. Castellani. This work was partly funded by NANOFORART—Nano-materials for the conservation and preservation of movable and immovable artworks, FP7-NMP European project (http://www.nanoforart.eu) and NANORESTART—NANOmaterials for the REStoration of works of ART, EU programme Horizon 2020 (www.nanorestart.eu).

References

Alemán JV, Chadwick AV, He J et al (2007) Definitions of terms relating to the structure and processing of sols, gels, networks, and inorganic-organic hybrid materials (IUPAC Recommendations 2007). Pure Appl Chem. doi:10.1351/pac200779101801

Almdal K, Dyre J, Hvidt S, Kramer O (1993) Towards a phenomenological definition of the term "gel". Polym Gels Netw 1:5–17. doi:10.1016/0966-7822(93)90020-I

Angelova LV, Terech P, Natali I et al (2011) Cosolvent gel-like materials from partially hydrolyzed poly(vinyl acetate)s and borax. Langmuir ACS J Surf Colloids 27:11671–11682. doi:10.1021/la202179e

Arnott S, Fulmer A, Scott WE et al (1974) The agarose double helix and its function in agarose gel structure. J Mol Biol 90:269–284. doi:10.1016/0022-2836(74)90372-6

Baglioni P, Chelazzi D (2013) Nanoscience for the conservation of works of art. Royal Society of Chemistry

Baglioni M, Rengstl D, Berti D et al (2010) Removal of acrylic coatings from works of art by means of nanofluids: understanding the mechanism at the nanoscale. Nanoscale 2:1723. doi:10.1039/c0nr00255k

Baglioni M, Giorgi R, Berti D, Baglioni P (2012) Smart cleaning of cultural heritage: a new challenge for soft nanoscience. Nanoscale 4:42. doi:10.1039/c1nr10911a

Baglioni M, Raudino M, Berti D et al (2014a) Nanostructured fluids from degradable nonionic surfactants for the cleaning of works of art from polymer contaminants. Soft Matter 10:6798–6809. doi:10.1039/C4SM01084A

Baglioni P, Chelazzi D, Giorgi R (2014b) Nanotechnologies in the conservation of cultural heritage: a compendium of materials and techniques. Springer, Berlin

Baglioni M, Jàidar Benavides Y, Berti D et al (2015) An amine-oxide surfactant-based microemulsion for the cleaning of works of art. J Colloid Interface Sci 440:204–210. doi:10.1016/j.jcis.2014.10.003

Banik G, Cremonesi P, de la Chappelle A, Montalbano L (2003) Nuove metodologie nel resaturo del materiale cartaceo. Il Prato, Padova

Bonini M, Lenz S, Giorgi R, Baglioni P (2007) Nanomagnetic sponges for the cleaning of works of art. Langmuir 23:8681–8685. doi:10.1021/la701292d

Bonini M, Lenz S, Falletta E et al (2008) Acrylamide-based magnetic nanosponges: a new smart nanocomposite material. Langmuir 24:12644–12650. doi:10.1021/la802425k

Borgioli L, Caminati G, Gabrielli G, Ferroni E (1995) Removal of hydrophobic impurities from pictorial surfaces by means of heterogeneous systems. Sci Technol Cult Herit J 4:67–74
Burnstock A, Kieslich T (1996) A study of the clearance of solvent gels used for varnish removal from paintings. James & James, London, pp 253–262
Burnstock A, White R (2000) A preliminary assessment of the aging/degradation of Ethomeen C-12 residues from solvent gel formulations and their potential for inducing changes in resinous paint media
Burnstock A, Learner T, Learner T, Learner T (1992) Changes in the surface characteristics of artificially aged mastic varnishes after cleaning using alkaline reagents. Stud Conserv 37:165–184
Carretti E, Dei L, Miliani C, Baglioni P (2001) Oil-in-water microemulsions to solubilize acrylic copolymers: application in cultural heritage conservation. In: Koutsoukos PPG (ed) Trends in colloid and interface science XV. Springer, Berlin, pp 63–67
Carretti E, Dei L, Baglioni P (2003a) Solubilization of acrylic and vinyl polymers in nanocontainer solutions. application of microemulsions and micelles to cultural heritage conservation. Langmuir 19:7867–7872. doi:10.1021/la034757q
Carretti E, Dei L, Baglioni P, Weiss RG (2003b) Synthesis and characterization of gels from polyallylamine and carbon dioxide as gellant. J Am Chem Soc 125:5121–5129. doi:10.1021/ja034399d
Carretti E, Dei L, Macherelli A, Weiss RG (2004) Rheoreversible polymeric organogels: the art of science for art conservation. Langmuir ACS J Surf Colloids 20:8414–8418. doi:10.1021/la0495175
Carretti E, Dei L, Weiss RG (2005) Soft matter and art conservation. Rheoreversible gels and beyond. Soft Matter 1:17–22. doi:10.1039/b501033k
Carretti E, Giorgi R, Berti D, Baglioni P (2007) Oil-in-water nanocontainers as low environmental impact cleaning tools for works of art: two case studies. Langmuir 23:6396–6403. doi:10.1021/la700487s
Carretti E, Dei L, Weiss RG, Baglioni P (2008) A new class of gels for the conservation of painted surfaces. J Cult Herit 9:386–393. doi:10.1016/j.culher.2007.10.009
Carretti E, Grassi S, Cossalter M et al (2009) Poly(vinyl alcohol)—borate hydro/cosolvent gels: viscoelastic properties, solubilizing power, and application to art conservation. Langmuir 25:8656–8662. doi:10.1021/la804306w
Carretti E, Bonini M, Dei L et al (2010a) New frontiers in materials science for art conservation: responsive gels and beyond. Acc Chem Res 43:751–760. doi:10.1021/ar900282h
Carretti E, Natali I, Matarrese C et al (2010b) A new family of high viscosity polymeric dispersions for cleaning easel paintings. J Cult Herit 11:373–380. doi:10.1016/j.culher.2010.04.002
Casoli A, Di Diego Z, Isca C (2014) Cleaning painted surfaces: evaluation of leaching phenomenon induced by solvents applied for the removal of gel residues. Environ Sci Pollut Res Int 21:13252–13263. doi:10.1007/s11356-014-2658-5
Chevalier A, Chelazzi D, Baglioni P et al (2008) Extraction d'adhésifs de rentoilage en peinture de chevalet: nouvelle approche. Allied Publishers, New Delhi, pp 581–589
Cosgrove T (2010) Colloid science: principles, methods and applications. Wiley, London
Cremonesi P (2006) Applicazione di metodologie di intervento più recenti per la pulitura del materiale cartaceo. In: Atti delle giornate di studio Problemi di Restauro. Il Prato, pp 39–46
Danielsson I, Lindman B (1981) The definition of microemulsion. Colloids Surf 3:391–392. doi:10.1016/0166-6622(81)80064-9
Djabourov M, Nishinari K, Ross-Murphy SB (2013) Physical gels from biological and synthetic polymers. Cambridge University Press, Cambridge
Domingues JAL, Bonelli N, Giorgi R et al (2013) Innovative hydrogels based on semi-interpenetrating p(HEMA)/PVP networks for the cleaning of water-sensitive cultural heritage artifacts. Langmuir 29:2746–2755. doi:10.1021/la3048664
Domingues J, Bonelli N, Giorgi R, Baglioni P (2014) Chemical semi-IPN hydrogels for the removal of adhesives from canvas paintings. Appl Phys A 114:705–710. doi:10.1007/s00339-013-8150-0

Evans DF, Wennerström H (1999) The colloidal domain: where physics, chemistry, biology, and technology meet. Wiley, London
Fanun M (2008) Microemulsions: properties and applications. CRC Press, Boca Raton
Flory PJ (1953) Principles of polymer chemistry. Cornell University Press, Ithaca
Giorgi R, Baglioni M, Berti D, Baglioni P (2010) New methodologies for the conservation of cultural heritage: micellar solutions, microemulsions, and hydroxide nanoparticles. Acc Chem Res 43:695–704. doi:10.1021/ar900193h
Goldberg LA (1989) A fresh face for Samuel Gompers: methyl cellulose poultice cleaning. J Am Inst Conserv 28:19–29. doi:10.1179/019713689806046228
Gorel F (2010) Assessment of agar gel loaded with micro-emulsion for the cleaning of porous surfaces
Grassi S, Favaro M, Tomasin P, Dei L (2009) Nanocontainer aqueous systems for removing polymeric materials from marble surfaces: a new and promising tool in cultural heritage conservation. J Cult Herit 10:347–355. doi:10.1016/j.culher.2008.10.003
Gulotta D, Saviello D, Gherardi F et al (2014) Setup of a sustainable indoor cleaning methodology for the sculpted stone surfaces of the Duomo of Milan. Herit Sci 2:1–13. doi:10.1186/2050-7445-2-6
Hermans PH (1949) Gels. In: Kruyt HR (ed) Colloid science. Elsevier Publishing Company, Amsterdam, pp 483–651
Holmberg K, Jönsson B, Kronberg B, Lindman B (2002) Surfactants and polymers in aqueous solution. Wiley, London
Khandekar N, Phenix A, Sharp J (1994) Pilot study into the effects of solvents on artificially aged egg tempera films. Conservator 18:62–72. doi:10.1080/01410096.1994.9995086
Kopeček J, Yang J (2007) Hydrogels as smart biomaterials. Polym Int 56:1078–1098. doi:10.1002/pi.2253
Langevin D (1988) Microemulsions. Acc Chem Res 21:255–260. doi:10.1021/ar00151a001
Laughlin RG (1994) The aqueous phase behavior of surfactants. Academic Press, London
Lloyd DJ (1926) The problem of gel structure. In: Alexander J (ed) Colloid chemistry: theoretical and applied. The Chemical Catalogue Company, New York, pp 767–782
LoNostro P, Choi S-M, Ku C-Y, Chen S-H (1999) Fluorinated microemulsions: a study of the phase behavior and structure. J Phys Chem B 103:5347–5352. doi:10.1021/jp9827025
Mao R, Tang J, Swanson BG (2001) Water holding capacity and microstructure of gellan gels. Carbohydr Polym 46:365–371. doi:10.1016/S0144-8617(00)00337-4
Marchiafava V, Bartolozzi G, Cucci C, et al (2014) Colour measurements for monitoring the conservation of contemporary artworks
Mazzuca C, Micheli L, Cervelli E et al (2014) Cleaning of paper artworks: development of an efficient gel-based material able to remove starch paste. ACS Appl Mater Interfaces 6:16519–16528. doi:10.1021/am504295n
Micheli L, Mazzuca C, Cervelli E, Palleschi A (2014) New strategy for the cleaning of paper artworks: a smart combination of gels and biosensors. Adv Chem 2014:e385674. doi:10.1155/2014/385674
Mitchell DJ, Ninham BW (1981) Micelles, vesicles and microemulsions. J Chem Soc Faraday Trans 2 Mol Chem Phys 77:601–629. doi:10.1039/F29817700601
Natali I, Carretti E, Angelova L et al (2011) Structural and mechanical properties of "peelable" organoaqueous dispersions with partially hydrolyzed Poly(vinyl acetate)-Borate networks: applications to cleaning painted surfaces. Langmuir 27:13226–13235. doi:10.1021/la2015786
Phenix A, Sutherland K (2001) The cleaning of paintings: effects of organic solvents on oil paint films. Rev Conserv 2:47–60
Pizzorusso G, Fratini E, Eiblmeier J et al (2012) Physicochemical characterization of acrylamide/bisacrylamide hydrogels and their application for the conservation of easel paintings. Langmuir 28:3952–3961. doi:10.1021/la2044619
Qiu Z, Texter J (2008) Ionic liquids in microemulsions. Curr Opin Colloid Interface Sci 13:252–262. doi:10.1016/j.cocis.2007.10.005
Robinson BH (2003) Self-assembly. IOS Press

Stauffer D, Coniglio A, Adam M (1982) Gelation and critical phenomena. In: Dušek K (ed) Polymer networks. Springer, Berlin, pp 103–158
Stavroudis C, Doherty T, Wolbers R (2005) A new approach to cleaning i: using mixtures of concentrated stock solutions and a database to arrive at an optimal aqueous cleaning system. WAAC Newsl 27:17–28
Stockmayer WH (1944) Theory of molecular size distribution and gel formation in branched polymers II. General cross linking. J Chem Phys 12:125–131. doi:10.1063/1.1723922
Stubenrauch C (2008) Microemulsions: background, new concepts, applications, perspectives. Wiley, London
Stulik D, Miller D, Khandekar N et al (2004) Solvent gels for the cleaning of works of art: the residue question. Getty Publications, Los Angeles
Takahashi R, Akutu M, Kubota K, Nakamura K (1999) Characterization of gellan gum in aqueous NaCl solution. In: Nishinari K (ed) Physical chemistry and industrial application of gellan gum. Springer, Berlin, pp 1–7
Wichterle O, Lím D (1960) Hydrophilic gels for biological use. Nature 185:117–118. doi:10.1038/185117a0
Wolbers R (2000) Cleaning painted surfaces: aqueous methods. Archetype, London
Wolbers R, Sterman N, Stavroudis C (1988) Notes for the workshop on new methods in the cleaning of paintings. The Getty Conservation Institute, Marina del Rey
Zallen R (1983) The physics of amorphous solids. Wiley, New York
Zana R (1987) Surfactant solutions: new methods of investigation. M. Dekker